Metallogeny of the Powell Block, Rouyn-Noranda Mining District, Québec

by

Marina Decker Schofield

A thesis submitted in partial fulfillment of the requirements
for the degree of Doctor of Philosophy (PhD)
in Mineral Deposits and Precambrian Geology

The Faculty of Graduate Studies
Laurentian University
Sudbury, Ontario, Canada

© Marina Decker Schofield, 2022

THESIS DEFENCE COMMITTEE/COMITÉ DE SOUTENANCE DE THÈSE
Laurentian Université/Université Laurentienne
Office of Graduate Studies/Bureau des études supérieures

Title of Thesis Titre de la thèse	Metallogeny of the Powell Block, Rouyn-Noranda Mining District, Québec
Name of Candidate Nom du candidat	Schofield, Marina
Degree Diplôme	Doctor of Philosophy
Program Programme	Mineral Deposits and Precambrian Geology
Date of Defence Date de la soutenance	February 08, 2023

APPROVED/APPROUVÉ

Thesis Examiners/Examinateurs de thèse:

Dr. Harold Gibson
(Co-Supervisor/Co-directeur(trice) de thèse)

Dr. Bruno Lafrance
(Co-Supervisor/Co-directeur(trice) de thèse)

Dr. Howard Poulsen
(Committee member/Membre du comité)

Dr. Peter Hollings
(External Examiner/Examinateur externe)

Dr. Ming Cai
(Internal Examiner/Examinateur interne)

Approved for the Office of Graduate Studies
Approuvé pour le Bureau des études supérieures
Tammy Eger, PhD
Vice-President Research (Office of Graduate Studies)
Vice-rectrice à la recherche (Bureau des études supérieures)
Laurentian University / Université Laurentienne

ACCESSIBILITY CLAUSE AND PERMISSION TO USE

I, **Marina Schofield**, hereby grant to Laurentian University and/or its agents the non-exclusive license to archive and make accessible my thesis, dissertation, or project report in whole or in part in all forms of media, now or for the duration of my copyright ownership. I retain all other ownership rights to the copyright of the thesis, dissertation or project report. I also reserve the right to use in future works (such as articles or books) all or part of this thesis, dissertation, or project report. I further agree that permission for copying of this thesis in any manner, in whole or in part, for scholarly purposes may be granted by the professor or professors who supervised my thesis work or, in their absence, by the Head of the Department in which my thesis work was done. It is understood that any copying or publication or use of this thesis or parts thereof for financial gain shall not be allowed without my written permission. It is also understood that this copy is being made available in this form by the authority of the copyright owner solely for the purpose of private study and research and may not be copied or reproduced except as permitted by the copyright laws without written authority from the copyright owner.

Abstract

The Rouyn-Noranda mining district of Québec is located along the southern margin of the Abitibi greenstone belt of the Archean Superior Province. It hosts 22 Cu-Zn-Au-Ag volcanogenic massive sulfide (VMS) deposits, distributed amongst four fault blocks (Hunter, Flavrian, Powell and Horne). The Powell Block hosts the Au-rich Quemont VMS deposit and separates the Horne deposit, a world class Au-rich VMS deposit, from conventional VMS deposits (≤ 1 g/t Au) north of the Beauchastel fault. The structural and stratigraphic evolution of the Powell Block is poorly constrained and as a result, the time-stratigraphic position of the Quemont deposit relative to the Horne deposit and deposits of the Flavrain Block is uncertain, as are the processes responsible for the anomalous gold content of the Horne and Quemont deposits. Gold-quartz-carbonate and quartz-sulfide (Cu-Ag-Zn) epigenetic veins are also present, but their origin and relative timing remain enigmatic.

The Powell Block can be subdivided into two distinctive domains, the Brownlee and Joliet domains, representing two overlapping volcanic centres. These two domains both consist of lower Blake River Group volcanic strata that differ slightly in age and volcanic history. The Brownlee domain is characterized by mafic dominated, bimodal volcanism (ca. 2701 Ma), whereas the Joliet domain is characterized by a thick sequence of felsic coherent and volcaniclastic units (≥2702 Ma). Two base metal mineralizing hydrothermal events are recognized. An early event is related to voluminous felsic volcanism, concomitant subsidence and the formation of the Quemont and Horne deposits in the Joliet domain and Horne block, respectively. These two deposits formed within the district's largest monogenic felsic volcanic centre in a subaqueous setting that was locally emergent. Given this setting, the Au-rich Quemont and Horne deposits may have had a more direct magmatic input resulting in higher Au grades than the Cu-Zn VMS deposits of the

Flavrian Block, which formed in a mafic dominated, bimodal, effusive and perhaps, a deeper water volcanic setting. A later hydrothermal event at ca. 2699~2695 Ma is related to the formation of disseminated, vein and breccia hosted (e.g. Joliet Breccia) quartz-sulfide (Cu-Ag-Zn) mineral occurrences, with variations in deposit characteristics reflecting differences in depth of formation and proximity to a magmatic source. The lateral zoning of alteration types, compositional gains and losses, and metal tenor are similar to VMS footwall alteration zones within the district and elsewhere, and these breccias and veins are part of a broad continuum of subsurface, cross-stratal magmatic-hydrothermal mineralization to seafloor, stratiform, VMS mineralization, a spectrum akin to the porphyry-epithermal continuum of modern subaerial volcanic arcs.

Approximately 30–40 m.y. later, gold-quartz-carbonate veins were emplaced during N-S shortening of the volcanic rocks. Superposition of alteration related to these younger veins perturbed and masked regional alteration patterns related to the Quemont and Horne deposits, but due to their restricted distribution and comparatively low-grade, did not substantially affect the original gold tenor of these VMS deposits.

Keywords: volcanogenic massive sulfide deposits; orogenic gold deposits; magmatic-hydrothermal deposits; superposition; Archean; volcanology; structural geology; metallogeny

Co-Authorship Statement

The work presented in this dissertation has benefitted from the scientific guidance and supervision of several collaborators, listed as co-authors. This thesis was conceived by Drs. Harold Gibson and Howard Poulsen and supervised by Drs. Harold Gibson, and Bruno Lafrance with input from committee member Dr. Howard Poulsen as part of the Metal Earth research initiative.

Field work and sample collection was completed by the candidate with the assistance of B. Courchesne (2017), D. Leung (2017), D. Dickson (2018), B. Smith (2019), M. Langa (2019) and H. Seibel (2020). Field work was completed over four field seasons: (1) June-August (2017); (2) May-August (2018); (3) May-August (2019); (4) September (2020). An area approximately 3 km by 4 km area was mapped at a scale of 1:10 000, with additional detailed mapping at 1:100 scale.

Samples were collected and cut by the candidate. Thin sections were prepared by Willard Desjardins at Laurentian University. Additional thin sections were prepared by Vancouver Petrographics and Precision Petrographics. Lithogeochemistry samples were sent to ALS laboratories for whole rock crushing and analysis. Six samples were processed for zircon U-Pb ID TIMS by Dr. Mike Hamilton at the Jack Satterly lab at the University of Toronto. Dr. Jeffrey Marsh conducted LA-ICP-MS analysis of monazite at the Mineral Exploration Research Centre Isotope Geochemistry Laboratory of Laurentian University. Whole-rock and mineral (quartz) $\delta^{18}O$ analysis was completed at Laval University by Christophe Scheffer, Benoit Quesnel and Georges Beaudoin. Petrographic analysis was conducted by the candidate at Laurentian University. All initial interpretations of the data and the first drafts were prepared by the candidate with guidance and reviews from the co-authors.

Acknowledgments

First and foremost, I would like to thank my supervisors Dr. Harold Gibson and Dr. Bruno Lafrance for their endless support, guidance, constructive feedback and helpful discussions throughout this project. I would also like to express my gratitude towards Dr. Howard Poulsen for his input and support as committee member, and for always playing the role of "devil's advocate" to help me become a better researcher. I feel incredibly fortunate to have had such an amazing committee. Their knowledge, expertise, supervising styles, enthusiasm and positivity complemented each other, and I have evolved and grown immensely as a geologist under their supervision.

Financial support for this project was provided by Canada First Research Excellence Fund, Northern Ontario Heritage Fund Corporation, and the Mineral Exploration Research Centre at Laurentian University. Additional funding was provided by the Goodman School of Mines PhD Scholarship.

Many thanks to all the professors in the Harquail School of Earth Science, in particular Dr. Ross Sherlock, Dr. Dan Kontak, and Dr. Doug Tinkham, for helpful discussions. Dr. Gerald Riverin and Mr. Jean Goutier are thanked for providing critical historical data. Dr. Ray Goldie and Mr. Sylvain Piccard are also thanked for providing useful reference samples for this study.

Thank you to everyone I worked with during my summers in Rouyn-Noranda. Thanks to my field assistants Brittany Courchesne (2017), Derek Leung (2017), David Dickson (2018), Brandon Smith (2019), Michael Langa (2019) and Henning Seibel (2020). Dr. Taus Jorgensen thank you for your guidance with fieldwork and lab work and for many helpful discussions over dumplings at Horizon Thai.

I would also like to thank my family and friends for their endless encouragement and support, which has been invaluable throughout this project. Thanks to my Sudbury friends for the many coffee breaks, potlucks, board game nights, and weekend adventures to Killarney. Thanks to my father, Larry Schofield, for inspiring my initial love of geology. Thanks to my mother, Gladys Schofield, my sisters, Meredith and Melody Schofield, and my friends back home, for your understanding during my long absences and the many care packages throughout the years. Lastly, I thank Henning Seibel for always believing in me, and making me laugh when I need it most, I love you.

Table of Contents

Thesis Defence Committee /Comité de soutenance de thèse ii

Abstract iii

Co-Authorship Statement v

Acknowledgments vi

Table of Contents viii

List of Tables xv

List of Figures xvi

List of Appendices xix

Chapter 1 1

1 Introduction to thesis 1

1.1 Background 1

1.2 Research Problem 6

1.3 Thesis Objectives 8

1.4 Structure of the Thesis 9

1.5 Statement of Original Contributions 12

1.6 References 13

Chapter 2 21

2 Recognizing subsurface breccias in Archean terranes: implications for district scale metallogeny 21

2.1 Abstract 21

2.2 Introduction 22

2.3 Geological setting of the Joliet Breccia 24

2.3.1 Description of the Joliet Breccia 27

2.4 Methodology 30

2.5 Results 31

2.5.1 Lithogeochemistry 31

2.5.2 Zircon U-Pb ID-TIMS geochronology 31

2.5.3 Structural Analysis 32

2.5.4 Mineralization 33

2.6 Discussion 40

2.6.1 Previously proposed model for the Joliet Breccia 41

2.6.2 Possible fragmentation processes for the Joliet Breccia 42

2.6.3 Distinguishing subsurface vs. surface breccias in the ancient rock record 46

2.6.4 Mineralization and associated hydrothermal alteration 47

2.6.5 Comparison to other known breccias within the Rouyn-Noranda mining district . 51

2.6.6 Metallogenic context of the Joliet Breccia within the Rouyn-Noranda mining district… 53

2.7 Conclusions 55

2.8 Acknowledgements 57

2.9 Figures 58

2.10 Tables 73

2.11 References 76

2.12 Appendices 87

Chapter 3 127

3 Discriminating superimposed alteration associated with epigenetic base and precious metal vein systems in the Rouyn-Noranda mining district, Québec; Implications for exploration in ancient volcanic districts 127

3.1 Abstract 127

3.2 Introduction 128

3.3 Regional Geology of the Rouyn-Noranda mining district 130

3.4 Methodology 133

3.5 Geology of the Powell Block 133

3.6 Structural analysis 135

3.7 Cu-Zn-Ag prospects and occurrences 136

3.7.1 Cu-Zn-Ag vein petrography and paragenesis 138

3.7.2 Hydrothermal alteration associated with Cu-Zn-Ag veins 139

Albite-chlorite alteration (spilitization): 139

Spotted (sericite-chlorite) alteration: 140

Chlorite alteration: 141

3.8 Au deposits and occurrences 142

3.8.1 Gold-quartz-carbonate vein petrography and paragenesis 143

3.8.2 Hydrothermal alteration associated with gold-quartz-carbonate veins 144

Chlorite-calcite-albite alteration: 144

Hematite alteration: 144

Albite-sericite ± calcite alteration: 144

Ankerite - sericite ± fuchsite alteration: 145

3.9 U-Pb TIMS Geochronology 145

3.10 Oxygen isotopic analysis 147

3.11 Discussion 149

3.11.1 Timing of gold-quartz-carbonate vein versus quartz-sulfide Cu-Zn-Ag rich vein mineralization 149

3.11.2 Quartz-sulfide Cu-Zn-Ag rich veins, emplacement and origin 149

3.11.3 Gold-quartz-carbonate veins, emplacement and origin 151

3.11.4 Comparison of alteration signatures associated with both vein systems 152

3.11.5 Significance of the superposition of alteration events on the district-scale alteration patterns. 154

3.12 Conclusions 156

3.13 Acknowledgements 158

3.14 Figures 159

3.15 Tables 174

3.16 References 175

3.17 Appendix 190

Chapter 4 248

4 Volcanic reconstruction of Lower Blake River Group strata of the Powell Block, Rouyn-Noranda Mining District, Québec; Implications for the timing and setting of base metal mineralization 248

4.1 Abstract 248

4.2 Introduction 249

4.3 Terminology 251

4.4 Geology of the Rouyn-Noranda Mining District 252

4.5 Volcanogenic massive sulfide deposits 253

4.6 Deformation and metamorphism 255

4.7 Methodology 257

4.8 Stratigraphic relationships of 2702-2700 Ma Blake River Group Strata within the Powell Block 258

4.8.1 Brownlee domain 259

4.8.2 Joliet domain 266

4.9 Lithogeochemistry of volcanic units of the Powell Block 268

4.10 Intrusions 268

4.10.1 Early mafic dikes/sills 269

4.10.2 Early felsic dikes/sills 269

4.10.3 Powell Pluton 270

4.10.4 Joliet tonalite suite 271

4.11 U-Pb ID TIMS Zircon Geochronology 272

4.11.1 Powell rhyolite 272

4.11.2 Brownlee rhyolite 272

4.11.3 Felsic dikes 273

4.12 Base metal mineralization 274

4.13 Discussion 276

4.13.1 Lithostratigraphic and chronostratigraphic considerations 276

4.13.2 Structural evolution of the Powell Block 277

4.13.3 Interpretation of volcanic lithofacies of the Brownlee domain 279

4.13.4 Interpretation of the volcanic lithofacies of the Joliet domain 287

4.13.5 Volcanic reconstruction of the LBRG within the Powell Block 290

4.13.6 Timing and setting of base metal mineralization within the Powell and Horne Blocks… 291

4.13.7 Implications for the Rouyn-Noranda mining district 293

4.14 Conclusions 295

4.15 Acknowledgements 296

4.16 References 297

4.17 Tables 308

4.18 Figures 316

4.19 Appendices 338

Chapter 5 361

5 Concluding statements 361

5.1 Conclusions 361

5.1 Future work 363

5.2 References 364

Appendices 366

Appendix A 366

List of Tables

Table 2-1: Zircon U-Pb isotopic data for eastern Powell block tonalite samples. 73

Table 2-2: Average values for select trace and major elements by lithology. 74

Table 2-3: Distinguishing characteristics of breccias. 75

Table 3-1: Zircon U-Pb isotopic data for tonalite intrusions. 174

Table 3-2: Summary table of measured $\delta^{18}O_{quartz}$ and calculated $\delta^{18}O_{H2O}$ values for veins. 175

Table 4-1: Zircon CA-ID-TIMS U-Pb isotopic data for Powell Block rhyolites. 308

Table 4-2: Characteristic features of formations and members of LBRG strata of the Powell Block 310

Table 4-3: Summary of base metal deposits and occurrences within the Powell Block, Rouyn-Noranda. 314

List of Figures

Figure 1.1 Geological map of the Abitibi Greenstone belt 4

Figure 1.2 Geological map of the Rouyn-Noranda mining district 5

Figure 2.1: Regional geology map of the Noranda volcanic complex. 58

Figure 2.2: Geological setting of the Joliet Breccia. 59

Figure 2.3: Geological map of the Joliet Breccia. 60

Figure 2.4: Photographs showing characteristic features of the main lithologies. 61

Figure 2.5: Whole-rock lithogeochemical classification of the main lithologies. 63

Figure 2.6: Zircon grain images and Concordia diagrams for ID-TIMS U-Pb analyses 64

Figure 2.7: Alteration and metal distribution map of the Joliet Breccia, with summary stereonet plot and rose diagrams. 65

Figure 2.8: Photographs showing characteristic textures of sulfide minerals and hydrothermal cement. 66

Figure 2.9: LAICPMS monazite maps and data. 68

Figure 2.10: Photographs showing characteristic features of the main alteration types. 69

Figure 2.11: Schematic diagram illustrating the interpreted model of formation of the Joliet Breccia. 71

Figure 2.12: Relative and absolute timing of relevant major geological events. 72

Figure 3.1: Regional geology map of the Rouyn-Noranda mining district. 159

Figure 3.2: Geology map of the Powell Block. 160

Figure 3.3: Geological map and stereonet projections of the Powell syncline and Powell fault 161

Figure 3.4: Outcrop photographs of structural features of D_2 and D_3. 162

Figure 3.5: Structural maps of the Powell fault. 163

Figure 3.6: Geological and alteration maps of Cu-Zn-Ag prospects. 164
Figure 3.7: Ternary plots of metal tenor for Cu-Zn-Ag veins compared to typical base metal deposits. 165
Figure 3.8: Photographs of textures of Cu-Zn-Ag veins and associated alteration. 166
Figure 3.9: SEM-EDS mineral chemistry results for chlorite and carbonate. 167
Figure 3.10: Geology and alteration maps for gold-quartz-carbonate vein deposits and occurrences. 168
Figure 3.11: Photographs of characteristic textures of the gold-quartz-carbonate-veins and associated alteration. 169
Figure 3.12: Results of ID-TIMS U-Pb analysis of two tonalite samples. 171
Figure 3.10: whole-rock and quartz $\delta^{18}O$ values. 172
Figure 3.14: Schematic diagram of relative timing and general morphology of Cu-Zn-Ag veins and gold-quartz-carbonate veins. 173
Figure 4.1: Regional geology map of the Rouyn-Noranda mining district. 316
Figure 4.2: Lithological compilation map of the Lower Blake River Group strata of the Powell Block. 317
Figure 4.3: Lithostratigraphic map with location of stratigraphic transects. 318
Figure 4.4: Stratigraphic columns for the transects shown in Figure 3. 319
Figure 4.5: Characteristic features of the Brownlee rhyolite formations..... 320
Figure 4.6: Lithogeochemistry data for the main volcanic units of the Powell Block. 321
Figure 4.7: Characteristic features of the Lower and Upper Powell Basalt members of the Powell formation. 322
Figure 4.8: Characteristic features of the Lower Marker member of the Powell formation. 323

Figure 4.9: Detailed stratigraphic section and photographs of the lower marker member of the Powell formation. 324
Figure 4.10: Characteristic features of the Powell rhyolite member of the Powell formation. .. 325
Figure 4.11: Characteristic features of the Powell tuff member of the Powell formation. 326
Figure 4.12: Characteristic features of the Héré Creek rhyolite formation. 327
Figure 4.13: Detailed stratigraphic sections of the contact between the Powell and Héré Creek rhyolite formations. 328
Figure 4.14: Characteristic features of the Joliet formation. 329
Figure 4.15: Characteristic features of dikes found in the study area. 330
Figure 4.16: Graphical summary of volcanic strata and intrusions within the study area. 331
Figure 4.17: Zircon grain images and concordia diagrams for ID-TIMS U-Pb analyses. 332
Figure 4.18: Summary diagram showing U-Pb zircon ages for the district 333
Figure 4.19: Sample location map for Brownlee rhyolite area. 334
Figure 4.20: Schematic reconstruction of the interpreted hydrothermal system that formed the Cu-Zn-Ag veins. 335
Figure 4.21: Whole rock lithogeochemistry for rhyolite units within the Powell Block compared to the Horne rhyolite. 336
Figure 4.22: Schematic cross-section through the Noranda subsidence structure. 337

List of Appendices

A 2-1: Detailed analytical methodology 87

A 2-2: LAICPMS U-Pb data 98

A 2-3: Multi element geochemistry 116

A 2-4: Whole-rock geochemistry 120

A 2-5: Alteration geochemistry plots 124

A 3-1: Multi element geochemistry of veins 190

A 3-2: Whole rock lithogeochemistry 192

A 3-3: Whole-rock $\delta^{18}O$ results 212

A 3-4: Quartz $\delta^{18}O$ results 214

A 3-5: SEM-EDS Chlorite and Carbonate data 215

A 4-1: Whole-rock lithogeochemistry results of the Powell Block 338

A 4-2: Regional whole-rock lithogeochemistry comparison 357

Chapter 1

1 Introduction to thesis

1.1 Background

Volcanogenic massive sulfide (VMS) deposits form at or near the seafloor as strata-bound mounds or subseafloor replacement bodies, commonly underlain by discordant stockwork vein mineralization (Franklin et al., 1981; Lydon, 1988; Barrie and Hannington, 1999; Large et al., 2001; Franklin et al., 2005). These deposits are polymetallic (Cu-Zn-Pb±Au±Ag), making them less vulnerable to metal price fluctuations (Mercier-Langevin et al., 2011) and they constitute an important source of metals in Canada, making up 27% of its Cu production, 49% of its Zn, 20% of its Pb, 40% of its Ag and 3% of its Au (Galley et al., 2007). VMS deposits form during extension in a variety of tectonic and geological settings (Franklin et al., 2005). Syn-volcanic structures control the location of VMS deposits by providing cross-stratal permeability for the upflow of hydrothermal fluids, which precipitate massive sulfide mineralization at or just below seafloor during hiatuses in volcanism (Gibson et al., 1999). These structures can be repeatedly reactivated through time and control the location of volcanic vents and associated VMS deposits at different stratigraphic levels as a volcanic complex grows, making them important exploration targets (Knuckey et al., 1982; Gibson and Watkinson, 1990; Setterfield et al., 1995). During orogenesis these volcanic complexes can be strongly deformed (Allen et al., 2002), making it difficult to ascertain timing and mechanism of formation of these deposits and complicating exploration strategies. In addition, during deformation VMS deposits can be overprinted by orogenic gold mineralization (e.g. Tourigny et al., 1989; Marquais et al., 1990; Yeats and Groves, 1998), which

has led to debates regarding the relative roles of orogenic and synvolcanic processes for gold enrichment of VMS deposits (Poulsen and Hannington, 1996).

The Blake River Group (BRG) is one of the most prolific base-metal and gold producing volcanic successions within the Abitibi Greenstone belt of Canada and hosts ~90% of the VMS-related gold (Fig. 1.1; Dubé and Mercier-Langevin, 2020). It comprises a 12,000 to 15,000 m thick, bimodal submarine volcanic assemblage that is bound to the north by the Porcupine Destor Fault system and to the south by the Larder Lake-Cadillac Fault system (Barager, 1968; Goodwin and Ridler, 1970; McNicoll et al., 2014), which are major structural features that coincide with intense carbonate alteration and orogenic-style Au mineralization (Poulsen, 2017 and references therein). Several distinct volcanic centres, characterized by thickening of the volcanic successions, an increased proportion of felsic volcanic rocks, and the presence of synvolcanic intrusions and associated synvolcanic faults, are present in the BRG, however not all of these volcanic centres are associated with VMS deposits (e.g. Ben Nevis; Péloquin et al., 2008). The Rouyn-Noranda mining district comprises several volcanic centres. It hosts 22 Cu-Zn-Au-Ag volcanogenic massive sulfide (VMS) deposits and 17 orogenic gold deposits (Fig. 1.2; Gibson and Watkinson, 1990). Most of the VMS deposits are small (<5 million tonnes), base metal-rich (Cu, Zn) lenses, which formed largely as mounds on the ancient seafloor and have average Au grades of ≤1 g/t Au (Gibson and Watkinson, 1990; Kerr and Gibson, 1993; Monecke et al., 2017). However, the Horne (167 Mt at 2.99 g/t Au, 15.3 g/t Ag, 0.84% Cu, and 0.63% Zn; combined past production and new measured, indicated and inferred Horne 5 resource; Krushnisky et al., 2020) and Quemont (14 Mt at 5.5 g/t Au, 331 g/t Ag 1.32% Cu, and 2.44% Zn) VMS deposits, constitute some of the largest synvolcanic gold deposits (Mercier Langevin et al., 2011) and are among the top 1% of the world's VMS deposits in terms of total original reserves (Galley et al., 2007).

Volcanic units in the Noranda camp comprise an approximately 6,000 m thick, bimodal (mafic-dominated) sequence (Spence and de Rosen-Spence, 1975; de Rosen Spence, 1976; Gélinas et al., 1983), which is bisected by numerous faults and distributed amongst four main fault blocks (Fig. 1.2; Hunter, Flavrian, Powell, and Horne). The Quemont and Horne deposits occur in the Powell and Horne blocks, respectively. Volcanic products are predominantly effusive volcanic flows, with minor pyroclastic activity marked locally by bedded tuffs and lenses of coarse breccia occurring proximal to interpreted eruptive centres (Spence and de Rosen-Spence, 1975). Cross-cutting the volcanic stratigraphy are the subvolcanic Flavrian and Powell plutons, interpreted to be synvolcanic with overlying VMS hosting volcanic stratigraphy (Goldie, 1976; Kennedy, 1985; Galley, 2003). The Powell intrusion is a 1 km thick, sill-like intrusion that dips ~60° to the northeast (Keating, 1992; Goldie, 1976; Carrier et al., 2000). It is interpreted to represent the heat source that drove hydrothermal circulation during formation of some of the VMS deposits in the district (Goldie, 1976; Campbell et al., 1981; Kennedy, 1985; Galley, 2003; Gibson and Galley, 2007). It also hosts gold-quartz-carbonate vein mineralization (e.g. Silidor and Powell-Rouyn; Carrier et al., 2000) and the Don-Rouyn deposit, which is interpreted as an Archean porphyry-type deposit (Kotila, 1975; Goldie et al., 1979; Jébrak et al., 1997).

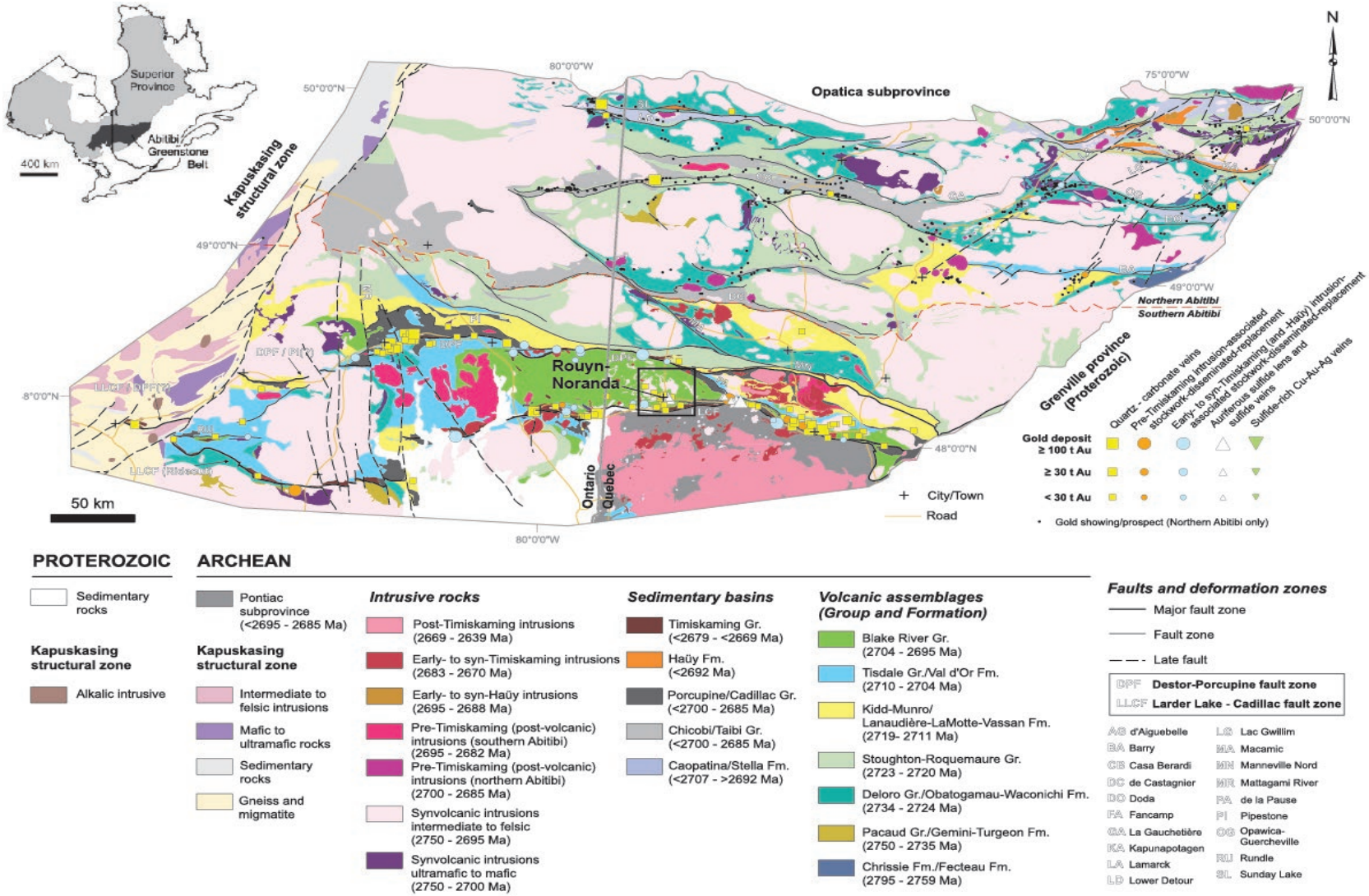

Figure 1.1 Geological map of the Abitibi Greenstone belt

Inset shows the location of the Abitibi Greenstone belt within the Superior Province. Location of the Rouyn-Noranda mining district (Fig. 1.2) highlighted in black rectangle. Modified from Dubé and Mercier-Langevin (2020).

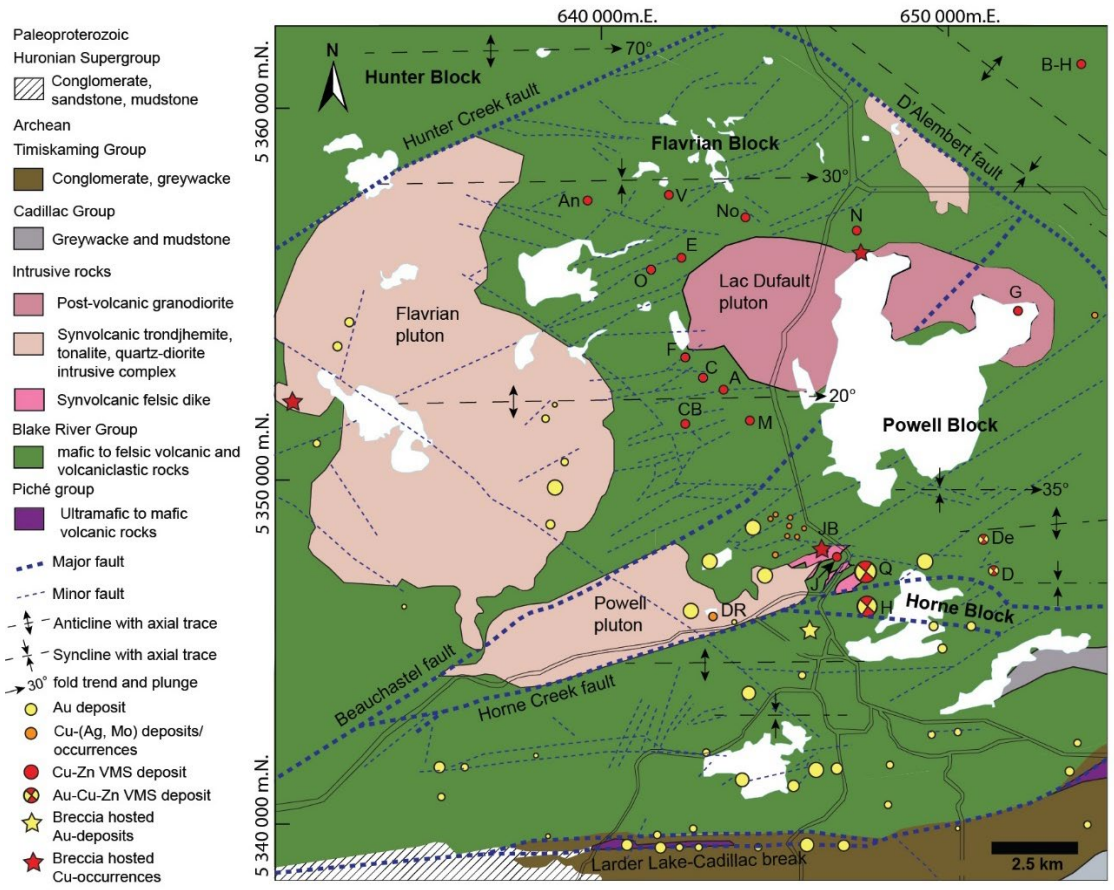

Figure 1.2 Geological map of the Rouyn-Noranda mining district

Regional geology map of the Rouyn-Noranda mining district modified from Poulsen (2017) and McNicoll et al. (2014), showing spatial distribution of the various mineral occurrences and deposits. The yellow circles are scaled to reflect the relative gold tonnage. Deposit names and occurrences are abbreviated: A = Amulet A, An = Ansil, B-H = Bouchard-Hebert, C = Amulet C, CB = Corbet, De = Deldona, D = Delbridge, DR = Don Rouyn, E = East Waite, F = Amulet F, G = Gallen, H = Horne, J = Joliet, JB = Joliet Breccia, M = Millenbach, No = Norbec, N = Newbec, O = Old Waite, Q = Quemont, V = Vauze.

At least three deformation events have been documented in the district, which have affected the geometry of the volcanic strata and associated VMS deposits. An early D_1 event produced large E-W to NW trending F_1 folds, which lack an axial planar cleavage (Fig. 1.2; Dimroth et al., 1983; Hubert et al., 1984; Hubert, 1990). This event tilted the volcanic rocks of the Blake River Group prior to the deposition of the Timiskaming group resulting in an angular unconformity between

the two groups (Wilson, 1956; Wilson, 1962; Poulsen, 2017 and references therein). The D_2 event was the main period of regional deformation, characterized by N-S shortening at ca. 2670–2660 Ma (e.g. Kerrich and Kyser, 1994; Bedeaux et al., 2017; Dubé and Mercier-Langevin, 2020). This coincides with peak metamorphism in the southern Abitibi greenstone belt, which occurred between ~2669–2653 Ma (Powell et al., 1995; Piette-Lauzière et al., 2019; Dubé and Mercier-Langevin, 2020). Subsequently, a NW-SE shortening D_3 event resulted in dextral movement along E-W striking faults (Kerrich and Kyser, 1994; Dimroth et al., 1983; Hubert et al., 1984; Hubert, 1990; Carrier et al., 2000; Bedeaux et al., 2017; Poulsen, 2017).

1.2 Research Problem

The Powell Block hosts the Au-rich Quemont VMS deposit (14 Mt at 5.5 g/t Au, 331 g/t Ag 1.32% Cu, and 2.44% Zn) and separates the Horne deposit, a world class Au-rich VMS deposit (54 Mt at 6.1 g/t Au, 13 g/t Ag, and 2.2% Cu), from more conventional Cu-Zn VMS deposits (≤ 1 g/t Au) north of the Beauchastel fault (Gibson and Galley, 2007). As such, the Powell Block is a keystone in understanding the metallogeny of the district. Despite years of research, uncertainty remains as to the volcanic and deformation history, as well as the metallogeny of the Powell Block. Early maps (Wilson, 1941; Morris, 1957; Morris, 1959; De Rosen Spence, 1976; Lichtblau, 1989) lack significant structural information regarding folds and foliations in the area. In addition, while numerous faults have been mapped or inferred in the area, their 3D geometry, kinematics, and displacements are poorly constrained (e.g. Powell Fault). Reconstructing the volcanic environment of the Powell Block at the time of formation of the Quemont deposit will contribute to a better understanding of why some districts or rock formations contain major Au-rich VMS deposits adjacent to Au-poor VMS deposits.

Several researchers have documented the lithofacies in the camp and inferred correlations between the various fault blocks (Spence and De Rosen Spence, 1975; De Rosen Spence, 1976; Gibson, 1990; Gibson and Watkinson, 1990; Kerr and Gibson, 1993; Lichbtlau and Dimroth, 1980; Lichtblau, 1989; Moore et al., 2016), however, there is no consensus for correlations across the Beauchastel and Horne Creek faults (Monecke et al., 2017). Recent U-Pb ID TIMS zircon geochronology has also challenged previous lithostratigraphic correlations across the Beauchastel fault (McNicoll et al., 2014), and therefore the time-stratigraphic position of the Quemont and Horne deposits relative to the deposits of the Flavrian block remains uncertain. Thus, it is unknown if the Quemont and Horne deposits are more Au-enriched because of temporal changes in the volcanic hydrothermal system, overprinting by a younger orogenic system, or due to more favourable syn-volcanic conditions during the same time-stratigraphic interval as the other VMS deposits of the district. It has been postulated that the anomalous size and grade of the Quemont and Horne deposits is linked to their location at the presumed southern caldera margin of the Noranda volcanic complex and therefore involved a more direct input of magmatic volatiles ± metals (e.g. Sharman et al., 2015; Krushnisky et al., 2020). The inferred boundaries for the "Caldera structure" of the Noranda camp are interpreted to be the Hunter Creek fault to the north, with the Quemont feeder dike in the Powell Block marking the southern margin (De Rosen Spence, 1976; Lichtblau, and Dimroth, 1980). However, these structures lack proper documentation and therefore a synvolcanic origin has not been demonstrated. One of the best documented examples of synvolcanic feeder dykes within the Noranda camp is the NW trending McDougall-Despina fault set, extending from the eastern margin of the Flavrian intrusion in the Flavrian block (Setterfield, et al., 1995). Several subsidiary structures in the Powell Block exhibit similar characteristics to the McDougall-Despina fault set. They are locally intruded by felsic dikes and

contain quartz-Cu-Zn-Ag vein mineralization, which has not been previously characterized and thus they may represent early synvolcanic structures that could provide a window into the deep plumbing system that fed overlying VMS deposits. A detailed structural study, paired with documentation of the lithofacies within adjacent fault blocks, will provide the context to interpret the presence of synvolcanic structures, and the role they may have played during mineralization.

Likewise, due to the poorly constrained structural history of the Powell Block, there are uncertainties regarding the relative timing and mechanism of formation of the gold-quartz-carbonate veins (e.g. McMurchy, 1948; Carrier et al., 2000). In addition, the nature and spatial extent of this hydrothermal overprint and effect on regional scale alteration patterns for VMS deposits has yet to be investigated. Detailed mapping and sampling at several of these deposits and comparison with the structural chronology documented throughout the Powell Block will allow for a revised interpretation of the timing of these veins, as well as an assessment of their alteration footprint. Findings from this research project will have implications on our understanding of Au-enrichment processes and for exploration models in the Abitibi and globally.

1.3 Thesis Objectives

The main objective of the thesis is to constrain the metallogeny of the Powell Block by reconstructing its structural and stratigraphic evolution and establishing the spatial and temporal distribution of the synvolcanic and syntectonic base and precious metal mineralization and alteration within that framework. Fulfilment of this objective requires answers to the following questions:

- What is the age and characteristic features of the lower Blake River Group volcanic strata of the Powell Block? Can they be correlated with the strata in the adjacent Flavrian and Horne blocks?
- What is the nature of the Joliet Breccia? Is it a phreatic seafloor crater correlated with the host volcanic strata or a younger magmatic or magmatic-hydrothermal breccia unrelated to its host rocks?
- What is the sequence of deformation events within the Powell Block and how has folding and faulting affected the geometry of the volcanic strata? What kinematic indicators are present on bounding faults, particularly the Powell fault?
- Where do the quartz-sulfide (Cu-Ag-Zn) veins fit within the deformation history of the Powell Block and Rouyn-Noranda mining district? Did they form at the same time as the gold-quartz-carbonate veins or are they synvolcanic and related to VMS mineralization? If the latter, are they blind veins without an associated massive sulphide lens, remnant roots of an eroded massive sulfide lens or is there potential for undiscovered VMS deposits? Or are they related to a younger unrecognized mineralization and alteration event?
- What is the timing and spatial distribution of the gold-quartz-carbonate mineralization? Has this event affected regional VMS alteration patterns for the district?

1.4 Structure of the Thesis

This thesis is organized into five chapters. The following three chapters (2-4) are written as manuscripts published or intended for publication in peer-reviewed scientific journals. As a result, there is inevitable repetition of content in the introduction and background geology sections of

these chapters. Chapter 5 summarizes the main conclusions from these three manuscripts and comments on future work needed to answer questions arising from the thesis.

Chapter 2 is a manuscript entitled **"Recognizing subsurface breccias in Archean terranes: implications for district scale metallogeny"**, which has been published in Precambrian Research (published 2021, vol. 361, 106264). This manuscript is co-authored by H.L. Gibson, B. Lafrance, K.H. Poulsen, J. Marsh, M.A. Hamilton, and T.R.C. Jørgensen. This chapter presents a detailed description of the Joliet Breccia Cu-occurrence, including its host rocks, alteration and metal zoning, and mineralization. Two new U-Pb TIMS ID zircon ages for tonalite intrusions are presented, in addition to a U-Pb La-ICP-MS hydrothermal monazite age, which constrain the timing of brecciation and mineralization. The characteristic features of the Joliet Breccia combined with the new ages indicate that this is a younger, discordant, subsurface magmatic-hydrothermal deposit unrelated to its host volcanic strata. The similarities in alteration style and metal tenor of the Joliet Breccia with the VMS deposits of the district are used to infer that this style of mineralization represents the deep plumbing system of VMS deposits forming higher in the stratigraphic sequence analogues to the porphyry-epithermal continuum of subaerial volcanic arcs.

Chapter 3 is a manuscript entitled **"Discriminating superimposed alteration associated with epigenetic base and precious metal vein systems in the Rouyn-Noranda mining district, Québec: implications for exploration in ancient volcanic districts"**, which has been submitted to Economic Geology. The manuscript is co-authored by B. Lafrance, H.L. Gibson, K.H. Poulsen, C. Scheffer, B. Quesnel, G. Beaudoin, and M.A. Hamilton. This chapter presents detailed descriptions of the two epigenetic vein sets within the district, quartz-Cu-Zn-Ag and gold-quartz-

carbonate veins, in order to establish their relative timing and mechanism of formation. $\delta^{18}O$ values for quartz from both vein types is used to interpret possible fluid sources and compare to typical VMS and orogenic signatures. The metal tenor and $\delta^{18}O$ values for the quartz-Cu-Zn-Ag veins are comparable to the Joliet Breccia and VMS deposits, suggesting these veins are related to the same hydrothermal system, and represent the deep plumbing system for VMS deposits that formed higher in the stratigraphic pile, superimposed on older volcanic strata. The gold-quartz-carbonate veins are comparable to typical orogenic deposits. Furthermore, this chapter presents the first detailed description of their associated alteration haloes and demonstrates that these epigenetic veins have perturbed regional alteration patterns associated with VMS systems, which has been overlooked in the past.

Chapter 4 is a manuscript entitled **"Volcanic reconstruction of Lower Blake River Group strata of the Powell Block, Rouyn-Noranda mining district Québec; Implications for the timing and setting of base metal mineralization"** (to be submitted to Canadian Journal of Earth Sciences). This manuscript is co-authored by H.L. Gibson, B. Lafrance, M.A. Hamilton, K.H. Poulsen, and T.R.C. Jørgensen. This chapter provides two new U-Pb TIMS ID zircon ages for two rhyolites within the lower volcanic strata of the Powell Block and together with a previous published age for a cross-cutting intrusion (Chapter 1) constrain the age of the Powell and Brownlee formations. The lithofacies and geochemistry of the Lower Blake River Group strata of the Powell Block are described and an interpretation of the volcanic setting of the Powell Block is provided. Correlations are proposed between the Powell Block and the Horne Block along with a new interpretation for the setting of the Quemont and Horne deposits.

1.5 Statement of Original Contributions

The following is a summary of original contributions presented by the candidate in this study:

1) Documented for the first time the superposition of Upper Blake River Group mineralization on Lower Blake River Group strata.
2) Demonstrated that the Joliet Breccia is an Upper Blake River Group magmatic-hydrothermal breccia, in contrast to earlier interpretations that it is a phreatic breccia correlated with the host volcanic strata (LBRG) of the Quemont Au-rich VMS deposit.
3) Proposed a new structural interpretation involving regional folding associated with reverse faulting along east-west striking faults, followed by dextral reactivation of the faults.
4) Revised the timing of the gold-quartz-carbonate vein emplacement to early syn-D_2 (N-S shortening) ca. 2670-2660 Ma, in contrast to earlier interpretations of emplacement post-D_3.
5) Demonstrated for the first time that superposition of alteration related to the younger gold-quartz-carbonate veins and related shear zones results in mixed alteration signatures that mask alteration related to the VMS mineralization.
6) Revised the stratigraphy of the Lower Blake River Group strata within the Powell Block, which suggests that the strata are products from two separate volcanic centres.
7) Correlated the host volcanic strata of the Quemont and Horne Au-rich VMS deposits, which suggests that the Au-rich VMS deposits are linked to a ca. 2702 Ma voluminous felsic volcanic centre, centred on the Horne Creek Fault and suggests that the higher Au-grades may be due to a greater input of magmatic-hydrothermal fluid.

1.6 References

Allen, R.L., Weihed, P., The Global VMS Research Project Team. 2002. Global comparisons of volcanic-associated massive sulphide deposits. In: Blundell, D. J., Neubauer, F., Quadt, A. von (Eds.), The timing and Location of Major Ore Deposits in an Evolving Orogen. Geological Society London Special Publication, 13-38.

Baragar, W. R. A. 1968. Major-element geochemistry of the Noranda volcanic belt, Quebec-Ontario; Canadian Journal of Earth Sciences, 5, 773-790.

Barrie, C. T., and Hannington, M.D. 1999. Classification of volcanic-associated massive sulfide deposits based on host-rock composition; Reviews in Economic Geology, 8, 1-11.

Bedeaux, P., Pilote, P., Daigneault, R., Rafini, S. 2017. Synthesis of the structural evolution and associated gold mineralization of the Cadillac Fault, Abitibi, Canada; Ore Geology Reviews, 82, 49-69.

Campbell, I.H., Franklin, J. M., Gorton, M.P., Hart, T. R., Scott, S.D. 1981. The role of subvolcanic sills in the generation of massive sulfide deposits; Economic Geology, 76, 2248-2253.

Carrier, A., Jébrak, M., Angelier, J., Holyland, P. 2000. The Silidor deposit, Rouyn-Noranda District, Abitibi Belt: geology, structural evolution, and paleostress modeling of an Au quartz vein-type deposit in an Archean trondjhemite; Economic Geology, 95, 1049-1065.

De Rosen Spence, A.F. 1976. Stratigraphy, Development and petrogenesis of the central Noranda volcanic pile, Noranda, Québec. PhD thesis. University of Toronto, Toronto, Ontario.

Dimroth, E., Imreh, L., Goulet, N., Rocheleau, M. 1983. Evolution of the south-central segment of the Archean Abitibi Belt, Quebec. Part II: Tectonic evolution and geomechanical model; Canadian Journal of Earth Sciences, 20, 1355-1373.

Dubé, B., and Mercier-Langevin, P. 2020. Gold deposits of the Archean Abitibi Greenstone belt, Canada, in: Sillitoe, R. H., Goldfard, R. J., Robert, F., Simmons, S. F. (Eds.) Geology of the world's major gold deposits and provinces, SEG Special Publication 23, 669-708.

Franklin, J.M., Sangster, D/M., and Lydon, J.W. 1981. Volcanic-associated massive sulfide deposits; Economic Geology 75th Anniversary Volume, 485-627.

Franklin, J.M., Gibson, H.L., Jonasson, I.R. and Galley, A.G. 2005. Volcanogenic massive sulfide deposits, *in* Hedenquist, J.W, Thompson, J.F.H., Goldfarb, R.J. and Richards, J.P., eds., Economic Geology 100th Anniversary Volume, Society of Economic Geologists Inc., 523-560.

Galley, A. 2003. Composite synvolcanic intrusions associated with Precambrian VMS-related hydrothermal systems; Mineralium Deposita, 38, 443-473.

Galley, A.G., Hannington, M.D., and Jonasson, I.R. 2007. Volcanogenic massive sulphide deposits, *in* Goodfellow, W.D., ed., Mineral Deposits of Canada: A synthesis of Major Deposit-Types, District Metallogeny, the Evolution of Geological Provinces, and Exploration Methods: Geological Association of Canada, Mineral Deposits Division, Special Publication No. 5, 141-161.

Gélinas, L., Trudel, P., and Hubert, C. 1983. Chemostratigraphic division of the Blake River Group, Rouyn-Noranda area, Abitibi, Quebec, Canadian Journal of Earth Sciences, 21, 220-231.

Gibson, H. L. 1990. The mine sequence of the Central Noranda volcanic complex: geology, alteration, massive sulfide deposits and volcanological reconstruction. Ph.D. thesis, Carleton University, Ottawa, Ontario.

Gibson, H.L., Watkinson, D.H. 1990. Volcanogenic Massive Sulphide Deposits of the Noranda Cauldron and Shield Volcano, Québec. Can. Inst. Min. Metall. Special Volume 43, 119–132.

Gibson, H. L., Morton, R. L., and Hudak, G. J. 1999. Submarine volcanic processes, deposits, and environments favorable for the location of volcanic-associated massive sulfide deposits. Reviews in Economic Geology 8, 13-51.

Gibson, H. L., and Galley, A. G. 2007. Volcanogenic massive sulphide deposits of the Archean Noranda District, Quebec, Geological Association of Canada, Mineral Deposits Division. Special Publication 5, 533-552.

Goldie, R. 1976. The Flavrian and Powell Plutons, Noranda area, Québec: A geological investigation of the Flavrian and Powell Plutons and their relationships to other rocks and structures of the Noranda area; unpublished PhD thesis, Queen's University, Kingston, Ontario; 381 p.

Goldie, R., Kotila, B., Seward, D. 1979. The Don Rouyn Mine: An Archean porphyry copper deposit near Noranda, Québec; Scientific Communications, 1680-1684.

Goodwin, A. M., and Ridler, R. H. 1970. The Abitibi orogenic belt, in Symposium on basins and geosynclines of the Canadian Shield, Canadian Geological Survey Paper 70-40, 1-24.

Hubert, C., Trudel, P., Gélinas, L. 1984. Archean wrench fault tectonics and structural

evolution of the Blake River Group, Abitibi belt, Québec; Canadian Journal of Earth Sciences, 21, 1024-1032.

Hubert, C. 1990. Geologic framework, evolution and structural setting of gold and base metal deposits of the Abitibi Greenstone Belt, Canada; in S. E. Ho, F. Robert and D.I. Groves (eds) Gold and Base Metal Mineralization in the Abitibi Subprovince with Emphasis on the Quebec Segment; Short Course Notes, University of Western Australia, Geology Department Publication No. 24, 53-62.

Jebrak, M., Harnois, L., Carrier, A., and Lafrance, J. 1997. The Don Rouyn-Cu-Au porphyry system; *in* J. F. Couture, and F. Robert eds., Atypical gold deposits in the Abitibi Belt, Geological Association of Canada, Field Trip B5 guide, Ottawa, 1997, 72-78.

Keating, P. 1992. Interpretation of the gravity anomaly field in the Noranda Val d'or region, Abitibi Greenstone belt, Canadian Shield; Canadian Journal of Earth Sciences, 25, 962-971.

Kennedy, L. P. 1985. The geology and geochemistry of the Archean Flavrian Pluton, Noranda, Quebec, Unpublished PhD thesis, The University of Western Ontario, London, Ontario, Canada, 491 p.

Kerr, D. J., and Gibson, H. L. 1993. A comparison of the Horne volcanogenic massive sulfide deposit and intracauldron deposits of the Mine sequence, Noranda, Quebec; Economic Geology, 88, 1419-1422.

Kerrich, R., and Kyser, T. K. 1994. 100 ma timing paradox of Archean gold, Abitibi greenstone-belt (Canada) – new evidence from U-Pb and Pb-Pb evaporation ages of hydrothermal zircons; Geology, 22, 1131-1134.

Knuckey, M. J., Comba, C.D.A., Riverin, G. 1982. Structure, metal zoning and alteration at the millenbach deposit, Noranda, Quebec. *In* Precambrian Sulphide Deposits. *Edited by* R.W. Hutchinson, C.D. Spence, and J.M. Franklin. Geological Association of Canada Special Paper 25, 255-295.

Kotila, B.W. 1975. An Archean porphyry copper deposit: The Don Rouyn mine, Noranda, Québec, Kingston, Ontario; unpublished B.Sc. thesis, Queen's University, Kingston, Ontario; 21 p.

Krushnisky, A. 2018. Controls on gold enrichment at the Horne 5 Archean VMS deposit, Abitibi Greenstone Belt, Québec; Unpublished MSc thesis, Université du Québec, Institute national de la recherché scientifique, 238 p.

Krushnisky, A., Mercier-Langevin, P., Ross, P.S., Goutier, J., Pilote, C, Bernier, C. 2020. Geology and gold enrichment at the Horne 5 Archean volcanogenic massive sulpide deposit, Abitibi greenstone belt, Québec: a synthesis. *In* Targeted Geoscience Initiative 5: contributions to the understanding of Canadian gold systems. *Edited by* P. Mercier-Langevin, C.J.M. Lawley, S, Castonguay, 31-44. https://doi.org/10.4095/323663

Large. R.R., McPhie, J., Gemmell, J.B., Herrmann, W., and Davidson, G.J. 2001. The spectrum of ore deposit types, volcanic environments, alteration halos and related exploration vectors in submarine volcanic successions: Some examples from Australia: Economic Geology, 96, 1037-1054.

Lichtblau, A. P. 1989. Stratigraphy and facies at the south margin of the Archean Noranda Caldera. MSc thesis, L'Université du Québec a Chicoutimi, Québec, Canada, 148 p.

Lichtblau, A. P., and Dimroth, E. 1980. Stratigraphy and facies at the south margin of the

Archean Noranda Caldera, Noranda, Quebec. Current research, Part A, Geological Survey of Canada, Paper 80-1A, 68-76.

Lydon, J.W. 1988. Ore deposit models: Volcanogenic massive sulfide deposits. Part 1: A descriptive model; Geoscience Canada, 11, 195-202.

Marquais, P., Hubert, C., Brow, A.C., and Rigg, D.M. 1990. Overprinting of early, redistributed Fe and Pb-Zn mineralization by late-stage Au-Ag-Cu deposition at the Dumagami mine, Bousquet district, Abitibi, Quebec: Canadian Journal of Earth Sciences, 27, 1651-1671.

McMurchy, R.C. 1948. Powell-Rouyn mine in Structural geology of Canadian ore deposits, Canadian Institute of Mining and Metallurgy, 581-589.

McNicoll, V., Goutier, J., Dubé, B., Mercier-Langevin, P., Ross, P.S., Dion, C., Monceck, T., Legault, M., Percival, J., Gibson, H. 2014. U-Pb geochronology of the Blake River Group, Abitibi greenstone belt, Québec, and implications for base metal exploration; Economic Geology, 109, 27–59.

Mercier-Langevin, P., Hannington, M.D., Dubé, B., Bécu, V. 2011. The gold content of volcanogenic massive sulfide deposits; Mineralium Deposita, 46, 509-539.

Monecke, T., Gibson, H. L., Goutier, J. 2017. Volcanogenic massive sulfide deposits of the Noranda camp; Reviews in Economic Geology, 19, 169-223

Moore, L. N., Daigneault, R., Aird, H.M., Banerjee, N.R., Mueller, W.U. 2016. Reconstruction and evolution of Archean intracaldera facies: the Rouyn-Pelletier Caldera Complex of the Blake River Group, Abitibi greenstone belt, Canada, Canadian Journal of Earth Sciences, 53, 355-377.

Morris, H. R. 1957. Héré Fault Copper Ltd. Surface Geology, Anglo-Rouyn and North Part of

Powell-Rouyn properties, Rouyn Twp., N.W. Québec; unpublished geological map, 3 sheets, one inch to 200 feet.

Morris, H.R. 1959. Joliet-Québec Mines Ltd. Surface Geology, Rouyn Twp., N.W. Québec; unpublished geological map, 3 sheets, one inch to 200 feet.

Péloquin, A.S., Piercey, S.J., and Hamilton, M.A. 2008. The Ben Nevis Complex, Ontario, Canada: Part of the Late Volcanic Phase of the Blake River Group, Abitibi Subprovince; Economic Geology, 103, 1219-1241.

Piette-Lauzière, N., Guillmette, C., Bouvier, A., Perrouty, S., Pilote, P., Gaillard, N., Lypaczewski, P., Linnen, R. L., Olivo, G. R. 2019. The timing of prograde metamorphism in the Pontiac Subprovince, Superior craton; implications for Archean geodynamics and gold mineralization; Precambrian Research, 320, 111-136.

Poulsen, K. H. 2017. The Larder Lake Cadillac Break and its gold districts; Reviews in Economic Geology, 19, 133-167.

Poulsen, K.H., and Hannington, M.D. 1996. Volcanic-associated massive sulphide gold, in Eckstrand, O.R., Sinclair, W.D., and Thorpe, R.I., eds., Geology of Canadian mineral deposit types: Geology of Canada, 8, 183-196.

Powell, W.G., Carmichael, D.M., Hodgson, C.J. 1995. Conditions and timing of metamorphism in the southern Abitibi Greenstone Belt, Québec; Canadian Journal of Earth Sciences, 32, 787–805

Setterfield, T. N., Hodder, R. W., Gibson, H. L., Watkins, J. J. 1995. The McDougall-Despina Fault set, Noranda, Quebec: Evidence for fault-controlled volcanism and hydrothermal fluid flow; Exploration Mining Geology, 4, 381-393.

Sharman, E. R., Taylor, B. E., Minarik, W. G., Dubé, B., Wing, B. A. 2015. Sulfur isotope and trace element data from ore sulfides in the Noranda district (Abitibi, Canada): implications for volcanogenic massive sulfide deposit genesis; Mineralium Deposita, 50, 591-606.

Spence, C. D., de Rosen-Spence, A. F. 1975. The place of sulfide mineralization in the volcanic sequence at Noranda, Quebec, Economic Geology, 70, 90-101.

Tourigny, G., Brown, A.C., Hubert, C., and Crépeau, R. 1989. Synvolcanic and syntectonic gold mineralization at the Bousquet Mine, Abitbi greenstone belt; Economic Geology, 84, 1875-1890.

Wilson, M. E. 1941. Geological Survey of Canada Memoir 229, 162 p.

Wilson, M.E. 1956. Early Precambrian rocks of the Timiskaming region, Quebec and Ontario, Canada; Geological Society of America Bulletin, 67, 1397-1430.

Wilson, M.E. 1962. Rouyn-Beauchastel map areas; Geological Survey of Canada memoir 315, 140 p.

Yeats, C.J, and Groves, D.I. 1998. The Archean Mount Gibson gold deposits, Yilgarn craton, Western Australia: Products of combined syn-volcanic and syntectonic alteration and mineralisation; Ore Geology Reviews, 13, 103-129.

Chapter 2

2 Recognizing subsurface breccias in Archean terranes: implications for district scale metallogeny

2.1 Abstract

Breccias are common in ancient and modern volcanic terranes, where they form at and below surface through volcanic, hydrovolcanic, magmatic, or tectonic mechanisms. They are critical for volcanic reconstruction as stratigraphic markers and indicators of geodynamic change and since they can be associated with mineralization their genesis is also important from an exploration perspective. Their origin can be difficult to ascertain in ancient terranes that have undergone polyphase deformation and associated metamorphism. The Joliet Breccia is a subeconomic Cu-Ag prospect within the Neoarchean Rouyn-Noranda mining district, in the Abitbi greenstone belt, Canada. It was previously interpreted as a phreatic breccia formed on the seafloor. This study presents new data indicating that the Joliet Breccia is a subsurface magmatic-hydrothermal breccia. Specifically, the recognition of gradational contacts with host rocks and between internal breccia domains, lack of sedimentary features and the spatial and temporal association with a tonalite intrusion strongly supports this interpretation. The angular, poorly sorted, lithic clasts derived from the immediate host rocks, hydrothermal cement, complete absence of a rock flour matrix, and presence of a radial and concentric fracture pattern extending into the host rocks, further supports a subsurface magmatic-hydrothermal emplacement mechanism.

A new TIMS U-Pb zircon age of 2698.0 ± 0.9 Ma (2σ) for a tonalite block within the breccia constrains the maximum age of brecciation. Four LA-ICP-MS U-Pb dates on hydrothermal

monazite (2693.7 ± 1.0/8.9 Ma; 2696.9 ± 0.45/8.9 Ma; 2698.7 ± 1.4/8.9 Ma; 2701.2 ± 0.33/8.9 Ma; 2s/2s_{sys}) found in the cement of the Breccia indicate brecciation and mineralization occurred shortly after the emplacement of the tonalite. Similarly, the ca. 2697 Ma St. Jude intrusive breccia indicates a localized ca. 2699–2695 Ma magmatic-hydrothermal event superimposed on ca. 2704–2701 Ma strata. These breccias are temporally correlative with the youngest units of the Blake River Group strata and associated ca. 2698–2695 Ma volcanogenic massive sulfide (VMS) deposits, which suggests an indirect genetic link between these two hydrothermal systems. The VMS deposits may represent the near surface, distal manifestations of a deeper magmatic-hydrothermal system akin to the porphyry-intermediate sulfidation epithermal continuum in modern subaerial volcanic arcs.

2.2 Introduction

Breccias are common to volcano-plutonic systems, and subsurface breccias are a frequent host to porphyry (e.g., El Teniente, Chile and Toquepala, Peru) and epithermal base and precious metal deposits (e.g., Red Mountain, Colorado; Pascua-Lama, Chile-Argentina; La Coipa, Chile; Wau, Papua New Guinea), making them preferred exploration targets because of their commonly high metal contents (Sillitoe, 1985; Sawkins, 1990). In addition, unique extrusive breccias serve as stratigraphic markers and provide insights into the changing dynamics of volcanic complexes, making their correct identification critical for volcanic reconstruction. In ancient volcanic successions, such as Precambrian greenstone belts, descriptions of subsurface breccias are rare, and there are few examples of mineralized breccias (e.g., Chadbourne, Québec, Walker and Cregheur, 1982; Newbec, Québec, Smith, 1983; Biedelman Bay intrusive complex, Ontario, Galley et al., 2000; St. Jude, Québec, Galley and van Breemen, 2002; Côté Au deposit, Ontario, Katz et al., 2017; Queylus, Québec, Mathieu and Racicot, 2019). The apparent paucity of

subsurface breccias in ancient greenstone belts may, in part, be due to limited exposure and, in many cases, substantial deformation and alteration, making it difficult to distinguish subsurface versus surface emplacement.

The Joliet Breccia is hosted by ca. <2702–2699.5 Ma Blake River Group (McNicoll et al., 2014) strata of the Noranda volcanic complex and spatially associated with the past-producing Joliet Cu (Sabina, 2003) and Quemont Zn-Cu-Au-Ag massive sulfide deposits (Fig. 2.1). Since Wilson (1941), it has been interpreted as an extrusive steam explosion breccia, related to the emplacement of a quartz feldspar porphyritic rhyolite dike (Quemont feeder dike; De Rosen Spence, 1976; Lichtblau and Dimroth, 1980). Lichtblau and Dimroth (1980) expanded this interpretation and correlated the Joliet Breccia to the host <2702–2699.5 Ma strata, in particular to a proximal volcaniclastic unit referred to as the "upper marker horizon", emphasizing a genesis at the seafloor. Their model interpreted layering in the Joliet Breccia to be bedding and they interpreted the tonalite blocks as an intact and unrelated younger intrusion. However, their observations do not preclude a subsurface emplacement mechanism for the Joliet Breccia and similarities to younger (ca. 2698 Ma) discordant mineralized breccia bodies within the Rouyn-Noranda mining district (Fig. 2.1) were not considered.

This study presents results of new detailed mapping, petrography, geochemistry and geochronology to unravel the timing, emplacement mechanism, and origin of the Joliet Breccia and its associated mineralization within the context of the broader metallogeny of the Rouyn-Noranda mining district. We explore the temporal relationship between the Joliet Breccia and other intrusive breccias, and with the volcanism and plutonism that constructed the Noranda volcanic complex and associated ore deposits. Ultimately, using the Joliet Breccia as a type example, we

present criteria that aid distinguishing surface and subsurface breccias in ancient terranes, which has significant ramifications for volcanic reconstruction and exploration.

2.3 Geological setting of the Joliet Breccia

The Rouyn-Noranda mining district is located within the Blake River Group of the southern Abitibi greenstone belt of the Superior Province (Fig. 2.1). Volcanic rocks of the district comprise the Noranda Subgroup (DeRosen Spence, 1976; Goodwin, 1980), a 6,000 m thick bimodal volcanic complex of the Blake River Group (Fig. 2.1), which was constructed over a 7 m.y. period (McNicoll et al. 2014). The Noranda Subgroup was subdivided into informal lithostratigraphic formations (De Rosen Spence, 1976; Gibson, 1990) and subsequently into informal chronostratigraphic "formations" by McNicoll et al. (2014). McNicoll et al. (2014) recognized a regional time gap in Noranda Subgroup volcanism at 2700–2698.5 Ma, with VMS deposits occurring in strata older (e.g., Horne, Quemont deposits) and younger (Bouchard-Hebert deposit) than this break. The Joliet Breccia is located in older ca. 2702–2699.5 Ma volcanic strata of the Powell Block (Fig. 2.1). The region has undergone four increments of deformation, the greatest strain related to north-south shortening that occurred <2669–>2639 Ma (Dubé and Mercier-Langevin, 2020), and folded the volcanic strata into a series of open, gently east-plunging anticlines and synclines, and an associated axial planar E-W cleavage (Goulet, 1978; Dimroth et al., 1983; Hubert et al., 1984; Wilkinson et al., 1999; Bedeaux et al., 2017; Poulsen, 2017).

The Joliet Breccia occurs along the northern margin of the northernmost Quemont feeder dike, one of three ENE trending, quartz-feldspar-porphyritic rhyolite intrusions (Fig. 2.2), which are interpreted to be feeder dikes to a quartz-feldspar-porphyritic rhyolite flow that comprises the hanging wall to the Quemont VMS deposit (De Rosen Spence, 1976; Lichtblau, 1989; McNicoll

et al., 2014). The dikes also cross-cut northwesterly-striking volcanic rocks of the Joliet formation (De Rosen Spence, 1976).

The northernmost dike is approximately 350 m wide, has a strike length of 1300 m, dips steeply to the north at 85° and contains ~5% quartz (0.5–1 mm) and 1% plagioclase phenocrysts (0.5–1 mm). The southernmost dike, which is compositionally, mineralogically and texturally similar yielded a ca. 2702.0 ± 0.8 Ma U-Pb zircon age (07-JG-9035; McNicoll et al., 2014). McNicoll et al. (2014) defined this sample as the extrusive Quemont rhyolite flow, however the contact relationships are not exposed, and this sample was taken from an area denoted to be the intrusive Quemont feeder dike by DeRosen Spence (1976). Sample 18MDS-0107 (Fig. 2.3) of the northernmost dike, collected for this study, did not yield zircon grains; however, the three feeder dikes are interpreted to be the same age and a product of the same volcanic event (De Rosen Spence, 1976; Lichtblau and Dimroth, 1980; Lichtblau, 1989; McNicoll et al., 2014).

To the southwest, the Quemont feeder dikes are cross-cut by the Powell tonalite of the composite Flavrian-Powell Intrusive Complex (Fig. 2.2). Smaller tonalite intrusions locally cross-cut the Quemont feeder dike and one in particular coincides with the Joliet Breccia, and is henceforth referred to as the "Joliet tonalite". The northernmost Quemont feeder dike marks a significant synvolcanic fault (Fig. 2.2) that separates andesites of the Powell formation to the north from rhyolite flows of the Joliet formation to the south (De Rosen Spence, 1976; Lichtblau, 1989). Volcanic strata of the Powell formation strike WNW, dip ~80° east and consist of massive amygdaloidal andesite, overlain by a conformable mafic volcaniclastic unit referred to as the "upper marker horizon" by Lichtblau (1989), herein referred to as the upper marker unit. The contact between the andesite and the Quemont feeder dike is sharp, irregular, and discordant. The contact between the Joliet Breccia and the upper marker unit is not exposed. The upper marker

unit is conformably overlain by massive andesite. East-northeast striking, boudinaged, aphyric rhyolite dikes oriented subparallel to the Quemont feeder dike, cross-cut the andesite (Fig. 2.3).

Volcanic strata south of the northernmost dike (Fig. 2.2) consist of the aphyric, coherent to brecciated rhyolite of the Joliet formation, which is host to the Joliet Cu-deposit, and is conformably overlain by crudely bedded, polymictic volcaniclastic units of the Quemont formation (Lichtblau, 1989). The gold-rich Quemont VMS deposit occurs at the contact between the Joliet formation and the Quemont formation, southeast of the Joliet Breccia (Fig. 2.2). The contact between the Joliet formation and northernmost Quemont feeder dike is sharp and discordant.

An E-W striking, moderately dipping cleavage cross-cuts all units within the map area (Hubert et al., 1984), including the Joliet Breccia. This is parallel to the main foliation observed elsewhere within the Rouyn-Noranda mining district that is commonly axial planar to E-W trending folds and is related to a north-south shortening event, which is interpreted as broadly coeval with the main regional dynamothermal metamorphic planar fabric which affects the Blake River Group volcanic rocks and younger Timiskaming Group sedimentary rocks (Fig. 2.1) at Noranda and elsewhere implying that it formed after 2669 Ma, the maximum age for Timiskaming deposition (Wilkinson et al., 1999; Bedeaux et al., 2017; Poulsen, 2017).

Cross-cutting relationships and the established age of deformation constrains formation of the Joliet Breccia between ca. 2702.0 ± 0.8 Ma and >2669 Ma. This approximately 34-million-year window questions whether the Joliet Breccia timing is related to early Blake River Group volcanism or to early post-Timiskaming deformation, as previously interpreted for the Chadbourne breccia (Walker and Cregheur, 1982) or alternatively to intervening geological events.

2.3.1 Description of the Joliet Breccia

The Joliet Breccia is 250 m by 150 m in area, has a crude, elliptical form (Fig. 2.3), straddles the contact between the Quemont feeder dike and the upper marker unit, and encompasses several masses composed of intact tonalite. Based on the relative abundance of felsic and mafic clasts the Joliet Breccia is divisible into three WSW striking domains: felsic, transitional and mafic. The three domains do not have an annular distribution within the Joliet Breccia, but reflect their immediate host rocks and show a south to north progression from felsic to transitional to mafic dominated clast domains, which terminate against the host Quemont feeder dike and the upper marker unit to the north (Fig. 2.3). Internal domain contacts and the contact between the breccia and the host rocks are gradational. The breccia noticeably lacks sedimentary features such as bedding. Clasts within all domains are poorly size-sorted and have distinctly angular, rectangular to tabular shapes with curviplanar margins. They are commonly oriented with their long axis parallel to the internal contacts between domains. The breccia is typically clast supported with a cement (10–20 %) comprising prismatic comb textured quartz (3–5 mm long) ± acicular Fe-chlorite rosettes ± sulfides (Fig. 2.4A) that grew syntaxially from clast margins. There is no evidence of a finer clastic, or rock-flour matrix component.

The outer limit of the Joliet Breccia is defined by an asymmetrically developed, 6 m wide zone of altered conjugate fractures containing localized areas of *in situ* breccia within the Quemont feeder dike and upper marker unit (Fig. 2.3). The *in situ* breccia reflects an inward and progressive increase in void space marked by an increase in quartz infill along the conjugate fractures grading into localized areas of monomictic, jig-saw fit breccia, wherein tabular clasts of the host Quemont feeder dike are rotated and clast margins mirror the orientation of the conjugate fractures. The contact between *in situ* brecciated Quemont feeder dike and the felsic dominated domain of the

Joliet Breccia is gradational and defined by the first appearance of breccia with quartz infilled open void space >10 % by area. The felsic dominated domain of the Joliet Breccia is a monomictic, jig-saw fit breccia containing >70 % quartz-feldspar porphyritic rhyolite clasts of the host Quemont feeder dike that range in size from generally 1–70 cm, with rare blocks up to 2–3 m diameter (Fig. 2.4B). The cement is dominantly quartz (Fig. 2.4C), with a gradational increase in interstitial chlorite that imparts an angular patchy morphology (Fig. 2.4D) towards the WNW in proximity to the transitional domain. The quartz-feldspar porphyritic rhyolite clasts have distinctive white silicified rims where associated with chlorite cement (Fig. 2.4D).

The transitional domain (Fig. 2.4E) is a polymictic breccia containing 40–60 % pervasively chloritized and locally spotted mafic clasts and ≤60 % quartz-feldspar porphyritic rhyolite clasts. Thin, west-southwest trending septa or lenses of the felsic dominated domain occur within the transitional domain; the contacts between these domains are parallel to the strike of the Quemont feeder dike (Fig. 2.3). Relative to the felsic dominated domain, clasts within the transitional domain are rotated, more equant and rectangular in form, and are smaller, with an average clast size of 5–14 cm.

The mafic dominated domain is a polymictic breccia containing >60 % mafic clasts (Fig. 2.4F). Clasts range in size from 3–60 cm, with local blocks >2 m. Thin, west-southwest trending septa or lenses of the transitional domain occur within the southern part of the mafic dominated domain; their orientation is parallel to the strike of the Quemont feeder dike. The five felsic clast types are representative of adjacent host rocks and include: i) quartz-feldspar porphyritic rhyolite clasts of the Quemont feeder dike; ii) clasts of the felsic dominated domain (jig-saw fit-texture of quartz-feldspar porphyritic rhyolite clasts separated by vuggy quartz; Fig. 2.4G); iii) silicified spherulitic, quartz microporphyritic rhyolite (≤1 mm, ~1 % quartz); iv)

aphyric-aphanitic rhyolite, identical to aphyric felsic dikes within the adjacent host rocks; and v) medium-grained tonalite (Fig. 2.4H). The five mafic clasts types are identical to the host volcanic strata and include: i) aphanitic to fine-grained massive andesite (Fig. 2.4H); ii) amygdaloidal (10 %, 0.5–5 cm diameter amygdales) massive andesite; iii) plagioclase-phyric massive andesite; IV) plagioclase crystal lapilli-tuff (upper marker unit), consisting of scoriaceous plagioclase-phyric clasts in a matrix of plagioclase crystals and fine, ash-sized material with chloritized sideromelane shards; and V) blocks of finely bedded mafic tuff. The contact between the mafic dominated domain and the upper marker unit is not exposed, but conjugate fractures are recognized in one outcrop of the upper marker unit immediately adjacent to the Joliet Breccia.

Large tonalite blocks, within the mafic dominated domain, range in size from decimetres (Fig. 2.4H) to 40 m x 25 m mega blocks. The outcrop pattern for the tonalite megablocks (Fig. 2.3) suggest they are remnants of a tonalite dike or plug; contacts with the surrounding mafic dominated breccia are not chilled (Fig. 2.4I) and are marked by broken quartz crystals within the tonalite (Fig. 2.4J). The tonalite is equigranular to porphyritic, consisting of 40–50 % medium-grained quartz and altered albite phenocrysts within a fine-grained spherulitic groundmass (50–60 %) of quartz, albite, sericite and chlorite. Phenocrysts have distinctive, fine-grained, spherulitic coronas defined by radiating quartz, sericite and altered albite (Fig. 2.4K). Quartz phenocrysts (10–20 %, 1-2 mm) are euhedral to subhedral and smokey grey in colour. Albite phenocrysts (25–35 %, 2-5 mm) are subhedral to euhedral tabular crystals that are intensely altered to sericite, but preserve remnant polysynthetic twinning. The groundmass is a fine-grained mosaic of quartz and albite ± fine-grained euhedral pyrite (1–3 %), cross-cut by arcuate perlitic fractures altered to sericite ± chlorite. The groundmass mosaic comprises spherulites showing all degrees of recrystallization from sector recrystallized spherulites (Fig. 2.4L) to quartz grains with irregular to rounded

(anhedral) outlines and containing internal radiating feldspar laths. The tonalite contains irregular, chloritized, quartz-porphyritic xenoliths.

2.4 Methodology

Detailed mapping was conducted over the span of two months aided by high resolution digital aerial photos at 1:500 scale and compiled at 1:2000 scale. Petrography was completed on polished slabs and on polished thin sections through standard transmitted and reflected light microscopy. Mineralogy was verified using the Scanning Electron Microscope (SEM) and energy-dispersive spectroscopy (EDS) at the Mineral Exploration Research Centre Isotope Geochemistry Laboratory of Laurentian University. High precision isotope-dilution – thermal ionization mass spectrometry (ID-TIMS) U-Pb zircon geochronology was completed at the Jack Satterly Geochronology Laboratory, University of Toronto. Laser ablation Inductively Coupled Mass Spectrometry (LA-ICPMS) U-Pb monazite geochronology was completed at the MERC Isotope Geochemistry Laboratory of Laurentian University. Details of analytical setup and results are provided in supplementary data file 1, and 2, respectively. Samples were submitted to ALS Geochemistry, in Sudbury, Ontario for crushing, pulverising and whole-rock geochemical analysis. Detailed description of all methodologies used can be found in supplementary data file 1. Results for the 53 analyzed samples for the metal zonation study are provided in supplementary data file 3. Whole rock data for the 25 analyzed samples used for lithological and alteration characterization are provided in supplementary data file 4.

2.5 Results

2.5.1 Lithogeochemistry

Whole-rock major and trace element analytical data from the Joliet tonalite, Quemont feeder dike and the Powell tonalite share similar geochemical characteristics. They plot as rhyodacite/dacite in the Pearce (1996) classification diagram (Fig. 2.5A), exhibit relatively flat chondrite-normalized REE patterns (La/Yb ratios 3–5), low Zr/Y ratios of 4–7, distinct negative Nb and Ti anomalies (Fig. 2.5B), have a transitional to calc-alkaline affinity (Fig. 2.5C), and are classified chemically as FIIIa/FIV rhyolites (Fig. 2.5D) (Hart et al., 2004). The mafic, chloritized clasts have a calc-alkaline affinity (Fig. 2.5C) and are basaltic in composition (Fig. 2.5A) with Zr/Y ratios of 5–7.5 and Y values of 20–30 ppm. The mafic clasts have negative Nb and Ti, anomalies and a relatively flat REE pattern (Fig. 2.5B) identical to the andesitic rocks of the Powell formation.

2.5.2 Zircon U-Pb ID-TIMS geochronology

Two samples were selected for U-Pb ID-TIMS analysis to provide a better temporal constraint on magmatism within the Powell Block. A sample of the eastern Powell tonalite (17MDS-0073; Fig. 2.1) that cross-cuts the northernmost Quemont feeder dike yielded a zircon population comprising irregular, cracked, broken, and rarely elongate forms generally lacking well-developed crystal faces (Fig. 2.6A). Chemical abrasion and subsequent analysis of three clearest single grains from this population overlap with each other and Concordia, and gives a weighted average $^{207}Pb/^{206}Pb$ age of 2701.0 ± 0.8 Ma with good fit (MSWD = 0.90; Fig. 2.6A, Table 1). This new age is within 2σ error of a 2700.1 ± 1.0 Ma U-Pb zircon age obtained by

McNicoll et al. (2014) for the lower Powell trondjhemite located to the southwest (06-CD-3038; Fig. 2.1) and is interpreted as the crystallization age for the Powell tonalite.

Sample 18MDS-0106 was collected from the largest tonalite megablock within the Joliet Breccia (Fig. 2.3). This sample yielded a robust population of clear and colourless, well faceted, stubby to elongate prismatic zircon grains (Fig. 2.6B). Analyses for three single, subequant to broken elongate euhedral crystals gave concordant to slightly discordant (1.5 %) results, with a relatively narrow range of overlapping model $^{207}Pb/^{206}Pb$ ages between 2697.5 and 2699.2 Ma (Table 1). A regression of the data, anchored at the origin, yields an age of 2698.0 ± 0.9 Ma (2σ; MSWD = 1.19; Fig. 2.6B), which is interpreted as the age of igneous crystallization of the tonalite block within the Joliet Breccia. This indicates that the Joliet tonalite is demonstrably younger than the Powell tonalite, and constrains a maximum age of formation for the Joliet Breccia.

2.5.3 Structural Analysis

The host rocks of the Joliet Breccia are cross-cut by a conjugate set of fractures that are oriented radial and concentric to the breccia within 6 m of the latter (Fig. 2.7). The fractures exhibit 15–60 cm spacing and are best developed along the ESE margin of the Joliet Breccia. They are ~1 mm wide, locally infilled by quartz ± sulfides, and are enveloped by the mineral association muscovite-quartz typical of sericite alteration (~4–8 cm wide), which is more resistant to weathering than the less altered host rock. Quartz within the fractures displays a euhedral comb habit oriented perpendicular to fracture walls. The mean orientation of the line of intersection between the fracture sets, as calculated using the Fisher analysis tool in Stereonet 10.0 ® (Allmendinger et al., 2012), is subvertical, plunging 88° towards 137° (Fig. 2.7). The main regional E-W striking cleavage overprints the sericite-quartz alteration halos of the fracture sets and all rock

types within the area. In addition, jogs in the breccia's outer contact correspond to minor sinistral fault offsets (Fig. 2.7).

2.5.4 Mineralization

Sulfide minerals occur in the hydrothermal cement of the Joliet Breccia (Fig. 2.8A-B) and, to a lesser extent, in local cross-cutting fractures (Fig. 2.8C). The dominant sulfide phases, in order of decreasing modal abundance, are pyrite, chalcopyrite and pyrrhotite.

2.5.4.1 Hydrothermal cement

White, coarse-grained comb quartz ± fibrous Fe-rich chlorite ± fibrous muscovite is the dominant hydrothermal cement of the Joliet Breccia, whereas sulfide minerals within vugs are spatially restricted and asymmetrically distributed (Fig. 2.8D). Pyrite occurs as euhedral to subhedral (0.5–4 mm) grains intergrown with comb quartz (Fig. 2.8D-E). Comb quartz crystals are fractured and overgrown by a finer grained, polygonal mosaic of grey quartz (Fig. 2.8E-F). Syn-deformational fringe structures occur around some pyrite grains within the quartz mosaic (Fig. 2.8E). Both generations of quartz exhibit undulose extinction, indicating some internal deformation, and have recrystallized grain boundaries (Fig. 2.8G). The distribution of the grey quartz mosaic is asymmetric with respect to the vug margins and locally cross-cuts comb quartz (Fig. 2.8F). Chalcopyrite and pyrrhotite typically occur intergrown with and interstitial to the polygonal grey-quartz as anhedral clusters ~0.1–1 mm in diameter (Fig. 2.8F-I). Where pyrite occurs with chalcopyrite it is corroded and fractured with numerous fine-grained inclusions and veinlets of chalcopyrite (Fig. 2.8I). Locally, sulfides are associated with ferroan dolomite and/or calcite (Figs. 2.4B and 8J) that cross-cuts clasts and vugs and infills remaining void space within vugs. In addition, all sulfides typically have red hematite rims (Fig. 2.8K), which imparts a red

stained appearance to associated quartz (Fig. 2.8B). Other accessory phases include euhedral to subhedral apatite (~20–50 μm), fibrous to bladed rutile (~20–100 μm in length) and subhedral monazite (~0.02–1 mm) (Fig. 2.8K). Silver and Bi tellurides occur as anhedral clusters (~20–80 μm in diameter) interstitial to and intergrown with chlorite and along microfractures (Fig. 2.8L). The Ag and Bi telluride clusters are zoned and consist of an outer rim of hessite (Ag_2Te), followed by coarser laths of tetradymite (Bi_2Te_2S) that generally point inward toward a wormy intergrowth core of hessite and galena.

2.5.4.2 Monazite U-Pb LA-ICP-MS geochronology

Monazite grains (0.01 – 1 mm) in two Joliet Breccia samples of mineralized chlorite filled vugs (e.g., Fig 2.8K) within the felsic-dominated domain were analyzed *in situ* by LA-ICPMS. Full details of the methodology, U-Pb geochronology and trace element data are presented in supplementary data files 1 and 2, with the compiled data summarized here. Full propagation of systematic uncertainties following the method of Horstwood et al. (2016), including the uncertainty in the primary reference material age and the long-term variance in the verification reference material dates, yields true uncertainties ($2S_{sys}$) for each weighted mean age of 8.9 Ma. The two largest monazite grains from sample 48 (Fig. 2.9A and B) yielded weighted mean $^{207}Pb/^{206}Pb$ ages of 2696.9 ± 0.45/8.9 Ma (Fig. 2.9D; $2s/2s_{sys}$; MSWD = 0.45; n = 120/134) and 2701.2 ± 0.33/8.9 Ma (Fig. 2.9E; $2s/2s_{sys}$; MSWD = 0.71; n = 409/431). Sixteen smaller grains from two sections of sample 47 yielded weighted means of 2693.7 ± 1.0/8.9 Ma (Fig. 2.9F; $2s/2s_{sys}$; MSWD = 1.09; n = 42/50; 10 grains) and 2698.7 ± 1.4/8.9 Ma (Fig. 2.9G; $2s/2s_{sys}$; MSWD = 2.5; n = 47/61; 6 grains), for each section respectively. A small percentage of analyses were >5% discordant outside of 2σ of the mean, representing younger (<~2670 Ma) or older (>~2710 Ma), and were excluded from the weighted mean calculations (see supplementary data file 1). These

ages indicate that brecciation and mineralization occurred between 2701~ 2693 Ma. Given the zircon U-Pb ID-TIMS age of 2698.0 ± 0.9 Ma for the tonalite megablock within the breccia, a permissible age range for brecciation and mineralization is 2698.9–2693 Ma, which is consistent with a minimal time gap between the crystallization of the tonalite and the mineralization. A number of grains displayed thin rims identified in high-contrast BSE, which were analyzed with a smaller spot size and yielded $^{207}Pb/^{206}Pb$ spot dates ranging from ~2700–2515 Ma, with small apparent sub-populations at ~2665 and 2620 Ma, indicating minor monazite growth or recrystallization during these time periods.

2.5.4.3 Vein mineralization

Cross-cutting, sulfide-bearing veins have sharp margins, typically range in width from 0.5–2 cm, are boudinaged, and strike 055° and dip 86°. The veins are zoned and have an outer margin of chlorite ± medium-coarse grained tabular quartz crystals and an interior of fine-grained, grey subhedral-euhedral granular quartz, acicular chlorite and sulfides. Sulfides are massive, vuggy and porous, consisting of subhedral to euhedral pyrite 0.5–1 mm diameter and anhedral interstitial chalcopyrite, rimmed by red iron-oxide. Locally, thin ~1 mm diameter, boudinaged calcite veins cross-cut the sulfide veins.

2.5.4.4 Metal zonation

Mapping indicates that the sulfide minerals are spatially restricted to the central area of the chloritized mafic dominated domain between tonalite blocks to the north and the felsic-transitional domains to the south. To determine spatial variations in metal tenor and association, 54 samples were collected along N-S and E-W oriented lines that cross the Joliet Breccia (Fig. 2.7).

There is considerable scatter in the absolute metal content of samples, reflecting the nugget-like distribution of sulfides within the breccia. Average values for select trace and major elements within each lithology are presented in Table 2. The Joliet Breccia is gold-poor, the highest value being 0.039 ppm Au, with an average value of 0.009 ppm Au. However, the breccia is relatively enriched in Ag, Bi, Te, Cu, Zn, As, Sn and W relative to the host rocks. In addition, the average value of Mo is slightly enriched in the felsic dominated domain, Joliet Breccia tonalite and Quemont feeder dike relative to more mafic lithologies.

2.5.4.5 Hydrothermal alteration

Four alteration types are recognized based on distinctive mineral associations. Mineral association refers to alteration or metamorphic minerals that occur together, are characteristic of a given alteration type, but may not be in equilibrium or have formed at the same time (Einaudi et al., 2003). All lithologies have experienced subgreenschist facies metamorphism, and virtually all samples contain some albite, quartz, chlorite ± sericite.

2.5.4.5.1 Quartz-albite alteration

Quartz-albite alteration is restricted to quartz-feldspar porphyritic rhyolite clasts derived from the Quemont feeder dike within the mafic dominated domain; it does not cross-cut the breccia. This alteration imparts a bleached, white appearance to clasts, in contrast to the yellow-beige or green alteration that characterizes sericite and chlorite alteration respectively (Fig. 2.10A). This alteration is fracture controlled and is manifest by a patchy to mesh textured distribution, with internal, angular areas between fractures of darker least altered rock. The contact between the darker least altered core areas and adjacent quartz-albite altered Quemont feeder dike is gradational over 0.5–1 mm and is cross-cut by fractures filled with vuggy quartz and sulfides that separate *in-*

situ brecciated, jig-saw fit clasts (Fig. 2.10B). The leucocratic, quartz-albite altered zones are fine-grained and consist of randomly oriented albite (~70–130 μm) and quartz (~120–250 μm) with trace chlorite (Fig. 2.10C). The darker, least altered areas between fractures preserve a fine-grained mosaic of anhedral rounded quartz and albite (~30–60 μm) as sector recrystallized spherulites, and anhedral, interstitial chlorite (~30 %).

2.5.4.5.2 Sericite alteration

The sericite alteration occurs in the coherent Quemont feeder dike and felsic clasts in the Joliet Breccia. It is characterized by a distinct, yellow-beige colouration and is subdivided into two alteration styles: 1) fracture controlled, and 2) pervasive. Fracture controlled sericitization occurs as haloes, on average 4–8 cm wide, that envelope conjugate fracture sets within the Quemont feeder dike (Fig. 2.10D). The fractures are also observed within large blocks of quartz-porphyritic rhyolite within the breccia. Pervasive sericite alteration is characteristic of the felsic dominated domain, where smaller clasts of Quemont feeder dike are pervasively sericitized (Fig. 2.4D). However, larger Quemont feeder dike clasts (≥0.5 m) within all domains of the breccia have preserved least altered interiors and a gradational boundary to a symmetrical, strongly sericitized clast margin (Fig. 2.10E-F). Sericite alteration consists of muscovite (20–30 %) and quartz (70–75 %) and minor chlorite (1–10 %). It is associated with complete destruction of feldspar, wherein albite is pseudomorphed by fine-grained sericite ± chlorite.

2.5.4.5.3 Chlorite alteration

Chlorite alteration is limited to the mafic dominated and transitional domains of the Joliet Breccia. It is manifest by green alteration rims that mantle dominantly mafic clasts (Fig. 2.10E and G), in addition to previously quartz-albite or sericite altered felsic clasts within the mafic

dominated domain (Fig. 2.10H). Clasts <40 cm in size are pervasively chloritized. Chlorite alteration obscures clast textures, and it is difficult in the field to distinguish chloritized clasts from chlorite cement (Fig. 2.10G). However, chlorite cement is restricted to vugs and tends to be coarser grained than chlorite within the altered margins of clasts (Fig. 2.10H). Chlorite alteration consists of fine-grained, distinctly green, Fe-rich chlorite, 60–70 %, quartz, 5–10 %, sericite 10–20 %, albite 5–10 % ± calcite ± chalcopyrite ± pyrite.

2.5.4.5.4 Spotted-textured alteration

The spotted-textured alteration manifests as ovoid, leucocratic "spots" 0.4–1 cm in diameter. Spotted-textured alteration is not uniformly distributed, and is limited to altered zones of clasts within the breccia and within sericite altered envelopes along conjugate fractures that occur up to 6m from the outer Joliet Breccia contact. The spots are concentrated either in the interior (Fig. 2.10G) or margin (Fig. 10I) of chloritized mafic and sericite altered felsic clasts (Fig. 2.10J). However, spotted-textured alteration does not occur within the tonalite. The spots comprise fine-grained muscovite and quartz ± rutile ± albite, in a chloritized matrix (Fig. 2.10K) and have diffuse margins with the host rock; where numerous, the spots impinge and appear to merge (Fig. 2.10L). The spots within mafic clasts are typically larger and occur as protuberances (Fig. 2.10I) in comparison to those within felsic clasts, which do not stand out as readily (Fig. 2.10J). The spots are typically flattened parallel to the main E-W striking regional cleavage (Fig. 2.10K).

2.5.4.5.5 Alteration geochemistry

The alteration products are partly controlled by the primary bulk composition of the protolith, which is evident in the spatial distribution of the alteration types (Fig. 2.7). The higher Fe, Mg, Mn and Sc values of the mafic dominated domain favours chloritization, whereas higher

K and Ba values of the felsic dominated domain, tonalite and fractured Quemont feeder dike favours sericitization. However, K, Ba, Fe, Sc and Mg are enriched in the felsic dominated and mafic dominated domains relative to the host Quemont feeder dike and Powell andesite (Table 2), indicating these elements were added by the hydrothermal fluid during alteration. In addition, average values for Ba, Fe, Sc and Mg are higher in the mafic and felsic dominated domains relative to the Joliet Breccia tonalite.

Compositional changes associated with each alteration type are calculated using Gresens (1967) mass change formula as modified by Babcock (1973), as outlined and graphically displayed in supplementary data file 5. Calculated compositional changes associated with each alteration type are consistent with the observed modal mineralogy. Sericite alteration is associated with significant gains in Si, Al, K, Rb, and Ba, and a decrease in Ca, Na, Mg, Mn, and Fe. Chlorite alteration is associated with gains in Al, Fe, Sc and Ti and losses in Si, Na, K, Ca, Mg, Ba, Sr, Rb and Cr. In addition, the LREE are depleted relative to the HREE and HFS, which indicates potential mobility. Compositional gains and losses associated with spotted-textured alteration include major gains in Al, Rb, K, Ba, Fe (± Mg ± Mn) and Ti and losses in Na, (± Mg ± Mn), Ca and Sr. Losses in Na and Ca, associated with sericite and chlorite alteration reflect destruction of feldspar. Progressive alteration is demonstrated by increased values in the Ishikawa alteration index (AI: 100*[K2O + MgO] / [K2O + MgO + Na_2O + CaO]) and chlorite carbonate pyrite index (CCPI: 100*[MgO + FeO] / [MgO + FeO + Na2O + K2O]; Fig. 2.2, supplementary data file 5). The spotted-textured samples appear to have intermediate AI and CCPI values between least altered and chlorite altered samples (Fig. 2.2, supplementary data file 5).

2.6 Discussion

We first discuss potential mechanism(s) and timing for Joliet Breccia fragmentation and emplacement, and then discuss the relationship and timing of the Joliet Breccia alteration and mineralization relative to the formation of the breccia and the larger-scale metallogeny of the Rouyn-Noranda mining district. Based on the geologic attributes for the Joliet Breccia established in this study through mapping, geochemistry, and geochronology, any model attempting to explain Joliet Breccia fragmentation and emplacement processes must satisfy the following constraints:

1. The gradational contacts between different breccia domains within the breccia, and between the Joliet Breccia and the immediate host rocks;
2. Fracturing and *in situ* brecciation of the host Quemont feeder dike in proximity to the Joliet Breccia;
3. Hydrothermal cement of the Joliet Breccia and surrounding *in situ* brecciated host rocks with a total absence of a fine-grained, clastic, ash-sized matrix;
4. Poor size sorting and absence of bedding, with breccia domains defined by dominant clast composition, which reflects the composition of adjacent host rocks;
5. Abundance of lithic clasts with an angular blocky to tabular morphology, including blocks of the upper marker unit;
6. Brecciation of a tonalitic intrusion and tonalite blocks in the Joliet Breccia;
7. A U-Pb zircon age of 2698.0 ± 0.9 Ma for the brecciated tonalite intrusion, and four hydrothermal monazite ages (2693.7 ± 1.0/8.9 Ma; 2696.9 ± 0.45/8.9 Ma; 2698.7 ± 1.4/8.9 Ma; 2701.2 ± 0.33/8.9 Ma; $2s/2s_{sys}$), which indicates that the brecciation and hydrothermal filling of vugs at the Joliet Breccia is 0.3–8.7 Ma younger than the 2702 ± 0.8 Ma synvolcanic Quemont feeder dike host and surrounding volcanic rocks;

8. Its formation prior to regional deformation, since the Joliet Breccia, host rocks, alteration and mineralization are overprinted by the regional ca. <2669–>2639 Ma age cleavage.

2.6.1 Previously proposed model for the Joliet Breccia

Wilson (1941), Lichtblau and Dimroth (1980), Lichtblau (1989), Dimroth and Rocheleau (1979) and De Rosen Spence (1976) attributed the formation of the Joliet Breccia to an explosive, subaqueous phreatic eruption and they invoked phreatic explosion breccia craters at Yellowstone (Muffler et al., 1971) as a subaerial analogue. The interpreted driving mechanism for brecciation was the heat of a cooling Quemont feeder dike. Dimroth and Rocheleau (1979) and Lichtblau (1989) interpreted the internal clast domains identified herein to be conformable depositional units deposited on the seafloor, which they subdivided into a lower "cycle 1", and an upper "cycle 2". "Cycle 1" was interpreted as an interbedded sequence of "mixed breccia" containing a few mafic blocks and "brecciated rhyolite", which corresponds to the transitional and felsic dominated domains of this study, respectively. They described "cycle 2", or the mafic dominated domain herein, as a mafic and mixed breccia, consisting of a chaotic assortment of angular Quemont feeder dike blocks and Powell andesite blocks, with an increase in proportion of andesite blocks towards the top of the sequence. They viewed the WSW striking breccia domains and the E-W trending long axis of the blocks within the breccia to define bedding and to mark the paleohorizontal. The western and eastern margins of the Joliet Breccia were described as the steeply dipping inner crater walls (Lichtblau, 1989). To justify the current geometry of the Joliet Breccia and host rocks, Lichtblau (1989) envisaged that originally, the Quemont feeder dike dipped shallowly towards the north and the base or deeper part of the explosion crater to lie to the south within the host Quemont feeder dike. Tonalite within the Joliet Breccia was interpreted as younger dikes cross-cutting the

breccia (Lichtblau, 1989) and thus post-dating and unrelated to the brecciation and mineralization events.

Lichtblau (1989) proposed that the upper marker unit of the Powell formation is the distal, basin-ward equivalent of "cycle 2", thus correlating the Joliet Breccia with the host volcanic strata ca. 2704–2701 Ma (McNicoll et al., 2014). However, blocks of the upper marker unit within the Joliet Breccia, and a new U-Pb zircon age of 2698.0 ± 0.9 Ma for a tonalite block within the breccia indicate that the Joliet Breccia is 0.3–8.7 Ma younger than the Quemont feeder dike, Powell formation and Quemont VMS deposit and is time equivalent to the youngest units of the Blake River Group (ca. <2699.5–2697 Ma; McNicol et al., 2014). Furthermore, the contacts between inferred beds, now interpreted as clast domains, are gradational as is the contact between the Joliet Breccia and host Quemont feeder dike, plus the complete lack of sedimentary features and blocks of younger tonalite indicate the Joliet Breccia formed in the subsurface and may or may not have breached the seafloor.

The occurrence of well bedded clasts of Powell tuff, massive amygdaloidal and pillowed andesite, and lapilli-tuff of the upper marker unit and massive aphanitic and quartz-microporphyritic rhyolite implies some vertical transport and or downward settling. The lack of a chilled margin and the presence of clasts of tonalite within the Joliet Breccia indicate that the tonalite was intruded prior to the formation of the mafic dominated domain of the Joliet Breccia.

2.6.2 Possible fragmentation processes for the Joliet Breccia

The abundance and anomalous size of lithic clasts with an anisometric clast size distribution within the Joliet Breccia, is consistent with sudden steam generation within the host rock and spalling, with high energy due to voluminous explosive vapor expansion (Fisher and

Schminke, 1984; Jébrak, 1997). Possible explosive fragmentation processes consistent with features of the Joliet Breccia include hydrovolcanic and magmatic-hydrothermal processes. Tectonic implosion may also produce similar features (Mitcham 1974; Sibson, 1986; Jébrak, 1997). All three fragmentation mechanisms can result in monomictic to polymictic breccias, gradational contacts with host rocks and an angular clast morphology (Table 3) depending on the nature of the host-rocks, intensity of the brecciation event and confining pressure, which dictates the amount of movement and particle attrition of the resultant breccia (Fisher and Schmincke, 1984). The angularity of clasts in the Joliet Breccia and lack of a clastic matrix indicates virtually no particle attrition, and the linear, dike parallel orientation of the clast domains rather than a symmetrical or annular distribution implies dominantly local derivation of clasts from the immediate host rocks, and minimal transport or fluidisation (Reynolds, 1954).

Explosive hydrovolcanic processes operate at or near surface, involve an external fluid source (meteoric or seawater), and are subdivided into phreatic and phreatomagmatic, based on evidence for indirect or direct contact with magma, respectively. A phreatic brecciation mechanism is caused by flashing of an external fluid to steam as a result of contact with hot rocks that were conductively heated by magma (Browne and Lawless, 2001). In contrast, a phreatomagmatic brecciation mechanism requires evidence for direct interaction between an external fluid and magma, as indicated by a juvenile component to the breccia that is usually present in the matrix (Lorenz, 1973; Fisher and Schmincke, 1984; White and Ross, 2011).

Tectonic-hydrothermal breccias form near surface in the upper 10–15 km of crust, associated with active faults and unlike hydrovolcanic breccias do not require a direct input of magmatically derived mass or energy (Sibson, 1986; Jébrak, 1997; Woodcock and Mort, 2008). Fault associated breccias are formed by a variety of physical processes, however, this discussion

is limited to fluid assisted brecciation, also known as implosion brecciation (Sibson, 1986), as it is the only viable tectonic-hydrothermal process that may produce the features observed in the Joliet Breccia. Implosion brecciation is triggered by a decrease in pressure at releasing bends or dilational jogs along fault surfaces and at intersections between two growing faults (Mitcham, 1974; Sibson, 1986; Jebrak, 1997).

Magmatic-hydrothermal brecciation requires the separation of a volatile phase from an associated crystallizing magma as a result of second boiling and subsequent decompression, vaporization and rapid volatile expansion to trigger an explosive event (Sillitoe, 2010), as opposed to the externally derived fluid involved in hydrovolcanic processes (Fisher and Schminke, 1984; Sillitoe, 2010). These systems are common in young arcs and active settings (e.g., El Teniente, central Chile; Camus, 1975), and their recognition in Archean greenstone belts is relatively rare (e.g., Côté Gold, Katz et al., 2017). The breccias are associated with plutons or stocks, and can host small volumes of fine-grained porphyritic intrusions in the form of dikes, small bodies, angular fragments and/or irregular, partly disaggregated masses, which indicates a temporal, spatial and likely genetic relationship to the breccia (Sillitoe, 1985).

The Joliet Breccia is spatially associated with a major synvolcanic structure now occupied by the Quemont feeder dike. The sharp, intrusive contact of the northernmost Quemont dike with the host volcanic strata is not sheared and evidence for lateral movement along the Quemont feeder dike is lacking. In addition, the anisometric clast size distribution and polymictic nature of the clasts in the Joliet Breccia and spatial association with intrusive rocks is atypical of implosion breccias (Table 3). Subseafloor phreatic, magmatic-hydrothermal and phreatomagmatic explosive activity remain as the most likely processes, but the latter is negated by the lack of a juvenile component as clasts or matrix in the Joliet Breccia. The main distinguishing feature that separates

phreatic breccias from magmatic-hydrothermal breccias is the widespread silicification that may be associated with the former, both as a pervasive replacement of clasts and as hydrothermal cement, with a close relationship between silicification and brecciation as an episodic self-sealing-rupture mechanism (Gibson et al., 1983; Sillitoe, 1985; Gibson, 2005). The spatial association with a tonalitic intrusion suggests the input of magmatic heat, ± volatiles ± metals to the system, likely at depth and generated from the same source as the Flavrian-Powell Intrusive Complex due to their similar mineralogy and geochemistry. This would be conducive to either a phreatic or magmatic-hydrothermal explosive event, depending on the indirect or direct role of magmatic volatiles, respectively. The radial and concentric orientations of the fractures surrounding the Joliet Breccia are suggestive of a uniaxial stress regime above a cylindrical stock typical of magmatic-hydrothermal environments (Koide and Bhattarcharji, 1975; Tosdal and Richards, 2001). This suggests that a magmatic-hydrothermal mechanism is the most likely brecciation process for the Joliet Breccia (Sillitoe and Sawkins, 1971).

A minimum of two brecciation events within the Joliet Breccia are indicated by the presence of blocks of *in situ* brecciated felsic dominated domain within the mafic dominated domain. In addition, the lack of the spotted-textured alteration within the tonalite, implies that it had not experienced the same degree of alteration as the pervasively sericitized and spotted felsic dominated domain. This, combined with the brecciated contact of the tonalite in the mafic dominated domain, and presence of cross-cutting sericitized fractures within the tonalite, suggests it was emplaced after the formation of the felsic dominated domain and prior to the formation of the mafic dominated domain (Fig. 2.11). The Joliet Breccia is broadly discordant based on cross-cutting relationships. Assuming formation driven by uniaxial extensional stresses, the long axis represented by the intersection of surrounding conjugate fractures would be parallel to the

orientation of the breccia body (Koide and Bhattarcharji, 1975; Tosdal and Richards, 2001), implying a possible sub-vertical geometry in this case (Fig. 2.3). These fractures were likely purely tensile as indicated locally by fibrous quartz growing perpendicular to the fracture margin.

2.6.3 Distinguishing subsurface vs. surface breccias in the ancient rock record

Distinguishing between surface and subsurface breccias is essential for stratigraphic reconstruction and exploration, particularly in VMS districts where coarse breccias, particularly those dominated by felsic clasts, commonly define favourable stratigraphic intervals associated with VMS deposits (Franklin et al., 2005). Using the Joliet Breccia as an example, features essential to recognizing subsurface breccias in ancient deformed terranes include:

1. Discordant contact with host rocks. This requires knowledge of the stratigraphy and structure, i.e., the development of the volcanic succession and deformation history;
2. Gradational contact with host rocks. Subsurface breccias are often surrounded by a gradational damage zone, associated with fracturing and *in situ* brecciation of host rocks;
3. A vuggy, open space matrix, which is characteristic of many subsurface breccias and is atypical of conformable volcanic breccias. In subsurface breccias the vuggy open-space matrix is typically infilled with hydrothermal minerals deposited syn or post brecciation. Some subsurface breccias are associated with a clastic, ash-sized matrix that may be massive and homogeneous or display fine lamination that developed during emplacement (Fisher and Schminke, 1984; Sawkins, 1990). In the latter, careful mapping to define contact relationships and to establish discordance are required;

4. Inter-breccia intrusions, and angular lithic blocks of intrusive rocks within the breccia;
5. Timing of the breccia and host rocks. This can be relative, based on cross-cutting relationships and relationship to tectonic fabrics (deformation history) or absolute, based on dating of blocks, matrix and host rocks.

2.6.4 Mineralization and associated hydrothermal alteration

Chalcopyrite, pyrite, and pyrrhotite mineralization occurs dominantly in the matrix of the breccia and, to a lesser extent, in veins that cut the breccia indicating that it was emplaced syn- to post-brecciation. Textural relationships such as the fractured, recrystallized and red staining of white coarse-grained comb quartz where associated with sulfides, and the observation that white comb quartz and sulfides occur together and separately within the breccia cement, suggest that the quartz formed early relative to the sulfides. The euhedral habit of the pyrite compared to the interstitial anhedral habit of chalcopyrite and pyrrhotite and the presence of corroded pyrite grains with cross-cutting chalcopyrite micro veinlets is likely related to post-mineralization deformation, wherein pyrrhotite and chalcopyrite are preferentially remobilized relative to pyrite (Gilligan and Marshall, 1987). This is supported by the presence of chalcopyrite interstitial to recrystallized quartz. Calcite veins cross-cutting Joliet Breccia clasts and matrix cement, and locally infilling remaining void space within matrix vugs represents the youngest event. The observed paragenesis of the hydrothermal cement at the Joliet Breccia is consistent with the expected paragenesis for magmatic-hydrothermal breccias, which typically consists of early tourmaline (where present), followed by quartz, then sulfides, and finally late carbonate minerals (Sillitoe and Sawkins, 1971; Sillitoe, 1985). The red staining results from oxidation of sulfides at surface.

The Joliet Breccia alteration consists of the low-temperature (<300˚C) mineral associations of chlorite, sericite and carbonate minerals (Sillitoe, 2010) consistent with many magmatic-hydrothermal breccias that have exclusively sericitic and/or chloritic alteration down to their roots (Table 3; Sillitoe and Sawkins, 1971), and notably is also typical of VMS deposits. The alteration types are divisible into pre-, syn-, and post- breccia events, based on textural and spatial relationships. The quartz-albite alteration is the earliest alteration as it is confined to select clasts within the Joliet Breccia where it is truncated by white comb quartz lining fracture controlled vugs. The sericite and chlorite alteration occurred syn-brecciation as indicated by their symmetrical, concentric pattern around clasts. However, chlorite alteration is later as evidenced by the presence of pervasively sericitized blocks of the felsic dominated domain, overprinted by chlorite alteration within the chloritized mafic dominated domain (Fig. 2.4I). In addition, the gradual increase in matrix chlorite towards the transitional domain and mafic dominated domain suggests that hydrothermal chlorite was superimposed on previously sericitized and cemented felsic dominated breccia and that the chlorite alteration followed the second brecciation event.

The compositional gains and losses attributed to chlorite and sericite alteration at the Joliet Breccia mimic those calculated by Riverin and Hodgson (1980) for the Millenbach VMS deposit within the Rouyn-Noranda mining district located a few km north of Joliet Breccia. Chlorite alteration is characterized by losses in Si, K, Na and Ca and gains in Fe. Similarly, spotted alteration is characterized by losses in Si, Na and Ca and gains in Al, K and Fe; sericite alteration shows Si and K gains and Na and Ca losses. The difference is Mg loss at the Joliet Breccia compared to Mg gain at Millenbach (supplementary data file 4; Fig. 2.9). The Fe/Mg ratio of chlorite is dominantly controlled by fluid composition, pH and temperature. The Mg content of chlorite in the upper parts of VMS systems is dominantly derived from interaction with seawater,

whereas deeper upwelling hydrothermal fluids have a higher Fe/Mg ratio (Shikazono and Kawahata, 1987). Thus, VMS alteration pipes at Noranda are characterized by an Fe-chlorite core grading upward and outward to Mg-chlorite and then sericite. The Millenbach samples reflect the Mg-rich chlorite present in the immediate sub-seafloor footwall rocks as opposed to the Joliet Breccia, which represents alteration within a deeper subsurface system.

The lateral and vertical zoning of alteration types, and metal tenor, as well as their timing is consistent with VMS footwall alteration zones at Noranda and elsewhere, with early quartz-albite alteration overprinted by an outer zone of sericite alteration and an inner chlorite alteration zone proximal to mineral occurrences and deposits (Riverin and Hodgson, 1980; Lesher et al., 1986; Maclean and Hoy, 1991; Franklin et al., 2005). In a VMS context, the quartz-albite alteration represents a semi-conformable alteration zone, which is interpreted to result from evolved seawater-rock interaction with down-welling modified seawater (Gibson et al., 1983). This laterally extensive alteration has been referred to as part of a self-sealing geothermal system at Noranda, wherein it served as an impermeable cap that focused subsequent VMS hydrothermal fluids to cross-cutting synvolcanic structures resulting in the superposition of discordant VMS alteration zones on regional quartz-albite alteration (Gibson et al., 1983).Thus, the lateral variation in alteration types within the Joliet Breccia may reflect a gradient in permeability, and likely temperature, with the highest water-rock ratio and temperature reflected by the internal chlorite alteration. This lateral zonation is also reflected in the Joliet Breccia metal tenors, with the highest values of Cu-Ag-Bi and Te located within the chlorite alteration of the mafic dominated domain. This metal zonation is typical of magmatic-hydrothermal deposits (Sillitoe, 2010) and VMS deposits due to the temperature dependent stability of CuCl complexes, wherein Cu becomes insoluble at temperatures < 300˚C, which results in Cu mineralization being concentrated in the

stockwork feeder zones and the base and interior of sulfide lenses (Lydon, 1988; Xiao et al., 1998; Franklin et al., 2005). In summary, the alteration mineralogy, attendant compositional changes and metal zonation are similar for the subsurface magmatic-hydrothermal Joliet Breccia and nearby seafloor VMS deposits, which may indicate similar fluid conditions and thus may further support a magmatic contribution to the VMS hydrothermal systems.

Wilson (1941) first noted the spotted-textured alteration in the Powell block and Lichtblau and Dimroth, (1980) and Lichtblau (1989), observed that it was particularly abundant within the Joliet Breccia. The clear fracture control of the spotted texture as haloes surrounding veins, and as rims surrounding clasts suggests a hydrothermal alteration origin. The spotted texture is similar to a well-known metamorphic texture within the Rouyn-Noranda mining district referred to as “dalmatianite” (De Rosen-Spence, 1969; Riverin and Hodgson, 1980), wherein cordierite porphyroblasts formed by contact metamorphism of Mg-altered mafic-intermediate volcanic rocks during intrusion of the ca. 2690 Ma post-volcanic Lac Dufault granitoid (Fig. 2.1). The cordierite porphyroblasts retrogressed to a subgreenschist facies mineral assemblage during regional metamorphism. The spotted-textured alteration in the Powell block is not associated with any known ca. 2690 Ma post-volcanic plutons, and if it is a retrogressed assemblage derived from an aluminosilicate porphyroblast, the precursor porphyroblast has not been identified. The spotted-texture alteration occurs in zones with a specific bulk composition, marked by gains in Rb, K, Ba, Mg and Fe and losses in Na and Ca, regardless of protolith, and appears to be geochemically intermediate between the sericite and chlorite alteration types. Therefore, the spotted texture is interpreted to represent either relict retrogressed porphyroblasts or new nodular chlorite-sericite intergrowths that preferentially developed in areas of intermediate alteration intensity.

2.6.5 Comparison to other known breccias within the Rouyn-Noranda mining district

The Joliet Breccia exhibits similarities to the Chadbourne, Newbec and St. Jude breccias (Fig. 2.1). The three breccia bodies and the Joliet Breccia are all spatially associated with intrusions, and are polymictic, with an abundance of andesitic blocks and variable proportions of felsic blocks. In addition, like the Joliet Breccia, the Chadbourne, and St. Jude breccias have: 1) gradational contacts with their host rocks, from an outer conjugate fracture set, to an incipient jig-saw fit breccia, to a rotated (±transported) matrix-clast supported breccia (Walker and Cregheur, 1982; Kennedy, 1985; Galley and van Breemen, 2002); 2) similar dimensions; and 3) a crudely elliptical morphology in plan view; the Newbec breccia has a triangular plan view (Smith, 1983). The key differences between these breccias are their matrix, metal content, and relative timing. The Joliet Breccia overlaps in time with the St. Jude breccia and possibly the Newbec breccia, however, the Chadbourne breccia is interpreted to be significantly younger (Fig. 2.12).

The Chadbourne breccia, one of the original discoveries in the camp, is an historic gold mine that produced 1.4 Mt of ore at a grade of 3.65 g/t Au. The breccia comprises andesitic blocks, with minor rhyolite blocks, in an open-space hydrothermal cement of quartz, albite, ankerite and dolomite with accessory pyrite, specularite and tourmaline. The timing of the Chadbourne breccia is poorly constrained. Walker and Cregheur (1982) suggested that the breccia was emplaced after the main regional post-Timiskaming (<2669 Ma) deformation, since the volcanic strata must have been tilted to steeper dips prior to emplacement. However, Dubé and Mercier Langevin (2020), consider the Chadbourne breccia to have been emplaced pre-Timiskaming (>2669 Ma). The Chadbourne mineralization occurs within the open-space breccia matrix and consists of native Au and Ag, Au-telluride, as well as microscopic Au inclusions within pyrite, chalcopyrite, and galena

and accessory magnetite (Walker and Cregheur, 1982). The mineralization is spatially associated with siliceous zones and is concentrated in cylindrical shoots with diameters up to 40m that parallel the plunge of the breccia, which is typical of structurally controlled gold-mineralization, with gold following the dilatant zones (Walker and Cregheur, 1982). The Chadbourne breccia is spatially associated with a major fault zone and a pre- to early- Timiskaming age syenite intrusion, which was interpreted as a heat source and potential fluid source to drive hydrothermal circulation (Walker and Cregheur, 1982; Dubé and Mercier-Langevin, 2020).

The Newbec Breccia is a subeconomic Cu-Mo-Zn occurrence that contains subrounded-subangular fragments of diorite, andesite, quartz-feldspar porphyry, tuff, gabbro, and anorthositic gabbro in a matrix of fractured and chlorite altered quartz-feldspar porphyry ± pyrrhotite ± chalcopyrite ± pyrite ± molybdenite ± sphalerite (Smith, 1983). Locally the matrix is open-space infill of crystalline quartz, chlorite, zoisite and ankerite (Smith, 1983). The timing of the Newbec breccia is poorly constrained. It was initially interpreted by Wilson (1941) as younger than the Lac Dufault intrusion due to the presence of angular fragments of granodiorite within the breccia adjacent to the contact. However, irregular offshoots of the granodiorite were observed to cross-cut the breccia leading Smith (1983) to interpret it as older than the Lac Dufault intrusion. The ~2690 Ma age for the Lac Dufault intrusion (Mortensen, 1993) makes the Newbec breccia pre-Timiskaming age. It was initially interpreted as a phreatic breccia that was overprinted by a magmatic brecciation event (Wilson, 1941). Smith (1983) interpreted the Newbec Breccia to have formed by a magmatic-hydrothermal fragmentation process.

The St. Jude Breccia, a subeconomic Au-Ag-Cu-Mo occurrence, comprises a polymictic breccia containing angular blocks of andesite wall-rock, and aphyric to porphyritic felsic intrusive blocks, in an igneous aplitic matrix (Galley and van Breemen, 2002). The brecciation event is

bracketed by the age of the host trondjhemite phase of the Flavrian-Powell Intrusive Complex ca. 2700 +3/-2 Ma and a cross-cutting quartz albite dike ca. 2696.6 ± 0.9Ma (McNicoll et al., 2014) and is interpreted as ca. 2698 Ma (Galley and van Breemen, 2002). Its location on the margin of the synvolcanic Flavrian-Powell Intrusive Complex and spatial association with a small trondjhemite intrusion internal to the breccia suggests that it formed by a magmatic-hydrothermal fragmentation process (Galley and van Breemen, 2002). The trondjhemite intrusion is locally *in-situ* brecciated, and occurs as block sized clasts within the breccia (Galley and van Breemen, 2002). The St. Jude breccia is enriched in magmatophile (Ag, Te, Se, Bi, Sn) elements and exhibits a metal zonation with an internal Mo-rich zone and an outer Cu-rich zone, associated with a proximal biotite alteration and a distal sericite alteration, typical of high-temperature intrusion related mineralization (Kennedy, 1985; Galley and van Breemen, 2002).

The Joliet mine, hosted by rhyolite breccia, produced 1,465,403 t averaging 0.905 % Cu, 8 g/t Ag, and 0.34 g/t Au (Sabina, 2003). Based on the ore outline displayed on historical company maps (Joliet-Quebec, 1948), at 100 m and 200 m depths, the orebody had a pipe-like shape with a diameter of 50 m and a long axis plunging moderately southward; however, it is now inaccessible and a detailed description of its mineralization and setting is lacking. The timing of the Joliet orebody is uncertain with the only age constraint being that it cross-cuts the Joliet Rhyolite, which is older than ca. 2702 Ma (McNicoll et al., 2014).

2.6.6 Metallogenic context of the Joliet Breccia within the Rouyn-Noranda mining district

Magmatism played a key role in the hydrothermal systems of the Rouyn-Noranda mining district, with VMS deposits forming at three intervals (ca. 2702 Ma, 2698–2697 Ma and 2696–

2695 Ma) during the 7 m.y. interval of BRG volcanism that constructed the Noranda volcanic complex (McNicoll et al., 2014). The VMS deposits of the Noranda volcanic complex are enriched in magmatophile elements and the relative role of seawater and magmatic hydrothermal fluid in subseafloor VMS hydrothermal systems has been debated (Hannington et al., 1999; Franklin et al., 2005; Mercier-Langevin et al., 2011). Enrichment in magmatophile elements and Au at active hydrothermal vents on the seafloor (e.g., Brothers Volcano, Kermadec Arc, New Zealand; De Ronde et al., 2011; Susu Knolls, Manus Basin, Yeats et al., 2014) has been interpreted to indicate a magmatic fluid contribution to a seawater dominated hydrothermal system and similar arguments have been made for Au-enrichment at Horne and Quemont (Sharman et al., 2015; Krushnisky, 2018; Krushnisky et al., 2020). The Joliet Breccia, which is enriched in magmatophile elements, but Au poor, post-dates the nearby Au-rich Quemont and Horne VMS deposits (ca. 2702 Ma), but is temporally coincident with the youngest volcanic units (2696–2695 Ma) and VMS deposits of the Noranda Subgroup (McNicoll et al., 2014).

The brecciation mechanisms for the Joliet Breccia have been presented as separate models, but in reality they may represent a continuum. Phreatic breccias form in the cooler, distal near surface or seafloor portions of a deeper magmatic-hydrothermal system and subsurface magmatic-hydrothermal breccias themselves can grade downwards into igneous breccias (Lawless and White, 1990). Given the temporal overlap, the Joliet and St. Jude breccias and possibly the Newbec breccia (Fig. 2.12), may all be products of the same ca. 2698 Ma magmatic-hydrothermal event that formed VMS deposits at the seafloor and magmatic hydrothermal breccias at different crustal levels and in proximity to a magmatic source. This is consistent with more recent work in the Bergslagen district, Sweden, where Allen et al. (1996), and Jansson and Allen (2011) invoked a continuum from deeper magmatic-hydrothermal processes to shallow

VMS processes. In the Bergslagen and the Rouyn-Noranda mining districts the two systems became superimposed following burial and resurgent magmatic-hydrothermal processes resulting in the source intrusions and associated mineral deposits eventually cross-cutting older volcanic strata.

Thus, although the mineralized Joliet Breccia, St. Jude and Newbec breccias are not genetically or temporally related to their older host strata or to older VMS deposits, it does not preclude a potential indirect genetic association between these mineralized breccias and temporally correlated ca. ≤2698 Ma VMS deposits. These variably mineralized subsurface breccias may provide additional evidence for a magmatic contribution to the VMS hydrothermal system, as suggested by previous workers (Poulsen and Franklin, 1981; Walford and Franklin, 1982; Kennedy, 1985; Gibson and Watkinson, 1990; Poulsen and Hannington, 1996; Hannington et al., 1999; Franklin et al., 2005; Dubé et al., 2007; De Ronde et al., 2011; Huston et al., 2011). Thus, in ancient VMS districts an intimate association between magmatic-hydrothermal and VMS deposits should be expected, and this relationship may be analogous to that of the porphyry-epithermal continuum documented in modern subaerial arcs (Sillitoe, 2010).

The Chadbourne breccia exhibits many similarities to the Joliet, St. Jude and Newbec breccias, but its interpreted later timing suggests it is not temporally or genetically related. The Chadbourne breccia is most likely post-volcanic and pre-syn Timiskaming deformation (Fig. 2.12; Dubé and Mercier-Langevin, 2020).

2.7 Conclusions

The Joliet Breccia is a subsurface breccia, indicated by its discordant relationship, gradational contacts with wallrocks, and ca. 2698.9–2693 Ma Ma age and is younger than the ca. <2702–

2699.5 Ma volcanic units, and associated VMS deposits. However, the location of the Joliet Breccia to a synvolcanic structure, marked by the ca. 2702 Ma Quemont feeder dike, attests to the continued reactivation of fundamental structures during the evolution of the Noranda volcanic complex and its hydrothermal systems. Subseafloor magmatic-hydrothermal explosive processes account for the features observed within the Joliet Breccia and its contact and timing with the host rocks. Initial brecciation could have been triggered by a decrease in permeability due to early quartz-albite alteration and a build-up of hydrothermal fluid pressure during renewed magmatic-hydrothermal processes.

The timing for the Joliet Breccia overlaps with other brecciation and mineralization events within the Rouyn-Noranda mining district, including the St. Jude breccia and possibly the Newbec breccia, which are both Cu-Mo deposits spatially associated with intrusions. However, the key difference between these prospects and the Joliet Breccia is their magmatic matrix and/or high-temperature alteration assemblage, which is typical of some but not all magmatic-hydrothermal systems. The Joliet Breccia is interpreted to have formed at a shallower crustal level relative to the Newbec and St. Jude intrusive breccias. This suggests that localized ca. 2699~2695 Ma magmatic-hydrothermal events were superimposed on older volcanic strata, with variations in individual deposit characteristics reflecting differences in depth of formation and proximity to magmatic source. This new interpretation highlights the difficulty in recognizing and classifying subsurface breccia bodies, particularly in deformed and metamorphosed terranes, which can have important implications on metallogeny. Establishing discordance, contact relationships, as well as relative and absolute timing requires knowledge of the stratigraphy and structure of the volcanic succession, a fundamental requisite to recognizing subsurface breccias.

The lateral zoning of alteration types, compositional gains and losses, metal tenor and association, as well as their relative timing within the Joliet Breccia are similar to VMS footwall alteration zones at Noranda and elsewhere (Riverin and Hodgson, 1980; Lesher et al., 1986; Franklin et al., 2005). The VMS deposits hosted by the youngest units of the Blake River Group are broadly coeval with the timing of the St. Jude, Joliet and possibly Newbec breccias. Thus, within the context of the metallogeny of the larger Rouyn-Noranda mining district these breccias may be part of a broad continuum of subsurface magmatic-hydrothermal, and seafloor VMS deposits, akin to the porphyry-intermediate sulfidation epithermal continuum of modern subaerial volcanic arcs.

2.8 Acknowledgements

The authors extend much appreciation to Dr. Richard Sillitoe and Dr. Patrick Mercier-Langevin for their expertise and insight, which greatly improved the manuscript. Field assistant Mr. Michael Langa is thanked for eager, competent and able assistance in the field. Yorbeau Resources Inc. are thanked for allowing the use of their rock saw facilities during the field season. Dr. Gérald Riverin and Mr. Jean Goutier are thanked for providing critical historical data. Financial support was provided by Metal Earth though a Canada First Research Excellence Fund (CFREF) grant, which comprises a tri-agency initiative of the Natural Sciences and Engineering Research Council (NSERC), Social Sciences and Humanities Research Council (SSHRC), and the Canadian Institutes of Health Research (CIHR). Funding was also provided by federal, provincial, and industry partners of the Mineral Exploration Research Centre (MERC; http://merc.laurentian.ca/research/metal-earth/). This publication is a Metal Earth contribution MERC-ME-2020-102.

2.9 Figures

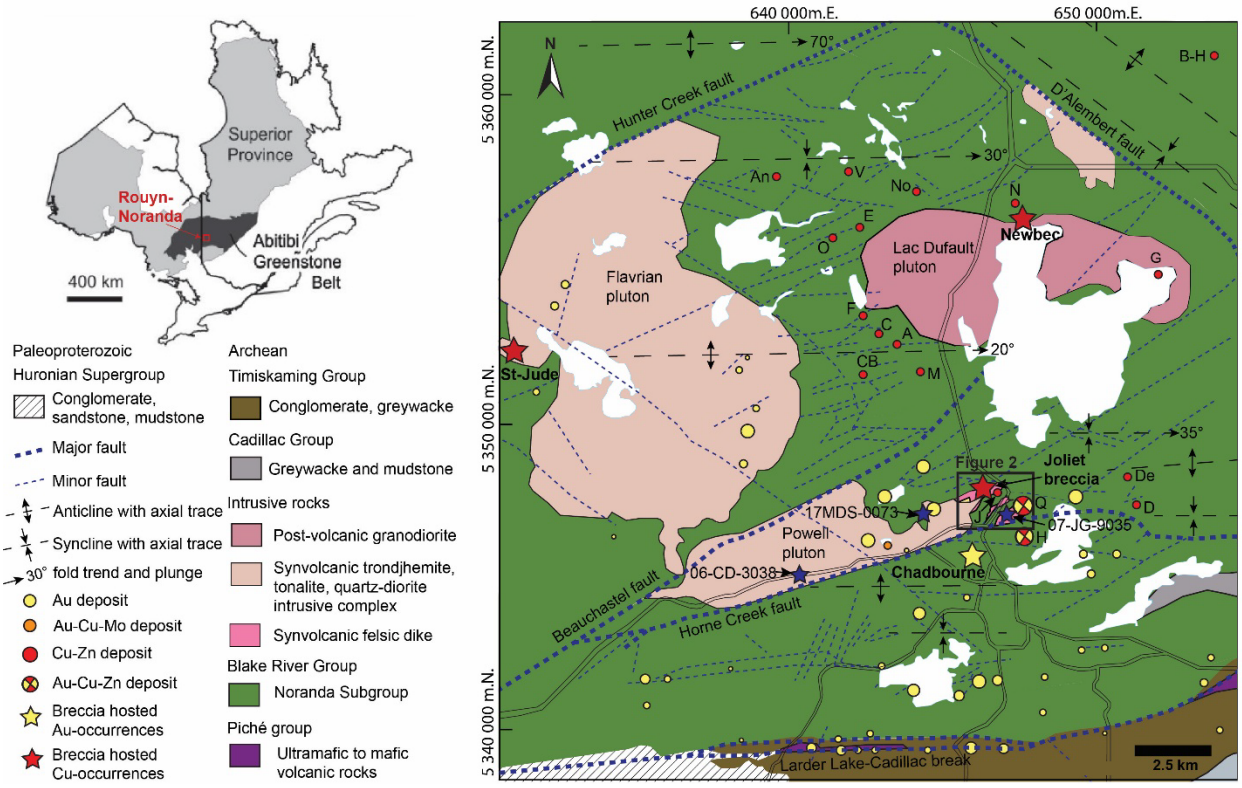

Figure 2.1: Regional geology map of the Noranda volcanic complex.

Regional map of the Noranda volcanic complex, modified from Poulsen (2017) and McNicoll et al. (2014). The Noranda volcanic complex comprises the Noranda Subgroup (Goodwin, 1980; De Rosen Spence, 1976) of the Blake River Group. The Noranda Subgroup represents 7 m.y. of continuous volcanism except for a distinct break in volcanism between 2700 and 2698.5 Ma with VMS deposits occurring in volcanic strata older and younger than this break. The locations of discordant breccia bodies are shown by red and yellow stars; the colour reflects the dominance of copper or gold respectively. Blue stars show the location of previously reported U-Pb ages in the Powell Block, which is the wedge shaped fault block bound to the north by the Beauchastel fault and to the south by the Horne Creek fault. Axial traces of regional synclines and anticlines from Hubert et al. (1984). VMS and orogenic gold deposits are shown by red and yellow circles respectively. The yellow circles are scaled to reflect the relative gold tonnage. (An = Ansil, V = Vauze, No = Norbec, N = Newbec, B-H = Bouchard-Hebert, O = Old Waite, E = East Waite, G = Gallen, F = Amulet F, C = Amulet C, A = Amulet A, CB = Corbet, M = Millenbach, J = Joliet, De = Deldona, D = Delbridge, Q = Quemont, H = Horne).

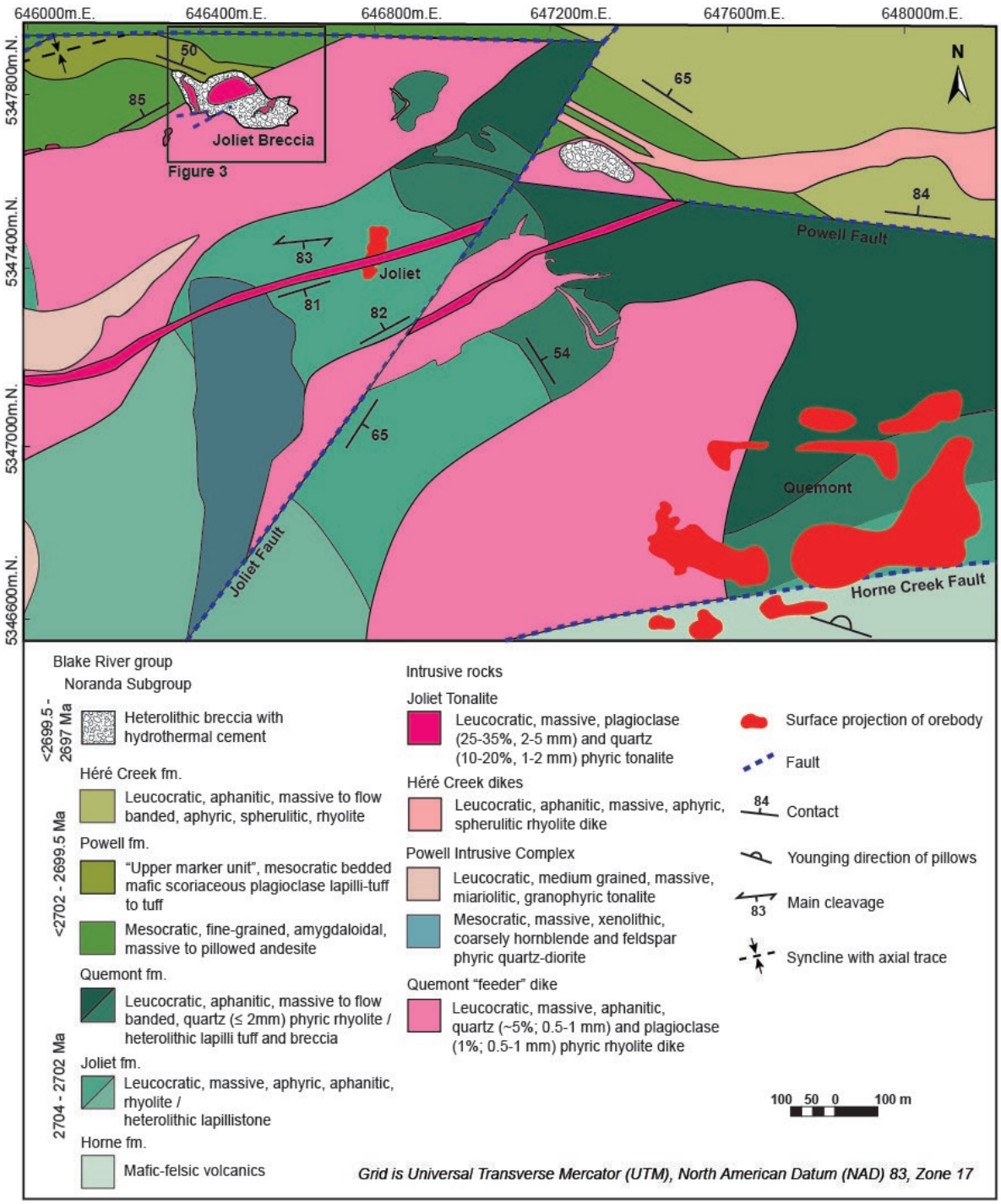

Figure 2.2: Geological setting of the Joliet Breccia.

Local geology map from rectangle outlined in Fig. 1 showing the distribution of mineral deposits within the Joliet Breccia area. Orebodies are vertical surface projections. Modified from Morris (1957, 1959), De Rosen Spence (1976), and Joliet-Quebec Mines Ltd. (1948). Original informal lithostratigraphic formations of De Rosen Spence (1976), shown as shades of green or blue to correspond to the informal chronostratigraphic divisions of McNicoll et al. (2014). Proterozoic diabase dikes are present in the map area but were omitted for clarity.

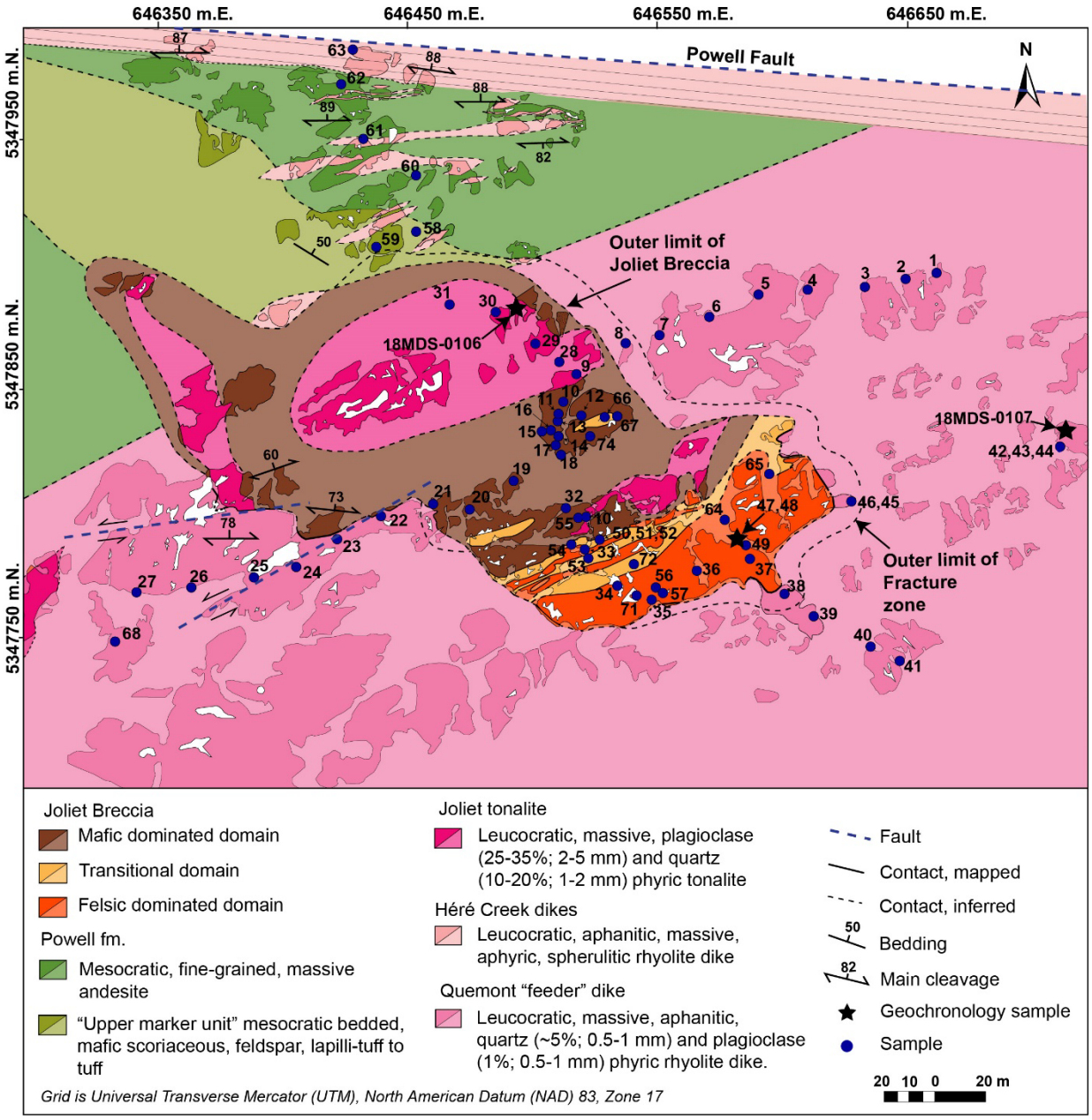

Figure 2.3: Geological map of the Joliet Breccia.

Geological map of the Joliet Breccia. Outcrop exposures are outlined; white patches denote areas covered by overburden. Lighter shades for each lithology show interpolation between outcrop exposures. The northwestern margin of the Joliet Breccia is poorly defined due to lack of outcrop exposure. Thin parallel lines within the Powell fault denote a zone of high strain and indicates the orientation of the shear fabric. Sample traverses for metal zonation are shown by blue dots. Samples collected for U-Pb TIMS geochronology are shown by black stars.

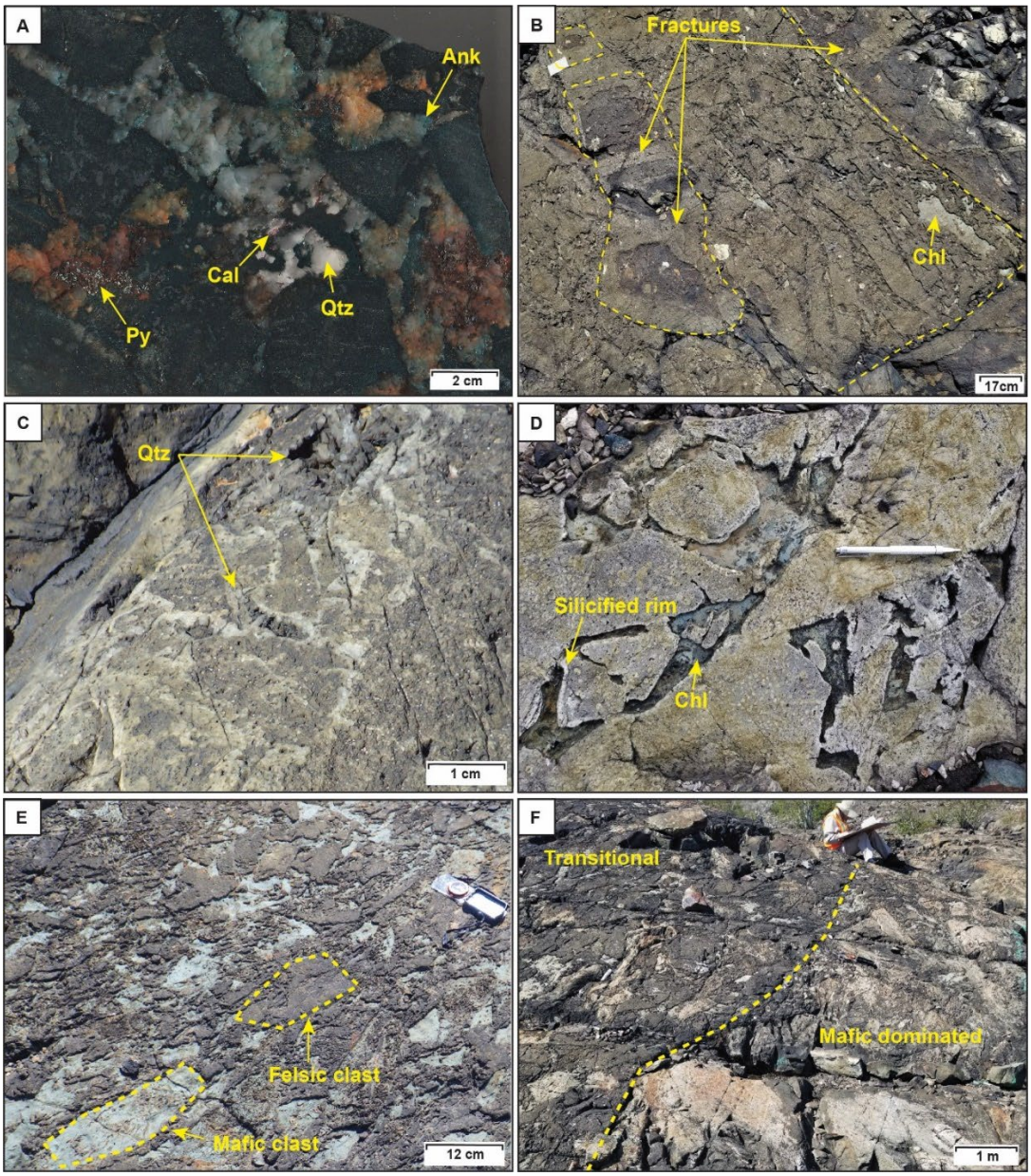

Figure 2.4: Photographs showing characteristic features of the main lithologies.

A) Mafic dominated domain of the Joliet Breccia. Note, angular tabular chlorite altered mafic fragments and a cement of white comb quartz, calcite, ankerite and pyrite. Ankerite is stained turquoise and calcite is stained pink following the method of Hitzman (1999) (polished stained slab); **B)** Felsic dominated domain of the Joliet Breccia. Note, jig-saw fit and elongate form of clasts, pervasive sericitization of smaller clasts, and larger blocks with internal fractures that are parallel to clast boundaries, with sericite alteration haloes that do not cross-cut the breccia (field photograph); **C)** Euhedral, pyramidal quartz cement, between in-situ, jig-saw fit clasts of the felsic dominated domain (field photograph); **D)** Chlorite cement within the felsic dominated domain. Note, the white silicified clast rims (field photograph); **E)** Transitional domain showing mafic and felsic clasts (field photograph); **F)** Contact between the transitional domain and the mafic dominated domain (field photograph).

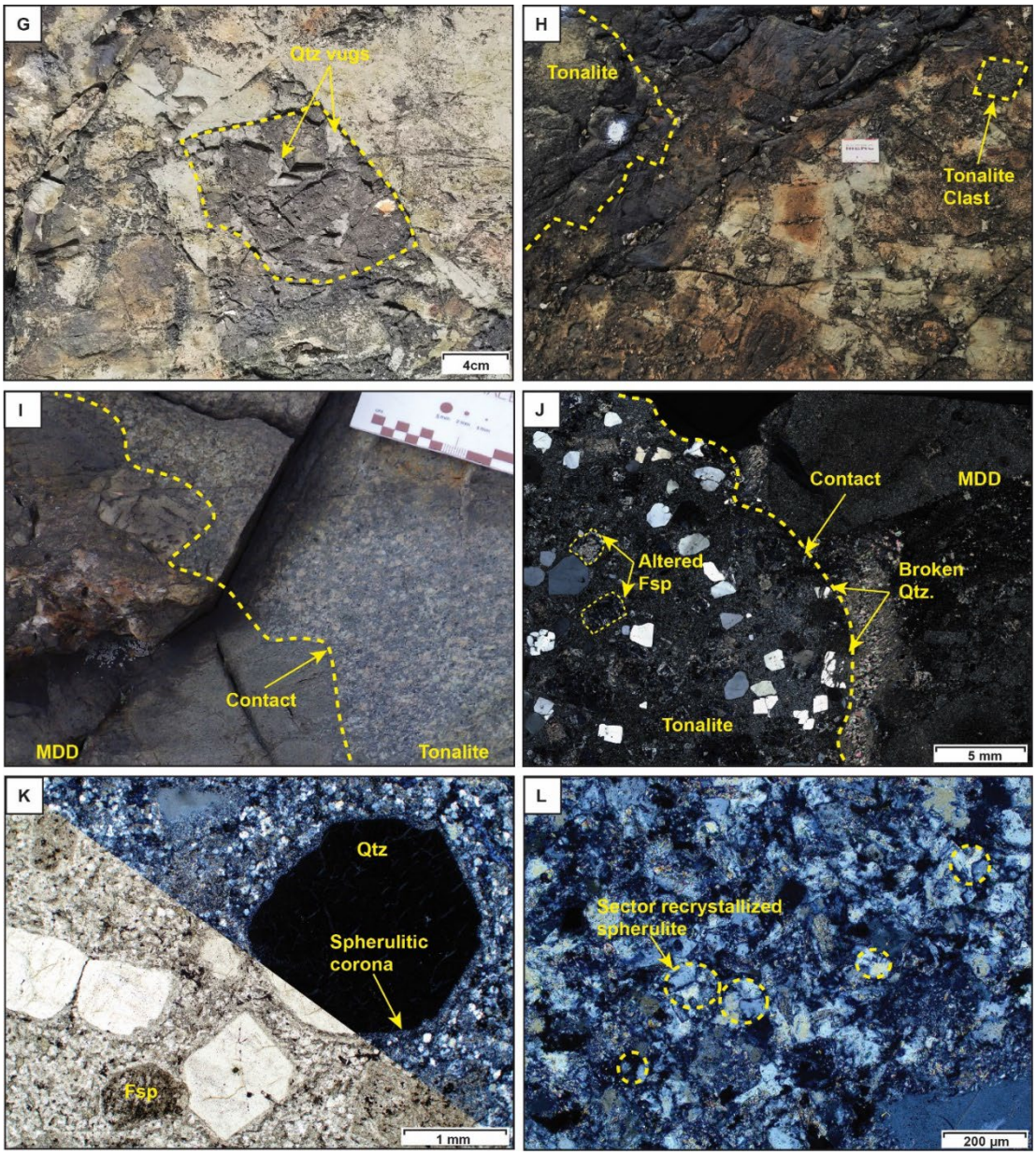

Figure 2.4 (continued): G) Large block of the felsic-dominated domain in the mafic-dominated domain. Note the internal jig saw fit texture of quartz-porphyritic blocks separated by vuggy quartz which is truncated by chlorite cement of the host mafic dominated domain (field photograph); **H)** Angular, tabular blocks of tonalite and andesite, within the mafic-dominated domain (field photograph); **I)** Joliet tonalite in contact with the mafic-dominated domain; note the difference in grain size and abundance of quartz phenocrysts relative to the Quemont feeder dike. Sharp, non-chilled, contact between the tonalite and mafic dominated domain (field photograph); **J)** Broken quartz crystals within Joliet tonalite at contact with mafic dominated domain (cross-polarized light); **K)** Joliet tonalite showing quartz and altered albite phenocrysts within an aphanitic, spherulitic groundmass (cross-polarized light (top right) / transmitted light (bottom left)). Note, spherulitic coronas surrounding phenocrysts; **L)** Spherulitic groundmass of the Joliet tonalite, showing sector recrystallized spherulites (cross-polarized light). (Ank = ankerite; Cal = calcite; Chl = chlorite; Fsp = feldspar; MDD = mafic dominated domain; Qtz = quartz).

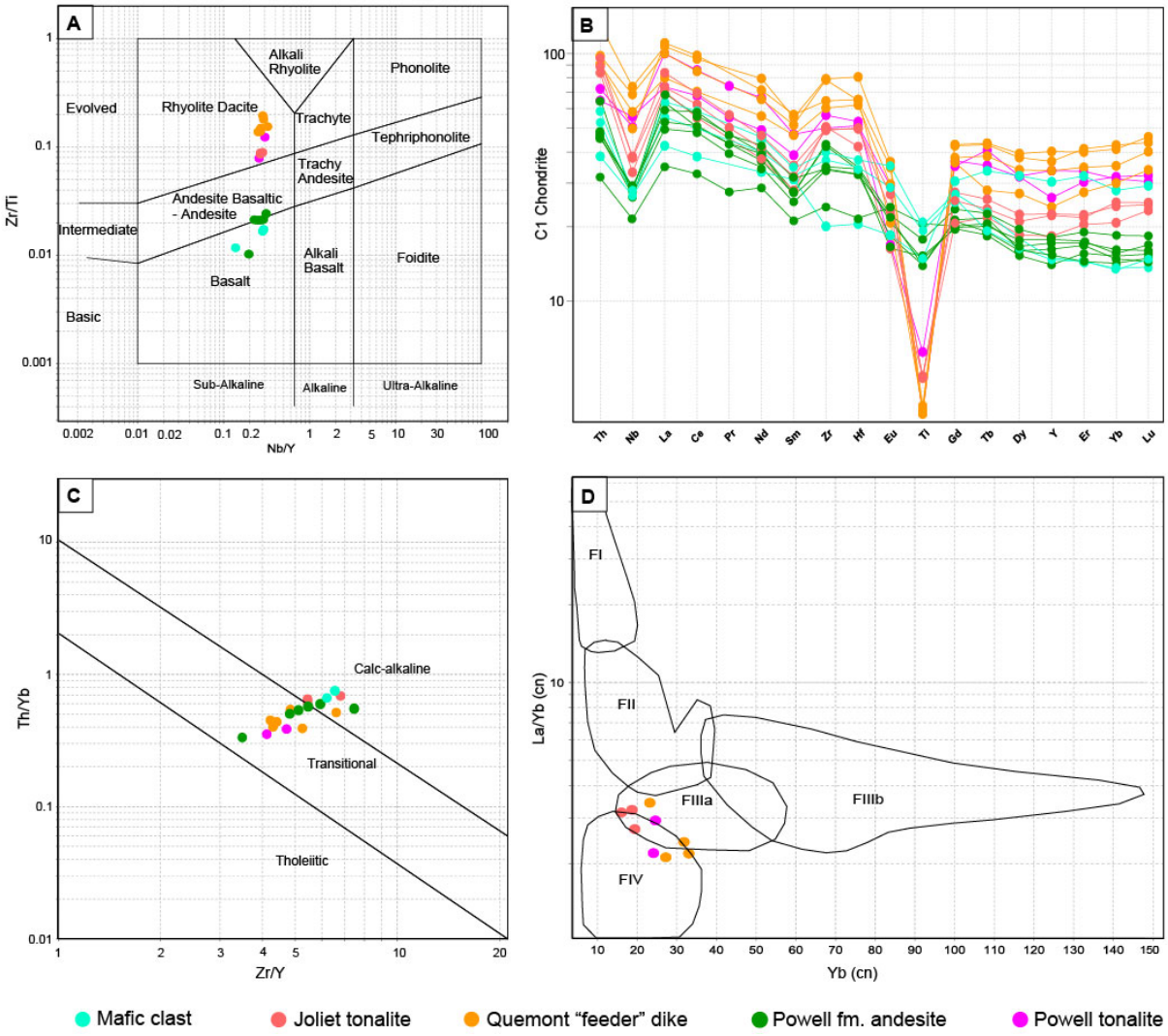

Figure 2.5: Whole-rock lithogeochemical classification of the main lithologies.

Geochemical classification of the main lithologies. A) Volcanic rock classification (Pearce, 1996); B) Spider diagram, chondrite normalized immobile trace elements (Sun and McDonough, 1989); C) Magma associations determined by Zr/Y vs Th/Yb ratios (Ross and Bedard, 2009); D) Rhyolite fertility classification (Hart et al., 2004).

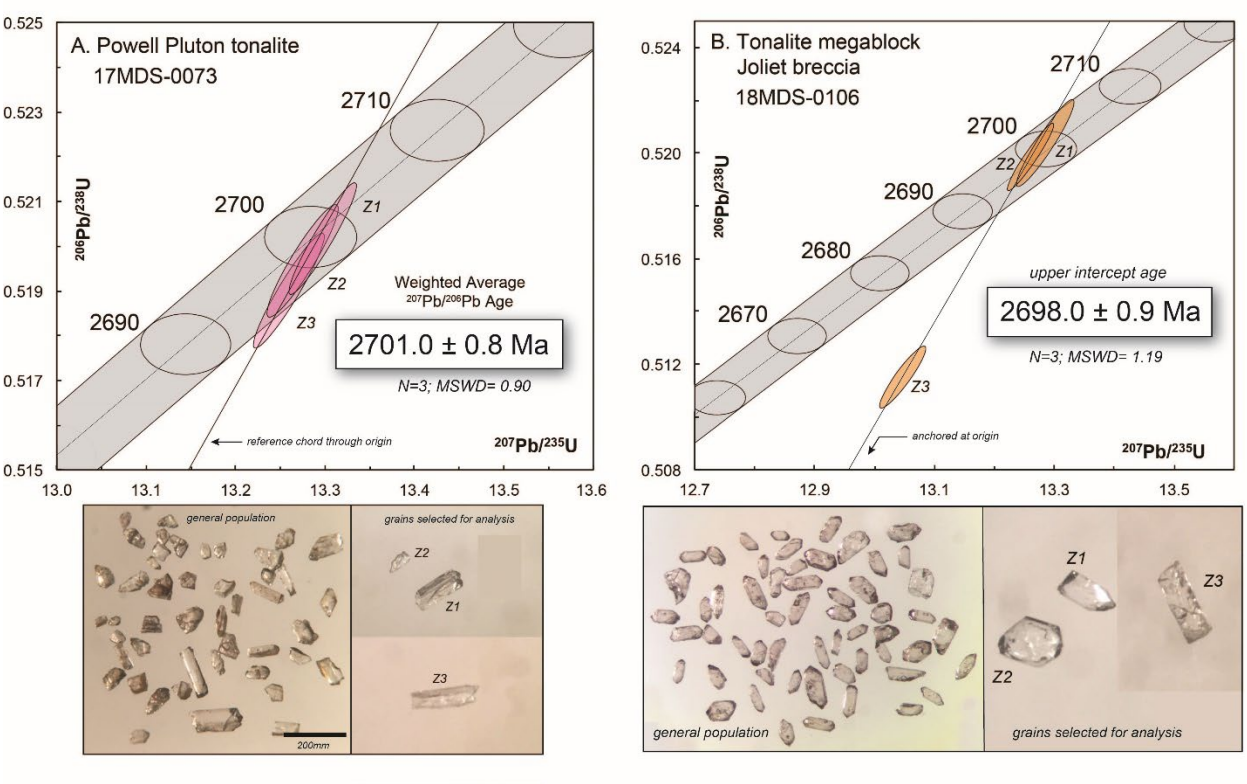

Figure 2.6: Zircon grain images and Concordia diagrams for ID-TIMS U-Pb analyses

Zircon grain images and Concordia diagrams for ID-TIMS U-Pb analyses from selected tonalite bodies in the eastern Powell Block.

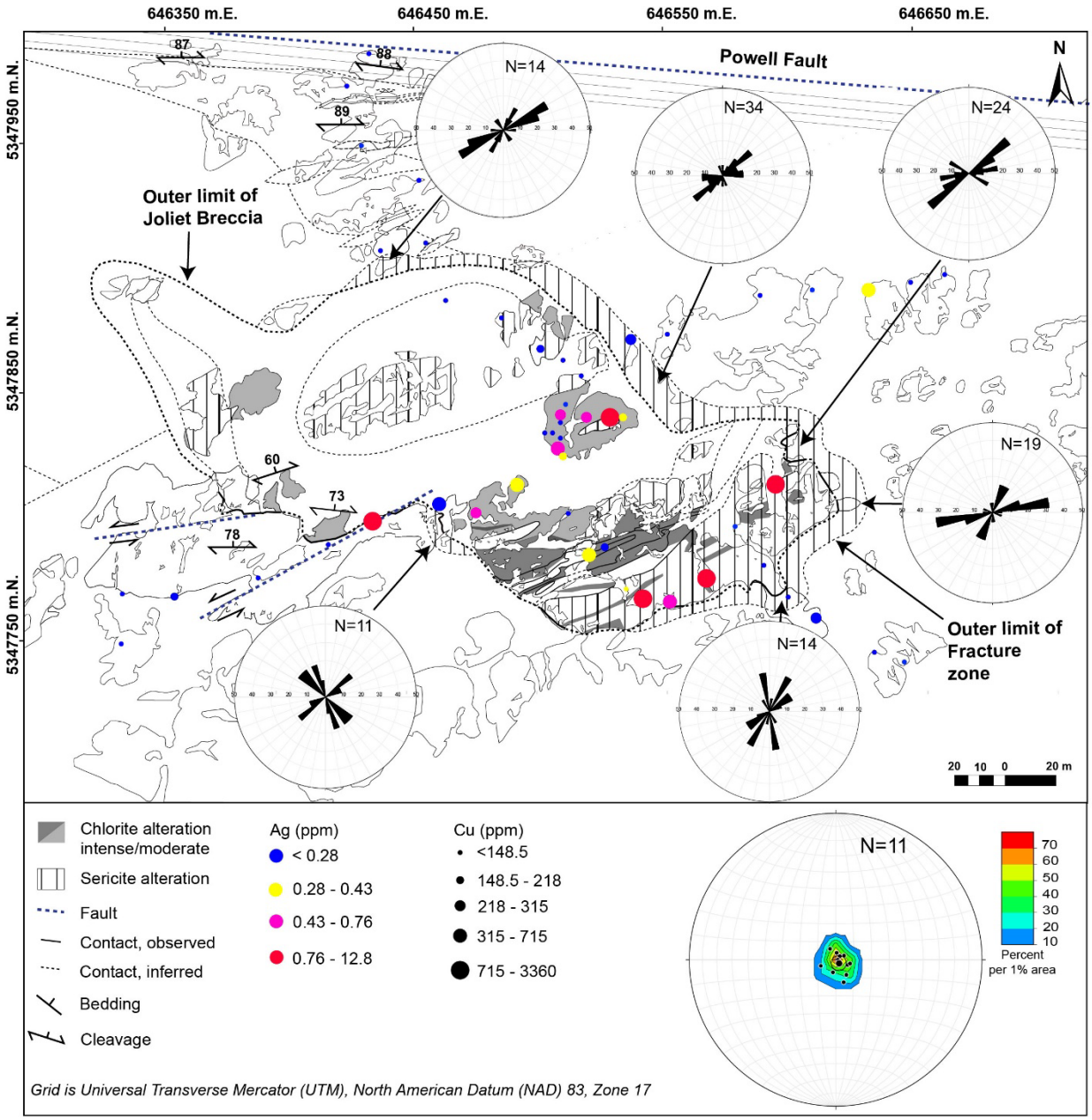

Figure 2.7: Alteration and metal distribution map of the Joliet Breccia, with summary stereonet plot and rose diagrams.

Spatial distribution of Ag and Cu within the Joliet Breccia. The Ag and Cu concentrations are illustrated by colour and size of the symbols, respectively. Rose diagram insets show variation in orientations of conjugate fracture sets within the QFP dike surrounding the margin of the Joliet Breccia. Note, fractures are oriented both subparallel and radial to the outer contact of the breccia. Stereonet inset shows the mean vector for the line of intersection between conjugate fractures.

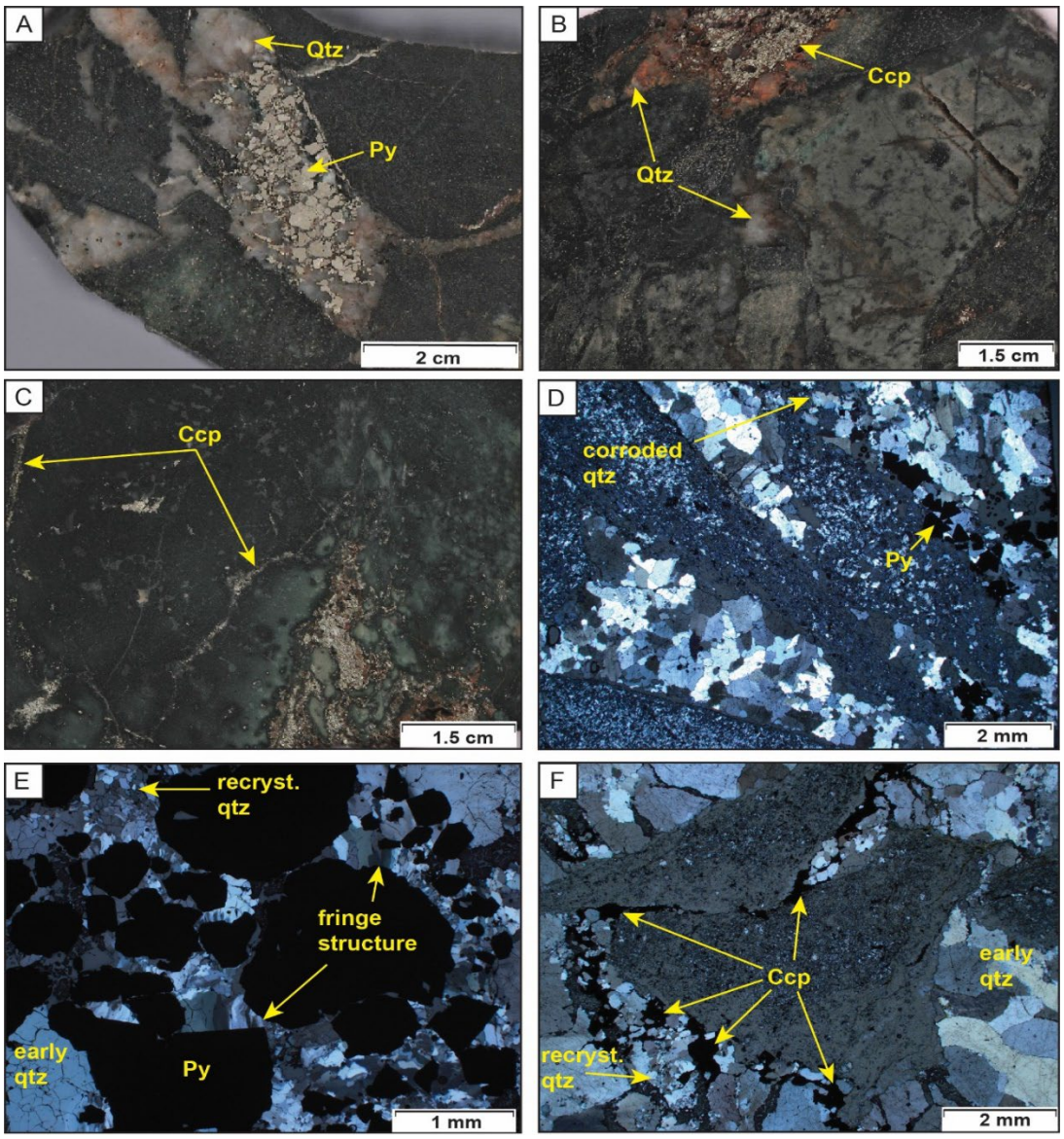

Figure 2.8: Photographs showing characteristic textures of sulfide minerals and hydrothermal cement.

A) Angular chloritized mafic clasts with a white comb quartz cement and coarse-grained euhedral pyrite (polished slab); **B)** Vug with strongly red stained quartz and internal massive chalcopyrite. Note the vug in the middle of the image, which lacks sulfides and appears pristine white (polished slab); **C)** Veinlets of chalcopyrite cross-cutting chloritized clasts and a vug associated with massive chalcopyrite, without quartz, and leucocratic alteration surrounding it (polished slab); **D)** Vug cement in bottom of image shows white comb quartz, without sulfides, compare to vug in top right of image which contains euhedral pyrite along the margin of the chloritized mafic clast (cross-polarized light); **E)** White comb quartz cement with undulose extinction that is overgrown by a fine-grained polygonal quartz mosaic with recrystallized grain boundaries. Note, euhedral pyrite with fringe structures (cross-polarized light); **F)** Angular chloritized mafic clast surrounded by white comb-quartz. Note, fracturing and recrystallization of quartz along grain boundaries infilled by anhedral chalcopyrite and chlorite (cross-polarized light);

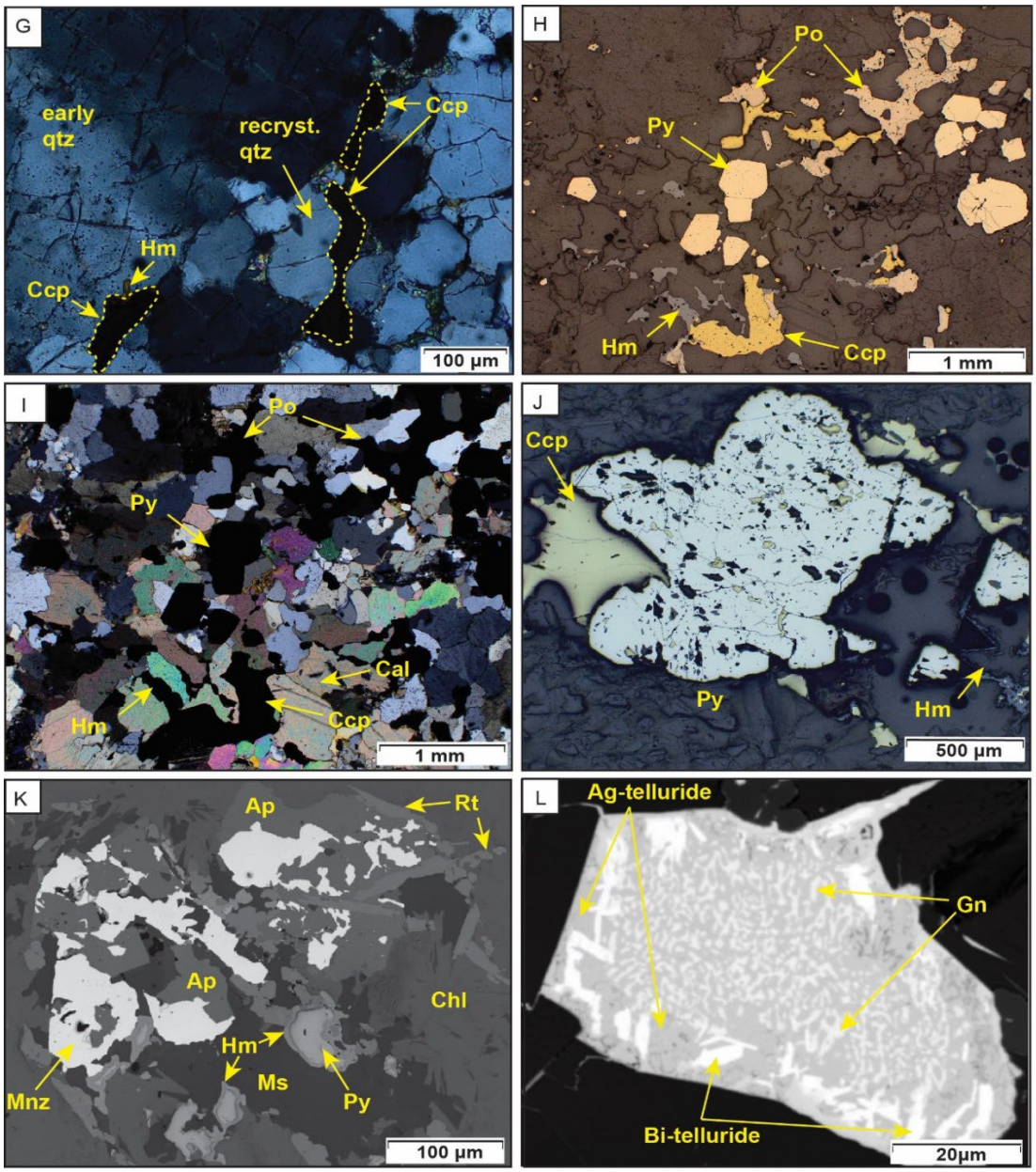

Figure 2.8 (continued): G) Fracturing and undulose extinction within early comb quartz (top left), which is overgrown by a polygonal quartz mosaic (bottom right). Chalcopyrite occurs interstitial to polygonal quartz; **H-I)** Euhedral pyrite, anhedral intergrown pyrrhotite and chalcopyrite, in a quartz, calcite vug (H = reflected and I = cross-polarized light); **J)** Euhedral to subhedral pyrite and interstitial anhedral chalcopyrite, note numerous inclusions and cross-cutting veinlets of chalcopyrite within pyrite (cross-polarized light); **K)** Subhedral pyrite with hematite rims, intergrown with apatite, monazite, rutile, muscovite and chlorite within vug (back-scattered electron image, SEM); **L)** Ag-Bi telluride interstitial to chlorite within vug (back-scattered electron image, SEM). (Ap = apatite, Cal = calcite, Ccp = chalcopyrite, Gn = galena, Hm = hematite, Mnz = monazite, Po = pyrrhotite, Py = pyrite, Qtz = quartz, Rt = rutile).

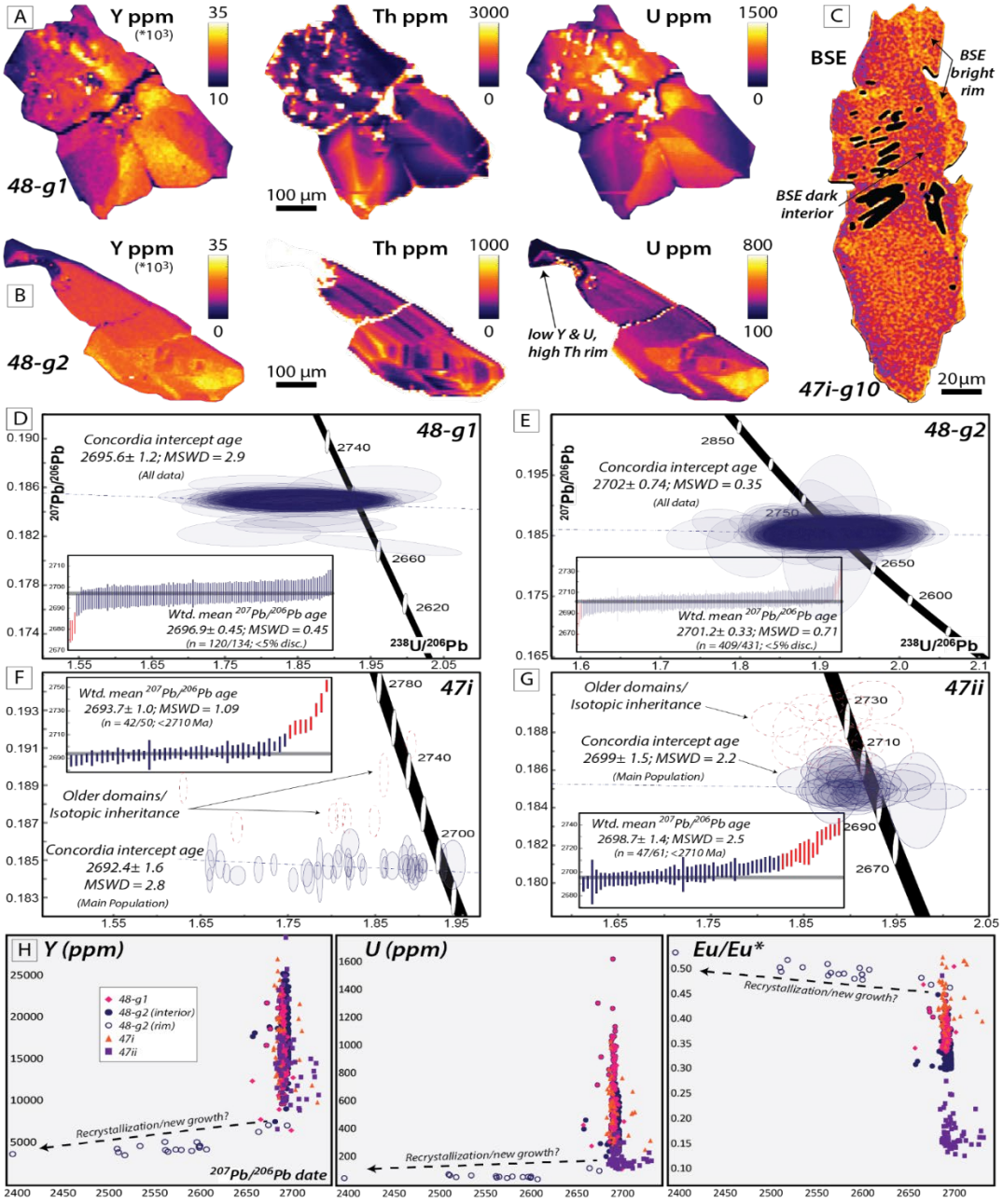

Figure 2.9: LAICPMS monazite maps and data.

LAICPMS monazite maps and data**; A-B)** Representative trace element concentration maps for monazite grains 1 and 2 from sample 48**; C)** Representative back scattered electron image of monazite from sample 47, showing a bright rim and a dark core**; D-E)** Concordia diagrams of all analyses for grains 1 and 2 from sample 48, with inset of weighted mean plots for <5% discordant analyses and 2σ outlier rejection**; F-G)** Concordia diagrams of all analyses for 16 grains from two subsamples of 47, with inset of weighted mean plots for <5% discordant analyses and 2σ outlier rejection**; H)** Plots of trace element concentration vs. $^{207}Pb/^{206}Pb$ spot date, showing similar range of concentrations for all grain interiors (except for 47ii), and depleted Y and U, and smaller Eu anomaly in thin rims of grains (interpreted as recrystallization or new growth).

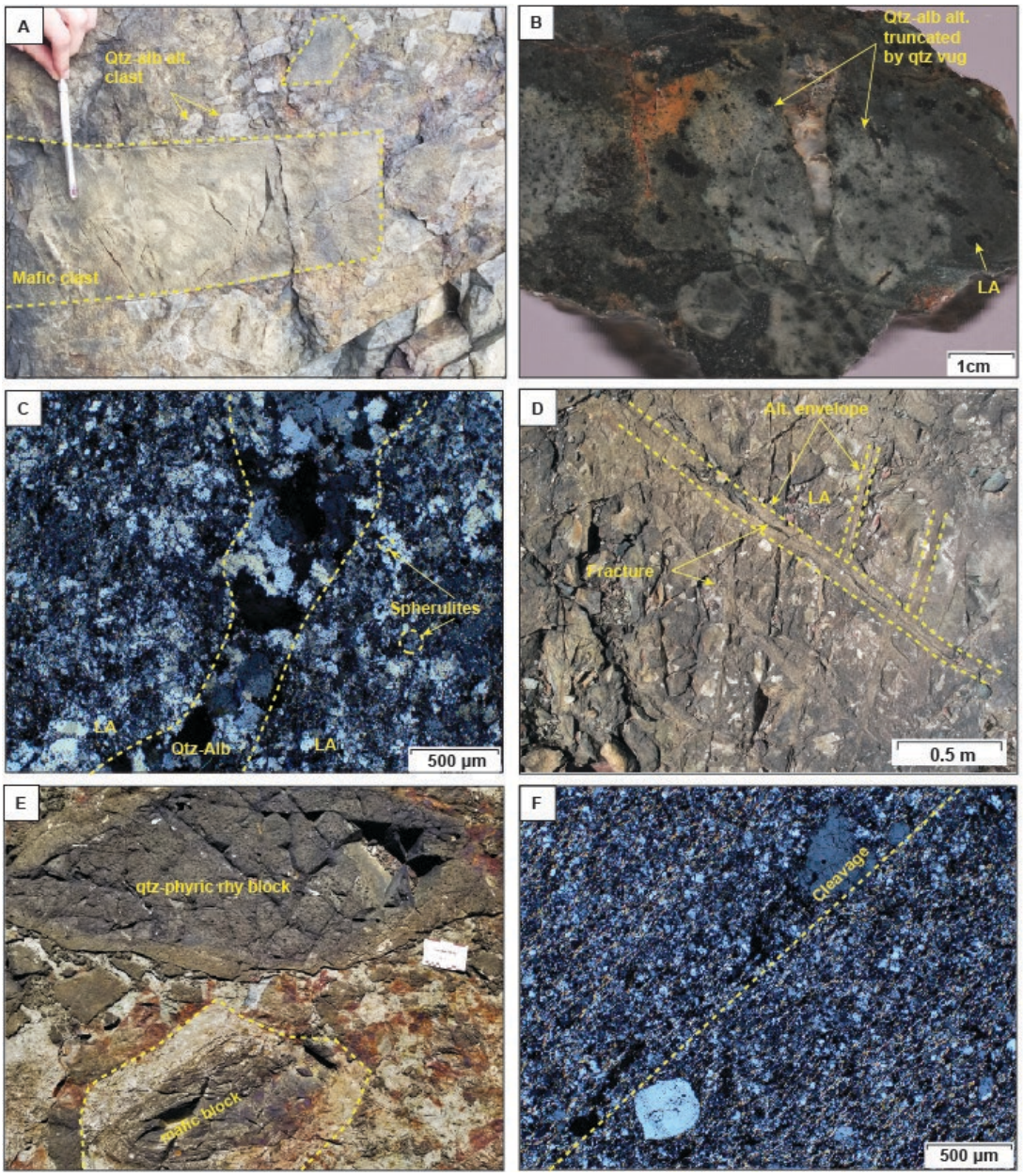

Figure 2.10: Photographs showing characteristic features of the main alteration types.

A) Quartz-albite altered clasts within the mafic dominated domain (field photograph); **B)** Quartz-albite alteration within a quartz-feldspar porphyritic rhyolite clast within the mafic dominated domain, note darker areas (least altered cores). Alteration truncated by quartz-vug. (polished slab); **C)** Diffuse, gradational contact between quartz-albite alteration and least altered quartz-feldspar porphyritic rhyolite clast. Note, change in quartz grain size, and destruction of spherulitic texture (cross-polarized light); **D)** Sericite alteration envelope surrounding fractures within the Quemont feeder dike; **E)** Chlorite and sericite alteration rims mantling clasts within the mafic dominated domain. Yellow, sericite rim around quartz porphyritic clasts, and green chlorite rims around mafic clasts (field photograph); **F)** Sericite alteration. Note well-developed foliation defined by sericite (cross-polarized light);

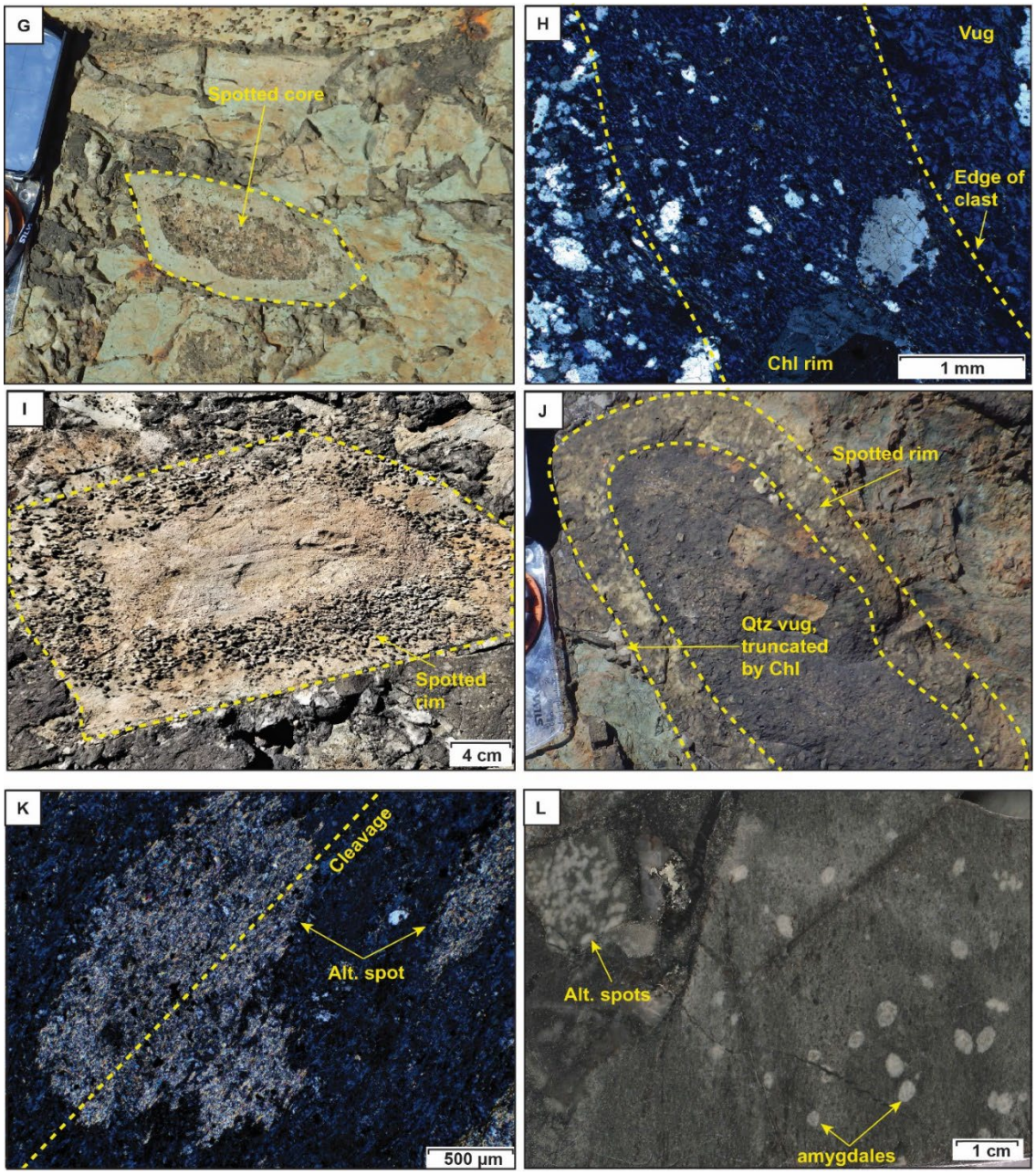

Figure 2.10 (continued): G) Intense chlorite alteration of mafic clast rims and weakly chloritized and spotted-textured core of mafic clasts, within mafic dominated domain (field photograph); **H)** Gradational contact with fine-grained chlorite alteration rim around quartz porphyritic rhyolite clast. Note, coarse grained chlorite in vug (cross-polarized light); **I)** Spotted-texture localized to rim of a weakly chloritized mafic clast (field photograph); **J)** Spotted-textured sericitic alteration rim around QP clast (field photograph); **K)** Alteration spot in chloritized mafic clast overprinted by regional cleavage. **L)** Grey alteration spots with diffuse margins within felsic clast, compared to amygdales in adjacent clast with sharp margins (polished slab). (Alt. = alteration, Chl = chlorite, LA = least altered, Qtz-Alb = quartz-albite).

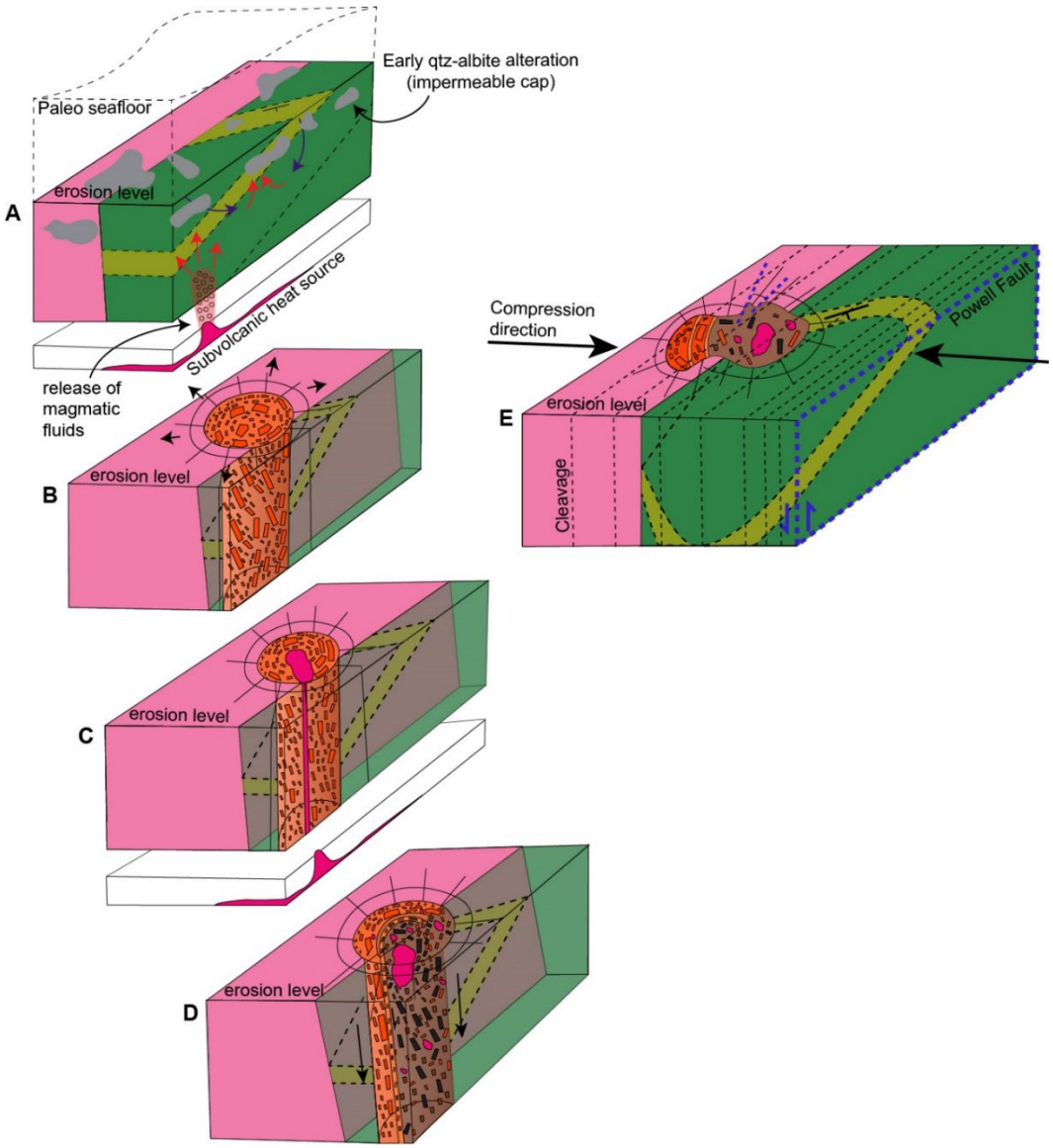

Figure 2.11: Schematic diagram illustrating the interpreted model of formation of the Joliet Breccia.

Schematic diagram illustrating the interpreted model of formation of the Joliet Breccia, not to scale; **A)** Pre-breccia quartz-albite alteration may have reduced the permeability of the immediate host rocks; **B)** Catastrophic release of a magmatic fluid that became impounded and over pressured, triggering a fragmentation event and formation of the felsic dominated breccia; **C)** Intrusion of the Joliet Breccia tonalite ; **D)** Second brecciation event and formation of the mafic dominated domain and associated chlorite alteration**.** Minor downward settling of breccia after fluid escapes and formation of the transitional domain. **E)** Current geometry of the Joliet Breccia after deformation. Colours match map legend from figure 3.

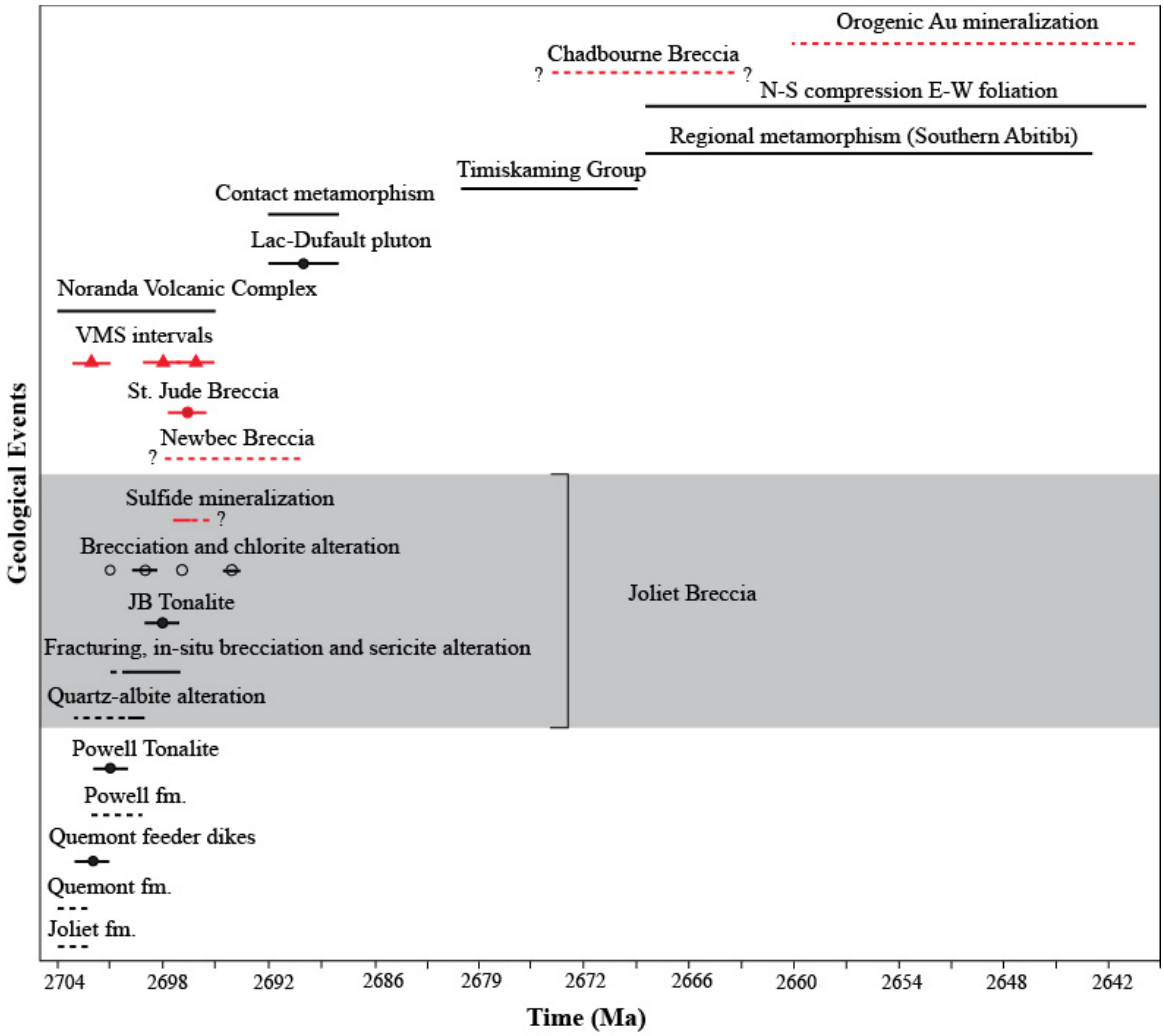

Figure 2.12: Relative and absolute timing of relevant major geological events.

Relative and absolute timing of relevant major geological events. Shaded grey rectangle shows events occurring within the Joliet Breccia. Dashed lines are the projected possible age ranges. Black solid circles show zircon U-Pb TIMS ages. The four black hollow circles for brecciation and chlorite alteration within the Joliet Breccia show monazite U-Pb LA-ICP-MS ages from this study with the solid line showing the range within 2σ. The Powell tonalite and Joliet Breccia ages are from this study. St. Jude Breccia (Galley and Van Breemen, 2002). Newbec Breccia (Smith, 1983). Lac Dufault pluton (Mortensen, 1993). Quemont feeder dike, Noranda volcanic complex and VMS intervals (McNicoll et al., 2014). Contact metamorphism (De Rosen Spence, 1969; Mortensen, 1933). Chadbourne breccia (Walker and Cregheur, 1982). Regional deformation and gold mineralization in the Abitibi greenstone belt (Bedeaux et al., 2017; Wilkinson et al., 1999; Dubé and Mercier-Langevin, 2020) and regional metamorphism (Powell et al., 1995).

2.10 Tables

Table 2-1: Zircon U-Pb isotopic data for eastern Powell block tonalite samples.

Fraction	Description	U (ppm)	Pb^T (pg)	Pb_C (pg)	Th/U	$^{206}Pb/^{204}Pb$	$^{206}Pb/^{238}U$	± 2s	$^{207}Pb/^{235}U$	± 2s	$^{207}Pb/^{206}Pb$	± 2s	$^{206}Pb/^{238}U$	± 2s	Ages (Ma) $^{207}Pb/^{235}U$	± 2s	Ages (Ma) $^{207}Pb/^{206}Pb$	± 2s	Disc. (%)
17MDS-0073; Powell pluton tonalite																			
Z1	1 clr, cls, lrg, el & irreg	856	2044.6	0.33	2.147	262028	0.520177	0.001005	13.29681	0.03087	0.185394	0.000149	2699.9	4.3	2701.0	2.2	2701.7	1.3	0.1
Z2	1 clr, cls, sm shard	232	145.78	1.48	0.799	5240	0.519688	0.001014	13.27452	0.03246	0.185257	0.000179	2697.9	4.3	2699.4	2.3	2700.5	1.6	0.1
Z3	1 clr, cls, lrg, el & irreg	233	183.43	0.93	2.102	8342	0.519029	0.001035	13.25888	0.03218	0.185274	0.000160	2695.1	4.4	2698.3	2.3	2700.7	1.4	0.3
18MDS-0106; Joliet Breccia tonalite																			
Z1	1 clr, cls, sm brkn el fct pr	61	35.43	0.46	0.433	4417	0.520416	0.001347	13.28258	0.03983	0.185110	0.000198	2700.9	5.7	2699.9	2.8	2699.2	1.8	-0.1
Z2	1 clr, cls, stubby fct pr	199	117.07	0.19	0.482	34863	0.519888	0.001032	13.25761	0.03152	0.184950	0.000145	2698.7	4.4	2698.2	2.2	2697.8	1.3	0.0
Z3	1 clr, cls, brkn el pr, sq, crk	137	164.48	1.97	0.633	4588	0.511588	0.000968	13.04357	0.03160	0.184916	0.000186	2663.4	4.1	2682.8	2.3	2697.5	1.7	1.5

Notes:
All analyzed fractions represent best optical quality (crack-, inclusion-, core-free), fresh (least altered) grains of zircon. Zircons were chemically abraded.
Abbreviations: Z - zircon; clr - clear; cls - colourless; crk - cracked; el - elongate; pr - prism/prismatic; fct - faceted; brkn - broken; sq - square cross-section; lrg - larger; sm - smaller; irr - irregular.
Pb^T is total amount (in picograms) of Pb.
Pb_C is total measured common Pb (in picograms) assuming the isotopic composition of laboratory blank: 206/204 - 18.221; 207/204 - 15.612; 208/204 - 39.360 (errors of 2%).
Pb/U atomic ratios are corrected for spike, fractionation, blank, and, where necessary, initial common Pb; 206Pb/204Pb is corrected for spike and fractionation.
Th/U is model value calculated from radiogenic 208Pb/206Pb ratio and 207Pb/206Pb age, assuming concordance.
Disc. (%) - per cent discordance for the given 207Pb/206Pb age.
Uranium decay constants are from Jaffey et al. (1971).

Table 2-2: Average values for select trace and major elements by lithology.

				Mafic dominated domain[1]			Felsic dominated domain[1]			JB Tonalite[1]			Quemont feeder dyke[1]			Powell andesite[2]		
		L.L.O.D	U.L.O.D	Avg.	Std.	No.[3]	Avg.	Std.	No.[3]	Avg.	Std.	No.[3]	Avg.	Std.	No.[3]	Avg.	Std.	No.[3]
Ag	*ppm*	*0.01*	*100*	1.2	3.1	16	0.8	0.7	6	0.11	0.1	6	0.1	0.1	17	0.3	0.0	4
As	*ppm*	*0.2*	*10,000*	3.8	6.5	16	0.5	0.3		1.02	0.7	6	0.6	0.4	17	0.3	0.2	4
Bi	*ppm*	*0.01*	*10,000*	0.9	1.3	16	0.5	0.4	6	0.27	0.2	6	0.2	0.2	17	0.0	0.0	4
Te	*ppm*	*0.05*	*500*	0.1	0.2	16	0.3	0.2	6	0.06	0.0	6	0.1	0.1	17	0.0	0.0	4
Sb	*ppm*	*0.05*	*10,000*	0.1	0.1	16	0.1	0.0	6	0.07	0.0	6	0.1	0.0	17	0.1	0.1	4
Sn	*ppm*	*0.2*	*500*	8.9	3.9	16	5.4	3.1	6	2.80	1.4	6	3.5	2.8	17	2.2	0.9	4
W	*ppm*	*0.1*	*10,000*	2.1	1.4	16	3.6	6.1	6	0.32	0.2	6	0.6	0.5	17	1.1	0.0	4
Li	*ppm*	*0.2*	*10,000*	41.4	9.3	16	29.1	29.9	6	17.35	1.7	6	10.6	4.3	17	21.4	8.5	4
Cu	*ppm*	*0.2*	*10,000*	510	909	16	553	479	6	60.68	56.2	6	124	176	17	98.5	181	4
Zn	*ppm*	*2*	*10,000*	197	64.4	16	97.7	92.9	6	63.00	25.2	6	71.1	33.8	17	221	155	4
Pb	*ppm*	*0.5*	*10,000*	1.6	1.1	16	1.5	0.5	6	1.25	0.3	6	1.9	1.5	17	2.4	2.8	4
Mo	*ppm*	*0.05*	*10,000*	1.1	0.5	16	4.1	3.4	6	2.82	0.8	6	2.9	0.6	17	0.8	0.3	4
S	*%*	*0.01*	*10*	0.8	1.1	16	0.1	0.1	6	0.42	0.3	6	0.2	0.2	17	0.1	0.1	4
Fe	*%*	*0.01*	*50*	10.7	2.4	16	7.4	7.2	6	3.29	0.6	6	3.4	0.5	17	7.5	0.3	4
Sc	*ppm*	*0.1*	*10,000*	27.9	5.8	16	16.7	7.4	6	9.63	1.9	6	12.3	1.2	17	25.8	4.5	4
Mg	*%*	*0.01*	*50*	2.4	0.6	16	1.7	2.0	6	0.54	0.1	6	0.4	0.2	17	3.9	0.9	4
Mn	*ppm*	*5*	*100,000*	1512	414	16	550	490	6	537	36.8	6	686	301	17	0.2	0.1	4
K	*%*	*0.01*	*10*	0.8	0.5	16	0.5	0.5	6	0.52	0.3	6	0.2	0.2	17	0.2	0.1	4
Rb	*ppm*	*0.1*	*10,000*	9.3	6.8	16	10.6	10.5	6	12.20	7.8	6	4.6	4.5	17	5.6	3.6	4
Sr	*ppm*	*0.2*	*10,000*	50.1	48.3	16	17.7	9.0	6	93.50	45.1	6	43.7	13.8	17	60.2	20.5	4
Ba	*ppm*	*10*	*10,000*	309	251	16	162	150	6	137	73.1	6	52.9	51.0	17	96.2	1.6	4
P	*ppm*	*10*	*10,000*	628	180	16	388	435	6	413	116.9	6	150	18.4	17	990	429	4
Na	*%*	*0.01*	*10*	1.2	1.0	16	1.6	1.5	6	2.74	0.4	6	3.7	0.3	17	3.5	0.4	4
Ca	*%*	*0.01*	*50*	1.0	1.0	16	0.1	0.1	6	1.26	0.6	6	0.6	0.4	17	2.0	1.2	4

[1]Data for mafic dominated domain, felsic dominated domain, Joliet tonalite and Quemont feeder dike from 4 acid digestion (ME-MS61)
[2]Data for Powell andesite from whole rock data (CCPKG01)
[3]Values below the detection were assigned half of the value of the detection limit
[4]Fe is corrected to sulfide free values, assuming all sulfides are present as pyrite using the equation:
$Fe_{sulfide\ free}$ = Fe $wt\%_{measured}$ - (46.55*S $wt\%_{measured}$)/53.45

Table 2-3: Distinguishing characteristics of breccias.

Category	Other names	Distinguishing textures	Diameter (m)	Geometry	Clast morphology	Clast size distribution	Matrix	Related intrusive rocks	Alteration	Examples	Ref.
Phreatic	Hydrothermal explosion/ eruption	Jig-saw fit, exfoliated fragments, sinter fragments (hydrothermally altered clasts)	up to ~500	pipes, but commonly irregular or pebble dikes	typically polymictic, angular-rounded	anisometric	rock flour (<50%) and/or hydrothermal cement	yes	widespread silicification common, argillic, advanced argillic, sericite, chlorite	Equity Silver, B.C. Canada; Round Mountain, Nevada;	Sillitoe (1985)
Implosion	Fluid-assisted breccia Hydrothermal breccia	Jig-saw fit	~50	steep tabular bodies, or pipes, occurs along dilational jogs in active structures	typically monomictic, angular	typically isometric	hydrothermal cement	no	variable	Martha Mine, New Zealand; Cinola deposit, B.C. Canada	Mitcham (1974), Sibson (1986), Jébrak (1997)
Magmatic-hydrothermal	Intrusion-related/ Porphyry	Jig-saw fit, sheeted contacts, shingle breccia, exfoliated fragments	50-300, locally >1000	single or multiple pipes	typically monomictic, angular-rounded	anisometric	rock flour (<30-50%) and/or hydrothermal cement	yes	biotite and/or k-silicate common, sericite, chlorite, quartz-topaz, tourmaline	Galore Creek, B.C. Canada; Red Mountain, Arizona	Sillitoe and Sawkins (1971), Sillitoe (1985), Sillitoe (2010)

2.11 References

Allen, R. L., Lundstrom, I., Ripa, M., Simeonov, A., Christofferson, H., 1996. Facies analysis of a 1.9 Ga, continental margin, back-arc, felsic caldera province with diverse Zn-Pb-Ag-(Cu-Au) sulfide and Fe oxide deposits, Bergslagen region, Sweden. Econ. Geol. 91, 979-1008.

Allmendinger, R.W., Cardozo, N., and Fisher, D., 2012. Structural geology algorithms: vectors and tensors: Cambridge University Press, Cambridge, 302 p.

Babcock, R.S., 1973. Computational models of metasomatic processes. Lithos. 6, 279-290.

Bedeaux, P., Pilote, P., Daigneault, R., Rafini, S., 2017. Synthesis of the structural evolution and associated gold mineralization of the Cadillac Fault, Abitibi, Canada. Ore Geol. Rev. 82, 49–69. https://doi.org/10.1016/j.oregeorev.2016.11.029

Browne, P.R.L., Lawless, J. V., 2001. Characteristics of hydrothermal eruptions, with examples from New Zealand and elsewhere. Earth Sci. Rev. 52, 299–331. https://doi.org/10.1016/S0012-8252(00)00030-1

Camus, F., 1975. Geology of the El Teniente orebody with emphasis on wallrock alteration. Econ. Geol. 70, 1341–1372.

De Ronde, C.E.J., Massoth, G.J., Butterfield, D.A., Christenson, B.W., Ishibashi, J., Ditchburn, R.G., Hannington, M.D., Brathwaite, R.L., Lupton, J.E., Kamenetsky, V.S., Graham, I.J., Zellmer, G.F., Dziak, R.P., Embley, R.W., Dekov, V.M., Munnik, F., Lahr, J., Evans, L.J., Takai, K., 2011. Submarine hydrothermal activity and gold-rich mineralization at Brothers Volcano , Kermadec Arc , New Zealand. Miner. Deposita. 46, 541–584. https://doi.org/10.1007/s00126-011-0345-8

De Rosen-Spence, A., 1969. Genèse des roches à cordierite-anthophyllite des gisements cupro-zincifères de la région de Rouyn-Noranda, Québec, Canada. Can. J. Earth Sci. 6, 1339–1345.

De Rosen Spence, A.F., 1976. Stratigraphy, Development and petrogenesis of the central Noranda volcanic pile, Noranda, Québec. PhD thesis. University of Toronto, Toronto, Ontario.

Dimroth, E., Rocheleau, M., 1979. Volcanology and Sedimentology of Rouyn-Noranda Area, Québec, in: Geological Association of Canada and Mineralogical Association of Canada Field Trip A-1 Guidebook. Université Laval, Québec, pp. 111–125.

Dimroth, E., Imreh, L., Goulet, N., and Rocheleau, M., 1983. Evolution of the south-central segment of the Archean Abitibi Belt, Québec. Part II : Tectonic evolution and geomechanical model. Can. J. Earth. Sci. 20, 1355-1373.

Dubé, B., Mercier-Langevin, P., Hannington, M.D., Lafrance, B., Gosselin, G., Gosselin, P., 2007. The Laronde Penna Au-rich volcanogenic massive sulfide deposit, Abitibi Greenstone Belt, Québec: Mineralogy and geochemistry of alteration and implications for genesis and exploration. Econ. Geol. 102, 633–666.

Dubé, B., and Mercier-Langevin, P., 2020. Gold deposits of the Archean Abitibi Greenstone belt, Canada, in: Sillitoe, R. H., Goldfard, R. J., Robert, F., Simmons, S. F. (Eds.) Geology of the world's major gold deposits and provinces, SEG Special Publication 23, pp. 669-708.

Einaudi, M.T., Hedenquist, J.W., Inan, E.E., 2003. Sulfidation state of fluids in active and extinct hydrothermal systems: transitions from porphyry to epithermal environments. SEG Special Publication 10, 285–314.

Fisher, R. V, Schmincke, H.U., 1984. Pyroclastic Rocks. Springer Berlin Heidelberg, Berlin, Heidelberg. https://doi.org/10.1007/978-3-642-74864-6

Franklin, J.M., Gibson, H.L., Jonasson, I.R., Galley, A.G., 2005. Volcanogenic Massive Sulfide Deposits. Econ. Geol. 100th Anniv., 523–560.

Galley, A., van Breemen, O., Franklin, J., 2000. The relationship between intrusion-hosted Cu-Mo mineralization and the VMS deposits of the Archean Sturgeon Lake mining camp, Northwestern Ontario. Econ. Geol. 95, 1543–1550. https://doi.org/10.2113/gsecongeo.95.7.1543

Galley, A.G., van Breemen, O., 2002. Timing of synvolcanic magmatism in relation to base-metal mineralization, Rouyn-Noranda, Abitibi volcanic belt, Québec. Geol. Surv. Canada Curr. Res. 2002-F8 1–9.

Gibson, H. L., 1990. The mine sequence of the Central Noranda volcanic complex: geology, alteration, massive sulfide deposits and volcanological reconstruction. Ph.D. thesis, Carleton University, Ottawa, Ontario.

Gibson, H.L., Watkinson, D.H., 1990. Volcanogenic Massive Sulphide Deposits of the Noranda Cauldron and Shield Volcano, Québec. Can. Inst. Min. Metall. Special Volume 43, 119–132.

Gibson, H.L., 2005. Chapter 12 Volcanic-hosted ore deposits, in: Martí, J., Ernst, G. (Eds.), Volcanoes and the Environment. Cambridge University Press, pp. 333–386.

Gibson, H.L., Watkinson, D.H., Comba, C.D.A., 1983. Silicification: hydrothermal alteration in an Archean geothermal system within the Amulet rhyolite formation, Noranda, Québec. Econ. Geol. 78, 954–971. https://doi.org/10.2113/gsecongeo.78.5.954

Gilligan, L. B., Marshall, B., 1987. Textural evidence for remobilization in metamorphic environments. Ore Geol. Rev. 2, 205-229. https://doi.org/10.1016/0169-1368(87)90029-1

Goodwin, A.M., 1980. Archean volcanic studies in the Timmins-Kirkland Lake-Noranda region of Ontario and Québec. Can. Geol. Surv. Bull. 278. https://doi.org/10.4095/106237

Goulet, N., 1978. Stratigraphy and structural relationships across the Cadillac – Larder Lake Fault, Rouyn – Beauchastel area, Québec. PhD thesis, Queen's University, Kingston, Ontario.

Gresens, R., 1967. Composition-volume relationships of metasomatism. Chem. Geol. 2, 47–65.

Hannington, M.D., Poulsen, K.H., Thompson, J.F.H., Sillitoe, R.H., 1999. Volcanogenic gold in the massive sulfide environment, in: Barrie, C.T., Hannington, M.D. (Eds.), Volcanic-Associated Massive Sulfide Deposits: Processes and Examples in Modern and Ancient Settings. Reviews in Economic Geology, 8, pp. 325–356.

Hart, T.R., Gibson, H.L., Lesher, C.M., 2004. Trace element geochemistry and petrogenesis of felsic volcanic rocks associated with volcanogenic massive Cu-Zn-Pb sulfide deposits. Econ. Geol. 99, 1003–1013.

Hitzman, M. W., 1999. Routine staining of drillcore to determine carbonate mineralogy and distinguish carbonate alteration textures. Miner. Deposita. 34,794-798.

Horstwood, M.S., Košler, J., Gehrels, G., Jackson, S.E., McLean, N.M., Paton, C., Pearson, N.J., Sircombe, K., Sylvester, P., Vermeesch, P., Bowring, J.F., Condon, D.J., Schoene, B., 2016. Community-derived standards for LA-ICP-MS U-(Th-) Pb geochronology–Uncertainty propagation, age interpretation and data reporting. *Geostand. Geoanal. Res.,* 40 (3), 311-332.

Hubert, C., Trudel, P., Gélinas, L., 1984. Archean wrench fault tectonics and structural evolution of the Blake River Group, Abitibi belt, Québec. Can J. Earth Sci. 21, 1024-1032.

Huston, D.L., Relvas, J.M.R.S., Gemmell, J.B., Drieberg, S., 2011. The role of granites in volcanic-hosted massive sulphide ore-forming systems : an assessment of magmatic – hydrothermal contributions. Miner. Deposita. 46, 473–507. https://doi.org/10.1007/s00126-010-0322-7

Jaffey, A.H., Flynn, K.F., Glendenin, L.E., Bentley, W.C. and Essling, A.M., 1971. Precision measurement of half-lives and specific activities of 235U and 238U; Phys. Rev. 4, 1889-1906.

Jansson, N.F., Allen, R.L., 2011. Timing of volcanism, hydrothermal alteration and ore formation at Garpenberg, Bergslagen, Sweden. GFF, 133, 3–18. https://doi.org/10.1080/11035897.2010.547597

Jébrak, M., 1997. Hydrothermal breccias in vein-type ore deposits: A review of mechanisms, morphology and size distribution. Ore Geol. Rev. 12, 111-134.

Joliet-Quebec Mines Ltd. 1948. Plan of surface geology and drilling, Rouyn Twp., N.W. Quebec, unpublished geological map, 1 sheet, one inch to 200 feet.

Katz, L.R., Kontak, D.J., Dubé, B., McNicoll, V., 2017. The geology , petrology , and geochronology of the Archean Coté Gold large-tonnage, low-grade intrusion-related Au(-Cu) deposit, Swayze greenstone belt, Ontario Canada. Can. J. Earth Sci. 54, 173–202. https://doi.org/dx.doi.org/10.1139/cjes-2016-0007

Kennedy, L.P., 1985. The geology and geochemistry of the Archean Flavrian pluton, Noranda, Québec. PhD thesis. The University of Western Ontario.

Koide, H., and Bhattarcharji, S., 1975. Formation of fractures around magmatic intrusions and their role in ore localization. Econ. Geol. 70, 781-799.

Krushnisky, A., 2018. Controls of gold enrichment at the Horne 5 Archean VMS deposit, Abitibi greenstone belt, Québec. MSc thesis. Institut national de la recherche scientifique – Centre Eau Terre Environment, Québec City, Québec.

Krushnisky, A., Mercier-Langevin, P., Ross, P.S., Goutier, J., Pilote, C, Bernier, C., 2020. Geology and gold enrichment at the Horne 5 Archean volcanogenic massive sulpide deposit, Abitibi greenstone belt, Québec: a synthesis, in: Mercier-Langevin, P., Lawley, C.J.M., Castonguay, S., (Eds.), Targeted Geoscience Initiative 5: contributions to the understanding of Canadian gold systems, pp. 31-44. https://doi.org/10.4095/323663

Lawless, J. V, White, P.J., 1990. Ore-related breccias: A revised genetical classification with particular reference to epithermal deposits, in: 12th New Zealand Geothermal Workshop. 197-202.

Lesher, C.M., Gibson, H.L., Campbell, I.H., 1986. Composition-volume changes during hydrothermal alteration of andesite at Buttercup Hill, Noranda District, Québec. Geochim. Cosmochim. Acta 50, 2693–2705. https://doi.org/10.1016/0016-7037(86)90219-X

Lichtblau, A., 1989. Stratigraphy and Facies at the south margin of the Archean Noranda Caldera. MSc thesis. l'Université du Québec à Chicoutimi, Chicoutimi, Québec.

Lichtblau, A., Dimroth, E., 1980. Stratigraphy and facies at the South margin, of the Archean Noranda Caldera, Noranda, Québec. Geol. Surv. Canada Curr. Res. Part A 69–76.

Lorenz, V., 1973. On the formation of maars. Bull. Volcanol. 37, 183–204.

Lydon, J.W., 1988. Ore deposit models: Volcanogenic massive sulfide deposits. Part 1: A descriptive model. Geosci. Can. 11, 195-202.

Maclean, W.H., Hoy, L.D., 1991. Geochemistry of hydrothermally altered rocks at the Horne Mine, Noranda, Québec. Econ. Geol. 86, 506–528. https://doi.org/10.2113/gsecongeo.86.3.506

Mathieu, L., Racicot, D., 2019. Petrogenetic study of the multiphase chibougamau pluton: Archaean magmas associated with Cu-Au magmato-hydrothermal systems, Minerals, 9 (3), 174. https://doi.org/10.3390/min9030174

Mercier-Langevin, P., Hannington, M.D., Dubé, B., Bécu, V., 2011. The gold content of volcanogenic massive sulfide deposits. Miner. Depos. 46, 509–539. https://doi.org/10.1007/s00126-010-0300-0

McNicoll, V., Goutier, J., Dubé, B., Mercier-Langevin, P., Ross, P.S., Dion, C., Monceck, T., Legault, M., Percival, J., Gibson, H., 2014. U-Pb geochronology of the Blake River Group, Abitibi greenstone belt, Québec, and implications for base metal exploration. Econ. Geol. 109, 27–59. https://doi.org/10.2113/econgeo.109.1.27

Mitcham, T., 1974. Origin of breccia pipes. Econ. Geol. 69, 412–413.

Morris, H. R. 1957. Héré Fault Copper Ltd. Surface Geology, Anglo-Rouyn and North Part of Powell-Rouyn properties, Rouyn Twp., N.W. Québec, unpublished geological map, 3 sheets, one inch to 200 feet.

Morris, H.R., 1959. Joliet-Québec Mines Ltd. Surface Geology, Rouyn Twp., N.W. Québec, unpublished geological map, 3 sheets, one inch to 200 feet.

Mortensen, J. K., 1993. U-Pb geochronology of the eastern Abitibi subprovince. Part 2. Noranda-Kirkland Lake area: Can. J. Earth. Sci. 30, 29-41.

Muffler, L., White, D., Truesdell, A., 1971. Hydrothermal explosion craters in Yellowstone National Park. Geol. Soc. Am. Bull. 82, 723–740.

Pearce, J.A., 1996. A user's guide to basalt discrimination diagrams, in: Bailes, A.H. (Eds.), Trace Element Geochemistry of Volcanic Rocks: Applications for Massive Sulfide Exploration. Geological Association of Canada, Short Course Notes, 12pp. 79-113.

Poulsen, K.H., 2017. Chapter 5 The Larder Lake-Cadillac Break and Its Gold Districts, in: Monecke, T., Mercier-Langevin, P., Dubé, B. (Eds.), Archean Base and Precious Metal Deposits, Southern Abitibi Greenstone Belt, Canada. Reviews in Economic Geology, 19, pp. 133–167.

Poulsen, K.H., Franklin, J.M., 1981. Copper and gold mineralization in an Archean trondjhemitic intrusion Sturgeon Lake, Ontario, in: Current Research Part A. Geological Survey of Canada, pp. 9–14.

Poulsen, K.H., Hannington, M.D., 1996. Volcanic-associated massive sulphide gold, in: Eckstrand, R.O., Sinclair, W.D., Thorpe, R.I. (Eds.), Geology of Canadian Mineral Deposit Types. pp. 183–196.

Powell, W.G., Carmichael, D.M., Hodgson, C.J., 1995. Conditions and timing of metamorphism in the southern Abitibi Greenstone Belt, Québec. Can. J. Earth Sci. 32, 787–805. https://doi.org/10.1139/e95-067

Reynolds, D.L., 1954. Fluidization as a geological process, and its bearing on the problem of

intrusive granites. Am. J. Sci. 252, 577-614. https://doi.org/10.2475/ajs.252.10.577

Riverin, G., Hodgson, C.J., 1980. Wall-rock alteration at the Millenbach Cu-Zn mine, Noranda, Québec. Econ. Geol. 75, 424–444. https://doi.org/10.2113/gsecongeo.75.3.424

Ross, P. S., and Bedard, J. H., 2009. Magmatic affinity of modern and ancient subalkaline volcanic rocks determined from trace-element discriminant diagrams. Can J. Earth Sci. 46, 823-839. https://doi.org/10.1139/e09-054

Sabina, A.P., 2003. Rocks and minerals for the collector: Kirkland Lake-Rouyn-Noranda-Val d'Or, Ontario and Québec. Geological Survey of Canada, Miscellaneous Report 77, 322 p.

Sawkins, F.J., 1990. Metal Deposits in Relation to Plate Tectonics, 2nd edition, 17. Springer-Verlag Berlin Heidelberg. 461 p. https://doi.org/10.1007/978-3-662-08681-0

Sharman, E.R., Taylor, B.E., Minarik, W.G., Dubé, B., Wing, B.A., 2015. Sulfur isotope and trace element data from ore sulfides in the Noranda district (Abitibi , Canada): implications for volcanogenic massive sulfide deposit genesis. Miner. Deposita. 50, 591–606. https://doi.org/10.1007/s00126-014-0559-7

Shikazono, N., & Kawahata, H., 1987. Compositional differences in chlorite from hydrothermally altered rocks and hydrothermal ore deposits. Can. Mineral. 25 (3), 465-474.

Sibson, R., 1986. Brecciation processes in fault zones: Inferences from earthquake rupturing. Pure and Applied Geophysics. 124 (1), 159-175.

Sillitoe, R.H., Sawkins, F.J., 1971. Geologic, Mineralogic and Fluid Inclusion Studies Relating to the Origin of Copper-bearing Tourmaline Breccia Pipes, Chile. Econ. Geol. 66, 1028–1041.

Sillitoe, R.H., 1985. Ore-Related Breccias in Volcanoplutonic Arcs. Econ. Geol. 80, 1467–1514.

Sillitoe, R.H., 2010. Porphyry copper systems. Econ. Geol. 105, 3–41. https://doi.org/10.2113/gsecongeo.105.1.3

Smith, W.K., 1983. A Petrographic Description of the Newbec Breccia, Noranda, Quebec. BSc thesis. University of Waterloo, Waterloo, Ontario.

Sun, S.S., McDonough, W. F., 1989. Chemical and isotopic systematics of oceanic basalts: implications for mantle composition and processes, in: Saunders, A. D., Norry, M. J. (Eds.), Magmatism and ocean basins. Geol. Soc. Lond. pp. 313-345.

Tosdal, R.M., Richards, J.P., 2001. Chapter 6 Magmatic and Structural Controls on the Development of Porphyry Cu ± Mo ± Au Deposits, in: Richards, J.P., Tosdal, R.M. (Eds.), Structural Controls on Ore Genesis. Reviews in Economic Geology, 14, pp. 157–181.

Walford, P.C., Franklin, J.M., 1982. The Anderson Lake Mine, Snow Lake, Manitoba. In: Hutchinson, R.W., Franklin, J.M., (Eds.) Precambrian sulphide deposits. Geol. Assoc. Can. Spec. Pap. 25, 481-523.

Walker, S.D., Cregheur, P., 1982. The Chadbourne Mine, Noranda, Quebec: A gold-bearing breccia, in: Hodder, R.W., Petruk, W., (Eds.), Geology of Canadian Gold Deposits. Canadian Institute of Mining and Metallurgy, Special Volume 24. pp. 58–66.

White, J.D.L., Ross, P.S., 2011. Maar-diatreme volcanoes: A review. J. Volcanol. Geotherm. Res. 201, 1–29.

Wilkinson, L., Cruden, A.R., Krogh, T.E., 1999. Timing and kinematics of post-Timiskaming deformation within the Larder Lake - Cadillac deformation zone, southwest Abitibi greenstone belt, Ontario, Canada. Can. J. Earth Sci. 36, 627–647.

https://doi.org/10.1139/e99-015

Wilson, M.E., 1941. Noranda district, Québec. Geological Survey of Canada, Memoir 229, 162 p. https://doi.org/10.4095/101612.

Woodcock, N.H., Mort, K., 2008. Classification of fault breccias and related fault rocks. Geol. Mag. 145 (3), 435-440. https://doi.org/10.1017/S0016756808004883

Xiao, Z., Gammons, C.H., Williams-Jones, A.E., 1998. Experimental study of copper (I) chloride complexing in hydrothermal solutions at 40-300C and saturated water vapor pressure. Geochemica Cosmochim. Acta 62, 2949–2964.

Yeats, C. J., Parr, J. M., Binns, R. A., Gemmell, J. B., Scott, S. D., 2014. The SuSu Knolls hydrothermal field, eastern Manus Basin, Papua New Guinea: An active submarine high-sulfidation copper-gold system. Econ. Geol. 109, 2207-2226.

2.12 Appendices

A 2-1: Detailed analytical methodology

Sample Preparation for whole-rock analysis:

Samples were first crushed to 2 mm, split using a riffle splitter, and a 250 g subsample was pulverized to 75 microns.

Samples for the metal zonation study were analysed for a suite of 36 major (with the exception of Si) and trace elements using a 4 acid digestion followed by ICP-MS and ICP-AES analytical techniques at ALS Geochemistry (ME-MS61). Samples (n = 15) with the highest Cu content were analyzed for Au using a fire assay fusion followed by ICP-AES.

Samples for complete lithological and alteration characterization were analyzed using five analytical methods to produce a complete suite of major and trace elements, C, S and specific gravity at ALS Geochemistry (***CCPKG01)***. Lithophile elements were obtained using Lithium Borate Fusion followed by ICP-MS analysis and base metals were obtained using 4-acid digestion, followed by ICP-AES analysis; Aqua regia digestion and ICP-MS analysis was used for select trace elements (As, Bi, Hg, In, Re, Sb, Se, Te, Tl). Specific gravity was calculated on pulverized material. Percent LOI was calculated from the difference between the samples weight before and after it was placed in an oven at 1000˚C for 1 hour. For S and C analysis the sample was combusted in a high frequency Leco Induction Furnace and measured using IR Spectroscopy.

Scanning electron microscopy (SEM)

Mineralogy was verified using the scanning electron microscope (SEM) and energy-dispersive spectroscopy (EDS) at the MERC Isotope Geochemistry Laboratory at Laurentian University. A

TESCAN VEGA3 SEM was used with a beam intensity of 18, at 15.00 kV and a working distance of 15 mm.

U-Pb zircon geochronology via isotope dilution – thermal ionization mass spectrometry (ID-TIMS) (Jack Satterly Geochronology Lab, University of Toronto; JSGL)

Heavy mineral concentrates were obtained at the JSGL using standard crushing, grinding and separation methods using a Wilfley table, magnetic and heavy liquid techniques. The mineral separates were then handpicked using a binocular microscope to obtain a representative population of best quality (crack, inclusion, core-free), fresh (least altered) grains of zircon; details of zircon morphology and quality are summarized in Table 1.

Analytical methods involved isotope dilution thermal ionization mass spectrometry (ID-TIMS) following chemical abrasion (CA, modified after Mattinson, 2005). Zircon grains that underwent CA treatment were annealed in quartz crucibles at 900°C for 2 days. Annealed grains were subsequently leached in approximately 0.10 ml of concentrated hydrofluoric (HF) acid for up to several hours in teflon vessels at 200°C. Weights of mineral fractions chosen for ID-TIMS analysis were estimated from scaled digital photomicrographs, using the density of zircon. Samples were washed briefly in 7N HNO_3 prior to dissolution. A mixed ^{205}Pb-^{235}U isotopic spike was added to the dissolution capsules during sample loading. Zircon grains were dissolved using concentrated HF in Teflon bombs at 200°C for 3-4 days, then dried and re-dissolved in 3N HCl overnight (Krogh, 1973). U and Pb were isolated using 50 microliter anion exchange columns using HCl elutions, dried down, and then loaded onto outgassed rhenium filaments with silica gel (Gerstenberger and Haase, 1997).

Pb and UO_2 were analyzed at the JSGL on a VG354 mass spectrometer using a Daly collector in pulse counting mode. The mass discrimination correction for this detector was constant at 0.07%/AMU. Thermal mass discrimination corrections are 0.10%/AMU for Pb and U. Dead time of the Daly system was 16 ns for Pb during the analytical period, monitored using the SRM982 Pb standard. Mass spectrometer data was reduced using in-house software (UtilAge program). All common Pb was assigned to procedural blank. Initial Pb from geological sources above 1 picogram was corrected using the Pb evolution model of Stacey and Kramers (1975). Plotting of Concordia curves and averaging of age results were carried out using the Isoplot 3.71 Add-In for MS Excel, of Ludwig (2009). Ages calculated are based on weighted averages of $^{207}Pb/^{206}Pb$ ages(ratios) or regressions using a modified version of the York (1969) algorithm, in which points are weighted proportional to the inverse of the square of the assigned errors, incorporating error correlations (see Ludwig, 2009). Although the Concordia curve bands shown in Fig. 6 incorporate uncertainties in the ^{235}U and ^{238}U decay constants, these are excluded from the final age calculations. All age errors and error ellipses are given at the 2 sigma or 95% level of confidence. Results are provided in Table 1 and displayed in Concordia plots in Figure 6.

Laser ablation Inductively Coupled Mass Spectrometry (LA ICP-MS), U-Pb monazite geochonrology:

Monazite U-Th-Pb and trace element (TE) analyses were conducted at the Mineral Exploration Research Centre Isotope Geochemistry Lab (MERC-IGL), at Laurentian University. Laser ablation sampling was performed using a Photon Machines Analyte G2 ArF excimer laser, with 193 nm wavelength, <5 ns pulse width, and HelEx II cell. U-Th-Pb isotope measurements were conducted using a Thermo Scientific Neptune Plus multicollector (MC) ICP-MS, equipped with Jet interface and nine Faraday cups. All MC-ICP-MS analyses were conducted in low resolution,

static mode to ensure maximum sensitivity and stability. TE measurements were conducted using a Thermo Scientific iCap-TQ ICP-MS in single quad mode to ensure maximum sensitivity on the low to intermediate mass range.

U-Th-Pb and TE measurements were conducted simultaneously on the Neptune Plus and iCap-TQ, respectively, by splitting the ablated aerosol downstream of the sample cell (LASS). Helium carrier gas flows through the ablation cell were 0.85-0.90 l/min (cup) and 0-0.10 l/min (cell), with 1.65 l/min Ar and 13-15 ml/min N_2 makeup gas added downstream of the cell. Ablation spot diameter was 20-35 µm during LASS analyses (depending on grain/domain size), with 30 second duration, laser fluence of 2 J/cm^2, and 7 Hz repetition rate, leaving estimated ablation pit depths of <10-15 µm. One session of U-Th-Pb analyses only was conducted using a 10 µm spots size, targeting thin rims observed in some grains in sample 48. Sixty seconds of background were measured at the beginning and end of the analytical session, with 30 seconds of background measured between each ablation.

For U-Th-Pb isotope analysis on the Neptune Plus, the ~15% Faraday cup mass range allows isotopes between ^{204}Hg/Pb to ^{238}U to be measured simultaneously, with the cup configuration shown in Table S1 and fictive mass of ~220.55 aligned with the center cup. All cups were coupled with 10^{11} Ω amplifiers, with the exception of L2, which was coupled with 10^{12} Ω amplifier for better precision on the low intensity ^{207}Pb signal. Ion beam drift from day to day was typically <0.05 amu, with flat top peak width typically ~0.2 amu, ensuring stable on-peak measurements throughout long-duration analytical sessions. Cool gas flows and RF power were set at 16 L/min and 1200 W, with Ar auxiliary gas flows of 0.75 L/min.

For trace element analysis on the iCap-TQ, the masses measured and associated dwell times are shown in Table S2. Cool gas, auxiliary gas, and RF power were set at 14 L/min, 0.8 L/min, and

1550 W, respectively, with no Ar makeup gas. Extraction lens and quadrupole entry lens voltages were tuned to maximize sensitivity in the low mass range, to compensate for the generally poorer low mass transmission.

The raw U-Th-Pb and TE data were synchronized in Iolite v.4, along with the laser log file, prior to processing, so that the same timeslices (selections) for each analysis were used in the calculations. Baseline subtraction, instrumental drift, and downhole fractionation corrections were performed with the U-Pb Geochronology data reduction scheme (DRS) implemented within Iolite (Paton et al., 2010; Petrus & Kamber, 2012), with U-Th-Pb isotope ratios normalized to the monazite reference material (RM) KM03-72 (1822 ± 2 Ma; MacLachlan et al., 2004). KM03-72 was analyzed three times at the beginning and end of each session, and once every ten unknowns throughout the session. Roughly four seconds at the beginning and one second at end of the ablation period were excluded from the selections in order to minimize potential fractionation effects, leaving ~25 seconds of signal for integration. Within run variance in the measured ratios for KM03-72 (i.e. the additional percent error required to achieve MSWD = 1) was propagated into the 2SE internal uncertainty for all unknowns. Additional uncertainty propagation was applied to the weighted mean $^{207}Pb/^{206}Pb$ ages of each grain/sample following the recommended method of Horstwood et al. (2016), which includes the uncertainty on the age of KM03-72 (0.11%) and the long term variance of $^{207}Pb/^{206}Pb$ ratios of monazite verification RMs run at the MERC-IGL (0.31%). Two verification RMs were analyzed during the sessions to ensure accuracy of the U-Pb ratios. Monazites A049 (1874 ± 3 Ma; Salli et al., 1983) and A276 (1911 ± 5 Ma; Merilainen et al., 1976), yielded weighed mean dates of 1877 ± 2 Ma and 1916 ± 3 Ma, respectively, during the sessions presented here, within uncertainty of their accepted ages.

Trace element data were processed using the Trace Element-Internal Standard DRS within Iolite v4, and normalized to the synthetic glass RM NIST610. An assumed stoichiometric concentration of 30 wt% Ce was used for all monazite, to account for differing ablation characteristics between the glass and monazite. The synthetic glass NIST612 was used to verify the accuracy of TE analysis, and all elements were within uncertainty of their published values.

Monazite petro-chronology

Eighteen monazite grains in four thins sections from two samples were analyzed *in-situ* by LA-ICPMS, with sample 48 having two large (0.5-1 mm diameter) grains and sample 47 having abundant smaller grains (Fig. 9) The two larger grains in sample 48 were initially mapped with 10 µm-wide line scans to evaluate their compositional variation, followed by simultaneous U-Pb and trace-element (LASS) spot analyses across most of the grains for fully-quantitative data. In subsequent spot analyses, a 35 µm spot was used on the sector-zoned grain (n = 134), and a smaller (20 µm) spot was used on the more oscillatory-zoned grain in order to capture potential core (n = 431)-rim (n = 19) age variation. High contrast BSE images of the smaller grains in two sections from sample 47 indicate that compositional variation exists within some of the grains, with BSE-darker interiors locally mantled by thin BSE-brighter rims. The interiors were analyzed with a larger spots size (20 µm) in the LASS configuration, enabling trace element concentrations to be measured along with U-Pb isotopes (n = 111). Simultaneous trace element analyses were not conducted with the smaller spots size (10 µm) required for the thin rims zones (n = 54).

Trace Element composition

Sample 48 - LA-ICPMS maps of the two large monazite grains in sample 48 displayed distinctive zonation in most trace element concentrations (e.g. REE, Th, & U), with one grain having predominantly sector-type zoning and the other having both sector- and oscillatory-type zoning characteristics (Fig. 9A & B). The oscillatory-zoned grain also had a thin, discontinuous rim with lower Y, HREE, and U and lower LREE and Th than the grain interior. Despite the internal compositional heterogeneity (zoning), both crystals have similar overall compositional characteristics, with concentrations almost entirely within the ranges of: Y ~1-2.5 wt%, Yb ~ 100-650 ppm, Th ~1000-3000 ppm, U ~200-1200 ppm, and Eu/Eu* ~0.30-0.45. The rim of the oscillatory-zoned grain has Y ~0.36-0.72 wt%, Yb ~ 90-150 ppm, Th ~2750-5650 ppm, U ~45-125 ppm, and Eu/Eu* ~0.45-0.55, each of which correlate linearly with the $^{207}Pb/^{206}Pb$ date determined for that spot (Fig. 9H).

Sample 47 – The interior of smaller grains in sample 47 mostly fall within the same compositional range as the larger grains in sample 48 (Fig. 9H). Concentrations almost entirely fall within the ranges of: Y ~1-3 wt%, Yb ~ 100-1300 ppm, Th ~50-1800 ppm, U ~100-1100 ppm, and Eu/Eu* ~0.10-0.55. The few older domains (>2710 Ma) typically have lower concentrations of all these elements, with Y mostly <1.5 wt%, Yb mostly < 500 ppm, Th mostly < 600 ppm, and U mostly < 600 ppm in both sections. The Eu/Eu* is distinctly different between the two sections, with section *i* having similar values to the grains in sample 48 (~0.35-0.55) and section *ii* having much lower values (~0.12-0.28). Overall the relatively low U and Th suggests a hydrous, late-magmatic or hydrothermal origin for the monazite (Schandl & Gorton, 2004).

U-Pb geochronology

Sample 48 – One-hundred and twenty-three 35 μm spot analyses of the more equant, sector-zoned grain in sample 48 yielded slightly reversely discordant ratios, with uncertainty ellipses overlapping Concordia (Fig. 9A, E). A discordia line fit to all analyses (with lower intercept anchored at 100 ± 50 Ma) yields an upper intercept date of 2695.6 ± 1.2 Ma (MSWD = 2.9). The high MSWD reflects a small number of younger, variably discordant spot dates as young as 2663 Ma. Excluding analyses that were <5% discordant and three additional spots dates between 2685-2675 (>2σ from the mean), the grain yields a weighted mean $^{207}Pb/^{206}Pb$ date of 2696.9 ± 0.45 Ma (MSWD = 0.45).

Four-hundred and thirty-one 20 μm spot analyses of the more elongate, oscillatory-zoned grain in sample 48 yielded mostly concordant ratios, with discordia line fit to all analyses (free regression lower intercept = 84 ± 110 Ma) yielding an upper intercept date of 2702 ± 0.74 Ma (MSWD = 0.35; Fig. 9B, F). Excluding analyses that were >5% discordant and spots dates between >2σ from the mean both older and younger), the grain yields a weighted mean $^{207}Pb/^{206}Pb$ date of 2701.2 ± 0.33 Ma (MSWD = 0.71).

Sample 47 – Fifty 25 μm spot analyses of ten grains in section *i*, yielded mostly reversely discordant analyses, forming two main linear arrays. A discordia line fit to the dominant array (with lower intercept anchored at 100 ± 50 Ma) yields an upper intercept date of 2692.4 ± 1.6 Ma (MSWD = 2.8). The high MSWD reflects some excess scatter in the $^{207}Pb/^{206}Pb$ ratio. A small number of older $^{207}Pb/^{206}Pb$ ratios (up to ~2740 Ma) suggest a significant component of isotopic inheritance in this samples. Excluding eight analyses >2σ from the mean (>2710 Ma), the section yields a weighted mean $^{207}Pb/^{206}Pb$ date of 2693.7 ± 1.0 Ma (MSWD = 1.9).

Sixty-one 25 µm spot analyses of six grains in section *ii*, yielded mostly concordant to slightly reversely discordant analyses. The main cluster yields an upper intercept date of 2699 ± 1.5 Ma (MSWD = 2.2). A moderate number of older $^{207}Pb/^{206}Pb$ ratios (up to ~2730 Ma) suggest a significant component of isotopic inheritance in this sample. Excluding 14 analyses >2σ from the mean (>2710 Ma), the section yields a weighted mean $^{207}Pb/^{206}Pb$ date of 2698.7± 1.4 Ma (MSWD = 2.5). MSWDs between 1.9-2.5 for the younger population in sample 47 suggest variable resetting of the U-Pb system by recrystallization/dissolution-precipitation between 2699-2693 Ma.

References

Gerstenberger, H. and Haase, G., 1997. A highly effective emitter substance for mass spectrometric Pb isotope ratio determinations. Chemical Geology 136, 309-312.

Horstwood, M.S.A., Kosler, J., Gehrels, G., Jackson, S.E., McLean, N.M., Paton, C., Pearson, N.J., Sircombe, K., Sylvester, P., Vermeesch, P., Bowring, J.F., Condon, D.J., Schoene, B., 2016. Community-derived standards for LA-ICP-MS U-Th-Pb geochronology e uncertainty propagation, age interpretation and data reporting. Geostandards and Geoanalytical Research. http://dx.doi.org/10.1111/j.1751-908X.2016.00379.x n/aen/a.

Krogh, T.E., 1973. A low contamination method for hydrothermal decomposition of zircon and extraction of U and Pb for isotopic age determinations. Geochimica et Cosmochimica Acta 37, 485-494.

Ludwig, K.R., 2009. User's manual for Isoplot 3.71 a geochronological toolkit for Excel. Berkeley Geochronological Center Special Publication 4, 72 p.

MacLachlan, K., Rayner, N., Dunning, G.R., Leugner, C., 2004. New results and ideas from the Rottenstone Domain Project. Summ. Investig. 2004, Vol. 2, Saskatchewan Geol. Surv. Saskatchewan Ind. Resour. Misc. Rep. 2004-4.2, CD-ROM, Pap. A-3, 21p. 4.2, 1–21.

Mattinson, J., 2005. Zircon U-Pb chemical abrasion (CA-TIMS) method: Combined annealing and multi-step partial dissolution analysis for improved precision and accuracy of zircon ages. Chemical Geololgy 220, 47-66.

Merilainen, K., 1976. The Granulite Complex and adjacent rocks in Lapland, Northern Finland. Geological Survey of Finland, Bulletin 281.

Paton, C., Woodhead, J., Hellstrom, J., Hergt, J., Greig, A. & Maas, R., 2010. Improved laser ablation U-Pb zircon geochronology through robust down-hole fractionation correction. G Cubed, 11, doi:10.1029/2009GC002618.

Petrus, J.A. and Kamber, B.S., 2012. VizualAge: A novel approach to laser ablation ICP-MS U-Pb geochronology data reduction. Geostandards and Geoanalytical Research 36(3), p. 247-270.

Salli, I., 1983. Geological map of Finland 1: 100,000. Explanation to the maps of rocks. Sheet 3314. Pre-Quaternary rocks of the Pielavesi map-sheet area.

Schandl, E.S. and Gorton, M.P., 2004. A textural and geochemical guide to the identification of hydrothermal monazite: Criteria for selection of samples for dating epigenetic hydrothermal ore deposits. Economic Geology. V.90, p. 1027-1035.

Stacey, J.S. and Kramers, J.D., 1975. Approximation of terrestrial lead isotope evolution by a two-stage model. Earth and Planetary Science Letters 26, 207-221.

York, D., 1969. Least-squares fitting of a straight line with correlated errors. Earth and Planetary Science Letters 5, 320-324.

A 2-2: LAICPMS U-Pb data

	Measured Ratios												Calculated Dates (Ma)						
	$^{206}Pb/^{238}U$	$^{206}Pb/^{238}U$ 2SE	$^{207}Pb/^{235}U$	$^{207}Pb/^{235}U$ 2SE	rho $^{206}Pb/^{238}U$ v $^{207}Pb/^{235}U$		$^{238}U/^{206}Pb$	$^{238}U/^{206}Pb$ 2SE	$^{207}Pb/^{206}Pb$	$^{207}Pb/^{206}Pb$ 2SE	rho $^{207}Pb/^{206}Pb$ v $^{238}U/^{206}Pb$		$^{206}Pb/^{238}U$	$^{206}Pb/^{238}U$ 2SE	$^{207}Pb/^{235}U$	$^{207}Pb/^{235}U$ 2SE	$^{207}Pb/^{206}Pb$	$^{207}Pb/^{206}Pb$ 2SE	% Disc.
Sample 48	**Grain1**																		
1	0.53595	0.02403	13.66067	0.82345	0.84849		1.86603	0.08380	0.18485	0.00054	0.11359		2766.43076	100.89879	2726.41645	56.99663	2696.13298	4.80138	-2.54110
2	0.54078	0.02427	13.78822	0.83201	0.77812		1.84942	0.08334	0.18489	0.00065	0.02900		2786.67171	101.60122	2735.16597	57.23475	2696.40937	5.83976	-3.23907
3	0.54135	0.02430	13.79345	0.83215	0.84712		1.84755	0.08364	0.18478	0.00059	0.13242		2789.01590	101.79746	2735.53217	57.24206	2695.40684	5.25712	-3.35635
4	0.54216	0.02435	13.82656	0.83450	0.84780		1.84482	0.08343	0.18496	0.00061	0.11187		2792.42184	101.92129	2737.78519	57.21814	2697.00816	5.41174	-3.41688
5	0.54284	0.02437	13.82159	0.83384	0.91836		1.84247	0.08326	0.18465	0.00052	-0.03661		2795.24705	101.93746	2737.46393	57.25136	2694.27207	4.66181	-3.61238
6	0.53991	0.02426	13.77060	0.83117	0.92184		1.85257	0.08374	0.18503	0.00053	0.10190		2782.98002	101.67233	2733.94284	57.22524	2697.74043	4.69300	-3.06289
7	0.54199	0.02436	13.81851	0.83408	0.89433		1.84545	0.08308	0.18492	0.00057	0.13037		2791.68675	101.85695	2737.23000	57.16004	2696.74631	5.10271	-3.40083
8	0.54089	0.02427	13.78204	0.83120	0.87956		1.84903	0.08323	0.18481	0.00054	0.01617		2787.13348	101.58607	2734.76415	57.15083	2695.74912	4.86718	-3.27879
9	0.54295	0.02454	13.84301	0.83830	0.97536		1.84278	0.08349	0.18490	0.00052	0.07328		2795.57737	102.56935	2738.75888	57.41921	2696.57796	4.66242	-3.54129
10	0.53643	0.02406	13.67665	0.82510	0.78127		1.86439	0.08413	0.18491	0.00064	-0.01177		2768.43589	101.06121	2727.48593	57.16022	2696.57557	5.74580	-2.59570
11	0.54072	0.02425	13.76695	0.82975	0.86375		1.84956	0.08339	0.18461	0.00052	0.01504		2786.43235	101.55076	2733.75511	57.10733	2693.95781	4.62273	-3.31874
12	0.53576	0.02406	13.65736	0.82391	0.93650		1.86684	0.08408	0.18490	0.00051	0.09541		2765.60197	101.04546	2726.15136	57.15821	2696.53583	4.58745	-2.49733
13	0.53743	0.02416	13.70523	0.82740	0.93396		1.86116	0.08411	0.18498	0.00054	0.03748		2772.57006	101.39352	2729.42985	57.25130	2697.29425	4.79303	-2.71502
14	0.53427	0.02398	13.61602	0.82119	0.88665		1.87198	0.08446	0.18487	0.00054	0.11553		2759.35712	100.84387	2723.29790	57.07144	2696.26418	4.82583	-2.28651
15	0.53774	0.02418	13.69314	0.82664	0.91801		1.86007	0.08397	0.18470	0.00056	0.13642		2773.88702	101.41834	2728.59833	57.33189	2694.70116	4.97225	-2.85469
16	0.53562	0.02407	13.65180	0.82395	0.92952		1.86738	0.08443	0.18488	0.00053	0.15976		2765.02255	101.16704	2725.75064	57.17509	2696.34725	4.70863	-2.48372
17	0.53483	0.02405	13.62300	0.82238	0.89574		1.87019	0.08486	0.18478	0.00057	0.19676		2761.69459	101.16837	2723.74436	57.26022	2695.41972	5.13626	-2.39979
18	0.53665	0.02410	13.67849	0.82556	0.84230		1.86374	0.08411	0.18488	0.00061	0.10424		2769.32560	101.19722	2727.60399	57.21789	2696.30012	5.41877	-2.63694
19	0.54177	0.02433	13.82133	0.83372	0.86854		1.84609	0.08332	0.18505	0.00056	0.27076		2790.78390	101.81158	2737.46519	57.19287	2697.84676	4.96666	-3.33014
20	0.53746	0.02417	13.69549	0.82692	0.92505		1.86104	0.08401	0.18483	0.00055	0.23312		2772.73022	101.42354	2728.76534	57.20940	2695.92494	4.87116	-2.77002
21	0.53589	0.02409	13.65327	0.82464	0.88989		1.86641	0.08424	0.18482	0.00058	0.00546		2766.14962	101.19028	2725.84405	57.18457	2695.79686	5.19418	-2.54335
22	0.53719	0.02411	13.67397	0.82510	0.68882		1.86164	0.08395	0.18461	0.00068	-0.01010		2771.66607	101.17303	2727.32908	57.20580	2693.91493	6.10613	-2.80521
23	0.52935	0.02391	13.47467	0.81585	0.97389		1.88999	0.08527	0.18467	0.00051	0.06540		2738.51640	100.76159	2713.28392	57.18506	2694.51581	4.59753	-1.60673
24	0.54048	0.02438	13.76532	0.83279	0.90000		1.85089	0.08368	0.18488	0.00059	0.16587		2785.32783	102.05016	2733.50351	57.34263	2696.34010	5.29803	-3.19487
25	0.53653	0.02417	13.68361	0.82707	0.91192		1.86438	0.08420	0.18501	0.00058	0.22274		2768.78785	101.43739	2727.91771	57.27031	2697.52969	5.19763	-2.57362
26	0.53039	0.02396	13.50020	0.81755	0.96656		1.88628	0.08538	0.18464	0.00053	0.05541		2742.90267	100.95306	2715.06853	57.28830	2694.26108	4.77521	-1.77336
27	0.53742	0.02427	13.70353	0.82995	0.97052		1.86160	0.08442	0.18498	0.00052	-0.02885		2772.44228	101.84186	2729.20106	57.34740	2697.23650	4.64096	-2.71262
28	0.53162	0.02400	13.54308	0.82001	0.95226		1.88183	0.08492	0.18482	0.00056	0.01473		2748.11483	100.99940	2718.07399	57.17737	2695.79611	5.01276	-1.90380
29	0.50977	0.02327	12.73325	0.78035	0.98721		1.96349	0.08903	0.18126	0.00068	-0.77287		2655.29631	99.24351	2659.45028	57.50580	2663.56955	6.21557	0.31157
30	0.53591	0.02413	13.66356	0.82627	0.92475		1.86646	0.08439	0.18497	0.00058	-0.09963		2766.20612	101.34179	2726.51367	57.38865	2697.10873	5.15209	-2.49791
31	0.53820	0.02430	13.72538	0.83104	0.94712		1.85880	0.08409	0.18495	0.00055	0.05222		2775.76529	101.85830	2730.72786	57.38643	2696.99100	4.93289	-2.83793
32	0.55674	0.02497	14.28731	0.86137	0.60293		1.79624	0.08050	0.18620	0.00065	-0.05080		2853.11165	103.36959	2768.91331	57.31251	2708.02087	5.78240	-5.08535
33	0.53714	0.02417	13.69951	0.82834	0.87503		1.86211	0.08425	0.18506	0.00063	-0.04920		2771.39913	101.46843	2729.01101	57.36252	2697.91583	5.58473	-2.65149
34	0.54008	0.02428	13.74007	0.82980	0.81829		1.85185	0.08322	0.18470	0.00057	0.14767		2783.71262	101.60835	2731.87335	57.18531	2694.75315	5.10399	-3.19571
35	0.54564	0.02461	13.88529	0.84014	0.95693		1.83336	0.08332	0.18465	0.00053	0.00349		2806.86721	102.75929	2741.72903	57.44160	2694.28054	4.76830	-4.01111
36	0.53886	0.02423	13.73249	0.82947	0.85941		1.85610	0.08414	0.18492	0.00058	0.17225		2778.59518	101.65190	2731.34226	57.27790	2696.71892	5.19234	-2.94668
37	0.53872	0.02424	13.72206	0.82917	0.91023		1.85662	0.08347	0.18483	0.00055	0.11859		2778.00979	101.53114	2730.60720	57.04830	2695.93975	4.90851	-2.95427
38	0.53710	0.02414	13.68188	0.82622	0.89104		1.86213	0.08417	0.18486	0.00054	0.15776		2771.22924	101.35458	2727.86573	57.24936	2696.22218	4.77636	-2.70663
39	0.53766	0.02417	13.71024	0.82783	0.86312		1.86016	0.08403	0.18507	0.00055	0.18637		2773.58205	101.40140	2729.83293	57.21764	2698.05311	4.91378	-2.72315

	Measured Ratios											Calculated Dates (Ma)						
	$^{206}Pb/^{238}U$	$^{206}Pb/^{238}U$ 2SE	$^{207}Pb/^{235}U$	$^{207}Pb/^{235}U$ 2SE	rho $^{206}Pb/^{238}U$ v $^{207}Pb/^{235}U$	$^{238}U/^{206}Pb$	$^{238}U/^{206}Pb$ 2SE	$^{207}Pb/^{206}Pb$	$^{207}Pb/^{206}Pb$ 2SE	rho $^{207}Pb/^{206}Pb$ v $^{238}U/^{206}Pb$	$^{206}Pb/^{238}U$	$^{206}Pb/^{238}U$ 2SE	$^{207}Pb/^{235}U$	$^{207}Pb/^{235}U$ 2SE	$^{207}Pb/^{206}Pb$	$^{207}Pb/^{206}Pb$ 2SE	% Disc.
Sample 48	**Grain1**																	
40	0.53334	0.02401	13.59929	0.82191	0.90566	1.87544	0.08489	0.18507	0.00057	0.13429	2755.40118	101.02687	2722.08978	57.24527	2698.00435	5.06636	-2.08307
41	0.53721	0.02417	13.69191	0.82731	0.91069	1.86184	0.08420	0.18497	0.00055	0.03060	2771.67821	101.43690	2728.52075	57.24644	2697.20541	4.92319	-2.68692
42	0.54045	0.02438	13.76735	0.83297	0.96756	1.85098	0.08390	0.18493	0.00050	0.05694	2785.20491	102.10073	2733.65082	57.42753	2696.85339	4.50471	-3.17217
43	0.53690	0.02419	13.67175	0.82680	0.93755	1.86313	0.08471	0.18475	0.00054	0.00683	2770.32248	101.62233	2727.07646	57.37020	2695.20223	4.79525	-2.71161
44	0.53665	0.02414	13.68309	0.82657	0.91900	1.86377	0.08433	0.18506	0.00054	0.06887	2769.34802	101.37382	2727.91692	57.20762	2697.99838	4.80726	-2.57641
45	0.53507	0.02411	13.60788	0.82251	0.94380	1.86950	0.08487	0.18461	0.00054	0.19515	2762.64944	101.37212	2722.66933	57.35432	2693.92235	4.85257	-2.48772
46	0.53337	0.02408	13.60458	0.82371	0.93964	1.87572	0.08537	0.18515	0.00059	0.03632	2755.44888	101.38450	2722.35147	57.55094	2698.74095	5.25325	-2.05803
47	0.53545	0.02409	13.64841	0.82458	0.90701	1.86801	0.08464	0.18501	0.00057	0.11513	2764.26861	101.27278	2725.50634	57.30205	2697.52439	5.04487	-2.41453
48	0.53079	0.02397	13.53709	0.81953	0.95447	1.88481	0.08541	0.18511	0.00055	0.07400	2744.60948	100.99261	2717.65722	57.31728	2698.42060	4.93337	-1.68289
49	0.53510	0.02404	13.62681	0.82223	0.86753	1.86902	0.08414	0.18485	0.00052	0.32269	2762.86378	100.97234	2724.07388	57.10036	2696.11785	4.68546	-2.41582
50	0.53596	0.02412	13.66324	0.82530	0.95444	1.86623	0.08474	0.18504	0.00050	0.14850	2766.43515	101.37340	2726.53856	57.29124	2697.76209	4.48137	-2.48237
51	0.53299	0.02396	13.58511	0.82028	0.93585	1.87657	0.08494	0.18492	0.00051	-0.01908	2753.95522	100.88142	2721.11994	57.22972	2697.26138	4.96472	-2.05863
52	0.53082	0.02384	13.51919	0.81566	0.89157	1.88413	0.08490	0.18478	0.00052	0.13599	2744.85528	100.45702	2716.55612	57.16426	2695.47460	4.64601	-1.79903
53	0.53258	0.02391	13.55951	0.81775	0.78728	1.87788	0.08482	0.18479	0.00058	0.27210	2752.25966	100.68194	2719.38349	57.13166	2695.55599	5.23087	-2.06026
54	0.53699	0.02418	13.67644	0.82631	0.95691	1.86279	0.08455	0.18482	0.00052	0.14358	2770.73226	101.56037	2727.41597	57.34937	2695.86174	4.62628	-2.70219
55	0.54219	0.02430	13.83404	0.83358	-0.02693	1.84438	0.08261	0.18474	0.00070	0.61413	2792.61453	101.54740	2738.40520	57.04637	2695.12211	6.30348	-3.49108
56	0.53925	0.02423	13.73059	0.82852	0.86249	1.85477	0.08386	0.18470	0.00056	0.21016	2780.22998	101.58858	2731.20978	57.30118	2694.73561	5.03243	-3.07508
57	0.51645	0.02322	13.25075	0.80449	0.35082	1.93646	0.08760	0.18599	0.00147	0.22574	2684.07367	98.81822	2697.55059	57.41320	2705.98154	13.00965	0.81622
58	0.53582	0.02409	13.64369	0.82363	0.90176	1.86673	0.08454	0.18479	0.00058	0.10011	2765.84656	101.24087	2725.17115	57.22408	2695.50633	5.15039	-2.54317
59	0.53674	0.02413	13.70171	0.82684	0.90451	1.86354	0.08436	0.18523	0.00057	0.20337	2769.69746	101.33673	2729.19391	57.20755	2699.49227	5.05478	-2.53476
60	0.53226	0.02394	13.56476	0.81915	0.94422	1.87930	0.08508	0.18493	0.00054	-0.03832	2750.86170	100.83970	2719.65808	57.29272	2696.85199	4.79587	-1.96337
61	0.53273	0.02399	13.58568	0.82058	0.96006	1.87781	0.08524	0.18503	0.00053	0.07627	2752.80548	101.02369	2721.08417	57.31947	2697.70208	4.72727	-2.00172
62	0.53758	0.02413	13.69353	0.82534	0.93972	1.86057	0.08397	0.18482	0.00052	0.11200	2773.24125	101.25040	2728.64059	57.18683	2695.81004	4.62323	-2.79208
63	0.54031	0.02438	13.78776	0.83380	0.95132	1.85172	0.08412	0.18514	0.00058	0.15667	2784.55673	102.16382	2734.99298	57.37184	2698.65336	5.13046	-3.08499
64	0.53976	0.02423	13.76598	0.83012	0.90040	1.85314	0.08374	0.18496	0.00056	0.12458	2782.33617	101.56999	2733.60850	57.18904	2697.03222	5.02315	-3.06591
65	0.53442	0.02396	13.61054	0.82015	0.92222	1.87156	0.08437	0.18478	0.00054	0.01986	2759.95922	100.76473	2722.88450	57.11871	2695.44796	4.81029	-2.33740
66	0.53745	0.02414	13.70234	0.82656	0.94041	1.86118	0.08381	0.18499	0.00055	0.02846	2772.64234	101.27053	2729.20190	57.23970	2697.31804	4.90714	-2.71670
67	0.53360	0.02398	13.60938	0.82097	0.97034	1.87462	0.08450	0.18501	0.00049	-0.02127	2756.50346	100.83700	2722.75425	57.09227	2697.52384	4.37404	-2.13965
68	0.53017	0.02380	13.49454	0.81316	0.93665	1.88672	0.08456	0.18471	0.00054	0.29705	2742.04894	100.24325	2714.77895	56.98532	2694.84734	4.83999	-1.72140
69	0.53464	0.02400	13.62548	0.82143	0.91788	1.87092	0.08446	0.18496	0.00057	0.09578	2760.85598	100.90258	2723.89595	57.15848	2697.05220	5.06463	-2.31101
70	0.53734	0.02418	13.69784	0.82726	0.94189	1.86178	0.08386	0.18498	0.00057	0.06989	2772.13059	101.41307	2728.83320	57.13306	2697.22432	5.11618	-2.70212
71	0.53664	0.02417	13.67950	0.82624	0.95367	1.86429	0.08394	0.18502	0.00056	0.12115	2769.19487	101.38062	2727.55243	57.14537	2697.59146	4.98885	-2.58571
72	0.53451	0.02393	13.62272	0.81977	0.90019	1.87120	0.08391	0.18501	0.00055	0.17678	2760.36528	100.54337	2723.74794	57.02355	2697.53625	4.89988	-2.27611
73	0.53238	0.02401	13.58427	0.82034	0.95926	1.87934	0.08547	0.18522	0.00055	0.36916	2751.26187	101.13456	2720.95276	57.24271	2699.42724	4.94810	-1.88403
74	0.55285	0.02479	14.07290	0.84823	0.87266	1.80925	0.08149	0.18479	0.00062	0.07692	2836.92907	102.99251	2754.48496	57.27931	2695.54621	5.53019	-4.98366
75	0.55984	0.02507	14.22121	0.85808	0.62694	1.78641	0.08043	0.18443	0.00081	-0.01704	2865.94132	103.69203	2764.43953	57.36321	2692.21039	7.26810	-6.06191
76	0.54138	0.02439	13.80148	0.83450	0.94884	1.84801	0.08467	0.18510	0.00059	-0.11264	2789.04136	102.30166	2735.91184	57.56716	2698.33821	5.24693	-3.25213
77	0.56176	0.02524	14.08863	0.85192	0.70475	1.78033	0.08026	0.18226	0.00088	0.07548	2873.84323	104.24622	2755.56745	57.81283	2672.63428	7.98374	-7.00139
78	0.54428	0.02427	13.86208	0.83279	0.76750	1.83743	0.08224	0.18495	0.00056	0.21166	2801.31591	101.38473	2740.27816	57.02788	2697.01996	5.01785	-3.72311
79	0.54332	0.02430	13.84634	0.83346	0.83735	1.84081	0.08266	0.18509	0.00060	0.08252	2797.27194	101.58462	2739.15885	57.04624	2698.17191	5.33461	-3.54274
80	0.54079	0.02420	13.77128	0.83050	0.76060	1.84945	0.08309	0.18496	0.00074	-0.03633	2786.69748	101.31938	2733.95321	57.39072	2696.99631	6.63925	-3.21891

	Measured Ratios											Calculated Dates (Ma)						
	$^{206}Pb/^{238}U$	$^{206}Pb/^{238}U$ 2SE	$^{207}Pb/^{235}U$	$^{207}Pb/^{235}U$ 2SE	rho $^{206}Pb/^{238}U$ v $^{207}Pb/^{235}U$	$^{238}U/^{206}Pb$	$^{238}U/^{206}Pb$ 2SE	$^{207}Pb/^{206}Pb$	$^{207}Pb/^{206}Pb$ 2SE	rho $^{207}Pb/^{206}Pb$ v $^{238}U/^{206}Pb$	$^{206}Pb/^{238}U$	$^{206}Pb/^{238}U$ 2SE	$^{207}Pb/^{235}U$	$^{207}Pb/^{235}U$ 2SE	$^{207}Pb/^{206}Pb$	$^{207}Pb/^{206}Pb$ 2SE	% Disc.
Sample 48	**Grain1**																	
81	0.53709	0.02408	13.68470	0.82434	0.92990	1.86233	0.08410	0.18513	0.00054	0.08073	2771.16719	101.12357	2728.01057	57.16244	2698.61083	4.84364	-2.61826
82	0.54332	0.02434	13.84351	0.83298	0.91932	1.84089	0.08250	0.18514	0.00053	0.26411	2797.26158	101.66024	2738.96620	56.91734	2698.69663	4.70553	-3.52362
83	0.54253	0.02441	13.81096	0.83332	0.95499	1.84391	0.08308	0.18496	0.00054	0.18906	2793.88685	102.02233	2736.64741	57.20948	2697.03387	4.84396	-3.46660
84	0.54030	0.02425	13.76250	0.82941	0.94704	1.85134	0.08313	0.18507	0.00053	0.14079	2784.60408	101.50393	2733.35945	56.98892	2698.07187	4.71927	-3.10752
85	0.54490	0.02447	13.87810	0.83648	0.94926	1.83577	0.08254	0.18506	0.00053	0.19897	2803.79508	102.13586	2741.27471	57.09246	2698.01695	4.74563	-3.77268
86	0.54476	0.02479	13.88163	0.84435	0.97268	1.83732	0.08072	0.18556	0.00067	-0.44229	2802.98951	102.76606	2741.20065	56.48832	2702.33986	5.92099	-3.59080
87	0.53428	0.02404	13.55595	0.81825	0.94635	1.87242	0.08434	0.18435	0.00056	0.09472	2759.29949	101.01159	2718.99387	57.05202	2691.62265	5.01370	-2.45268
88	0.53655	0.02398	13.66429	0.82108	0.88495	1.86395	0.08365	0.18505	0.00052	0.21401	2768.96228	100.67952	2726.66937	56.84977	2697.86109	4.62617	-2.56779
89	0.54809	0.02450	13.93166	0.83733	0.85746	1.82473	0.08199	0.18471	0.00053	0.24719	2817.16200	102.11843	2745.01531	57.00651	2694.81236	4.78805	-4.34301
90	0.55130	0.02466	14.01980	0.84389	0.69419	1.81412	0.08156	0.18478	0.00066	0.21464	2830.52594	102.57036	2750.96744	56.94005	2695.40995	5.93600	-4.77353
91	0.54458	0.02455	13.82214	0.83547	0.95406	1.83706	0.08454	0.18434	0.00059	-0.12433	2802.43214	102.81811	2737.38703	57.64678	2691.55084	5.27899	-3.95661
92	0.53691	0.02397	13.52133	0.81277	0.66464	1.86264	0.08338	0.18295	0.00058	0.25772	2770.46075	100.57890	2716.73124	56.71362	2678.98222	5.25952	-3.30192
93	0.54844	0.02455	13.96383	0.84012	0.88707	1.82363	0.08225	0.18496	0.00055	0.10052	2818.61714	102.34591	2747.17217	57.14252	2697.03071	4.90490	-4.31369
94	0.55627	0.02492	14.18906	0.85480	0.59620	1.79775	0.08058	0.18529	0.00060	0.01510	2851.18618	103.21619	2762.37892	57.17792	2699.94832	5.36381	-5.30438
95	0.54041	0.02417	13.75927	0.82779	0.82708	1.85067	0.08296	0.18495	0.00057	0.11168	2785.12971	101.19480	2733.19977	56.89841	2696.94869	5.12873	-3.16614
96	0.54343	0.02433	13.83981	0.83246	0.92110	1.84045	0.08237	0.18497	0.00052	0.23127	2797.73833	101.62472	2738.72453	56.89736	2697.18855	4.63533	-3.59397
97	0.55838	0.02510	14.22550	0.85777	0.92342	1.79149	0.08073	0.18503	0.00058	0.21425	2859.79130	103.86798	2764.69930	57.25200	2697.66060	5.17452	-5.66932
98	0.54703	0.02462	13.93781	0.84141	0.97029	1.82876	0.08269	0.18505	0.00051	-0.03637	2812.65532	102.67715	2745.28689	57.27317	2697.87862	4.58612	-4.08072
99	0.54777	0.02475	13.94910	0.84390	0.96920	1.82668	0.08242	0.18493	0.00054	0.09946	2815.63482	103.05594	2745.97172	57.29287	2696.81461	4.79926	-4.22001
100	0.54876	0.02466	13.99413	0.84378	0.93696	1.82279	0.08229	0.18510	0.00054	0.12591	2819.88800	102.70602	2749.17144	57.19250	2698.29407	4.82400	-4.31201
101	0.54844	0.02475	13.98967	0.84611	0.97712	1.82426	0.08270	0.18512	0.00051	-0.04998	2818.48361	103.11684	2748.75059	57.38793	2698.53015	4.58481	-4.25596
102	0.54800	0.02469	13.97332	0.84426	0.95236	1.82553	0.08240	0.18504	0.00055	0.01432	2816.68281	102.82893	2747.69334	57.18484	2697.77758	4.92006	-4.22146
103	0.55555	0.02485	14.17202	0.85303	0.75449	1.80013	0.08087	0.18511	0.00057	-0.05342	2848.17179	103.07020	2761.23130	57.15501	2698.37189	5.11572	-5.25951
104	0.55280	0.02477	14.05502	0.84646	0.79273	1.80918	0.08126	0.18449	0.00059	0.11760	2836.74514	102.87257	2753.35274	57.07973	2692.80648	5.29051	-5.07408
105	0.54149	0.02437	13.80550	0.83328	0.93933	1.84734	0.08320	0.18499	0.00055	0.14804	2789.57009	101.91323	2736.29555	57.04862	2697.29781	4.88751	-3.30776
106	0.54629	0.02453	13.95283	0.84159	0.91680	1.83091	0.08289	0.18527	0.00056	-0.02226	2809.65069	102.42637	2746.38243	57.25057	2699.85997	5.00121	-3.90763
107	0.57062	0.02554	14.57761	0.87767	0.61470	1.75255	0.07885	0.18530	0.00058	0.07322	2910.34411	104.91385	2788.03464	57.21332	2700.11549	5.15257	-7.22350
108	0.54018	0.02436	13.76312	0.83177	0.95913	1.85201	0.08411	0.18480	0.00054	0.12850	2784.03669	102.06842	2733.34259	57.33210	2695.65757	4.81105	-3.17450
109	0.54570	0.02452	13.92910	0.84044	0.91005	1.83290	0.08209	0.18513	0.00057	0.02911	2807.17365	102.19620	2744.77011	57.09787	2698.58187	5.07884	-3.86837
110	0.54723	0.02454	13.97876	0.84286	0.75830	1.82755	0.08222	0.18522	0.00063	0.00165	2813.61495	102.31549	2748.18504	57.25180	2699.37470	5.63853	-4.06027
111	0.54972	0.02466	14.03395	0.84617	0.74418	1.81930	0.08233	0.18510	0.00063	0.07215	2823.95919	102.73927	2751.92589	57.16238	2698.29088	5.60847	-4.45008
112	0.55250	0.02489	14.10341	0.85225	0.92288	1.81055	0.08217	0.18504	0.00059	0.11446	2835.44103	103.47887	2756.50982	57.54444	2697.80395	5.23256	-4.85417
113	0.54824	0.02464	14.01045	0.84584	0.89204	1.82439	0.08229	0.18534	0.00056	-0.02891	2817.75442	102.66578	2750.28871	57.26774	2700.49499	4.99911	-4.16145
114	0.52580	0.02396	13.42144	0.81664	0.97373	1.90375	0.08599	0.18501	0.00058	0.09146	2723.33953	101.06833	2709.29601	57.21268	2697.51063	5.15978	-0.94843
115	0.54935	0.02471	14.00590	0.84583	0.86057	1.82071	0.08221	0.18478	0.00062	0.08717	2822.39394	102.86299	2749.97726	57.32744	2695.44995	5.54869	-4.49774
116	0.55086	0.02474	14.09317	0.85016	0.80089	1.81558	0.08200	0.18543	0.00059	0.23423	2828.69563	102.95277	2755.92362	57.27406	2701.21427	5.28298	-4.50672
117	0.54360	0.02447	13.88103	0.83862	0.96024	1.84009	0.08299	0.18507	0.00051	0.06991	2798.37510	102.24013	2741.48824	57.36335	2698.10674	4.54990	-3.58309
118	0.54810	0.02467	14.01319	0.84686	0.81848	1.82484	0.08284	0.18524	0.00064	0.11899	2817.17064	102.87200	2750.48534	57.35025	2699.51328	5.73642	-4.17644
119	0.54611	0.02456	13.95855	0.84295	0.78521	1.83125	0.08285	0.18519	0.00054	0.18362	2808.95844	102.49340	2746.85504	57.15486	2699.13140	4.79536	-3.90988
120	0.55544	0.02501	14.17623	0.85693	0.89757	1.80077	0.08198	0.18490	0.00057	0.13757	2847.67554	103.86619	2761.44965	57.54179	2696.56190	5.14460	-5.30656

	Measured Ratios												Calculated Dates (Ma)							
	$^{206}Pb/^{238}U$	$^{206}Pb/^{238}U$ 2SE	$^{207}Pb/^{235}U$	$^{207}Pb/^{235}U$ 2SE	rho $^{206}Pb/^{238}U$ v $^{207}Pb/^{235}U$		$^{238}U/^{206}Pb$	$^{238}U/^{206}Pb$ 2SE	$^{207}Pb/^{206}Pb$	$^{207}Pb/^{206}Pb$ 2SE	rho $^{207}Pb/^{206}Pb$ v $^{238}U/^{206}Pb$		$^{206}Pb/^{238}U$	$^{206}Pb/^{238}U$ 2SE	$^{207}Pb/^{235}U$	$^{207}Pb/^{235}U$ 2SE	$^{207}Pb/^{206}Pb$	$^{207}Pb/^{206}Pb$ 2SE	% Disc.
Sample 48	**Grain1**																			
121	0.54455	0.02452	13.91341	0.84115	0.91450		1.83672	0.08362	0.18510	0.00054	0.11955		2802.40118	102.53446	2743.72885	57.50373	2698.33852	4.80598	-3.71334	
122	0.55294	0.02488	14.11158	0.85270	0.79163		1.80866	0.08210	0.18483	0.00053	0.24350		2837.35137	103.44227	2757.18702	57.37137	2695.89975	4.73668	-4.98534	
123	0.51826	0.02355	13.25942	0.80647	0.97594		1.93098	0.08750	0.18535	0.00056	-0.17271		2691.52916	99.92539	2697.88887	57.31051	2700.50604	4.97532	0.33352	
124	0.54576	0.02458	13.94447	0.84327	0.93066		1.83262	0.08295	0.18511	0.00052	0.17337		2807.45978	102.59646	2745.85339	57.40242	2698.43798	4.61335	-3.88329	
125	0.54931	0.02489	14.02528	0.85111	0.95264		1.82158	0.08313	0.18499	0.00058	0.04591		2822.03981	103.69104	2751.12056	57.70194	2697.36944	5.16316	-4.41774	
126	0.55079	0.02486	14.07214	0.85217	0.93791		1.81618	0.08245	0.18509	0.00056	0.04745		2828.30997	103.44322	2754.40372	57.56928	2698.24245	5.02617	-4.59877	
127	0.54375	0.02446	13.92182	0.84079	0.58825		1.83833	0.07690	0.18551	0.00069	0.15406		2799.07909	102.26951	2744.32528	57.28270	2701.93827	6.16720	-3.47046	
128	0.56216	0.02530	14.34076	0.86680	0.81630		1.77905	0.08086	0.18485	0.00062	-0.14209		2875.51602	104.56893	2772.41699	57.65408	2696.04124	5.57072	-6.24148	
129	0.54015	0.02433	13.78263	0.83378	0.85782		1.85150	0.08368	0.18485	0.00051	0.09350		2784.03699	101.88762	2734.83325	57.31801	2696.06690	4.57903	-3.15980	
130	0.55678	0.02508	14.23272	0.86100	0.90524		1.79628	0.08105	0.18522	0.00052	0.23377		2853.25645	103.89166	2765.27298	57.39230	2699.44047	4.66800	-5.39089	
131	0.54416	0.02451	13.77145	0.83263	0.85277		1.83796	0.08372	0.18339	0.00056	0.23077		2800.77167	102.51844	2734.04936	57.40557	2682.98723	5.07537	-4.20543	
132	0.53804	0.02424	13.74723	0.83200	0.90731		1.85886	0.08394	0.18516	0.00053	0.07991		2775.17790	101.64844	2732.36951	57.29720	2698.89123	4.70689	-2.74889	
133	0.53271	0.02408	13.45230	0.81617	0.97343		1.87800	0.08580	0.18300	0.00053	-0.37672		2752.70423	101.47363	2711.67845	57.64940	2679.49341	4.77952	-2.65960	
134	0.54855	0.02478	14.00732	0.84890	0.92028		1.82365	0.08230	0.18508	0.00061	0.09476		2818.99706	103.13902	2750.00917	57.51592	2698.15470	5.43961	-4.28671	
Sample 48	**Grain2 Core**																			
1	0.55401	0.01189	13.91051	0.56080	0.63790		1.80642	0.03973	0.18306	0.00182	-0.16956		2841.51508	49.52597	2747.84321	32.57033	2678.64814	16.59250	-5.73169	
2	0.53275	0.01119	13.55548	0.52222	0.74240		1.87793	0.03974	0.18517	0.00094	0.09693		2752.83972	47.12317	2718.81611	36.25323	2698.62583	8.43121	-1.96938	
3	0.51439	0.01176	13.05362	0.51157	0.83689		1.94738	0.04532	0.18533	0.00117	0.38585		2674.73126	50.21708	2682.83611	37.24835	2699.89747	10.42281	0.94089	
4	0.53666	0.01105	13.60773	0.52091	0.61266		1.86377	0.03839	0.18518	0.00093	0.10900		2769.37775	46.36143	2722.57379	36.26375	2698.78405	8.24297	-2.54908	
5	0.53125	0.01087	13.49866	0.51623	0.60071		1.88260	0.03834	0.18562	0.00088	-0.01138		2746.67870	45.71930	2714.97888	36.24661	2702.68168	7.88273	-1.60183	
6	0.53690	0.01097	13.63511	0.52186	0.55364		1.86277	0.03802	0.18552	0.00087	-0.09161		2770.40788	46.00489	2724.47799	36.39328	2701.86588	7.78676	-2.47408	
7	0.53181	0.01112	13.48354	0.51807	0.77529		1.88112	0.03893	0.18571	0.00078	0.07356		2748.91964	46.69769	2713.82996	36.28268	2703.59199	6.99921	-1.64893	
8	0.50935	0.01084	12.81086	0.50602	0.87375		1.96438	0.04178	0.18405	0.00121	-0.49600		2653.65862	46.27093	2665.08759	37.35751	2688.40623	10.89432	1.30942	
9	0.52349	0.01313	13.26922	0.66923	0.37335		1.91376	0.05035	0.18484	0.00500	0.13171		2713.28935	55.97897	2695.13922	47.20871	2703.19681	49.93997	-0.37197	
10	0.53015	0.01095	13.49058	0.51563	0.70918		1.88673	0.03876	0.18638	0.00078	0.11673		2741.97593	46.07152	2714.42525	36.07764	2709.51573	6.94033	-1.18383	
11	0.53828	0.01095	13.64260	0.52004	0.39427		1.85788	0.03774	0.18575	0.00086	0.12293		2776.22775	45.88320	2725.07169	36.22314	2703.91616	7.65636	-2.60467	
12	0.53957	0.01106	13.67256	0.52265	0.46393		1.85359	0.03821	0.18567	0.00096	0.15743		2781.59858	46.34519	2727.09722	36.21829	2703.09808	8.55116	-2.82214	
13	0.52796	0.01080	13.37117	0.51141	0.49445		1.89431	0.03867	0.18559	0.00096	0.07691		2732.81419	45.55396	2706.00939	36.21315	2702.36739	8.55794	-1.11412	
14	0.53075	0.01093	13.45982	0.51443	0.65367		1.88450	0.03878	0.18581	0.00083	0.08297		2744.52984	46.00503	2712.27090	36.18336	2704.41778	7.35507	-1.46153	
15	0.54260	0.01130	13.75674	0.52682	0.83181		1.84361	0.03813	0.18577	0.00068	0.03957		2794.19987	47.16840	2732.86854	36.17149	2704.15376	6.03825	-3.22261	
16	0.53009	0.01097	13.44216	0.51444	0.62902		1.88697	0.03909	0.18606	0.00095	0.11130		2741.72805	46.22864	2712.16134	39.01345	2706.58696	8.43919	-1.28171	
17	0.54089	0.01116	13.79022	0.53119	0.73708		1.84908	0.03792	0.18694	0.00126	-0.23670		2787.11546	46.61966	2735.16006	36.52080	2714.23914	11.08107	-2.61476	
18	0.50509	0.01063	12.73079	0.49168	0.67899		1.98077	0.04225	0.18463	0.00110	0.08809		2635.47270	45.62087	2659.54260	36.57350	2693.66051	9.87885	2.20787	
19	0.53844	0.01099	13.70617	0.52315	0.47568		1.85736	0.03786	0.18617	0.00089	0.08162		2776.87207	46.04832	2729.44668	36.04927	2707.56588	7.85378	-2.49584	
20	0.53268	0.01096	13.51508	0.51733	0.56949		1.87765	0.03867	0.18574	0.00094	0.06926		2752.64564	46.11742	2716.11017	36.31164	2703.73968	8.40989	-1.77669	
21	0.54405	0.01119	13.76440	0.52551	0.60715		1.83835	0.03780	0.18517	0.00081	0.09125		2800.32756	46.70638	2733.45688	36.14821	2698.77281	7.23201	-3.62653	
22	0.53443	0.01090	13.58550	0.51740	0.29325		1.87124	0.03826	0.18601	0.00085	0.17683		2760.08609	45.82736	2721.12204	36.05920	2706.18121	7.56585	-1.95301	
23	0.52393	0.01107	13.30038	0.51242	0.79582		1.90742	0.04310	0.18545	0.00089	0.18560		2718.36136	50.36753	2700.85582	36.28051	2701.17301	7.88268	-0.63231	
24	0.52424	0.01071	13.29117	0.50703	0.51811		1.90766	0.03906	0.18535	0.00083	-0.09303		2717.11169	45.32570	2700.39387	36.08022	2700.35109	7.40699	-0.61685	
25	0.53347	0.01101	13.64501	0.52903	0.50054		1.87478	0.03823	0.18660	0.00140	0.02325		2755.99086	46.17828	2725.10894	36.62117	2711.20416	12.40729	-1.62507	

	Measured Ratios											Calculated Dates (Ma)						
	$^{206}Pb/^{238}U$	$^{206}Pb/^{238}U$ 2SE	$^{207}Pb/^{235}U$	$^{207}Pb/^{235}U$ 2SE	rho $^{206}Pb/^{238}U$ v $^{207}Pb/^{235}U$	$^{238}U/^{206}Pb$	$^{238}U/^{206}Pb$ 2SE	$^{207}Pb/^{206}Pb$	$^{207}Pb/^{206}Pb$ 2SE	rho $^{207}Pb/^{206}Pb$ v $^{238}U/^{206}Pb$	$^{206}Pb/^{238}U$	$^{206}Pb/^{238}U$ 2SE	$^{207}Pb/^{235}U$	$^{207}Pb/^{235}U$ 2SE	$^{207}Pb/^{206}Pb$	$^{207}Pb/^{206}Pb$ 2SE	% Disc.
Sample 48	**Grain2 Core**																	
26	0.54254	0.01111	13.84934	0.53617	0.49982	1.84344	0.03753	0.18614	0.00140	-0.04266	2794.00627	46.36603	2739.01424	36.54093	2706.88056	12.46228	-3.11831
27	0.57061	0.01194	14.50024	0.55673	0.59777	1.75319	0.03720	0.18539	0.00099	0.25414	2910.16958	49.13076	2782.73257	36.42120	2702.38564	9.54040	-7.13993
28	0.53504	0.01132	13.63587	0.52640	0.83471	1.87003	0.03971	0.18607	0.00083	-0.04698	2762.43277	47.56389	2724.36122	36.45480	2706.77509	7.39554	-2.01481
29	0.52791	0.01089	13.47208	0.51517	0.67204	1.89461	0.03900	0.18622	0.00083	0.02583	2732.57790	45.92262	2713.12160	36.16505	2708.08237	7.35324	-0.89643
30	0.52146	0.01091	13.27823	0.51023	0.73248	1.91843	0.04012	0.18575	0.00090	0.07532	2705.20678	46.20537	2699.33339	36.17350	2703.82324	7.98221	-0.05114
31	0.52481	0.01088	13.33083	0.50894	0.72564	1.90595	0.03918	0.18523	0.00072	0.18491	2719.43970	45.93622	2703.19363	36.07621	2699.33289	6.47389	-0.73937
32	0.52644	0.01093	13.38382	0.51340	0.67510	1.90007	0.03930	0.18531	0.00092	0.05384	2726.33584	46.12575	2706.84556	36.32416	2699.92834	8.19652	-0.96861
33	0.52664	0.01086	13.39739	0.51207	0.68669	1.89918	0.03900	0.18536	0.00079	0.00003	2727.20966	45.81747	2707.87318	36.14668	2700.47517	7.06559	-0.98029
34	0.52439	0.01077	13.37254	0.51023	0.40256	1.90721	0.03923	0.18576	0.00092	0.24253	2717.73399	45.55252	2706.15281	36.04999	2703.89785	8.21173	-0.50911
35	0.52550	0.01075	13.41172	0.51107	0.38903	1.90308	0.03896	0.18580	0.00085	0.13687	2722.43456	45.43173	2708.94344	36.09964	2704.29195	7.57529	-0.66641
36	0.52486	0.01073	13.37058	0.51145	0.54135	1.90542	0.03880	0.18528	0.00093	-0.09440	2719.72071	45.34106	2705.96518	36.19235	2699.64305	8.30412	-0.73822
37	0.52170	0.01074	13.31370	0.50694	0.51221	1.91714	0.03954	0.18567	0.00080	0.32822	2706.31235	45.50915	2702.02698	36.03490	2703.18327	7.08127	-0.11562
38	0.53500	0.01095	13.68801	0.52084	0.42141	1.86932	0.03809	0.18569	0.00083	0.18205	2762.45309	45.96309	2728.25310	36.03471	2703.33846	7.38855	-2.13993
39	0.53657	0.01119	13.70951	0.52555	0.67285	1.86432	0.03851	0.18556	0.00092	0.18852	2768.93080	46.86805	2729.59721	36.27034	2702.17071	8.14640	-2.41104
40	0.53386	0.01105	13.65450	0.52214	0.63270	1.87361	0.03856	0.18569	0.00087	0.15452	2757.58750	46.38170	2725.83643	36.24162	2703.31928	7.74278	-1.96796
41	0.54130	0.01139	13.92409	0.53949	0.71473	1.84768	0.03866	0.18642	0.00115	-0.02948	2788.82973	47.58611	2744.40756	36.80924	2709.95092	10.18116	-2.82838
42	0.53330	0.01107	13.65069	0.52348	0.77637	1.87564	0.03883	0.18565	0.00079	-0.07006	2755.24745	46.53158	2725.51696	36.34801	2703.06515	7.06857	-1.89392
43	0.53284	0.01102	13.61116	0.52205	0.71971	1.87719	0.03865	0.18523	0.00087	-0.07325	2753.29940	46.31370	2722.77099	36.30376	2699.21154	7.72939	-1.96447
44	0.53324	0.01107	13.63161	0.52390	0.63586	1.87585	0.03888	0.18567	0.00090	-0.08994	2754.99405	46.52231	2724.15191	36.37639	2703.17236	7.99222	-1.88101
45	0.53301	0.01102	13.64425	0.52213	0.64544	1.87659	0.03860	0.18553	0.00087	0.11585	2754.01592	46.31176	2725.11318	36.09482	2701.87711	7.77730	-1.89319
46	0.53275	0.01094	13.68685	0.52348	0.55819	1.87730	0.03835	0.18597	0.00093	0.07729	2752.99028	45.96313	2728.07106	36.28349	2705.75262	8.21183	-1.71587
47	0.53381	0.01097	13.68613	0.52239	0.63036	1.87363	0.03848	0.18566	0.00079	0.06779	2757.40466	46.11305	2728.06423	36.19003	2703.14086	7.00322	-1.96793
48	0.53298	0.01101	13.64188	0.52301	0.66825	1.87665	0.03872	0.18530	0.00092	-0.01826	2753.91637	46.28967	2724.91083	36.39237	2699.85048	8.17301	-1.96324
49	0.79721	0.11684	22.54916	5.51255	0.40807	1.35325	0.18977	0.21050	0.05121	0.26278	3730.41787	410.42920	3090.78648	267.74489	2678.52327	441.65586	-28.19777
50	0.63624	0.03381	15.97726	1.45091	0.49198	1.60745	0.09097	0.18230	0.01445	0.13483	3163.83832	134.27065	2842.46887	101.75540	2613.12728	146.98210	-17.40642
51	0.52639	0.01083	13.50913	0.51567	0.57681	1.90007	0.03901	0.18561	0.00084	0.16850	2726.14498	45.73557	2715.74860	36.12272	2702.63543	7.46200	-0.86237
52	0.51811	0.01077	13.29009	0.50824	0.70830	1.93067	0.03990	0.18548	0.00081	0.19132	2691.03040	45.67537	2700.27153	36.11794	2701.47133	7.19808	0.38799
53	0.51370	0.01068	13.22229	0.50678	0.67711	1.94725	0.04042	0.18606	0.00091	0.12887	2672.29866	45.46368	2695.39560	36.26336	2706.60006	8.01206	1.28359
54	0.51423	0.01075	13.18833	0.50636	0.77230	1.94537	0.04049	0.18535	0.00083	0.03965	2674.53916	45.71868	2692.93452	36.24102	2700.30411	7.36979	0.96334
55	0.51225	0.01066	13.12332	0.50279	0.69962	1.95281	0.04056	0.18512	0.00086	0.13482	2666.09345	45.41951	2688.31339	36.11476	2698.22989	7.69338	1.20538
56	0.51221	0.01062	13.14943	0.50255	0.65009	1.95285	0.04028	0.18546	0.00084	0.23063	2665.95618	45.23417	2690.23961	36.01770	2701.32028	7.46344	1.32651
57	0.51585	0.01072	13.32193	0.50999	0.63507	1.93914	0.04012	0.18647	0.00092	0.21530	2681.42866	45.54077	2702.50634	36.28412	2710.23607	8.12759	1.07433
58	0.52330	0.01085	13.45504	0.51503	0.69688	1.91146	0.03927	0.18545	0.00084	0.10974	2713.06889	45.84483	2711.90355	36.07498	2701.22923	7.47151	-0.43639
59	0.51334	0.01074	13.21584	0.50641	0.77912	1.94879	0.04088	0.18561	0.00078	0.16967	2670.74268	45.77532	2694.94006	36.15486	2702.67473	6.95323	1.19562
60	0.51017	0.01054	13.17176	0.50320	0.69638	1.96059	0.04043	0.18611	0.00078	0.11792	2657.25306	44.98487	2691.84783	36.07947	2707.10716	6.89380	1.87615
61	0.50929	0.01059	13.09108	0.50179	0.77179	1.96413	0.04086	0.18525	0.00078	0.03376	2653.49128	45.24677	2685.98496	36.03708	2699.43424	6.96199	1.73142
62	0.52270	0.01077	13.43856	0.51456	0.72219	1.91353	0.03952	0.18526	0.00081	-0.11297	2710.53053	45.62206	2710.73854	36.17586	2699.50702	7.21358	-0.40669
63	0.52299	0.01068	13.44330	0.51222	0.55065	1.91223	0.03905	0.18519	0.00077	-0.00270	2711.82386	45.21724	2711.16872	35.95909	2698.99258	6.84097	-0.47316
64	0.51822	0.01067	13.32627	0.51064	0.57634	1.93003	0.03970	0.18524	0.00097	0.03393	2691.56499	45.28581	2702.79566	36.27699	2699.25190	8.69521	0.28559
65	0.52137	0.01065	13.46298	0.51415	0.42514	1.91818	0.03933	0.18594	0.00093	0.05029	2704.95112	45.14034	2712.50474	36.07368	2705.48289	8.26959	0.01966
66	0.52011	0.01066	13.39950	0.51153	0.50452	1.92291	0.03943	0.18549	0.00089	0.10909	2699.59810	45.20207	2708.04851	36.13820	2701.51432	7.85681	0.07098

	Measured Ratios											Calculated Dates (Ma)						
	$^{206}Pb/^{238}U$	$^{206}Pb/^{238}U$ 2SE	$^{207}Pb/^{235}U$	$^{207}Pb/^{235}U$ 2SE	rho $^{206}Pb/^{238}U$ v $^{207}Pb/^{235}U$		$^{238}U/^{206}Pb$	$^{238}U/^{206}Pb$ 2SE	$^{207}Pb/^{206}Pb$	$^{207}Pb/^{206}Pb$ 2SE	rho $^{207}Pb/^{206}Pb$ v $^{238}U/^{206}Pb$	$^{206}Pb/^{238}U$	$^{206}Pb/^{238}U$ 2SE	$^{207}Pb/^{235}U$	$^{207}Pb/^{235}U$ 2SE	$^{207}Pb/^{206}Pb$	$^{207}Pb/^{206}Pb$ 2SE	% Disc.
Sample 48	**Grain2 Core**																	
67	0.52576	0.01075	13.53430	0.51898	0.39280		1.90218	0.03886	0.18532	0.00110	0.03840	2723.52826	45.40373	2717.42481	36.25480	2699.82292	9.79956	-0.87039
68	0.52900	0.01080	13.63201	0.52422	0.34614		1.89052	0.03863	0.18548	0.00124	0.01953	2737.19442	45.55239	2724.16637	36.48952	2701.18077	11.06738	-1.31571
69	0.52574	0.01076	13.50565	0.51655	0.53388		1.90229	0.03916	0.18484	0.00093	-0.02802	2723.43148	45.50497	2716.54517	33.62082	2695.74897	8.34487	-1.01646
70	0.51502	0.01072	13.28594	0.51056	0.60623		1.94230	0.04002	0.18541	0.00097	0.14250	2677.89519	45.51410	2699.88278	36.39765	2700.72779	8.68425	0.85263
71	0.52559	0.01090	13.49996	0.51744	0.76130		1.90316	0.03975	0.18477	0.00080	-0.04268	2722.74225	46.10443	2715.02617	36.32021	2695.21030	7.16310	-1.01118
72	0.52094	0.01071	13.43821	0.51398	0.64597		1.91992	0.03946	0.18555	0.00086	-0.00710	2703.11129	45.38795	2710.73810	36.22719	2702.13764	7.63167	-0.03602
73	0.51477	0.01060	13.29604	0.50841	0.57299		1.94300	0.03999	0.18559	0.00083	0.14209	2676.87368	45.11534	2700.69629	36.12384	2702.49497	7.32718	0.95714
74	0.50280	0.01036	12.97724	0.49821	0.57623		1.98928	0.04083	0.18583	0.00097	0.02428	2625.72784	44.40810	2677.71195	36.24398	2704.46046	8.58961	2.99851
75	0.51381	0.01068	13.27528	0.50874	0.68129		1.94684	0.04022	0.18577	0.00089	0.14821	2672.75683	45.42408	2699.18019	36.03392	2704.03067	7.88870	1.17010
76	0.51314	0.01052	13.23761	0.50516	0.67600		1.94904	0.03993	0.18546	0.00074	-0.02603	2669.98655	44.82620	2696.57326	36.02517	2701.34019	6.60418	1.17430
77	0.52504	0.01076	13.58233	0.52150	0.31143		1.90489	0.03912	0.18600	0.00121	0.17843	2720.44996	45.49547	2720.74074	36.24104	2705.75371	10.74171	-0.54021
78	0.52764	0.01078	13.60730	0.51847	0.31603		1.89541	0.03851	0.18553	0.00094	0.22714	2731.45528	45.44141	2722.63245	36.00214	2701.86446	8.38873	-1.08334
79	0.51348	0.01051	13.22397	0.50584	0.52936		1.94772	0.03992	0.18506	0.00093	-0.00164	2671.42825	44.77216	2695.55455	36.07918	2697.70082	8.32723	0.98347
80	0.51544	0.01059	13.33774	0.50916	0.71866		1.94040	0.03961	0.18594	0.00073	-0.03632	2679.74909	44.99012	2703.68588	35.89775	2705.64006	6.42354	0.96617
81	0.51430	0.01055	13.32780	0.50927	0.48427		1.94469	0.03969	0.18619	0.00092	0.10740	2674.88986	44.87761	2702.96038	35.99547	2707.77182	8.10549	1.22928
82	0.50472	0.01047	13.01606	0.50111	0.58926		1.98187	0.04086	0.18525	0.00111	0.08378	2633.94819	44.81748	2680.47682	36.44027	2699.22644	9.97571	2.47834
83	0.51519	0.01068	13.27650	0.50868	0.65316		1.94159	0.04053	0.18512	0.00091	0.12237	2678.63984	45.50179	2699.26801	36.34230	2698.22855	8.08265	0.73129
84	0.52242	0.01071	13.48288	0.51577	0.65361		1.91443	0.03897	0.18526	0.00086	-0.04133	2709.38655	45.29399	2713.86988	36.42131	2699.55418	7.68162	-0.36290
85	0.51952	0.01078	13.42196	0.51529	0.79790		1.92541	0.03962	0.18543	0.00074	-0.12733	2697.03477	45.66979	2709.52430	36.21943	2701.10535	6.60616	0.15093
86	0.53028	0.01082	13.69535	0.52154	0.58943		1.88595	0.03821	0.18548	0.00072	-0.00382	2742.60494	45.53071	2729.56920	33.45540	2701.59406	6.43789	-1.49533
87	0.52756	0.01077	13.64976	0.52007	0.41339		1.89569	0.03860	0.18573	0.00085	0.24709	2731.11883	45.43032	2725.58065	36.04449	2703.68669	7.54444	-1.00443
88	0.52542	0.01075	13.58255	0.51878	0.64652		1.90237	0.04169	0.18555	0.00080	-0.04394	2722.07864	45.38132	2720.86197	36.17928	2702.12392	7.16935	-0.73307
89	0.52248	0.01068	13.48599	0.51547	0.57276		1.91416	0.03901	0.18561	0.00095	-0.10187	2709.63660	45.20348	2714.10561	36.19706	2702.59398	8.46286	-0.25991
90	0.52748	0.01087	13.61585	0.52186	0.65843		1.89622	0.03881	0.18540	0.00091	-0.00965	2730.72594	45.82204	2723.10993	36.33028	2700.68764	8.13006	-1.10001
91	0.51224	0.01061	13.22437	0.50619	0.77790		1.95274	0.04033	0.18543	0.00074	-0.00450	2666.07564	45.19746	2695.57362	36.12696	2701.10913	6.61736	1.31405
92	0.51043	0.01056	13.16712	0.50353	0.70529		1.95964	0.04038	0.18525	0.00080	0.11848	2658.36777	45.04090	2691.49190	36.22252	2699.47789	7.12955	1.54644
93	0.50899	0.01053	13.15481	0.50460	0.65692		1.96516	0.04036	0.18561	0.00094	0.05538	2652.23501	44.91420	2690.55139	36.22481	2702.59683	8.35504	1.89884
94	0.51195	0.01070	13.21617	0.50734	0.79150		1.95405	0.04045	0.18541	0.00080	0.05540	2664.81567	45.52972	2694.93421	36.16971	2700.91476	7.10943	1.35466
95	0.51372	0.01064	13.25282	0.50701	0.73632		1.94712	0.04008	0.18531	0.00078	0.08187	2672.38452	45.25890	2697.60867	36.13145	2700.01640	6.92707	1.03398
96	0.51182	0.01062	13.20913	0.50483	0.72360		1.95438	0.04031	0.18539	0.00077	0.18643	2664.29079	45.22352	2694.51123	36.13782	2700.77698	6.85564	1.36945
97	0.50721	0.01076	13.07654	0.50526	0.82611		1.97271	0.04154	0.18516	0.00087	0.01044	2644.50910	45.95329	2684.78052	36.39049	2698.58482	7.77005	2.04483
98	0.50387	0.01057	13.02318	0.50134	0.73472		1.98552	0.04186	0.18570	0.00095	0.10730	2630.24912	45.36222	2681.00104	36.33303	2703.34219	8.42266	2.77894
99	0.51002	0.01099	13.18434	0.51069	0.85549		1.96226	0.04181	0.18576	0.00085	0.11274	2656.42743	46.81934	2692.47968	36.37114	2703.97174	7.57351	1.78978
100	0.51129	0.01089	13.16023	0.50679	0.87927		1.95708	0.04102	0.18526	0.00075	-0.00958	2661.89185	46.30170	2690.86482	36.26260	2699.62887	6.70328	1.41768
101	0.51537	0.01076	13.30850	0.51264	0.80351		1.94107	0.04023	0.18559	0.00086	-0.10774	2679.39092	45.72509	2701.44153	36.28899	2702.43312	7.63091	0.85998
102	0.51908	0.01074	13.37403	0.51032	0.71317		1.92700	0.03951	0.18534	0.00076	0.08743	2695.18124	45.52120	2706.25761	36.03592	2700.30531	6.76801	0.19012
103	0.52340	0.01095	13.49699	0.51890	0.82143		1.91136	0.03962	0.18535	0.00078	-0.02098	2713.44363	46.26951	2714.75706	36.19544	2700.37622	6.93208	-0.48158
104	0.50691	0.01049	13.11485	0.50113	0.79123		1.97327	0.04065	0.18583	0.00064	0.07008	2643.33112	44.84813	2687.75574	36.03755	2704.71562	5.66681	2.32224
105	0.50447	0.01031	13.06029	0.49777	0.42169		1.98252	0.04030	0.18614	0.00088	0.22930	2632.92256	44.14051	2683.87169	35.82340	2707.28608	7.74275	2.82437
106	0.51952	0.01072	13.41190	0.51282	0.78372		1.92529	0.03974	0.18562	0.00070	-0.04531	2697.05302	45.46416	2708.89335	36.00285	2702.87035	6.21886	0.21569
107	0.50526	0.01051	13.03399	0.49853	0.70298		1.97985	0.04123	0.18553	0.00083	0.23856	2636.23764	45.01638	2681.90184	36.22238	2701.91708	7.38826	2.49141

	Measured Ratios											Calculated Dates (Ma)						
	$^{206}Pb/^{238}U$	$^{206}Pb/^{238}U$ 2SE	$^{207}Pb/^{235}U$	$^{207}Pb/^{235}U$ 2SE	rho $^{206}Pb/^{238}U$ v $^{207}Pb/^{235}U$	$^{238}U/^{206}Pb$	$^{238}U/^{206}Pb$ 2SE	$^{207}Pb/^{206}Pb$	$^{207}Pb/^{206}Pb$ 2SE	rho $^{207}Pb/^{206}Pb$ v $^{238}U/^{206}Pb$	$^{206}Pb/^{238}U$	$^{206}Pb/^{238}U$ 2SE	$^{207}Pb/^{235}U$	$^{207}Pb/^{235}U$ 2SE	$^{207}Pb/^{206}Pb$	$^{207}Pb/^{206}Pb$ 2SE	% Disc.
Sample 48	**Grain2 Core**																	
108	0.50627	0.01056	13.05278	0.50449	0.70058	1.97576	0.04125	0.18537	0.00110	-0.05735	2640.57958	45.20251	2683.18261	36.53908	2700.44791	9.78519	2.26724
109	0.50512	0.01037	12.96953	0.49464	0.60446	1.98006	0.04066	0.18471	0.00078	0.16621	2635.70638	44.40347	2677.28370	36.05916	2694.63568	6.99140	2.23581
110	0.46349	0.01179	12.27796	0.60930	0.22806	2.16194	0.05552	0.19065	0.00624	0.25679	2454.28647	51.97635	2622.11064	46.31256	2738.63779	52.91514	11.58591
111	0.50207	0.01045	12.90788	0.49410	0.77585	1.99243	0.04142	0.18515	0.00069	0.14575	2622.57912	44.83884	2672.72333	35.99062	2698.62232	6.19233	2.89956
112	0.51411	0.01065	13.16489	0.50514	0.55677	1.94541	0.04039	0.18415	0.00102	0.16991	2674.08803	45.36286	2691.39702	36.13600	2689.62738	9.13459	0.58111
113	0.51207	0.01062	13.20974	0.50707	0.57930	1.95344	0.04045	0.18571	0.00105	0.17023	2665.33989	45.24593	2694.47057	36.22321	2703.33158	9.29129	1.42540
114	0.52519	0.01072	13.55067	0.51599	0.44701	1.90425	0.03879	0.18592	0.00073	0.22489	2721.12672	45.29300	2718.70085	36.04178	2705.47159	6.52209	-0.57532
115	0.51885	0.01071	13.35528	0.51040	0.67786	1.92780	0.03989	0.18531	0.00081	0.15491	2694.20888	45.47352	2704.90483	36.17404	2700.01833	7.16982	0.21563
116	0.52112	0.01069	13.41031	0.51175	0.52786	1.91926	0.03900	0.18517	0.00087	0.24921	2703.84887	45.21970	2708.81469	36.12072	2698.69384	7.72596	-0.19066
117	0.52506	0.01072	13.49894	0.51532	0.45278	1.90475	0.03898	0.18523	0.00090	0.13107	2720.56936	45.34300	2715.03328	36.09033	2699.19005	8.05186	-0.78584
118	0.51489	0.01063	13.23336	0.50631	0.72176	1.94261	0.04006	0.18515	0.00079	0.03542	2677.38851	45.20965	2696.22404	36.11611	2698.54821	7.07275	0.79031
119	0.51719	0.01058	13.33999	0.50722	0.62019	1.93378	0.03937	0.18585	0.00064	0.26571	2687.19784	44.91613	2703.91863	35.88083	2704.85909	5.71801	0.65724
120	0.51995	0.01066	13.38504	0.51090	0.65758	1.92356	0.03933	0.18551	0.00077	0.05722	2698.91703	45.20564	2707.03202	36.00208	2701.81302	6.86810	0.10730
121	0.52123	0.01067	13.40444	0.51196	0.53645	1.91879	0.03923	0.18535	0.00088	0.09082	2704.34772	45.19537	2708.38405	36.18415	2700.34535	7.82486	-0.14800
122	0.52146	0.01069	13.45190	0.51506	0.54838	1.91798	0.03921	0.18597	0.00097	0.03474	2705.30217	45.25567	2711.67993	36.21509	2705.78839	8.59167	0.01797
123	0.52144	0.01066	13.40967	0.51037	0.48094	1.91798	0.03924	0.18542	0.00075	0.19886	2705.25637	45.16403	2708.82085	36.03682	2700.99900	6.66093	-0.15737
124	0.51988	0.01063	13.37779	0.50989	0.60465	1.92376	0.03927	0.18557	0.00075	0.05746	2698.61412	45.07296	2706.54689	35.93261	2702.34880	6.67552	0.13839
125	0.53439	0.01085	13.74450	0.52241	0.14222	1.87135	0.03804	0.18545	0.00078	0.25304	2759.91727	45.60593	2732.16905	35.99970	2701.30053	6.96895	-2.12386
126	0.51818	0.01063	13.32451	0.50870	0.50553	1.93014	0.03940	0.18546	0.00089	0.20906	2691.38837	45.09633	2702.74254	36.14670	2701.28322	7.93537	0.36765
127	0.52990	0.01077	13.59270	0.51576	0.30093	1.88722	0.03827	0.18494	0.00064	0.32813	2741.02418	45.35629	2721.69430	35.86891	2696.75114	5.74322	-1.61520
128	0.52820	0.01080	13.58889	0.51810	0.35377	1.89344	0.03865	0.18556	0.00089	0.24418	2733.82223	45.55732	2721.34017	36.03569	2702.17802	7.89587	-1.15751
129	0.52795	0.01080	13.58538	0.51792	0.44678	1.89434	0.03858	0.18563	0.00086	0.21777	2732.76169	45.51276	2721.09495	36.10820	2702.77995	7.65889	-1.09712
130	0.51754	0.01064	13.36131	0.50992	0.62428	1.93255	0.03951	0.18625	0.00080	0.15595	2688.68623	45.14386	2705.35845	36.02958	2708.40055	7.10753	0.73323
131	0.52803	0.01081	13.60181	0.51933	0.46011	1.89406	0.03853	0.18586	0.00092	0.16403	2733.11271	45.54214	2722.20939	36.07762	2704.78161	8.11753	-1.03659
132	0.53306	0.01092	13.72874	0.52411	0.37309	1.87622	0.03860	0.18586	0.00096	0.27793	2754.28835	45.96529	2730.99992	36.07462	2704.77839	8.54045	-1.79756
133	0.53293	0.01095	13.73429	0.52387	0.55814	1.87676	0.03861	0.18594	0.00083	0.22331	2753.70071	46.05730	2731.40155	36.17179	2705.60612	7.38525	-1.74654
134	0.53069	0.01097	13.66094	0.52342	0.70898	1.88480	0.03902	0.18556	0.00079	0.01867	2744.27371	46.22432	2726.24883	36.27313	2702.22973	7.03757	-1.53206
135	0.53211	0.01098	13.71578	0.52398	0.63944	1.87975	0.03877	0.18598	0.00083	0.18532	2750.22851	46.19443	2730.09264	36.14459	2705.98330	7.35000	-1.60878
136	0.52898	0.01102	13.60761	0.52066	0.76500	1.89108	0.03935	0.18562	0.00075	0.18328	2737.02682	46.43948	2722.57219	36.12924	2702.78206	6.67832	-1.25117
137	0.52748	0.01087	13.53546	0.51687	0.72318	1.89618	0.03883	0.18509	0.00073	0.04025	2730.74869	45.82335	2717.58549	36.13782	2698.10189	6.49096	-1.19553
138	0.52762	0.01089	13.57351	0.51855	0.74046	1.89571	0.03889	0.18555	0.00073	0.03933	2731.33898	45.89549	2720.22920	36.04016	2702.15586	6.46502	-1.06845
139	0.51503	0.01083	13.26151	0.50979	0.76019	1.94254	0.04054	0.18552	0.00081	0.15181	2677.88725	46.03601	2698.14114	36.16845	2701.91184	7.20607	0.89715
140	0.51500	0.01076	13.26907	0.50957	0.72498	1.94247	0.04024	0.18576	0.00091	0.11220	2677.80391	45.70627	2698.69161	36.32628	2703.94692	8.03370	0.97629
141	0.51723	0.01068	13.34428	0.51090	0.74708	1.93381	0.03981	0.18598	0.00078	-0.05456	2687.33407	45.36709	2704.09354	36.09044	2706.01071	6.95014	0.69499
142	0.51722	0.01069	13.34449	0.51006	0.61869	1.93387	0.03976	0.18599	0.00087	0.19523	2687.29038	45.38425	2704.13589	36.10933	2706.03176	7.71898	0.69741
143	0.51784	0.01067	13.35235	0.51202	0.63067	1.93148	0.03958	0.18546	0.00078	-0.01866	2689.93083	45.27577	2704.63643	35.94101	2701.36000	6.91183	0.42489
144	0.52012	0.01077	13.39517	0.51191	0.66579	1.92311	0.03964	0.18557	0.00082	0.19218	2699.60445	45.61888	2707.71891	36.26045	2702.29051	7.30325	0.09950
145	0.51981	0.01077	13.39385	0.51213	0.59337	1.92430	0.03976	0.18564	0.00091	0.25783	2698.26201	45.66045	2707.61688	36.13560	2702.82797	8.06649	0.16922
146	0.51879	0.01074	13.37945	0.51241	0.59589	1.92805	0.03994	0.18577	0.00095	0.18089	2693.95952	45.59844	2706.57253	36.24691	2703.99516	8.45764	0.37252
147	0.51668	0.01063	13.30870	0.50776	0.52726	1.93578	0.03979	0.18551	0.00085	0.24369	2685.00539	45.17709	2701.63459	36.03481	2701.70895	7.58202	0.62211
148	0.52754	0.01086	13.61031	0.52076	0.62570	1.89593	0.03879	0.18571	0.00088	0.04633	2731.01304	45.78829	2722.76344	36.10657	2703.53294	7.81568	-1.00622

	Measured Ratios											Calculated Dates (Ma)						
	$^{206}Pb/^{238}U$	$^{206}Pb/^{238}U$ 2SE	$^{207}Pb/^{235}U$	$^{207}Pb/^{235}U$ 2SE	rho $^{206}Pb/^{238}U$ v $^{207}Pb/^{235}U$		$^{238}U/^{206}Pb$	$^{238}U/^{206}Pb$ 2SE	$^{207}Pb/^{206}Pb$	$^{207}Pb/^{206}Pb$ 2SE	rho $^{207}Pb/^{206}Pb$ v $^{238}U/^{206}Pb$	$^{206}Pb/^{238}U$	$^{206}Pb/^{238}U$ 2SE	$^{207}Pb/^{235}U$	$^{207}Pb/^{235}U$ 2SE	$^{207}Pb/^{206}Pb$	$^{207}Pb/^{206}Pb$ 2SE	% Disc.
Sample 48	**Grain2 Core**																	
149	0.52124	0.01096	13.43440	0.51517	0.72455		1.91936	0.03980	0.18551	0.00089	0.28228	2704.27370	46.31788	2710.41798	36.15146	2701.73562	7.88104	-0.09385
150	0.52628	0.01094	13.53474	0.51932	0.80513		1.90072	0.03940	0.18507	0.00076	-0.08669	2725.63375	46.19803	2717.44444	36.23750	2697.89051	6.80605	-1.01786
151	0.51205	0.01067	13.22855	0.50904	0.71461		1.95360	0.04045	0.18588	0.00096	0.00825	2665.25212	45.44547	2695.76453	36.42055	2704.95147	8.59703	1.48952
152	0.50806	0.01052	13.09435	0.50065	0.71744		1.96879	0.04068	0.18542	0.00078	0.11109	2648.24212	44.96762	2686.26789	36.04168	2701.00240	6.95246	1.99228
153	0.51207	0.01054	13.18069	0.50170	0.66045		1.95323	0.03998	0.18515	0.00068	0.28070	2665.37239	44.90209	2692.55475	35.94043	2698.64821	6.06958	1.24845
154	0.51480	0.01061	13.26407	0.50837	0.72459		1.94288	0.03990	0.18523	0.00084	-0.12733	2677.01271	45.12506	2698.38011	36.03683	2699.28763	7.47124	0.83208
155	0.51450	0.01063	13.25527	0.50713	0.67957		1.94409	0.03990	0.18519	0.00083	0.08627	2675.72401	45.20710	2697.78371	35.99786	2698.94829	7.39696	0.86796
156	0.50363	0.01044	12.99705	0.49760	0.65776		1.98615	0.04115	0.18541	0.00089	0.16158	2629.26543	44.76779	2679.20845	36.09132	2700.82896	7.89045	2.72181
157	0.51731	0.01086	13.37085	0.51357	0.78608		1.93392	0.04031	0.18548	0.00073	0.10905	2687.57957	46.07080	2705.91207	36.11390	2701.58536	6.50398	0.52113
158	0.51756	0.01073	13.38554	0.51318	0.76229		1.93268	0.03993	0.18576	0.00080	-0.04340	2688.70987	45.56380	2706.98353	36.17955	2703.98873	7.11520	0.56826
159	0.51446	0.01073	13.32255	0.51181	0.82301		1.94448	0.04041	0.18597	0.00077	-0.09239	2675.51197	45.65248	2702.48417	36.21839	2705.88077	6.81189	1.13506
160	0.52960	0.01089	13.69415	0.52227	0.66774		1.88853	0.03861	0.18565	0.00074	0.12667	2739.71723	45.85763	2728.63204	36.11662	2703.05734	6.53903	-1.33809
161	0.51625	0.01076	13.32420	0.50951	0.67931		1.93770	0.04047	0.18530	0.00085	0.30915	2683.14485	45.76652	2702.69289	36.18685	2699.92440	7.57160	0.62537
162	0.52040	0.01078	13.43812	0.51291	0.73701		1.92210	0.03952	0.18525	0.00067	0.22788	2700.79320	45.65495	2710.77006	35.96927	2699.51847	5.97367	-0.04720
163	0.52005	0.01076	13.41858	0.51260	0.72014		1.92339	0.03938	0.18523	0.00075	0.14426	2699.28441	45.53972	2709.37773	36.07144	2699.35289	6.68189	0.00254
164	0.51947	0.01064	13.41051	0.51125	0.58445		1.92529	0.03920	0.18528	0.00077	0.09929	2696.86956	45.07598	2708.84874	35.90165	2699.75668	6.86961	0.10705
165	0.51925	0.01072	13.41256	0.51280	0.77928		1.92630	0.03964	0.18541	0.00071	-0.03527	2695.91822	45.45903	2708.93667	36.20593	2700.92079	6.34401	0.18556
166	0.51763	0.01070	13.37605	0.51116	0.69684		1.93235	0.03965	0.18550	0.00078	0.15320	2689.03689	45.39985	2706.37517	35.99489	2701.74640	6.99877	0.47264
167	0.51715	0.01065	13.36304	0.50977	0.73205		1.93405	0.03952	0.18551	0.00069	0.10335	2687.01981	45.18398	2705.48802	36.08771	2701.81744	6.17072	0.55071
168	0.51616	0.01063	13.36271	0.51075	0.64658		1.93778	0.03948	0.18584	0.00084	0.12732	2682.81060	45.12478	2705.42442	36.19885	2704.72924	7.43669	0.81700
169	0.51441	0.01064	13.29104	0.50796	0.73218		1.94450	0.03998	0.18575	0.00080	0.05234	2675.32027	45.24444	2700.34814	36.01465	2703.88158	7.12803	1.06758
170	0.51315	0.01064	13.26391	0.50630	0.73002		1.94935	0.04025	0.18542	0.00078	0.18535	2669.94489	45.30080	2698.44188	36.03404	2701.03363	6.94556	1.16440
171	0.51471	0.01056	13.31295	0.50953	0.57785		1.94316	0.03947	0.18581	0.00093	0.06139	2676.65866	44.85264	2701.87505	36.14712	2704.39993	8.27257	1.03641
172	0.51518	0.01057	13.27038	0.50631	0.79126		1.94142	0.03968	0.18511	0.00064	-0.07871	2678.62551	44.92329	2698.91103	36.04133	2698.28633	5.70333	0.73399
173	0.51705	0.01059	13.33092	0.50840	0.63435		1.93439	0.03970	0.18533	0.00076	0.15174	2686.57279	45.02411	2703.21778	36.07917	2700.19671	6.80074	0.50711
174	0.51799	0.01051	13.38187	0.50838	0.52600		1.92973	0.04318	0.18578	0.00069	0.14343	2690.63792	44.59587	2706.89458	35.93882	2704.24762	6.14035	0.50582
175	0.51492	0.01058	13.28919	0.50699	0.76938		1.94246	0.03946	0.18578	0.00072	0.04991	2677.50353	44.92346	2700.25313	36.01565	2704.24952	6.40843	0.99892
176	0.51494	0.01053	13.25618	0.50505	0.75510		1.94228	0.03932	0.18568	0.00068	0.03344	2677.62935	44.71464	2697.92865	35.72168	2703.38880	5.98998	0.96202
177	0.52747	0.01088	13.59319	0.51921	0.73763		1.89634	0.03855	0.18577	0.00068	0.17669	2730.67687	45.79145	2721.60673	35.84182	2704.18451	5.99194	-0.97018
178	0.52754	0.01076	13.57677	0.51868	0.74074		1.89586	0.03820	0.18553	0.00073	0.00858	2731.01937	45.30649	2720.45596	36.03306	2701.97638	6.48027	-1.06345
179	0.52895	0.01098	13.58742	0.52047	0.73997		1.89118	0.03884	0.18547	0.00074	0.17397	2736.90143	46.21761	2721.15138	36.02724	2701.42205	6.61108	-1.29633
180	0.52946	0.01103	13.55924	0.52085	0.81119		1.88947	0.03885	0.18523	0.00077	0.00865	2739.00562	46.36994	2719.13136	36.00980	2699.33132	6.89037	-1.44849
181	0.52717	0.01091	13.50221	0.51800	0.74646		1.89752	0.03878	0.18542	0.00084	0.04280	2729.38862	45.94948	2715.16890	36.10483	2700.96199	7.45690	-1.04150
182	0.52701	0.01075	13.48420	0.51417	0.75752		1.89777	0.03854	0.18535	0.00065	-0.03049	2728.80299	45.34873	2714.02367	35.95886	2700.40580	5.82344	-1.04065
183	0.51945	0.01074	13.26503	0.50711	0.74465		1.92569	0.03972	0.18538	0.00075	0.19018	2696.74799	45.53886	2698.49143	36.18072	2700.69693	6.71205	0.14643
184	0.51594	0.01076	13.14663	0.50340	0.81087		1.93900	0.04040	0.18517	0.00072	0.21050	2681.78730	45.76279	2690.00283	36.11817	2698.84100	6.40017	0.63591
185	0.52005	0.01084	13.27312	0.50873	0.78836		1.92365	0.03976	0.18559	0.00077	0.16617	2699.25526	45.90660	2699.01798	36.20533	2702.50835	6.88164	0.12052
186	0.51538	0.01088	13.10724	0.50363	0.84233		1.94142	0.04085	0.18512	0.00074	0.21275	2679.34226	46.26912	2687.10113	36.20289	2698.38793	6.62958	0.71083
187	0.51672	0.01087	13.14210	0.50618	0.89556		1.93627	0.04038	0.18528	0.00066	-0.08921	2685.05270	46.13483	2689.56789	36.16701	2699.83689	5.87857	0.55061
188	0.51611	0.01087	13.14074	0.50509	0.90587		1.93861	0.04054	0.18564	0.00061	0.02901	2682.44402	46.16223	2689.50311	36.15451	2703.05991	5.39041	0.76855
189	0.51556	0.01084	13.10556	0.50356	0.89976		1.94060	0.04058	0.18549	0.00061	0.00347	2680.14755	46.05168	2686.98089	36.13466	2701.71671	5.46008	0.80478

	Measured Ratios											Calculated Dates (Ma)						
	$^{206}Pb/^{238}U$	$^{206}Pb/^{238}U$ 2SE	$^{207}Pb/^{235}U$	$^{207}Pb/^{235}U$ 2SE	rho $^{206}Pb/^{238}U$ v $^{207}Pb/^{235}U$		$^{238}U/^{206}Pb$	$^{238}U/^{206}Pb$ 2SE	$^{207}Pb/^{206}Pb$	$^{207}Pb/^{206}Pb$ 2SE	rho $^{207}Pb/^{206}Pb$ v $^{238}U/^{206}Pb$	$^{206}Pb/^{238}U$	$^{206}Pb/^{238}U$ 2SE	$^{207}Pb/^{235}U$	$^{207}Pb/^{235}U$ 2SE	$^{207}Pb/^{206}Pb$	$^{207}Pb/^{206}Pb$ 2SE	% Disc.
Sample 48	**Grain2 Core**																	
190	0.51779	0.01080	13.15035	0.50464	0.82799		1.93208	0.04012	0.18543	0.00074	0.05329	2689.63948	45.85072	2690.22396	36.17250	2701.11781	6.55683	0.42676
191	0.51794	0.01075	13.11586	0.50119	0.83021		1.93137	0.04018	0.18491	0.00060	0.16828	2690.31646	45.68157	2687.83006	36.09312	2697.52087	5.82791	0.26779
192	0.51723	0.01078	13.12310	0.50238	0.83343		1.93412	0.04015	0.18549	0.00067	0.12501	2687.26480	45.75794	2688.31333	36.09122	2701.64017	5.98161	0.53494
193	0.52041	0.01074	13.19655	0.50344	0.76942		1.92203	0.03967	0.18548	0.00066	0.16911	2700.83558	45.52327	2693.64918	35.97754	2701.61018	5.90952	0.02868
194	0.51954	0.01071	13.17955	0.50233	0.64374		1.92522	0.03928	0.18564	0.00076	0.32435	2697.15383	45.35571	2692.44782	35.91443	2702.93912	6.75449	0.21450
195	0.53270	0.01087	13.49951	0.51438	0.47080		1.87736	0.03827	0.18543	0.00081	0.08146	2752.78348	45.69519	2715.10833	36.21786	2701.03389	7.23502	-1.87990
196	0.53624	0.01096	13.59791	0.51736	0.57316		1.86497	0.03783	0.18561	0.00069	0.05532	2767.66866	45.91275	2722.00511	35.97880	2702.78286	6.13573	-2.34442
197	0.56014	0.01174	14.32173	0.55576	0.80065		1.78539	0.03726	0.18664	0.00103	-0.30439	2867.16479	48.46760	2771.18114	36.86358	2712.01329	9.15388	-5.41132
198	0.51804	0.01056	12.86161	0.48943	0.44951		1.93048	0.03924	0.18156	0.00079	0.04860	2690.82360	44.80953	2669.45141	35.69069	2666.19906	7.15811	-0.91513
199	0.53522	0.01103	13.54861	0.51651	0.71687		1.86871	0.03835	0.18511	0.00068	0.07937	2763.34264	46.27043	2718.53511	36.06919	2698.25489	6.08341	-2.35540
200	0.53648	0.01105	13.61647	0.51972	0.69433		1.86433	0.03820	0.18536	0.00068	0.02617	2768.61079	46.32786	2723.23456	36.06458	2700.53471	6.03396	-2.45885
201	0.53604	0.01112	13.59209	0.51960	0.83053		1.86599	0.03842	0.18526	0.00064	-0.04149	2766.76783	46.60346	2721.51349	36.04278	2699.61250	5.72426	-2.42721
202	0.53996	0.01127	13.69115	0.52463	0.84008		1.85261	0.03850	0.18512	0.00068	-0.02495	2783.14671	47.12614	2728.33751	36.25155	2698.34516	6.10809	-3.04697
203	0.53797	0.01118	13.68049	0.52338	0.72539		1.85936	0.03837	0.18557	0.00079	0.11760	2774.83192	46.79040	2727.62872	36.03025	2702.28854	7.01241	-2.61433
204	0.53971	0.01119	13.72193	0.52541	0.75197		1.85331	0.03806	0.18543	0.00078	-0.02573	2782.12562	46.76512	2730.47308	36.24039	2702.33785	6.50765	-2.86787
205	0.53597	0.01113	13.62898	0.52087	0.79745		1.86629	0.03842	0.18536	0.00068	0.04822	2766.43177	46.64339	2724.08193	36.14005	2700.50911	6.06057	-2.38295
206	0.53591	0.01109	13.63676	0.51951	0.83228		1.86639	0.03843	0.18527	0.00050	0.09570	2766.20798	46.48961	2724.68259	35.91918	2700.64413	4.05068	-2.37017
207	0.52710	0.01094	13.44183	0.51290	0.83513		1.89768	0.03915	0.18563	0.00058	0.10854	2729.10597	46.14194	2711.03714	35.87700	2703.01411	5.18546	-0.95606
208	0.51781	0.01101	13.19207	0.50734	0.86792		1.93235	0.04078	0.18535	0.00071	0.16320	2689.65058	46.70829	2693.17675	36.23889	2700.42116	6.29816	0.40045
209	0.51653	0.01091	13.18871	0.50678	0.88190		1.93695	0.04058	0.18564	0.00066	0.04030	2684.27546	46.32579	2692.94699	36.21999	2703.01460	5.85627	0.69811
210	0.51808	0.01075	13.20758	0.50500	0.78456		1.93068	0.03990	0.18524	0.00070	0.00747	2690.94693	45.60992	2694.39605	36.03069	2699.45609	6.25515	0.31621
211	0.51944	0.01079	13.27726	0.50836	0.76360		1.92566	0.03961	0.18562	0.00077	-0.00508	2696.70405	45.68576	2699.33419	36.03568	2702.80301	6.82234	0.22616
212	0.51728	0.01079	13.20514	0.50529	0.85684		1.93384	0.03997	0.18528	0.00063	0.01714	2687.49336	45.77793	2694.20259	36.09697	2699.81156	5.57999	0.45835
213	0.51621	0.01069	13.16663	0.50131	0.80472		1.93763	0.03961	0.18503	0.00057	0.26194	2683.01713	45.35077	2691.54210	35.89233	2697.66210	5.12806	0.54584
214	0.51383	0.01062	13.11843	0.50060	0.75627		1.94657	0.03997	0.18511	0.00068	0.06809	2672.89400	45.18800	2688.04212	35.89921	2698.33340	6.01803	0.95176
215	0.52593	0.01085	13.48400	0.51382	0.76807		1.90177	0.03897	0.18559	0.00063	0.13333	2724.19851	45.79844	2714.02473	35.98474	2702.63657	5.55176	-0.79150
216	0.51174	0.01068	13.11928	0.50191	0.81225		1.95480	0.04098	0.18552	0.00069	0.13797	2663.93826	45.57063	2688.04957	36.23123	2701.93448	6.17070	1.42632
217	0.51946	0.01066	13.32753	0.50982	0.58797		1.92533	0.03916	0.18557	0.00090	-0.01280	2696.84412	45.16418	2702.92256	36.16447	2702.28697	8.01186	0.20182
218	0.52535	0.01074	13.41854	0.51087	0.38531		1.90367	0.03884	0.18472	0.00082	0.24527	2721.79716	45.37529	2709.43885	36.00131	2694.72091	7.33119	-0.99479
219	0.52518	0.01072	13.44887	0.51202	0.49364		1.90424	0.03878	0.18513	0.00075	0.08785	2721.09229	45.28999	2711.57549	35.94569	2698.41764	6.69086	-0.83329
220	0.52497	0.01074	13.47883	0.51375	0.50612		1.90506	0.03874	0.18560	0.00081	0.15206	2720.20010	45.35806	2713.65531	35.91052	2702.56219	7.23824	-0.64841
221	0.52295	0.01066	13.44620	0.51190	0.49498		1.91238	0.03885	0.18578	0.00076	0.12202	2711.63173	45.10345	2711.38646	36.00229	2704.23522	6.73947	-0.27277
222	0.52615	0.01079	13.50926	0.51352	0.69576		1.90087	0.03886	0.18553	0.00057	0.13754	2725.15658	45.53794	2715.83848	35.96157	2702.07626	5.07810	-0.84694
223	0.52766	0.01085	13.53665	0.51603	0.75669		1.89550	0.03856	0.18543	0.00065	0.07694	2731.52624	45.70272	2717.69841	36.03972	2701.11737	5.79594	-1.11326
224	0.52481	0.01094	13.44931	0.51468	0.85247		1.90613	0.03936	0.18531	0.00069	0.06222	2719.40423	46.15493	2711.50588	36.10811	2700.03696	6.18015	-0.71219
225	0.53021	0.01103	13.56813	0.51963	0.77884		1.88665	0.03852	0.18502	0.00075	0.08902	2742.22576	46.31571	2719.81120	36.06899	2697.44087	6.69378	-1.63316
226	0.52648	0.01085	13.50222	0.51615	0.71762		1.89981	0.03880	0.18532	0.00072	0.04015	2726.53678	45.73771	2715.23783	35.99304	2701.33036	6.90116	-0.92448
227	0.53314	0.01106	13.66971	0.52354	0.72691		1.87627	0.03858	0.18541	0.00082	0.11921	2754.53346	46.42513	2726.85594	36.24104	2700.85487	7.29899	-1.94874
228	0.53031	0.01091	13.61951	0.52073	0.79712		1.88608	0.03852	0.18579	0.00069	-0.12179	2742.68222	45.90382	2723.41315	36.15453	2704.31562	6.14400	-1.39887
229	0.52753	0.01084	13.52185	0.51541	0.74485		1.89600	0.03869	0.18552	0.00066	0.14089	2730.95844	45.70392	2716.66877	36.09116	2701.93136	5.87169	-1.06289
230	0.52362	0.01084	13.44220	0.51339	0.77261		1.91035	0.03977	0.18582	0.00069	0.19414	2714.40260	45.91783	2711.04380	36.13298	2704.62540	6.14626	-0.36020

	Measured Ratios											Calculated Dates (Ma)						
	$^{206}Pb/^{238}U$	$^{206}Pb/^{238}U$ 2SE	$^{207}Pb/^{235}U$	$^{207}Pb/^{235}U$ 2SE	rho $^{206}Pb/^{238}U$ v $^{207}Pb/^{235}U$	$^{238}U/^{206}Pb$	$^{238}U/^{206}Pb$ 2SE	$^{207}Pb/^{206}Pb$	$^{207}Pb/^{206}Pb$ 2SE	rho $^{207}Pb/^{206}Pb$ v $^{238}U/^{206}Pb$	$^{206}Pb/^{238}U$	$^{206}Pb/^{238}U$ 2SE	$^{207}Pb/^{235}U$	$^{207}Pb/^{235}U$ 2SE	$^{207}Pb/^{206}Pb$	$^{207}Pb/^{206}Pb$ 2SE	% Disc.
Sample 48	**Grain2 Core**																	
231	0.51020	0.01064	13.04857	0.50052	0.82000	1.96077	0.04092	0.18505	0.00068	0.04673	2657.34472	45.43007	2682.90626	36.24748	2697.79614	6.04864	1.52225
232	0.51790	0.01069	13.23817	0.50733	0.71618	1.93136	0.04006	0.18502	0.00084	0.08891	2690.18688	45.43296	2696.53647	36.09356	2697.38945	7.52950	0.26773
233	0.51933	0.01073	13.23990	0.50702	0.80811	1.92609	0.03980	0.18481	0.00071	-0.09934	2696.22678	45.50778	2696.66869	36.12894	2695.59978	6.35376	-0.02325
234	0.52837	0.01075	13.49076	0.51233	0.62915	1.89283	0.03845	0.18534	0.00062	0.22049	2734.52893	45.32034	2714.56200	36.01679	2700.37507	5.50700	-1.24899
235	0.50609	0.01073	12.86570	0.49601	0.90772	1.97715	0.04194	0.18480	0.00064	-0.03126	2639.67475	45.92875	2669.50616	36.36063	2695.56689	5.75771	2.11739
236	0.51337	0.01065	13.08260	0.50012	0.81492	1.94856	0.04042	0.18535	0.00067	0.17163	2670.89270	45.37653	2685.42539	35.89572	2700.42243	5.95829	1.10561
237	0.51616	0.01057	13.14339	0.50265	0.61403	1.93773	0.03969	0.18535	0.00087	0.06436	2682.80807	44.92619	2689.78964	36.17101	2700.34745	7.71267	0.65377
238	0.51842	0.01077	13.22008	0.50651	0.81812	1.92965	0.04007	0.18578	0.00071	0.05535	2692.32074	45.72614	2695.24619	36.12401	2704.24301	6.30334	0.44283
239	0.51829	0.01070	13.19726	0.50444	0.80359	1.92995	0.03980	0.18566	0.00068	0.05373	2691.83159	45.42666	2693.65995	36.16031	2703.19460	6.02677	0.42213
240	0.52318	0.01084	13.25525	0.50763	0.75286	1.91201	0.03973	0.18484	0.00079	0.10035	2712.52186	45.88399	2697.76099	36.24127	2695.81401	7.04958	-0.61595
241	0.53162	0.01075	13.51296	0.51388	0.42926	1.88110	0.03800	0.18559	0.00072	-0.01087	2748.26410	45.24088	2716.09069	35.86302	2702.53742	6.37237	-1.66384
242	0.52370	0.01064	13.31948	0.50681	0.38791	1.90969	0.03907	0.18586	0.00080	0.30790	2714.80600	45.08368	2702.45222	35.98772	2704.88825	7.11985	-0.36532
243	0.53373	0.01100	13.54368	0.51785	0.79171	1.87411	0.03892	0.18540	0.00068	0.11113	2757.03643	46.30931	2718.13133	36.15245	2700.84662	6.09729	-2.03805
244	0.53603	0.01102	13.58953	0.51906	0.69639	1.86598	0.03828	0.18549	0.00076	0.12148	2766.72433	46.23767	2721.34742	36.15271	2701.65210	6.77135	-2.35196
245	0.52652	0.01098	13.26993	0.50856	0.75855	1.89800	0.04172	0.18434	0.00083	0.28128	2726.61966	46.20145	2698.79969	35.93958	2691.27969	7.43081	-1.29611
246	0.53542	0.01105	13.53335	0.51896	0.77051	1.86819	0.03817	0.18498	0.00079	0.01870	2764.12602	46.29627	2717.35565	36.05157	2697.09753	7.09960	-2.42494
247	0.53334	0.01093	13.49247	0.51425	0.72207	1.87531	0.03824	0.18544	0.00067	0.12727	2755.44075	45.92681	2714.61378	36.05098	2701.24637	5.95217	-1.96681
248	0.51756	0.01049	12.80006	0.48691	0.34521	1.93221	0.03912	0.18134	0.00077	0.03632	2688.80097	44.56479	2664.93879	35.88627	2664.16884	7.03886	-0.91610
249	0.53085	0.01106	13.37588	0.51370	0.72837	1.88444	0.03886	0.18483	0.00090	0.10237	2744.90463	46.50040	2706.26785	36.27479	2695.62637	8.00941	-1.79526
250	0.53528	0.01128	13.49474	0.51991	0.83493	1.86913	0.03897	0.18498	0.00080	0.01962	2763.45993	47.28147	2714.56345	36.27665	2697.05967	7.13912	-2.40279
251	0.52914	0.01113	13.21795	0.50995	0.83329	1.89074	0.03889	0.18333	0.00083	-0.07427	2737.64822	46.73821	2694.96694	36.25065	2682.21361	7.48043	-2.02490
252	0.54139	0.01113	13.66236	0.52106	0.51841	1.84744	0.03790	0.18526	0.00086	0.28626	2789.18957	46.53746	2726.43435	36.19113	2699.50205	7.64912	-3.21554
253	0.53717	0.01101	13.53112	0.51382	0.60443	1.86186	0.03829	0.18506	0.00064	0.35599	2771.53836	46.20548	2717.38696	35.99334	2697.84377	5.70405	-2.65898
254	0.52400	0.01090	13.25897	0.50763	0.71704	1.90895	0.03922	0.18561	0.00079	0.20889	2716.01034	45.99842	2698.03425	36.00102	2702.71801	7.00173	-0.48941
255	0.52450	0.01081	13.24097	0.50484	0.60931	1.90693	0.03915	0.18484	0.00077	0.19713	2718.15803	45.68300	2696.83111	36.10600	2695.80423	6.95634	-0.82239
256	0.51489	0.01104	13.04869	0.50277	0.81045	1.94352	0.04155	0.18543	0.00088	0.26847	2677.21833	46.95879	2682.82437	36.27220	2701.02395	7.80941	0.88919
257	0.51219	0.01110	13.01454	0.50264	0.83841	1.95406	0.04227	0.18578	0.00087	0.30069	2665.65350	47.29700	2680.30944	36.25045	2704.09501	7.70743	1.44210
258	0.50788	0.01070	12.85502	0.49174	0.57201	1.96986	0.04133	0.18493	0.00102	0.47046	2647.39255	45.70950	2668.87416	35.85795	2696.45932	9.06575	1.85340
259	0.51346	0.01120	13.02855	0.50559	0.88954	1.94939	0.04254	0.18519	0.00080	0.12103	2671.03143	47.71559	2681.23440	36.65861	2698.94847	7.07616	1.04518
260	0.51289	0.01102	13.00450	0.50434	0.87901	1.95116	0.04198	0.18487	0.00081	-0.07632	2668.67289	46.96430	2679.49773	36.54635	2696.04523	7.22132	1.02569
261	0.50473	0.01089	12.88492	0.49755	0.87396	1.98277	0.04254	0.18597	0.00078	0.17596	2633.81184	46.59646	2670.88206	36.39273	2705.92958	6.88870	2.73815
262	0.51344	0.01115	13.08570	0.50843	0.88072	1.94931	0.04217	0.18544	0.00082	0.01034	2670.97894	47.44318	2685.34102	36.55913	2701.17598	7.28384	1.13056
263	0.51720	0.01089	13.23624	0.50856	0.74369	1.93434	0.04072	0.18604	0.00090	0.15212	2687.12717	46.27445	2696.34472	36.17941	2706.44040	7.95280	0.71873
264	0.51614	0.01077	13.17304	0.50648	0.66579	1.93807	0.04053	0.18511	0.00092	0.04150	2682.66390	45.80570	2691.81236	36.33671	2698.14543	8.26159	0.57710
265	0.51358	0.01069	13.12419	0.50153	0.59064	1.94764	0.04055	0.18539	0.00090	0.28686	2671.80139	45.53200	2688.42529	36.10748	2700.61839	7.98542	1.07856
266	0.52307	0.01073	13.40047	0.50942	0.28646	1.91183	0.03925	0.18567	0.00074	0.12465	2712.19195	45.41371	2708.19648	35.96621	2703.25443	6.54355	-0.32953
267	0.51792	0.01070	13.21190	0.50337	0.77564	1.93115	0.03952	0.18477	0.00060	-0.05987	2690.26827	45.38174	2694.76926	35.86262	2695.30821	5.35116	0.18734
268	0.51924	0.01068	13.27695	0.50484	0.49480	1.92608	0.03948	0.18499	0.00071	0.23061	2695.90366	45.29065	2699.44509	35.90274	2697.23024	6.29437	0.04921
269	0.52504	0.01086	13.49917	0.51571	0.60585	1.90497	0.03912	0.18560	0.00087	0.28338	2720.46172	45.84425	2715.03685	35.98634	2702.53308	7.70736	-0.65903
270	0.52883	0.01112	13.62446	0.52404	0.77615	1.89175	0.03944	0.18605	0.00087	0.04653	2736.36731	46.81214	2723.64532	36.41707	2706.51933	7.72091	-1.09079
271	0.52087	0.01065	13.36810	0.50834	0.36676	1.91994	0.03925	0.18522	0.00074	0.11305	2702.86022	45.13930	2705.90561	35.86584	2699.20940	6.61854	-0.13507

	Measured Ratios											Calculated Dates (Ma)						
	$^{206}Pb/^{238}U$	$^{206}Pb/^{238}U$ 2SE	$^{207}Pb/^{235}U$	$^{207}Pb/^{235}U$ 2SE	rho $^{206}Pb/^{238}U$ v $^{207}Pb/^{235}U$		$^{238}U/^{206}Pb$	$^{238}U/^{206}Pb$ 2SE	$^{207}Pb/^{206}Pb$	$^{207}Pb/^{206}Pb$ 2SE	rho $^{207}Pb/^{206}Pb$ v $^{238}U/^{206}Pb$	$^{206}Pb/^{238}U$	$^{206}Pb/^{238}U$ 2SE	$^{207}Pb/^{235}U$	$^{207}Pb/^{235}U$ 2SE	$^{207}Pb/^{206}Pb$	$^{207}Pb/^{206}Pb$ 2SE	% Disc.
Sample 48	**Grain2 Core**																	
272	0.51496	0.01055	13.22201	0.50383	0.55834		1.94204	0.03974	0.18517	0.00077	-0.01473	2677.75357	44.89479	2695.48700	36.02072	2698.80104	6.89112	0.78601
273	0.51721	0.01062	13.30543	0.50833	0.58667		1.93365	0.03958	0.18539	0.00086	-0.02484	2687.30851	45.09936	2701.37988	36.04320	2700.67985	7.59872	0.49757
274	0.51442	0.01062	13.27009	0.50800	0.55035		1.94436	0.04004	0.18571	0.00096	0.17324	2675.40383	45.19538	2698.82258	36.07262	2703.45980	8.55892	1.04866
275	0.51937	0.01065	13.36623	0.50974	0.50741		1.92567	0.03920	0.18526	0.00084	0.17140	2696.44395	45.10993	2705.71870	36.18601	2699.54166	7.51909	0.11488
276	0.52550	0.01070	13.55149	0.51549	0.15085		1.90306	0.03861	0.18563	0.00085	0.34422	2722.42987	45.18982	2718.77457	35.99056	2702.81364	7.50487	-0.72054
277	0.52019	0.01077	13.37575	0.51180	0.75486		1.92289	0.03971	0.18504	0.00076	0.05954	2699.89894	45.65851	2706.32559	36.17033	2697.61616	6.75687	-0.08455
278	0.51766	0.01088	13.30339	0.51028	0.85474		1.93268	0.04013	0.18497	0.00068	0.15084	2689.06462	46.12931	2701.15585	36.14108	2697.04180	6.08379	0.29665
279	0.51095	0.01061	13.16527	0.50485	0.71826		1.95777	0.04047	0.18549	0.00087	0.07339	2660.54878	45.21577	2691.30604	36.32716	2701.55906	7.74344	1.54142
280	0.50671	0.01052	13.03180	0.50042	0.66928		1.97414	0.04059	0.18518	0.00097	0.10161	2642.45543	44.94688	2681.66718	36.30045	2698.74312	8.61121	2.13013
281	0.50753	0.01058	13.04910	0.50149	0.79171		1.97105	0.04083	0.18515	0.00082	-0.01317	2645.94818	45.20882	2682.90999	36.16027	2698.55678	7.29604	1.98827
282	0.52140	0.01078	13.42503	0.51359	0.77595		1.91843	0.03935	0.18548	0.00073	0.02897	2705.00586	45.60395	2709.80504	36.04469	2701.56145	6.47640	-0.12733
283	0.52114	0.01072	13.40050	0.51183	0.68174		1.91927	0.03931	0.18531	0.00078	0.10709	2703.93068	45.38389	2708.10581	36.19436	2700.05108	6.93955	-0.14348
284	0.52648	0.01108	13.52925	0.52055	0.80900		1.90036	0.03975	0.18527	0.00082	0.10276	2726.41659	46.75002	2717.00252	36.36041	2699.60219	7.34116	-0.98350
285	0.50997	0.01083	13.09830	0.50533	0.90187		1.96211	0.04127	0.18525	0.00067	-0.03416	2656.27610	46.15390	2686.37893	36.32667	2699.56871	5.99696	1.62982
286	0.51748	0.01078	13.31102	0.50970	0.71347		1.93314	0.03972	0.18564	0.00085	0.23659	2688.35035	45.69697	2701.73365	36.08577	2702.88625	7.50257	0.54070
287	0.52154	0.01089	13.39645	0.51527	0.85039		1.91814	0.03957	0.18539	0.00074	-0.12316	2705.57274	46.02598	2707.68668	36.23126	2700.72225	6.58508	-0.17928
288	0.51429	0.01079	13.20547	0.50997	0.77342		1.94530	0.04009	0.18543	0.00096	-0.01869	2674.76479	45.79848	2694.04998	36.25019	2700.91442	8.58285	0.97764
289	0.52027	0.01070	13.34212	0.51035	0.60062		1.92248	0.03909	0.18531	0.00090	0.15700	2700.25967	45.29395	2703.95459	36.03137	2699.88844	8.00396	-0.01375
290	0.51612	0.01060	13.23371	0.50403	0.49352		1.93793	0.03977	0.18548	0.00084	0.40878	2682.61505	45.06604	2696.33366	36.10693	2701.46168	7.45536	0.70255
291	0.52286	0.01065	13.39369	0.50889	0.43294		1.91278	0.03888	0.18505	0.00070	0.34568	2711.23741	45.07221	2707.72713	35.88735	2698.96099	6.72439	-0.45280
292	0.52694	0.01078	13.48276	0.51370	0.74154		1.89806	0.03876	0.18522	0.00063	0.04844	2728.46735	45.49701	2713.93812	35.91903	2699.26579	5.65026	-1.07026
293	0.50809	0.01098	12.98604	0.50460	0.83565		1.96984	0.04247	0.18526	0.00096	0.07476	2648.15073	46.90022	2678.11594	36.82310	2699.42209	8.50158	1.93612
294	0.52925	0.01076	13.57592	0.51679	0.28113		1.88960	0.03850	0.18600	0.00084	0.27494	2738.26420	45.38076	2720.46528	35.95474	2706.07234	7.40702	-1.17563
295	0.53585	0.01092	13.71541	0.52144	0.31929		1.86636	0.03818	0.18566	0.00078	0.37500	2766.02306	45.84989	2730.16096	35.99124	2703.14283	6.96474	-2.27331
296	0.52307	0.01076	13.38415	0.50970	0.69616		1.91218	0.03919	0.18578	0.00064	0.29338	2712.12694	45.52728	2707.00956	36.00251	2704.29506	5.64219	-0.28877
297	0.53053	0.01107	13.56345	0.52063	0.83745		1.88564	0.03885	0.18554	0.00072	-0.03006	2743.52164	46.51980	2719.43661	36.20402	2702.08338	6.45564	-1.51040
298	0.52754	0.01113	13.46467	0.51848	0.84268		1.89657	0.03954	0.18524	0.00077	0.04936	2730.88350	46.86334	2712.46616	36.18249	2699.37767	6.89037	-1.15369
299	0.52719	0.01126	13.44303	0.52005	0.85409		1.89814	0.03982	0.18511	0.00083	0.04258	2729.32998	47.37311	2710.85641	36.28726	2698.16007	7.39287	-1.14204
300	0.52358	0.01116	13.38315	0.51668	0.88887		1.91117	0.04029	0.18544	0.00065	0.03758	2714.11169	47.12648	2706.67725	36.23637	2701.23054	5.73167	-0.47460
301	0.51982	0.01108	13.26648	0.51080	0.83008		1.92500	0.04098	0.18538	0.00081	0.23606	2698.15914	46.97930	2698.46405	36.28198	2700.60485	7.24988	0.09064
302	0.52215	0.01097	13.31660	0.51095	0.83116		1.91602	0.03989	0.18528	0.00073	0.13843	2708.12118	46.36832	2702.09169	36.09343	2699.82267	6.46608	-0.30643
303	0.52209	0.01092	13.31551	0.51058	0.82317		1.91616	0.03979	0.18532	0.00072	0.08839	2707.87905	46.17800	2702.02218	36.09879	2700.17100	6.41138	-0.28465
304	0.52677	0.01085	13.43894	0.51302	0.76865		1.89878	0.03886	0.18538	0.00067	0.03530	2727.73229	45.75672	2710.82488	35.96897	2700.71189	5.97082	-0.99058
305	0.52600	0.01087	13.39985	0.51352	0.66822		1.90162	0.03903	0.18515	0.00089	0.07299	2724.48091	45.87077	2708.00032	36.20077	2698.51028	7.95856	-0.95323
306	0.52778	0.01148	13.53795	0.53256	0.91576		1.89646	0.04009	0.18683	0.00101	-0.43620	2731.74390	48.19676	2719.25500	39.17895	2713.31755	8.84651	-0.67453
307	0.51567	0.01071	13.38936	0.51468	0.62883		1.93983	0.04049	0.18879	0.00107	0.08714	2680.68350	45.58082	2707.19632	36.38581	2730.44630	9.29211	1.85635
308	0.51808	0.01065	13.27504	0.50703	0.69137		1.93055	0.03961	0.18628	0.00077	0.06496	2690.97910	45.22393	2699.22657	35.93871	2708.60864	6.80570	0.65513
309	0.51428	0.01058	13.13984	0.50168	0.61499		1.94485	0.03977	0.18578	0.00082	0.17633	2674.79406	44.98673	2689.56699	36.02454	2704.14696	7.30934	1.09739
310	0.52447	0.01069	13.40571	0.51062	0.63264		1.90685	0.03857	0.18593	0.00076	0.02532	2718.08296	45.15503	2708.52741	35.91354	2705.56934	6.70966	-0.46038
311	0.53893	0.01188	13.77087	0.53433	0.91735		1.85762	0.04072	0.18586	0.00071	0.29456	2778.51382	49.69174	2733.58346	36.63635	2704.91482	6.33542	-2.64886
312	0.52890	0.01123	13.49847	0.52007	0.84840		1.89187	0.04004	0.18564	0.00078	0.11559	2736.56677	47.31227	2714.82351	36.31537	2702.99723	6.88097	-1.22670

	Measured Ratios											Calculated Dates (Ma)						
	$^{206}Pb/^{238}U$	$^{206}Pb/^{238}U$ 2SE	$^{207}Pb/^{235}U$	$^{207}Pb/^{235}U$ 2SE	rho $^{206}Pb/^{238}U$ v $^{207}Pb/^{235}U$		$^{238}U/^{206}Pb$	$^{238}U/^{206}Pb$ 2SE	$^{207}Pb/^{206}Pb$	$^{207}Pb/^{206}Pb$ 2SE	rho $^{207}Pb/^{206}Pb$ v $^{238}U/^{206}Pb$	$^{206}Pb/^{238}U$	$^{206}Pb/^{238}U$ 2SE	$^{207}Pb/^{235}U$	$^{207}Pb/^{235}U$ 2SE	$^{207}Pb/^{206}Pb$	$^{207}Pb/^{206}Pb$ 2SE	% Disc.
Sample 48	**Grain2 Core**																	
313	0.53313	0.01083	13.56626	0.51644	0.36322		1.87579	0.03806	0.18501	0.00074	0.01460	2754.59821	45.52403	2719.79032	36.07802	2697.34795	6.64894	-2.07835
314	0.53096	0.01083	13.54933	0.51647	0.53308		1.88355	0.03820	0.18551	0.00081	0.25180	2745.47738	45.56888	2718.58789	35.96380	2703.14352	6.69764	-1.54195
315	0.52944	0.01084	13.48386	0.51405	0.63036		1.88784	0.04132	0.18520	0.00069	0.15119	2739.04571	45.63717	2714.00344	35.98354	2699.09301	6.15187	-1.45864
316	0.52807	0.01088	13.41971	0.51129	0.68913		1.89409	0.03881	0.18511	0.00071	0.27191	2733.24933	45.86995	2709.50998	36.05563	2698.25133	6.26781	-1.28045
317	0.52791	0.01077	13.45324	0.51177	0.34237		1.89445	0.03859	0.18566	0.00079	0.33759	2732.59036	45.42611	2711.89568	35.89666	2703.13479	7.04437	-1.07794
318	0.52200	0.01068	13.29590	0.50601	0.63463		1.91598	0.03888	0.18547	0.00069	0.27227	2707.58782	45.17190	2700.77378	35.85355	2701.46526	6.15231	-0.22613
319	0.52580	0.01088	13.36757	0.50934	0.67862		1.90236	0.03901	0.18529	0.00074	0.37566	2723.64716	45.88982	2705.82864	36.03400	2701.08203	6.11431	-0.82849
320	0.53032	0.01096	13.45577	0.51374	0.71994		1.88613	0.03862	0.18513	0.00079	0.08019	2742.70132	46.09332	2712.00712	36.04973	2698.42062	7.04698	-1.61449
321	0.52957	0.01092	13.47737	0.51449	0.76259		1.88876	0.03867	0.18548	0.00069	0.06751	2739.53966	45.96192	2713.52301	35.97929	2701.62518	6.12368	-1.38397
322	0.52594	0.01086	13.38209	0.51108	0.65852		1.90182	0.03891	0.18548	0.00081	0.19764	2724.21704	45.79963	2706.81161	36.15994	2701.55369	7.22303	-0.83192
323	0.52649	0.01090	13.35846	0.51081	0.70118		1.89988	0.03897	0.18500	0.00080	0.15381	2726.55311	45.94551	2705.11243	36.10491	2697.26653	7.16925	-1.07412
324	0.53780	0.01142	13.68294	0.54907	0.74024		1.85968	0.03918	0.18513	0.00181	-0.34012	2774.19081	47.80701	2727.74210	37.56286	2698.28961	16.09146	-2.73598
325	0.51795	0.01075	13.15789	0.50404	0.81598		1.93129	0.04020	0.18523	0.00071	-0.03983	2690.35544	45.67106	2690.79750	36.25592	2699.35425	6.33446	0.33448
326	0.50535	0.01046	12.82037	0.48992	0.79232		1.97936	0.04102	0.18503	0.00068	0.06856	2636.65735	44.80868	2666.34679	35.94450	2697.55445	6.04801	2.30963
327	0.52634	0.01117	13.34511	0.51436	0.83492		1.90106	0.04033	0.18491	0.00082	0.10452	2725.76653	47.16831	2704.01620	36.49105	2696.43931	7.24838	-1.07593
328	0.52689	0.01086	13.37301	0.51129	0.73029		1.89833	0.03896	0.18511	0.00075	0.02744	2728.26678	45.82920	2706.14906	35.92520	2698.23625	6.73005	-1.10072
329	0.51469	0.01057	13.09643	0.49974	0.70078		1.94327	0.03974	0.18560	0.00072	0.04660	2676.54134	44.96416	2686.45608	35.90977	2702.66706	6.39164	0.97610
330	0.51702	0.01068	13.13990	0.50202	0.80519		1.93460	0.03954	0.18539	0.00066	-0.01617	2686.45743	45.29986	2689.56157	36.04610	2700.80543	5.87264	0.53409
331	0.53517	0.01116	13.54839	0.52107	0.70421		1.86922	0.03840	0.18468	0.00096	0.04989	2763.07049	46.72670	2718.34658	36.39477	2694.27203	8.54775	-2.48993
332	0.51950	0.01095	13.29289	0.51252	0.56744		1.92589	0.04053	0.18594	0.00120	0.05419	2696.88475	46.44355	2700.31067	36.23570	2707.79926	11.78499	0.40471
333	0.53005	0.01108	13.47093	0.51771	0.83698		1.88737	0.03916	0.18534	0.00075	-0.06668	2741.49957	46.63470	2712.93432	36.41576	2700.30762	6.72811	-1.50253
334	0.53233	0.01097	13.53541	0.51630	0.66295		1.87893	0.03841	0.18546	0.00075	0.18418	2751.16586	46.08910	2717.60077	35.95559	2701.40859	6.66126	-1.80859
335	0.52389	0.01094	13.34865	0.51140	0.75646		1.90951	0.03955	0.18579	0.00080	0.18098	2715.50835	46.22591	2704.39030	36.14496	2704.26292	7.10247	-0.41412
336	0.52512	0.01089	13.32056	0.50984	0.80712		1.90488	0.03943	0.18494	0.00069	-0.01444	2720.74008	46.02716	2702.41580	36.00016	2696.73351	6.14800	-0.88235
337	0.51660	0.01069	13.14310	0.50281	0.81897		1.93623	0.03995	0.18547	0.00067	-0.07076	2684.65055	45.43107	2689.76365	35.96980	2701.49568	5.95943	0.62746
338	0.52078	0.01099	13.27337	0.51053	0.85458		1.92117	0.04053	0.18578	0.00073	0.05202	2702.30729	46.58092	2698.96812	36.29589	2704.24533	6.46875	0.07172
339	0.51615	0.01104	13.13605	0.50818	0.83122		1.93875	0.04132	0.18550	0.00088	0.08360	2682.58082	46.89171	2689.04185	36.32517	2701.62441	7.86187	0.70990
340	0.51501	0.01096	13.10999	0.50651	0.81631		1.94291	0.04116	0.18552	0.00089	0.06838	2677.76407	46.59600	2687.19223	36.37267	2701.83936	7.95100	0.89908
341	0.51379	0.01062	13.07191	0.50064	0.64688		1.94679	0.04008	0.18537	0.00090	0.07647	2672.68259	45.19214	2684.62145	36.17459	2700.44305	7.96419	1.03867
342	0.53257	0.01087	13.52037	0.51531	0.47816		1.87782	0.03834	0.18494	0.00082	0.02547	2752.23357	45.71513	2716.56398	36.03807	2696.66568	7.29835	-2.01901
343	0.54144	0.01137	13.79737	0.52931	0.81306		1.84773	0.03843	0.18562	0.00075	0.14540	2789.30530	47.46943	2735.63092	36.20401	2702.75967	6.68834	-3.10277
344	0.52556	0.01107	13.49668	0.52086	0.89868		1.90365	0.03970	0.18688	0.00066	-0.25249	2722.53941	46.70786	2714.66545	36.40737	2714.00068	5.81538	-0.31363
345	0.53395	0.01099	13.71072	0.52417	0.81354		1.87317	0.03832	0.18699	0.00069	-0.24178	2757.99978	46.12676	2729.73249	36.18468	2714.95447	6.05208	-1.56074
346	0.53091	0.01087	13.52080	0.51435	0.72511		1.88375	0.03827	0.18538	0.00059	0.01186	2745.26041	45.69578	2716.63066	35.94259	2700.77168	5.27859	-1.62056
347	0.53672	0.01100	13.64732	0.51965	0.61611		1.86342	0.03827	0.18508	0.00071	0.13116	2769.64055	46.16476	2725.42096	36.11236	2698.04454	6.30539	-2.58503
348	0.52959	0.01076	13.45991	0.51076	0.21239		1.88828	0.03839	0.18497	0.00064	0.15922	2739.72222	45.35315	2712.41098	35.87919	2697.07368	5.69391	-1.55667
349	0.51830	0.01062	13.18224	0.50200	0.58895		1.92963	0.03969	0.18509	0.00072	0.15854	2691.92001	45.12767	2692.65611	36.00485	2698.08636	6.46701	0.22907
350	0.53346	0.01085	13.56613	0.51587	0.37790		1.87463	0.03825	0.18504	0.00074	0.03767	2755.98319	45.64881	2719.80228	36.00364	2697.65566	6.58915	-2.11640
351	0.52931	0.01077	13.47013	0.51125	0.29436		1.88930	0.03843	0.18516	0.00064	0.21678	2738.53715	45.38434	2713.12589	35.76998	2698.77027	5.72146	-1.45212
352	0.52852	0.01075	13.46530	0.51105	0.44826		1.89213	0.03853	0.18529	0.00064	0.06069	2735.20312	45.34001	2712.78665	35.90315	2699.89371	5.69218	-1.29092
353	0.52329	0.01093	13.33944	0.51012	0.83018		1.91171	0.03987	0.18541	0.00066	0.20624	2712.95683	46.23372	2703.77222	36.13693	2700.95188	5.84411	-0.44250

	Measured Ratios											Calculated Dates (Ma)						
	$^{206}Pb/^{238}U$	$^{206}Pb/^{238}U$ 2SE	$^{207}Pb/^{235}U$	$^{207}Pb/^{235}U$ 2SE	rho $^{206}Pb/^{238}U$ v $^{207}Pb/^{235}U$	$^{238}U/^{206}Pb$	$^{238}U/^{206}Pb$ 2SE	$^{207}Pb/^{206}Pb$	$^{207}Pb/^{206}Pb$ 2SE	rho $^{207}Pb/^{206}Pb$ v $^{238}U/^{206}Pb$	$^{206}Pb/^{238}U$	$^{206}Pb/^{238}U$ 2SE	$^{207}Pb/^{235}U$	$^{207}Pb/^{235}U$ 2SE	$^{207}Pb/^{206}Pb$	$^{207}Pb/^{206}Pb$ 2SE	% Disc.
Sample 48	**Grain2 Core**																	
354	0.51437	0.01078	13.07065	0.50103	0.90547	1.94495	0.04047	0.18481	0.00056	-0.01300	2675.09107	45.82192	2684.51082	36.01592	2695.66105	5.01674	0.76895
355	0.51655	0.01080	13.16047	0.50393	0.81451	1.93666	0.04055	0.18530	0.00071	0.16159	2684.40515	45.92221	2690.99425	36.25162	2700.01600	6.32363	0.58154
356	0.51544	0.01078	13.11727	0.50205	0.84671	1.94085	0.04056	0.18509	0.00065	0.15353	2679.66794	45.83585	2687.90130	36.17971	2698.16382	5.80669	0.69023
357	0.53276	0.01096	13.58208	0.51741	0.69598	1.87739	0.03862	0.18539	0.00068	0.22893	2752.99074	46.11085	2720.87968	36.09985	2700.78335	6.05845	-1.89639
358	0.51932	0.01076	13.25458	0.50613	0.85432	1.92611	0.03944	0.18563	0.00058	0.05421	2696.20676	45.55830	2697.77442	35.85802	2703.00290	5.17789	0.25206
359	0.50387	0.01075	12.83338	0.49389	0.87979	1.98595	0.04203	0.18527	0.00070	0.21221	2630.17491	46.02360	2667.16671	36.15372	2699.66910	6.23433	2.64219
360	0.52860	0.01087	13.50285	0.51573	0.72210	1.89213	0.03862	0.18578	0.00074	0.00603	2735.48874	45.79373	2715.30038	36.16087	2704.18835	6.61120	-1.14423
361	0.52820	0.01091	13.48973	0.51809	0.51904	1.89339	0.03904	0.18549	0.00110	0.14249	2733.82873	45.99268	2714.45776	36.24491	2701.69956	9.76503	-1.17524
362	0.51950	0.01067	13.20350	0.50351	0.60587	1.92526	0.03925	0.18489	0.00078	0.18046	2696.98534	45.20544	2694.15071	36.02680	2696.23643	7.01698	-0.02777
363	0.52290	0.01080	13.31835	0.50916	0.64178	1.91286	0.03919	0.18530	0.00085	0.17289	2711.38349	45.64746	2702.28420	36.00667	2699.90991	7.52055	-0.42316
364	0.52530	0.01076	13.36848	0.50949	0.63547	1.90394	0.03870	0.18511	0.00072	0.11948	2721.57185	45.42695	2705.88804	36.09208	2698.26047	6.48825	-0.85654
365	0.52701	0.01089	13.43984	0.51376	0.66283	1.89796	0.03910	0.18553	0.00083	0.18168	2728.76511	45.95876	2710.85908	36.27137	2701.90466	7.40417	-0.98434
366	0.51628	0.01073	13.18077	0.50597	0.68129	1.93757	0.04025	0.18577	0.00094	0.09839	2683.25159	45.60993	2692.39664	36.30525	2704.03245	8.32767	0.77447
367	0.51488	0.01067	13.15192	0.50409	0.67283	1.94274	0.04003	0.18590	0.00091	0.10995	2677.33276	45.36303	2690.36333	36.18361	2705.14062	8.04408	1.03864
368	0.52510	0.01082	13.37509	0.51227	0.67072	1.90480	0.03910	0.18539	0.00088	-0.00595	2720.68879	45.68645	2706.25942	36.21671	2700.63007	7.84901	-0.73727
369	0.51206	0.01063	13.03935	0.50084	0.71996	1.95349	0.04028	0.18533	0.00091	0.01110	2665.31428	45.27613	2682.21004	36.16330	2700.06454	8.09486	1.30380
370	0.52234	0.01084	13.31297	0.50905	0.69961	1.91503	0.03981	0.18552	0.00081	0.22676	2708.99850	45.91676	2701.89520	36.04516	2701.85599	7.20766	-0.26366
371	0.51073	0.01051	13.03983	0.49899	0.47650	1.95838	0.04017	0.18588	0.00100	0.21464	2659.65246	44.81636	2682.31679	35.99842	2706.59242	8.24556	1.76489
372	0.52510	0.01081	13.37800	0.51084	0.53738	1.90478	0.03925	0.18551	0.00089	0.24403	2720.70195	45.69122	2706.52278	36.17423	2701.71235	7.94087	-0.69797
373	0.52648	0.01093	13.33028	0.51208	0.79211	1.89999	0.03958	0.18440	0.00081	-0.11440	2726.48682	46.19418	2703.03676	36.36037	2691.84523	7.27735	-1.27056
374	0.54600	0.01112	13.98481	0.53533	0.75355	1.83162	0.03699	0.18623	0.00084	-0.53801	2808.48543	46.30801	2748.45646	35.70612	2708.11713	7.43977	-3.57375
375	0.53340	0.01094	13.57806	0.51777	0.54042	1.87506	0.03858	0.18545	0.00082	0.20322	2755.69844	46.01212	2720.57979	36.26345	2701.22881	7.34225	-1.97662
376	0.52487	0.01095	13.31526	0.50985	0.76391	1.90595	0.03989	0.18484	0.00077	0.17178	2719.64795	46.31526	2702.03081	36.15224	2695.84059	6.93238	-0.87538
377	0.53399	0.01127	13.60730	0.52309	0.83248	1.87368	0.03939	0.18568	0.00077	0.11942	2758.02327	47.31650	2722.45807	36.41630	2703.29328	6.79901	-1.98439
378	0.53291	0.01088	13.55209	0.51467	0.50897	1.87669	0.03827	0.18527	0.00065	0.35309	2753.64456	45.74466	2718.84889	35.92580	2699.75287	5.74012	-1.95710
379	0.52618	0.01071	13.39073	0.50894	0.59817	1.90061	0.03867	0.18542	0.00062	0.03609	2725.31342	45.24818	2707.51259	35.85281	2701.08358	5.56420	-0.88907
380	0.52689	0.01075	13.39082	0.50987	0.60781	1.89714	0.04158	0.18509	0.00071	0.03071	2728.31323	45.34650	2707.48584	35.96708	2698.12177	6.38439	-1.10660
381	0.52981	0.01084	13.50639	0.51526	0.51356	1.88771	0.03850	0.18577	0.00085	0.13799	2740.59332	45.66293	2715.56863	36.03221	2704.04786	7.52155	-1.33349
382	0.52728	0.01101	13.40721	0.51231	0.87280	1.89722	0.03995	0.18514	0.00069	0.17884	2729.85705	46.51300	2708.57165	36.01137	2698.57062	6.13570	-1.14608
383	0.53152	0.01100	13.50208	0.51567	0.72314	1.88188	0.03864	0.18508	0.00074	0.17804	2747.74788	46.22563	2715.24815	36.09120	2698.02074	6.60763	-1.80974
384	0.53311	0.01102	13.56341	0.51774	0.77895	1.87623	0.03860	0.18539	0.00066	0.10904	2754.45911	46.29388	2719.54392	36.07895	2700.80563	5.90413	-1.94788
385	0.52016	0.01119	13.44738	0.61113	0.86609	1.92398	0.04085	0.18740	0.00253	-0.72627	2699.55452	47.33851	2708.25541	36.30431	2716.49058	19.89260	0.62737
386	0.52414	0.01083	13.32915	0.50842	0.78104	1.90834	0.03906	0.18531	0.00064	0.13601	2716.61567	45.71901	2703.09195	36.00674	2700.11963	5.70981	-0.60723
387	0.51806	0.01072	13.19373	0.50379	0.75210	1.93079	0.03975	0.18558	0.00071	0.16073	2690.84097	45.49651	2693.42730	36.01381	2702.45978	6.32295	0.43179
388	0.52520	0.01071	13.34718	0.50676	0.52994	1.90419	0.03904	0.18514	0.00060	0.24319	2721.15186	45.31596	2704.45481	35.86637	2698.55596	5.37702	-0.83038
389	0.52364	0.01069	13.30844	0.50558	0.58098	1.90988	0.03896	0.18514	0.00062	0.20884	2714.54987	45.23485	2701.69966	35.81897	2698.61852	5.48851	-0.58689
390	0.53498	0.01092	13.60820	0.51724	0.50958	1.86937	0.03831	0.18542	0.00062	0.20044	2762.38201	45.89846	2722.73970	36.11337	2701.06562	5.55125	-2.21969
391	0.53892	0.01142	13.70112	0.52749	0.88979	1.85663	0.03924	0.18518	0.00066	0.03280	2778.69200	47.82341	2728.93142	36.32021	2698.88678	5.92782	-2.87204
392	0.51820	0.01085	13.21029	0.50518	0.85578	1.93052	0.04007	0.18579	0.00059	0.22687	2691.39812	45.99885	2694.58620	36.05281	2704.36266	5.22817	0.48170
393	0.52258	0.01096	13.30620	0.51032	0.83561	1.91439	0.04022	0.18546	0.00064	0.10582	2709.96287	46.42498	2701.36065	36.24577	2701.46675	5.74170	-0.31351
394	0.51065	0.01074	12.99442	0.49848	0.89289	1.95919	0.04095	0.18518	0.00061	0.05482	2659.22414	45.78769	2678.98523	36.05552	2698.96241	5.41627	1.49436
395	0.52041	0.01093	13.27343	0.50890	0.85883	1.92241	0.04026	0.18559	0.00066	0.10437	2700.75445	46.31553	2699.03463	36.13920	2702.58412	5.83619	0.06775

	Measured Ratios											Calculated Dates (Ma)						
	$^{206}Pb/^{238}U$	$^{206}Pb/^{238}U$ 2SE	$^{207}Pb/^{235}U$	$^{207}Pb/^{235}U$ 2SE	rho $^{206}Pb/^{238}U$ v $^{207}Pb/^{235}U$		$^{238}U/^{206}Pb$	$^{238}U/^{206}Pb$ 2SE	$^{207}Pb/^{206}Pb$	$^{207}Pb/^{206}Pb$ 2SE	rho $^{207}Pb/^{206}Pb$ v $^{238}U/^{206}Pb$	$^{206}Pb/^{238}U$	$^{206}Pb/^{238}U$ 2SE	$^{207}Pb/^{235}U$	$^{207}Pb/^{235}U$ 2SE	$^{207}Pb/^{206}Pb$	$^{207}Pb/^{206}Pb$ 2SE	% Disc.
Sample 48	**Grain2 Core**																	
396	0.52911	0.01084	13.54194	0.51898	0.61455		1.89007	0.03864	0.18603	0.00096	-0.13584	2737.69386	45.68219	2718.07910	36.15873	2706.42975	8.50808	-1.14199
397	0.51886	0.01064	13.23409	0.50436	0.59181		1.92755	0.03968	0.18553	0.00075	0.11621	2694.29206	45.19796	2696.34980	35.98886	2702.01937	6.69211	0.28680
398	0.51897	0.01067	13.27361	0.50466	0.73629		1.92720	0.03943	0.18595	0.00057	0.28986	2694.75965	45.25710	2699.20998	35.86554	2705.83626	5.09409	0.41104
399	0.53444	0.01098	13.62684	0.51837	0.44417		1.87141	0.03827	0.18535	0.00080	0.42481	2760.06357	46.09822	2724.02040	36.01142	2700.38616	7.06226	-2.16218
400	0.53180	0.01103	13.68751	0.52964	0.36307		1.88059	0.03885	0.18677	0.00149	0.21466	2748.98419	46.38857	2728.18390	36.62802	2712.86980	13.07918	-1.31374
401	0.51640	0.01059	13.13310	0.50066	0.50921		1.93672	0.03957	0.18498	0.00088	0.10234	2683.84295	44.97420	2689.11383	36.00178	2696.99949	7.79942	0.49021
402	0.52477	0.01071	13.44658	0.51104	0.13566		1.90571	0.03888	0.18615	0.00080	0.41730	2719.34710	45.26299	2711.44688	35.84301	2707.43713	7.07365	-0.43797
403	0.52709	0.01078	13.46866	0.51325	0.39648		1.89738	0.03885	0.18553	0.00085	0.20831	2729.14677	45.52858	2712.94764	35.99184	2701.97225	7.54466	-0.99571
404	0.52902	0.01078	13.56189	0.51474	0.26752		1.89035	0.03854	0.18596	0.00068	0.20351	2737.29714	45.43935	2719.54292	35.94479	2705.89274	6.07335	-1.14728
405	0.51785	0.01067	13.21609	0.50472	0.59598		1.93143	0.03951	0.18523	0.00084	0.15186	2689.96640	45.25666	2695.02546	36.11643	2699.26488	7.53207	0.34567
406	0.51324	0.01066	13.16298	0.50434	0.70286		1.94895	0.04018	0.18609	0.00086	0.08790	2670.35809	45.34773	2691.15837	36.29923	2706.89243	7.67779	1.36814
407	0.52040	0.01076	13.38213	0.51026	0.61891		1.92201	0.03950	0.18656	0.00079	0.29181	2700.80923	45.55614	2706.84568	35.98661	2711.14605	6.97781	0.38273
408	0.51003	0.01056	13.06858	0.50019	0.72606		1.96117	0.04021	0.18594	0.00075	0.04996	2656.66511	45.01941	2684.39077	36.02530	2705.64191	6.62487	1.84354
409	0.51396	0.01057	13.13933	0.50037	0.71985		1.94600	0.04003	0.18534	0.00064	0.13858	2673.45365	45.02506	2689.57982	35.95331	2700.40218	5.67252	1.00800
410	0.50684	0.01045	12.93870	0.49327	0.61875		1.97340	0.04056	0.18505	0.00077	0.24456	2643.04758	44.68999	2675.04797	35.97870	2697.68388	6.88539	2.06717
411	0.52144	0.01109	13.36630	0.51485	0.83786		1.91895	0.04085	0.18576	0.00080	0.13979	2705.04547	46.99278	2705.52680	36.49133	2704.00988	7.11948	-0.03828
412	0.51276	0.01062	13.14292	0.50337	0.80742		1.95072	0.04050	0.18565	0.00072	-0.11359	2668.32250	45.28829	2689.73183	36.09069	2703.11925	6.41310	1.30407
413	0.51991	0.01067	13.31288	0.50733	0.64545		1.92369	0.03944	0.18518	0.00077	0.00652	2698.72615	45.24645	2701.95399	35.94246	2698.87874	6.82401	0.00565
414	0.51368	0.01069	13.21125	0.50476	0.71484		1.94736	0.04054	0.18612	0.00079	0.28484	2672.21532	45.53766	2694.66784	36.14140	2707.16835	6.96761	1.30802
415	0.51052	0.01052	13.06967	0.49943	0.68951		1.95916	0.04042	0.18523	0.00078	0.03943	2658.79209	44.91609	2684.50236	36.03997	2699.32376	6.96365	1.52444
416	0.52372	0.01069	13.59476	0.51784	0.37398		1.90957	0.03905	0.18778	0.00086	0.13806	2714.90881	45.24864	2721.76336	36.01763	2721.84876	7.50140	0.25562
417	0.50369	0.01252	13.37509	0.64800	0.30481		1.98794	0.04987	0.19194	0.00560	0.17873	2629.17143	53.75509	2703.95461	46.15442	2752.96427	49.05321	4.70844
418	0.50748	0.01096	12.94545	0.50183	0.90201		1.97217	0.04247	0.18448	0.00073	0.01034	2645.54207	46.84325	2675.21518	36.57198	2692.65038	6.58539	1.78067
419	0.51248	0.01094	13.09060	0.50649	0.84013		1.95258	0.04165	0.18466	0.00086	0.02338	2666.97534	46.61025	2685.76576	36.57215	2694.13300	7.70644	1.01829
420	0.51259	0.01064	13.16980	0.50364	0.74254		1.95143	0.04024	0.18572	0.00077	0.14676	2667.58158	45.30064	2691.68851	36.07227	2703.69060	6.79636	1.35362
421	0.51087	0.01054	13.11253	0.50096	0.67307		1.95788	0.04025	0.18535	0.00073	0.11544	2660.24555	44.93979	2687.59208	36.03591	2700.37119	6.47114	1.50834
422	0.53039	0.01085	13.79520	0.52558	0.45270		1.88565	0.03839	0.18798	0.00086	0.16730	2743.03453	45.66761	2735.60869	36.07724	2723.57623	7.51329	-0.70937
423	0.50438	0.01058	12.94094	0.49602	0.87564		1.98349	0.04134	0.18541	0.00062	0.08095	2632.42018	45.29912	2675.11337	36.00655	2700.99848	5.53982	2.60514
424	0.50225	0.01055	12.87210	0.49369	0.87181		1.99193	0.04195	0.18518	0.00064	0.06892	2623.29768	45.27346	2670.06974	36.10159	2698.97699	5.72413	2.88489
425	0.50628	0.01078	12.98186	0.50007	0.88564		1.97642	0.04178	0.18523	0.00069	0.10640	2640.50636	46.08123	2677.99464	36.23145	2699.32211	6.18276	2.22744
426	0.51161	0.01077	13.13360	0.50513	0.87475		1.95556	0.04113	0.18542	0.00068	-0.03866	2663.30881	45.91880	2688.97787	36.22602	2701.01974	6.09719	1.41594
427	0.50169	0.01054	12.87143	0.49529	0.83994		1.99417	0.04168	0.18529	0.00077	-0.03487	2620.88713	45.19857	2669.95734	36.24457	2699.83559	6.83322	3.01228
428	0.52018	0.01059	13.39731	0.51087	0.60464		1.92252	0.03899	0.18603	0.00083	-0.26560	2699.92775	44.87777	2707.91194	35.98543	2706.40053	7.36536	0.23974
429	0.51577	0.01078	13.30333	0.50895	0.69479		1.93958	0.04025	0.18608	0.00088	0.39979	2681.08609	45.78838	2701.20111	36.09458	2706.75018	7.86589	0.95723
430	0.49755	0.01044	12.77991	0.49224	0.79710		2.01073	0.04205	0.18548	0.00086	-0.01735	2603.10654	44.91964	2663.21710	36.24575	2701.49499	7.69810	3.77966
431	0.50877	0.01083	13.07978	0.50214	0.74602		1.96677	0.04182	0.18563	0.00094	0.40210	2651.15164	46.27593	2685.13796	36.28457	2702.77141	8.33450	1.94707
Sample 48	**Grain2 Rim**																	
1	0.54410	0.01148	13.65670	0.54697	0.46223		1.83831	0.03868	0.18209	0.00214	-0.03615	2800.49485	47.89353	2725.69838	38.06957	2670.42995	19.31367	4.64435
2	0.50253	0.01180	11.87129	0.53569	0.59632		1.99161	0.04643	0.17137	0.00336	-0.11613	2624.34533	50.55367	2592.78737	41.17269	2568.12933	32.38569	2.14210
3	0.48993	0.01171	11.38779	0.52039	0.71455		2.04413	0.04893	0.16871	0.00316	-0.27945	2569.87233	50.66340	2552.82848	42.49274	2540.98379	31.26708	1.12412
4	0.52359	0.01148	12.60619	0.51763	0.52518		1.91189	0.04221	0.17504	0.00237	0.01605	2713.98985	48.62171	2649.05636	38.33697	2603.10438	22.52410	4.08570

	Measured Ratios											Calculated Dates (Ma)						
	$^{206}Pb/^{238}U$	$^{206}Pb/^{238}U$ 2SE	$^{207}Pb/^{235}U$	$^{207}Pb/^{235}U$ 2SE	rho $^{206}Pb/^{238}U$ v $^{207}Pb/^{235}U$	$^{238}U/^{206}Pb$	$^{238}U/^{206}Pb$ 2SE	$^{207}Pb/^{206}Pb$	$^{207}Pb/^{206}Pb$ 2SE	rho $^{207}Pb/^{206}Pb$ v $^{238}U/^{206}Pb$	$^{206}Pb/^{238}U$	$^{206}Pb/^{238}U$ 2SE	$^{207}Pb/^{235}U$	$^{207}Pb/^{235}U$ 2SE	$^{207}Pb/^{206}Pb$	$^{207}Pb/^{206}Pb$ 2SE	% Disc.
Sample 48	**Grain2 Rim**																	
1	0.54410	0.01148	13.65670	0.54697	0.46223	1.83831	0.03868	0.18209	0.00214	-0.03615	2800.49485	47.89353	2725.69838	38.06957	2670.42995	19.31367	4.64435
2	0.50253	0.01180	11.87129	0.53569	0.59632	1.99161	0.04643	0.17137	0.00336	-0.11613	2624.34533	50.55367	2592.78737	41.17269	2568.12933	32.38569	2.14210
3	0.48993	0.01171	11.38779	0.52039	0.71455	2.04413	0.04893	0.16871	0.00316	-0.27945	2569.87233	50.66340	2552.82848	42.49274	2540.98379	31.26708	1.12412
4	0.52359	0.01148	12.60619	0.51763	0.52518	1.91189	0.04221	0.17504	0.00237	0.01605	2713.98985	48.62171	2649.05636	38.33697	2603.10438	22.52410	4.08570
5	0.48223	0.01136	11.09011	0.49198	0.66885	2.07619	0.04932	0.16699	0.00292	-0.17172	2536.57446	49.47495	2528.82929	41.39839	2524.45872	29.56607	0.47764
6	0.45850	0.01604	9.82695	0.59422	0.75421	2.18807	0.07600	0.15546	0.00490	-0.20196	2431.91173	70.80494	2414.98227	55.46410	2402.04159	54.26626	1.22826
7	0.49354	0.01068	11.63996	0.48323	0.44228	2.02799	0.04434	0.17158	0.00265	0.01511	2585.66348	46.16796	2573.95556	38.95685	2568.81758	25.82157	0.65151
8	0.50955	0.01076	12.27732	0.49758	0.17275	1.96356	0.04149	0.17544	0.00261	0.23408	2654.52867	45.96186	2624.45783	38.04728	2606.28106	24.70360	1.81756
9	0.50183	0.01071	12.08901	0.49937	0.22927	1.99130	0.03981	0.17545	0.00291	0.18033	2621.39626	46.06323	2609.53374	39.38154	2605.61259	27.79152	0.60211
10	0.47471	0.01004	10.83749	0.44384	0.34617	2.10766	0.04452	0.16638	0.00256	-0.00599	2504.02317	43.87459	2507.74786	37.90759	2517.45370	25.74445	-0.53636
11	0.48900	0.01044	11.63152	0.47104	0.41989	2.04636	0.04384	0.17325	0.00230	0.08793	2566.12938	45.23017	2573.87082	38.03600	2586.01142	22.42429	-0.77479
12	0.50709	0.01425	12.29315	0.63830	0.51655	1.97626	0.05681	0.17636	0.00527	0.02035	2643.41938	61.17575	2624.10303	47.84498	2613.54921	49.04017	1.12998
13	0.49242	0.01053	11.61851	0.48727	0.13908	2.03223	0.04405	0.17201	0.00320	0.23738	2580.88772	45.55679	2572.04484	39.18416	2571.60369	30.94063	0.35972
14	0.50869	0.01068	12.18542	0.48932	0.44527	1.96451	0.04434	0.17439	0.00212	0.01185	2650.84820	45.63869	2617.62052	37.71824	2597.43967	20.28345	2.01477
15	0.49735	0.01100	11.96653	0.49800	0.55242	2.01300	0.04470	0.17536	0.00253	-0.03760	2601.99403	47.37600	2599.87843	38.81453	2605.80206	24.00815	-0.14635
16	0.47603	0.01063	10.83939	0.43633	0.64837	2.10342	0.04614	0.16608	0.00177	0.05291	2509.52905	46.27293	2510.80980	34.84649	2516.13465	17.90914	-0.26322
17	0.54082	0.01119	13.55098	0.53157	0.25937	1.84955	0.03841	0.18331	0.00174	0.22124	2786.76809	46.84825	2720.09867	34.41147	2681.02842	15.67616	3.79435
18	0.50905	0.01180	12.02318	0.50552	0.54625	1.96812	0.04482	0.17274	0.00269	0.07311	2651.86968	50.21097	2603.99903	39.78215	2580.11176	25.99405	2.70594
19	0.54522	0.01122	13.80784	0.53192	0.22104	1.83446	0.03774	0.18557	0.00150	0.24342	2805.20070	46.80277	2736.26194	36.43531	2701.60848	13.36428	3.69286
Sample 47i																	
Mnz1_1	0.53781	0.00127	14.05393	0.08566	0.56319	1.85964	0.00441	0.18955	0.00094	-0.21008	2774.21531	5.33522	2752.96269	5.81655	2737.00029	8.19469	-1.35970
Mnz1_2	0.52877	0.00125	13.94337	0.05751	0.58963	1.89142	0.00446	0.19120	0.00060	-0.00393	2736.20315	5.25563	2745.70833	3.89327	2751.54738	5.11274	0.55766
Mnz1_3	0.53053	0.00229	13.48463	0.06873	0.81507	1.88572	0.00793	0.18461	0.00055	-0.03174	2743.50416	9.60900	2713.94462	4.79370	2693.80235	4.89176	-1.84504
Mnz1_4	0.52749	0.00087	13.39677	0.05079	0.47443	1.89590	0.00314	0.18442	0.00061	0.04460	2730.83543	3.68054	2707.88203	3.57710	2692.03375	5.49821	-1.44135
Mnz1_5	0.52625	0.00104	13.37734	0.05239	0.57930	1.90042	0.00375	0.18456	0.00059	0.00939	2725.58213	4.38771	2706.50069	3.70383	2693.31115	5.31957	-1.19819
Mnz1_6	0.53033	0.00095	13.48093	0.05015	0.58746	1.88577	0.00336	0.18446	0.00056	-0.04683	2742.80524	3.98779	2713.80599	3.51680	2692.40792	5.01003	-1.87183
Mnz1_7	0.52875	0.00103	13.44149	0.05057	0.64437	1.89144	0.00370	0.18443	0.00054	-0.07467	2736.13330	4.35244	2711.03340	3.56030	2692.19248	4.83682	-1.63216
Mnz1_8	0.54966	0.00063	13.95527	0.04568	0.55525	1.81938	0.00208	0.18402	0.00050	-0.22526	2823.72814	2.60834	2746.56610	3.09420	2688.56449	4.51025	-5.02735
Mnz1_9	0.54461	0.00091	13.85373	0.04919	0.49394	1.83629	0.00308	0.18438	0.00057	0.07752	2802.70038	3.80685	2739.62710	3.36856	2691.67120	5.13113	-4.12492
Mnz1_10	0.54961	0.00090	14.00686	0.04598	0.51842	1.81959	0.00298	0.18472	0.00052	0.08611	2823.52416	3.74632	2750.06079	3.11232	2694.79821	4.63365	-4.77683
Mnz2_1	0.55364	0.00132	14.11309	0.06108	0.62439	1.80648	0.00431	0.18477	0.00062	-0.01368	2840.22449	5.47067	2757.14052	4.09663	2695.16680	5.55355	-5.38214
Mnz2_2	0.55976	0.00090	14.27100	0.10657	0.00341	1.78651	0.00287	0.18448	0.00142	0.19452	2865.62157	3.70890	2767.79635	7.07662	2692.56522	12.70691	-6.42719
Mnz3_1	0.55505	0.00136	14.34080	0.06497	0.65251	1.80187	0.00441	0.18724	0.00065	-0.10233	2846.07223	5.62916	2772.33514	4.29656	2717.07874	5.69520	-4.74751
Mnz4_1	0.54982	0.00102	14.02126	0.05399	0.47781	1.81891	0.00338	0.18488	0.00063	0.08997	2824.40923	4.25400	2750.99192	3.65929	2696.09776	5.59218	-4.75915
Mnz4_2	0.55263	0.00143	14.29248	0.06774	0.69102	1.80981	0.00471	0.18752	0.00065	-0.18597	2836.04248	5.95148	2769.08183	4.50664	2719.49626	5.73854	-4.28558
Mnz4_3	0.54094	0.00146	13.96829	0.05970	0.59073	1.84895	0.00502	0.18711	0.00069	0.09877	2787.32197	6.12358	2747.36905	4.06545	2715.84834	6.07063	-2.63172
Mnz5_1	0.53503	0.00187	13.62793	0.06919	0.78393	1.86958	0.00657	0.18471	0.00060	-0.09580	2762.50880	7.85001	2723.93556	4.82659	2694.61040	5.36933	-2.51979
Mnz5_2	0.55022	0.00120	14.20161	0.05863	0.48199	1.81767	0.00397	0.18720	0.00068	-0.00982	2826.03073	4.97873	2763.08805	3.90980	2716.72137	5.97054	-4.02358
Mnz5_3	0.54932	0.00251	14.07252	0.07428	0.76222	1.82133	0.00818	0.18590	0.00062	0.13948	2822.12715	10.40913	2754.31812	4.97704	2705.25309	5.54092	-4.32026
Mnz17a_1	0.52798	0.00156	13.44760	0.07553	0.65473	1.89412	0.00559	0.18438	0.00079	-0.14942	2732.90266	6.57413	2711.52236	5.30783	2691.83319	7.03513	-1.52571
Mnz17a_2	0.52530	0.00123	13.37189	0.04444	0.86375	1.90393	0.00449	0.18473	0.00032	-0.13017	2721.55325	5.22170	2706.16150	3.14405	2694.98153	2.82970	-0.98597

	Measured Ratios												Calculated Dates (Ma)						
	$^{206}Pb/^{238}U$	$^{206}Pb/^{238}U$ 2SE	$^{207}Pb/^{235}U$	$^{207}Pb/^{235}U$ 2SE	rho $^{206}Pb/^{238}U$ v $^{207}Pb/^{235}U$		$^{238}U/^{206}Pb$	$^{238}U/^{206}Pb$ 2SE	$^{207}Pb/^{206}Pb$	$^{207}Pb/^{206}Pb$ 2SE	rho $^{207}Pb/^{206}Pb$ v $^{238}U/^{206}Pb$		$^{206}Pb/^{238}U$	$^{206}Pb/^{238}U$ 2SE	$^{207}Pb/^{235}U$	$^{207}Pb/^{235}U$ 2SE	$^{207}Pb/^{206}Pb$	$^{207}Pb/^{206}Pb$ 2SE	% Disc.
Sample 47i																			
Mnz17a_3	0.52497	0.00092	13.35760	0.03325	0.77129		1.90502	0.00332	0.18465	0.00029	0.01937		2720.18284	3.87049	2705.20046	2.35213	2694.32332	2.64161	-0.95978
Mnz17a_4	0.52644	0.00093	13.38243	0.03058	0.68811		1.89968	0.00337	0.18441	0.00030	-0.03879		2726.42100	3.91619	2706.96480	2.15913	2692.11607	2.72470	-1.27427
Mnz17a_5	0.51861	0.00091	13.23888	0.06586	0.48447		1.92824	0.00336	0.18490	0.00082	-0.16431		2693.29194	3.84431	2696.80055	4.69525	2696.54318	7.30590	0.12057
Mnz17a_6	0.54532	0.00097	13.91297	0.04384	0.76360		1.83392	0.00327	0.18488	0.00038	-0.30072		2805.65655	4.04866	2743.69708	2.98070	2696.27414	3.42963	-4.05680
Mnz17a_7	0.55311	0.00092	14.14983	0.04835	0.77623		1.80806	0.00299	0.18530	0.00045	-0.42330		2838.08501	3.80083	2759.67984	3.23986	2700.05080	3.96945	-5.11228
Mnz17a_8	0.55690	0.00163	14.20122	0.07128	0.82648		1.79602	0.00530	0.18468	0.00057	-0.33485		2853.71235	6.74372	2762.97823	4.77197	2694.39111	5.06993	-5.91307
Mnz17a_9	0.56344	0.00175	14.34716	0.08536	0.80066		1.77401	0.00515	0.18405	0.00069	-0.37243		2882.12778	6.73394	2772.69282	5.65775	2690.03822	6.64135	-7.14077
Mnz17b_1	0.56457	0.00168	14.37181	0.07575	0.81734		1.77163	0.00526	0.18433	0.00061	-0.33034		2885.39568	6.91841	2774.28156	4.98650	2691.22247	5.47446	-7.21506
Mnz17b_2	0.57674	0.00095	14.70728	0.04871	0.69147		1.73399	0.00285	0.18475	0.00048	-0.34020		2935.40758	3.87276	2796.37765	3.14280	2695.10845	4.27141	-8.91612
Mnz17b_3	0.59113	0.00257	15.00825	0.08033	0.90867		1.69244	0.00738	0.18418	0.00041	-0.09520		2993.79458	10.42103	2815.46328	5.08673	2690.00299	3.70202	-11.29336
Mnz17b_4	0.59537	0.00116	15.12009	0.05418	0.82179		1.67977	0.00327	0.18431	0.00042	-0.30953		3011.13286	4.68997	2822.69784	3.40742	2691.75032	3.57467	-11.86524
Mnz17b_5	0.60228	0.00092	15.25594	0.06118	0.78355		1.66044	0.00254	0.18393	0.00054	-0.50536		3039.01075	3.70654	2831.18418	3.82420	2687.66647	4.83615	-13.07247
Mnz17c_1	0.59809	0.00160	15.21940	0.07993	0.79295		1.67228	0.00447	0.18478	0.00061	-0.37107		3022.04476	6.44322	2828.78185	4.99989	2695.24370	5.49366	-12.12510
Mnz17c_2	0.60247	0.00145	15.31028	0.07819	0.74012		1.66006	0.00402	0.18473	0.00068	-0.32161		3039.71260	5.84146	2834.47037	4.86906	2694.76859	6.06321	-12.80051
Mnz17c_3	0.60127	0.00150	15.33777	0.07335	0.67810		1.66331	0.00415	0.18550	0.00075	-0.23823		3034.90987	6.05188	2836.29066	4.55463	2701.71101	6.63009	-12.33288
Mnz17c_4	0.61362	0.00133	15.93269	0.06624	0.60673		1.62984	0.00355	0.18882	0.00066	-0.08381		3084.43913	5.32966	2872.59818	3.96729	2730.93353	5.71161	-12.94450
Mnz21_1	0.59129	0.00180	15.18590	0.08861	0.84084		1.69158	0.00515	0.18671	0.00067	-0.46399		2994.55623	7.28307	2826.61278	5.54221	2712.33266	5.95510	-10.40520
Mnz21_2	0.58274	0.00140	14.79383	0.07217	0.85478		1.71628	0.00415	0.18450	0.00057	-0.57335		2959.84290	5.72268	2801.82503	4.63045	2692.79570	5.06178	-9.91710
Mnz21_3	0.56951	0.00139	14.42148	0.06145	0.77487		1.75614	0.00428	0.18396	0.00052	-0.29752		2905.74362	5.71482	2777.65723	4.03435	2687.98004	4.65036	-8.10138
Mnz21_4	0.56055	0.00100	14.24199	0.04361	0.74424		1.78409	0.00317	0.18445	0.00039	-0.08999		2868.87349	4.11343	2765.86174	2.90632	2692.48280	3.44670	-6.55123
Mnz21_5	0.55484	0.00076	14.08795	0.04122	0.76137		1.80239	0.00245	0.18424	0.00038	-0.36522		2845.26249	3.13516	2755.55582	2.77144	2690.56060	3.43200	-5.74980
Mnz21_6	0.54886	0.00095	13.96590	0.05229	0.77589		1.82208	0.00315	0.18453	0.00049	-0.37798		2820.40697	3.95743	2747.25332	3.54320	2693.11918	4.34521	-4.72641
Mnz21_7	0.53734	0.00081	13.68446	0.04396	0.64537		1.86113	0.00279	0.18462	0.00047	-0.21562		2772.26502	3.37940	2728.01512	3.03076	2693.89199	4.17445	-2.90929
Mnz24_1	0.53775	0.00096	13.73493	0.05678	0.58086		1.85974	0.00333	0.18482	0.00064	-0.14388		2773.99391	4.02330	2731.42809	3.90841	2695.61205	5.67144	-2.90776
Mnz24_2	0.53125	0.00123	13.58555	0.06266	0.69690		1.88257	0.00439	0.18505	0.00063	-0.17785		2746.68611	5.19292	2721.03948	4.37399	2697.62305	5.67790	-1.81875
Mnz25_1	0.52513	0.00110	13.39521	0.05867	0.70472		1.90450	0.00399	0.18463	0.00060	-0.35112		2720.84381	4.63530	2707.72498	4.13166	2693.89835	5.38277	-1.00024
Mnz27_1	0.51579	0.00300	13.19449	0.11981	0.78481		1.93911	0.01132	0.18476	0.00107	-0.18197		2681.22601	12.77293	2693.48080	8.60486	2695.20223	9.51111	0.51856
Mnz31_1	0.52861	0.00127	13.48996	0.07569	0.70965		1.89201	0.00456	0.18487	0.00078	-0.36390		2735.53694	5.37198	2714.26081	5.29341	2695.94759	6.96702	-1.46848
Mnz31_2	0.53015	0.00137	13.54927	0.08860	0.78840		1.88655	0.00484	0.18524	0.00088	-0.50368		2742.02792	5.75593	2718.28912	6.16255	2699.08734	7.83649	-1.59093
Sample 47ii																			
Mnz3_1	0.53680	0.00673	14.03311	0.38888	0.50575		1.86302	0.02339	0.18934	0.00058	-0.02745		2770.01498	28.23096	2751.81321	26.33585	2735.52770	5.00848	-1.26072
Mnz3_2	0.52975	0.00657	13.51193	0.37250	0.35924		1.88777	0.02346	0.18474	0.00056	0.03897		2740.39271	27.70790	2716.01311	26.03713	2694.91260	4.96367	-1.68763
Mnz3_3	0.53144	0.00666	13.65798	0.37796	0.26540		1.88192	0.02353	0.18633	0.00076	0.25304		2747.45860	28.01279	2726.13288	26.18671	2708.95489	6.71526	-1.42135
Mnz3_4	0.52808	0.00660	13.45557	0.37296	0.39327		1.89376	0.02364	0.18469	0.00068	-0.00773		2733.34606	27.85331	2712.00323	26.13704	2694.36988	6.05586	-1.44658
Mnz3_5	0.53295	0.00674	13.59117	0.37674	0.53125		1.87650	0.02371	0.18488	0.00061	-0.04281		2753.85211	28.33691	2722.10833	27.62757	2697.07125	5.72805	-2.10528
Mnz3_6	0.52861	0.00664	13.77468	0.38236	0.54298		1.89189	0.02376	0.18905	0.00061	-0.10269		2735.55990	28.00503	2734.18942	26.30830	2732.94841	5.31049	-0.09556
Mnz3_7	0.52425	0.00658	13.53754	0.37727	0.68183		1.90766	0.02395	0.18741	0.00072	-0.40042		2717.12950	27.84603	2717.67072	26.27112	2718.52340	6.30769	0.05127
Mnz3_8	0.51940	0.00646	13.20418	0.36403	0.35945		1.92538	0.02401	0.18471	0.00060	0.01046		2696.61729	27.43325	2694.24644	25.90767	2694.63494	5.31419	-0.07357
Mnz3_9	0.52079	0.00664	13.24178	0.36661	0.60712		1.92040	0.02454	0.18490	0.00048	0.08940		2702.46538	28.15187	2696.94636	26.19331	2696.39705	4.30965	-0.22505
Mnz3_10	0.52383	0.00668	13.30879	0.36950	0.52075		1.90922	0.02436	0.18467	0.00060	-0.02687		2715.36162	28.25022	2701.66455	26.24043	2694.26236	5.31913	-0.78312
Mnz3_11	0.52168	0.00667	13.28647	0.36845	0.54761		1.91712	0.02463	0.18507	0.00053	0.07747		2706.24137	28.26930	2700.09733	26.20634	2697.92721	4.75359	-0.30817

	Measured Ratios												Calculated Dates (Ma)							
	$^{206}Pb/^{238}U$	$^{206}Pb/^{238}U$ 2SE	$^{207}Pb/^{235}U$	$^{207}Pb/^{235}U$ 2SE	rho $^{206}Pb/^{238}U$ v $^{207}Pb/^{235}U$		$^{238}U/^{206}Pb$	$^{238}U/^{206}Pb$ 2SE	$^{207}Pb/^{206}Pb$	$^{207}Pb/^{206}Pb$ 2SE	rho $^{207}Pb/^{206}Pb$ v $^{238}U/^{206}Pb$		$^{206}Pb/^{238}U$	$^{206}Pb/^{238}U$ 2SE	$^{207}Pb/^{235}U$	$^{207}Pb/^{235}U$ 2SE	$^{207}Pb/^{206}Pb$	$^{207}Pb/^{206}Pb$ 2SE	% Disc.
Sample 47ii																				
Mnz3_12	0.52526	0.00666	13.41557	0.37030	0.26227		1.90393	0.02414	0.18557	0.00057	0.20455		2721.42202	28.14766	2709.25772	26.09136	2702.34970	5.06491	-0.70577	
Mnz3_13	0.52777	0.00695	13.50318	0.37359	0.49291		1.89486	0.02490	0.18585	0.00064	-0.16403		2732.03286	29.31551	2715.34523	26.13118	2704.80407	5.67575	-1.00668	
Mnz3_14	0.53417	0.00677	13.74896	0.38099	0.45584		1.87218	0.02375	0.18693	0.00062	-0.03073		2758.98091	28.46697	2732.42356	26.16443	2714.37324	5.45301	-1.64339	
Mnz3_15	0.52774	0.00669	13.43250	0.37210	0.51214		1.89497	0.02400	0.18483	0.00056	-0.17708		2731.89488	28.22830	2710.42125	26.18460	2695.71755	4.97933	-1.34203	
Mnz3_16	0.52333	0.00666	13.30840	0.37003	0.56861		1.91105	0.02433	0.18463	0.00065	-0.10557		2713.24427	28.16907	2701.58658	26.25781	2693.88374	5.86677	-0.71868	
Mnz3_17	0.52776	0.00668	13.57447	0.37833	0.47598		1.89502	0.02400	0.18666	0.00079	-0.05826		2731.95289	28.19631	2720.23776	26.32064	2711.76503	7.01748	-0.74445	
Mnz3_18	0.52814	0.00665	13.57933	0.37610	0.37260		1.89356	0.02386	0.18648	0.00062	0.03933		2733.59028	28.04585	2720.67664	26.13507	2710.36711	5.50678	-0.85683	
Mnz5_1	0.52694	0.00664	13.42187	0.37203	0.60675		1.89788	0.02396	0.18477	0.00058	-0.17429		2728.51724	28.05293	2709.64037	26.21985	2695.21713	5.19737	-1.23553	
Mnz5_2	0.52844	0.00677	13.53015	0.37581	0.66074		1.89272	0.02412	0.18579	0.00059	0.03660		2734.80480	28.53129	2717.20870	26.17414	2704.29541	5.23268	-1.12818	
Mnz6_1	0.52911	0.00671	13.51278	0.37417	0.71546		1.89020	0.02401	0.18530	0.00051	-0.18594		2737.66368	28.29534	2716.02650	26.15271	2700.70680	4.32775	-1.36842	
Mnz6_2	0.50237	0.00678	12.78216	0.36023	0.87442		1.99178	0.02699	0.18460	0.00058	-0.10160		2623.75227	29.09106	2663.30939	26.54051	2693.69720	5.13653	2.59661	
Mnz6_3	0.51050	0.00680	13.06858	0.36680	0.81943		1.95983	0.02616	0.18562	0.00060	-0.02223		2658.59772	29.01560	2684.25515	26.54478	2702.80458	5.30657	1.63559	
Mnz6_4	0.53316	0.00678	13.66260	0.37914	0.55181		1.87588	0.02382	0.18591	0.00064	0.01649		2754.68506	28.48544	2726.42978	26.19485	2705.31106	5.65162	-1.82508	
Mnz6_5	0.54894	0.00703	14.27788	0.39738	0.47334		1.82200	0.02327	0.18866	0.00074	0.07896		2820.69494	29.24617	2768.11439	26.40466	2729.43667	6.47129	-3.34348	
Mnz6_6	0.54069	0.00697	13.82953	0.38559	0.81081		1.84982	0.02371	0.18542	0.00060	-0.30967		2786.27970	29.11517	2737.90115	26.24835	2701.01500	5.35343	-3.15677	
Mnz6_7	0.51160	0.00674	13.07378	0.36767	0.83180		1.95552	0.02563	0.18515	0.00069	-0.22233		2663.29961	28.71832	2684.56422	26.46696	2698.48345	6.14397	1.30384	
Mnz6_8	0.52547	0.00660	13.45018	0.37229	0.54875		1.90320	0.02387	0.18548	0.00065	-0.12534		2722.29628	27.89161	2711.63448	26.10396	2701.45240	5.75964	-0.77158	
Mnz6_9	0.53462	0.00684	13.63830	0.37908	0.76110		1.87076	0.02390	0.18485	0.00054	-0.29199		2760.83377	28.72453	2724.75049	26.27997	2695.98335	4.83998	-2.40545	
Mnz6_10	0.52883	0.00672	13.47872	0.37579	0.75758		1.89116	0.02399	0.18459	0.00065	-0.47811		2736.47547	28.32518	2713.55641	26.22650	2693.50316	5.79324	-1.59541	
Mnz9_1	0.53359	0.00688	13.61990	0.38192	0.64120		1.87447	0.02430	0.18500	0.00083	-0.10101		2756.47840	28.94878	2723.37883	26.40410	2697.15289	7.37110	-2.19956	
Mnz9_2	0.53168	0.00727	13.73001	0.39932	0.74292		1.88194	0.02585	0.18730	0.00124	-0.19384		2748.31046	30.60881	2730.47740	27.49332	2717.05159	10.86719	-1.15047	
Mnz9_3	0.53173	0.00686	13.58103	0.40420	0.77051		1.88093	0.02415	0.18518	0.00165	-0.56874		2748.68411	28.85610	2720.11761	27.95351	2697.98789	14.68983	-1.87904	
Mnz9_4	0.53104	0.00676	13.58276	0.38602	0.59847		1.88341	0.02391	0.18545	0.00114	-0.28304		2745.75654	28.43822	2720.49513	26.85458	2702.26394	9.67030	-1.60949	
Mnz9_5	0.52421	0.00677	13.44977	0.37636	0.60544		1.90807	0.02488	0.18608	0.00078	-0.03575		2716.92669	28.67100	2711.47735	26.49165	2706.67025	6.90950	-0.37893	
Mnz9_6	0.52485	0.00668	13.41271	0.37723	0.65415		1.90558	0.02417	0.18522	0.00085	-0.28439		2719.67207	28.23251	2708.76331	26.57223	2698.95497	7.60835	-0.76760	
Mnz9_7	0.52794	0.00666	13.54696	0.37654	0.42123		1.89439	0.02397	0.18614	0.00074	0.09115		2732.71275	28.12040	2718.36346	26.25627	2707.28897	6.59839	-0.93909	
Mnz9_8	0.52285	0.00671	13.35159	0.37392	0.53332		1.91303	0.02459	0.18523	0.00090	0.02786		2711.18323	28.42423	2704.50373	26.33759	2699.02537	7.96469	-0.45045	
Mnz9_9	0.52264	0.00653	13.31383	0.37024	0.65779		1.91342	0.02388	0.18472	0.00071	-0.43073		2710.37231	27.65236	2701.94788	26.23721	2694.61839	6.39109	-0.58464	
Mnz9_10	0.52514	0.00664	13.35196	0.37003	0.51440		1.90440	0.02405	0.18435	0.00059	0.01874		2720.91273	28.04232	2704.72008	26.09415	2691.39543	5.28290	-1.09673	
Mnz9_11	0.54158	0.00714	14.05853	0.40264	0.68282		1.84711	0.02453	0.18816	0.00111	-0.20407		2789.90648	29.88645	2753.07967	27.08799	2724.75101	9.69318	-2.39125	
Mnz9_12	0.52814	0.00678	13.78114	0.38577	0.65405		1.89384	0.02428	0.18918	0.00077	-0.10101		2733.53755	28.58852	2734.48111	26.55195	2733.90405	6.68053	0.01341	
Mnz9_13	0.52347	0.00657	13.36194	0.37119	0.31479		1.91043	0.02402	0.18510	0.00073	0.05894		2713.84526	27.80717	2705.41477	26.20494	2698.10760	6.51795	-0.58329	
Mnz9_14	0.52009	0.00703	13.61268	0.39080	0.88285		1.92396	0.02644	0.18970	0.00084	-0.48330		2699.32179	29.89612	2722.41751	27.24979	2738.34852	7.26112	1.42519	
Mnz9_15	0.54178	0.00757	13.99354	0.39697	0.74280		1.84700	0.02538	0.18715	0.00093	0.16100		2790.62582	31.56709	2748.87376	26.63092	2716.15276	8.15778	-2.74186	
Mnz9_16	0.51712	0.00751	13.35260	0.38598	0.75853		1.93430	0.02741	0.18713	0.00112	0.14173		2686.84532	31.79345	2704.73659	27.12826	2716.19503	9.84134	1.08055	
Mnz9_17	0.51957	0.00660	13.28519	0.36884	0.69319		1.92503	0.02445	0.18533	0.00062	-0.15299		2697.27906	28.00996	2699.91425	26.11818	2700.19362	5.47184	0.10794	
Mnz9_18	0.51792	0.00660	13.21254	0.36764	0.62910		1.93115	0.02473	0.18490	0.00071	-0.07176		2690.29548	28.06031	2694.70547	26.21272	2696.25603	6.32909	0.22107	
Mnz9_19	0.50696	0.00653	12.90154	0.38187	-0.00782		1.97257	0.02529	0.18438	0.00208	0.24330		2643.64969	27.89937	2672.33788	28.08512	2691.58326	18.79772	1.78087	
Mnz9_20	0.53910	0.00319	13.69453	0.09244	0.08181		1.85599	0.01111	0.18536	0.00088	0.16200		2779.44694	13.40005	2728.49993	6.39179	2700.31161	7.82415	-2.93060	
Mnz9_21	0.52751	0.00110	13.39739	0.06720	0.68507		1.89588	0.00397	0.18509	0.00096	0.29926		2730.92920	4.66115	2707.81497	4.73553	2697.64473	8.51225	-1.23383	
Mnz8_1	0.53646	0.00199	13.62495	0.07244	0.30998		1.86468	0.00691	0.18473	0.00071	-0.05636		2768.47575	8.34697	2723.70462	5.03159	2694.72636	6.39519	-2.73680	

	Measured Ratios												Calculated Dates (Ma)							
	$^{206}Pb/^{238}U$	$^{206}Pb/^{238}U$ 2SE	$^{207}Pb/^{235}U$	$^{207}Pb/^{235}U$ 2SE	rho $^{206}Pb/^{238}U$ v $^{207}Pb/^{235}U$		$^{238}U/^{206}Pb$	$^{238}U/^{206}Pb$ 2SE	$^{207}Pb/^{206}Pb$	$^{207}Pb/^{206}Pb$ 2SE	rho $^{207}Pb/^{206}Pb$ v $^{238}U/^{206}Pb$		$^{206}Pb/^{238}U$	$^{206}Pb/^{238}U$ 2SE	$^{207}Pb/^{235}U$	$^{207}Pb/^{235}U$ 2SE	$^{207}Pb/^{206}Pb$	$^{207}Pb/^{206}Pb$ 2SE	% Disc.	
Sample 47ii																				
Mnz8_2	0.52619	0.00080	13.51774	0.05484	0.45449		1.90056	0.00288	0.18604	0.00072	0.01544		2725.34181	3.36028	2716.37467	3.83338	2706.40785	6.38629	-0.69960	
Mnz8_3	0.52515	0.00111	13.45855	0.06109	0.46870		1.90439	0.00399	0.18520	0.00080	0.15280		2720.94541	4.68930	2712.19298	4.28593	2698.91451	7.19795	-0.81629	
Mnz8_4	0.52047	0.00195	13.25165	0.06218	0.88000		1.92197	0.00732	0.18447	0.00080	0.35428		2701.06243	8.30242	2697.51492	4.44734	2692.27828	7.16951	-0.32627	
Mnz8_5	0.52975	0.00435	13.44034	0.09355	0.42472		1.89053	0.01473	0.18418	0.00069	0.38370		2739.78444	18.15827	2710.60563	6.50289	2689.77864	6.16094	-1.85910	
Mnz8_6	0.50988	0.00198	12.98497	0.08641			1.96144	0.00765	0.18441	0.00112	0.18252		2656.09531	8.46087	2678.42644	6.30884	2691.90068	10.07615	1.33011	

A 2-3: Multi element geochemistry

SAMPLE	Lithology	Easting	Northing	Ti	Al	Fe	Mg	Mn	Na	K	Ca	Ba	Sr	P	Au	Ag	As	Be	Bi	Cd	Ce	Co	Cr	Cs	Cu	Ga	Ge
				%	%	%	%	ppm	%	%	%	ppm	ppm	ppm	ppm	ppm	ppm	ppm	ppm	ppm	ppm	ppm	ppm	ppm	ppm	ppm	ppm
MERN19MDS0125DG01	QFP dyke	646662	5347897	0.085	5.82	3.39	0.35	808	3.84	0.12	0.28	30	41.2	170		0.03	0.9	0.67	0.13	0.51	52.3	1.2	22	0.08	84.5	18.55	0.11
MERN19MDS0125DG02	QFP dyke	646649	5347895	0.061	5.82	3.64	0.71	899	3.63	0.03	0.46	10	40.8	120		0.01	0.6	0.5	0.02	0.29	51.1	0.8	46	0.05	12.7	19.15	0.17
MERN19MDS0125DG03	QFP dyke	646632	5347892	0.086	5.74	3.3	0.62	442	3.74	0.03	0.33	10	40.1	130	0.008	0.31	0.5	0.5	0.25	0.09	48	2.4	43	<0.05	715	18.75	0.09
MERN19MDS0125DG04	QFP dyke	646610	5347890	0.083	5.82	3.4	0.11	993	4.03	0.25	0.46	50	35	170		0.02	<0.2	0.83	0.14	0.32	57.4	1.4	23	0.15	27.3	20.8	0.11
MERN19MDS0125DG05	QFP dyke	646590	5347889	0.057	5.94	4.53	0.45	711	3.57	0.03	0.16	10	24.4	180		0.01	<0.2	0.65	0.01	0.28	53.6	1.8	22	0.05	15.1	20.3	0.1
MERN19MDS0125DG07	QFP dyke	646550	5347872	0.097	5.74	3.86	0.52	1480	3.68	0.03	0.82	10	29.1	170		0.01	<0.2	0.73	0.05	0.16	51.7	2	27	<0.05	29.1	17.35	0.1
MERN19MDS0125DG08	QFP dyke	646536	5347870	0.077	5.76	3.94	0.73	540	3.47	0.02	0.1	10	21.2	160	0.001	0.14	0.3	0.51	0.07	0.19	49.2	1.6	24	<0.05	265	19.65	0.1
MERN19MDS0125EG09	Tonalite	646517	5347856	0.189	6.84	3.42	0.48	503	2.46	0.6	1.26	180	126	440		0.16	1.1	0.82	0.29	0.03	34.7	10.3	27	0.44	55.1	16.55	0.07
MERN19MDS0125BG10	MDD	646511	5347845	0.654	8.91	7.29	1.97	1640	2.45	0.58	4.19	160	181.5	550		0.02	0.4	0.88	0.11	0.64	7	11	13	0.46	5.6	18.55	0.05
MERN19MDS0125BG11	MDD	646509	5347841	0.594	9.99	12	2.29	1220	2.45	0.93	0.99	250	97.9	630		0.71	24.8	1.34	2.89	0.09	41.5	91.9	33	0.52	241	20.6	0.09
MERN19MDS0125BG12	MDD	646519	5347840	0.361	7.94	11.7	2.51	1560	1.47	0.55	1.55	160	51.9	480	0.002	0.69	1.2	0.49	2.2	2.87	11.5	34	31	0.42	315	17.3	0.07
MERN19MDS0125BG13	MDD	646509	5347838	0.503	9.04	11.2	3.56	1760	1.18	0.38	1.42	90	80.9	450		0.03	<0.2	0.86	0.09	0.04	10.55	10	45	0.39	2.5	20.1	0.07
MERN19MDS0125BG14	MDD	646509	5347832	0.702	9.34	9.88	2.11	1230	1.73	1.21	1.5	360	57.8	760		0.28	2.5	0.83	0.89	0.11	14.95	26.3	18	0.63	123	20.4	0.11
MERN19MDS0125BG15	MDD	646503	5347834	0.591	9.62	9.58	2.16	1440	2.04	0.95	1.55	290	94.8	740		0.04	0.3	0.91	0.32	0.06	11.15	11.7	23	0.51	36.6	19.5	0.05
MERN19MDS0125BG16	MDD	646506	5347834	0.615	11.1	12.9	2.71	1920	3.16	0.42	1.54	140	82	770		0.13	0.4	0.78	0.21	0.86	10.7	12.4	22	0.29	92	20.7	0.12
MERN19MDS0125BG17	MDD	646508	5347828	0.488	7.22	13.8	3.05	1700	0.36	0.34	0.56	110	11	790	0.002	0.54	9	0.41	0.75	0.52	11.75	24.7	21	0.21	354	19.45	0.09
MERN19MDS0125BG18	MDD	646510	5347825	0.592	7.67	9.44	2.48	1110	2.24	0.19	0.88	60	53.7	950		0.35	2	0.77	0.41	1.51	28.3	24.7	14	0.23	198.5	17.65	0.11
MERN19MDS0125BG19	MDD	646491	5347814	0.343	7.12	8.09	1.84	1140	0.76	1.04	0.35	390	17	450	<0.001	0.43	0.4	0.66	0.05	0.18	38.1	11	15	0.36	422	19.15	0.13
MERN19MDS0125BG20	MDD	646473	5347803	0.566	10.4	13.65	2.46	1800	0.46	2.1	0.13	690	15.8	640	0.023	0.76	11.4	1.26	0.67	0.14	2.09	28.9	34	0.43	251	27	0.07
MERN19MDS0125BG21	MDD	646459	5347805	0.476	7.88	13.85	3.31	2390	0.31	0.69	0.65	250	8.9	500	0.001	0.22	1	0.59	0.21	0.36	2.4	16.4	36	0.2	390	27	0.08
MERN19MDS0125DG22	QFP dyke	646437	5347800	0.158	5.9	9.04	1.12	603	0.12	0.89	0.04	440	7	220	0.005	1.26	2.1	0.53	0.47	0.05	38.8	19.3	11	0.26	2120	20.3	0.1
MERN19MDS0125DG23	QFP dyke	646420	5347791	0.138	5.86	3.38	0.69	534	2.92	0.49	0.49	130	34.1	160		0.1	1.5	0.79	0.57	0.1	46.3	7	27	0.22	64.8	18.3	0.16
MERN19MDS0125DG24	QFP dyke	646403	5347780	0.136	6	3.62	0.16	453	3.93	0.45	0.99	190	61.1	150		<0.01	0.2	1.04	0.03	0.06	56.4	0.5	34	0.29	34.8	20.6	0.15
MERN19MDS0125DG25	QFP dyke	646386	5347775	0.129	5.88	2.82	0.12	325	4.17	0.27	0.92	80	69.6	130		0.01	0.9	0.89	0.03	0.14	53.8	0.3	34	0.17	14.8	19.15	0.18
MERN19MDS0125DG26	QFP dyke	646361	5347771	0.134	5.89	2.74	0.27	649	3.95	0.09	0.97	70	62.4	150		0.04	1	0.9	0.89	0.04	52.7	2.9	27	0.09	218	18.05	0.17
MERN19MDS0125DG27	QFP dyke	646341	5347772	0.121	5.64	2.82	0.19	1080	3.75	0.34	1.86	120	52.4	120		0.01	1	0.78	0.06	0.16	46	1	23	0.19	14.2	18.6	0.16
MERN19MDS0125EG28	Tonalite	646510	5347862	0.184	7.31	3.6	0.45	511	2.38	0.49	1.85	130	146.5	500		0.11	0.5	0.99	0.37	0.07	40.2	9.1	20	0.31	59.4	16.7	0.13
MERN19MDS0125EG29	Tonalite	646500	5347869	0.165	7.17	4.19	0.59	526	2.5	1.03	0.89	220	64.7	470		0.28	1.6	0.78	0.66	0.13	39.4	9.7	43	0.42	170	16.2	0.09
MERN19MDS0125EG30	Tonalite	646484	5347880	0.201	7.38	3.57	0.5	562	2.69	0.59	1.57	170	106.5	460		0.07	1.9	0.92	0.18	0.03	31	7.6	38	0.37	38.9	16.7	0.13
MERN19MDS0125EG31	Tonalite	646465	5347885	0.181	6.77	2.96	0.56	599	3	0.38	1.77	110	96.5	430		0.03	0.9	0.83	0.08	0.07	38	5.4	29	0.28	27.1	15.8	0.08
MERN19MDS0125BG32	MDD	646512	5347803	0.465	7.16	14.25	2.64	1860	0.06	0.51	0.17	240	6.5	790		0.07	1	0.58	0.06	0.17	4.37	10.6	16	0.2	79.3	25.8	0.05
MERN19MDS0125AG33	FDD	646520	5347787	0.071	5.61	6	0.83	641	1.32	0.65	0.09	230	18.1	180	<0.001	0.43	0.5	0.67	0.02	0.1	44.1	6.1	20	0.18	394	18.95	0.08
MERN19MDS0125AG34	FDD	646533	5347772	0.083	5.7	3.28	0.5	245	3.75	0.06	0.07	20	27.6	170		0.36	0.4	0.43	0.2	0.06	62.2	2.8	13	<0.05	63.9	15.3	0.09
MERN19MDS0125AG35	FDD	646547	5347766	0.097	5.65	3.06	0.68	214	3.13	0.25	0.07	60	21.9	170	0.003	1.34	0.6	0.48	0.44	0.03	68	4.2	18	0.11	1060	13.25	0.1
MERN19MDS0125AG36	FDD	646565	5347778	0.117	6.31	5.34	1.09	319	1.01	1.04	0.07	300	23.5	310	0.005	1.99	0.9	0.84	1.08	0.02	45.5	5.4	15	0.39	1140	20.1	0.09
MERN19MDS0125AG37	FDD	646587	5347783	0.115	5.6	5.33	1.54	379	0.19	1.09	0.06	350	12.2	230		0.07	0.2	0.87	0.32	0.02	86.4	6.2	20	0.38	27	21.5	0.15
MERN19MDS0125DG38	QFP dyke	646600	5347768	0.092	5.98	3.98	0.56	647	3.43	0.21	0.22	40	43.6	140		0.03	0.3	0.85	0.03	0.28	53.4	2.2	24	0.14	106	16.9	0.08
MERN19MDS0125DG39	QFP dyke	646612	5347760	0.136	5.89	3.71	0.54	492	3.65	0.14	0.56	40	33.2	160	0.002	0.06	0.3	0.63	0.06	0.39	55	1.8	29	0.1	273	19.15	0.09
MERN19MDS0125DG40	QFP dyke	646635	5347747	0.134	5.76	3.55	0.39	393	3.74	0.05	0.31	30	47.4	140		0.18	0.6	0.93	0.11	0.34	47.4	2.2	17	0.05	148.5	18.1	0.16
MERN19MDS0125DG41	QFP dyke	646647	5347742	0.141	5.73	3.43	0.53	803	3.43	0.04	0.95	30	58.8	160		0.02	0.3	0.85	0.03	0.11	46.7	1.3	28	0.05	15	21.5	0.07
MERN19MDS0125CG51	TD	646526	5347790	0.383	6.82	18.15	2.9	1850	0.03	0.08	0.05	80	3.2	200		0.27	<0.2	0.42	0.1	0.35	1.38	13.3	33	<0.05	151	34.2	0.09

SAMPLE	Lithology	Easting	Northing	Ti	Al	Fe	Mg	Mn	Na	K	Ca	Ba	Sr	P	Au	Ag	As	Be	Bi	Cd	Ce	Co	Cr	Cs	Cu	Ga	Ge
				%	%	%	%	ppm	%	%	%	ppm	ppm	ppm	ppm	ppm	ppm	ppm	ppm	ppm	ppm	ppm	ppm	ppm	ppm	ppm	ppm	ppm
MERN19MDS0125AG57	FDD	646551	5347769	0.481	11.1	21.9	5.76	1500	0.02	0.05	0.26	10	2.7	1270	<0.001	0.71	<0.2	0.44	0.9	<0.02	22.3	26.5	9	0.08	632	50.6	0.16
MERN19MDS0125FG58	Rhyolite dyke	646452	5347913	0.137	5.45	2.33	1.16	436	3.45	0.05	1.54	30	60.5	110		0.04	3.2	0.54	0.08	0.14	27	11.3	64	0.07	69.7	12.5	0.06
MERN19MDS0125HG59	UM	646436	5347908	0.515	8.64	7.38	2.73	1220	3.08	0.14	4.7	60	162.5	460		0.04	<0.2	0.26	0.07	0.18	8.72	20.4	27	0.08	17.3	14.8	<0.05
MERN19MDS0125GG60	Andesite	646452	5347937	0.492	8.45	6.73	4.29	666	3.13	1.16	1.14	470	76.1	380		0.02	<0.2	0.35	0.01	0.06	5.46	28.9	21	0.64	1.8	18.65	0.06
MERN19MDS0125GG61	Andesite	646493	5347917	0.424	8.15	9	4.65	610	1.34	1.03	0.19	250	36.4	380		0.12	1.1	0.62	0.51	0.1	9.21	25.2	27	0.45	80.7	21.7	0.07
MERN19MDS0125GG62	Andesite	646421	5347973	0.357	8.69	8.3	4.35	928	2.87	0.18	2.84	60	90.1	450		0.11	0.2	0.48	26.1	0.06	5.21	30.8	34	0.13	61.9	19.05	0.05
MERN19MDS0125FG63	Rhyolite dyke	646426	5347987	0.097	5.78	2.2	0.97	216	1.89	1.14	0.22	350	23.2	140		0.03	0.2	0.54	0.03	0.07	51.6	4.2	28	0.47	21.1	11.15	0.09
MERN19MDS0125AG64	FDD	646576	5347798	0.084	5.66	3.73	0.74	637	3.25	0.08	0.67	20	19.3	140		0.02	0.5	0.54	0.01	0.19	59.1	1.6	39	0.07	9.7	17.8	0.17
MERN19MDS0125AG65	FDD	646594	5347816	0.328	7.46	15.65	2.08	913	0.07	0.44	0.15	220	6.1	730	0.019	2.1	1.3	0.39	1.57	0.11	5.12	19.7	25	0.2	1480	24.2	0.06
MERN19MDS0125CG66	TD	646528	5347840	0.44	8.65	12.8	1.74	1380	0.29	1.53	0.1	1040	22.7	620	0.039	12.8	2.9	0.86	4.71	0.21	0.75	26.9	23	0.36	3360	23.4	0.11
MERN19MDS0125BG67	MDD	646533	5347840	0.453	7.77	13	2.47	1440	0.25	0.73	0.18	280	12.9	710		0.43	0.5	0.56	0.27	0.4	12.25	20.4	24	0.32	174	20.9	0.1
MERN19MDS0125DG68	QFP dyke	646366	5347750	0.108	5.97	3.68	0.43	407	3.66	0.19	0.32	40	48.8	140		0.05	0.8	0.73	0.29	0.13	52.2	2.8	24	0.13	72.9	19.5	0.18

SAMPLE	Lithology	Easting	Northing	Hf	In	La	Li	Mo	Nb	Ni	Pb	Rb	Re	S	Sb	Sc	Se	Sn	Ta	Te	Th	Tl	U	V	W	Y	Zn	Zr
				ppm	ppm	ppm	ppm	ppm	ppm	ppm	ppm	ppm	ppm	%	ppm	ppm	ppm	ppm	ppm	ppm	ppm	ppm	ppm	ppm	ppm	ppm	ppm	ppm
MERN19MDS0125DG01	QFP dyke	646662	5347897	6.2	0.266	22.5	10.3	2.25	7.6	1.9	7.4	3.5	<0.002	0.15	0.2	12.2	<1	9.5	0.47	0.05	2.32	0.03	0.5	5	0.4	15.9	101	224
MERN19MDS0125DG02	QFP dyke	646649	5347895	6.1	0.087	22	16.2	3.85	6.2	1.1	2.3	0.9	<0.002	0.01	0.08	10.7	1	1.1	0.4	<0.05	2.26	<0.02	0.5	1	0.6	12.7	102	225
MERN19MDS0125DG03	QFP dyke	646632	5347892	5.1	0.305	20.5	15.2	3.83	8.5	1.7	1	0.6	<0.002	0.11	0.08	11.4	1	2.3	0.5	0.15	2.31	<0.02	0.6	1	0.5	16.7	93	215
MERN19MDS0125DG04	QFP dyke	646610	5347890	5.8	0.199	28.7	5.8	3.45	7.2	1.3	1.6	7.6	<0.002	0.31	0.07	14	1	9.3	0.48	<0.05	2.35	0.04	0.6	5	0.4	17.3	52	229
MERN19MDS0125DG05	QFP dyke	646590	5347889	6.1	0.148	22.6	18	2.74	4.9	1.4	1.8	0.8	<0.002	<0.01	0.2	14.1	<1	1.5	0.34	<0.05	2.3	<0.02	0.6	6	0.1	13.5	147	244
MERN19MDS0125DG07	QFP dyke	646550	5347872	5.5	0.126	22.3	13.7	3.03	8.5	2	1.1	0.8	<0.002	0.05	0.06	12.4	1	8.7	0.52	<0.05	2.29	<0.02	0.6	5	0.2	15.6	106	226
MERN19MDS0125DG08	QFP dyke	646536	5347870	6	0.164	21.2	13.7	2.59	7.1	1.7	2.4	0.4	<0.002	0.03	0.05	12.6	1	1.9	0.44	0.05	2.35	<0.02	0.6	4	0.2	16.1	106	242
MERN19MDS0125EG09	Tonalite	646517	5347856	3	0.032	15.7	16.6	2.09	7.7	2.3	1.2	14.3	<0.002	0.6	0.06	9.1	1	3.3	0.53	0.07	2.26	0.07	0.6	20	0.4	11.4	46	104.5
MERN19MDS0125BG10	MDD	646511	5347845	0.7	0.128	2.8	45.8	2.26	2.1	12.4	0.6	8.1	0.006	0.05	0.1	29.5	1	7.1	0.12	<0.05	0.36	0.08	0.1	307	0.5	11.8	176	30.3
MERN19MDS0125BG11	MDD	646509	5347841	0.8	0.132	17.4	41.4	0.78	2.6	18.6	2.5	9.2	<0.002	4.34	0.28	32.1	5	9.3	0.13	0.29	0.41	0.1	0.2	288	1	21.5	155	34.9
MERN19MDS0125BG12	MDD	646519	5347840	0.9	0.37	4.5	44.1	1.79	2.1	20.2	2	8.9	<0.002	1.85	0.15	30.3	2	10.2	0.11	0.1	0.42	0.07	0.1	291	0.8	7.8	344	38.4
MERN19MDS0125BG13	MDD	646509	5347838	0.5	0.109	4.7	61	0.88	1.7	31.7	<0.5	6.8	0.003	0.02	0.11	38.1	1	12.1	0.09	<0.05	0.31	0.05	0.1	305	0.5	8.6	199	21.5
MERN19MDS0125BG14	MDD	646509	5347832	2.1	0.096	7	35.1	0.64	4.1	11.7	1.7	26.5	<0.002	1.34	0.15	31.7	2	8.3	0.25	0.1	0.94	0.13	0.3	328	1.3	18.5	125	78.2
MERN19MDS0125BG15	MDD	646503	5347834	0.7	0.138	4.3	42.1	0.95	1.9	11.6	0.7	14.6	0.002	0.14	0.11	31.9	<1	7.4	0.1	0.07	0.33	0.11	0.1	305	1.3	13.9	111	28.8
MERN19MDS0125BG16	MDD	646506	5347834	0.8	0.095	3.9	50.3	0.53	2	10.6	1.4	2.7	<0.002	0.11	0.11	33.3	1	5	0.11	<0.05	0.29	0.05	0.1	343	2.2	17.4	249	28.8
MERN19MDS0125BG17	MDD	646508	5347828	2.8	0.157	5.2	51.9	1.65	3.7	18.3	2.8	1.8	<0.002	0.94	0.15	23.8	2	5.2	0.24	0.12	0.65	0.04	0.3	293	2.3	14	213	109.5
MERN19MDS0125BG18	MDD	646510	5347825	3.3	0.149	12.6	39.4	1.12	4.7	15.7	4.8	4.7	<0.002	1.27	0.11	26.1	1	9.5	0.32	0.07	1.31	0.03	0.3	270	1.1	14.9	224	129.5
MERN19MDS0125BG19	MDD	646491	5347814	5.4	0.212	18.2	27.2	1.19	6.7	8.8	0.7	18.2	<0.002	0.02	0.06	19.5	1	5.7	0.52	<0.05	2.07	0.08	0.6	150	3	13.8	118	198
MERN19MDS0125BG20	MDD	646473	5347803	1	0.475	0.7	33	0.39	2.2	13.8	2.4	12.7	<0.002	0.37	0.08	32.6	2	11.8	0.11	0.34	0.13	0.21	0.1	348	4.1	2.8	213	34.6
MERN19MDS0125BG21	MDD	646459	5347805	1.9	0.234	0.9	36.5	0.9	4.3	15	1.6	2.8	<0.002	0.08	0.08	26.6	1	4.8	0.22	0.06	0.31	0.08	0.3	271	2.1	4.7	232	69
MERN19MDS0125EG22	QFP dyke	646437	5347800	5.3	1.245	16.2	24	1.1	8.4	3.7	1.6	16.1	<0.002	0.52	0.07	14.2	2	8.4	0.54	0.22	2.12	0.07	0.6	47	2.5	8.5	98	194.5
MERN19MDS0125DG23	QFP dyke	646420	5347791	5.9	0.106	21.4	9.3	2.91	13.3	1	1.3	14.1	<0.002	0.37	0.05	12.2	<1	3.4	0.79	0.06	2.34	0.07	0.6	3	0.7	21.5	59	222
MERN19MDS0125DG24	QFP dyke	646403	5347780	6.2	0.136	24.1	3.9	3.33	14.6	1.4	1.3	13.6	<0.002	0.04	0.1	12.9	<1	2.3	0.88	<0.05	2.47	0.06	0.6	4	2.1	41.4	29	228
MERN19MDS0125DG25	QFP dyke	646386	5347775	6.1	0.118	23.9	3.7	3.58	13.7	0.9	1.8	8.4	<0.002	0.03	0.11	12.5	1	2.1	0.85	<0.05	2.35	0.05	0.6	1	1.2	18.8	24	218
MERN19MDS0125DG26	QFP dyke	646361	5347771	5.5	0.175	22.7	8.8	3.01	12.8	0.9	1.5	2.4	<0.002	0.27	0.1	12.8	1	3.4	0.74	0.35	2.39	<0.02	0.6	2	0.6	27.5	45	211
MERN19MDS0125DG27	QFP dyke	646341	5347772	5.5	0.14	21.1	6.2	2.19	12	0.8	1.1	8.8	<0.002	0.19	0.08	11.2	1	1.6	0.77	<0.05	2.03	0.04	0.5	1	1.7	15.5	36	192.5
MERN19MDS0125EG28	Tonalite	646510	5347862	3.6	0.046	19.1	18.3	1.86	7.8	2.2	1.6	11	<0.002	0.88	0.08	9.4	1	2.8	0.54	0.07	2.28	0.05	0.6	20	0.3	12.9	49	119.5
MERN19MDS0125EG29	Tonalite	646500	5347869	2.9	0.123	19.5	14.7	4.08	6.5	2.6	1.6	24.4	<0.002	0.39	0.1	9	1	4.9	0.46	0.09	2.32	0.12	0.6	19	0.6	19.2	76	102
MERN19MDS0125EG30	Tonalite	646484	5347880	3.3	0.06	13.7	17.5	3.16	8.4	2.4	1.4	14.1	<0.002	0.44	0.12	9.3	1	2.6	0.59	0.05	2.41	0.07	0.6	19	0.2	13.4	50	101.5
MERN19MDS0125EG31	Tonalite	646465	5347885	3.2	0.041	17.8	17.2	2.79	7.9	3.6	0.9	8.8	<0.002	0.19	<0.05	7.7	<1	2.5	0.53	<0.05	2.32	0.04	0.6	19	0.1	11.7	48	117.5
MERN19MDS0125BG32	MDD	646512	5347803	3	0.115	1.5	41.9	0.98	4.8	17.1	0.6	2.6	<0.002	0.04	0.09	25.4	<1	6.1	0.27	<0.05	0.46	0.05	0.3	276	6	3.4	254	132
MERN19MDS0125AG33	FDD	646520	5347787	5.8	0.195	19.2	15.4	1.6	5.8	1.4	1.2	10.6	<0.002	0.03	0.07	12.6	1	5.2	0.37	<0.05	2.26	0.05	0.6	7	0.4	12.1	90	230
MERN19MDS0125AG34	FDD	646533	5347772	5.9	0.124	27.5	8.8	3.12	6.8	0.9	1.9	0.9	<0.002	0.01	0.11	11.6	1	1.1	0.42	0.13	2.13	<0.02	0.6	7	0.6	14.5	38	239
MERN19MDS0125AG35	FDD	646547	5347766	5.7	0.487	31.3	11.2	10.75	8.5	2.4	1.4	4.8	<0.002	0.17	0.06	11.3	1	4	0.52	0.23	2.29	0.03	0.7	5	0.8	15.3	40	228
MERN19MDS0125AG36	FDD	646565	5347778	5.2	0.887	19.7	22.8	3.91	6.3	1.7	2.2	22.6	<0.002	0.13	0.1	15	2	9.1	0.4	0.49	2.17	0.11	0.5	14	1.3	11.9	62	201
MERN19MDS0125AG37	FDD	646587	5347783	5.5	0.095	36.4	28.2	3.52	10.4	2.3	1	23.9	<0.002	0.03	0.05	19.3	<1	9	0.5	0.21	2.13	0.11	0.9	25	2.4	14.7	73	231
MERN19MDS0125DG38	QFP dyke	646600	5347768	6.2	0.086	23.2	13.1	2.12	8.8	1.4	1.6	5.3	<0.002	0.03	0.08	9.1	<1	1	0.55	<0.05	2.44	0.04	0.6	2	0.7	14.7	73	253
MERN19MDS0125DG39	QFP dyke	646612	5347760	5.6	0.123	23.8	9.6	2.98	13.7	1.7	1.1	3.3	0.002	0.13	0.05	11.8	<1	1.8	0.8	<0.05	2.29	0.02	0.6	5	0.3	17.2	52	231
MERN19MDS0125DG40	QFP dyke	646635	5347747	6.4	0.107	20.9	8.2	2.34	14.4	0.8	1.8	1.1	<0.002	0.71	0.06	12.9	1	1.9	0.83	0.21	2.41	<0.02	0.6	2	0.2	30.2	41	229
MERN19MDS0125DG41	QFP dyke	646647	5347742	5.5	0.202	20.2	10.3	2.16	14.4	1.2	1.1	0.9	<0.002	0.03	0.05	13.2	<1	4.2	0.81	<0.05	2.53	<0.02	0.7	3	0.3	51.9	64	230
MERN19MDS0125CG51	TD	646526	5347790	1	0.151	0.5	51.4	0.87	3	14.6	<0.5	0.4	<0.002	0.01	0.08	20	1	5.9	0.09	<0.05	0.08	<0.02	0.1	432	3.5	0.9	360	42.3

SAMPLE	Lithology	Easting	Northing	Hf	In	La	Li	Mo	Nb	Ni	Pb	Rb	Re	S	Sb	Sc	Se	Sn	Ta	Te	Th	Tl	U	V	W	Y	Zn	Zr
				ppm	ppm	ppm	ppm	ppm	ppm	ppm	ppm	ppm	ppm	%	ppm	ppm	ppm	ppm	ppm	ppm	ppm	ppm	ppm	ppm	ppm	ppm	ppm	ppm
MERN19MDS0125AG57	FDD	646551	5347769	4.9	0.44	9.4	88.3	1.47	8.3	8.2	1.3	0.5	<0.002	0.07	0.08	30.5	1	4.2	0.31	0.52	0.81	<0.02	0.5	284	16	6.8	283	192.5
MERN19MDS0125FG58	Rhyolite dyke	646452	5347913	6.1	0.028	11.7	9.3	6.79	7.3	4.1	1.9	1.2	<0.002	0.05	0.06	6.8	<1	0.8	0.58	<0.05	3.34	<0.02	0.9	26	0.1	26.9	34	255
MERN19MDS0125HG59	UM	646436	5347908	0.6	0.129	3.3	11	3.44	2.1	17.2	1	0.9	<0.002	0.04	0.11	31.2	<1	4.2	0.11	<0.05	0.34	<0.02	0.1	282	0.2	10.3	91	21.3
MERN19MDS0125GG60	Andesite	646452	5347937	0.8	0.042	2.2	33.3	0.56	2	18.8	0.5	7.7	<0.002	0.01	<0.05	29.5	<1	0.6	0.11	<0.05	0.25	0.1	0.1	299	0.1	9.9	124	31.9
MERN19MDS0125GG61	Andesite	646493	5347917	0.6	0.124	3.5	54	0.35	1.8	19.2	0.6	9.9	<0.002	0.2	1.61	23	1	3.6	0.09	0.21	0.15	0.17	0.1	288	1.1	3.2	178	23.7
MERN19MDS0125GG62	Andesite	646421	5347973	0.6	0.168	2.2	71.9	0.65	1.9	32.7	4.6	1.8	<0.002	0.17	0.08	30.2	1	7.3	0.12	16.15	0.28	0.04	0.1	265	0.8	2.9	185	28
MERN19MDS0125FG63	Rhyolite dyke	646426	5347987	6.2	0.031	22.4	12.9	2.74	6.1	1.5	1.3	27.1	<0.002	0.01	<0.05	7.1	<1	1.8	0.46	<0.05	3.33	0.15	0.8	3	0.2	18.1	47	254
MERN19MDS0125AG64	FDD	646576	5347798	5.3	0.064	26.1	9.7	3.19	8.2	1.6	1.1	2	<0.002	0.01	<0.05	12.2	<1	1.2	0.51	<0.05	2.19	<0.02	0.5	2	0.6	12.6	58	198.5
MERN19MDS0125AG65	FDD	646594	5347816	2.7	0.672	1.7	48.2	1.39	2.8	14.9	3.4	2.5	<0.002	0.27	0.33	25	2	5.9	0.17	0.4	0.43	0.03	0.2	245	3.7	2.9	257	106.5
MERN19MDS0125CG66	TD	646528	5347840	0.9	3.4	<0.5	39.9	0.79	2	13.1	1.7	7.2	<0.002	0.93	0.25	24.8	10	20.6	0.1	0.74	0.13	0.09	0.1	281	2.4	1.2	204	36.1
MERN19MDS0125BG67	MDD	646533	5347840	3.1	0.228	4.7	48.4	0.93	5.3	16.4	0.8	6.4	<0.002	0.07	0.08	27.2	1	11	0.3	0.05	0.67	0.07	0.3	227	1.9	5.4	232	121
MERN19MDS0125DG68	QFP dyke	646366	5347750	5.8	0.183	22.9	14.6	3.29	10.9	0.6	1.6	5.3	<0.002	0.5	0.07	12.4	1	3.7	0.68	0.09	2.4	0.03	0.6	2	0.7	15.6	78	215

A 2-4: Whole-rock geochemistry

Number	Field Description	Alteration	UTM-East	UTM-North	SiO2	TiO2	Al2O3	Fe2O3t	Cr2O3	MnO	MgO	CaO	SrO	BaO
					%	%	%	%	%	%	%	%	%	%
MERN17MDS0041AG03	Powell tonalite	L-A	644674	5347418	75.5	0.26	11.95	4.88	0	0.05	1.55	0.08	0	0.01
MERN18MDS0087AG01	Powell tonalite	spotted	644635	5347296	68.9	0.45	13.1	8.22	0	0.1	3.52	0.2	0	0.02
MERN17MDS0073AG01	Powell Tonalite	L-A	644512	5347244	76.7	0.26	11.7	4.11	0	0.04	1.32	0.16	0	0.01
MERN18MDS0106AG01	Joliet Tonalite	L-A	646474	5347883	71.3	0.36	13.65	4.61	0.003	0.08	0.78	2.61	0.01	0.01
MERN19MDS0125EG09	Joliet tonalite	L-A	646517	5347856	71	0.36	14.25	5.19	0.006	0.08	0.87	1.87	0.01	0.02
MERN19MDS0125EG28	Joliet tonalite	L-A	646510	5347862	70	0.35	13.95	5.13	0.005	0.07	0.79	2.51	0.02	0.01
MERN18MDS0107AG01	QFP dyke	L-A	646710	5347834	74.2	0.24	10.9	4.48	0.002	0.12	0.34	2.08	0.01	0.06
MERN19MDS0125AG49	QFP dyke clast	L-A (Core of clast)	646586	5347789	75.2	0.27	10.75	6.09	0.003	0.03	1.44	0.11	0.01	0.02
MERN19MDS0125DG42	QFP dyke	L-A	646712	5347827	76.8	0.26	11.45	5.5	0.004	0.09	0.55	0.67	0.01	0.02
MERN19MDS0125AG70	QFP dyke clast	Spotted	646551	5347769	74	0.26	11.05	7.32	0.002	0.05	2.11	0.06	0.01	0.04
MERN19MDS0125AG49	QFP dyke clast	sericite	646586	5347789	75.9	0.27	10.4	7.1	0.003	0.04	1.79	0.05	0.01	0.05
MERN19MDS0125DG43	QFP dyke	sericite	646712	5347827	80.1	0.26	12.2	2.2	0.004	0.02	0.31	0.09	0.01	0.14
MERN18MDS0098AG05	Powell Andesite	weakly altered	644616	5348043	57.9	0.98	14.6	11.8	0.01	0.22	6.65	0.28	0.01	0.01
MERN18MDS0098AG07	Powell Andesite	L-A	644616	5348043	53	1.02	15.45	10.3	0.01	0.31	6.23	3.37	0.01	0.01
MERN18MDS0099AG01	Powell Andesite	L-A	644419	5347923	52.8	1.39	13.75	10.2	0	0.42	3.98	3.8	0.01	0.01
MERN18MDS0113AG01	Powell Andesite	L-A	645805	5347679	59.1	1.24	13.65	9.49	0.003	0.12	6.55	0.47	0.01	0.01
MERN18MDS0124AG01	Powell Andesite	L-A	644476	5348228	54.6	1.06	13.65	9.99	0.009	0.22	7.35	2.56	0.01	0.01
MERN19MDS0125BG54B	Mafic clast	L-A (Core of clast)	646515	5347789	45.1	0.64	17.95	14.8	0.005	0.32	3.21	5.39	0.01	0.06
MERN19MDS0125BG55a	Mafic clast (amyg.)	L-A (Core of clast)	646518	5347800	53.4	1.4	15.6	13.25	0.002	0.23	3.33	3.44	0.01	0.04
MERN19MDS0125DG48	patchy chlorite	chlorite	646586	5347789	28.1	1.56	21	32.9	0.003	0.19	8.06	0.3	0.01	0.01
MERN19MDS0125AG50	patchy chlorite	chlorite	646527	5347791	45.1	1.2	15.4	25.7	0.016	0.24	5.16	0.22	0.01	0.01
MERN19MDS0125BG54	Mafic clast	chlorite (rim)	646515	5347789	38.4	0.72	19.65	25.6	0.006	0.27	5.45	0.5	0.01	0.03
MERN19MDS0125BG55b	Mafic clast (amyg.)	chlorite (rim)	646518	5347800	57.4	1.35	15	12.55	0.002	0.19	3.43	1.94	0.01	0.02
MERN19MDS0125AG52	Mafic clast	Spotted	646522	5347784	46.2	0.77	19.85	19.35	0.008	0.2	4.7	0.19	0.01	0.06
MERN19MDS0125AG53	Mafic clast	Spotted	646522	5347784	44.5	1.01	18.7	22	0.005	0.19	4.51	0.2	0.01	0.04
MERN18MDS0098AG08	Andesite	Spotted	644616	5348043	54.1	0.98	14.95	14.6	0.02	0.25	7.23	0.22	0.01	0.04
MERN18MDS0098AG04	Andesite	Spotted	644609	5348031	56	1	14.95	14.8	0.01	0.27	6.96	0.23	0.01	0.04

Number	Na2O	K2O	P2O5	LOI	Total	VFF	C	S	H20+	Cl	F	S.G.	Ag	As	Ba	Bi	Cd	Ce	Co
	%	%	%				%	%	%	ppm	ppm		ppm	ppm	ppm	ppm	ppm	ppm	ppm
MERN17MDS0041AG03	4.65	0.34	0.03	1.6	100.9	1.01	0.02	0.01	1.54	25	440	2.67	0.25	0.2	64.3	0.03	0.25	52	2
MERN18MDS0087AG01	2.31	0.95	0.09	2.82	100.68	1.02	0.03	0.01	3.32	110	710	2.68	0.25	0.05	130		0.25	40.2	4
MERN17MDS0073AG01	4.87	0.37	0.06	1.23	100.83	1.01	0.04	0.01	1.18	25	300	2.72	0.25	0.1	56	0.03	0.25	119	1
MERN18MDS0106AG01	4.5	0.38	0.1	2.78	101.67	1.02	0.42	0.1		25	290	2.74	0.25	0.6	89.4	0.05	0.6	33.1	6
MERN19MDS0125EG09	3.39	0.74	0.11	2.88	100.78	1.02	0.33	0.53					0.25	1.4	184	0.3	0.25	37.2	13
MERN19MDS0125EG28	3.15	0.57	0.11	3.4	100.07	1.03	0.46	0.8					0.25	1.1	132	0.37	0.25	40.7	10
MERN18MDS0107AG01	3.07	1.24	0.04	2.79	99.57	1.03	0.46	0.02		25	480	2.75	0.25	4.6	497	0.02	0.25	44.4	0.5
MERN19MDS0125AG49	3.06	0.74	0.03	1.89	99.63	1.02	0.01	0.6		25	230	2.77	2	0.8	160	1.16	0.25	48.2	11
MERN19MDS0125DG42	4.43	0.47	0.03	1.36	101.63	1.00	0.12	0.04		25	260	2.72	0.25	0.2	178	0.04	0.25	42.9	1
MERN19MDS0125AG70	0.29	1.64	0.03	2.45	99.3	1.03	0.01	0.01					0.25	0.8	338	0.22	0.25	57.9	6
MERN19MDS0125AG49	0.31	1.6	0.04	2.52	100.07	1.03	0.01	0.48		25	340	2.8	1.2	1	435	1.32	0.25	53.7	13
MERN19MDS0125DG43	0.23	3.59	0.04	1.8	100.98	1.01	0.01	0.02		25	1010	2.8	0.25	0.05	1230	0.02	0.25	57.7	0.5
MERN18MDS0098AG05	3.23	0.05	0.14	4.02	99.88	1.04	0.02	0.04	4.62	50	470	2.75	0.25	0.3	21.9	0.13	0.25	33.8	28
MERN18MDS0098AG07	3.73	0.45	0.16	6.14	100.18	1.06	0.73	0.01	4.05	25	610	2.67	0.25	0.05	83		0.9	29.2	19
MERN18MDS0099AG01	4.7	0.16	0.34	6.45	98.01	1.09	1.33	0.16	2.68	25	520	2.69	0.25	0.4	62.7		0.9	18.2	18
MERN18MDS0113AG01	4.16	0.1	0.17	3.86	100.32	1.05	0.06	0.02		25	530	2.69	0.25	0.3	68.4	0.01	0.5	29.2	23
MERN18MDS0124AG01	4.83	0.26	0.17	3.34	100.36	1.06	0.01	0.01		25	610	2.7	0.25	0.2	80.5	0.01	1	32.3	28
MERN19MDS0125BG54B	1.18	2.23	0.1	7.48	98.47	1.10	1.23	0.7		25	590	2.74	1.3	4.1	502	1.76	0.25	14.2	25
MERN19MDS0125BG55A	2	1.29	0.21	5.25	99.44	1.06	0.67	0.54		25	600	2.71	0.6	7.1	323	1.74	0.25	33.4	49
MERN19MDS0125DG48	0.05	0.07	0.22	7.11	99.56	1.08	0.02	0.17		180	680	2.76	0.7	0.3	23.9	0.67	0.25	32.3	23
MERN19MDS0125AG50	0.04	0.06	0.12	5.29	98.55	1.07	0.04	0.02		180	470	2.82	0.25	0.05	22.7	0.06	0.5	9.6	15
MERN19MDS0125BG54	0.55	0.93	0.11	5.87	98.09	1.08	0.13	0.38		25	510	2.84	2.4	1.8	228	0.45	0.25	43.6	23
MERN19MDS0125BG55B	2.54	0.8	0.22	4.36	99.8	1.05	0.35	0.08		25	570	2.77	0.25	0.3	214	0.18	0.25	28.8	13
MERN19MDS0125AG52	0.4	2.08	0.1	5.25	99.16	1.06	0.03	0.05		25	740	2.72	0.8	0.05	552	0.09	3.1	12.5	13
MERN19MDS0125AG53	0.56	1.39	0.13	5.16	98.4	1.07	0.01	0.26		25	620	2.81	2	1.3	395	0.16	0.25	21.5	22
MERN18MDS0098AG08	0.05	1.53	0.15	5.09	99.21	1.06	0.02	0.01	6.14	25	790	2.76	0.25	0.05	369		0.25	29.5	24
MERN18MDS0098AG04	0.39	1.22	0.16	4.73	100.76	1.04	0.01	0.05	6.28	50	520	2.85	0.25	0.3	355		0.25	27.5	29

Number	Cr	Cs	Cu	Dy	Er	Eu	Ga	Gd	Ge	Hf	Hg	Ho	In	La	Li	Lu	Mo	Nb	Nd	Ni	Pb
	ppm	ppm	ppm	ppm	ppm	ppm	ppm	ppm	ppm	ppm	ppm	ppm	ppm	ppm	ppm	ppm	ppm	ppm	ppm	ppm	ppm
MERN17MDS0041AG03	10	0.15	7	8.01	4.97	1.68	19.4	7.51	2.5	5.4	0	1.7	0.04	23.5	10	0.81	1	12.3	30.7	1	2
MERN18MDS0087AG01	20	0.25	15	7.9	5.38	0.95	22.1	7.01	2.5	5.5	0	1.7	0.05	16.9	40	0.75	0.5	13.3	22.3	2	1
MERN17MDS0073AG01	10	0.23	24	9.02	5.58	3.46	18.2	10.25	2.5	2.8	0	1.9	0.04	58.9	10	0.69	1	12.2	58.8	2	1
MERN18MDS0106AG01	10	0.2	19	4.62	3.31	0.93	16.4	4.17	2.5	4.4	0.003	1.1	0.06	16.3	20	0.58	1	8	17.2	12	1
MERN19MDS0125EG09	30	0.47	57	5.2	3.51	1.3	17.4	5.11	2.5	5.2	0.006	1.2	0.02	16.9	20	0.62	3	9.1	18.9	4	4
MERN19MDS0125EG28	20	0.34	60	5.48	3.56	1.51	16.8	5.45	2.5	5.1	0.003	1.2	0.03	19.1	20	0.6	2	9.1	21	0.5	2
MERN18MDS0107AG01	10	0.41	6	8.26	5.84	1.72	20.4	7.46	2.5	5.9	0.003	1.9	0.04	20.3	10	0.95	1	14.4	26.1	2	1
MERN19MDS0125AG49	20	0.16	2870	8.5	5.59	1.05	16.6	8.09	2.5	6.1	0.01	1.8	0.83	20.8	20	0.96	1	14	28.8	2	1
MERN19MDS0125DG42	10	0.14	30	8.61	5.74	1.72	18.5	7.8	2.5	6.6	0.003	1.8	0.06	18.9	20	1.02	2	14.3	26.1	1	1
MERN19MDS0125AG70	10	0.44	15	6.66	4.39	1.16	22	7.19	2.5	6.7	0.003	1.4	0.06	25.2	20	0.83	1	11.8	32	6	5
MERN19MDS0125AG49	20	0.36	312	8.72	5.57	1.05	20.2	8.98	2.5	6.2	0.003	1.8	0.13	23.5	20	0.97	2	13.3	31.2	6	1
MERN19MDS0125DG43	10	1.2	13	9.93	6.56	2.1	27.5	8.74	2.5	8.5	0.003	2.2	0.03	25.1	<10	1.16	1	17.9	36.7	3	1
MERN18MDS0098AG05	80	0.18	444	3.88	2.27	1.2	17.7	4.16	2.5	3.3	0	0.8	0.14	13.3	30	0.36	1	6.7	18.9	73	3
MERN18MDS0098AG07	80	0.23	9	4.19	2.7	1.13	19.3	3.81	2.5	3.4	0	0.9	0.12	11.7	20	0.4	1	6.7	17.2	70	1
MERN18MDS0099AG01	20	0.08	336	3.85	2.59	1.26	18.4	3.76	2.5	2.1	0	0.8	0.13	7.6	10	0.37	1	4.8	12.2	10	6
MERN18MDS0113AG01	5	0.22	12	4.67	2.97	1.22	19.5	4.56	2.5	3.5	0.003	1	0.06	14.2	30	0.44	0.5	6.1	16.3	13	1
MERN18MDS0124AG01	50	0.57	2	3.65	2.43	0.89	15.5	3.79	2.5	3.4	0.003	0.8	0	15.4	20	0.37	0.5	6.4	17.5	52	1
MERN19MDS0125BG54B	40	0.65	159	2.09	1.06	0.63	19.7	1.96	2.5	0.6	0.003	0.4	0.14	7.2	30	0.18	0.5	1.7	7.7	28	1
MERN19MDS0125BG55A	10	0.48	184	4.23	2.24	1.9	19.7	5.22	2.5	3.7	0.003	0.8	0.16	14.1	30	0.35	1	6.4	20	20	1
MERN19MDS0125DG48	10	0.17	316	8.55	5.13	0.74	45.8	7.5	2.5	3.9	0.003	1.7	0.35	14.8	100	0.74	1	18.5	19.1	15	1
MERN19MDS0125AG50	120	0.14	145	4.98	3.13	0.54	29.8	3.96	2.5	1.7	0.003	1.1	0.13	4.3	60	0.52	1	4.5	6.6	19	1
MERN19MDS0125BG54	40	0.29	2580	3.42	1.81	1.51	29.2	4.92	2.5	0.6	0.003	0.7	0.99	22	50	0.26	1	2	21.7	37	2
MERN19MDS0125BG55B	10	0.33	69	3.95	2.26	1.58	19.1	5.06	2.5	3.5	0.003	0.8	0.1	12.4	30	0.33	1	6.2	17.7	17	1
MERN19MDS0125AG52	80	0.56	824	3.72	2.17	0.58	27.9	3.22	2.5	0.6	0.003	0.8	0.34	8.3	50	0.27	0.5	2.6	7.6	22	1
MERN19MDS0125AG53	30	0.45	1500	7.46	4.85	0.98	28.6	5.74	2.5	2	0.005	1.6	0.71	9.2	50	0.68	1	6	14.2	17	1
MERN18MDS0098AG08	90	0.62	61	4.35	2.8	0.74	19	4.05	2.5	3.2	0	0.9	0.1	12	30	0.38	1	6.5	17	71	1
MERN18MDS0098AG04	80	0.41	525	3.64	2.21	0.9	18.5	3.76	2.5	3.1	0	0.8	0.14	10.8	30	0.34	1	6.6	14.8	72	1

Number	Rb	Re	Sb	Sc	Se	Sm	Sn	Sr	Ta	Tb	Te	Th	Tl	Tm	U	V	W	Y	Yb	Zn	Zr
	ppm	ppm	ppm	ppm	ppm	ppm	ppm	ppm	ppm	ppm	ppm	ppm	ppm	ppm	ppm	ppm	ppm	ppm	ppm	ppm	ppm
MERN17MDS0041AG03	7.2	0	0.03	12	0.1	7.15	2	18.6	0.7	1.31	0	2.07	0.01	0.72	0.54	2.5	2	40.7	5.36	149	192
MERN18MDS0087AG01	16.1	0	0.03	16	0.1	5.78	4	14.9	0.7	1.48	0	1.82	0.01	0.77	0.66	11	1	51.4	5.15	371	212
MERN17MDS0073AG01	7.6	0	0.03	10	0.1	12.2	2	34.7	0.5	1.49	0	2.95	0.01	0.75	0.41	2.5	1	45	5.07	111	101
MERN18MDS0106AG01	7.7	0.0005	0.05	9	0.1	4.2	4	143	0.5	0.8	0	2.38	0.01	0.49	0.64	19	0.5	28.2	3.46	98	192
MERN19MDS0125EG09	15.7	0.0005	0.11	10	0.3	4.76	4	139	0.7	0.86	0.1	2.71	0.01	0.59	0.71	27	1	34	4.16	54	185
MERN19MDS0125EG28	11.5	0.0005	0.07	9	0.5	5.2	3	155	0.6	0.93	0.1	2.47	0.01	0.57	0.67	25	1	34	3.96	50	185
MERN18MDS0107AG01	25.3	0.0005	0.06	12	0.1	6.74	2	51.4	0.8	1.37	0	2.43	0.01	0.92	0.65	2.5	1	49.3	6.21	65	259
MERN19MDS0125AG49	11	0.001	0.025	12	1.7	7.08	9	21.8	0.9	1.43	0.8	2.47	0.01	0.92	0.85	8	3	52.3	6.16	52	225
MERN19MDS0125DG42	9.5	0.0005	0.025	12	0.1	7.16	4	56.6	1	1.44	0	2.62	0.01	0.94	0.73	2.5	2	52.8	5.98	102	233
MERN19MDS0125AG70	26.3	0.0005	0.05	15	0.1	8.35	10	11.7	0.9	1.01	0.1	2.53	0.01	0.71	0.92	14	3	36.3	4.91	71	240
MERN19MDS0125AG49	27.1	0.0005	0.025	13	0.7	7.86	13	11	0.9	1.47	0.9	2.5	0.01	0.93	0.93	12	3	52.8	5.55	63	223
MERN19MDS0125DG43	74.1	0.0005	0.025	15	0.1	8.37	18	20.3	1.1	1.61	0	3.76	0.02	1.1	0.83	2.5	2	62.6	6.93	29	303
MERN18MDS0098AG05	0.6	0	0.05	21	0.5	4.55	1	13.1	0.3	0.77	0.1	1.31	0.01	0.31	0.34	128	1	22.9	2.3	373	126
MERN18MDS0098AG07	9.1	0	0.03	21	0.2	3.83	2	44	0.3	0.7	0	1.23	0.01	0.36	0.28	133	1	26	2.47	412	126
MERN18MDS0099AG01	2.9	0	0.19	29	0.7	2.94	3	79.5	0.2	0.7	0	0.83	0.01	0.36	0.22	171	1	24.5	2.5	143	85
MERN18MDS0113AG01	1.9	0.001	0.025	21	0.1	3.92	2	39.6	0.4	0.8	0	1.8	0.01	0.45	0.43	272	1	26.8	2.96	187	158
MERN18MDS0124AG01	6.9	0.0005	0.025	25	0.2	3.97	1	60.2	0.3	0.65	0	1.32	0.03	0.38	0.41	198	1	20.7	2.43	81	154
MERN19MDS0125BG54B	38	0.003	0.05	28	1.1	1.8	13	49.2	0.1	0.34	0.2	0.62	0.01	0.18	0.58	255	2	10.4	1.08	148	20
MERN19MDS0125BG55A	23.6	0.003	0.025	26	0.6	4.91	9	54	0.5	0.79	0.1	1.58	0.01	0.34	0.36	393	3	21.9	2.12	174	144
MERN19MDS0125DG48	1.9	0.0005	0.025	25	0.4	5.4	13	2.6	0.7	1.35	0.4	1.36	0.01	0.76	0.58	357	42	49.3	4.89	285	148
MERN19MDS0125AG50	1	0.001	0.025	29	0.1	2.17	7	2.7	0.2	0.77	0	0.66	0.01	0.52	0.26	347	8	29.9	3.32	373	59
MERN19MDS0125BG54	16.7	0.002	0.07	27	1.6	5.3	11	10.9	0.1	0.6	0.1	0.49	0.01	0.27	0.1	324	4	16.9	1.67	259	23
MERN19MDS0125BG55B	15.1	0.002	0.025	26	0.2	4.64	9	51.6	0.5	0.68	0	1.44	0.01	0.39	0.44	382	3	21.8	2.18	181	136
MERN19MDS0125AG52	30.1	0.0005	0.025	26	0.3	2.32	18	20.3	0.1	0.58	0	0.39	0.01	0.28	0.14	354	4	20.4	1.84	363	25
MERN19MDS0125AG53	22.7	0.0005	0.025	23	1.3	4.34	11	15.5	0.3	1.15	0.1	1.02	0.01	0.75	0.25	338	6	43.6	4.36	233	71
MERN18MDS0098AG08	26	0	0.03	22	0.1	4.12	4	3.6	0.3	0.73	0	1.28	0.01	0.36	0.33	130	1	26.7	2.56	534	126
MERN18MDS0098AG04	17.2	0	0.05	19	0.7	3.66	3	4.3	0.3	0.68	0	1.24	0.01	0.34	0.31	124	1	22.5	2.15	430	123

A 2-5: Alteration geochemistry plots

Compositional changes due to alteration were calculated using Gresen's (1967) equation as modified by Babcock (1973), equation 1, and are displayed in graphically (Fig. 1).

$$\Delta Xn = a(K_v * X_i^B \rho^B / \rho^A) - X_i^A \quad \text{equation 1}$$

Where ΔXn is the magnitude of chemical transfer. X_i is the composition of element i within the altered rock (B) and least altered protolith (A), ρ is the density and a is the grams of parent rock (100g). K_v is the ratio between the final and initial volume. For the purposes of this study constant volume is assumed, which is supported by the preservation of delicate textures and allows comparison with previous work (e.g. Riverin and Hodgson, 1980).

Due to the superposition of alteration types and intensity of the alteration within the JB least altered precursors were collected from host rocks outside of the JB, which are texturally, mineralogically and geochemically similar to clasts within the JB. The least altered felsic precursor is a sample from the Quemont feeder dike (MERN19MDS0125DG42) that preserved primary volcanic features (e.g. spherulitic groundmass, visible feldspar microlites and phenocrysts showing minimal sausseritization), contained < 10 % sericite, and < 20 % chlorite. Similarly, a sample of the least altered Powell andesite (MERN18MDS098AG07) was used as a precursor for the mafic blocks. The mafic precursor has a preserved feldspar dominant pilotaxitic groundmass, feldspar microporphyritic texture with phenocrysts showing minimal sausseritization, a groundmass containing < 20 % chlorite.

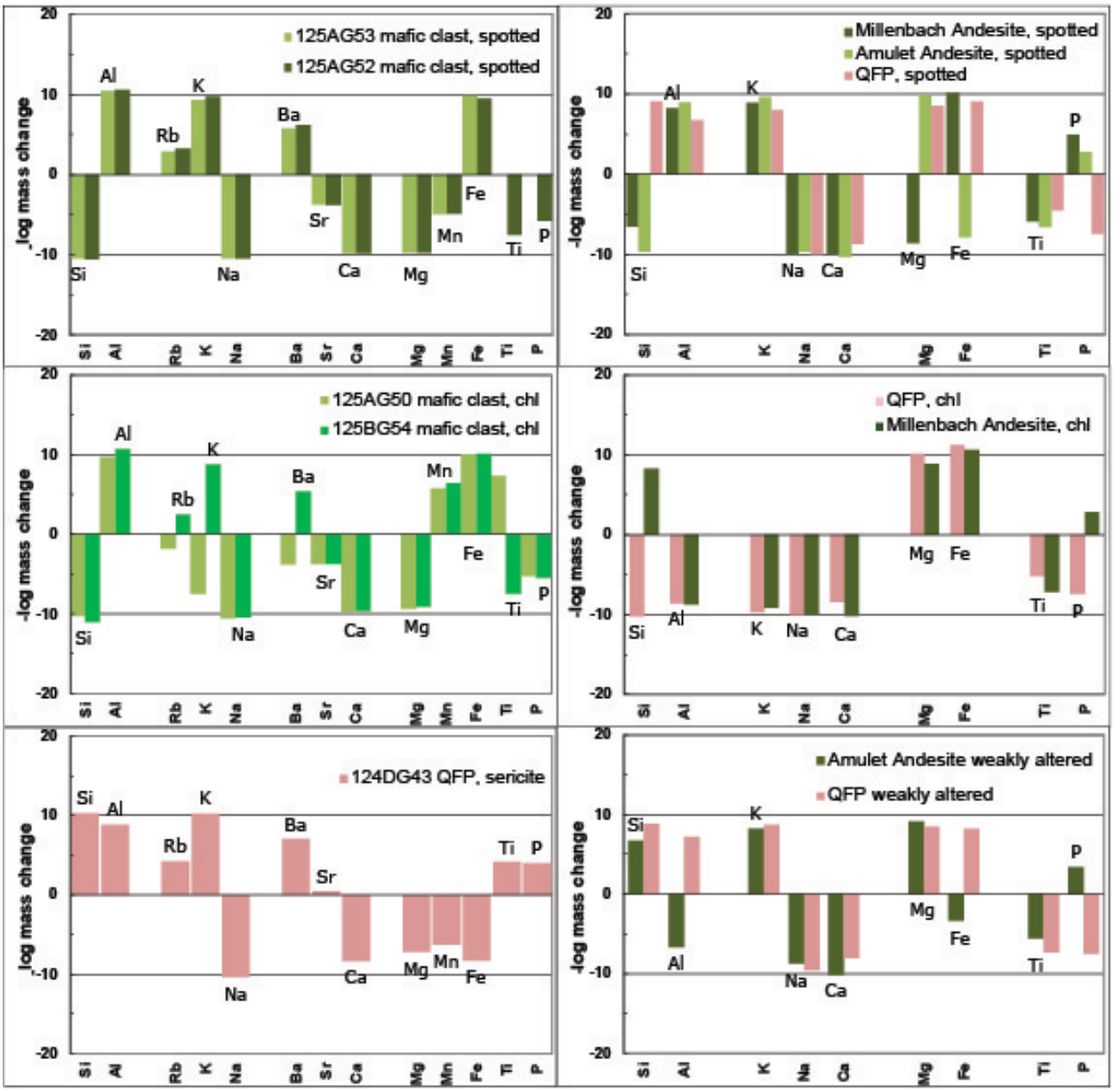

Figure 1: Calculated mass change of elements for each alteration type, relative to a least altered protolith, assuming constant volume. Whole-rock geochemical data from this study (A, C, and E) compared with data from Riverin and Hodgson (1980) for similar VMS related alteration types in the central Rouyn-Noranda mining district (B, D and F). All samples were normalized to volatile free and sulfide free values prior to plotting. QFP = Quartz feldspar porphyritic rhyolite dike; chl = chlorite.

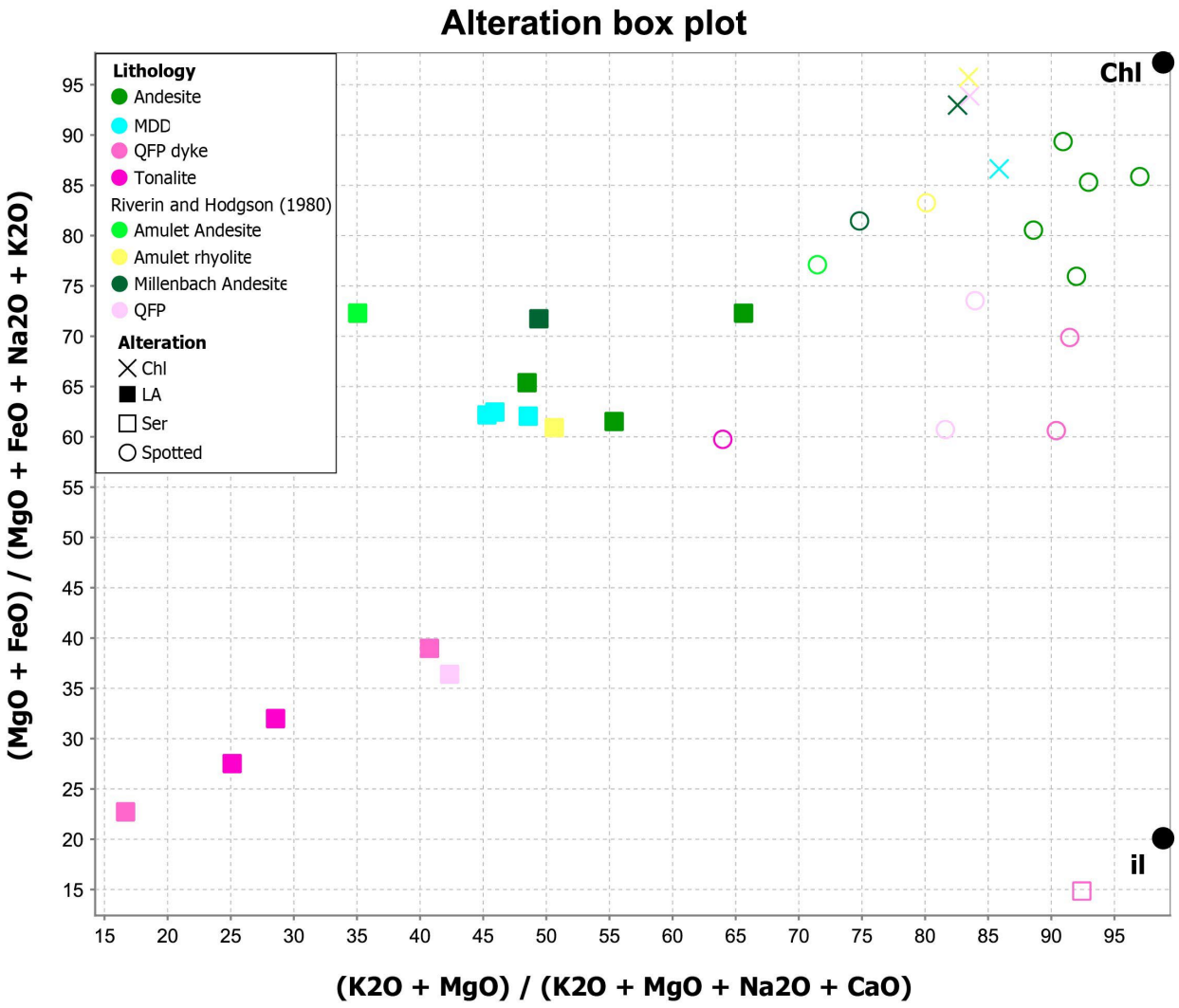

Figure 2: Box plot (Large et al., 2001). Spotted alteration textured samples plot within an intermediate range between least altered precursors and most intensely chlorite altered samples (Chl = chlorite; LA = least altered, Ser = sericite).

Chapter 3

3 Discriminating superimposed alteration associated with epigenetic base and precious metal vein systems in the Rouyn-Noranda mining district, Québec; Implications for exploration in ancient volcanic districts

3.1 Abstract

The Rouyn-Noranda mining district of Québec contains 20 Cu-Zn (±Au ±Ag) volcanogenic massive sulfide (VMS) deposits including the giant and gold-rich Quemont and Horne deposits. Mineralized epigenetic veins are also present, but their origin and relative timing remain enigmatic. The nature and extent of their alteration signatures and the effect of their superposition on district scale alteration patterns is unknown. The quartz-sulfide Cu-Zn-Ag veins are characterized by $\delta^{18}O_{quartz}$ values of 8.5 ± 0.8‰, reflecting $\delta^{18}O_{fluid}$ compositions of -0.4‰ to 3.1‰ (250–350°C), typical of Archean seawater. They are associated with a proximal Fe-rich chlorite alteration and marginal spotted sericite-chlorite alteration, with whole rock $\delta^{18}O$ values of 2.9–5.9‰ and are interpreted as a deeper crustal manifestation of a VMS system. Younger gold-quartz-carbonate veins were emplaced along mechanical anisotropies created by mafic dikes during N-S compression and the formation of regional east-trending faults, folds and cleavage. They are characterized by $\delta^{18}O_{quartz}$ values of 11.3 ± 0.8‰, reflecting $\delta^{18}O_{fluid}$ composition of 2.4–5.9‰ (250-350°C), typical of a metamorphic fluid, possibly mixed with a lower $\delta^{18}O$ upper crustal fluid and are associated with ankerite, calcite, muscovite, chlorite, albite, quartz ± hematite alteration with whole rock $\delta^{18}O$ values of 5.8–10.3‰. ID-TIMS U-Pb zircon ages for two tonalite intrusions constrain the maximum age of the Cu-Zn-Ag veins to 2697.6 ± 0.7 Ma, and the

minimum age to 2695.3 ± 1.0 Ma, which is also the maximum age of the gold-quartz-carbonate veins. Superposition of alteration related to the gold-quartz-carbonate veins on previously chlorite and sericite altered rocks have resulted in mixed alteration signals with whole rock $\delta^{18}O$ values ~6-8‰, which has perturbed and masked regional alteration patterns related to older VMS mineralization, such as the Quemont and Horne deposits. These results indicate that defining alteration vectors in camps that have superimposed hydrothermal systems requires full consideration of the hydrothermal history of the camp and if such constraints are lacking, whole rock $\delta^{18}O$ values should not be used as a stand-alone exploration method.

3.2 Introduction

Quartz-sulfide(-oxide) veins associated with phyllosilicate mineral alteration assemblages are ubiquitous to virtually all hydrothermal ore deposits (e.g. porphyry, epithermal, volcanogenic massive sulfide (VMS) and orogenic gold) regardless of age or tectonic setting. The internal textures of these veins are typically non unique, and where overprinted by subsequent deformation events, early vein types (e.g. porphyry, epithermal, VMS) may be similar to later orogenic veins (Robert and Poulsen, 2001). Further complexity arises when multiple deposit types are superposed within a district, a common feature of modern evolving orogens (Sillitoe, 1978; Sawkins, 1990; Blundell, 2002) and greenstone belts globally (Hutchinson, 1987; Dubé and Mercier-Langevin, 2020; Tripp et al., 2020). In regard to the latter, the origin of fracture and vein-controlled Cu-Au mineralization associated with phyllosilicate alteration at the Archean Boddington deposit within the Saddleback greenstone belt, Yilgarn Craton, Western Australia, has remained enigmatic due to similarities with more than one deposit type (Turner et al., 2020 and references therein). However, it has recently been interpreted as a product of three superposed mineralization types: early “porphyry style” quartz-sulfide Cu (±Au) vein mineralization, intrusion-related Au-Cu-Mo-

Bi mineralization, and younger orogenic Au mineralization (Turner et al., 2020). Likewise, the origin of the Cu-Au veins of the Archean Chapais-Chibougamau mining camp, Abitibi greenstone belt, Canada, have long been debated as either syntectonic or magmatic-hydrothermal (Watkins and Riverin, 1982; Guha et al., 1983; Pilote et al., 1995; Leclerc et al., 2012; Dubé and Mercier-Langevin, 2020). These veins are hosted by brittle-ductile shear zones, which are associated with tonalite and quartz diorite dike swarms and quartz, carbonate, sericite, chlorite alteration assemblages. They are now interpreted as magmatic-hydrothermal in origin, with the shear zones superposed during later deformation and associated locally with orogenic gold mineralization (Dubé and Mercier-Langevin, 2020). Where superposition of mineralization has occurred, the proper identification of ore deposit types is critical to understand how these deposits form, their paleohydrothermal systems and associated magmatic and tectonic processes, all of which are important in the planning of successful exploration programs.

The Rouyn-Noranda mining district of Québec (Fig. 3.1), which contains 20 volcanogenic massive sulfide (VMS) deposits, 19 orogenic gold-quartz-carbonate vein deposits, and several enigmatic breccia hosted and vein style Cu-Zn-Ag prospects, occurrences and deposits (Gibson and Galley, 2007), is an example of a complex mining district where the recognition and effects of superimposed mineralization types has been largely overlooked. The Cu-Zn-Ag prospects and occurrences, which comprise quartz-sulfide veins with local vein stockworks and disseminated sulfides, have been interpreted as epigenetic and either younger than the gold-quartz-carbonate veins (McMurchy, 1948) or older than those veins and related to Cu-(Mo) intrusion-related deposits (Kirkham, 1972; Kotila, 1975; Goldie et al., 1979; Kennedy, 1985; Jebrak et al., 1997; Galley and van Breemen, 2002). They have also been interpreted as synvolcanic and related to VMS mineralization (Lichtblau, 1979) especially in the Central Noranda camp (Gibson et al.,

1983; Zubowski, 2011). Likewise, the timing of the gold-quartz-carbonate vein deposits is controversial and they have been interpreted as syn-tectonic (Riverin et al., 1990; Robert et al., 1996) or post-tectonic (McMurchy, 1948; Carrier et al., 2000) relative to the main period of N-S shortening across the district. The relative timing of the Cu-Zn-Ag quartz veins and Au-quartz-carbonate veins has not been demonstrated, nor has the alteration associated with each, where superposed, been defined.

Different tools may be used to determine the timing and origin of multi generational veins, including overprinting relationships between the veins, their associated alteration assemblages and regional structural fabrics, as well as geochronology and the mineral and isotopic chemistry of the veins and alteration assemblages. This study shows how, using new and pre-existing data, those tools are applied to interpret the vein history of the Rouyn-Noranda mining district. More specifically herein, we: 1) demonstrate the relative chronology of the two vein types with respect to each other and regional structural fabrics; 2) present new interpretations for their emplacement and origin; 3) characterize and contrast their alteration and oxygen isotopic signatures; and 4) for the first time, evaluate the effects of their superimposed alteration on mineralogical, geochemical and isotopic alteration vectors used for VMS and gold exploration.

3.3 Regional Geology of the Rouyn-Noranda mining district

Rouyn-Noranda is a gold and base metal mining district within the 2704–2695 Ma Blake River Group in the Abitibi Subprovince of the Archean Superior Province (Fig. 3.1). It is centred on a 6 km thick bimodal volcanic package of the Noranda volcanic complex, which is interpreted to have formed as a submarine shield volcano with a diameter of 40–50 km (De Rosen-Spence, 1976). Volcanic strata and their massive sulfide deposits are subdivided into older (2703–2701

Ma) and younger (2699–2695 Ma) Blake River Group, separated by a brief hiatus in volcanism at ~2700 Ma (McNicoll et al., 2014). The VMS deposits are localized along NE- and NW-striking synvolcanic structures (Scott, 1980; Knuckey et al., 1982; Knuckey and Watkins, 1982; Setterfield et al., 1995) and the Flavrian Powell Intrusive Complex along the western margin of the district has been interpreted as the synvolcanic heat source driving hydrothermal circulation and the formation of some of the VMS deposits within the district (Gibson and Galley, 2007).

The Noranda volcanic complex is located ~5 km north of the Larder Lake Cadillac Break, a major east-west striking belt-scale structure (Fig. 3.1) associated with alluvial-fluvial successions of polymictic conglomeratic rocks, cross-bedded sandstone, and alkali-shoshonitic volcanic rocks of the Timiskaming Group and numerous orogenic gold deposits (Poulsen, 2017; Dubé and Mercier-Langevin, 2020). The district has undergone at least three deformational events. A pre-Timiskaming deformation event produced E-W to NW trending F_1 folds, which lack an axial planar cleavage, and is expressed by an angular unconformity between the folded and tilted ca. 2704–2695 Ma Blake River Group metavolcanic rocks and the ca. 2676–2669 Ma Timiskaming Group (Wilson, 1956; Poulsen, 2017). The main post-Timiskaming deformation in the district occurred between ca. 2670–2660 Ma, with the most intense strain in proximity to the Larder Lake Cadillac Break (Bedeaux et al., 2017; Daigneault et al., 2002; Robert et al., 2005; Dubé and Mercier-Langevin, 2020). Subsequently, northwest-southeast directed shortening resulted in dextral transcurrent reactivation of the Larder Lake Cadillac and Porcupine Destor faults (Dimroth et al., 1983; Hubert et al., 1984; Wilkinson et al., 1999; Daigneault et al., 2002; Ispolatov et al., 2008; Bleeker, 2012; Poulsen, 2017; Bedeaux et al., 2017). In accordance with most past studies in the Rouyn-Noranda mining district, the main post-Timiskaming folding event is referred to as

"D2" and the dextral transcurrent event as "D3" (Goulet, 1978; Dimroth et al., 1983; Hubert et al., 1984).

Gold deposits within the district are located along the Larder Lake Cadillac Break, related second and third order structures (e.g. Horne Creek Fault) or within competent intrusive bodies (e.g. Flavrian and Powell intrusive complex). The timing of orogenic gold mineralization within the southern Abitibi greenstone belt remains controversial, but most authors agree that a major gold mineralization event occurred during the main period of regional deformation, characterized by N-S shortening at ca. 2670–2660 Ma (e.g. Kerrich and Kyser, 1994; Bedeaux et al., 2017; Dubé and Mercier-Langevin, 2020). This coincides with peak metamorphism in the southern Abitibi greenstone belt, which occurred between ~2669–2653 Ma (Powell et al., 1995; Piette-Lauzière et al., 2019; Dubé and Mercier-Langevin, 2020).

Regional metamorphism of the Noranda district resulted in subgreenschist to greenschist facies assemblages (Powell et al., 1995) that are superimposed on older amphibolite facies assemblages that define a 2.5 km wide contact metamorphic aureole around the post-volcanic, 2690.3 +2.2/-2.0 Ma (Mortensen, 1993) Lac Dufault pluton. The aureole is defined by hornblende and biotite in unaltered volcanic rocks, and a spotted cordierite, biotite, anthophyllite and cummingtonite assemblages in hydrothermally altered volcanic rocks associated with VMS deposits (De Rosen Spence, 1969; Hall, 1982; Fitchett, 2012). Pristine cordierite is rare and has retrograded to a fine-grained mineral association of sericite (muscovite and paragonite), quartz, biotite and chlorite during later regional metamorphism (Cooke et al., 1931; Walker, 1930; Wilson, 1941; De Rosen-Spence, 1969; Fitchett, 2012). All lithologies discussed in this study are metamorphosed so the "meta" prefix is omitted for brevity.

3.4 Methodology

Detailed field mapping and sampling of both Cu-Zn-Ag quartz sulfide and gold-quartz-carbonate veins was conducted at a scale of 1:100 using aerial drone images as base maps. Sampling transects were oriented perpendicular to the veins in order to determine the extent of their alteration footprints. Mineralized samples were analyzed for metal tenor and representative altered and least altered samples were analyzed for whole-rock compositions at ALS Geochemistry, Sudbury, Ontario. Results are included in Appendix Table A1 and A2. Selected splits of the pulverized samples were also submitted for whole-rock $\delta^{18}O$ analysis (n = 85). Results are included in Appendix Table A3. In addition, representative samples of quartz (n = 11) from each of the veins was sent for $\delta^{18}O_{quartz}$ analysis at Laval University; results are included in Appendix Table A4. Mineralogical compositions were determined using the Scanning Electron Microscope (SEM) and energy-dispersive spectroscopy (EDS) at the Mineral Exploration Research Centre Isotope Geochemistry Laboratory of Laurentian University. A TESCAN VEGA3 SEM was used with a beam intensity of 18 nA, at 15.00 kV and a working distance of 15 mm. Results are included in Appendix Table A5. High precision isotope-dilution – thermal ionization mass spectrometry (ID-TIMS) U-Pb zircon geochronology (Table 1) was completed at the Jack Satterly Geochronology Laboratory (JSGL), University of Toronto. Full details on sample preparation and analytical techniques are included in Appendix A6.

3.5 Geology of the Powell Block

The Powell Block (PB) is bound to the north by the Beauchastel Fault and to the south by the Horne Creek Fault and contains an abundance of these two enigmatic vein types within spatial proximity (Fig. 3.2). It comprises a bimodal transitional to calc-alkaline volcanic sequence of

effusive mafic volcanic rocks, intercalated with lesser, localized aphyric and quartz-phyric rhyolite flow dome complexes and minor volcaniclastic rocks. The strata have an overall NNW strike and moderate to steep ENE dip of 70–80° but are offset along NE to ENE striking faults and folded into E-W trending, moderately E plunging anticlines and synclines (Fig. 3.1, 3.3). To the west, the volcanic strata are intruded by the subvolcanic Powell intrusive complex, which comprises sill-like bodies of quartz diorite and younger tonalite and trondjhemite (Goldie, 1976). The age of the volcanic package within the study area is constrained to ca. 2702–2700 Ma (McNicoll et al., 2014; Schofield et al., 2021) but a younger ca. 2698 Ma magmatic event is locally superposed on the volcanic rocks as evidenced by the Joliet Breccia and related copper mineralization (Schofield et al., 2021).

Numerous felsic, mafic and composite dikes occur throughout the Powell Block. They typically strike ENE and coincide with stratigraphic offsets. A quartz feldspar porphyritic rhyolite dike was dated at 2702.0 ± 0.8 Ma (Fig. 3.2; McNicoll et al., 2014). Younger lamprophyre, mafic and syenite dikes strike NNE to NNW, crosscut the Powell intrusion, ENE striking dikes, and all volcanic strata within the Powell block. Proterozoic diabase dikes crosscut all units as well as most faults (Fig. 3.2) and represent the youngest intrusive event (Carrier et al., 2000).

Rocks of the Powell Block have undergone higher strain than the northern Flavrian Block of the Noranda volcanic complex (Dimroth et al., 1983; Hubert et al., 1984). In the Powell Block, the D1 event is not expressed by mesoscopic and macroscopic structural features and may simply have contributed to the moderate eastward dips of the volcanic strata. Later deformation events imparted structural fabrics on the rocks of the Powell Block and are described below.

3.6 Structural analysis

The D_2 deformation event produced the most prominent structures in the Powell Block, including the Powell syncline (Fig. 3.3), a regional cleavage, a shape and mineral stretching lineation, a bedding-cleavage intersection lineation, and major E-W striking brittle-ductile shear zones (Fig. 3.4A-F). The regional S_2 cleavage is present across the Powell Block but is more prominent in hydrothermally altered rocks, where it is expressed as a penetrative continuous slaty cleavage defined by chlorite and sericite. In weak to moderate altered massive felsic rocks, it forms an anastomosing sericitic fabric that imparts a pseudo-clastic appearance to the rocks. Pillows in volcanic flows, clasts in volcaniclastic units (Fig. 3.4A), and ovoid metasomatic spots (Fig. 3.4B), are flattened parallel to the S_2 cleavage and elongate parallel to an L_2 shape stretching lineation. The mineral stretching lineation is restricted to E-W striking shear zones (Fig. 3.5A-D) and defined by yellow grooves of sericite and ribs of quartz. Structural measurements of bedding, lineations and cleavage were taken along the limbs and hinge of the F_2 Powell syncline. Poles to folded bedding define a great circle whose pole coincides with data points for the bedding-cleavage intersection lineation (Fig. 3.3) and mineral and shape stretching lineation (Fig. 3.5C). The lineation data points (average plunge of 73° towards 103°) fall within the plane of the regional cleavage (average strike of 085° and dip of 81°), which bisects the interlimb angle (78°) of the fold. This confirms that the Powell syncline, regional cleavage, and the shape and mineral stretching lineation, are coeval F_2, S_2 and L_2 structural features, respectively, which formed during the D_2 deformation event.

The Powell syncline is truncated to the north by the Powell Fault. The latter is expressed as a ~2–10m wide, strongly foliated zone, which strikes ENE (099°) and dips steeply (81°) to the south (Fig. 3.5). It is characterized by the intensification of the S_2 cleavage into a sericitic and

chloritic phyllonitic foliation (Fig. 3.4C) and by a pronounced subvertical mineral stretching lineation, which is parallel to the L_2 shape and mineral stretching lineation. This suggests that the Powell Fault formed during the D_2 deformation event. Shear sense indicators, including sigma shaped clasts (Fig. 3.4D), S-C fabrics (Fig. 3.4E) and shear bands, are observed on vertical surfaces perpendicular to foliation and parallel to lineation. They indicate north-side-up movement parallel to the mineral stretching lineation.

The phyllonitic foliation along the Powell Fault is overprinted by dextral shear bands, Z-folded quartz veins, and a penetrative S_3 crenulation cleavage (078°/75º; Fig. 3.4F). The latter is axial planar to Z-shaped drag folds and is further expressed as a spaced (~2–7 mm) fracture cleavage within massive felsic rocks and weakly to moderately altered basalt, and as a continuous, chloritic and sericitic, slaty cleavage in altered basalt. These shear sense indicators, together with the progressive clockwise (~17°) rotation of the S_2 cleavage with increasing proximity to the Powell fault, suggest that the Powell Fault was reactivated as a dextral transcurrent fault during a D_3 deformation event.

3.7 Cu-Zn-Ag prospects and occurrences

Cu-Zn-Ag prospects and minor occurrences are abundant in the Powell Block northwest of the Joliet Breccia (Fig. 3.2). All were studied in detail but only two, well exposed representative examples, the Powell F-zone and Powell D-zone (Fig. 3.6), which encompass the range of features observed at these occurrences, are described below.

The Powell F-zone occurrence consists of a ~1 m wide quartz, chalcopyrite, pyrite, sphalerite vein with a strike length of 90m (Fig. 3.6). The vein occurs along the margin of a 30 m wide NE striking aphanitic, aphyric, spherulitic felsic dike (Fig. 3.6). The dike has irregular lobate

flow banded to brecciated margins and the vein is observed to crosscut both its brecciated margin and more massive interior. The felsic dike marks a distinctive stratigraphic offset. The regional E-W-striking S_2 cleavage overprints both the felsic dike and the vein. The vein strikes NE (056°), and dips steeply (80°) to the SE (App. Fig. A1). It pinches and swells along strike and is locally offset by E-W and NNW striking faults. Smaller (5–20 cm wide), oblique (030°) quartz-sulfide veins that branch off from the main vein are also offset by a brittle E-W striking fault. The S_2 cleavage overprints the brittle fault and wraps around the competent segments of the offset vein. Disseminated sulfide minerals in the host rocks within 8 m of the vein give the rock a rusty weathered appearance.

The Powell D-Zone consists of a ~150 m by ~90 m area of predominantly fracture controlled to disseminated sulfide minerals. It is located on the west side of a NE striking fault infilled by a sulfide vein (Fig. 3.6). The vein is ~30 cm wide and has a strike length of ~70 m and is enveloped by a ~7 m wide zone of stockwork to disseminated sulfide minerals. The vein terminates to the SW in a branching network of sulfide veins and disseminated sulfides. The large area of disseminated to fracture-controlled mineralization is characterized by a concentric distribution of sulfides in plan view decreasing in abundance from the centre outwards (Fig. 3.6). Its mineralized centre is a breccia consisting of angular vuggy patches of quartz and sulfide minerals between angular fragments of the host andesite. The breccia is surrounded by a zone of disseminated to fracture-controlled mineralization, itself surrounded by a zone of weakly mineralized, dominantly fracture controlled mineralization. The fractures typically strike NE and are overprinted by a conjugate set of thin, planar NNW and E-W striking sulfide filled fractures (<1 mm in thickness), which have no discernible alteration halo.

The host rocks at the Powell D-zone consist of massive andesitic flows striking approximately WNW and dipping moderately to the NNE. Several WNW striking intrusions cut the andesitic flows, including ≤ 1 m thick, subparallel, aphyric, spherulitic, flow-banded rhyolite sills/dikes, and a larger, irregular quartz (1–2 mm; 20%) feldspar (2-3 mm; 30–40%) porphyritic tonalite intrusion which is overprinted by the sulfide mineralization. The tonalite intrusion contains fine-grained disseminated sulfides and its outer margin is locally marked by a pronounced ~0.5 m wide zone of sheeted ~1 mm wide sulfide fractures, which are oriented perpendicular and parallel to the tonalite contact and locally crosscut the tonalite.

There is no compliant estimate of tonnage and grade for these prospects and occurrences. Lichtblau (1979) provided a non-compliant estimate of 22,680 tonnes of mineralization at a grade of 7.88% Cu, 118.3 g/t Ag and 0.24 g/t Au for the Powell F-zone occurrence. Grab samples from this study of the Powell F-zone and Powell D-zone veins assayed 1.6% Cu, 0.5 ppm Au, 43.6 ppm Ag and 0.11% Zn, and 1.3% Cu, 0.14% Zn and 16.4 ppm Ag, respectively (Table A1). Three grab samples of the disseminated mineralization at Powell D-zone averaged 0.08% Cu, 0.2 ppm Au, 6 ppm Ag, and 0.04% Zn (Table A1). The metal tenor for these prospects and occurrences is similar to that of the Joliet Breccia (Schofield et al., 2021) and overlaps with the typical range for Cu-Zn VMS deposits (e.g. Franklin et al., 1981; Fig. 3.7).

3.7.1 Cu-Zn-Ag vein petrography and paragenesis

The Cu-Zn-Ag veins are zoned and consist of an outer banded margin and an inner vuggy and porous centre. The outer vein margin is locally banded by alternating thin slivers of altered wall rock and bands of quartz with lesser pyrite and chalcopyrite (Figs. 3.8A-B). The banding is commonly asymmetrically developed, e.g., at Powell F-Zone, and in places only occurs at the margin between the vein and the more competent felsic dike. Where banding is not present, there

is a gradation between the medium-grained, vuggy, white quartz margin of the veins and the sulfide-dominated center of the veins (Fig. 3.8C). The vein centers consist of massive pyrite ± pyrrhotite ± chalcopyrite, and minor fine-grained grey quartz surrounding rare fragments of altered wall rocks and inclusions of white quartz (Figs. 3.8B-C). Similar textures are observed in the breccia at the Powell D-zone, but the mineral infill is restricted to angular vugs between clasts of altered wall rock (Fig. 3.8D). The observation of quartz-dominant vein margins grading inwards to a pyrite-dominant core, suggests that pyrite was deposited later than the quartz. The banded margins and presence of fragments of quartz and altered wall rock internal to the veins suggest that there may have been multiple periods of dilation, opening of the veins and fractures, and subsequent mineral deposition and sealing. Pyrite, in the centre of the vein, consists of angular fragments with jig-saw fit margins (Fig. 3.8B) and more rounded fragments with corroded and abraded grain surfaces. Microfractures transect the grains in both cases (Fig. A2 A-D). Anhedral inclusions of galena, sphalerite, chalcopyrite and Ag- and Bi-tellurides occur as small blebs that align along the fractures and in vugs (Fig. A2 A-F). The mineral associations, textures, and paragenesis for the Cu-Zn-Ag prospects is similar to those for the Joliet Breccia (e.g. Schofield et al., 2021) and are typical of Cu-Zn VMS deposits (e.g. Franklin et al., 1981).

3.7.2 Hydrothermal alteration associated with Cu-Zn-Ag veins

Two main types of alteration (Fig. 3.8E-H) surround all the Cu-Zn-Ag occurrences: fine grained chlorite and spotted sericite-chlorite (Fig. 3.6). Both overprint an older, more pervasive and district-scale spilitic (albite-chlorite) alteration (Gibson et al., 1983; Hannington et al., 2003; Fig. 3.6).

Albite-chlorite alteration (spilitization): All volcanic units within the study area appear to have undergone an early spilite alteration and thus this alteration type makes up the background

composition as there is no unaltered volcanic protolith for comparison. This alteration is characterized by quartz, albite, chlorite and rutile and is locally observed as relic patches within chlorite and spotted sericite-chlorite alteration zones (e.g. Schofield et al., 2021). Epidote is rare and actinolite is only present locally as a pseudomorph of pyroxene phenocrysts within medium to coarse-grained massive porphyritic mafic flows or intrusions. Chlorite is typically Mg-rich (Mg-pycnochlorite), exhibits anomalous brown-blue birefringence, and is interstitial to albite microlites. This splitic alteration is pervasive throughout the Rouyn-Noranda district and has been interpreted to be a product of the interaction between volcanic rocks and relatively cold down-drawn seawater within a shallow sub-seafloor hydrothermal system (Gibson et al., 1983; L'Heureux, 1992; Franklin et al., 2005; Schofield et al., 2021).

During this alteration, albite, pycnochlorite (Fig. 3.9) and quartz formed at the expense of primary volcanic glass, calcic feldspar, epidote and clinopyroxene. Lithogeochemical data show the distinctive high Na_2O and low K_2O compositions that are typical of spilites (Fig. A3; Hughes, 1973).

Spotted (sericite-chlorite) alteration: The background regional spilite alteration is locally overprinted by discordant spotted sericite - chlorite alteration. This is a fracture-controlled alteration, which is commonly observed as 4~30 cm wide haloes surrounding sulfide veinlets (Fig. 3.8E-F). This alteration occurs in association with the Cu-Zn-Ag veins and as a 0.5 m wide halo surrounding the younger tonalite intrusion at the Powell D-zone. The spots visually resemble varioles and consist of ovoid clusters (0.2–1 cm diameter) of fine-grained sericite (muscovite) within a chloritized matrix (Fig. 3.8G-H). They can be distinguished from varioles by their localization along discordant fractures and veins. Contacts between the ovoid sericite clusters and the chloritic groundmass are typically diffuse (Fig. 3.8G). The sericite clusters are observed distal

to veins as very small spots (2–3 mm diameter) that merge into larger spots (0.5–1 cm diameter) with increasing proximity to the veins (Fig. 3.8G) and concomitant increase in chlorite in the groundmass at the expense of albite microlites. These clusters are typically concentrically zoned with albite and muscovite rich cores, surrounded by muscovite and chlorite rich margins (Fig. 3.8G-H). The original composition of the host rock controls the composition of the chlorite, with chlorite found in spotted felsic rocks exhibiting a higher Fe-content than chlorite in spotted mafic rocks (Fig. 3.9). The only phase preserved in the matrix from the precursor spilitized host rock is fine-grained disseminated quartz, which also occurs as inclusions within the spots. This alteration results in gains in K ± Fe and losses in Na ± Mg (Fig. A3).

Ankerite locally overprints spotted andesite in crosscutting quartz-carbonate veinlets and as disseminated carbonate. Fine-grained, euhedral to subhedral ankerite typically occurs along the outer margins of alteration spots where it replaces fine-grained muscovite.

Chlorite alteration: Massive, discordant and fracture-controlled chlorite alteration is best developed immediately adjacent to the Cu-Zn-Ag veins (Fig. 3.8F). The chlorite is fine-grained and replaced the groundmass in coherent mafic and felsic volcanic flows and hypabyssal intrusive rocks. It is more laterally extensive in permeable volcaniclastic units where it has replaced the hyaloclastite and tuffaceous matrix between more competent clasts. It overprints and is in sharp contact with the spotted alteration texture (Fig. 3.8F). This pervasive chlorite alteration is texturally destructive and has obliterated pre-existing feldspar microlites or phenocrysts. The only other mineral phases that occur with the fine-grained chlorite (60%) are disseminated, fine grained, subhedral quartz (25%) and subhedral to euhedral rutile (15%). Chlorite is Fe-rich and the replacement of muscovite by Fe-rich chlorite reflects gains in Fe, Mg and H_2O and losses in K (Fig. A3).

3.8 Au deposits and occurrences

Au deposits in the Powell Block are dominantly confined to the Powell intrusive complex and are typically associated with NNW striking mafic dikes. Several of the historically mined veins are no longer accessible; however, the two best surface exposures, Silidor and Vox (Fig. 3.10A-E) were studied in detail to characterize this style of mineralization.

The Silidor vein strikes on average 330° and dips 50° ENE (Fig. A1) with an average width of ~3.5 m. It is located within tonalite of the Powell Intrusive Complex (Fig. 3.2) in association with highly altered mafic dikes (Fig. 3.10A). Tonalite in immediate proximity to the vein is heavily fractured and contains numerous ~1 mm wide anastomosing fractures filled with chlorite and carbonate and trace amounts of disseminated pyrite.

The contact with the vein is marked by a carbonate-fuchsite breccia, comprising altered fragments of tonalite in a carbonate, chlorite ± quartz matrix, with trace amounts of disseminated pyrite and fuchsite (Fig. 3.11A). The breccia locally has jigsaw fit fragments. Several parallel, thin, secondary quartz veins are hosted by the breccia and mafic dike(s) (Fig. 3.11B). In addition, numerous 1–2 cm wide NNE striking (Fig. A1) fibrous quartz ± ankerite ± specular hematite veins crosscut the host rocks (Fig. 3.11C-D) and the main NNW quartz vein but are also locally folded and rotated into the footwall of the vein. The main Silidor vein and parallel secondary veins are folded (Fig. 3.11B-C) into open, moderately NE-plunging folds with an interlimb angle of ~120°. The regional E-W striking and steeply S-dipping cleavage is oriented at a high angle (45°–90°) to the folded vein and is axial planar to the folds (Fig. A1). This cleavage is most strongly developed in the mafic dike and carbonate matrix of the footwall breccia where it is expressed as a spaced and anastomosing cleavage defined by chlorite (Fig. 3.11A, D). Late E-W striking sinistral and dextral faults offset the Silidor vein laterally by up to 50 m (Carrier et al., 2000).

The Vox vein is hosted by an older quartz (~5%; 0.5–1 mm) feldspar (1%; 0.5–1 mm) porphyritic rhyolite dike, which is cut by the Powell quartz-diorite (Fig. 3.10B). The vein does not coincide with a mafic dike but with a structure that dextrally offsets by 20 m in map view a porphyritic tonalite dike that cuts across the older rhyolite dike. The Vox vein is on average 1–2 m thick, but it pinches and swells (up to 5 m thick) along strike. Where thickest, it contains angular altered wall-rock fragments. There are several smaller, 10–20 cm wide subparallel quartz-breccia veins, which crosscut the host rocks in the hanging wall up to ~100 m away from the main Vox vein. These veins are all folded into open, moderately E-plunging folds, and crosscut by an E-W striking, steeply dipping cleavage. Extensional, NNE striking, subvertical, fibrous quartz ± ankerite ± specular hematite veins, varying in width from 7 to 12 cm, cut across the NNW striking veins and are locally folded and rotated into the veins and parallel structures.

3.8.1 Gold-quartz-carbonate vein petrography and paragenesis

The gold-quartz-carbonate veins have a white quartz banded (Fig. 3.11E) to brecciated (Fig. 3.11F) outer margin and a massive, white to smoky grey, quartz inner centre. Locally, sulfide minerals fill vugs lined with quartz (Fig. 3.11G). Pyrite grains in the veins and the altered wall rocks are subhedral to euhedral and are internally porous. Aggregates of pyrite grains locally exhibit triple point junctions (Fig. A4). Gold occurs in the veins and altered wall rocks as electrum inclusions and pore fillings in pyrite, along fractures transecting pyrite grains, and along pyrite grain boundaries (Fig. A4) in association with chalcopyrite, galena, and tellurides as anhedral intergrown blebs (Fig. A4). Pyrite also contains inclusions of apatite, quartz, rutile, muscovite, chlorite and ferroan dolomite (Fig. A4), which formed during the alteration of the vein wall rocks as described below.

3.8.2 Hydrothermal alteration associated with gold-quartz-carbonate veins

Alteration associated with the gold-quartz-carbonate veins consists of chlorite, hematite, albite, carbonate (ankerite and calcite), fuchsite and sericite. The abundance of these minerals changes with proximity to the veins and to some degree by the composition of the immediate host rocks (Fig. 3.10C-D). Apatite, rutile and pyrite are accessory phases observed in all alteration types.

Chlorite-calcite-albite alteration: This is the most distal alteration. It extends from ~30-300 m from the vein margins (Fig. 3.10C). It consists of fine-grained groundmass chlorite, calcite and albite and gives the rock a dark-green appearance. Chlorite is Mg-rich (Mg-pychnochlorite/ripidolite) relative to chlorites associated with the Cu-Zn-Ag veins (Fe-pychnochlorite/ripidolite) and tends to be more enriched in Mg in mafic rock units and in Fe in felsic rock units (Fig. 3.9). It is also relatively Fe-rich compared to the chlorite (clinochlore) found in background mafic rocks (mafic dike, lamprophyre, glomeroporphyritic gabbro) (Fig. 3.9).

Hematite alteration: The chlorite-calcite-albite alteration is overprinted by hematite alteration, which extends for ~30–200 m into the host rocks (Fig. 3.10C-D). It is most prominent within tonalite, where it imparts a red-rusty appearance. It consists of fine-grained, disseminated specular hematite (~25%), albite, ankerite, calcite, chlorite, apatite, rutile ± ilmenite. It is also concentrated in alteration haloes associated with numerous ~0.1–1 cm wide brittle fractures in the tonalite, and along fracture planes as veinlets of medium grained specular hematite. This alteration is most abundant in the hanging wall of the veins.

Albite-sericite ± calcite alteration: This is the most proximal alteration associated with the gold-quartz-carbonate veins within highly siliceous felsic host rocks that lack ferromagnesian minerals

(e.g. rhyolite flows; Fig. A5). It consists of fine-grained granoblastic albite, quartz, muscovite, ± calcite within ~30–50 m of the veins, imparting a bleached, beige appearance in contrast to the dark-green chlorite-calcite-albite alteration.

Ankerite - sericite ± fuchsite alteration: This is the most proximal alteration associated with the gold-quartz-carbonate veins within the tonalite and mafic dike host rocks (Fig. 3.10C-D). It consists of ankerite ± calcite, muscovite ± fuchsite, albite, and quartz within ~30–50 m of the veins, coloring the rock bleached beige (Fig. 3.11H-I). It is also found in association with E-W striking brittle-ductile shear zones across the Powell Block, and locally overprints the spotted alteration associated with Cu-Zn-Ag occurrences. Within tonalite, this alteration type consists of ~25% ankerite, ~40% quartz, ~25% albite, ~5% chlorite and ~5% muscovite. It is a texturally destructive alteration, which replaces the primary graphic (intergrowth of feldspar and quartz) texture of the tonalite with fine-grained granoblastic quartz and ankerite (Fig. 3.11I). Similarly, ankerite pervasively replaced the mafic dikes and at Silidor forms the matrix of the breccia at the contact between the mafic dike and quartz vein.

3.9 U-Pb TIMS Geochronology

Two felsic intrusive units were sampled for high resolution U-Pb zircon geochronology. The first is a quartz-feldspar-porphyritic tonalite dike (sample 20MDS-201B; Fig. 3.12A–C), which is overprinted by disseminated to stockwork Cu mineralization at the Powell D-Zone Cu occurrence. Dating of this unit provides a maximum age limit for the mineralization as well as a temporal context for its emplacement relative to known regional volcanism (and associated VMS mineralization) and younger magmatic-hydrothermal breccia systems (Schofield et al., 2021). The second dated unit is a tonalite dike that is crosscut by the Vox vein and its associated Fe-carbonate

alteration (20MDS-186B; Fig. 3.12D–E). To the NE of the Vox occurrence this same dike also crosscuts the Joliet Cu deposit (Fig. 3.2), which is a steeply plunging deposit of similar morphology, metal tenor and alteration as that of the Joliet Breccia (Schofield et al., 2021). It thus provides a minimum age for Cu mineralization and a maximum age for Au mineralization.

Zircon recovered from the quartz-feldspar-porphyritic tonalite dike at the Powell D-Zone yielded a population of small, clear, short, stubby, prismatic, colorless to pale yellow zircon grains (Fig. 3.12C). A few grains show good oscillatory zoning and small mineral inclusions of apatite and an opaque oxide (ilmenite?). U-Pb isotopic analysis of four, best-quality single grain zircon fractions from sample 20MDS-201B show a linear array of concordant to slightly reverse discordant data, with a narrow range of $^{207}Pb/^{206}Pb$ ages between 2697.4 and 2698.0 Ma (Table 1, Fig. 3.12B). Th/U ratios are very consistent (0.41-0.48) and typical of igneous zircons (Kirkland et al., 2015). The data yielded a calculated weighted average $^{207}Pb/^{206}Pb$ age of 2697.6 ± 0.7 Ma (N = 4, MSWD = 0.24; probability of fit = 87%) from the four fractions, which is interpreted to be the crystallization age of the tonalite and the maximum age for the emplacement of the stockwork and disseminated Cu-Zn-Ag mineralization that overprints the tonalite.

Zircon grains in sample 20MDS-186B are also well-formed, sharp and small, but are mostly altered, cracked or broken, clouded and colourless to brown (Fig. 3.12E). U-Pb isotopic analyses of three, best-quality single grain zircon fractions show a linear array of slightly reverse discordant data, with $^{207}Pb/^{206}Pb$ ages between 2694.6 and 2696.0 Ma (Table 1, Fig. 3.12D). Th/U ratios range from 0.51-0.62 and are typical of igneous zircons (Kirkland et al., 2015). A weighted average $^{207}Pb/^{206}Pb$ age calculated from all three fractions is 2695.3 ± 1.0 Ma (MSWD = 1.0; probability of fit = 37%) and represents an accurate date for the crystallization of the tonalite dike.

This also provides a minimum age for the Joliet Cu deposit, and a maximum age for overprinting Fe-carbonate alteration accompanying intrusion of the late, crosscutting, gold-bearing Vox vein.

3.10 Oxygen isotopic analysis

The histogram of all whole rock $\delta^{18}O$ samples from the mafic and felsic host rocks at the Cu-Zn-Ag occurrences shows a range from 2.9–5.9‰ (x = 4.8‰ ± 0.6; Fig. 3.13A; App. Table A3). These values are on average lower than the background mafic and felsic whole rock $\delta^{18}O$ values within the Powell block 4.4–7.7‰ (x = 5.9‰ ± 1.1; Fig. 3.13A-B; App. Table A3). The background values represent the least altered samples, which were selected from the study area based on petrographic observations (preserved primary textures, minimal modal abundance of alteration minerals) and/or lithogeochemical assessment (Ishikawa alteration index (AI): AI < 65 (mafic), AI < 85 (felsic); Fig. A3; Ishikawa et al., 1976). Least altered mafic samples from this study have $\delta^{18}O$ values between 4.4 and 5.4‰. Least altered felsic samples have $\delta^{18}O$ values slightly higher than the mafic samples and range from 5.5 to 7.7‰ (Fig. 3.13). By comparison, a histogram for all whole rock $\delta^{18}O$ samples from the altered host rocks of the gold-quartz-carbonate vein deposits illustrate a range from 5.8–10.3‰ (x = 7.7‰ ± 1.2; Fig. 3.13A; App. Table A3). These values are on average higher than the background values within the Powell block and the altered wall rocks associated with the Cu-Zn-Ag prospects (Fig. 3.13A-B).

The alteration surrounding the individual Cu-Zn-Ag occurrences typically extends for a minimum of ~50–100 m (Fig. 3.6), however, collectively these closely spaced occurrences and their associated alteration span an area of ~3.5 km^2 with $\delta^{18}O_{whole\ rock}$ values dominantly <6‰ (Fig. 3.2). Within ~20–50 m of the gold-quartz-carbonate veins and E-W striking shear zones the whole rock $\delta^{18}O$ values increase by ~2–5‰ (Fig. 3.2, 3.10C-D), which if superimposed on

previously lower $\delta^{18}O$ chlorite-sericite altered rocks associated with the Cu-Zn-Ag veins results in an apparent "least altered" $\delta^{18}O_{whole\ rock}$ value (~6-8‰; Fig. 3.10D). For example, all the samples collected in proximity to the Powell-Rouyn vein (Fig. 3.13B, A5) exhibit $\delta^{18}O_{whole\ rock}$ values of 6.4-7.3‰, which falls within the background least altered $\delta^{18}O_{whole\ rock}$ values, compared to the ~8-10‰ $\delta^{18}O_{whole\ rock}$ values found surrounding the Vox and Silidor veins (Fig. 3.10C-D). The Powell-Rouyn vein is superposed on an area of pervasive chlorite-sericite alteration with $\delta^{18}O_{whole\ rock}$ values <6‰ (Fig. 3.2).

Six vein quartz samples from the Cu-Zn-Ag veins yield $\delta^{18}O_{quartz}$ values that range from 6.4–9.4‰ with an average of 8.5 ± 0.8‰ (Fig. 3.13B; App. Table A4). The $\delta^{18}O_{quartz}$ values (n = 5) for quartz in the gold-quartz-carbonate veins range from 9.3–12.6‰ with an average value of 11.3 ± 0.8‰ (Fig. 3.13B; App. Table A4). This agrees with the previously reported $\delta^{18}O_{quartz}$ value (n = 6) for the Silidor vein of 10.1 ± 1.2‰ (Carrier et al., 2000). Using the isotopic fractionation equation between quartz and H_2O from Sharp et al. (2016) with an inferred temperature range of 250–350°C, which is typical for VMS systems (e.g. Cathles, 1993; Hannington et al., 2003), the range of $\delta^{18}O_{fluid}$ from which the quartz in the Cu-Zn-Ag veins crystallized is -0.4‰ to 3.1‰ (Table 2; Fig. 3.13B; Matsuhisa et al., 1979; Sharp et al., 2016;). This is consistent with the reported -2‰ to 4‰ $\delta^{18}O_{fluid}$ range for VMS hydrothermal fluids (Huston, 1999). In contrast, the $\delta^{18}O_{quartz}$ values for the gold-quartz-carbonate veins are similar to the typical range for orogenic gold mineralization throughout the Superior Province, which is ~12.5-15‰ $\delta^{18}O_{quartz}$ (McCuaig and Kerrich, 1998; Goldfarb et al., 2005; Quesnel et al, in press). Using a temperature range of 250-350°C, typical for orogenic systems and consistent with the estimated P-T conditions for the Blake River Group in the Rouyn-Noranda area (270°C; Powell et al., 1995), the calculated $\delta^{18}O_{fluid}$ composition for the gold-quartz-carbonate veins is 2.4–5.9‰ (Table 2; Fig. 3.13B; Matsuhisa et

al., 1979; Sharp et al., 2016;). This is in agreement with a metamorphic fluid source (Beaudoin and Pitre, 2005; Beaudoin and Chiaradia, 2016; Quesnel et al., in press), but it also partially overlaps with the estimated ranges for magmatic and Archean seawater fluids (Fig. 3.13B), which might suggest fluid mixing and involvement of more than one fluid source.

3.11 Discussion

3.11.1 Timing of gold-quartz-carbonate vein versus quartz-sulfide Cu-Zn-Ag rich vein mineralization

Two lines of field evidence suggest that the Cu-Zn-Ag veins are older than the gold-quartz-carbonate veins: 1) The spotted alteration associated with the Cu-Zn-Ag veins overprints the volcanic rocks at the Vox occurrence and is itself overprinted by ankerite proximal to ~E-W striking brittle-ductile shear zones; and 2) Minor quartz-sulfide veins, disseminated sulfides and/or associated alteration are locally crosscut by quartz-carbonate veins of similar orientation to the main gold-quartz-carbonate veins at the Powell-F zone. This is further supported by the new ID-TIMS U-Pb zircon ages for the two tonalite intrusions, which constrain the minimum age of the Cu-mineralization and maximum age of the Au-mineralization to 2695.3 ± 1.0 Ma.

3.11.2 Quartz-sulfide Cu-Zn-Ag rich veins, emplacement and origin

Quartz-sulfide Cu-Zn-Ag mineralized zones and their associated alteration haloes are crosscut by the main E-W striking S_2 cleavage. This indicates that the veins were emplaced prior to D_2, either during D_1 or earlier volcanic or magmatic events. The veins are spatially associated with brittle NE striking structures, which have typically been interpreted as re-activated synvolcanic structures (De Rosen Spence, 1976; Lichtblau and Dimroth, 1980; Dimroth et al.,

1982). The NE structures associated with the Cu-Zn-Ag veins are marked by stratigraphic offsets and contain spherulitic felsic dikes and intrusion-related breccias, consistent with a synvolcanic origin.

The Cu-Zn-Ag veins in the Powell Block crosscut older (2703–2701 Ma) Blake River Group strata, as do the McDougall and C-Shaft veins in the Flavrian Block and the Joliet Breccia in the Powell Block (Gibson et al., 1983; Zubowski, 2011; Schofield et al., 2021). Furthermore, the ID-TIMS U-Pb zircon age of 2697.6 ± 0.7 Ma for the altered Powell D-Zone tonalite reported herein accords well with the 2698.0 ± 0.9 Ma age of an altered tonalite intrusion at the Joliet Breccia (Schofield et al., 2021). The two intrusions are similar in age to the upper Blake River Group strata (2699–2695 Ma) and associated VMS hydrothermal system (e.g., Bouchard Hebert VMS deposit, Fig. 3.1). The similarities between the quartz-sulfide Cu-Zn-Ag rich veins, the Joliet Breccia mineralization, McDougall-Despina and C-Shaft quartz-sulfide veins, in terms of metal association, textures, paragenesis, and alteration styles (e.g. Zubowski, 2011; Schofield et al., 2021), are consistent with their formation from the same hydrothermal system, which is interpreted as the "deep structural roots" or "upflow zones" for a VMS hydrothermal system (Fig. 3.14A) that may have fed stratigraphically higher and younger VMS deposits (e.g. Gibson et al. 1983; Cathles, 1993; Zubowski, 2011; Schofield et al., 2021).

The spotted alteration texture associated with the veins resembles dalmatianite, a cordierite porphyryoblastic rock associated with VMS deposits in the contact metamorphic aureole of Lac Dufault pluton in the Flavrian Block to the north (Fig. 3.1). Like dalmatianite, the spotted alteration texture developed in altered rocks with a bulk composition reflecting the transition from sericite to chlorite alteration (Franklin et al., 2005; Schofield et al., 2021). However, the spots are texturally distinctive from retrogressed cordierite porphyroblastic dalamatianite alteration. The

concentric zoning of the spots is unusual for retrogressed porphyroblasts and suggests a primary metasomatic or early diagenetic origin. The albite rich cores of the spots indicate that the spots may have nucleated on pre-existing albite microlites and/or phenocrysts of previously spilitized lithologies. The presence of a similar style of spots in chlorite and sericite altered rocks at the Corbet VMS deposit (Knuckey and Watkins, 1982), the Joliet Breccia (Schofield et al., 2021) and overprinting the No.14 lens of the Millenbach VMS deposit (Fig. 3.1; Riverin, 1977) implies that this texture is patchily distributed in altered rocks throughout the Noranda Volcanic Complex, but is likely younger than the ca. 2703–2701 Ma VMS mineralization.

3.11.3 Gold-quartz-carbonate veins, emplacement and origin

McMurchy (1948) and Carrier et al. (2000) interpreted the gold-quartz-carbonate veins as "late-orogenic" deposits emplaced during post-D_2 regional folding and post-D_3, reverse-dextral shearing along major E-W striking faults. Carrier et al. (2000) suggested that the gold-quartz-carbonate veins occupy NW-striking reverse shear zones, which formed during NE-SW bulk shortening associated with sinistral reactivation of the major E-W striking faults (Horne and Beauchastel faults). However, apart from the lack of evidence for sinistral reactivation of the major E-W striking faults (e.g., Powell fault, Fig. 3.5) and for reverse shearing along the veins exposed at surface, the veins are folded with the S_2 cleavage axial planar to the folds, so they cannot be late-orogenic as proposed by McMurchy (1948) and Carrier et al. (2000).

The gold-quartz-carbonate veins vary in orientation along strike and the poles to individual vein segments define a great circle (Fig. 3.10E), which is similar in orientation to the great circle defined by the poles to bedding measured in the hinge and limbs of the Powell syncline, indicating that the veins were folded during the deformation event that produced the Powell syncline. The pole to the great circle defined by the folded veins represents the axis of the folds overprinting the

veins. It plunges moderately to the ENE and lies along the regional S_2 cleavage. This structural relationship, together with the observed overprinting of the vein alteration halos by the cleavage, suggest that the veins were emplaced during D_2, as were most gold deposits in the southern Abitibi greenstone belt (Dubé and Mercier-Langevin, 2020) including the nearby Donalda deposit (Riverin et al., 1990; Robert et al., 1996). The NNW strike of the veins is largely controlled by the mechanical anisotropies created by rheological contrasts between the mafic dikes and host tonalite (e.g. Belkabir et al., 1993; Blenkinsop et al., 2020). Because the strike of the mafic dikes is within ~20° of the N-S bulk shortening direction during the D_2 event (Fig. 3.14B), the dike-tonalite contacts acted as planes of weakness that underwent a dextral shear traction as they opened up parallel to the bulk extension direction (e.g. Sibson, 2001; Lafrance, 2004). Gold-bearing hydrothermal fluids flowed into the newly created NNW-striking fractures and deposited quartz veins (Silidor), and where offset markers are present (Vox vein), displaced those markers in a dextral manner.

3.11.4 Comparison of alteration signatures associated with both vein systems

The strong lithological control on the alteration mineralogy associated with the gold-quartz-carbonate veins suggests a rock dominated hydrothermal system, with the requirement of primary ferromagnesian minerals to form ankerite. Within felsic dominated successions, this results in cryptic alteration signatures (albite - sericite ± calcite), which are similar to regional synvolcanic spilitic alteration. In contrast, the quartz-sulfide Cu-Zn-Ag rich veins, exhibit consistent alteration mineralogy, which is controlled by primary permeability, regardless of initial host-rock composition, suggesting a fluid dominated hydrothermal system. While both hydrothermal systems introduce chlorite into the mineral assemblage, they appear to form chlorite

with distinguishable compositional differences (Fig. 3.9). Likewise, these two hydrothermal systems have contrasting effects on whole rock $\delta^{18}O$ values.

Whole rock $\delta^{18}O$ values ultimately depend on the oxygen isotope composition of the constituent minerals and the modal mineralogy of the rock, thus composition in part controls the whole rock $\delta^{18}O$ values. For example, pristine rhyolite typically has a $\delta^{18}O$ value ~2‰ higher than their mafic counterparts (Beaudoin et al., 2014). Hydrothermal alteration modifies the oxygen isotope composition of fresh rocks because of the formation of new minerals at the expense of primary minerals (Muehlenbachs, 1986). Altered mafic and felsic samples that are spatially associated with the Cu-Zn-Ag prospects and Au occurrences display lower and higher whole rock $\delta^{18}O$ values, respectively, relative to the background values of their least altered precursors (Fig. 3.13A-B). The difference in whole rock $\delta^{18}O$ values for altered rocks associated with both types of veins could be controlled by different fluid sources, temperatures of alteration, or fluid/rock ratio.

Chlorite and sericite mineral assemblages and isotopically light whole rock $\delta^{18}O$ values of 2.9–5.9‰ within the altered rocks adjacent to the Cu-Zn-Ag occurrences are consistent with hydrothermal alteration driven by modified Archean seawater (Fig. 3.13C; Pope et al., 2012; Johnson and Wing, 2020). In contrast, the gold-quartz-carbonate veins are characterized by relatively isotopically heavy whole rock $\delta^{18}O$ values of 5.8–10.3‰ and carbonate (ankerite ± calcite), albite, sericite, fuchsite, hematite, chlorite mineral associations, which is consistent with hydrothermal alteration driven by interaction with a metamorphic fluid (Fig. 3.13C; Sheppard, 1986) possibly mixed with a lower $\delta^{18}O$ upper crustal fluid, such as Archean seawater trapped in the volcanic rocks porosity (Fig. 3.13C). Mixing between these two fluid types was also invoked for the Val d'Or district, 100 km to the east (Beaudoin and Pitre, 2005) and for quartz-tourmaline-

carbonate veins along the Larder Lake Cadillac fault within the Rouyn-Noranda mining district (Raymond, 2022). Likewise, despite the similarities in textures of quartz within the gold-quartz-carbonate and Cu-Zn-Ag veins, quartz from the two vein sets can be clearly distinguished by different $\delta^{18}O_{quartz}$ values which are relatively higher for the gold-quartz-carbonate veins at an average of 11.3 ± 0.8‰ compared to an average of 8.5 ± 0.8‰ for the Cu-Zn-Ag veins (Fig. 3.13B). This is consistent with different fluid sources for the two vein systems and associated alteration (Fig. 3.13B; Table 2).

3.11.5 Significance of the superposition of alteration events on the district-scale alteration patterns

In a landmark study, Cathles (1993) used whole rock oxygen isotope data to distinguish district-scale, higher-temperature, VMS chlorite and sericite altered up-flow zones characterized by whole-rock $\delta^{18}O$ values <6‰ from lower temperature, albite, epidote, carbonate and/or quartz altered down-flow zones characterized by whole-rock $\delta^{18}O$ values of 8.5–14‰. Cathles (1993) interpreted rocks with whole rock $\delta^{18}O$ values between 6–8‰ as unaltered. Taylor et al. (2014) refined the pattern of oxygen-isotope anomalies in the Powell Block and, along with Cathles (1993) and Hannington et al. (2003), interpreted the extensive areas of sericite-quartz alteration and whole-rock $\delta^{18}O$ values of 8.5–14‰ associated with the Horne and Quemont deposits in terms of semi-conformable synvolcanic "downflow zones" due to seawater recharge. It was proposed that this anomalously high whole rock $\delta^{18}O$ alteration signature for the Horne and Quemont deposits located stratigraphically above lower whole rock $\delta^{18}O$ alteration signatures defined by MacLean and Hoy (1991) might be a useful exploration vector for specifically large and Au-rich VMS deposits (Cathles, 1993). However, in all these studies the effect of an orogenic gold system superimposed upon a VMS system was not considered or was assumed to have had a negligible

effect (e.g. Maclean and Hoy, 1991: Taylor et al., 2014). As such, it is noteworthy that there is considerable overlap between the documented range of whole-rock $\delta^{18}O$ values associated with orogenic systems (e.g. McCuaig and Kerrich, 1998; Beaudoin, 2011) and seawater recharge zones associated with VMS deposits (e.g. Cathles, 1993; Taylor et al., 2014).

This study shows that alteration of the host volcanic rocks during the Cu-Zn-Ag vein-forming event lowered their $\delta^{18}O$ values to 2.9–7.7‰ (Fig. 3.14A), but subsequent overprinting alteration associated with the later gold-quartz-carbonate veins locally increased their $\delta^{18}O$ values to ~5.8–10.3‰ (Fig. 3.14B). Thus, the whole-rock $\delta^{18}O$ values in the Powell Block are dominantly related to the alteration signatures associated with one of the two younger vein mineralization events and locally represent averages of two or more alteration events (Fig. 3.14B). In addition, many of the interpreted VMS related "downflow zones" delineated by relatively enriched $\delta^{18}O$ values, overlap with known orogenic deposits and major structures such as the Horne Creek fault, and Larder Lake Cadillac Break, which are known to have localized orogenic ore forming fluids (e.g. Riverin et al., 1990; Robert et al., 1996; Dubé and Mercier-Langevin, 2020). Likewise, this study has demonstrated that the juxtaposition of orogenic related albite ± ankerite ± calcite ± sericite alteration on VMS and/or magmatic-hydrothermal related chlorite-sericite alteration can produce lower whole rock $\delta^{18}O$ values than what might be expected for typical orogenic deposits and may result in the misinterpretation that such rocks are unaltered. This has been problematic for the use of whole-rock $\delta^{18}O$ values to discern VMS alteration patterns in the Powell block. For example, Taylor et al (2014) did not detect distinct zones of VMS-related alteration in the footwall to the Quemont VMS deposit in part because the superposition of orogenic gold alteration on VMS altered rocks effectively masked the early VMS alteration and lead to interpretations that the rocks were unaltered. The intense quartz-sericite alteration surrounding the Horne and Quemont VMS

deposits, characterized by anomalously high whole rock $\delta^{18}O$ values of 6.6–11.6‰ (MacLean and Hoy, 1991; Taylor et al., 2014) overlaps with the 5.8–10.3‰ $\delta^{18}O_{whole\ rock}$ range associated with the orogenic overprint documented throughout the Powell Block in this study. Both deposits occur proximal to the Horne Creek Fault (Fig. 3.1), and Krushnisky (2018) described a 10m wide fault zone associated with intense sericite, hematite, and Fe-carbonate alteration crosscutting the Horne mineralization, which is consistent with an orogenic gold alteration overprint.

3.12 Conclusions

The Powell Block contains an abundance of two types of epigenetic quartz veins: quartz-sulfide Cu-Zn-Ag rich veins and gold-quartz-carbonate veins. Field relationships suggest that the Cu-Zn-Ag veins formed earlier than the gold-quartz-carbonate veins and that the two are genetically unrelated. This is further supported by the contrasting alteration mineral associations, lithogeochemical and isotopic alteration signatures, metal tenors and $\delta^{18}O_{quartz}$ values for both vein styles (11.3 ± 0.8‰ for the Au veins and 8.5 ± 0.8‰ for the Cu-Zn-Ag veins), which indicate that different fluid sources are likely for the two vein systems. Assuming a temperature range of 250–350°C, which is typical for VMS systems, the range of $\delta^{18}O_{fluid}$ from which the quartz in the Cu-Zn-Ag veins crystallized is -0.4‰ to 3.1‰. In contrast, using the same temperature range, which is also common in orogenic systems, the calculated $\delta^{18}O_{fluid}$ composition for the gold-quartz-carbonate veins is 2.4–5.9‰. In addition, new ID-TIMS U-Pb zircon ages for two tonalite intrusions constrain the maximum age for the Cu-mineralization to 2697.6 ± 0.7 Ma, and a minimum age at 2695.3 ± 1.0 Ma; the younger age also defines a maximum age for emplacement of the gold-quartz carbonate veins.

Despite the different timing for the formation of the two vein systems, in both cases pre-existing structures controlled the hydrothermal fluid flow and ultimately dictated the orientation of the resulting hydrothermal veins and their subsequent deformation style. Early ENE striking Cu-Zn-Ag veins may have utilized pre-existing structures marked by older (ca. 2703–2701 Ma) Blake River Group felsic dikes, but clearly were emplaced during a younger ca. 2698 Ma Blake River Group magmatic-hydrothermal event. The veins may represent a relatively deeper manifestation of a ca. 2699-2695 Ma VMS system that formed in rocks at a higher stratigraphic level. In contrast, the gold-quartz-carbonate veins were emplaced along pre-existing mechanical anisotropies created by NNW striking mafic dikes, ~40–30 m.y. after the Cu-Zn-Ag veins during early D_2 N-S shortening at ca. 2670–2660 Ma.

Both vein sets are associated with fracture-controlled to pervasive hydrothermal alteration, which overprints rocks that were subject to early seafloor spilitization. Thus, superposition of at least three independent types of alteration is observed within the Powell block and in the larger Rouyn-Noranda Mining District: 1) early quartz-albite (spillitization); 2) chlorite and spotted sericite-chlorite alteration characterized by Fe-rich chlorite, and whole rock $\delta^{18}O$ values of 2.9–5.9‰; and 3) carbonate, sericite, chlorite and hematite alteration, characterized by Mg-rich chlorite, and whole rock $\delta^{18}O$ values of 5.8–10.3‰ (Fig. 3.14). Moreover, where the carbonate alteration associated with the gold-quartz-carbonate veins and shear zones is superimposed on the chlorite and spotted sericite-chlorite alteration associated with the Cu veins, an increase of ~2–5‰ whole-rock $\delta^{18}O$ values occurs. The whole-rock $\delta^{18}O$ values from samples that have experienced more than one hydrothermal alteration event are thus an average of the individual signatures, and this juxtaposition of orogenic related alteration, on VMS and/or magmatic-hydrothermal related alteration can produce lower whole rock $\delta^{18}O$ values than what might be expected for typical

orogenic deposits and result in the misinterpretation of such rocks as either unaltered or altered by VMS related "downflow" zones. This is problematic for the use of whole-rock $\delta^{18}O$ values to discern regional scale alteration patterns for VMS deposits within any area that has multiple superposed mineralization events. Since superposed mineralization events are ubiquitous in ancient volcanic districts, whole-rock $\delta^{18}O$ values should not be used as a stand alone method to provide vectors to mineralization, particularly at the greenfield exploration stage . The results of this study provide a guide for using a combination of detailed field observations including overprinting relationships between veins, their associated alteration assemblages and regional structural fabrics, as well as geochronology, mineral and isotopic chemistry, to help decipher and vector within volcanic rocks that are modified by superimposed hydrothermal events.

3.13 Acknowledgements

The authors extend much appreciation to Mr. Sylvain Picard for providing access to historical samples and data for the Silidor deposit. Dr. Gérald Riverin and Mr. Jean Goutier are also thanked for providing critical historical data. Dr. Taus Jørgensen is thanked for helpful discussions and providing invaluable logistical assistance during field work. Field assistants Ms. Brittany Courchesne, Mr. David Dickson and Mr. Michael Langa are thanked for eager, competent and able assistance in the field. Yorbeau Resources Inc. are thanked for allowing the use of their rock saw facilities during the field season. Financial support was provided by Metal Earth though a Canada First Research Excellence Fund (CFREF) grant, which comprises a tri-agency initiative of the Natural Sciences and Engineering Research Council (NSERC), Social Sciences and Humanities Research Council (SSHRC), and the Canadian Institutes of Health Research (CIHR). Funding was also provided by federal, provincial, and industry partners of the Mineral Exploration

Research Centre (MERC; http://merc.laurentian.ca/research/metal-earth/). This publication is a Metal Earth contribution MERC-ME-2021-68.

3.14 Figures

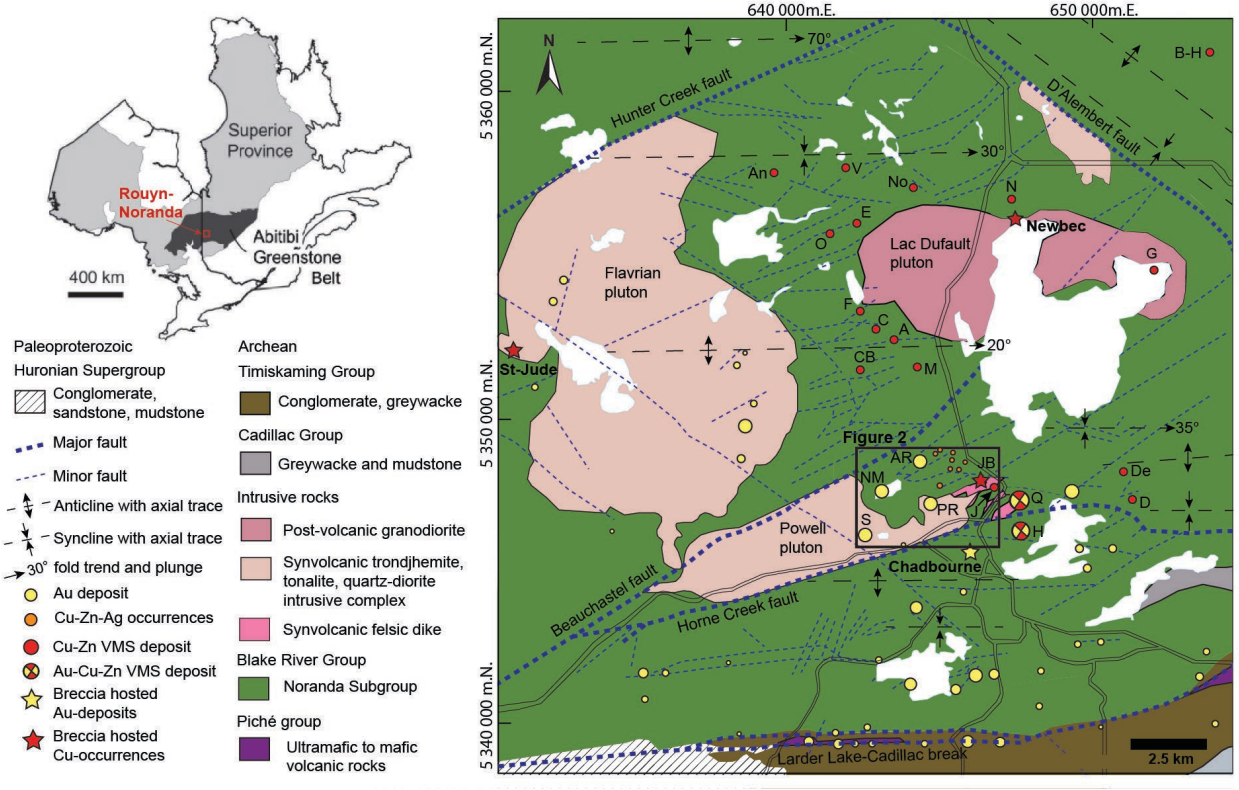

Figure 3.1: Regional geology map of the Rouyn-Noranda mining district.

Regional geology map of the Rouyn-Noranda mining district modified from Schofield et al., (2021) and references therein, showing spatial distribution of the various mineral occurrences and deposits. The yellow circles are scaled to reflect the relative gold tonnage. Abbreviated VMS deposits are: A = Amulet A, An = Ansil, B-H = Bouchard-Hebert, C = Amulet C, CB = Corbet, De = Deldona, D = Delbridge, E = East Waite, F = Amulet F, G = Gallen, H = Horne, J = Joliet, M = Millenbach, No = Norbec, N = Newbec, O = Old Waite, Q = Quemont, V = Vauze. Abbreviation for other deposits are: AR = Anglo-Rouyn; JB = Joliet Breccia; NM = New Marlon; PR = Powell Rouyn; S = Silidor. Location for Figure 2 is highlighted by the black rectangle.

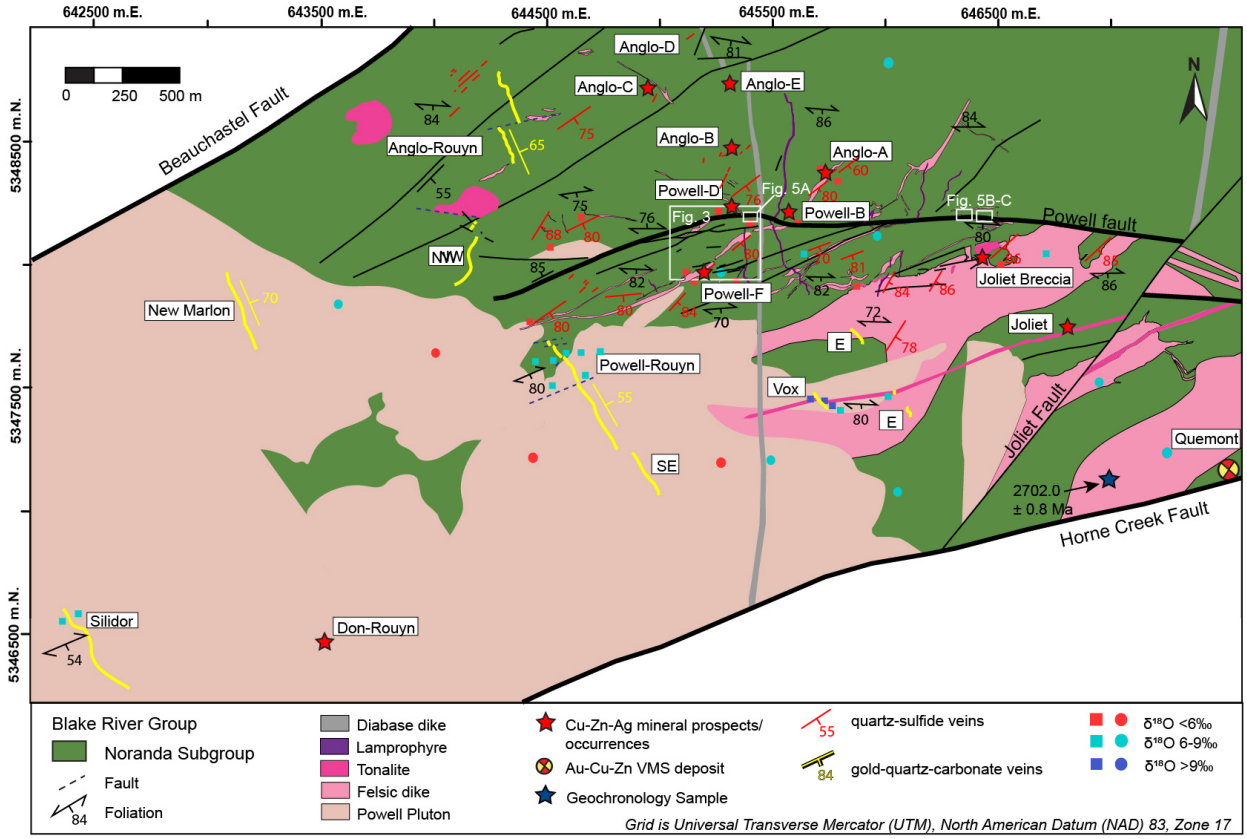

Figure 3.2: Geology map of the Powell Block.

Geology map of the Powell Block, modified from Morris (1957;1959), showing the distribution and orientations of the gold-quartz-carbonate veins (yellow) and quartz-sulfide Cu-Zn-Ag veins (red). Whole rock $\delta^{18}O$ data localities from this study and previous studies (Cathles, 1993; Taylor et al., 2014) are shown by squares and circles, respectively, color coded to reflect the typical ranges used for VMS exploration in the district (Cathles, 1993; Taylor et al., 2014). Note higher whole rock $\delta^{18}O$ values proximal to the gold-quartz-carbonate veins and lower whole rock $\delta^{18}O$ values proximal to the quartz-sulfide Cu-Zn-Ag veins.

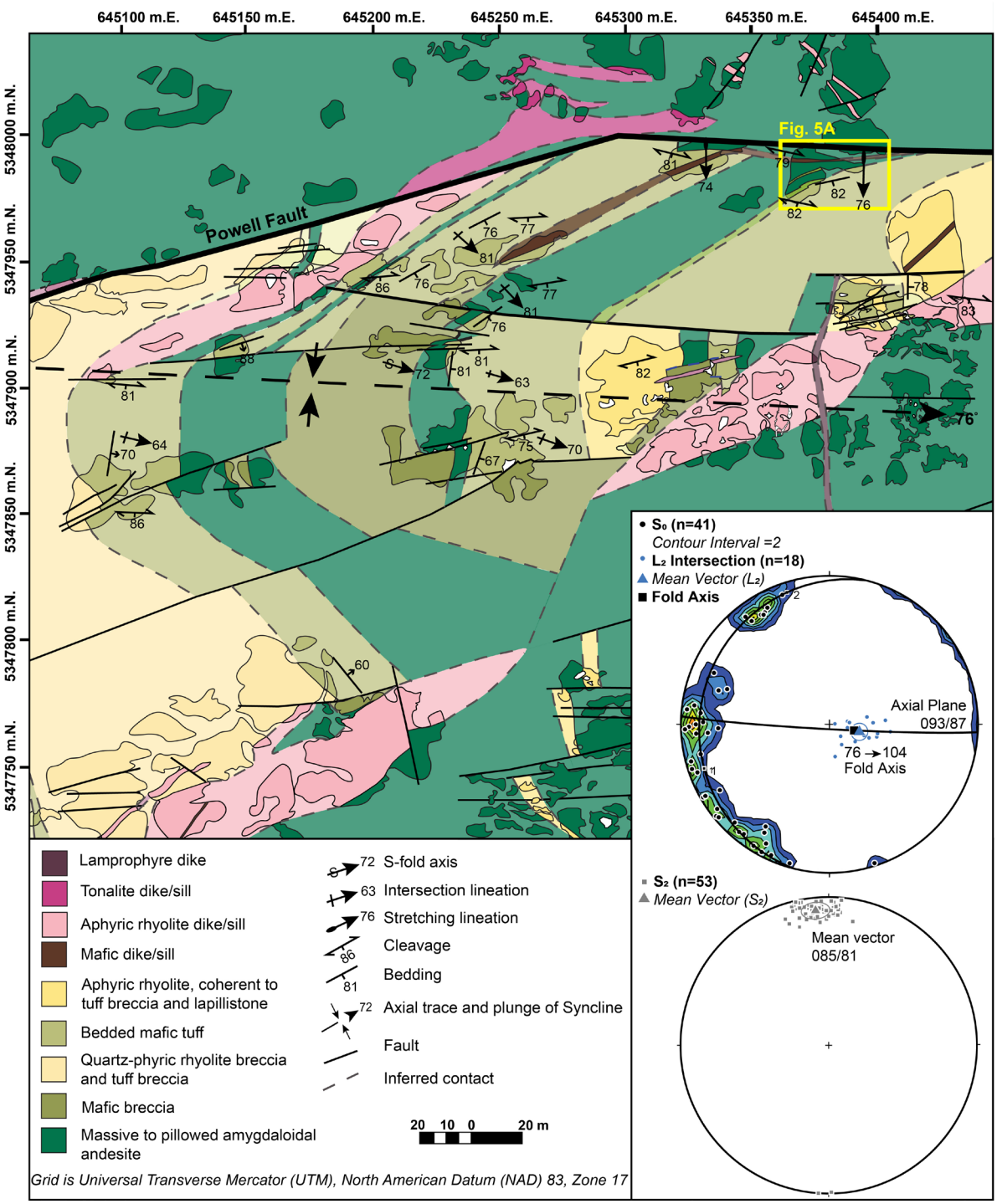

Figure 3.3: Geological map and stereonet projections of the Powell syncline and Powell fault.

Geological map of the Powell syncline and Powell Fault and equal area, lower hemisphere stereonet projections of structural measurements from the Powell syncline; stereonet plots generated with Stereonet® (Allmendinger et al., 2012). The trend and plunge of the fold axis have been interpreted from the pole to the great circle that best fits the distribution of poles of bedding measurements. Contours of poles to bedding measurements are calculated as percent of total

number of data points per 1% area with contour intervals of 2. The calculated fold axis orientation overlaps with the mean vector of the measured intersection lineations between bedding and foliation. The orientation of the axial plane was determined from its mapped surface trace combined with the computed fold axis.

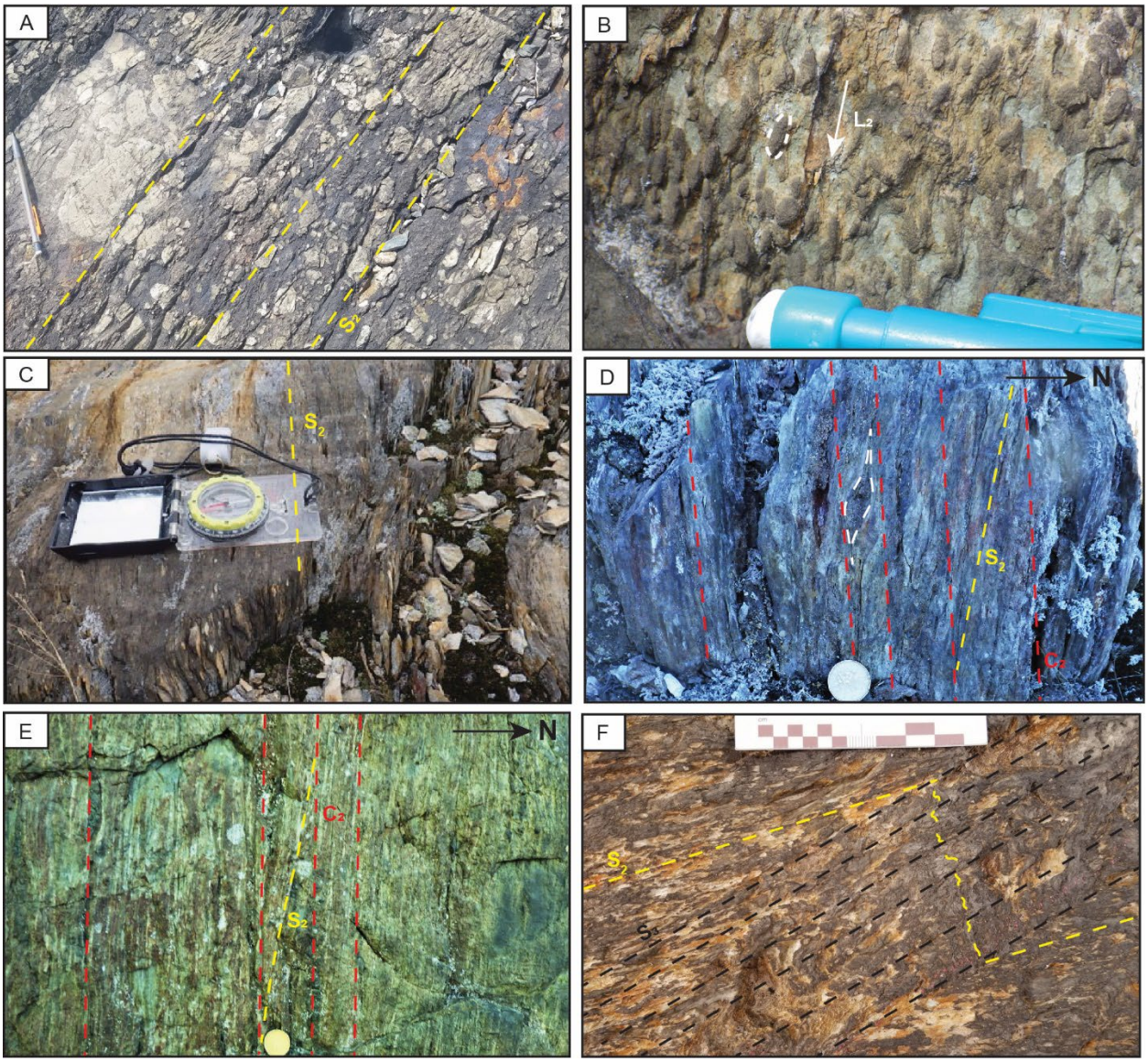

Figure 3.4: Outcrop photographs of structural features of D_2 and D_3.

Outcrop photographs of the main structural elements of the D_2 and D_3 deformation increments within the Powell block: **A)** The S_2 foliation defined by elongate and aligned clasts in weakly altered rhyolite lapillistone; **B)** Deformed spotted alteration in the Powell fault showing a subvertical shape lineation of individual spots; **C)** Sericitic phyllonitic S_2 fabric within the Powell fault; **D)** Vertical surface across the Powell fault showing S-C fabrics and asymmetrical sigmoidal clast indicating N over S movement; **E)** Vertical view of the Powell fault showing S-C fabrics indicating N over S movement; **F)** S_2 foliation crenulated by S_3 spaced cleavage within Powell fault.

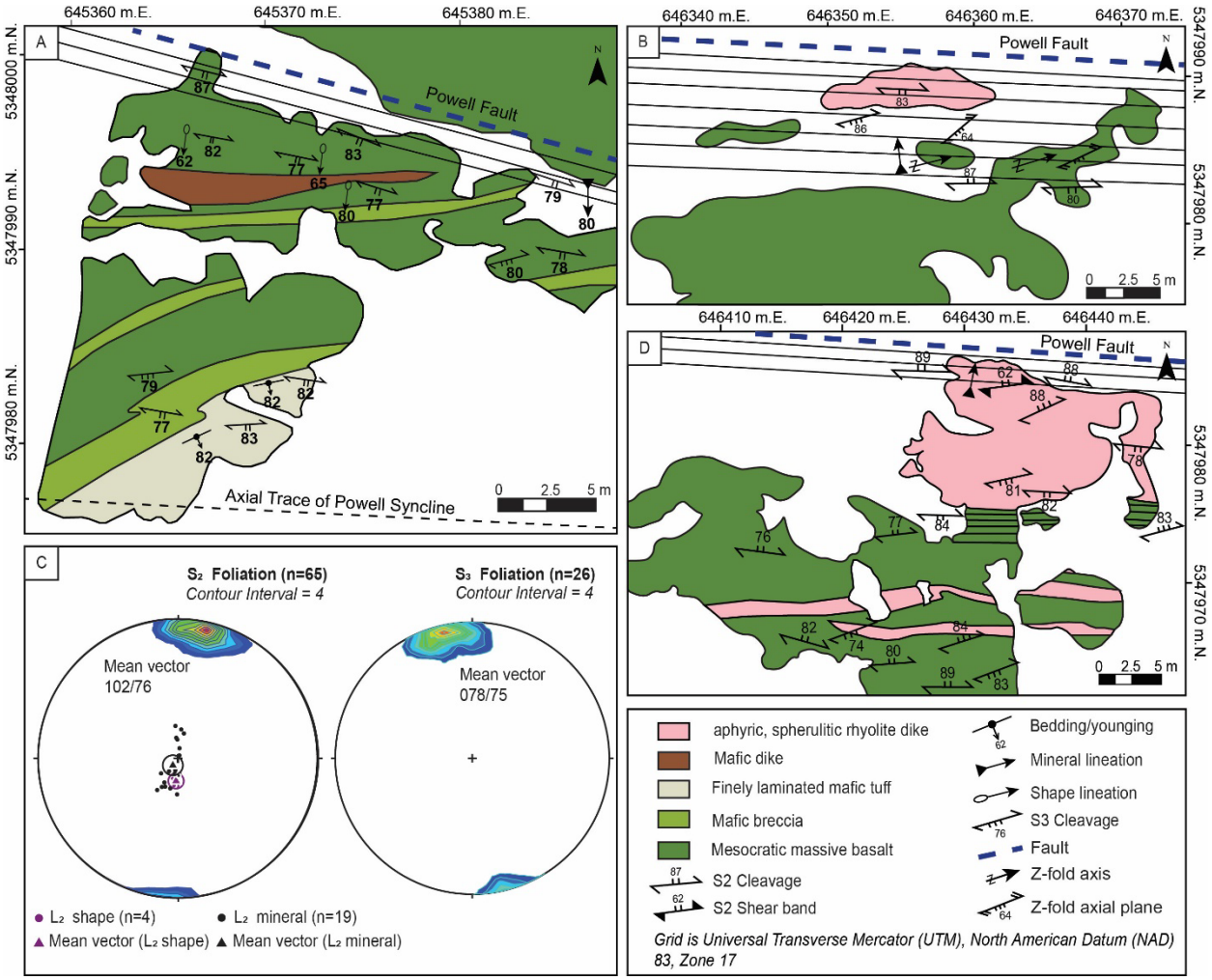

Figure 3.5: Structural maps of the Powell fault.

Structural maps of key outcrops along the Powell fault: western exposure (**A**) and eastern exposures (**B, D**). Equal area, lower hemisphere, stereonet projections (**C**) summarize foliation and lineation measurements along the Powell fault. Stereonet plots generated with Stereonet® (Allmendinger et al., 2012). Contours of poles to bedding measurements are calculated as percent of total number of data points per 1% area with contour intervals of 4.

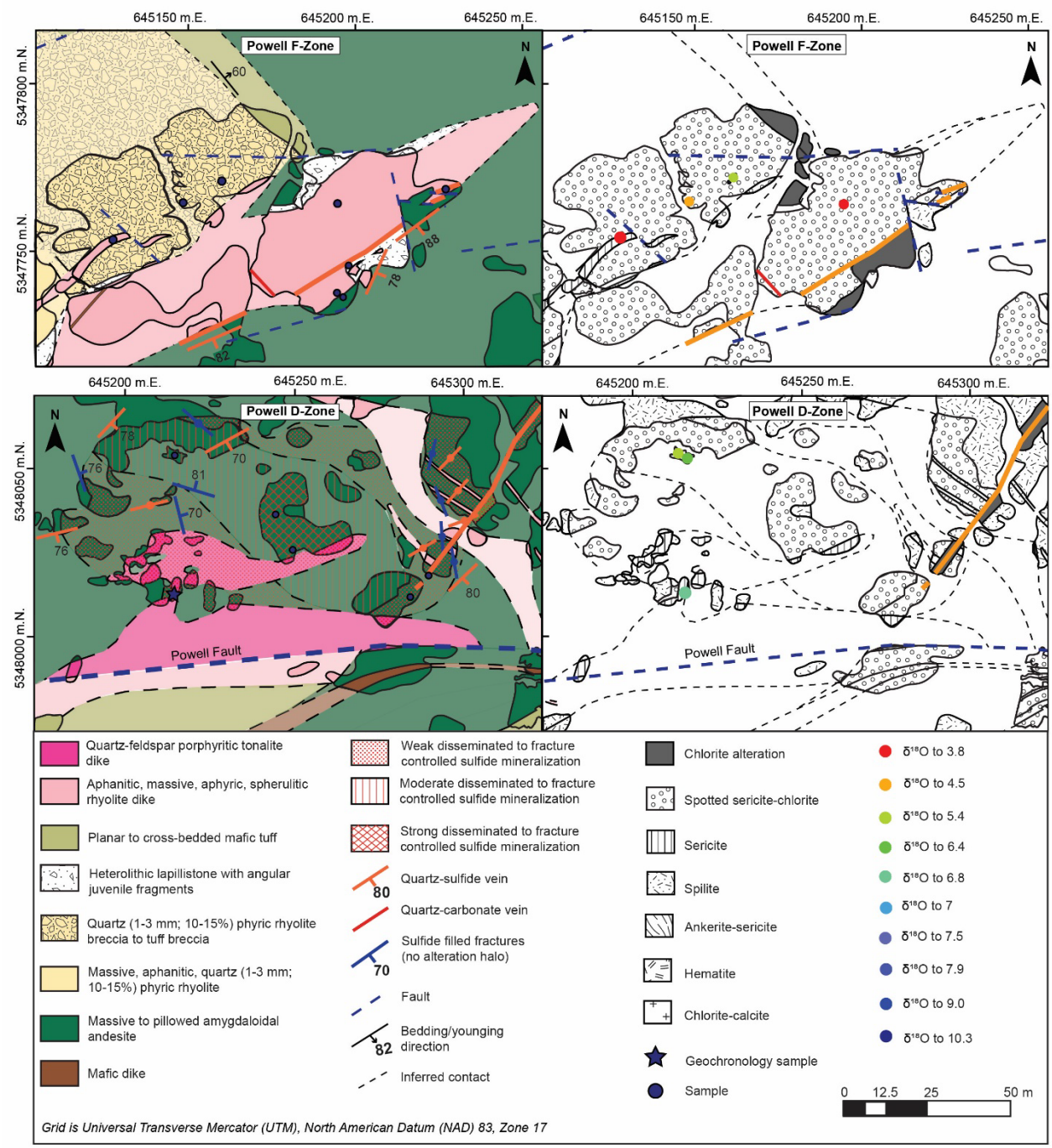

Figure 3.6: Geological and alteration maps of Cu-Zn-Ag prospects.

Geological and alteration maps of the Powell F-zone and Powell D-zone Cu-Zn-Ag prospects. Sample locations are shown in blue circles, for whole-rock geochemistry, multi-element, thin section and/or $\delta^{18}O$ analysis. Whole rock $\delta^{18}O$ values color coded to reflect their variation. Note the alteration associated with these veins extend into the host rocks for ~100m from the veins and is associated with whole rock $\delta^{18}O$ values <7‰. Blue star shows the location for tonalite dike U-Pb geochronology sample 20MDS-201B in the Powell D-zone.

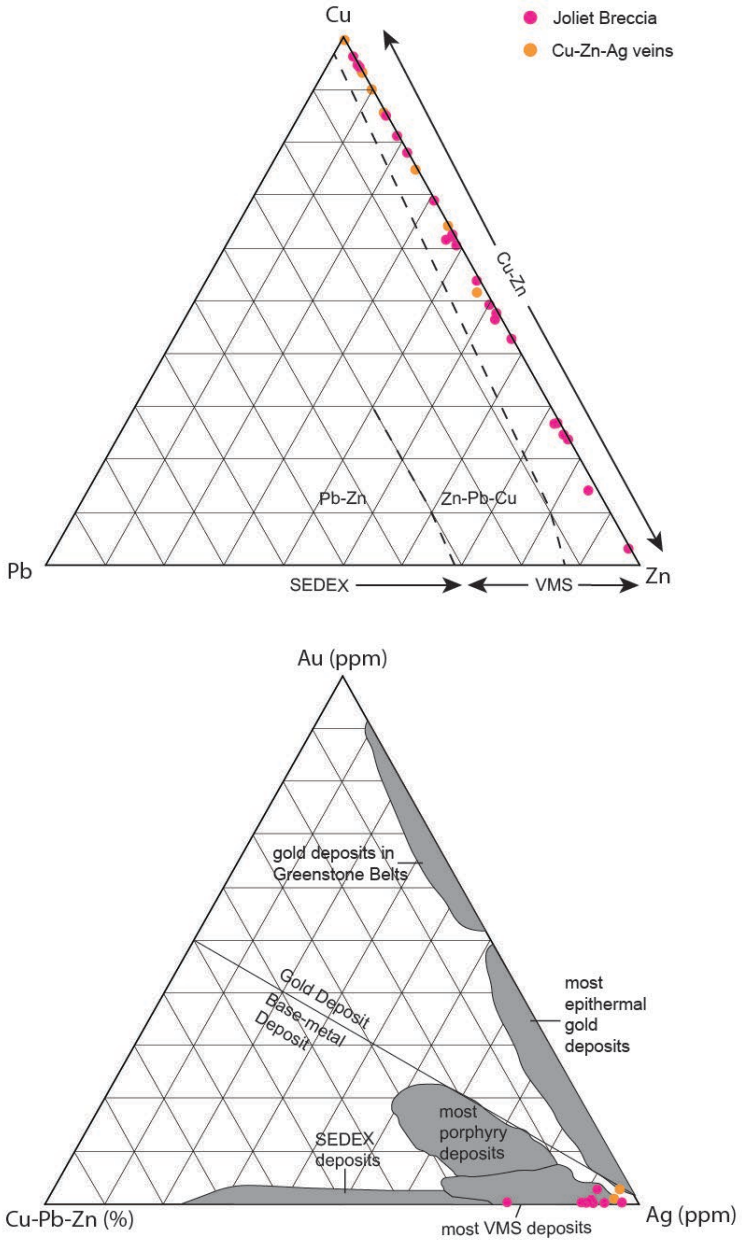

Figure 3.7: Ternary plots of metal tenor for Cu-Zn-Ag veins compared to typical base metal deposits.

Ternary plots modified from Franklin et al. (1981) and Hannington et al. (1999) showing the metal tenor of the quartz sulfide veins compared to the Joliet Breccia (Schofield et al., 2021) and typical base metal deposits. The veins and Joliet Breccia overlap with the Cu-Zn VMS field.

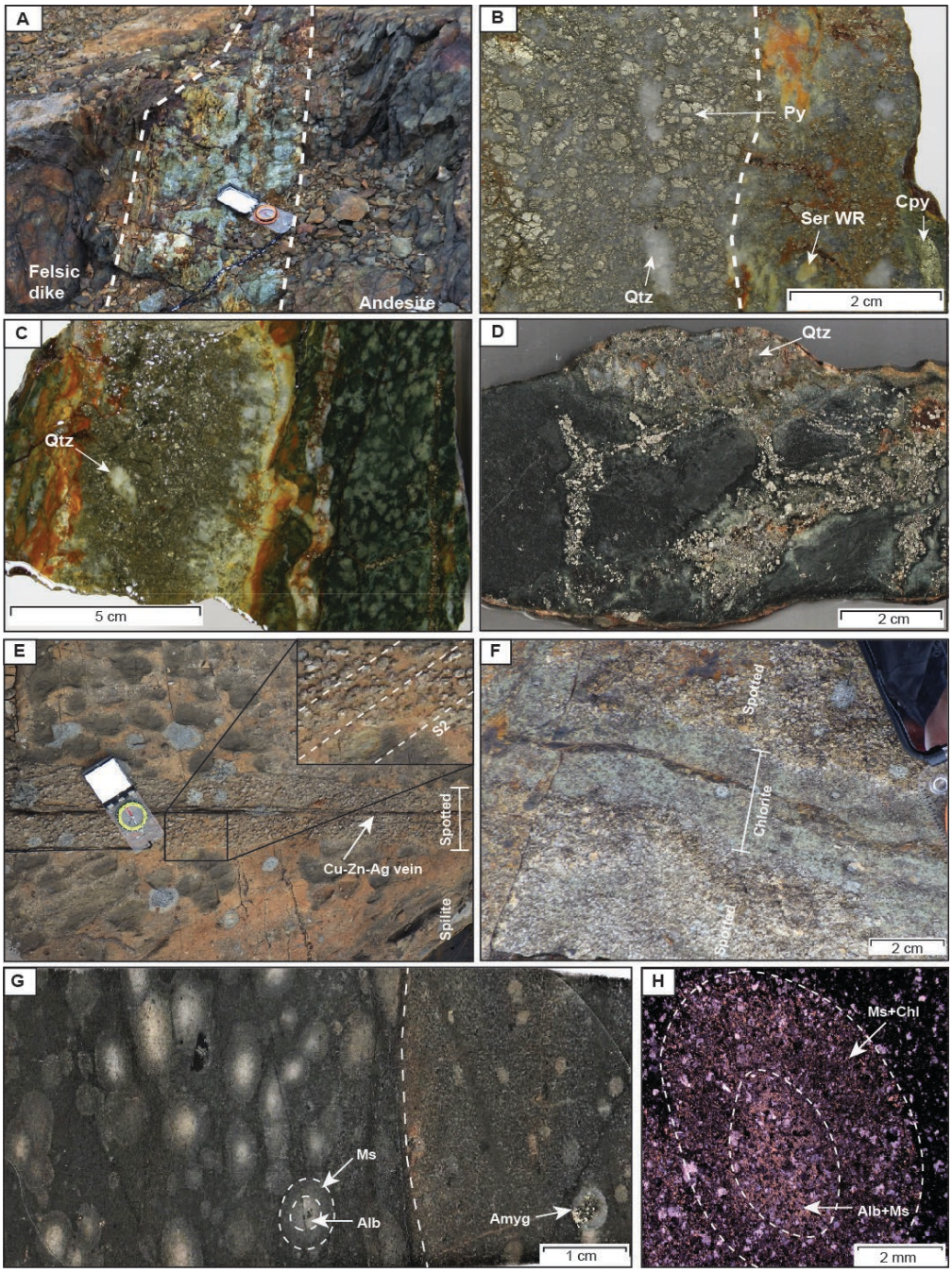

Figure 3.8: Photographs of textures of Cu-Zn-Ag veins and associated alteration.

Photographs of showing the range of macroscopic textures of the quartz-sulfide Cu-Zn-Ag veins and associated alteration. **A)** Powell F-Zone vein, showing outer banded margin adjacent to aphyric rhyolite dike and more massive interior; **B)** Anglo D-zone vein with angular jig-saw fit pyrite and fine-grained grey quartz. Note, angular fragments of white quartz and sericitized wallrock; **C)** Anglo D-Zone vein showing white, medium grained, euhedral quartz along the sharp planar margin of the vein with host andesite, and a massive pyrite dominant core with an angular fragment of quartz. Note the spotted alteration texture in the host andesite; **D**) Powell D-zone

showing angular fragments of andesite cemented by quartz and pyrite; **E)** Quartz-sulfide Cu-Zn-Ag vein with associated halo of spotted sericite-chlorite alteration crosscutting spilitized andesite, Powell F-zone area. Note, the very sharp contact of the alteration halo and overprinting S_2 cleavage, which corresponds to shortening of the alteration spots in a direction perpendicular to it (the larger beige and gray patches represent lichen on the outcrop surface); **F)** Quartz-sulfide Cu-Zn-Ag vein from Anglo-A zone. Note, the alteration zoning from a marginal halo of spotted sericite-chlorite alteration to a proximal Fe-rich chlorite alteration and the overprinting S_2 cleavage; **G)** Channel sample through contact between spotted alteration halo and spilitized amygdaloidal andesite from Powell F-zone. Note, the concentric zoning of the alteration spots with white albite and muscovite rich cores and beige muscovite and chlorite rich rims in a chloritized groundmass (polished slab); **H)** Close-up of concentrically zoned alteration spot from sample shown in Fig. 9C (photomicrograph). Cpy = chalcopyrite; Py = pyrite; Qtz = quartz; Ser WR = sericitized wallrock.

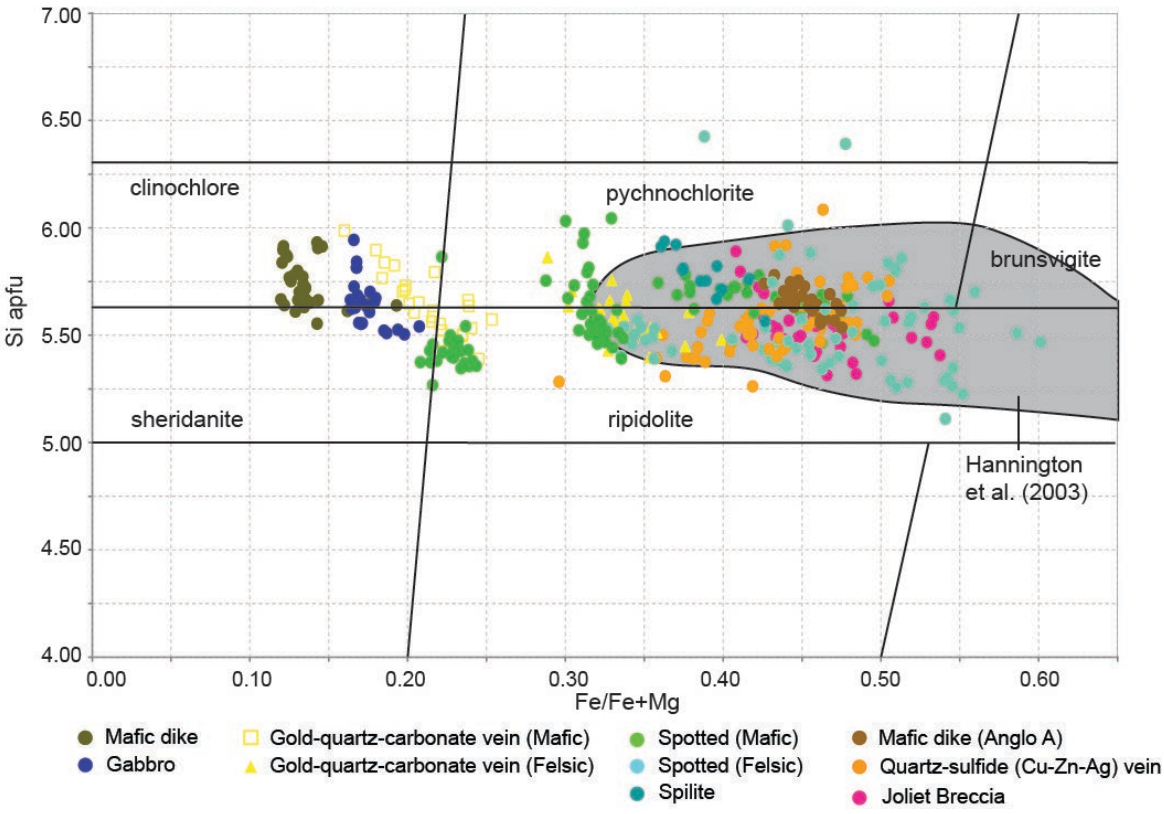

Figure 3.9: SEM-EDS mineral chemistry results for chlorite and carbonate.

SEM-EDS mineral chemistry results. **A)** Chlorite composition, nomenclature for ranges of chlorites from Hey (1954). Felsic protoliths trend towards higher Fe-chlorite compositions, compared to mafic protoliths but the highest Fe-chlorites occur in both mafic and felsic lithologies that are most proximal to Cu-Zn-Ag prospects and occurrences. Chlorite associated with the alteration haloes surrounding the Au-deposits are more Mg-rich than the chlorite associated with the Cu-Zn-Ag prospects and occurrences. Grey shaded area shows range of chlorite composition for VMS deposits in Noranda from Hannington et al. (2003).

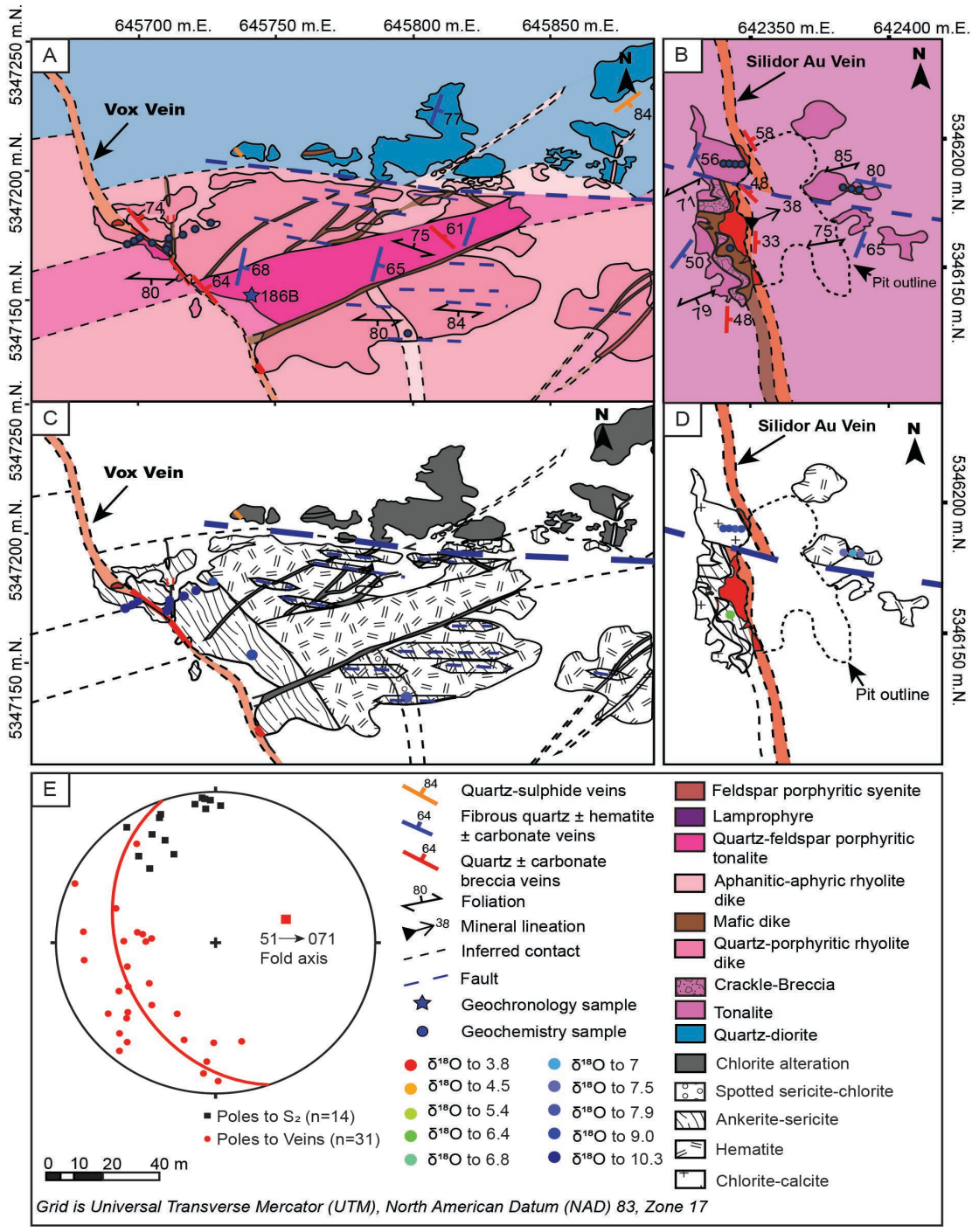

Figure 3.10: Geology and alteration maps for gold-quartz-carbonate vein deposits and occurrences.

Geology (**A-B**) and alteration maps (**C-D**) for two well-exposed gold-quartz-carbonate-vein deposits and occurrences in the Powell-Block, Rouyn-Noranda, Québec. Sample locations are shown in blue circles, for whole-rock geochemistry, multi-element, thin section and/or $\delta^{18}O$ analysis. White star shows the location for tonalite dike U-Pb geochronology sample 20MDS-186B at the Vox occurrence. Whole rock $\delta^{18}O$ values color coded to reflect their variation. Note,

patches of chlorite and spotted-sericite alteration, overprinted by ankerite-sericite alteration at the Vox occurrence has relatively high whole rock $\delta^{18}O$ values compared to the same alteration shown in Figure 6. Equal area, lower hemisphere, stereonet projection (**E**) summarizes structural measurements taken along the gold-quartz-carbonate veins. Stereonet plots generated with Stereonet® (Allmendinger et al., 2012).

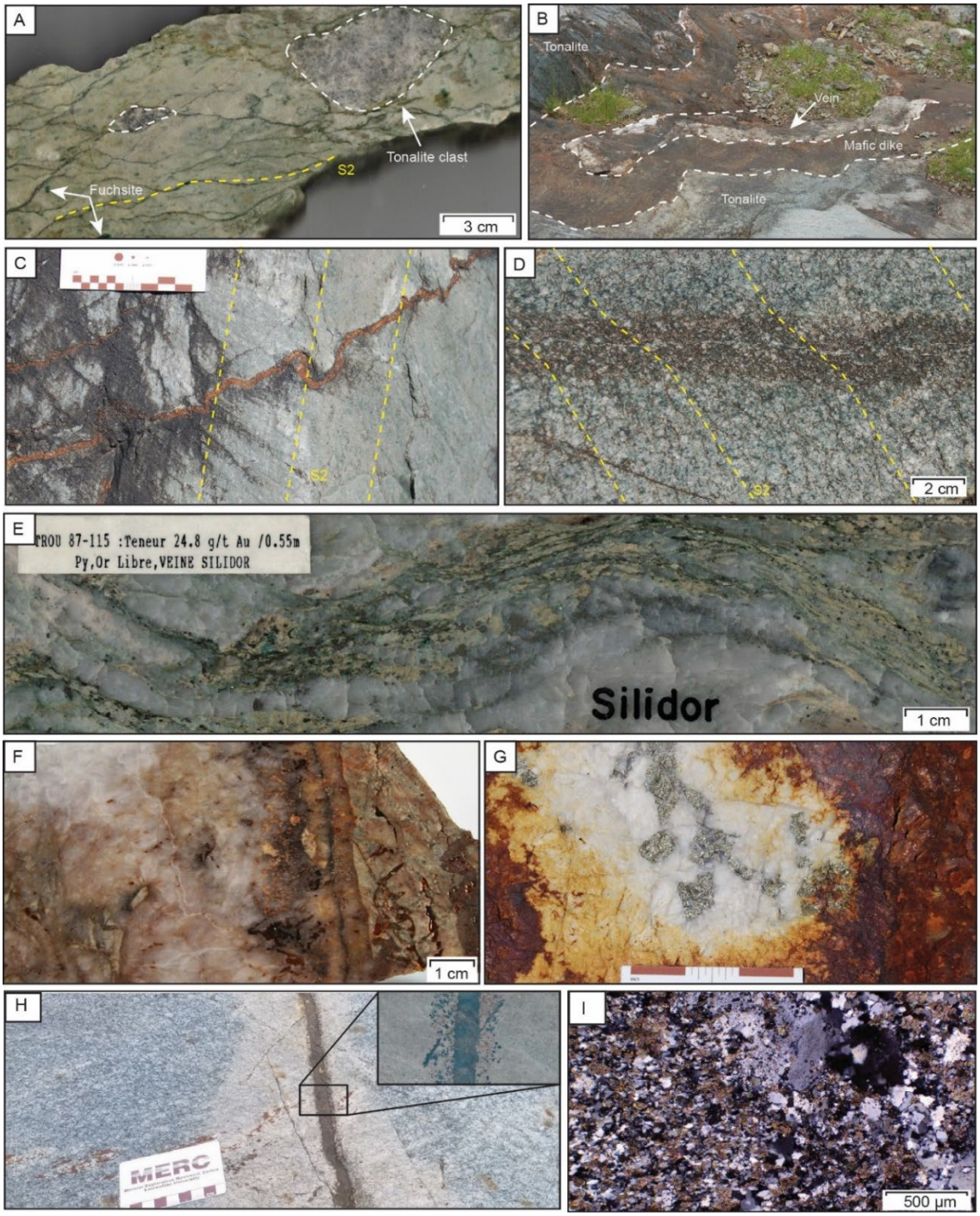

Figure 3.11: Photographs of characteristic textures of the gold-quartz-carbonate-veins and associated alteration.

Hand sample and outcrop photos demonstrating the characteristic textures of the gold-quartz-carbonate-veins and associated alteration found in the Powell Block. **A)** Channel sample of carbonate-fuchsite breccia in the footwall of the Silidor vein, with the S_2 cleavage overprinting the matrix of the breccia; **B)** Outcrop image of footwall mafic dike and parallel quartz vein, crosscutting tonalite. The thin quartz vein is parallel to the main Silidor vein and both the dike and the vein are folded into an open, moderately NE plunging fold. Photo is taken looking down plunge of the fold. Field of view is approximately 2m; **C)** Folded oblique fibrous ankerite veins at the Silidor deposit; **D)** Thin quartz veinlet with ankerite-sericite alteration halo crosscutting the hanging wall tonalite at the Silidor deposit. Note the overprinting cleavage; **E)** Historic drillcore display sample from hole 87-115 provided by Sylvain Piccard. Banded margin of Silidor vein, showing slivers of altered wall rock and disseminated pyrite, note the folded nature of the vein and the foliated wall rock slivers; **F)** Polished slab of Powell-Rouyn Au vein showing angular altered clasts of host-rock within the massive quartz vein. Note euhedral pyrite within altered wall rock, and ankerite intergrown with quartz on the margin of the vein (right); **G)** Outcrop surface of the vein showing a vuggy texture of quartz with sulfides found internal to the quartz vugs; **H)** Chlorite calcite altered Powell tonalite from the hanging wall of the Silidor vein, crosscut by a bleached ankerite, calcite and sericite halo associated with a 1cm wide ankerite and hematite vein (outcrop). Inset shows stained (Hitzman, 1999) hand sample with ankerite (blue) and calcite (pink) disseminations surrounding ankerite vein (hand sample); **I)** Most proximal, intense carbonate alteration in hanging wall of Silidor vein. Graphic textured tonalite completely overprinted by granoblastic carbonate texture.

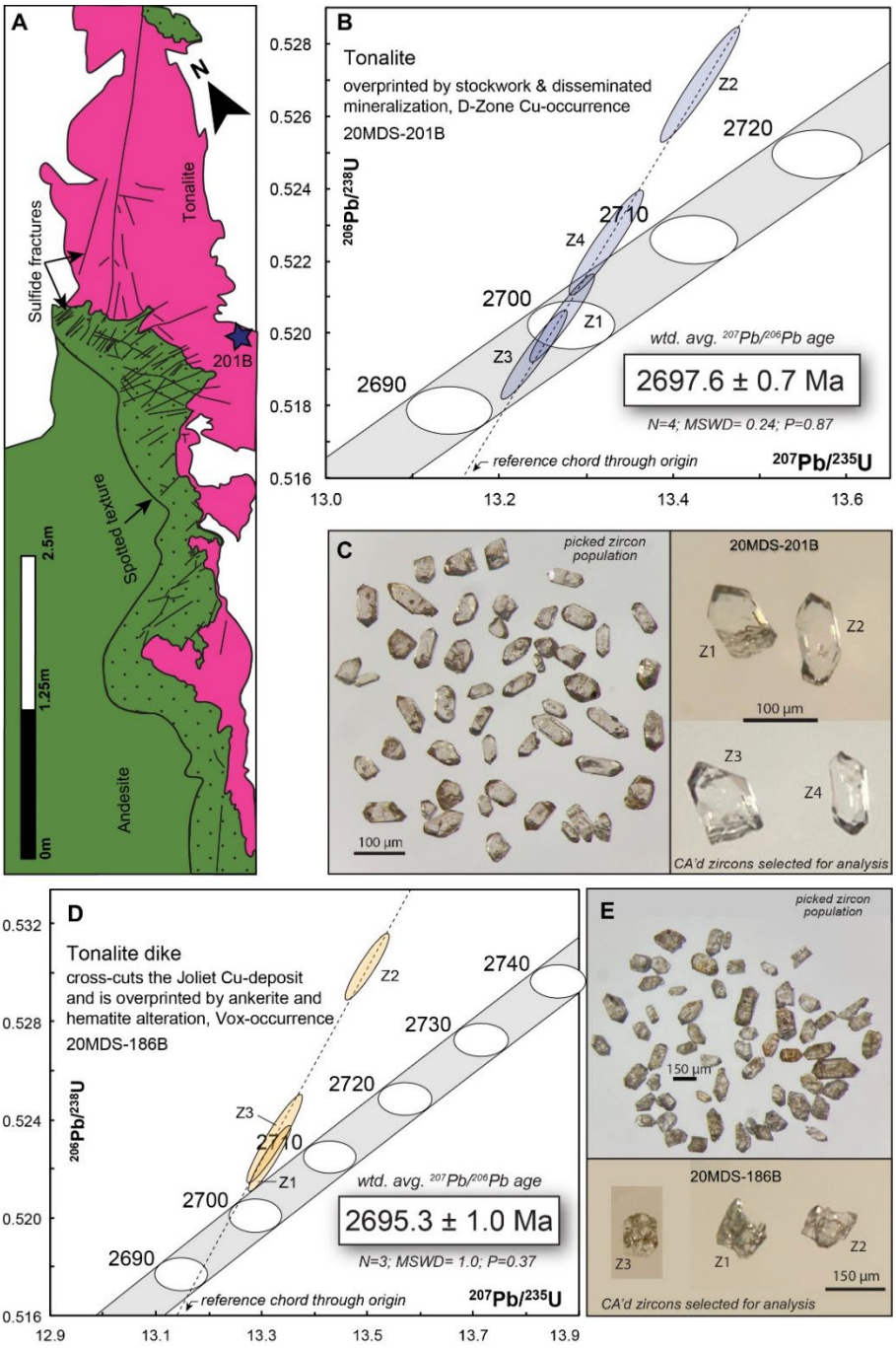

Figure 3.12: Results of ID-TIMS U-Pb analysis of two tonalite samples.

Results of ID-TIMS U-Pb analysis of two tonalite samples. **A)** Detailed outcrop sketch of tonalite intrusion at Powell D-zone from location shown in Fig. 3, illustrating the relationship between the sulfide mineralization and the intrusion as well as the location of the geochronology sample; **B)** Concordia diagram and **C)** Zircon grain images for ID-TIMS U-Pb analysis; **D)** Concordia diagram for sample of tonalite dike from the Vox gold occurrence (see Fig. 10B for location); E) Zircon grain images for ID-TIMS U-Pb analysis.

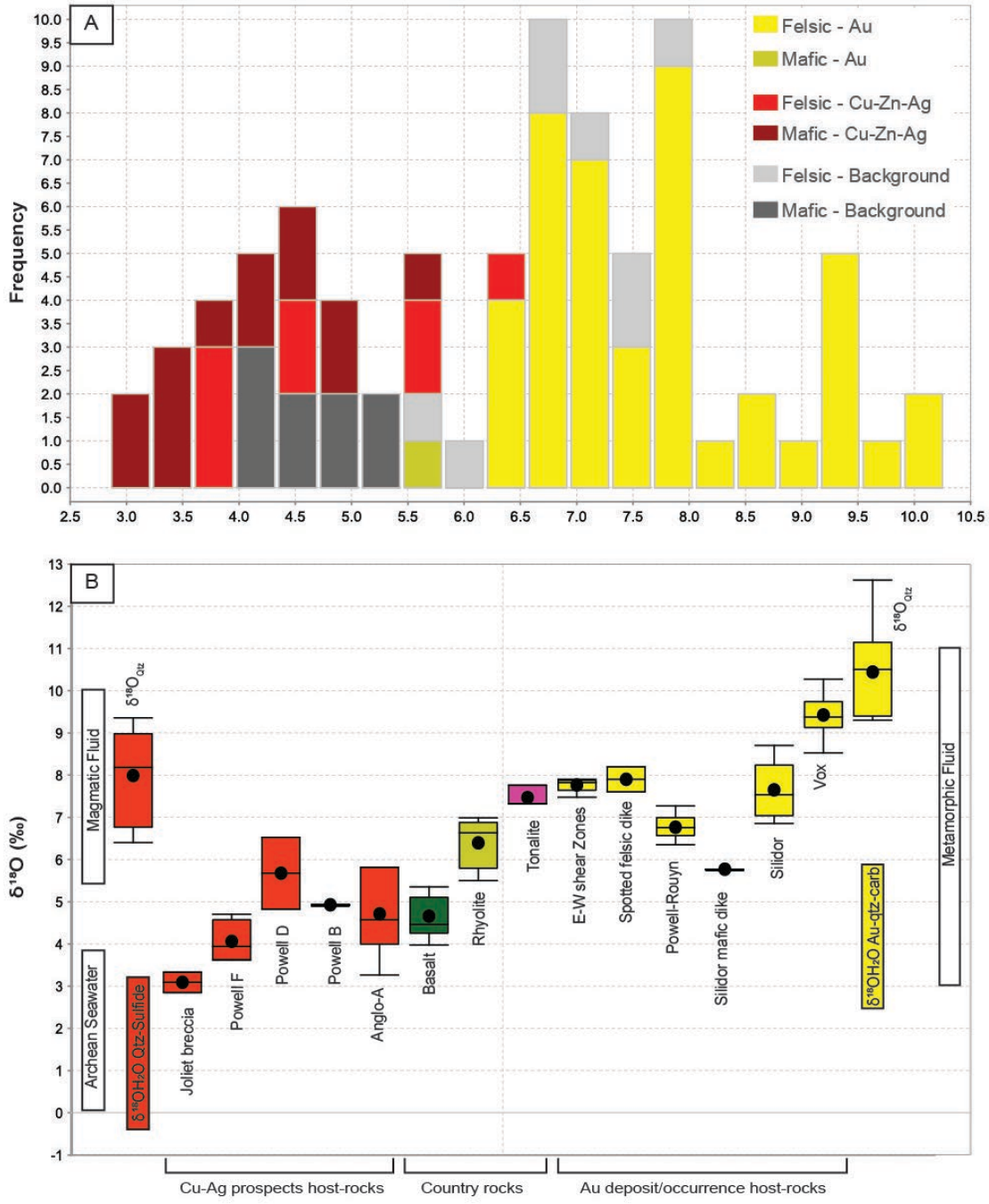

Figure 3.13: whole-rock and quartz $\delta^{18}O$ values.

A) Histogram of whole-rock $\delta^{18}O$ values for lithologies distal to mineralization (grey) and within alteration haloes associated with the quartz-sulfide Cu-Zn-Ag veins (red) and gold-quartz-carbonate-veins (yellow). Data is grouped into 20 bins, 0.371‰ wide. The shades within each group reflect the mafic and felsic composition range; **B)** Comparison of whole-rock $\delta^{18}O$ values for altered host rocks associated with Cu-Zn-Ag and Au mineral prospects, occurrences and deposits with the background country rock values for the main lithologies in the Powell Block. Quartz $\delta^{18}O$ values from quartz-sulfide Cu-Zn-Ag veins and gold-quartz-carbonate veins are

shown on far left and right of the diagram, respectively. The $\delta^{18}O$ H_2O values calculated from the mean $\delta^{18}O$ quartz values and estimated temperature range from the two vein types (Table 2) are also plotted in comparison to the range of $\delta^{18}O$ values for the possible fluid sources (Sheppard, 1986; Pope et al., 2012; Johnson and Wing, 2020).

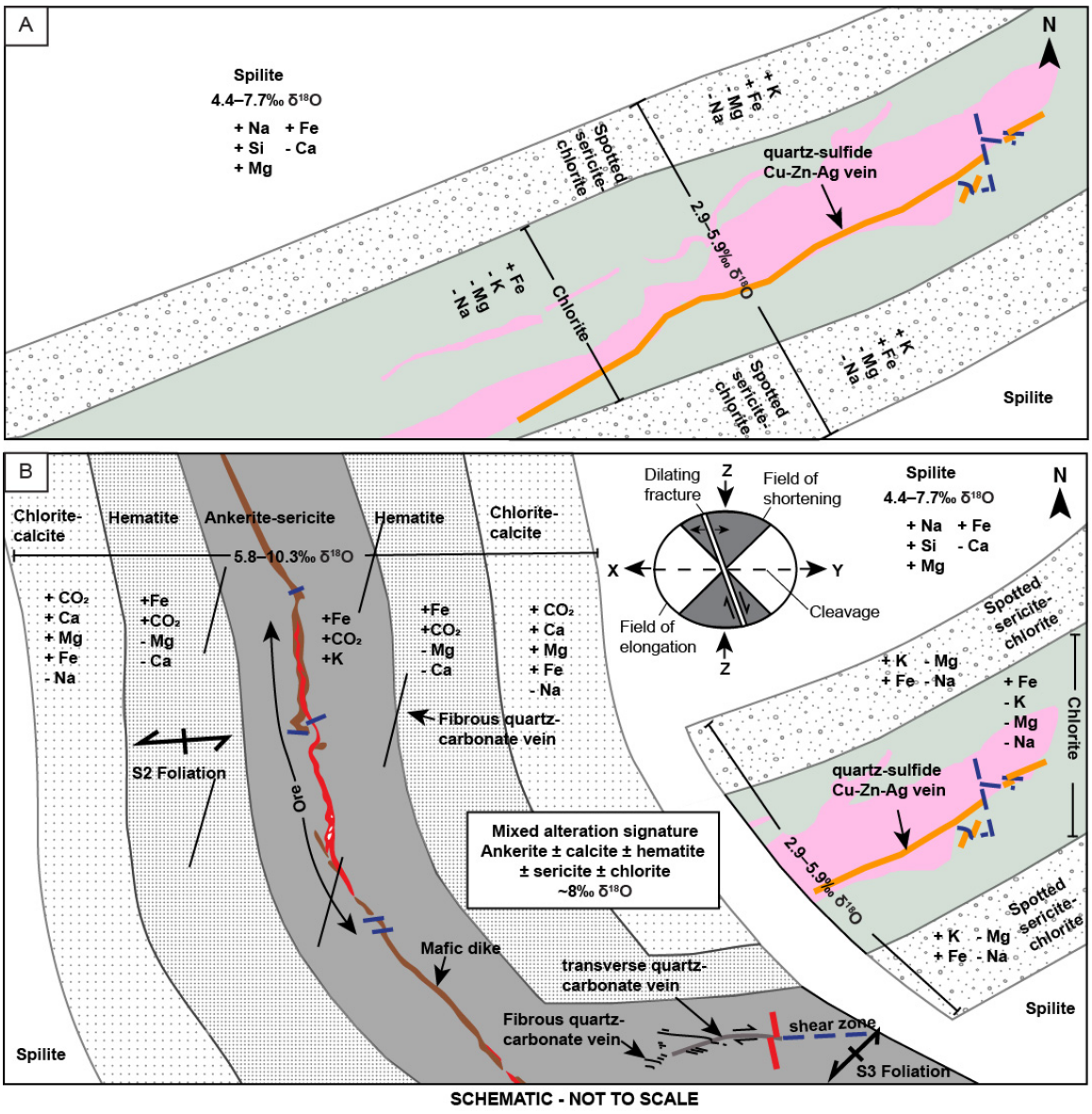

Figure 3.14: Schematic diagram of relative timing and general morphology of Cu-Zn-Ag veins and gold-quartz-carbonate veins.

Schematic diagram illustrating the relative timing and general morphology of the quartz-sulfide Cu-Zn-Ag rich (**A**) and gold-quartz-carbonate (**B**) vein types, using the Powell F-Zone and Powell-Rouyn (1550' level from McMurchy, 1958) vein traces for reference. The mineralogical, chemical and isotopic changes associated with their alteration envelopes are shown schematically, along with the mixed alteration signal within their overlap zone. The strain ellipse during D_2 is shown with the orientation of pre-existing fractures that are expected to dilate; Note that a component of dextral shear is also permissible along a NNW oriented structure.

3.15 Tables

Table 3-1: Zircon U-Pb isotopic data for tonalite intrusions.

Fraction	Description	U ppm	Pb^T pg	Pb_C pg	Th/U	$^{206}Pb/^{204}Pb$	$^{206}Pb/^{238}U$	± 2σ	$^{207}Pb/^{235}U$	± 2σ	$^{207}Pb/^{206}Pb$	± 2σ	Ages (Ma) $^{206}Pb/^{238}U$	± 2σ	Ages (Ma) $^{207}Pb/^{235}U$	± 2σ	Ages (Ma) $^{207}Pb/^{206}Pb$	± 2σ	Disc (%)
20MDS-186B; tonalite dike crosscuts Joliet Cu deposit and overprinted by ankerite and hematite alteration at Vox-occurrence.																			
Z1	1 clr, cls, blocky frag	259	110.26	0.38	0.617	15802	0.522503	0.00109 1	13.31 029	0.032 54	0.1847 56	0.0001 65	2709.8	4.6	2701.9	2.3	2696.0	1.5	-0.6
Z2	1 clr, cls, blocky frag	130	80.56	0.84	0.612	5273	0.530245	0.00109 6	13.49 552	0.034 18	0.1845 91	0.0001 96	2742.5	4.6	2715.0	2.4	2694.6	1.7	-2.2
Z3	1 clr cls, brkn half-pr	326	194.48	2.75	0.512	3998	0.523305	0.00145 9	13.32 063	0.042 50	0.1846 16	0.0002 12	2713.2	6.2	2702.6	3.0	2694.8	1.9	-0.8
20MDS-201B; tonalite overprinted by stockwork & disseminated Cu mineralization, D-Zone Cu occurrence.																			
Z1	1 clr, cls, sharp, fctd, brkn pr	196	115.22	0.11	0.468	57313	0.520385	0.00099 6	13.27 214	0.030 68	0.1849 76	0.0001 48	2700.8	4.2	2699.2	2.2	2698.0	1.3	-0.1
Z2	1 euh, clr, cls 2:1 pr	65	37.99	0.20	0.405	10968	0.526845	0.00129 5	13.43 226	0.037 60	0.1849 12	0.0001 57	2728.1	5.5	2710.5	2.6	2697.4	1.4	-1.4
Z3	1 lrg, clr cls, brkn gemmy pr	230	135.08	0.58	0.477	13171	0.519373	0.00100 8	13.24 045	0.031 13	0.1848 94	0.0001 55	2696.5	4.3	2696.9	2.2	2697.3	1.4	0.0
Z4	1 sm, clr, cls gemmy 2:1 pr	175	51.76	0.33	0.472	8850	0.522480	0.00118 8	13.32 392	0.035 13	0.1849 53	0.0001 73	2709.7	5.0	2702.9	2.5	2697.8	1.5	-0.5

All analyzed fractions represent best optical quality (inclusion- & core-free), fresh (least altered) grains of zircon. Zircons were chemically abraded.
Abbreviations: Z - zircon; clr - clear; cls - colourless; pr - prism/prismatic; fctd - faceted; frag - fragment; brkn - broken; lrg]- larger; sm - smaller.
Pb^T is total amount (in picograms) of
Pb.
Pb_C is total measured common Pb (in picograms) assuming the isotopic composition of laboratory blank: 206/204 - 18.49±0.4%; 207/204 - 15.59±0.4%; 208/204 - 39.36±0.4%.
Pb/U atomic ratios are corrected for spike, fractionation, blank, and, where necessary, initial common Pb; 206Pb/204Pb is corrected for spike and fractionation.
Th/U is model value calculated from radiogenic 208Pb/206Pb ratio and 207Pb/206Pb age, assuming concordance.
Disc. (%) - per cent discordance for the given 207Pb/206Pb age.
Uranium decay constants are from Jaffey et al. (1971).

Table 3-2: Summary table of measured $\delta^{18}O_{quartz}$ and calculated $\delta^{18}O_{H2O}$ values for veins.

	Quartz-sulfide Cu-Zn-Ag veins	**Gold-quartz-carbonate veins**
Hydrothermal system	VMS	Orogenic gold
Temperature range	250–350°C	250–350°C
$\delta^{18}O_{quartz}$ values	6.4–9.4	9.3–12.6
Mean $\delta^{18}O_{quartz}$ values for veins	8.5	11.3
$\delta^{18}O_{H2O}$ range calculated from minimum $\delta^{18}O_{quartz}$	-2.5–1	0.4–3.9
$\delta^{18}O_{H2O}$ range calculated from maximum $\delta^{18}O_{quartz}$	0.5–4	3.7–7.2
$\delta^{18}O_{H2O}$ range calculated from mean $\delta^{18}O_{quartz}$ (using Qtz-H_2O from Sharp 2016)	-0.4 to 3.1	2.4 to 5.9

Note: stable isotope fractionation factor for Qtz-H2O system computed using equation from Sharp et al., (2016)

3.16 References

Allmendinger, R.W., Cardozo, N., and Fisher, D., 2012, Structural geology algorithms: vectors and tensors; Cambridge University Press, Cambridge, 302 p.

Beaudoin, G., 2011, The stable isotope geochemistry of orogenic gold deposits, *in* Barra, F., Reich, M., Campos, E., Tornos, F. eds., Proceedings of the Eleventh Biennial SGA Meeting, Antogfagasta, Chile, p. 556–558

Beaudoin, G., and Chiaradia, M., 2016. Fluid mixing in orogenic gold deposits: evidence from the H-O-Sr isotope composition of the Val d'Or vein field (Abitbi, Canada); Chemical Geology, v. 437, p. 7-18.

Beaudoin, G., and Pitre, D., 2005. Stable isotope geochemistry of the Archean Val-d'Or (Canada) orogenic gold vein field; Mineralium Deposita, v. 40, p. 59-75.

Beaudoin, G., Mercier-Langevin, P., Dubé, B., and Taylor, B.E., 2014, Low-temperature alteration at the world-class La Ronde Penna Archean Au-rich volcanogenic massive sulfide deposit, Abitibi Subprovince, Québec, Canada: Evidence from whole-rock oxygen isotopes; Economic Geology, v. 109, p. 167-182.

Bedeaux, P., Pilote, P., Daigneault, R., Rafini, S., 2017, Synthesis of the structural evolution and associated gold mineralization of the Cadillac Fault, Abitibi, Canada; Ore Geology Reviews, v. 82, p. 49-69.

Belkabir, A., Robert, F., Vu, L., Hubert, C., 1993, The influence of dikes on auriferous shear zone development within granitoid intrusions: the Bourlamaque pluton, Val-d'Or district, Abitbi greenstone belt; Canadian Journal of Earth Sciences, v. 30, p. 1924-1933.

Bleeker, W., 2012, Lode gold deposits in ancient deformed and metamorphosed terranes: The role of extension in the formation of Timiskaming basins and large gold deposits, Abitibi greenstone belt – a discussion; Ontario Geological Survey Open File Report 6280, 47-1 – 47-12.

Blenkinsop, T.G., Oliver, N.H.S., Dirks, P.G.H.M., Nugus, M., Tripp, G., Sanislav, I., 2020, Structural geology applied to the evaluation of hydrothermal fold deposits; in Rowland, J.V., and Rhys, D.A., eds., Applied structural geology of ore-forming hydrothermal systems, SEG special publication 21, 1-23.

Blundell, D.J., 2002, The timing and location of major ore deposits in an evolving orogeny: the geodynamic context; *in* D.J. Blundell, F. Neubauer, A. von Quadt eds., The timing and location of major ore deposits in an evolving orogen, Geological Society of London Special Publication 24, p. 1-12

Carrier, A., Jébrak, M., Angelier, J., Holyland, P., 2000, The Silidor deposit, Rouyn-Noranda District, Abitibi Belt: geology, structural evolution, and paleostress modeling of an Au quartz vein-type deposit in an Archean trondjhemite; Economic Geology, v. 95, p. 1049-1065.

Cathles, L. M., Spooner, E. T. C., Barrie, C. T., 1993, Oxygen isotope alteration in the Noranda mining district, Abitibi greenstone belt, Québec; Economic Geology, v. 88, p. 1483-1511. https://doi.org/10.2113/gsecongeo.88.6.1483

Clayton, R. N., and Mayeda, T. K., 1963, The use of bromine pentafluoride in the extraction of oxygen from oxides and silicates for isotopic analysis; Geochimica et Cosmochimica Acta, v. 27, p. 43-52.

Cooke, H.C., James, W.F., Mawdsley, J.B., 1931, Geology and ore deposits of Rouyn-Harricanaw Region, Quebec; Geological Survey of Canada, Memoir 166, 314pp.

Daigneault, R., Mueller, W.U., Chown, E.H., 2002, Oblique Archean subduction: accretion and exhumation of an oceanic arc during dextral transpression, Southern Volcanic Zone, Abitibi Subprovince Canada; Precambrian Research, v. 115, p. 261-290.

De Rosen-Spence, A., 1969, Genèse des roches à cordierite-anthophyllite des gisements cupro-zincifères de la région de Rouyn-Noranda, Québec, Canada; Canadian Journal of Earth Sciences, v. 6, p. 1339–1345.

De Rosen Spence, A.F., 1976, Stratigraphy, Development and petrogenesis of the central Noranda volcanic pile, Noranda, Québec; unpublished PhD thesis. University of Toronto, Toronto, Ontario.

Dimroth, E., Imreh, L., Rocheleau, M., Goulet, N., 1982, Evolution of the south-central part of the Archean Abitibi Belt, Québec. Part I: Stratigraphy and paleogeographic model; Canadian Journal of Earth Sciences, v. 19, p. 1729-1758.

Dimroth, E., Imreh, L., Goulet, N., Rocheleau, M., 1983, Evolution of the south-central segment of the Archean Abitibi Belt, Quebec. Part II: Tectonic evolution and geomechanical model; Canadian Journal of Earth Sciences, v. 20, p. 1355-1373.

Dubé, B., and Gosselin, P., 2007, Greenstone-hosted quartz-carbonate vein deposits; *in* W.D. Goodfellow ed., Mineral Deposits of Canada: A Synthesis of Major Deposit-Types, District Metallogeny, the Evolution of Geological Provinces, and Exploration Methods: Geological Association of Canada, Mineral Deposits Division, Special Publication No. 5, p. 49-73.

Dubé, B., and Mercier-Langevin, P., 2020, Gold deposits of the Archean Abitibi Greenstone belt, Canada; *in* R.H. Sillitoe, R.J. Goldfard, F. Robert, S.F. Simmons eds., Geology of the world's major gold deposits and provinces, SEG Special Publication 23, p. 669-708.

Eilu, P. K., Mathison, C. I., Groves, D. I., Allardyce, W. J., 1999, Atlas of alteration assemlages, styles and zoning in orogenic lode-gold deposits in a variety of host rock and metamorphic settings; Geology and Geophysics Department (Centre for Strategic Mineral Deposits) & UWA Extension, The University of Western Australia, Publication 30, 50 p.

Fitchett, C., 2012, Metamorphic phase equilibria of hydrothermally altered rocks, Noranda district, Abitibi Subprovince, Québec; unpublished MSc thesis, Laurentian University, Sudbury, Ontario; 148 p.

Franklin, J.M., Sangster, D/M., and Lydon, J.W., 1981, Volcanic-associated massive sulfide deposits; Economic Geology 75th Anniversary Volume, 485-627.

Franklin, J.M., Gibson, H.L., Jonasson, I.R. and Galley, A.G., 2005, Volcanogenic massive sulfide deposits, *in* Hedenquist, J.W, Thompson, J.F.H., Goldfarb, R.J. and Richards, J.P., eds., Economic Geology 100th Anniversary Volume, Society of Economic Geologists Inc., p.523-560.

Galley, A.G., van Breemen, O., 2002, Timing of synvolcanic magmatism in relation to base-metal mineralization, Rouyn-Noranda, Abitibi volcanic belt, Québec; Geological Survey of Canada Current Research 2002-F8, p. 1-9.

Gibson, H. L., Watkinson, D.H., Comba, C.D.A., 1983, Silicification: Hydrothermal alteration in an Archean geothermal system within the Amulet rhyolite formation, Noranda, Quebec; Economic Geology, v. 78, p. 954-971.

Gibson, H.L. and Galley, A.G., 2007, Volcanogenic massive sulphide deposits of the Archean, Noranda District, Quebec; in Mineral Deposits of Canada, edited by W. D. Goodfellow, Geological Association of Canada, Mineral Deposits Division, Special Publication no.5, p.533-552.

Goldfarb, R. J., and Groves, D. I., 2015, Orogenic gold: Common or evolving fluid and metal sources through time; Lithos, v. 233, p. 2-26.

Goldie, R., 1976, The Flavrian and Powell Plutons, Noranda area, Québec: A geological investigation of the Flavrian and Powell Plutons and their relationships to other rocks and structures of the Noranda area; unpublished PhD thesis, Queen's University, Kingston, Ontario; 381 p.

Goldie, R., Kotila, B., Seward, D., 1979, The Don Rouyn Mine: An Archean porphyry copper deposit near Noranda, Québec; Scientific Communications, p. 1680-1684.

Goulet, N., 1978, Stratigraphy and structural relationships across the Cadillac-Larder Lake Fault, Rouyn-Beauchastel area, Quebec: unpublished PhD thesis, Queen's University, Kingston, Ontario, 141p.

Guha, J., Archambault, G., Leroy, J., 1983, A correlation between the evolution of mineralizing fluids and the geomechanical development of a shear zone as illustrated by the Henderson 2 Mine, Québec; Economic Geology, v. 78, p. 1605-1618.

Hall, B. V., 1982, Geochemistry of the alteration pipe at the Amulet Upper A deposit, Noranda, Québec; Canadian Journal of Earth Sciences, v. 19, p. 2060-2084.

Hannington, M.D., Poulsen, K.H., Thompson, J.F.H., and Sillitoe, R.H., 1999, Volcanogenic gold in the massive sulfide environment; in C.T. Barrie, and M.D. Hannington, (eds) Volcanic-Associated Massive Sulfide Deposits: Processes and Examples in Modern and Ancient Settings; Reviews in Economic Geology, 8, p. 325-356.

Hannington, M. D., Santaguida, F., Kjarsgaard, I. M., Cathles, L. M., 2003, Regional-scale hydrothermal alteration in the Central Blake River Group, westerm Abitibi subprovince, Canada: implications for VMS prospectivity; Mineralium Deposita, v. 38, p. 393-422.

Hitzman, M.W., 1999, Routine staining of drill core to determine carbonate mineralogy and distinguish carbonate alteration textures; Mineralium deposita, v. 34, p. 794-798.

Hoefs, J., 2015, Stable Isotope Geochemistry; Seventh Edition, Springer, 402 pp. https://doi.org/10.1007/978-3-319-19716-6

Hubert, C., Trudel, P., Gélinas, L., 1984, Archean wrench fault tectonics and structural evolution of the Blake River Group, Abitibi belt, Québec; Canadian Journal of Earth Sciences, v. 21, p. 1024-1032.

Hubert, C., 1990, Geologic framework, evolution and structural setting of gold and base metal deposits of the Abitibi Greenstone Belt, Canada; in S. E. Ho, F. Robert and D.I. Groves (eds) Gold and Base Metal Mineralization in the Abitibi Subprovince with Emphasis on the Quebec Segment; Short Course Notes, University of Western Australia, Geology Department Publication No. 24, p. 53-62

Hughes, C. J., 1973, Late Precambrian volcanic rocks of Avalon, Newfoundland–A spilite/keratophyre province: Recognition and implications; Canadian Journal of Earth Sciences, v. 10, p. 272-282.

Huston, D.L., 1999, Stable isotopes and their significance for understanding the genesis of volcanic-hosted massive sulfide deposits: a review; Reviews in Economic Geology, v. 10, p. 151-180.

Hutchinson, R.W., 1987, Metallogeny of Precambrian gold deposits: space and time relationships; Economic Geology, v. 82, 1993-2007.

Ishikawa, Y., Sawaguchi, T., Iwaya, S., and Horiuchi, M., 1976, Delineation of prospecting targets for Kuroko deposits based on modes of volcanism of underlying dacite and alteration halos; Mining Geology, v. 26, p. 105-117.

Ispolatov, V., Lafrance, B., Dubé, B., Creaser, R., and Hamilton, M., 2008, Geologic and structural setting of gold mineralization in the Kirkland Lake-Larder Lake gold belt, Ontario; Economic Geology, v. 103, p. 1309-1340.

Jebrak, M., Harnois, L., Carrier, A., and Lafrance, J., 1997, The Don Rouyn-Cu-Au porphyry system; *in* J. F. Couture, and F. Robert eds., Atypical gold deposits in the Abitibi Belt, Geological Association of Canada, Field Trip B5 guide, Ottawa, 1997, p. 72-78.

Johnson, B.W., Wing, B. A., 2020, Limited Archean continental emergence reflected in an early Archean 18O-enriched ocean; Nature Geoscience, v. 13, p. 243-248.

Kennedy, L.P., 1985, The geology and geochemistry of the Archean Flavrian pluton, Noranda, Québec; unpublished PhD thesis, University of Western Ontario, London, Ontario.

Kerrich, R., and Kyser, T. K., 1994, 100 ma timing paradox of Archean gold, Abitibi greenstone-belt (Canada) – new evidence from U-Pb and Pb-Pb evaporation ages of hydrothermal zircons; Geology, v. 22, p. 1131-1134.

Kirkham, R.V., 1972, Geology of Copper and Molybdenum deposits; in Report of Activities, Part A, Geological Survey of Canada, Paper 72-1A, p. 82-87.

Kirkland, C.L., Smithies, R.H., Taylor, R.J.M., Evans, N. and McDonald, B., 2015, Zircon Th/U ratios in magmatic environs. Lithos, v. 212, p. 397-414.

Knuckey, M. J., Comba, C.D.A., Riverin, G., 1982, Structure, metal zoning and alteration at the millenbach deposit, Noranda, Quebec; *in* R.W. Hutchinson, C.D. Spence, and J.M. Franklin eds., Precambrian Sulphide Deposits, Geological Association of Canada Special Paper 25, p. 255-295.

Knuckey, M.J., and Watkins, J.J., 1982, The geology of the Corbet massive sulphide deposit Noranda district, Québec, Canada; *in* R.W. Hutchinson, C.D. Spence, and J.M. Franklin

eds., Precambrian Sulphide Deposits, Geological Association of Canada Special Paper 25, p. 297-317.

Kotila, B.W., 1975, An Archean porphyry copper deposit: The Don Rouyn mine, Noranda, Québec, Kingston, Ontario; unpublished B.Sc. thesis, Queen's University, Kingston, Ontario; 21 p.

Krushnisky, A., 2018, Controls on gold enrichment at the Horne 5 Archean VMS deposit, Abitibi Greenstone Belt, Québec; Unpublished MSc thesis, Université du Québec, Institute national de la recherché scientifique, 238 p.

Lafrance, B., 2004, Conjugate oblique-extension veins in shear and tensile fracture systems at the Komis gold mine and Mufferaw gold prospect, Northern Saskatchewan; Exploration and Mining Geology, v. 13, pp. 129-137.

Leclerc, F., Harris, L.B., Bédard, J.H., Breemen, O.V., Goulet, N., 2012, Structural and stratigraphic controls on magmatic, volcanogenic, and shear zone-hosted mineralization in the Chapais-Chibougamau Mining Camp, Northeastern Abitibi, Canada; Economic Geology, v. 107, p. 963-989.

Lichtblau, A., 1979, Property acquisition proposal Powell-Rouyn Gold Mines, Unpublished report, Falconbridge Copper, 17 p.

Lichtblau, A., Dimroth, E., 1980, Stratigraphy and facies at the South margin, of the Archean Noranda Caldera, Noranda, Québec; Geological Survey of Canada Current Research Part A, p. 69–76.

L'Heureux, M., 1992, Caractérisation géochimique des volcanites et d'une cheminée d'altération dans la partie oust du bloc de Powell, Rouyn-Noranda, Québec, Unpublished MSc Thesis, L'Université du Québec a Chicoutimi, 116 p.

Maclean, W.H., Hoy, L. D.,1991, Geochemistry of hydrothermally altered rocks at the Horne Mine, Noranda, Quebec; Economic Geolgy, v. 86, p. 506-528.

Matsuhisa, Y., Goldsmith, J.R., Clayton, R. N., 1979, Oxygen isotopic fractionation in the system quartz-albite-anorthite-water; Geochimica et Cosmochimica Acta, v. 43, p. 1131-1140.

McCuaig, T.C., Kerrich, R., 1994, P-T-t-deformation-fluid characteristics of lode gold deposits: Evidence from alteration systematics; Geological Association of Canada, short course notes, 11, p. 339-379.

McMurchy, R.C., 1948, Powell-Rouyn mine in Structural geology of Canadian ore deposits, Canadian Institute of Mining and Metallurgy, p. 581-589.

McNicoll, V., Goutier, J., Dubé, B., Mercier-Langevin, P., Ross, P.S., Dion, C., Monceck, T., Legault, M., Percival, J., Gibson, H., 2014, U-Pb geochronology of the Blake River Group, Abitibi greenstone belt, Québec, and implications for base metal exploration; Economic Geology, v. 109, p. 27–59. https://doi.org/10.2113/econgeo.109.1.27

Morris, H. R., 1957, Héré Fault Copper Ltd. Surface Geology, Anglo-Rouyn and North Part of Powell-Rouyn properties, Rouyn Twp., N.W. Québec; unpublished geological map, 3 sheets, one inch to 200 feet.

Morris, H.R., 1959, Joliet-Québec Mines Ltd. Surface Geology, Rouyn Twp., N.W. Québec; unpublished geological map, 3 sheets, one inch to 200 feet.

Mortensen, J.K., 1993, U-Pb geochronology of the eastern Abitibi Subprovince: Part 2: Noranda-Kirkland Lake area; Canadian Journal of Earth Sciences, v. 30 p.29-41

Muehlenbachs, K., 1986, Alteration of the oceanic crust and the 18O history of seawater; *in* J.W. Valley, H.P. Taylor, J. O'Neil, eds., Reviews in Mineralogy, Mineralogical Society of America, v.16, p. 425-444.

Piette-Lauzière, N., Guillmette, C., Bouvier, A., Perrouty, S., Pilote, P., Gaillard, N., Lypaczewski, P., Linnen, R. L., Olivo, G. R., 2019, The timing of prograde metamorphism in the Pontiac Subprovince, Superior craton; implications for Archean geodynamics and gold mineralization; Precambrian Research, v. 320, p. 111-136.

Pilote, P., Robert, F., Sinclair, W.D., Kirkham, R.V., Daigneault, R., 1995, Porphyry-type mineralization in the Doré Lake Complex: Clark Lake and Merrill Island area; Geological Survey of Canada Open File 3143, 65-86.

Pope, E.C., Bird, D. K., Rosing, M. T., 2012, Isotope composition and volume of Earth's early oceans; The Proceedings of the National Academy of Sciences, v. 109, p. 4371–4376.

Poulsen, K.H., 2017, The Larder Lake-Cadillac Break and Its Gold Districts; *in* T. Monecke, P. Mercier-Langevin, B. Dubé eds., Archean Base and Precious Metal Deposits, Southern Abitibi Greenstone Belt, Canada. Reviews in Economic Geology, v. 19, p. 133–167.

Powell, W.G., Carmichael, D.M., Hodgson, C.J., 1995, Conditions and timing of metamorphism in the southern Abitibi Greenstone Belt, Québec; Canadian Journal of Earth Sciences, v. 32, p. 787–805. https://doi.org/10.1139/e95-067

Quesnel, B., Scheffer, C., Beaudoin, G., 2023, The light stable isotope (H, B, C, N, O, Si, S) composition of orogenic gold deposits. Isotopes in mineral exploration. In: Nature, S. (Ed.), Isotopes in Mineral Exploration. SGA Special Publication (In press).

Raymond, G., 2022, Variation spatiale des conditions de circulation des fluides à l'origine de la minéralisation en or orogénique dans le segment Augmitto-Bouzan (sous-province de l'Abitibi, Québec, Canada) ; unpublished MSc thesis, Université Laval, Québec City, Québec.

Riverin, G., 1977, Wall-rock alteration at the Millenbach mine, Noranda, Québec; unpublished PhD thesis, Queen's University, Kingston, Ontario.

Riverin, G., Bernard, D., Boily, B., 1990, The Donalda gold deposit, Rouyn-Noranda, Québec; *in* M. Rive, P. Verpaelst, Y. Gagnon, J.M. Lulin, G. Riverin, A. Simard, eds., The Northwestern Québec polymetallic belt, Canadian Institute of Mining and Metallurgy, special volume 43, p. 199-209.

Robert, F., Boullier, A-M., and Firdaous, K., 1996, Geometric aspects of a large extensional vein, Donalda deposit, Rouyn-Noranda, Québec, Geological Survey of Canada, Current Research 1996-C Canadian Shield, p. 147-155.

Robert, F., Poulsen, K.H., Cassidy, K.F., and Hodgson, C.J., 2005, Gold metallogeny of the Superior and Yilgarn cratons, Economic Geology 100th Anniversary Volume, p. 1001-1033.

Robert, F., and Poulsen, K.H., 2001, Vein formation and deformation in greenstone gold deposits, Reviews in Economic Geology, v. 14, p. 111-155.

Schofield, M., Gibson, H., Lafrance, B., Poulsen, K. H., Marsh, J., Hamilton, M. A., Jørgensen, T.R.C., 2021, Recognizing subsurface breccias in Archean terranes: implications for district scale metallogeny; Precambrian Research, v. 361, 106264. https://doi.org/10.1016/j.precmres.2021.106264

Scott, S.D., 1980, Geology and structural control of Kuroko-type massive sulphide deposits; in The Continental Crust and Its Mineral Deposits, edited by D.W. Strangway; Geological Association of Canada, Special Paper 20, p.705-721

Sawkins, F.J., 1990, Metal deposits in relation to plate tectonics, edited by A. El Goresy, W. von Engelhardt, T. Hahn; Springer-Verlag Berlin Heidelberg, 475 p.

Setterfield, T. N., Hodder, R.W., Gibson, H. L., Watkins, J.J., 1995, The McDougall-Despina Fault set, Noranda, Québec: evidence for fault-controlled volcanism and hydrothermal fluid flow; Exploration and Mining Geology, v. 4, p. 381-393.

Sharp Z.D., Gibbons J.A., Maltsev O., Atudorei V., Pack A., Sengupta S., Shock E.L., Knauth L.P., 2016, A calibration of the triple oxygen isotope fractionation in the SiO_2-H_2O system and applications to natural samples; Geochimica et Cosmochimica Acta, v. 186, p.105-119.

Sheppard, S.M.F., 1986. Characterization and isotopic variations in natural waters; Reviews in Mineralogy and Geochemistry, v. 16, p. 165-183.

Sibson, R.H.,2001, Seismogenic framework for hydrothermal transport and ore deposition; in Structural Controls on Ore Genesis, edited by J.P Richards and R.M. Tosdal, Reviews in Economic Geology, v. 14, p. 25-50.

Sillitoe, R.H., 1978, Metallogenic evolution of a collisional mountain belt in Pakistan: a preliminary analysis; Journal Geological Society of London, v. 135, 377-387.

Taylor, B. E., De Kemp, E., Grunsky, E., Martin, L., Maxwell, G., Rigg, D., Goutier, J., Lauzière, K., and Dubé, B., 2014, Three-dimensional visualization of the Archean Horne and Quemont Au-Bearing Volcanogenic Massive Sulfide Hydrothermal Systems, Blake River Group, Québec; Economic Geology, v. 109, p. 183-203.

Tripp, G.T., Tosdal, R.M., Blenkinsop, T., Rogers, J. R., Halley, S., 2020, Neoarchean eastern goldfields of Western Australia; *in* R.H. Sillitoe, R.J. Goldfard, F. Robert, S.F. Simmons eds., Geology of the world's major gold deposits and provinces, SEG Special Publication 23, p. 709-734.

Turner, S.J., Reynolds, G., Hagemann, S.G., 2020, Boddington: An enigmatic giant Archean Gold-Copper (Molybdenum-Silver) Deposit in the Southwest Yilgarn Craton, Western Australia; *in* R.H. Sillitoe, R.J. Goldfard, F. Robert, S.F. Simmons eds., Geology of the world's major gold deposits and provinces, SEG Special Publication 23, p. 275-288.

Walker, T. L., 1930, Dalmatianite, the spotted greenstone from the Amulet mine, Noranda, Québec; University of Toronto, geological series, 29, 9-12.

Watkins, D.H., and Riverin, G., 1982, Geology of the Opemiska copper-gold deposits at Chapais, Quebec; in Hutchinson, R.W., Spence, C.D., Franklin, J.M. eds., Precambrian Sulphide Deposits, Geological Association of Canada Special Paper 25, 427-446

Wilkinson, L., Cruden, A.R., Krogh, T.E., 1999, Timing and kinematics of post-Timiskaming deformation within the Larder Lake - Cadillac deformation zone, southwest Abitibi greenstone belt, Ontario, Canada; Canadian Journal of Earth Sciences, v. 36, p. 627–647.

Wilson, M.E., 1941, Noranda district, Québec; Geological Survey of Canada, Memoir 229, 162 p. https://doi.org/10.4095/101612.

Zubowski, S., 2011, Characterization of hydrothermal fluids within synvolcanic faults of the ~2.7Ga, Mine Sequence, Noranda District, Québec, Unpublished MSc thesis, Laurentian University, Sudbury, Ontario, 168 p.

3.17 Appendix

A 3-1: Multi element geochemistry of veins

					178DG04 Quartz-sulfide vein	0061AG04 Powell F	0180AG01 Anglo C	201AG06 Powell D (vein)	201AG04 Powell D (dissem)	201AG07 Powell D (dissem)	0074AG02 Powell D (dissem)	197AG01 Here Cu Vein	127AG05 Silidor
					646610 m.E. 5347386 m.N.	645225 m.E. 5347768 m.N.	644958 m.E. 5348515 m.N.	645340 m.E. 5348020 m.N.	645293 m.E. 5348039 m.N.	645329 m.E. 5348011 m.N.	645300 m.E. 5348033 m.N.	644177 m.E. 5348703 m.N.	642344 m.E. 5346167 m.N.
		LLOD	ULOD	Analysis									
Cu	%	0.001	40	Cu-OG62		1.565	18.6	1.31					
Cu	ppm	0.2	10000	ME-MS61	60.6	>10000	>10000	>10000	756	904	801	6470	105.5
Sn	ppm	0.2	500	ME-MS61	1.3	54.7	22.9	36.1	107	38.8	80.7	4.7	<0.2
Au	ppm			Au-ICP21		0.449					0.165		
Ag	ppm	0.01	100	ME-MS61	0.1	43.6	98.5	16.35	2.93	9.6	5.62	9.77	585
Al	%	0.01	50	ME-MS61	7.13	6.57	0.55	5.25	7.72	6.58	7.03	0.61	0.09
As	ppm	0.2	10000	ME-MS61	1.7	8.7	18.6	60.2	0.4	1	0.6	34.6	1.8
Ba	ppm	10	10000	ME-MS61	120	190	<10	10	280	370	360	10	20
Be	ppm	0.05	1000	ME-MS61	0.64	0.47	<0.05	0.26	0.36	0.44	0.5	<0.05	<0.05
Bi	ppm	0.01	10000	ME-MS61	0.12	4.79	6.17	2.9	2.03	3.32	2.71	14.35	356
Ca	%	0.01	50	ME-MS61	0.27	0.05	0.01	0.1	0.43	0.05	0.41	0.01	0.19
Cd	ppm	0.02	1000	ME-MS61	0.1	3.95	14.45	8.96	1.46	0.17	0.78	5.96	0.24
Ce	ppm	0.01	500	ME-MS61	31.9	23.3	0.77	10.5	14.9	28.1	23.9	1.05	0.16
Co	ppm	0.1	10000	ME-MS61	8.6	27.9	103.5	394	23.3	7.7	10.4	134	18.6
Cr	ppm	1	10000	ME-MS61	66	45	23	30	22	26	26	23	25
Cs	ppm	0.05	500	ME-MS61	0.3	0.44	<0.05	0.05	0.3	0.36	0.55	<0.05	<0.05
Fe	%	0.01	50	ME-MS61	5.67	8.2	19.65	19.7	11.35	8.48	7.16	10.45	15.4
Ga	ppm	0.05	10000	ME-MS61	19.55	29.9	3.12	18.8	21.3	17.35	18.4	3.73	0.27
Ge	ppm	0.05	500	ME-MS61	0.1	0.31	0.48	0.18	0.07	0.07	0.11	0.19	0.19
Hf	ppm	0.1	500	ME-MS61	4.6	3	0.1	2.6	3.6	3.1	3.2	0.1	<0.1
In	ppm	0.005	500	ME-MS61	0.027	4.98	35.2	7.57	0.372	2.48	0.304	3.79	0.018

					178DG04	0061AG04	0180AG01	201AG06	201AG04	201AG07	0074AG02	197AG01	127AG05
K	**%**	**0.01**	**10**	**ME-MS61**	0.42	2.17	0.01	0.02	1.54	1.47	1.88	0.04	0.02
La	**ppm**	**0.5**	**10000**	**ME-MS61**	16.4	9.4	<0.5	4.9	5.3	12.4	8.9	0.5	<0.5
Li	**ppm**	**0.2**	**10000**	**ME-MS61**	16.3	5.5	1.9	12.4	19.9	12	14	1.5	0.3
Mg	**%**	**0.01**	**50**	**ME-MS61**	1.29	0.99	0.2	3.15	3	2	2.09	0.21	0.08
Mn	**ppm**	**5**	**10000**	**ME-MS61**	890	108	115	1690	1800	1140	1220	115	76
Mo	**ppm**	**0.05**	**10000**	**ME-MS61**	4.77	1.32	5.94	12.35	0.96	1.87	1.13	2.44	3.81
Na	**%**	**0.01**	**10**	**ME-MS61**	3.22	0.2	0.01	0.01	0.07	0.1	0.09	0.01	0.05
Nb	**ppm**	**0.1**	**500**	**ME-MS61**	5.1	2.8	0.2	4.3	6.7	4.8	5.4	0.1	<0.1
Ni	**ppm**	**0.2**	**10000**	**ME-MS61**	5.7	18.9	8.3	26.6	21.9	6.2	10	21.9	122.5
P	**ppm**	**10**	**10000**	**ME-MS61**	520	460	30	410	760	590	480	30	10
Pb	**ppm**	**0.5**	**10000**	**ME-MS61**	1.9	19.2	11.1	17.1	2.1	2.9	3.5	7.8	1110
Rb	**ppm**	**0.1**	**10000**	**ME-MS61**	11.2	44.3	0.2	0.6	17.4	36.1	48.8	0.7	0.4
Re	**ppm**	**0.002**	**50**	**ME-MS61**	<0.002	<0.002	<0.002	0.002	<0.002	<0.002	<0.002	<0.002	<0.002
S	**%**	**0.01**	**10**	**ME-MS61**	0.17	3.45	>10.0	>10.0	1.02	0.23	0.7	9.16	>10.0
Sb	**ppm**	**0.05**	**10000**	**ME-MS61**	0.07	0.31	0.77	0.36	<0.05	0.07	0.06	0.17	0.08
Sc	**ppm**	**0.1**	**10000**	**ME-MS61**	19.3	24.2	1.7	16.6	25.9	22.6	23.5	1.5	0.3
Se	**ppm**	**1**	**1000**	**ME-MS61**	0.5	99	179	51	2	3	3	80	57
Sr	**ppm**	**0.2**	**10000**	**ME-MS61**	28.8	11.1	0.8	1.9	6.3	7.3	5.5	0.9	6.3
Ta	**ppm**	**0.05**	**100**	**ME-MS61**	0.31	0.21	<0.05	0.27	0.39	0.31	0.35	<0.05	<0.05
Te	**ppm**	**0.05**	**500**	**ME-MS61**	0.13	3.54	12.55	3.69	0.25	2.27	1	4.82	490
Th	**ppm**	**0.01**	**10000**	**ME-MS61**	1.74	1.25	0.06	1.05	0.96	1.26	1.2	0.07	0.01
Ti	**%**	**0.005**	**10**	**ME-MS61**	0.177	0.2	0.022	0.393	0.57	0.423	0.497	0.011	<0.005
Tl	**ppm**	**0.02**	**10000**	**ME-MS61**	0.05	0.11	0.07	0.3	0.21	0.2	0.26	<0.02	<0.02
U	**ppm**	**0.1**	**10000**	**ME-MS61**	0.5	0.3	<0.1	0.4	0.4	0.3	0.3	<0.1	<0.1
V	**ppm**	**1**	**10000**	**ME-MS61**	44	167	13	112	204	168	168	17	1
W	**ppm**	**0.1**	**10000**	**ME-MS61**	0.4	0.5	0.1	0.5	4.4	2.6	3	0.1	0.1
Y	**ppm**	**0.1**	**500**	**ME-MS61**	17.1	7.5	0.7	30.7	17	9.7	21.1	0.8	0.3
Zn	**ppm**	**2**	**10000**	**ME-MS61**	55	1130	1180	1440	420	149	266	452	3
Zr	**ppm**	**0.5**	**500**	**ME-MS61**	161.5	108.5	5.1	97.4	136.5	113.5	125	4.4	<0.5

A 3-2: Whole rock lithogeochemistry

	Field Number	Lab ID	Rock Type	Alteration	UTM-East	UTM-North	SiO2_wt%	TiO2_wt%	Al2O3_wt%	Fe2O3t_wt%	MnO_wt%	MgO_wt%	CaO_wt%	SrO wt%	BaO wt%	Na2O_wt%	K2O_wt%	P2O5_wt%	LOI_%	Total_wt%	C_%
Method					NAD 83	NAD 83	ME-ICP06	ME-ICP06	ME-ICP06	ME-ICP06	ME-ICP06	ME-ICP06	ME-ICP06	ME-ICP06	ME-ICP06	ME-ICP06	ME-ICP06	ME-ICP06	OA-GRA05		C-IR07
Detection Limit							0.01	0.01	0.01	0.01	0.01	0.01	0.01	0.01	0.01	0.01	0.01	0.01	0.01		0.01
1	MERN17MDS0044AG02	X258412	Aphyric rhyolite	Ser	644493	5347553	68.60	0.47	11.65	10.45	0.06	2.97	0.13	0.01	0.06	0.08	1.44	0.10	3.08	99.09	0.01
2	MERN17MDS0045AG02	X258413	Aphyric rhyolite	Ser	644405	5347521	65.90	0.80	13.30	9.34	0.08	4.58	0.32	0.01	0.05	0.08	2.00	0.27	3.69	100.41	0.01
3	MERN18MDS0104CG04	X258471	Aphyric rhyolite	Ser	644494	5347556	69.10	0.52	12.90	8.63	0.06	4.56	0.09	0.01	0.07	0.10	1.77	0.10	3.61	101.51	<0.01
4	MERN19MDS0129AG07	X261180	Aphyric rhyolite	Alb-Ser	644505	5347412	70.60	0.43	10.80	9.18	0.03	2.98	0.12	0.01	0.04	0.11	1.55	0.10	2.99	98.93	0.02
5	MERN19MDS0129AG08	X261181	Aphyric rhyolite	Alb-Ser	644504	5347410	69.70	0.49	11.95	8.14	0.02	3.45	0.14	0.01	0.04	0.13	1.86	0.11	3.03	99.06	0.01
6	MERN19MDS0129AG09	X261182	Aphyric rhyolite	Alb-Ser	644503	5347409	70.70	0.46	11.55	8.42	0.02	3.38	0.12	0.01	0.04	0.11	1.73	0.11	3.01	99.65	<0.01
7	MERN19MDS0129AG10	X261183	Aphyric rhyolite	Alb-Ser	644503	5347408	75.80	0.40	10.40	7.68	0.02	3.05	0.12	0.01	0.03	0.11	1.56	0.09	2.63	101.89	0.01
8	MERN19MDS0129AG11	X261184	Aphyric rhyolite	Alb-Ser	644503	5347408	69.70	0.44	11.40	8.72	0.02	3.40	0.13	0.01	0.04	0.11	1.68	0.10	3.09	98.83	0.01
9	MERN19MDS0129AG12	X261185	Aphyric rhyolite	Alb-Ser	644503	5347408	72.00	0.44	11.20	7.92	0.02	2.96	0.13	0.01	0.04	0.12	1.82	0.11	2.87	99.63	0.01
10	MERN19MDS0129AG13	X261186	Aphyric rhyolite	Alb-Ser	644502	5347407	70.00	0.42	10.95	8.82	0.02	3.24	0.13	0.01	0.03	0.10	1.56	0.09	3.04	98.4	0.01
11	MERN19MDS0129AG14	X261187	Aphyric rhyolite	Alb-Ser	644502	5347407	70.80	0.43	10.50	8.82	0.02	3.18	0.12	0.01	0.03	0.09	1.45	0.09	2.96	98.49	0.01
12	MERN19MDS0129AG15	X261188	Aphyric rhyolite	Alb-Ser	644502	5347407	70.80	0.42	10.95	8.67	0.02	3.10	0.11	0.01	0.03	0.10	1.62	0.09	2.90	98.81	0.01
13	MERN19MDS0129AG16	X261189	Aphyric rhyolite	Alb-Ser	644510	5347419	68.30	0.48	12.20	9.39	0.03	3.49	0.14	0.01	0.04	0.12	1.76	0.12	3.24	99.31	0.01
14	MERN19MDS0129AG18	X261190	Aphyric rhyolite	Ank-Ser	644556	5347359	70.10	0.44	11.45	6.04	0.05	2.97	0.64	0.01	0.03	0.21	2.44	0.10	3.53	98	0.23
15	MERN19MDS0129AG19	X261191	Aphyric rhyolite	Ank-Ser	644555	5347358	66.00	0.45	11.45	7.25	0.07	3.32	0.69	0.01	0.03	0.13	2.24	0.10	3.82	95.55	0.27
16	MERN19MDS0129AG20	X261192	Aphyric rhyolite	Alb-Ser	644554	5347358	73.10	0.46	12.20	6.95	0.04	3.24	0.20	0.01	0.03	0.12	2.41	0.12	2.99	101.86	0.04
17	MERN19MDS0129AG21	X261193	Aphyric rhyolite	Alb-Ser	644551	5347357	66.40	0.43	11.35	9.81	0.05	5.63	0.23	0.01	0.02	0.07	1.11	0.10	3.81	99.01	0.04
18	MERN19MDS0129AG22	X261139	Aphyric rhyolite	Alb-Ser	644548	5347355	71.40	0.51	11.95	7.94	0.03	3.44	0.18	0.01	0.03	0.64	1.80	0.10	3.13	101.15	0.04
19	MERN19MDS0129AG23	X261194	Aphyric rhyolite	Alb-Ser	644546	5347353	73.30	0.25	11.20	8.14	0.03	2.47	0.03	0.01	0.03	0.27	2.08	0.01	2.57	100.38	<0.01
20	MERN19MDS0155AG01	X261150	Aphyric rhyolite	Spilite	644016	5347982	72.00	0.46	11.50	7.13	0.05	2.66	0.36	0.01	0.01	3.60	0.14	0.10	1.99	99.99	0.06
21	MERN19MDS0177BG02	X261160	Aphyric rhyolite	Spilite	646423	5347441	77.80	0.24	12.00	3.90	0.05	1.67	0.15	0.01	0.02	4.15	0.68	0.04	1.27	101.97	0.01
22	MERN19MDS0178CG03	X261165	Aphyric rhyolite	Spilite	646610	5347387	75.20	0.23	11.90	3.04	0.03	1.31	0.22	0.01	0.02	4.28	0.79	0.05	1.12	98.19	0.02
23	MERN19MDS0150AG03	X261143	Aphyric rhyolite	Spilite	646455	5348483	82.90	0.22	8.96	1.93	0.02	0.71	0.53	0.01	0.01	4.10	0.39	0.01	0.78	100.57	0.08
24	MERN19MDS0150BG02	X261142	Aphyric rhyolite	Spilite	646471	5348498	76.60	0.34	11.90	3.25	0.06	1.30	1.29	0.01	0.01	5.11	0.42	0.05	1.65	101.98	0.22
25	MERN19MDS0150CG01	X261141	Aphyric rhyolite	Spilite	646482	5348491	71.90	0.40	12.60	5.69	0.08	2.81	0.70	0.01	0.04	3.53	1.07	0.06	2.50	101.38	0.11
26	MERN19MDS0151AG01	X261144	Aphyric rhyolite	Spilite	646382	5348652	74.80	0.39	12.10	4.30	0.04	1.01	0.89	0.01	0.05	2.68	1.82	0.06	2.22	100.36	0.2
27	MERN19MDS0151AG02	X261145	Aphyric rhyolite	Spilite	646382	5348652	68.50	0.37	12.00	7.97	0.07	1.19	1.68	0.01	0.02	4.53	0.49	0.07	2.28	99.17	0.35
28	MERN19MDS0165AG01	X261156	Aphyric rhyolite	Spotted	645687	5348449	71.60	0.39	11.65	5.32	0.04	2.00	0.37	0.01	0.04	3.43	0.91	0.06	2.31	98.12	0.14
29	MERN19MDS0183AG01	X261169	Aphyric rhyolite	Spilite	645151	5348837	75.00	0.38	12.40	4.15	0.02	1.95	0.09	0.01	0.02	5.27	0.36	0.05	1.52	101.21	0.01
30	MERN19MDS0184AG01	X261170	Aphyric rhyolite	Spilite	645088	5348911	75.40	0.37	11.55	3.52	0.03	1.97	0.24	0.01	0.01	5.13	0.23	0.05	1.44	99.94	0.04
31	MERN18MDS0120AG01	X258479	Aphyric rhyolite	Chl	645686	5348384	75.30	0.35	13.65	4.06	0.09	4.17	0.10	0.01	0.02	0.14	2.06	0.07	3.19	101.35	0.005
32	MERN18MDS0103EG05	X258473	Aphyric rhyolite	Spotted	645415	5347965	75.80	0.22	11.40	5.50	0.03	3.16	0.10	0.01	0.08	0.18	1.87	0.04	2.83	101.21	<0.01
33	MERN17MDS0030BG01	X258496	Aphyric felsic dike	Spotted	645036	5347711	73.90	0.34	11.40	8.33	0.08	2.23	0.05	0.01	0.08	0.18	1.75	0.07	2.76	101.17	<0.01
34	MERN17MDS0033AG03	X258403	Aphyric felsic dike	Spotted	644497	5347308	76.30	0.26	10.75	4.87	0.04	2.39	0.17	0.01	0.03	0.10	2.33	0.09	2.50	99.83	0.02
35	MERN17MDS0033AG06	X258419	Aphyric felsic dike	Spotted	644491	5347311	74.50	0.26	11.25	6.45	0.07	3.59	0.05	0.01	0.03	0.10	1.99	0.03	2.96	101.28	0.01
36	MERN17MDS0033AG07	X258404	Aphyric felsic dike	Spotted	644462	5347319	74.10	0.23	11.05	6.14	0.04	1.12	0.54	0.01	0.03	3.52	1.14	0.04	1.57	99.52	0.1
37	MERN17MDS0033AG09	X258420	Aphyric felsic dike	Spotted	644451	5347324	75.90	0.25	11.30	5.52	0.02	0.37	0.73	0.01	0.01	5.38	0.55	0.04	0.67	100.75	0.12
38	MERN17MDS0034AG03	X258406	Aphyric felsic dike		644450	5347291	73.30	0.28	12.00	5.11	0.06	2.80	0.13	0.01	0.03	2.54	1.28	0.05	2.28	99.86	0.01
39	MERN17MDS0050AG01	X258472	Aphyric felsic dike		644379	5347443	70.70	0.34	11.80	8.15	0.10	2.69	0.04	0.01	0.08	0.11	2.65	0.06	2.74	99.46	<0.01
40	MERN18MDS0086AG04	X258438	Aphyric felsic dike	Ser	645190	5347767	73.40	0.35	11.05	7.03	0.05	1.90	0.05	0.01	0.07	0.18	1.83	0.05	2.56	98.52	0.01

	Field Number	Lab ID	Rock Type	Alteration	UTM-East	UTM-North	S_%	H20+_%	S.G.	Ag ppm	As ppm	Au_ppm	Ba ppm	Bi ppm	Cd ppm	Ce ppm	Co ppm	Cr ppm	Cs ppm	Cu ppm	Dy ppm
Method					**NAD 83**	**NAD 83**	**S-IR08**	**OA-IR06**	**OA-GRA08b**	**ME-4ACD81**	**ME-MS42**	**Au-ICP21**	**ME-MS81**	**ME-MS42**	**ME-4ACD81**	**ME-MS81**	**ME-4ACD8**	**ME-MS81**	**ME-MS81**	**ME-4ACD81**	**ME-MS81**
Detection Limit							**0.01**	**0.01**		**0.5**	**0.1**		**0.5**	**0.01**	**0.5**	**0.1**	**1**	**1**	**0.05**	**1**	**0.05**
1	MERN17MDS0044AG02	X258412	Aphyric rhyolite	Ser	644493	5347553	0.01	3.94	2.78	0.25	0.4		509	0.17	0.25	42.3	11	10	0.31	15	9.79
2	MERN17MDS0045AG02	X258413	Aphyric rhyolite	Ser	644405	5347521	0.04	3.93	2.76	0.25	0.1		459	0.17	0.25	47.5	12	10	0.54	8	7.91
3	MERN18MDS0104CG04	X258471	Aphyric rhyolite	Ser	644494	5347556	0.005		2.72	0.25	1.1		520	0.06	0.5	53.6	15	10	0.31	25	5.83
4	MERN19MDS0129AG07	X261180	Aphyric rhyolite	Alb-Ser	644505	5347412	0.08	4.55	2.85												
5	MERN19MDS0129AG08	X261181	Aphyric rhyolite	Alb-Ser	644504	5347410	0.02	4.51	2.78												
6	MERN19MDS0129AG09	X261182	Aphyric rhyolite	Alb-Ser	644503	5347409	0.02	4.25	2.86												
7	MERN19MDS0129AG10	X261183	Aphyric rhyolite	Alb-Ser	644503	5347408	0.02	3.92	2.83												
8	MERN19MDS0129AG11	X261184	Aphyric rhyolite	Alb-Ser	644503	5347408	0.02	4.38	2.79												
9	MERN19MDS0129AG12	X261185	Aphyric rhyolite	Alb-Ser	644503	5347408	<0.01	3.96	2.79												
10	MERN19MDS0129AG13	X261186	Aphyric rhyolite	Alb-Ser	644502	5347407	0.02	4.25	2.79												
11	MERN19MDS0129AG14	X261187	Aphyric rhyolite	Alb-Ser	644502	5347407	0.08	4.02	2.85												
12	MERN19MDS0129AG15	X261188	Aphyric rhyolite	Alb-Ser	644502	5347407	0.04	4.05	2.84												
13	MERN19MDS0129AG16	X261189	Aphyric rhyolite	Alb-Ser	644510	5347419	0.02	4.65	2.8												
14	MERN19MDS0129AG18	X261190	Aphyric rhyolite	Ank-Ser	644556	5347359	0.03	3.43	2.82												
15	MERN19MDS0129AG19	X261191	Aphyric rhyolite	Ank-Ser	644555	5347358	0.07	3.96	2.73												
16	MERN19MDS0129AG20	X261192	Aphyric rhyolite	Alb-Ser	644554	5347358	0.06	3.83	2.83												
17	MERN19MDS0129AG21	X261193	Aphyric rhyolite	Alb-Ser	644551	5347357	0.02	5.29	2.82												
18	MERN19MDS0129AG22	X261139	Aphyric rhyolite	Alb-Ser	644548	5347355	0.03	3.97	2.82												
19	MERN19MDS0129AG23	X261194	Aphyric rhyolite	Alb-Ser	644546	5347353	0.12	3.45	2.74												
20	MERN19MDS0155AG01	X261150	Aphyric rhyolite	Spilite	644016	5347982	<0.01			0.25	0.1		30.9	0.02	<0.5	74.1	4	20	0.05	12	9.05
21	MERN19MDS0177BG02	X261160	Aphyric rhyolite	Spilite	646423	5347441	<0.01			0.25	0.1		130	0.02	<0.5	36.2	2	20	0.24	6	6.43
22	MERN19MDS0178CG03	X261165	Aphyric rhyolite	Spilite	646610	5347387	<0.01			0.25	0.3		147	0.04	<0.5	37.4	2	30	0.27	2	7.05
23	MERN19MDS0150AG03	X261143	Aphyric rhyolite	Spilite	646455	5348483	<0.01	0.76	2.71												
24	MERN19MDS0150BG02	X261142	Aphyric rhyolite	Spilite	646471	5348498	<0.01	1.23	2.76												
25	MERN19MDS0150CG01	X261141	Aphyric rhyolite	Spilite	646482	5348491	0.01	2.65	2.77												
26	MERN19MDS0151AG01	X261144	Aphyric rhyolite	Spilite	646382	5348652	<0.01	1.81	2.72												
27	MERN19MDS0151AG02	X261145	Aphyric rhyolite	Spilite	646382	5348652	<0.01			0.25	0.4		177.5	0.01	<0.5	64.2	2	20	0.28	2	8.17
28	MERN19MDS0165AG01	X261156	Aphyric rhyolite	Spotted	645687	5348449	0.39	2.3	2.73												
29	MERN19MDS0183AG01	X261169	Aphyric rhyolite	Spilite	645151	5348837	0.03	1.67	2.75												
30	MERN19MDS0184AG01	X261170	Aphyric rhyolite	Spilite	645088	5348911	0.01	1.56	2.75												
31	MERN18MDS0120AG01	X258479	Aphyric rhyolite	Chl	645686	5348384	0.005		2.73	0.25	2		208	0.02	0.25	42.4	1	5	0.31	37	5.77
32	MERN18MDS0103EG05	X258473	Aphyric rhyolite	Spotted	645415	5347965	0.005		2.79	0.25	0.2		762	0.06	0.25	54.6	7	10	0.33	10	8.16
33	MERN17MDS0030BG01	X258496	Aphyric felsic dike	Spotted	645036	5347711	0.01		2.75												
34	MERN17MDS0033AG03	X258403	Aphyric felsic dike	Spotted	644497	5347308	0.04	2.81	2.81	0.5	0.8		260	1.43	3	11.4	4	10	0.45	13	5.96
35	MERN17MDS0033AG06	X258419	Aphyric felsic dike	Spotted	644491	5347311	0.06	3.29	2.74												
36	MERN17MDS0033AG07	X258404	Aphyric felsic dike	Spotted	644462	5347319	0.11	1.18	2.73	0.25	0.2		211	0.18	0.25	31.2	5	10	0.45	29	6.09
37	MERN17MDS0033AG09	X258420	Aphyric felsic dike	Spotted	644451	5347324	0.03	0.46	2.73												
38	MERN17MDS0034AG03	X258406	Aphyric felsic dike		644450	5347291	0.04	2.25	2.76	0.25	0.1		305	0.08	0.25	49.3	7	10	0.41	30	8.33
39	MERN17MDS0050AG01	X258472	Aphyric felsic dike		644379	5347443	0.07		2.73												
40	MERN18MDS0086AG04	X258438	Aphyric felsic dike	Ser	645190	5347767	0.03	2.68	2.74	0.25	0.3		630	0.12	0.25	47.3	5	10	0.27	25	6.56

	Field Number	Lab ID	Rock Type	Alteration	UTM-East	UTM-North	Er ppm	Eu ppm	Ga_ppm	Gd_ppm	Ge_ppm	Hf_ppm	Hg_ppm	Ho_ppm	In_ppm	La_ppm	Li_ppm	Lu_ppm	Mo_ppm	Nb_ppm	Nd_ppm
Method					**NAD 83**	**NAD 83**	**ME-MS81**	**ME-MS81**	**ME-MS81**	**ME-MS81**	**ME-MS81**	**ME-MS81**	**ME-MS42**	**ME-MS81**	**ME-MS42**	**ME-MS81**	**ME-4ACD81**	**ME-MS81**	**ME-4ACD81**	**ME-MS81**	**ME-MS81**
Detection Limit							**0.03**	**0.03**	**0.1**	**0.05**	**5**	**0.2**	**0.005**	**0.01**	**0.005**	**0.1**	**10**	**0.01**	**1**	**0.2**	**0.1**
1	MERN17MDS0044AG02	X258412	Aphyric rhyolite	Ser	644493	5347553	6.15	1.22	18.8	8.21	2.5	7.1	0	2.18	0.02	17.4	20	0.9	1	11.8	24.2
2	MERN17MDS0045AG02	X258413	Aphyric rhyolite	Ser	644405	5347521	4.69	1	19.9	8.13	2.5	5.3	0	1.73	0.02	19.7	30	0.69	2	10	28.7
3	MERN18MDS0104CG04	X258471	Aphyric rhyolite	Ser	644494	5347556	4.2	0.55	15.3	5.65	2.5	4.8	0.0025	1.3	0.046	23.7	30	0.64	1	8.7	28.8
4	MERN19MDS0129AG07	X261180	Aphyric rhyolite	Alb-Ser	644505	5347412															
5	MERN19MDS0129AG08	X261181	Aphyric rhyolite	Alb-Ser	644504	5347410															
6	MERN19MDS0129AG09	X261182	Aphyric rhyolite	Alb-Ser	644503	5347409															
7	MERN19MDS0129AG10	X261183	Aphyric rhyolite	Alb-Ser	644503	5347408															
8	MERN19MDS0129AG11	X261184	Aphyric rhyolite	Alb-Ser	644503	5347408															
9	MERN19MDS0129AG12	X261185	Aphyric rhyolite	Alb-Ser	644503	5347408															
10	MERN19MDS0129AG13	X261186	Aphyric rhyolite	Alb-Ser	644502	5347407															
11	MERN19MDS0129AG14	X261187	Aphyric rhyolite	Alb-Ser	644502	5347407															
12	MERN19MDS0129AG15	X261188	Aphyric rhyolite	Alb-Ser	644502	5347407															
13	MERN19MDS0129AG16	X261189	Aphyric rhyolite	Alb-Ser	644510	5347419															
14	MERN19MDS0129AG18	X261190	Aphyric rhyolite	Ank-Ser	644556	5347359															
15	MERN19MDS0129AG19	X261191	Aphyric rhyolite	Ank-Ser	644555	5347358															
16	MERN19MDS0129AG20	X261192	Aphyric rhyolite	Alb-Ser	644554	5347358															
17	MERN19MDS0129AG21	X261193	Aphyric rhyolite	Alb-Ser	644551	5347357															
18	MERN19MDS0129AG22	X261139	Aphyric rhyolite	Alb-Ser	644548	5347355															
19	MERN19MDS0129AG23	X261194	Aphyric rhyolite	Alb-Ser	644546	5347353															
20	MERN19MDS0155AG01	X261150	Aphyric rhyolite	Spilite	644016	5347982	5.69	2.41	18.8	9.42	<5	6.6	<0.005	1.84	0.031	33.6	20	0.74	1	11	40.5
21	MERN19MDS0177BG02	X261160	Aphyric rhyolite	Spilite	646423	5347441	4.42	0.8	16.4	5.67	<5	5.4	<0.005	1.44	0.006	16.7	10	0.76	2	8.2	19.5
22	MERN19MDS0178CG03	X261165	Aphyric rhyolite	Spilite	646610	5347387	4.88	0.72	15.9	5.99	<5	6.1	<0.005	1.6	0.005	16.7	10	0.79	2	8.1	20.7
23	MERN19MDS0150AG03	X261143	Aphyric rhyolite	Spilite	646455	5348483															
24	MERN19MDS0150BG02	X261142	Aphyric rhyolite	Spilite	646471	5348498															
25	MERN19MDS0150CG01	X261141	Aphyric rhyolite	Spilite	646482	5348491															
26	MERN19MDS0151AG01	X261144	Aphyric rhyolite	Spilite	646382	5348652															
27	MERN19MDS0151AG02	X261145	Aphyric rhyolite	Spilite	646382	5348652	5.49	1.34	19	7.76	<5	7.1	<0.005	1.8	0.021	27.5	20	0.85	1	9.4	32.6
28	MERN19MDS0165AG01	X261156	Aphyric rhyolite	Spotted	645687	5348449															
29	MERN19MDS0183AG01	X261169	Aphyric rhyolite	Spilite	645151	5348837															
30	MERN19MDS0184AG01	X261170	Aphyric rhyolite	Spilite	645088	5348911															
31	MERN18MDS0120AG01	X258479	Aphyric rhyolite	Chl	645686	5348384	4.24	1.03	16	5.59	2.5	6.4	0.0025	1.33	0.014	20.3	20	0.74	0.5	11.5	23.2
32	MERN18MDS0103EG05	X258473	Aphyric rhyolite	Spotted	645415	5347965	5.69	0.75	16.6	7.45	2.5	7.3	0.0025	1.83	0.022	25.5	20	0.94	0.5	12.6	29.7
33	MERN17MDS0030BG01	X258496	Aphyric felsic dike	Spotted	645036	5347711															
34	MERN17MDS0033AG03	X258403	Aphyric felsic dike	Spotted	644497	5347308	3.95	0.67	17.1	4.52	2.5	4.6	0.17	1.31	0.56	4.9	20	0.59	0.5	12.3	9
35	MERN17MDS0033AG06	X258419	Aphyric felsic dike	Spotted	644491	5347311															
36	MERN17MDS0033AG07	X258404	Aphyric felsic dike	Spotted	644462	5347319	4.32	1.13	19.1	5.35	2.5	4.8	0	1.44	0.01	15.7	10	0.68	3	13.1	19.8
37	MERN17MDS0033AG09	X258420	Aphyric felsic dike	Spotted	644451	5347324															
38	MERN17MDS0034AG03	X258406	Aphyric felsic dike		644450	5347291	5.58	1.27	16.9	7.33	2.5	7.9	0.01	1.81	0.01	22.6	20	0.84	1	12.9	26.5
39	MERN17MDS0050AG01	X258472	Aphyric felsic dike		644379	5347443															
40	MERN18MDS0086AG04	X258438	Aphyric felsic dike	Ser	645190	5347767	4.09	0.31	17.4	6.28	2.5	7	0	1.35	0.02	20.5	10	0.67	1	11.4	25.5

	Field Number	Lab ID	Rock Type	Alteration	UTM-East	UTM-North	Ni_ppm	Pb_ppm	Rb_ppm	Re_ppm	Sb_ppm	Sc_ppm	Se_ppm	Sm_ppm	Sn_ppm	Sr_ppm	Ta_ppm	Tb_ppm	Te_ppm	Th_ppm	Tl_ppm
Method					**NAD 83**	**NAD 83**	**ME-4ACD81**	**ME-4ACD81**	**ME-MS81**	**ME-MS42**	**ME-MS42**	**ME-4ACD81**	**ME-MS42**	**ME-MS81**	**ME-MS81**	**ME-MS81**	**ME-MS81**	**ME-MS81**	**ME-MS42**	**ME-MS81**	**ME-MS42**
Detection Limit							**1**	**2**	**0.2**	**0.001**	**0.05**	**1**	**0.2**	**0.03**	**1**	**0.1**	**0.1**	**0.01**	**0.01**	**0.05**	**0.02**
1	MERN17MDS0044AG02	X258412	Aphyric rhyolite	Ser	644493	5347553	2	3	24.4	0	0.03	16	0.3	5.96	4	6.8	0.7	1.55	0.02	2.78	0.01
2	MERN17MDS0045AG02	X258413	Aphyric rhyolite	Ser	644405	5347521	3	3	36.8	0	0.03	15	0.1	6.96	3	10.4	0.6	1.32	0.06	2.23	0.01
3	MERN18MDS0104CG04	X258471	Aphyric rhyolite	Ser	644494	5347556	9	1	28.6	0.0005	0.05	12	0.1	6.25	5	7	0.5	1.02	0.02	2.73	0.01
4	MERN19MDS0129AG07	X261180	Aphyric rhyolite	Alb-Ser	644505	5347412															
5	MERN19MDS0129AG08	X261181	Aphyric rhyolite	Alb-Ser	644504	5347410															
6	MERN19MDS0129AG09	X261182	Aphyric rhyolite	Alb-Ser	644503	5347409															
7	MERN19MDS0129AG10	X261183	Aphyric rhyolite	Alb-Ser	644503	5347408															
8	MERN19MDS0129AG11	X261184	Aphyric rhyolite	Alb-Ser	644503	5347408															
9	MERN19MDS0129AG12	X261185	Aphyric rhyolite	Alb-Ser	644503	5347408															
10	MERN19MDS0129AG13	X261186	Aphyric rhyolite	Alb-Ser	644502	5347407															
11	MERN19MDS0129AG14	X261187	Aphyric rhyolite	Alb-Ser	644502	5347407															
12	MERN19MDS0129AG15	X261188	Aphyric rhyolite	Alb-Ser	644502	5347407															
13	MERN19MDS0129AG16	X261189	Aphyric rhyolite	Alb-Ser	644510	5347419															
14	MERN19MDS0129AG18	X261190	Aphyric rhyolite	Ank-Ser	644556	5347359															
15	MERN19MDS0129AG19	X261191	Aphyric rhyolite	Ank-Ser	644555	5347358															
16	MERN19MDS0129AG20	X261192	Aphyric rhyolite	Alb-Ser	644554	5347358															
17	MERN19MDS0129AG21	X261193	Aphyric rhyolite	Alb-Ser	644551	5347357															
18	MERN19MDS0129AG22	X261139	Aphyric rhyolite	Alb-Ser	644548	5347355															
19	MERN19MDS0129AG23	X261194	Aphyric rhyolite	Alb-Ser	644546	5347353															
20	MERN19MDS0155AG01	X261150	Aphyric rhyolite	Spilite	644016	5347982	<1	2	2.4	<0.001	<0.05	14	0.2	10.3	1	31.6	0.7	1.53	0.01	2.71	<0.02
21	MERN19MDS0177BG02	X261160	Aphyric rhyolite	Spilite	646423	5347441	<1	2	12.5	0.001	<0.05	7	<0.2	4.94	1	29.6	0.7	0.94	0.02	2.95	<0.02
22	MERN19MDS0178CG03	X261165	Aphyric rhyolite	Spilite	646610	5347387	<1	<2	14.8	0.001	<0.05	8	<0.2	5.15	1	24.9	0.7	1.03	0.01	3.15	<0.02
23	MERN19MDS0150AG03	X261143	Aphyric rhyolite	Spilite	646455	5348483															
24	MERN19MDS0150BG02	X261142	Aphyric rhyolite	Spilite	646471	5348498															
25	MERN19MDS0150CG01	X261141	Aphyric rhyolite	Spilite	646482	5348491															
26	MERN19MDS0151AG01	X261144	Aphyric rhyolite	Spilite	646382	5348652															
27	MERN19MDS0151AG02	X261145	Aphyric rhyolite	Spilite	646382	5348652	2	<2	9.2	<0.001	<0.05	12	<0.2	7.73	2	54.5	0.7	1.28	<0.01	4.08	<0.02
28	MERN19MDS0165AG01	X261156	Aphyric rhyolite	Spotted	645687	5348449															
29	MERN19MDS0183AG01	X261169	Aphyric rhyolite	Spilite	645151	5348837															
30	MERN19MDS0184AG01	X261170	Aphyric rhyolite	Spilite	645088	5348911															
31	MERN18MDS0120AG01	X258479	Aphyric rhyolite	Chl	645686	5348384	1	1	35.3	0.0005	0.025	10	0.1	5.58	1	11.3	0.7	1.02	0.01	3.49	0.01
32	MERN18MDS0103EG05	X258473	Aphyric rhyolite	Spotted	645415	5347965	1	1	30.3	0.0005	0.05	9	0.1	6.98	6	7.2	0.8	1.38	0.03	4.04	0.01
33	MERN17MDS0030BG01	X258496	Aphyric felsic dike	Spotted	645036	5347711															
34	MERN17MDS0033AG03	X258403	Aphyric felsic dike	Spotted	644497	5347308	6	1	40	0	0.03	14	0.1	2.75	39	6.4	0.7	0.84	0.04	1.85	0.01
35	MERN17MDS0033AG06	X258419	Aphyric felsic dike	Spotted	644491	5347311															
36	MERN17MDS0033AG07	X258404	Aphyric felsic dike	Spotted	644462	5347319	2	2	22.1	0	0.03	11	0.1	4.96	5	47.1	0.7	0.98	0.04	2.11	0.01
37	MERN17MDS0033AG09	X258420	Aphyric felsic dike	Spotted	644451	5347324															
38	MERN17MDS0034AG03	X258406	Aphyric felsic dike		644450	5347291	1	1	22.4	0	0.03	9	0.3	7.09	2	29.6	0.7	1.35	0.02	4.04	0.01
39	MERN17MDS0050AG01	X258472	Aphyric felsic dike		644379	5347443															
40	MERN18MDS0086AG04	X258438	Aphyric felsic dike	Ser	645190	5347767	1	3	28.7	0	0.38	10	0.2	5.54	3	7.3	0.8	1.08	0.07	3.53	0.01

	Field Number	Lab ID	Rock Type	Alteration	UTM-East	UTM-North	Tm_ppm	U_ppm	V_ppm	W_ppm	Y_ppm	Yb_ppm	Zn_ppm	Zr_ppm
Method					**NAD 83**	**NAD 83**	**ME-MS81**	**ME-MS81**	**ME-MS81**	**ME-MS81**	**ME-MS81**	**ME-MS81**	**ME4ACD81**	**ME-MS81**
Detection Limit							**0.01**	**0.05**	**5**	**1**	**0.1**	**0.03**	**2**	**2**
1	MERN17MDS0044AG02	X258412	Aphyric rhyolite	Ser	644493	5347553	0.93	0.83	2.5	2	55	6.31	41	260
2	MERN17MDS0045AG02	X258413	Aphyric rhyolite	Ser	644405	5347521	0.72	0.65	23	2	43.7	4.81	77	217
3	MERN18MDS0104CG04	X258471	Aphyric rhyolite	Ser	644494	5347556	0.62	0.72	68	2	34.8	4.18	298	215
4	MERN19MDS0129AG07	X261180	Aphyric rhyolite	Alb-Ser	644505	5347412					43.5			233
5	MERN19MDS0129AG08	X261181	Aphyric rhyolite	Alb-Ser	644504	5347410					47.9			249
6	MERN19MDS0129AG09	X261182	Aphyric rhyolite	Alb-Ser	644503	5347409					46.9			250
7	MERN19MDS0129AG10	X261183	Aphyric rhyolite	Alb-Ser	644503	5347408					44.3			226
8	MERN19MDS0129AG11	X261184	Aphyric rhyolite	Alb-Ser	644503	5347408					46.7			228
9	MERN19MDS0129AG12	X261185	Aphyric rhyolite	Alb-Ser	644503	5347408					48.8			238
10	MERN19MDS0129AG13	X261186	Aphyric rhyolite	Alb-Ser	644502	5347407					43.2			221
11	MERN19MDS0129AG14	X261187	Aphyric rhyolite	Alb-Ser	644502	5347407					47.6			239
12	MERN19MDS0129AG15	X261188	Aphyric rhyolite	Alb-Ser	644502	5347407					37.8			228
13	MERN19MDS0129AG16	X261189	Aphyric rhyolite	Alb-Ser	644510	5347419					53.2			262
14	MERN19MDS0129AG18	X261190	Aphyric rhyolite	Ank-Ser	644556	5347359					48.2			238
15	MERN19MDS0129AG19	X261191	Aphyric rhyolite	Ank-Ser	644555	5347358					47.5			236
16	MERN19MDS0129AG20	X261192	Aphyric rhyolite	Alb-Ser	644554	5347358					46.8			244
17	MERN19MDS0129AG21	X261193	Aphyric rhyolite	Alb-Ser	644551	5347357					49.8			228
18	MERN19MDS0129AG22	X261139	Aphyric rhyolite	Alb-Ser	644548	5347355					53			291
19	MERN19MDS0129AG23	X261194	Aphyric rhyolite	Alb-Ser	644546	5347353					40.6			180
20	MERN19MDS0155AG01	X261150	Aphyric rhyolite	Spilite	644016	5347982	0.83	0.68	<5	<1	50.6	5.2	69	257
21	MERN19MDS0177BG02	X261160	Aphyric rhyolite	Spilite	646423	5347441	0.73	0.83	8	1	41.6	4.43	30	210
22	MERN19MDS0178CG03	X261165	Aphyric rhyolite	Spilite	646610	5347387	0.75	0.92	8	1	43.9	5.14	25	218
23	MERN19MDS0150AG03	X261143	Aphyric rhyolite	Spilite	646455	5348483					39.2			214
24	MERN19MDS0150BG02	X261142	Aphyric rhyolite	Spilite	646471	5348498					29			269
25	MERN19MDS0150CG01	X261141	Aphyric rhyolite	Spilite	646482	5348491					50.2			298
26	MERN19MDS0151AG01	X261144	Aphyric rhyolite	Spilite	646382	5348652					48.2			286
27	MERN19MDS0151AG02	X261145	Aphyric rhyolite	Spilite	646382	5348652	0.86	1.17	7	1	49.4	5.69	42	278
28	MERN19MDS0165AG01	X261156	Aphyric rhyolite	Spotted	645687	5348449					35.1			271
29	MERN19MDS0183AG01	X261169	Aphyric rhyolite	Spilite	645151	5348837					27.3			282
30	MERN19MDS0184AG01	X261170	Aphyric rhyolite	Spilite	645088	5348911					55			271
31	MERN18MDS0120AG01	X258479	Aphyric rhyolite	Chl	645686	5348384	0.68	0.92	7	0.5	35.9	4.52	188	286
32	MERN18MDS0103EG05	X258473	Aphyric rhyolite	Spotted	645415	5347965	0.88	1.04	5	1	48.3	5.91	140	318
33	MERN17MDS0030BG01	X258496	Aphyric felsic dike	Spotted	645036	5347711					41.9			267
34	MERN17MDS0033AG03	X258403	Aphyric felsic dike	Spotted	644497	5347308	0.58	0.42	18	2	33.4	4.12	819	176
35	MERN17MDS0033AG06	X258419	Aphyric felsic dike	Spotted	644491	5347311					32.5			201
36	MERN17MDS0033AG07	X258404	Aphyric felsic dike	Spotted	644462	5347319	0.64	0.71	2.5	1	32.8	4.29	77	178
37	MERN17MDS0033AG09	X258420	Aphyric felsic dike	Spotted	644451	5347324					47.8			204
38	MERN17MDS0034AG03	X258406	Aphyric felsic dike		644450	5347291	0.81	0.96	6	1	46.6	6.17	91	289
39	MERN17MDS0050AG01	X258472	Aphyric felsic dike		644379	5347443					39			272
40	MERN18MDS0086AG04	X258438	Aphyric felsic dike	Ser	645190	5347767	0.64	0.92	7	3	35.2	4.35	101	256

	Field Number	Lab ID	Rock Type	Alteration	UTM-East	UTM-North	SiO2_wt%	TiO2_wt%	Al2O3_wt%	Fe2O3t_wt%	MnO_wt%	MgO_wt%	CaO_wt%	SrO wt%	BaO wt%	Na2O_wt%	K2O_wt%	P2O5_wt%	LOI_%	Total_wt%	C_%
Method					**NAD 83**	**NAD 83**	**ME-ICP06**	**ME-ICP06**	**ME-ICP06**	**ME-ICP06**	**ME-ICP06**	**ME-ICP06**	**ME-ICP06**	**ME-ICP06**	**ME-ICP06**	**ME-ICP06**	**ME-ICP06**	**ME-ICP06**	**OA-GRA05**		**C-IR07**
Detection Limit							**0.01**	**0.01**	**0.01**	**0.01**	**0.01**	**0.01**	**0.01**	**0.01**	**0.01**	**0.01**	**0.01**	**0.01**	**0.01**		**0.01**
41	MERN18MDS0086AG05	X258439	Aphyric felsic dike	Spotted	645190	5347765	73.50	0.34	10.90	7.60	0.04	2.98	0.07	0.01	0.06	0.14	1.45	0.05	2.91	100.04	0.01
42	MERN18MDS0086AG08	X258440	Aphyric felsic dike	Spotted	645186	5347742	75.60	0.37	11.80	5.63	0.02	2.51	0.07	0.01	0.12	0.18	1.92	0.05	2.73	101	0.02
43	MERN18MDS0087CG02	X258445	Aphyric felsic dike	Spotted	644635	5347296	75.90	0.22	11.45	5.77	0.08	2.53	0.14	0.01	0.02	1.41	1.45	0.03	2.30	101.3	0.05
44	MERN18MDS0098BG09	X258450	Aphyric felsic dike	Spilite	644647	5348093	75.60	0.31	11.90	4.58	0.07	2.85	0.11	0.01	0.01	4.71	0.05	0.04	1.74	101.96	0.01
45	MERN18MDS0100BG02	X258454	Aphyric felsic dike	Spotted	644482	5347947	79.00	0.41	4.39	10.45	0.04	1.80	0.20	0.01	0.01	0.02	0.34	0.15	3.33	100.14	0.02
46	MERN18MDS0103BG02	X258490	Aphyric felsic dike	Spotted	645414	5347964	72.60	0.35	11.40	6.35	0.07	3.42	0.05	0.01	0.06	0.15	1.77	0.06	2.81	99.09	<0.01
47	MERN18MDS0104BG03	X261053	Aphyric felsic dike	Spotted	644494	5347556	73.40	0.39	13.65	6.13	0.03	2.83	0.08	0.01	0.07	0.12	2.28	0.07	2.85	100.4	0.005
48	MERN18MDS0108BG02	X261059	Aphyric felsic dike	Spilite	645622	5347834	75.00	0.39	13.65	4.92	0.04	2.77	0.11	0.01	0.01	3.27	0.63	0.07	2.31	101.17	0.12
49	MERN18MDS0113BG02	X258476	Aphyric felsic dike		645805	5347679	72.10	0.50	13.65	6.53	0.06	3.32	0.12	0.01	0.09	0.94	1.92	0.09	2.77	100.19	0.01
50	MERN18MDS0114BG03	X258498	Aphyric felsic dike	Spotted	645819	5347735	77.20	0.22	10.60	4.38	0.03	2.42	0.07	0.01	0.03	2.09	1.02	0.04	2.02	100.12	<0.01
51	MERN20MDS0186CG14	C079654	Aphyric felsic dike	Spotted	645800	5347138	69.50	0.43	13.35	4.64	0.03	3.78	0.13	0.01	0.04	1.35	2.03	0.08	2.91	98.27	<0.01
52	MERN17MDS0061DG05	X258416	Qtz-phyric rhyolite	Spotted	645168	5347780	75.90	0.28	11.65	7.76	0.03	1.33	0.06	0.01	0.16	0.19	2.05	0.05	2.44	101.9	0.13
53	MERN17MDS0061DG06	X258417	Qtz-phyric rhyolite	Spotted	645166	5347775	75.30	0.26	11.05	8.07	0.04	1.72	0.03	0.01	0.10	0.15	1.75	0.05	2.49	101.01	0.04
54	MERN17MDS0061DG07	X258421	Qtz-phyric rhyolite	Spotted	645148	5347763	76.20	0.29	11.10	6.18	0.03	1.81	0.06	0.01	0.12	0.16	1.94	0.04	2.37	100.3	0.01
55	MERN17MDS0061DG08	X258422	Qtz-phyric rhyolite	Spotted	645141	5347766	77.70	0.26	10.20	5.86	0.04	1.70	0.05	0.01	0.12	0.16	1.82	0.04	2.38	100.33	0.04
56	MERN17MDS0061DG09	X258423	Qtz-phyric rhyolite	Spotted	645142	5347760	74.80	0.28	10.90	6.19	0.03	2.24	0.05	0.01	0.09	0.17	1.78	0.04	2.55	99.12	0.01
57	MERN18MDS0085BG01	X258433	Qtz-phyric rhyolite	Spotted	645738	5348189	76.40	0.27	9.56	6.21	0.07	1.52	0.07	0.01	0.07	0.32	1.74	0.04	2.07	98.34	0.02
58	MERN18MDS0085BG02	X258434	Qtz-phyric rhyolite	Spotted	645723	5348170	79.70	0.25	9.53	5.34	0.06	1.03	0.07	0.01	0.08	0.14	1.99	0.04	1.81	100.04	0.02
59	MERN18MDS0110AG01	X258497	Qtz-phyric rhyolite	Spilite	645673	5347845	77.10	0.28	13.65	4.94	0.05	2.69	0.05	0.01	0.05	0.74	1.73	0.04	2.56	101.63	0.02
60	MERN19MDS0126AG01	X261138	Qtz-phyric rhyolite	Spilite	646496	5348024	71.60	0.36	13.20	4.22	0.07	2.50	0.55	0.01	0.02	4.35	0.89	0.07	2.00	99.83	0.1
61	MERN18MDS0113CG03	X261057	Qtz-phyric rhyolite dike	Spilite	645805	5347679	77.30	0.23	13.65	3.95	0.04	0.87	1.12	0.01	0.01	5.59	0.06	0.04	1.36	101.98	0.2
62	MERN19MDS0175AG01	X261158	Qtz-phyric rhyolite dike	Spilite	646460	5347507	75.20	0.23	10.25	5.74	0.09	1.35	0.36	0.01	0.01	3.95	0.10	0.01	1.50	98.78	0.08
63	MERN19MDS0125DG01	X261095	Qtz-phyric rhyolite dike	Spilite	646662	5347897	74.40	0.26	10.80	4.77	0.10	0.58	0.36	0.01	0.01	4.94	0.14	0.02	1.33	97.7	0.12
64	MERN19MDS0125DG04	X261092	Qtz-phyric rhyolite dike	Spilite	646610	5347890	75.20	0.28	11.35	5.17	0.13	0.20	0.64	0.01	0.01	5.40	0.32	0.05	1.42	100.18	0.21
65	MERN19MDS0125DG07	X261093	Qtz-phyric rhyolite dike	Spilite	646550	5347872	72.50	0.25	10.60	5.43	0.19	0.86	1.06	0.01	0.01	4.70	0.04	0.02	2.38	98.04	0.39
66	MERN19MDS0125DG23	X261107	Qtz-phyric rhyolite dike	Spilite	646420	5347791	75.20	0.25	11.50	5.04	0.07	1.23	0.67	0.01	0.01	3.95	0.60	0.03	1.76	100.32	0.11
67	MERN19MDS0125DG24	X261105	Qtz-phyric rhyolite dike	Spilite	646403	5347780	75.60	0.24	11.45	5.34	0.06	0.28	1.32	0.01	0.02	5.19	0.52	0.01	1.41	101.45	0.25
68	MERN19MDS0125DG27	X261110	Qtz-phyric rhyolite dike	Spilite	646341	5347772	75.70	0.22	10.90	4.13	0.14	0.33	2.57	0.01	0.01	4.99	0.40	0.02	2.30	101.72	0.54
69	MERN20MDS186AG04	C079672	Qtz-phyric rhyolite dike	Ank-Ser	645699	5347175	83.50	0.14	7.89	3.17	0.08	0.14	0.52	0.01	0.01	4.26	0.21	0.02	0.85	100.79	0.11
70	MERN20MDS186AG05	X261198	Qtz-phyric rhyolite dike	Ank-Ser	645696	5347174	77.30	0.22	10.75	4.56	0.07	0.08	0.32	0.01	0.01	5.80	0.19	0.06	0.51	99.87	0.06
71	MERN20MDS186AG06	X261199	Qtz-phyric rhyolite dike	Ank-Ser	645693	5347172	73.80	0.21	10.20	9.30	<0.01	0.13	0.15	0.01	0.01	5.24	0.32	0.04	0.43	99.83	0.02
72	MERN20MDS186AG07	C079676	Qtz-phyric rhyolite dike	Ank-Ser	645708	5347170	80.40	0.22	10.25	3.05	0.06	0.20	0.64	0.01	0.06	5.53	0.25	0.06	1.10	101.83	0.18
73	MERN20MDS186AG08	C079675	Qtz-phyric rhyolite dike	Ank-Ser	645709	5347171	76.30	0.23	10.45	4.49	0.07	0.30	0.83	0.01	0.07	5.92	0.07	0.06	1.39	100.19	0.3
74	MERN20MDS186AG09	X261200	Qtz-phyric rhyolite dike	Ank-Ser	645710	5347172	76.00	0.24	10.80	4.27	0.06	0.58	1.26	0.01	0.01	5.48	0.55	0.06	1.80	101.11	0.45
75	MERN20MDS186AG10	C079651	Qtz-phyric rhyolite dike	Ank-Ser	645717	5347173	77.60	0.24	11.35	3.74	0.04	0.17	0.88	0.01	0.01	5.70	0.47	0.03	0.84	101.07	0.16
76	MERN20MDS186AG11	C079652	Qtz-phyric rhyolite dike	Ank-Ser	645720	5347175	74.30	0.24	11.05	3.82	0.04	0.38	1.23	0.01	0.01	5.47	0.25	0.04	1.20	98.03	0.22
77	MERN20MDS186AG12	C079674	Qtz-phyric rhyolite dike	Ank-Ser	645728	5347180	75.00	0.25	11.40	5.01	0.04	0.16	1.28	0.01	0.02	5.34	0.47	0.03	1.17	100.18	0.22
78	MERN18MDS0107AG01	X258465	Qtz-phyric rhyolite dike	Spilite	646710	5347834	74.20	0.24	10.90	4.48	0.12	0.34	2.08	0.01	0.06	3.07	1.24	0.04	2.79	99.57	0.46
79	MERN19MDS0125DG42	X261131	Qtz-phyric rhyolite dike	Spilite	646712	5347827	76.80	0.26	11.45	5.50	0.09	0.55	0.67	0.01	0.02	4.43	0.47	0.03	1.36	101.63	0.12
80	MERN19MDS0125DG43	X261129	Qtz-phyric rhyolite dike	Ser	646712	5347827	80.10	0.26	12.20	2.20	0.02	0.31	0.09	0.01	0.14	0.23	3.59	0.04	1.80	100.98	0.01
81	MERN17MDS0041AG03	X258411	Powell Tonalite	Spilite	644674	5347418	75.50	0.26	11.95	4.88	0.05	1.55	0.08	0.01	0.01	4.65	0.34	0.03	1.60	100.9	0.02
82	MERN17MDS0073AG01	X258418	Powell Tonalite	Spilite	644512	5347244	76.70	0.26	11.70	4.11	0.04	1.32	0.16	0.01	0.01	4.87	0.37	0.06	1.23	100.83	0.04

	Field Number	Lab ID	Rock Type	Alteration	UTM-East	UTM-North	S_%	H20+_%	S.G.	Ag ppm	As ppm	Au_ppm	Ba ppm	Bi ppm	Cd ppm	Ce ppm	Co ppm	Cr ppm	Cs ppm	Cu ppm	Dy ppm
Method					NAD 83	NAD 83	S-IR08	OA-IR06	OA-GRA08b	ME-4ACD81	ME-MS42	Au-ICP21	ME-MS81	ME-MS42	ME-4ACD81	ME-MS81	ME-4ACD8	ME-MS81	ME-MS81	ME-4ACD81	ME-MS81
Detection Limit							0.01	0.01		0.5	0.1		0.5	0.01	0.5	0.1	1	1	0.05	1	0.05
41	MERN18MDS0086AG05	X258439	Aphyric felsic dike	Spotted	645190	5347765	0.01	3.03	2.73	0.25	0.2		485	0.03	0.25	38.4	8	5	0.27	5	6.31
42	MERN18MDS0086AG08	X258440	Aphyric felsic dike	Spotted	645186	5347742	0.01	2.62	2.75	0.25	0.1	<0.001	1085	1.09	0.25	36.3	11	10	0.31	4	6.58
43	MERN18MDS0087CG02	X258445	Aphyric felsic dike	Spotted	644635	5347296	0.01	2.4	2.7	0.25	0.05		218		0.25	124	2	10	0.34	9	10.75
44	MERN18MDS0098BG09	X258450	Aphyric felsic dike	Spilite	644647	5348093	0.01	1.4	2.68	0.25	0.05		26.2		0.25	40	5	20	0.05	7	5.88
45	MERN18MDS0100BG02	X258454	Aphyric felsic dike	Spotted	644482	5347947	3.36	1.84	2.79	7.9	8.4	0.09	113.5		0.25	14.4	43	20	0.11	16000	3.93
46	MERN18MDS0103BG02	X258490	Aphyric felsic dike	Spotted	645414	5347964	0.01		2.74												
47	MERN18MDS0104BG03	X261053	Aphyric felsic dike	Spotted	644494	5347556	0.005		2.74	0.25	0.1		611	0.08	0.25	46.9	9	5	0.44	4	6.02
48	MERN18MDS0108BG02	X261059	Aphyric felsic dike	Spilite	645622	5347834	0.005		2.72	0.25	0.05		109.5	0.01	0.25	42.6	4	10	0.16	4	6.08
49	MERN18MDS0113BG02	X258476	Aphyric felsic dike		645805	5347679	0.005		2.73	0.25	<0.1		856	0.03	0.25	37.5	5	10	0.62	36	5.75
50	MERN18MDS0114BG03	X258498	Aphyric felsic dike	Spotted	645819	5347735	0.03		2.73												
51	MERN20MDS0186CG14	C079654	Aphyric felsic dike	Spotted	645800	5347138	<0.01	3.19	2.78												
52	MERN17MDS0061DG05	X258416	Qtz-phyric rhyolite	Spotted	645168	5347780	0.12	2.75	2.76	0.25	0.4		1355	0.92	0.25	49.7	8	10	0.32	13	9.84
53	MERN17MDS0061DG06	X258417	Qtz-phyric rhyolite	Spotted	645166	5347775	0.07	2.97	2.78	0.8	0.6		885	0.29	0.25	49.7	10	10	0.32	358	7.81
54	MERN17MDS0061DG07	X258421	Qtz-phyric rhyolite	Spotted	645148	5347763	0.01	2.47	2.81												
55	MERN17MDS0061DG08	X258422	Qtz-phyric rhyolite	Spotted	645141	5347766	0.06	2.48	2.8												
56	MERN17MDS0061DG09	X258423	Qtz-phyric rhyolite	Spotted	645142	5347760	0.01	2.95	2.73												
57	MERN18MDS0085BG01	X258433	Qtz-phyric rhyolite	Spotted	645738	5348189	0.03	1.94	2.85	0.25	1.2		620		0.25	26.8	9	10	0.28	476	7.5
58	MERN18MDS0085BG02	X258434	Qtz-phyric rhyolite	Spotted	645723	5348170	0.02	2.06	2.82	0.25	2.4		679		0.25	34.2	10	20	0.27	123	7.7
59	MERN18MDS0110AG01	X258497	Qtz-phyric rhyolite	Spilite	645673	5347845	0.005		2.71	0.25	0.05		350	0.01	0.25	42.5	5	5	0.35	3	7.52
60	MERN19MDS0126AG01	X261138	Qtz-phyric rhyolite	Spilite	646496	5348024	0.02			0.25	0.7		211	0.08	<0.5	54.9	5	20	0.26	50	8.13
61	MERN18MDS0113CG03	X261057	Qtz-phyric rhyolite dike	Spilite	645805	5347679	0.15		2.72	0.25	0.1		73.1	0.03	0.25	82.6	4	10	0.08	33	9.96
62	MERN19MDS0175AG01	X261158	Qtz-phyric rhyolite dike	Spilite	646460	5347507	0.09	1.85	2.73												
63	MERN19MDS0125DG01	X261095	Qtz-phyric rhyolite dike	Spilite	646662	5347897	0.14	1.42	2.8												
64	MERN19MDS0125DG04	X261092	Qtz-phyric rhyolite dike	Spilite	646610	5347890	0.28	0.75	2.83												
65	MERN19MDS0125DG07	X261093	Qtz-phyric rhyolite dike	Spilite	646550	5347872	0.06	1.63	2.82												
66	MERN19MDS0125DG23	X261107	Qtz-phyric rhyolite dike	Spilite	646420	5347791	0.36	2.18	2.78												
67	MERN19MDS0125DG24	X261105	Qtz-phyric rhyolite dike	Spilite	646403	5347780	0.04	0.83	2.81												
68	MERN19MDS0125DG27	X261110	Qtz-phyric rhyolite dike	Spilite	646341	5347772	0.17	0.88	2.78												
69	MERN20MDS186AG04	C079672	Qtz-phyric rhyolite dike	Ank-Ser	645699	5347175	0.1	0.41	2.77												
70	MERN20MDS186AG05	X261198	Qtz-phyric rhyolite dike	Ank-Ser	645696	5347174	0.11	0.43	2.64												
71	MERN20MDS186AG06	X261199	Qtz-phyric rhyolite dike	Ank-Ser	645693	5347172	0.01	0.58	2.77												
72	MERN20MDS186AG07	C079676	Qtz-phyric rhyolite dike	Ank-Ser	645708	5347170	0.37	0.77	2.71												
73	MERN20MDS186AG08	C079675	Qtz-phyric rhyolite dike	Ank-Ser	645709	5347171	0.32	0.62	2.77												
74	MERN20MDS186AG09	X261200	Qtz-phyric rhyolite dike	Ank-Ser	645710	5347172	0.33	0.38	2.75												
75	MERN20MDS186AG10	C079651	Qtz-phyric rhyolite dike	Ank-Ser	645717	5347173	0.15	0.3	2.71												
76	MERN20MDS186AG11	C079652	Qtz-phyric rhyolite dike	Ank-Ser	645720	5347175	0.03	0.64	2.7												
77	MERN20MDS186AG12	C079674	Qtz-phyric rhyolite dike	Ank-Ser	645728	5347180	0.03	0.77	2.77												
78	MERN18MDS0107AG01	X258465	Qtz-phyric rhyolite dike	Spilite	646710	5347834	0.02		2.75	0.25	4.6		497	0.02	0.25	44.4	0.5	10	0.41	6	8.26
79	MERN19MDS0125DG42	X261131	Qtz-phyric rhyolite dike	Spilite	646712	5347827	0.04		2.72	0.25	0.2		177.5	0.04	0.25	42.9	1	10	0.14	30	8.61
80	MERN19MDS0125DG43	X261129	Qtz-phyric rhyolite dike	Ser	646712	5347827	0.02		2.8	0.25	0.05		1230	0.02	0.25	57.7	0.5	10	1.2	13	9.93
81	MERN17MDS0041AG03	X258411	Powell Tonalite	Spilite	644674	5347418	0.01	1.54	2.67	0.25	0.2		64.3	0.03	0.25	52	2	10	0.15	7	8.01
82	MERN17MDS0073AG01	X258418	Powell Tonalite	Spilite	644512	5347244	0.01	1.18	2.72	0.25	0.1		56	0.03	0.25	119	1	10	0.23	24	9.02

	Field Number	Lab ID	Rock Type	Alteration	UTM-East	UTM-North	Er ppm	Eu ppm	Ga_ppm	Gd_ppm	Ge_ppm	Hf_ppm	Hg_ppm	Ho_ppm	In_ppm	La_ppm	Li_ppm	Lu_ppm	Mo_ppm	Nb_ppm	Nd_ppm
Method					**NAD 83**	**NAD 83**	**ME-MS81**	**ME-MS81**	**ME-MS81**	**ME-MS81**	**ME-MS81**	**ME-MS81**	**ME-MS42**	**ME-MS81**	**ME-MS42**	**ME-MS81**	**ME-4ACD81**	**ME-MS81**	**ME-4ACD81**	**ME-MS81**	**ME-MS81**
Detection Limit							**0.03**	**0.03**	**0.1**	**0.05**	**5**	**0.2**	**0.005**	**0.01**	**0.005**	**0.1**	**10**	**0.01**	**1**	**0.2**	**0.1**
41	MERN18MDS0086AG05	X258439	Aphyric felsic dike	Spotted	645190	5347765	4.49	0.36	15.5	5.19	2.5	6.2	0	1.4	0.02	15.9	10	0.65	1	12.7	20.8
42	MERN18MDS0086AG08	X258440	Aphyric felsic dike	Spotted	645186	5347742	4.95	0.42	16.9	5.29	2.5	7.1	0	1.53	0.01	14	10	0.78	1	12.5	19.4
43	MERN18MDS0087CG02	X258445	Aphyric felsic dike	Spotted	644635	5347296	6.66	2.21	19.5	11.6	2.5	5.4	0	2.27	0.04	53.5	30	1	0.5	13.2	61.5
44	MERN18MDS0098BG09	X258450	Aphyric felsic dike	Spilite	644647	5348093	4.22	1.29	17.8	5.11	2.5	4.8	0	1.29	0.02	16.6	10	0.68	1	12.6	22.3
45	MERN18MDS0100BG02	X258454	Aphyric felsic dike	Spotted	644482	5347947	2.62	0.67	7.9	3.58	2.5	0.9	0.02	0.9	3.36	6.1	10	0.31	6	2.1	9.3
46	MERN18MDS0103BG02	X258490	Aphyric felsic dike	Spotted	645414	5347964															
47	MERN18MDS0104BG03	X261053	Aphyric felsic dike	Spotted	644494	5347556	4.38	0.76	14.5	5.67	2.5	6.1	0.0025	1.39	0.032	21.5	20	0.71	0.5	10.9	26
48	MERN18MDS0108BG02	X261059	Aphyric felsic dike	Spilite	645622	5347834	4.29	1.13	13.7	5.83	2.5	5.9	0.0025	1.4	0.012	19.9	10	0.69	1	9.9	23.3
49	MERN18MDS0113BG02	X258476	Aphyric felsic dike		645805	5347679	4.27	0.82	14.8	5.3	2.5	5.6	0.0025	1.35	0.077	17.7	20	0.72	0.5	10.1	20.9
50	MERN18MDS0114BG03	X258498	Aphyric felsic dike	Spotted	645819	5347735															
51	MERN20MDS0186CG14	C079654	Aphyric felsic dike	Spotted	645800	5347138															
52	MERN17MDS0061DG05	X258416	Qtz-phyric rhyolite	Spotted	645168	5347780	6.06	0.57	16.4	8.67	2.5	7.7	0	2.05	0.01	23.3	10	0.92	1	12.8	27.7
53	MERN17MDS0061DG06	X258417	Qtz-phyric rhyolite	Spotted	645166	5347775	5.27	0.57	16	7.5	2.5	7.3	0	1.69	0.1	23.2	10	0.81	3	11.9	27.6
54	MERN17MDS0061DG07	X258421	Qtz-phyric rhyolite	Spotted	645148	5347763															
55	MERN17MDS0061DG08	X258422	Qtz-phyric rhyolite	Spotted	645141	5347766															
56	MERN17MDS0061DG09	X258423	Qtz-phyric rhyolite	Spotted	645142	5347760															
57	MERN18MDS0085BG01	X258433	Qtz-phyric rhyolite	Spotted	645738	5348189	5.25	0.4	16.7	5.54	2.5	7.9		1.66		11.9	10	0.8	3	10.7	14.6
58	MERN18MDS0085BG02	X258434	Qtz-phyric rhyolite	Spotted	645723	5348170	4.81	0.35	16.4	6.68	2.5	7.4		1.69		14.1	10	0.75	2	9.9	18.7
59	MERN18MDS0110AG01	X258497	Qtz-phyric rhyolite	Spilite	645673	5347845	5.3	0.77	15.3	6.57	2.5	6.9	0.0025	1.75	0.021	19.6	10	0.87	1	11.3	23.6
60	MERN19MDS0126AG01	X261138	Qtz-phyric rhyolite	Spilite	646496	5348024	5.26	1.17	17.8	7.07	<5	7.2	<0.005	1.81	0.025	24.1	10	0.81	1	11.3	29.8
61	MERN18MDS0113CG03	X261057	Qtz-phyric rhyolite dike	Spilite	645805	5347679	6.96	1.83	20.7	9.85	2.5	6.6	0.0025	2.23	0.019	32	<10	1.14	1	15.3	41.7
62	MERN19MDS0175AG01	X261158	Qtz-phyric rhyolite dike	Spilite	646460	5347507															
63	MERN19MDS0125DG01	X261095	Qtz-phyric rhyolite dike	Spilite	646662	5347897															
64	MERN19MDS0125DG04	X261092	Qtz-phyric rhyolite dike	Spilite	646610	5347890															
65	MERN19MDS0125DG07	X261093	Qtz-phyric rhyolite dike	Spilite	646550	5347872															
66	MERN19MDS0125DG23	X261107	Qtz-phyric rhyolite dike	Spilite	646420	5347791															
67	MERN19MDS0125DG24	X261105	Qtz-phyric rhyolite dike	Spilite	646403	5347780															
68	MERN19MDS0125DG27	X261110	Qtz-phyric rhyolite dike	Spilite	646341	5347772															
69	MERN20MDS186AG04	C079672	Qtz-phyric rhyolite dike	Ank-Ser	645699	5347175															
70	MERN20MDS186AG05	X261198	Qtz-phyric rhyolite dike	Ank-Ser	645696	5347174															
71	MERN20MDS186AG06	X261199	Qtz-phyric rhyolite dike	Ank-Ser	645693	5347172															
72	MERN20MDS186AG07	C079676	Qtz-phyric rhyolite dike	Ank-Ser	645708	5347170															
73	MERN20MDS186AG08	C079675	Qtz-phyric rhyolite dike	Ank-Ser	645709	5347171															
74	MERN20MDS186AG09	X261200	Qtz-phyric rhyolite dike	Ank-Ser	645710	5347172															
75	MERN20MDS186AG10	C079651	Qtz-phyric rhyolite dike	Ank-Ser	645717	5347173															
76	MERN20MDS186AG11	C079652	Qtz-phyric rhyolite dike	Ank-Ser	645720	5347175															
77	MERN20MDS186AG12	C079674	Qtz-phyric rhyolite dike	Ank-Ser	645728	5347180															
78	MERN18MDS0107AG01	X258465	Qtz-phyric rhyolite dike	Spilite	646710	5347834	5.84	1.72	20.4	7.46	2.5	5.9	0.0025	1.9	0.041	20.3	10	0.95	1	14.4	26.1
79	MERN19MDS0125DG42	X261131	Qtz-phyric rhyolite dike	Spilite	646712	5347827	5.74	1.72	18.5	7.8	2.5	6.6	0.0025	1.82	0.055	18.9	20	1.02	2	14.3	26.1
80	MERN19MDS0125DG43	X261129	Qtz-phyric rhyolite dike	Ser	646712	5347827	6.56	2.1	27.5	8.74	2.5	8.5	0.0025	2.23	0.031	25.1	<10	1.16	1	17.9	36.7
81	MERN17MDS0041AG03	X258411	Powell Tonalite	Spilite	644674	5347418	4.97	1.68	19.4	7.51	2.5	5.4	0	1.7	0.04	23.5	10	0.81	1	12.3	30.7
82	MERN17MDS0073AG01	X258418	Powell Tonalite	Spilite	644512	5347244	5.58	3.46	18.2	10.25	2.5	2.8	0	1.87	0.04	58.9	10	0.69	1	12.2	58.8

	Field Number	Lab ID	Rock Type	Alteration	UTM-East	UTM-North	Ni_ppm	Pb_ppm	Rb_ppm	Re_ppm	Sb_ppm	Sc_ppm	Se_ppm	Sm_ppm	Sn_ppm	Sr_ppm	Ta_ppm	Tb_ppm	Te_ppm	Th_ppm	Tl_ppm
Method					**NAD 83**	**NAD 83**	**ME-4ACD81**	**ME-4ACD81**	**ME-MS81**	**ME-MS42**	**ME-MS42**	**ME-4ACD81**	**ME-MS42**	**ME-MS81**	**ME-MS81**	**ME-MS81**	**ME-MS81**	**ME-MS81**	**ME-MS42**	**ME-MS81**	**ME-MS42**
Detection Limit							**1**	**2**	**0.2**	**0.001**	**0.05**	**1**	**0.2**	**0.03**	**1**	**0.1**	**0.1**	**0.01**	**0.01**	**0.05**	**0.02**
41	MERN18MDS0086AG05	X258439	Aphyric felsic dike	Spotted	645190	5347765	2	1	20.5	0	0.05	10	0.2	4.7	4	5.8	0.6	1.08	0.02	3.63	0.01
42	MERN18MDS0086AG08	X258440	Aphyric felsic dike	Spotted	645186	5347742	3	3	26.7	0	0.03	10	0.1	4.75	3	9.5	0.7	1.01	0.81	3.87	0.01
43	MERN18MDS0087CG02	X258445	Aphyric felsic dike	Spotted	644635	5347296	9	1	23.1	0	0.05	12	0.2	12.9	6	11.6	0.8	1.95	0.01	2.48	0.01
44	MERN18MDS0098BG09	X258450	Aphyric felsic dike	Spilite	644647	5348093		2	0.7	0	0.03	14	0.2	5.3	1	27.1	0.7	0.97	0.01	2.02	0.01
45	MERN18MDS0100BG02	X258454	Aphyric felsic dike	Spotted	644482	5347947		7	6.5	0	0.1	6	20.8	2.47	2	5.5	0.05	0.65	1.78	0.3	0.01
46	MERN18MDS0103BG02	X258490	Aphyric felsic dike	Spotted	645414	5347964															
47	MERN18MDS0104BG03	X261053	Aphyric felsic dike	Spotted	644494	5347556		1	38.8	0.0005	0.025	11	0.1	6.03	6	6.8	0.7	1.03	0.01	3.47	0.01
48	MERN18MDS0108BG02	X261059	Aphyric felsic dike	Spilite	645622	5347834		1	10.9	0.0005	0.025	9	0.1	5.7	4	14.1	0.6	1.07	0.01	3.02	0.01
49	MERN18MDS0113BG02	X258476	Aphyric felsic dike		645805	5347679		2	33.9	0.0005	0.025	13	0.1	4.9	7	9.8	0.6	0.95	0.03	2.91	0.01
50	MERN18MDS0114BG03	X258498	Aphyric felsic dike	Spotted	645819	5347735															
51	MERN20MDS0186CG14	C079654	Aphyric felsic dike	Spotted	645800	5347138															
52	MERN17MDS0061DG05	X258416	Qtz-phyric rhyolite	Spotted	645168	5347780		2	29.9	0	0.03	9	0.3	7.28	5	6.7	0.8	1.51	0.51	4.21	0.01
53	MERN17MDS0061DG06	X258417	Qtz-phyric rhyolite	Spotted	645166	5347775		1	26.4	0	0.03	8	1.7	7.25	6	5.5	0.7	1.26	0.16	3.9	0.01
54	MERN17MDS0061DG07	X258421	Qtz-phyric rhyolite	Spotted	645148	5347763															
55	MERN17MDS0061DG08	X258422	Qtz-phyric rhyolite	Spotted	645141	5347766															
56	MERN17MDS0061DG09	X258423	Qtz-phyric rhyolite	Spotted	645142	5347760															
57	MERN18MDS0085BG01	X258433	Qtz-phyric rhyolite	Spotted	645738	5348189		3	33.2			9		3.76	5	6.8	0.8	1.15		3.34	
58	MERN18MDS0085BG02	X258434	Qtz-phyric rhyolite	Spotted	645723	5348170		1	32			8		5.08	3	4.5	0.8	1.15		3.18	
59	MERN18MDS0110AG01	X258497	Qtz-phyric rhyolite	Spilite	645673	5347845		1	30.6	0.0005	0.025	9	0.1	5.88	3	9.2	0.7	1.29	0.005	3.56	0.01
60	MERN19MDS0126AG01	X261138	Qtz-phyric rhyolite	Spilite	646496	5348024	<1	<2	16	<0.001	<0.05	11	<0.2	7.1	1	49.6	0.8	1.23	0.03	3.71	0.02
61	MERN18MDS0113CG03	X261057	Qtz-phyric rhyolite dike	Spilite	645805	5347679	<1	2	0.9	0.0005	0.025	12	0.1	9.99	1	70.1	0.9	1.76	0.02	2.79	0.01
62	MERN19MDS0175AG01	X261158	Qtz-phyric rhyolite dike	Spilite	646460	5347507	<1														
63	MERN19MDS0125DG01	X261095	Qtz-phyric rhyolite dike	Spilite	646662	5347897															
64	MERN19MDS0125DG04	X261092	Qtz-phyric rhyolite dike	Spilite	646610	5347890															
65	MERN19MDS0125DG07	X261093	Qtz-phyric rhyolite dike	Spilite	646550	5347872															
66	MERN19MDS0125DG23	X261107	Qtz-phyric rhyolite dike	Spilite	646420	5347791															
67	MERN19MDS0125DG24	X261105	Qtz-phyric rhyolite dike	Spilite	646403	5347780	2														
68	MERN19MDS0125DG27	X261110	Qtz-phyric rhyolite dike	Spilite	646341	5347772															
69	MERN20MDS186AG04	C079672	Qtz-phyric rhyolite dike	Ank-Ser	645699	5347175															
70	MERN20MDS186AG05	X261198	Qtz-phyric rhyolite dike	Ank-Ser	645696	5347174															
71	MERN20MDS186AG06	X261199	Qtz-phyric rhyolite dike	Ank-Ser	645693	5347172	1														
72	MERN20MDS186AG07	C079676	Qtz-phyric rhyolite dike	Ank-Ser	645708	5347170	1														
73	MERN20MDS186AG08	C079675	Qtz-phyric rhyolite dike	Ank-Ser	645709	5347171															
74	MERN20MDS186AG09	X261200	Qtz-phyric rhyolite dike	Ank-Ser	645710	5347172	6														
75	MERN20MDS186AG10	C079651	Qtz-phyric rhyolite dike	Ank-Ser	645717	5347173															
76	MERN20MDS186AG11	C079652	Qtz-phyric rhyolite dike	Ank-Ser	645720	5347175	2														
77	MERN20MDS186AG12	C079674	Qtz-phyric rhyolite dike	Ank-Ser	645728	5347180															
78	MERN18MDS0107AG01	X258465	Qtz-phyric rhyolite dike	Spilite	646710	5347834	1	1	25.3	0.0005	0.06	12	0.1	6.74	2	51.4	0.8	1.37	0.01	2.43	0.01
79	MERN19MDS0125DG42	X261131	Qtz-phyric rhyolite dike	Spilite	646712	5347827		1	9.5	0.0005	0.025	12	0.1	7.16	4	56.6	1	1.44	0.01	2.62	0.01
80	MERN19MDS0125DG43	X261129	Qtz-phyric rhyolite dike	Ser	646712	5347827	1	1	74.1	0.0005	0.025	15	0.1	8.37	18	20.3	1.1	1.61	0.01	3.76	0.02
81	MERN17MDS0041AG03	X258411	Powell Tonalite	Spilite	644674	5347418	0.5	2	7.2	0	0.03	12	0.1	7.15	2	18.6	0.7	1.31	0.02	2.07	0.01
82	MERN17MDS0073AG01	X258418	Powell Tonalite	Spilite	644512	5347244	3	1	7.6	0	0.03	10	0.1	12.2	2	34.7	0.5	1.49	0.02	2.95	0.01

	Field Number	Lab ID	Rock Type	Alteration	UTM-East	UTM-North	Tm_ppm	U_ppm	V_ppm	W_ppm	Y_ppm	Yb_ppm	Zn_ppm	Zr_ppm
Method					**NAD 83**	**NAD 83**	**ME-MS81**	**ME-MS81**	**ME-MS81**	**ME-MS81**	**ME-MS81**	**ME-MS81**	**ME4ACD81**	**ME-MS81**
Detection Limit							**0.01**	**0.05**	**5**	**1**	**0.1**	**0.03**	**2**	**2**
41	MERN18MDS0086AG05	X258439	Aphyric felsic dike	Spotted	645190	5347765	0.93	0.89	2.5	2	42.9	4.57	135	243
42	MERN18MDS0086AG08	X258440	Aphyric felsic dike	Spotted	645186	5347742	0.72	0.97	6	1	46	4.97	41	285
43	MERN18MDS0087CG02	X258445	Aphyric felsic dike	Spotted	644635	5347296	0.62	0.81	2.5	1	66.9	6.5	248	210
44	MERN18MDS0098BG09	X258450	Aphyric felsic dike	Spilite	644647	5348093		0.53	2.5	1	36.3	4.18	95	189
45	MERN18MDS0100BG02	X258454	Aphyric felsic dike	Spotted	644482	5347947		0.23	17	8	27.9	1.99	42	34
46	MERN18MDS0103BG02	X258490	Aphyric felsic dike	Spotted	645414	5347964					43.9			252
47	MERN18MDS0104BG03	X261053	Aphyric felsic dike	Spotted	644494	5347556		0.89	11	3	37.2	4.53	127	273
48	MERN18MDS0108BG02	X261059	Aphyric felsic dike	Spilite	645622	5347834		0.78	9	1	36.5	4.42	139	260
49	MERN18MDS0113BG02	X258476	Aphyric felsic dike		645805	5347679		0.72	43	1	35.7	4.58	119	249
50	MERN18MDS0114BG03	X258498	Aphyric felsic dike	Spotted	645819	5347735					35.8			258
51	MERN20MDS0186CG14	C079654	Aphyric felsic dike	Spotted	645800	5347138					34.5			233
52	MERN17MDS0061DG05	X258416	Qtz-phyric rhyolite	Spotted	645168	5347780		1.03	11	4	50.5	6.36	89	284
53	MERN17MDS0061DG06	X258417	Qtz-phyric rhyolite	Spotted	645166	5347775		0.91	11	5	41.7	5.58	107	270
54	MERN17MDS0061DG07	X258421	Qtz-phyric rhyolite	Spotted	645148	5347763					49.5			307
55	MERN17MDS0061DG08	X258422	Qtz-phyric rhyolite	Spotted	645141	5347766					48.3			250
56	MERN17MDS0061DG09	X258423	Qtz-phyric rhyolite	Spotted	645142	5347760					55.5			300
57	MERN18MDS0085BG01	X258433	Qtz-phyric rhyolite	Spotted	645738	5348189		0.89	22	2	43.2	5.05	68	275
58	MERN18MDS0085BG02	X258434	Qtz-phyric rhyolite	Spotted	645723	5348170		0.88	12	1	44.7	5.28	43	256
59	MERN18MDS0110AG01	X258497	Qtz-phyric rhyolite	Spilite	645673	5347845		0.94	14	1	45.7	5.51	136	287
60	MERN19MDS0126AG01	X261138	Qtz-phyric rhyolite	Spilite	646496	5348024	0.83	1.03	48	1	49.5	5.4	74	278
61	MERN18MDS0113CG03	X261057	Qtz-phyric rhyolite dike	Spilite	645805	5347679	0.73	1.03	2.5	1	57.7	7.34	32	280
62	MERN19MDS0175AG01	X261158	Qtz-phyric rhyolite dike	Spilite	646460	5347507	0.75				47.5			236
63	MERN19MDS0125DG01	X261095	Qtz-phyric rhyolite dike	Spilite	646662	5347897					48.6			209
64	MERN19MDS0125DG04	X261092	Qtz-phyric rhyolite dike	Spilite	646610	5347890					53.3			221
65	MERN19MDS0125DG07	X261093	Qtz-phyric rhyolite dike	Spilite	646550	5347872					56.9			212
66	MERN19MDS0125DG23	X261107	Qtz-phyric rhyolite dike	Spilite	646420	5347791					55.6			221
67	MERN19MDS0125DG24	X261105	Qtz-phyric rhyolite dike	Spilite	646403	5347780	0.86				58.1			236
68	MERN19MDS0125DG27	X261110	Qtz-phyric rhyolite dike	Spilite	646341	5347772					51			215
69	MERN20MDS186AG04	C079672	Qtz-phyric rhyolite dike	Ank-Ser	645699	5347175					30.5			133
70	MERN20MDS186AG05	X261198	Qtz-phyric rhyolite dike	Ank-Ser	645696	5347174					56			239
71	MERN20MDS186AG06	X261199	Qtz-phyric rhyolite dike	Ank-Ser	645693	5347172	0.68				70.4			219
72	MERN20MDS186AG07	C079676	Qtz-phyric rhyolite dike	Ank-Ser	645708	5347170	0.88				49.7			213
73	MERN20MDS186AG08	C079675	Qtz-phyric rhyolite dike	Ank-Ser	645709	5347171					50			221
74	MERN20MDS186AG09	X261200	Qtz-phyric rhyolite dike	Ank-Ser	645710	5347172	0.58				50.2			231
75	MERN20MDS186AG10	C079651	Qtz-phyric rhyolite dike	Ank-Ser	645717	5347173					52.2			229
76	MERN20MDS186AG11	C079652	Qtz-phyric rhyolite dike	Ank-Ser	645720	5347175	0.64				55.5			237
77	MERN20MDS186AG12	C079674	Qtz-phyric rhyolite dike	Ank-Ser	645728	5347180					54.4			243
78	MERN18MDS0107AG01	X258465	Qtz-phyric rhyolite dike	Spilite	646710	5347834	0.81	0.65	2.5	1	49.3	6.21	65	259
79	MERN19MDS0125DG42	X261131	Qtz-phyric rhyolite dike	Spilite	646712	5347827		0.73	2.5	2	52.8	5.98	102	233
80	MERN19MDS0125DG43	X261129	Qtz-phyric rhyolite dike	Ser	646712	5347827	0.64	0.83	2.5	2	62.6	6.93	29	303
81	MERN17MDS0041AG03	X258411	Powell Tonalite	Spilite	644674	5347418	0.69	0.54	2.5	2	40.7	5.36	149	192
82	MERN17MDS0073AG01	X258418	Powell Tonalite	Spilite	644512	5347244	0.75	0.41	2.5	1	45	5.07	111	101

	Field Number	Lab ID	Rock Type	Alteration	UTM-East	UTM-North	SiO2_wt%	TiO2_wt%	Al2O3_wt%	Fe2O3t_wt%	MnO_wt%	MgO_wt%	CaO_wt%	SrO wt%	BaO wt%	Na2O_wt%	K2O_wt%	P2O5_wt%	LOI_%	Total_wt%	C_%
Method					**NAD 83**	**NAD 83**	**ME-ICP06**	**ME-ICP06**	**ME-ICP06**	**ME-ICP06**	**ME-ICP06**	**ME-ICP06**	**ME-ICP06**	**ME-ICP06**	**ME-ICP06**	**ME-ICP06**	**ME-ICP06**	**ME-ICP06**	**OA-GRA05**		**C-IR07**
Detection Limit							**0.01**	**0.01**	**0.01**	**0.01**	**0.01**	**0.01**	**0.01**	**0.01**	**0.01**	**0.01**	**0.01**	**0.01**	**0.01**		**0.01**
83	MERN18MDS0087AG01	X258444	Powell Tonalite	Spotted	644635	5347296	68.90	0.45	13.10	8.22	0.10	3.52	0.20	0.01	0.02	2.31	0.95	0.09	2.82	100.68	0.03
84	MERN19MDS0128BG02	X261173	Powell Tonalite	Ank-Ser	644626	5347381	76.20	0.23	11.80	3.81	0.10	0.66	0.83	0.01	0.02	4.50	0.82	0.02	1.81	100.8	0.15
85	MERN19MDS0128BG03	X261174	Powell Tonalite	Ank-Ser	644626	5347381	70.10	0.24	11.25	4.89	0.10	0.98	1.04	0.01	0.02	3.27	1.07	0.02	2.42	95.4	0.23
86	MERN19MDS0128BG04	X261175	Powell Tonalite	Ank-Ser	644626	5347380	77.30	0.23	11.85	4.32	0.11	0.67	0.39	0.01	0.02	4.31	0.93	0.03	1.64	101.8	0.07
87	MERN19MDS0128BG05	X261176	Powell Tonalite	Ank-Ser	644626	5347382	72.20	0.16	10.80	4.50	0.06	1.19	0.48	0.01	0.01	4.10	0.51	0.03	1.93	95.97	0.18
88	MERN19MDS0128BG06	X261177	Powell Tonalite	Ank-Ser	644626	5347382	67.80	0.15	9.85	7.68	0.12	2.00	0.83	0.01	0.01	2.49	0.57	0.02	3.16	94.68	0.33
89	MERN19MDS0128BG07	X261178	Powell Tonalite	Ank-Ser	644626	5347382	73.60	0.20	10.40	5.68	0.15	1.47	1.29	0.01	0.01	3.62	0.70	0.04	3.10	100.26	0.53
90	MERN19MDS0128BG08	X261179	Powell Tonalite	Ank-Ser	644626	5347382	73.90	0.27	11.60	4.82	0.11	0.80	0.53	0.01	0.02	4.33	1.05	0.04	2.09	99.56	0.31
91	MERN20MDS127AG01	C079662	Powell Tonalite	Ank-Ser	642390	5346179	75.90	0.29	12.55	3.10	0.04	0.74	0.94	0.01	0.02	4.59	0.66	0.06	1.74	100.63	0.23
92	MERN20MDS127AG02_dist h	C079664	Powell Tonalite	Ank-Ser	642390	5346179	78.20	0.31	12.80	1.27	0.03	0.22	0.92	0.01	0.03	5.09	0.91	0.07	1.31	101.17	0.2
93	MERN20MDS127AG02_prox h	C079663	Powell Tonalite	Ank-Ser	642390	5346179	69.50	0.30	13.30	2.52	0.13	0.79	3.32	0.01	0.03	5.47	0.89	0.06	3.77	100.09	1.03
94	MERN20MDS127AG03	C079665	Powell Tonalite	Ank-Ser	642390	5346179	75.90	0.28	12.70	3.12	0.02	0.61	0.61	0.01	0.02	4.89	0.59	0.04	1.26	100.04	0.1
95	MERN20MDS127AG06	C079667	Powell Tonalite	Ank-Ser	642348	5346189	72.60	0.22	9.38	3.80	0.06	1.13	1.92	0.01	0.01	4.40	0.69	0.02	4.29	98.53	0.71
96	MERN20MDS127AG07	C079668	Powell Tonalite	Ank-Ser	642348	5346189	73.30	0.27	12.10	4.39	0.02	0.65	1.06	0.01	0.02	5.00	0.96	0.05	1.70	99.52	0.24
97	MERN20MDS127AG08	C079669	Powell Tonalite	Ank-Ser	642347	5346188	73.70	0.27	12.30	4.34	0.02	0.71	0.86	0.01	0.02	5.14	0.90	0.05	1.53	99.84	0.2
98	MERN20MDS127AG09	C079670	Powell Tonalite	Ank-Ser	642347	5346188	74.50	0.27	12.50	4.21	0.03	0.63	1.16	0.01	0.01	5.73	0.70	0.06	1.56	101.36	0.29
99	MERN18MDS0106AG01	X261056	Joliet tonalite	Spilite	646474	5347883	71.30	0.36	13.65	4.61	0.08	0.78	2.61	0.01	0.01	4.50	0.38	0.10	2.78	101.67	0.42
100	MERN19MDS0125EG09	X261074	Joliet tonalite	Spilite	646517	5347856	71.00	0.36	14.25	5.19	0.08	0.87	1.87	0.01	0.02	3.39	0.74	0.11	2.88	100.78	0.33
101	MERN19MDS0125EG28	X261109	Joliet tonalite	Spilite	646510	5347862	70.00	0.35	13.95	5.13	0.07	0.79	2.51	0.02	0.01	3.15	0.57	0.11	3.40	100.07	0.46
102	MERN20MDS186BG13	C079653	Joliet tonalite	Hmt	645742	5347150	77.50	0.18	12.60	3.27	0.05	0.09	0.20	0.01	0.04	5.71	0.89	0.04	0.77	101.35	0.03
103	MERN20MDS200BG01	C079656	Joliet tonalite	Spotted	645997	5347208	75.70	0.11	11.50	3.23	0.03	0.29	0.87	0.01	0.05	3.51	1.79	0.03	1.55	98.66	0.18
104	MERN20MDS201BG08	C079661	Joliet tonalite	Ser	645262	5348013	70.30	0.29	13.25	7.22	0.12	1.37	0.11	0.01	0.03	0.16	3.12	0.07	3.35	99.39	0.01
105	MERN19MDS0141CG04	X261140	Joliet tonalite	Spilite	645996	5347739	75.70	0.20	10.90	5.43	0.07	0.77	0.04	0.01	0.02	3.49	1.29	0.03	1.56	99.5	0.04
106	MERN17MDS0035BG03	X258461	Andesite	Chl	644426	5347363	63.70	1.16	13.45	9.13	0.05	5.93	0.50	0.01	0.02	1.56	1.02	0.34	3.77	100.63	0.02
107	MERN18MDS0099AG05i	X258489	Andesite	Chl	644451	5347921	53.30	1.51	14.60	18.00	0.18	6.31	0.49	0.01	0.02	0.38	0.71	0.37	4.61	100.48	<0.01
108	MERN18MDS0099AG05ii	X261052	Andesite	Chl	644451	5347921	57.80	1.60	15.20	13.90	0.15	4.66	0.63	0.01	0.05	0.13	2.00	0.39	4.18	100.69	0.04
109	MERN18MDS0099AG05iii	X258486	Andesite	Spotted	644451	5347921	55.80	1.46	14.45	15.45	0.17	5.42	0.79	0.01	0.03	0.97	0.93	0.37	4.35	100.19	0.08
110	MERN18MDS0101AG01	X258460	Andesite	Spotted	644602	5347975	60.80	1.27	13.20	13.85	0.12	4.61	0.85	0.01	0.04	0.08	1.46	0.59	3.89	100.76	<0.01
111	MERN18MDS0101BG02	X258468	Andesite	Spotted	644613	5347950	59.40	1.23	13.35	15.10	0.13	5.81	0.85	0.01	0.03	0.10	1.05	0.56	4.26	101.87	0.01
112	MERN18MDS0124AG01	X258500	Andesite	Spilite	644476	5348228	54.60	1.06	13.65	9.99	0.22	7.35	2.56	0.01	0.01	4.83	0.26	0.17	3.34	100.36	0.01
113	MERN19MDS0156AG02	X261151	Andesite	Spotted	644520	5348365	62.10	0.75	14.15	10.85	0.09	4.38	0.13	0.01	0.07	0.04	2.79	0.11	3.80	99.26	0.01
114	MERN19MDS0158AG01	X261155	Andesite	Spilite	644520	5348391	56.80	1.04	15.50	8.05	0.15	5.94	1.34	0.01	0.01	5.32	0.09	0.16	3.90	98.31	0.2
115	MERN18MDS0098AG04	X258447	Andesite	Spotted	644609	5348031	56.00	1.00	14.95	14.80	0.27	6.96	0.23	0.01	0.04	0.39	1.22	0.16	4.73	100.76	0.01
116	MERN18MDS0098AG05	X258442	Andesite	Spilite	644616	5348043	57.90	0.98	14.60	11.80	0.22	6.65	0.28	0.01	0.01	3.23	0.05	0.14	4.02	99.88	0.02
117	MERN18MDS0098AG06	X258499	Andesite	Spilite	644609	5348031	54.90	0.99	15.30	12.20	0.24	6.96	0.29	0.01	0.01	3.52	0.08	0.18	4.23	98.9	0.01
118	MERN18MDS0098AG07	X258448	Andesite	Spilite	644616	5348043	53.00	1.02	15.45	10.30	0.31	6.23	3.37	0.01	0.01	3.73	0.45	0.16	6.14	100.18	0.73
119	MERN18MDS0098AG08	X258449	Andesite	Spotted	644616	5348043	54.10	0.98	14.95	14.60	0.25	7.23	0.22	0.01	0.04	0.05	1.53	0.15	5.09	99.21	0.02
120	MERN18MDS0099AG01	X258451	Andesite	Spilite	644419	5347923	52.80	1.39	13.75	10.20	0.42	3.98	3.80	0.01	0.01	4.70	0.16	0.34	6.45	98.01	1.33
121	MERN18MDS0099AG02	X258452	Andesite	Spotted	644419	5347923	60.20	1.36	14.05	12.90	0.13	4.52	0.80	0.01	0.05	0.12	1.65	0.58	3.93	100.29	0.02
122	MERN18MDS0100AG01	X258453	Andesite	Spotted	644482	5347947	57.90	1.26	12.95	16.15	0.09	4.08	0.74	0.01	0.04	0.04	0.99	0.54	3.91	98.69	0.02
123	MERN19MDS0153BG02	X261148	Andesite	Spilite	646297	5348043	56.50	1.20	14.90	11.20	0.23	6.33	0.26	0.01	0.01	3.46	0.12	0.15	3.98	98.33	0.01
124	MERN20MDS201AG01	C079657	Andesite	Spilite	645265	5348054	57.30	1.03	15.80	11.40	0.26	4.69	1.12	0.01	0.02	3.09	0.91	0.17	3.38	99.18	0.01

	Field Number	Lab ID	Rock Type	Alteration	UTM-East	UTM-North	S_%	H20+_%	S.G.	Ag ppm	As ppm	Au_ppm	Ba ppm	Bi ppm	Cd ppm	Ce ppm	Co ppm	Cr ppm	Cs ppm	Cu ppm	Dy ppm
Method					**NAD 83**	**NAD 83**	**S-IR08**	**OA-IR06**	**OA-GRA08b**	**ME-4ACD81**	**ME-MS42**	**Au-ICP21**	**ME-MS81**	**ME-MS42**	**ME-4ACD81**	**ME-MS81**	**ME-4ACD8**	**ME-MS81**	**ME-MS81**	**ME-4ACD81**	**ME-MS81**
Detection Limit							**0.01**	**0.01**		**0.5**	**0.1**		**0.5**	**0.01**	**0.5**	**0.1**	**1**	**1**	**0.05**	**1**	**0.05**
83	MERN18MDS0087AG01	X258444	Powell Tonalite	Spotted	644635	5347296	0.01	3.32	2.68	0.25	0.05		129.5		0.25	40.2	4	20	0.25	15	7.9
84	MERN19MDS0128BG02	X261173	Powell Tonalite	Ank-Ser	644626	5347381	0.01	1.17	2.76												
85	MERN19MDS0128BG03	X261174	Powell Tonalite	Ank-Ser	644626	5347381	0.03	1.82	2.83												
86	MERN19MDS0128BG04	X261175	Powell Tonalite	Ank-Ser	644626	5347380	0.04	1.33	2.82												
87	MERN19MDS0128BG05	X261176	Powell Tonalite	Ank-Ser	644626	5347382	0.03	1.56	2.84												
88	MERN19MDS0128BG06	X261177	Powell Tonalite	Ank-Ser	644626	5347382	0.02	3.22	2.81												
89	MERN19MDS0128BG07	X261178	Powell Tonalite	Ank-Ser	644626	5347382	0.21	2.09	2.76												
90	MERN19MDS0128BG08	X261179	Powell Tonalite	Ank-Ser	644626	5347382	0.21	5.25	2.78												
91	MERN20MDS127AG01	C079662	Powell Tonalite	Ank-Ser	642390	5346179	0.13	1.1	2.72												
92	MERN20MDS127AG02_dist h	C079664	Powell Tonalite	Ank-Ser	642390	5346179	0.21	0.72	2.63	0.25	0.3		281	0.23	<0.5	32	4	30	0.37	24	4.62
93	MERN20MDS127AG02_prox h	C079663	Powell Tonalite	Ank-Ser	642390	5346179	0.2	0.69	2.7	0.25	0.3		313	0.22	<0.5	43.5	6	30	0.52	39	4.72
94	MERN20MDS127AG03	C079665	Powell Tonalite	Ank-Ser	642390	5346179	0.17	1.09	2.71												
95	MERN20MDS127AG06	C079667	Powell Tonalite	Ank-Ser	642348	5346189	2.23	0.57	2.71												
96	MERN20MDS127AG07	C079668	Powell Tonalite	Ank-Ser	642348	5346189	0.88	1.18	2.73												
97	MERN20MDS127AG08	C079669	Powell Tonalite	Ank-Ser	642347	5346188	0.25	1.12	2.75												
98	MERN20MDS127AG09	C079670	Powell Tonalite	Ank-Ser	642347	5346188	0.34	0.81	2.71												
99	MERN18MDS0106AG01	X261056	Joliet tonalite	Spilite	646474	5347883	0.1		2.74	0.25	0.6		89.4	0.05	0.6	33.1	6	10	0.2	19	4.62
100	MERN19MDS0125EG09	X261074	Joliet tonalite	Spilite	646517	5347856	0.53			0.25	1.4		184	0.3	0.25	37.2	13	30	0.47	57	5.2
101	MERN19MDS0125EG28	X261109	Joliet tonalite	Spilite	646510	5347862	0.8			0.25	1.1		131.5	0.37	0.25	40.7	10	20	0.34	60	5.48
102	MERN20MDS186BG13	C079653	Joliet tonalite	Hmt	645742	5347150	0.16	0.51	2.71												
103	MERN20MDS200BG01	C079656	Joliet tonalite	Spotted	645997	5347208	0.23	0.94	2.7												
104	MERN20MDS201BG08	C079661	Joliet tonalite	Ser	645262	5348013	1.19	3.11	2.81	0.5	0.1		281	0.43	1.7	29.9	8	10	0.48	245	4.31
105	MERN19MDS0141CG04	X261140	Joliet tonalite	Spilite	645996	5347739	0.07			0.25	0.1		185	0.04	<0.5	51.4	1	10	0.72	14	10.7
106	MERN17MDS0035BG03	X258461	Andesite	Chl	644426	5347363	<0.01		2.75	0.25	0.2		230	0.05	0.25	37.6	11	10	0.34	10	7.25
107	MERN18MDS0099AG05i	X258489	Andesite	Chl	644451	5347921	<0.01		2.75												
108	MERN18MDS0099AG05ii	X261052	Andesite	Chl	644451	5347921	<0.01		2.74												
109	MERN18MDS0099AG05iii	X258486	Andesite	Spotted	644451	5347921	0.04		2.73												
110	MERN18MDS0101AG01	X258460	Andesite	Spotted	644602	5347975	0.01		2.75												
111	MERN18MDS0101BG02	X258468	Andesite	Spotted	644613	5347950	0.08		2.69												
112	MERN18MDS0124AG01	X258500	Andesite	Spilite	644476	5348228	0.01		2.7	0.25	0.2		80.5	0.01	1	32.3	28	50	0.57	2	3.65
113	MERN19MDS0156AG02	X261151	Andesite	Spotted	644520	5348365	<0.01	5.17	2.73												
114	MERN19MDS0158AG01	X261155	Andesite	Spilite	644520	5348391	0.01	4.18	2.78												
115	MERN18MDS0098AG04	X258447	Andesite	Spotted	644609	5348031	0.05	6.28	2.85	0.25	0.3		355		0.25	27.5	29	80	0.41	525	3.64
116	MERN18MDS0098AG05	X258442	Andesite	Spilite	644616	5348043	0.04	4.62	2.75	0.25	0.3		21.9	0.13	0.25	33.8	28	80	0.18	444	3.88
117	MERN18MDS0098AG06	X258499	Andesite	Spilite	644609	5348031	0.01		2.78												
118	MERN18MDS0098AG07	X258448	Andesite	Spilite	644616	5348043	0.01	4.05	2.67	0.25	0.05		83		0.9	29.2	19	80	0.23	9	4.19
119	MERN18MDS0098AG08	X258449	Andesite	Spotted	644616	5348043	0.01	6.14	2.76	0.25	0.05		369		0.25	29.5	24	90	0.62	61	4.35
120	MERN18MDS0099AG01	X258451	Andesite	Spilite	644419	5347923	0.16	2.68	2.69	0.25	0.4		62.7		0.9	18.2	18	20	0.08	336	3.85
121	MERN18MDS0099AG02	X258452	Andesite	Spotted	644419	5347923	0.01	5.37	2.78	0.25	0.1		430		0.25	25.5	21	5	0.31	2	5.39
122	MERN18MDS0100AG01	X258453	Andesite	Spotted	644482	5347947	0.01	5.73	3.05	0.25	0.2		370		0.6	25	23	5	0.26	6	3.53
123	MERN19MDS0153BG02	X261148	Andesite	Spilite	646297	5348043	0.33			0.25	5.1		41.7	0.4	<0.5	27.9	25	10	0.1	37	4.18
124	MERN20MDS201AG01	C079657	Andesite	Spilite	645265	5348054	<0.01	4.64	2.9	0.25	0.5		142.5	0.01	1.5	32.5	8	30	0.35	9	4.2

	Field Number	Lab ID	Rock Type	Alteration	UTM-East	UTM-North	Er ppm	Eu ppm	Ga_ppm	Gd_ppm	Ge_ppm	Hf_ppm	Hg_ppm	Ho_ppm	In_ppm	La_ppm	Li_ppm	Lu_ppm	Mo_ppm	Nb_ppm	Nd_ppm
Method					**NAD 83**	**NAD 83**	**ME-MS81**	**ME-MS81**	**ME-MS81**	**ME-MS81**	**ME-MS81**	**ME-MS81**	**ME-MS42**	**ME-MS81**	**ME-MS42**	**ME-MS81**	**ME-4ACD81**	**ME-MS81**	**ME-4ACD81**	**ME-MS81**	**ME-MS81**
Detection Limit							**0.03**	**0.03**	**0.1**	**0.05**	**5**	**0.2**	**0.005**	**0.01**	**0.005**	**0.1**	**10**	**0.01**	**1**	**0.2**	**0.1**
83	MERN18MDS0087AG01	X258444	Powell Tonalite	Spotted	644635	5347296	5.38	0.95	22.1	7.01	2.5	5.5	0	1.69	0.05	16.9	40	0.75	0.5	13.3	22.3
84	MERN19MDS0128BG02	X261173	Powell Tonalite	Ank-Ser	644626	5347381															
85	MERN19MDS0128BG03	X261174	Powell Tonalite	Ank-Ser	644626	5347381															
86	MERN19MDS0128BG04	X261175	Powell Tonalite	Ank-Ser	644626	5347380															
87	MERN19MDS0128BG05	X261176	Powell Tonalite	Ank-Ser	644626	5347382															
88	MERN19MDS0128BG06	X261177	Powell Tonalite	Ank-Ser	644626	5347382															
89	MERN19MDS0128BG07	X261178	Powell Tonalite	Ank-Ser	644626	5347382															
90	MERN19MDS0128BG08	X261179	Powell Tonalite	Ank-Ser	644626	5347382															
91	MERN20MDS127AG01	C079662	Powell Tonalite	Ank-Ser	642390	5346179															
92	MERN20MDS127AG02_dist h	C079664	Powell Tonalite	Ank-Ser	642390	5346179	3.52	0.82	13.5	4.1	<5	5.9	<0.005	1.1	0.008	16.1	<10	0.63	2	8.2	16.5
93	MERN20MDS127AG02_prox h	C079663	Powell Tonalite	Ank-Ser	642390	5346179	3.48	1.14	16.1	4.65	<5	6.2	<0.005	1	0.042	22.4	<10	0.66	2	8.6	22.4
94	MERN20MDS127AG03	C079665	Powell Tonalite	Ank-Ser	642390	5346179															
95	MERN20MDS127AG06	C079667	Powell Tonalite	Ank-Ser	642348	5346189															
96	MERN20MDS127AG07	C079668	Powell Tonalite	Ank-Ser	642348	5346189															
97	MERN20MDS127AG08	C079669	Powell Tonalite	Ank-Ser	642347	5346188															
98	MERN20MDS127AG09	C079670	Powell Tonalite	Ank-Ser	642347	5346188															
99	MERN18MDS0106AG01	X261056	Joliet tonalite	Spilite	646474	5347883	3.31	0.93	16.4	4.17	2.5	4.4	0.0025	1.05	0.055	16.3	20	0.58	1	8	17.2
100	MERN19MDS0125EG09	X261074	Joliet tonalite	Spilite	646517	5347856	3.51	1.3	17.4	5.11	2.5	5.2	0.006	1.19	0.019	16.9	20	0.62	3	9.1	18.9
101	MERN19MDS0125EG28	X261109	Joliet tonalite	Spilite	646510	5347862	3.56	1.51	16.8	5.45	2.5	5.1	0.0025	1.2	0.027	19.1	20	0.6	2	9.1	21
102	MERN20MDS186BG13	C079653	Joliet tonalite	Hmt	645742	5347150															
103	MERN20MDS200BG01	C079656	Joliet tonalite	Spotted	645997	5347208															
104	MERN20MDS201BG08	C079661	Joliet tonalite	Ser	645262	5348013	3.16	1.03	17	3.42	<5	4.7	<0.005	0.99	0.094	14.4	10	0.66	2	8.6	15.7
105	MERN19MDS0141CG04	X261140	Joliet tonalite	Spilite	645996	5347739	7.26	1.48	20.2	8.87	<5	8.4	<0.005	2.35	0.013	20	10	1.13	1	13.5	32.6
106	MERN17MDS0035BG03	X258461	Andesite	Chl	644426	5347363	4.38	1.18	21.5	7.01	2.5	4.3	0.0025	1.66	0.018	15.6	40	0.68	0.5	8.5	22.6
107	MERN18MDS0099AG05i	X258489	Andesite	Chl	644451	5347921															
108	MERN18MDS0099AG05ii	X261052	Andesite	Chl	644451	5347921															
109	MERN18MDS0099AG05iii	X258486	Andesite	Spotted	644451	5347921															
110	MERN18MDS0101AG01	X258460	Andesite	Spotted	644602	5347975															
111	MERN18MDS0101BG02	X258468	Andesite	Spotted	644613	5347950															
112	MERN18MDS0124AG01	X258500	Andesite	Spilite	644476	5348228	2.43	0.89	15.5	3.79	2.5	3.4	0.0025	0.81	0.0025	15.4	20	0.37	0.5	6.4	17.5
113	MERN19MDS0156AG02	X261151	Andesite	Spotted	644520	5348365															
114	MERN19MDS0158AG01	X261155	Andesite	Spilite	644520	5348391															
115	MERN18MDS0098AG04	X258447	Andesite	Spotted	644609	5348031	2.21	0.9	18.5	3.76	2.5	3.1	0	0.8	0.14	10.8	30	0.34	1	6.6	14.8
116	MERN18MDS0098AG05	X258442	Andesite	Spilite	644616	5348043	2.27	1.2	17.7	4.16	2.5	3.3	0	0.8	0.14	13.3	30	0.36	1	6.7	18.9
117	MERN18MDS0098AG06	X258499	Andesite	Spilite	644609	5348031															
118	MERN18MDS0098AG07	X258448	Andesite	Spilite	644616	5348043	2.7	1.13	19.3	3.81	2.5	3.4	0	0.89	0.12	11.7	20	0.4	1	6.7	17.2
119	MERN18MDS0098AG08	X258449	Andesite	Spotted	644616	5348043	2.8	0.74	19	4.05	2.5	3.2	0	0.88	0.1	12	30	0.38	1	6.5	17
120	MERN18MDS0099AG01	X258451	Andesite	Spilite	644419	5347923	2.59	1.26	18.4	3.76	2.5	2.1	0	0.8	0.13	7.6	10	0.37	1	4.8	12.2
121	MERN18MDS0099AG02	X258452	Andesite	Spotted	644419	5347923	3.45	1.18	21.1	5.79	2.5	3	0	1.16	0.03	10.5	20	0.51	1	5.8	16.5
122	MERN18MDS0100AG01	X258453	Andesite	Spotted	644482	5347947	2.53	0.73	19	4.22	2.5	2.5	0	0.8	0.06	10.2	20	0.34	1	5.1	16.1
123	MERN19MDS0153BG02	X261148	Andesite	Spilite	646297	5348043	2.67	0.84	21.3	4.35	<5	3.7	<0.005	0.93	0.043	12.2	20	0.41	2	6.1	15.9
124	MERN20MDS201AG01	C079657	Andesite	Spilite	645265	5348054	2.62	1.42	15.7	4.18	<5	3.4	<0.005	0.83	0.195	14.2	20	0.38	1	6.2	18.6

	Field Number	Lab ID	Rock Type	Alteration	UTM-East	UTM-North	Ni_ppm	Pb_ppm	Rb_ppm	Re_ppm	Sb_ppm	Sc_ppm	Se_ppm	Sm_ppm	Sn_ppm	Sr_ppm	Ta_ppm	Tb_ppm	Te_ppm	Th_ppm	Tl_ppm
Method					**NAD 83**	**NAD 83**	**ME-4ACD81**	**ME-4ACD81**	**ME-MS81**	**ME-MS42**	**ME-MS42**	**ME-4ACD81**	**ME-MS42**	**ME-MS81**	**ME-MS81**	**ME-MS81**	**ME-MS81**	**ME-MS81**	**ME-MS42**	**ME-MS81**	**ME-MS42**
Detection Limit							**1**	**2**	**0.2**	**0.001**	**0.05**	**1**	**0.2**	**0.03**	**1**	**0.1**	**0.1**	**0.01**	**0.01**	**0.05**	**0.02**
83	MERN18MDS0087AG01	X258444	Powell Tonalite	Spotted	644635	5347296	2	1	16.1	0	0.03	16	0.1	5.78	4	14.9	0.7	1.48	0.01	1.82	0.01
84	MERN19MDS0128BG02	X261173	Powell Tonalite	Ank-Ser	644626	5347381															
85	MERN19MDS0128BG03	X261174	Powell Tonalite	Ank-Ser	644626	5347381															
86	MERN19MDS0128BG04	X261175	Powell Tonalite	Ank-Ser	644626	5347380															
87	MERN19MDS0128BG05	X261176	Powell Tonalite	Ank-Ser	644626	5347382															
88	MERN19MDS0128BG06	X261177	Powell Tonalite	Ank-Ser	644626	5347382															
89	MERN19MDS0128BG07	X261178	Powell Tonalite	Ank-Ser	644626	5347382															
90	MERN19MDS0128BG08	X261179	Powell Tonalite	Ank-Ser	644626	5347382															
91	MERN20MDS127AG01	C079662	Powell Tonalite	Ank-Ser	642390	5346179															
92	MERN20MDS127AG02_dist h	C079664	Powell Tonalite	Ank-Ser	642390	5346179	5	<2	20.5	<0.001	<0.05	6	<0.2	3.69	2	79.4	1.1	0.72	0.08	3.2	<0.02
93	MERN20MDS127AG02_prox h	C079663	Powell Tonalite	Ank-Ser	642390	5346179	2	<2	23.2	<0.001	<0.05	6	0.2	5.05	2	109.5	0.7	0.74	0.07	3.72	<0.02
94	MERN20MDS127AG03	C079665	Powell Tonalite	Ank-Ser	642390	5346179															
95	MERN20MDS127AG06	C079667	Powell Tonalite	Ank-Ser	642348	5346189															
96	MERN20MDS127AG07	C079668	Powell Tonalite	Ank-Ser	642348	5346189															
97	MERN20MDS127AG08	C079669	Powell Tonalite	Ank-Ser	642347	5346188															
98	MERN20MDS127AG09	C079670	Powell Tonalite	Ank-Ser	642347	5346188															
99	MERN18MDS0106AG01	X261056	Joliet tonalite	Spilite	646474	5347883	12	1	7.7	0.0005	0.05	9	0.1	4.2	4	142.5	0.5	0.8	0.01	2.38	0.01
100	MERN19MDS0125EG09	X261074	Joliet tonalite	Spilite	646517	5347856	4	4	15.7	0.0005	0.11	10	0.3	4.76	4	139	0.7	0.86	0.08	2.71	0.01
101	MERN19MDS0125EG28	X261109	Joliet tonalite	Spilite	646510	5347862	0.5	2	11.5	0.0005	0.07	9	0.5	5.2	3	154.5	0.6	0.93	0.06	2.47	0.01
102	MERN20MDS186BG13	C079653	Joliet tonalite	Hmt	645742	5347150															
103	MERN20MDS200BG01	C079656	Joliet tonalite	Spotted	645997	5347208															
104	MERN20MDS201BG08	C079661	Joliet tonalite	Ser	645262	5348013	4	<2	62.5	<0.001	<0.05	8	0.5	3.68	25	5.7	0.7	0.58	0.18	2.98	0.02
105	MERN19MDS0141CG04	X261140	Joliet tonalite	Spilite	645996	5347739	<1	<2	34.1	<0.001	<0.05	11	<0.2	8.26	2	24.6	1.1	1.57	0.03	3.44	0.02
106	MERN17MDS0035BG03	X258461	Andesite	Chl	644426	5347363	6	2	20.6	0.0005	0.09	24	0.1	5.81	2	17.6	0.6	1.22	0.02	1.5	0.01
107	MERN18MDS0099AG05i	X258489	Andesite	Chl	644451	5347921															
108	MERN18MDS0099AG05ii	X261052	Andesite	Chl	644451	5347921															
109	MERN18MDS0099AG05iii	X258486	Andesite	Spotted	644451	5347921															
110	MERN18MDS0101AG01	X258460	Andesite	Spotted	644602	5347975															
111	MERN18MDS0101BG02	X258468	Andesite	Spotted	644613	5347950															
112	MERN18MDS0124AG01	X258500	Andesite	Spilite	644476	5348228	52	1	6.9	0.0005	0.025	25	0.2	3.97	1	60.2	0.3	0.65	0.01	1.32	0.03
113	MERN19MDS0156AG02	X261151	Andesite	Spotted	644520	5348365															
114	MERN19MDS0158AG01	X261155	Andesite	Spilite	644520	5348391															
115	MERN18MDS0098AG04	X258447	Andesite	Spotted	644609	5348031	72	1	17.2	0	0.05	19	0.7	3.66	3	4.3	0.3	0.68	0.03	1.24	0.01
116	MERN18MDS0098AG05	X258442	Andesite	Spilite	644616	5348043	73	3	0.6	0	0.05	21	0.5	4.55	1	13.1	0.3	0.77	0.05	1.31	0.01
117	MERN18MDS0098AG06	X258499	Andesite	Spilite	644609	5348031															
118	MERN18MDS0098AG07	X258448	Andesite	Spilite	644616	5348043	70	1	9.1	0	0.03	21	0.2	3.83	2	44	0.3	0.7	0.01	1.23	0.01
119	MERN18MDS0098AG08	X258449	Andesite	Spotted	644616	5348043	71	1	26	0	0.03	22	0.1	4.12	4	3.6	0.3	0.73	0.01	1.28	0.01
120	MERN18MDS0099AG01	X258451	Andesite	Spilite	644419	5347923	10	6	2.9	0	0.19	29	0.7	2.94	3	79.5	0.2	0.7	0.01	0.83	0.01
121	MERN18MDS0099AG02	X258452	Andesite	Spotted	644419	5347923	2	1	28	0	0.03	26	0.1	4.48	3	9.8	0.3	0.99	0.01	1.01	0.01
122	MERN18MDS0100AG01	X258453	Andesite	Spotted	644482	5347947	1	1	16.3	0	0.03	25	0.2	3.98	2	10.9	0.2	0.62	0.01	0.91	0.01
123	MERN19MDS0153BG02	X261148	Andesite	Spilite	646297	5348043	13	2	2.1	0.001	<0.05	21	0.4	4.39	3	26.3	0.5	0.65	0.1	1.77	<0.02
124	MERN20MDS201AG01	C079657	Andesite	Spilite	645265	5348054	29	<2	20.4	0.001	<0.05	22	<0.2	3.79	19	31.3	0.4	0.65	<0.01	1.41	<0.02

	Field Number	Lab ID	Rock Type	Alteration	UTM-East	UTM-North	Tm_ppm	U_ppm	V_ppm	W_ppm	Y_ppm	Yb_ppm	Zn_ppm	Zr_ppm
Method					**NAD 83**	**NAD 83**	**ME-MS81**	**ME-MS81**	**ME-MS81**	**ME-MS81**	**ME-MS81**	**ME-MS81**	**ME4ACD81**	**ME-MS81**
Detection Limit							**0.01**	**0.05**	**5**	**1**	**0.1**	**0.03**	**2**	**2**
83	MERN18MDS0087AG01	X258444	Powell Tonalite	Spotted	644635	5347296	0.77	0.66	11	1	51.4	5.15	371	212
84	MERN19MDS0128BG02	X261173	Powell Tonalite	Ank-Ser	644626	5347381					28.1			238
85	MERN19MDS0128BG03	X261174	Powell Tonalite	Ank-Ser	644626	5347381					23.9			179
86	MERN19MDS0128BG04	X261175	Powell Tonalite	Ank-Ser	644626	5347380					26.9			176
87	MERN19MDS0128BG05	X261176	Powell Tonalite	Ank-Ser	644626	5347382					43.4			266
88	MERN19MDS0128BG06	X261177	Powell Tonalite	Ank-Ser	644626	5347382					148			283
89	MERN19MDS0128BG07	X261178	Powell Tonalite	Ank-Ser	644626	5347382					95			287
90	MERN19MDS0128BG08	X261179	Powell Tonalite	Ank-Ser	644626	5347382					48.3			163
91	MERN20MDS127AG01	C079662	Powell Tonalite	Ank-Ser	642390	5346179					35.4			202
92	MERN20MDS127AG02_dist h	C079664	Powell Tonalite	Ank-Ser	642390	5346179	0.51	0.88	18	2	32.5	3.9	6	208
93	MERN20MDS127AG02_prox h	C079663	Powell Tonalite	Ank-Ser	642390	5346179	0.58	1	21	15	30.6	4.03	12	217
94	MERN20MDS127AG03	C079665	Powell Tonalite	Ank-Ser	642390	5346179					32.3			192
95	MERN20MDS127AG06	C079667	Powell Tonalite	Ank-Ser	642348	5346189					30.7			143
96	MERN20MDS127AG07	C079668	Powell Tonalite	Ank-Ser	642348	5346189					34.8			166
97	MERN20MDS127AG08	C079669	Powell Tonalite	Ank-Ser	642347	5346188					34.4			177
98	MERN20MDS127AG09	C079670	Powell Tonalite	Ank-Ser	642347	5346188					34.3			175
99	MERN18MDS0106AG01	X261056	Joliet tonalite	Spilite	646474	5347883	0.49	0.64	19	0.5	28.2	3.46	98	192
100	MERN19MDS0125EG09	X261074	Joliet tonalite	Spilite	646517	5347856	0.59	0.71	27	1	34	4.16	54	185
101	MERN19MDS0125EG28	X261109	Joliet tonalite	Spilite	646510	5347862	0.57	0.67	25	1	34	3.96	50	185
102	MERN20MDS186BG13	C079653	Joliet tonalite	Hmt	645742	5347150					85			260
103	MERN20MDS200BG01	C079656	Joliet tonalite	Spotted	645997	5347208					104			183
104	MERN20MDS201BG08	C079661	Joliet tonalite	Ser	645262	5348013	0.52	0.79	34	2	27.9	3.9	433	169
105	MERN19MDS0141CG04	X261140	Joliet tonalite	Spilite	645996	5347739	1.13	0.91	<5	2	63.9	7.22	43	320
106	MERN17MDS0035BG03	X258461	Andesite	Chl	644426	5347363	0.67	0.46	61	2	42.5	4.19	78	157
107	MERN18MDS0099AG05i	X258489	Andesite	Chl	644451	5347921					23.2			84
108	MERN18MDS0099AG05ii	X261052	Andesite	Chl	644451	5347921					25.1			90
109	MERN18MDS0099AG05iii	X258486	Andesite	Spotted	644451	5347921					22.2			85
110	MERN18MDS0101AG01	X258460	Andesite	Spotted	644602	5347975					29.9			99
111	MERN18MDS0101BG02	X258468	Andesite	Spotted	644613	5347950					29.3			100
112	MERN18MDS0124AG01	X258500	Andesite	Spilite	644476	5348228	0.38	0.41	198	1	20.7	2.43	81	154
113	MERN19MDS0156AG02	X261151	Andesite	Spotted	644520	5348365					31.1			205
114	MERN19MDS0158AG01	X261155	Andesite	Spilite	644520	5348391					22.7			131
115	MERN18MDS0098AG04	X258447	Andesite	Spotted	644609	5348031	0.34	0.31	124	1	22.5	2.15	430	123
116	MERN18MDS0098AG05	X258442	Andesite	Spilite	644616	5348043	0.31	0.34	128	1	22.9	2.3	373	126
117	MERN18MDS0098AG06	X258499	Andesite	Spilite	644609	5348031					23.6			129
118	MERN18MDS0098AG07	X258448	Andesite	Spilite	644616	5348043	0.36	0.28	133	1	26	2.47	412	126
119	MERN18MDS0098AG08	X258449	Andesite	Spotted	644616	5348043	0.36	0.33	130	1	26.7	2.56	534	126
120	MERN18MDS0099AG01	X258451	Andesite	Spilite	644419	5347923	0.36	0.22	171	1	24.5	2.5	143	85
121	MERN18MDS0099AG02	X258452	Andesite	Spotted	644419	5347923	0.51	0.28	56	1	33.9	3.03	122	104
122	MERN18MDS0100AG01	X258453	Andesite	Spotted	644482	5347947	0.31	0.25	50	4	21.5	2.18	87	94
123	MERN19MDS0153BG02	X261148	Andesite	Spilite	646297	5348043	0.43	0.41	275	1	25.2	2.55	160	151
124	MERN20MDS201AG01	C079657	Andesite	Spilite	645265	5348054	0.34	0.37	204	3	23.3	2.43	265	132

	Field Number	Lab ID	Rock Type	Alteration	UTM-East	UTM-North	SiO2_wt%	TiO2_wt%	Al2O3_wt%	Fe2O3t_wt%	MnO_wt%	MgO_wt%	CaO_wt%	SrO wt%	BaO wt%	Na2O_wt%	K2O_wt%	P2O5_wt%	LOI_%	Total_wt%	C_%
Method					NAD 83	NAD 83	ME-ICP06	ME-ICP06	ME-ICP06	ME-ICP06	ME-ICP06	ME-ICP06	ME-ICP06	ME-ICP06	ME-ICP06	ME-ICP06	ME-ICP06	ME-ICP06	OA-GRA05		C-IR07
Detection Limit							0.01	0.01	0.01	0.01	0.01	0.01	0.01	0.01	0.01	0.01	0.01	0.01	0.01		0.01
125	MERN20MDS201AG03	C079658	Andesite	Spotted	645265	5348054	54.60	1.10	16.65	13.35	0.29	5.18	1.02	0.01	0.03	0.85	2.04	0.19	4.26	99.57	0.01
126	MERN17MDS0030AG02	X258481	Andesite	Spotted	645036	5347711	63.00	0.74	13.85	11.80	0.10	3.71	0.31	0.01	0.06	0.18	1.65	0.26	3.80	99.46	0.01
127	MERN17MDS0031AG07i	X258485	Andesite	Spilite	645240	5347733	62.30	1.20	14.70	8.08	0.20	5.94	0.42	0.01	0.01	4.44	0.09	0.16	3.83	101.36	0.26
128	MERN17MDS0031AG07ii	X261051	Andesite	Spotted	645240	5347733	54.80	1.22	14.90	12.25	0.12	8.92	0.26	0.01	0.02	0.69	0.61	0.17	5.34	99.3	0.05
129	MERN17MDS0064DG04	X258482	Andesite	Spilite	645355	5347769	63.20	1.23	14.95	8.37	0.10	5.97	0.26	0.01	0.01	4.50	0.04	0.18	3.17	101.97	0.04
130	MERN18MDS0084CG01	X258432	Andesite	Spotted	645667	5348114	63.90	0.98	11.10	15.60	0.19	4.26	0.27	0.01	0.01	0.46	0.33	0.15	3.60	100.85	0.03
131	MERN18MDS0085EG11	X258436	Andesite	Chl	645776	5348159	58.30	1.26	13.05	14.50	0.27	4.75	0.44	0.01	0.03	0.09	1.17	0.31	4.03	98.2	0.02
132	MERN18MDS0108AG01	X258470	Andesite	Spilite	645622	5347834	63.70	0.65	14.80	8.83	0.15	3.85	0.36	0.01	0.02	4.13	0.49	0.21	3.25	100.44	0.18
133	MERN18MDS0109AG01	X258474	Andesite	Spotted	645563	5347825	69.60	0.66	13.65	5.98	0.10	3.06	0.32	0.01	0.03	4.07	0.72	0.23	2.33	100.75	<0.01
134	MERN18MDS0112AG01	X258494	Andesite	Spilite	645748	5347867	52.50	1.33	13.65	11.35	0.24	7.78	1.63	0.01	0.01	3.97	0.08	0.14	5.05	100.71	0.27
135	MERN18MDS0113AG01	X258478	Andesite	Spilite	645805	5347679	59.10	1.24	13.65	9.49	0.12	6.55	0.47	0.01	0.01	4.16	0.10	0.17	3.86	100.32	0.06
136	MERN18MDS0114AG01	X258493	Andesite	Spotted	645819	5347735	60.00	1.21	13.50	12.50	0.09	5.06	0.79	0.01	0.04	0.46	1.24	0.32	4.38	99.59	0.16
137	MERN18MDS0114AG02	X258475	Andesite	Spotted	645819	5347735	60.90	1.24	13.65	12.20	0.11	6.65	0.35	0.01	0.03	0.12	1.06	0.23	4.62	101.31	0.03
138	MERN18MDS0118AG01	X258466	Andesite	Spilite	645590	5347983	59.70	1.39	14.50	10.05	0.08	4.16	0.72	0.01	0.01	4.05	0.27	0.36	3.19	98.48	0.06
139	MERN18MDS0118AG02	X258491	Andesite	Spilite	645590	5347983	61.00	1.39	13.65	9.69	0.20	4.01	0.97	0.01	0.01	4.55	0.04	0.36	2.98	99.35	0.08
140	MERN19MDS0153BG03	X261149	Andesite	Spilite	646297	5348043	63.50	1.10	13.25	8.05	0.13	5.00	0.26	0.01	0.01	3.55	0.22	0.15	2.83	98.05	0.02
141	MERN18MDS0119AG01	X258462	Andesite		645630	5348024	73.30	1.29	10.65	7.23	0.06	1.15	0.44	0.01	0.03	2.97	0.72	0.07	1.61	99.52	<0.01
142	MERN18MDS0085CG07	X258435	Mafic tuff	Spotted	645724	5348195	55.30	0.68	15.25	17.30	0.52	5.17	0.17	0.01	0.05	0.65	1.43	0.08	4.42	101.02	0.03
143	MERN18MDS0085CG12i	X258488	Mafic tuff	Spotted	645737	5348188	50.40	0.75	17.85	21.10	0.38	3.98	0.11	0.01	0.07	0.29	2.10	0.10	4.38	101.52	<0.01
144	MERN18MDS0085CG12ii	X258487	Mafic tuff	Chl	645737	5348188	50.20	0.73	17.30	19.95	0.36	3.76	0.12	0.01	0.07	0.30	2.15	0.09	4.28	99.32	0.01
145	MERN18MDS0115BG03	X258459	Mafic tuff	Spotted	645851	5347849	55.80	0.81	17.30	11.30	0.12	6.67	1.02	0.01	0.09	1.46	1.93	0.13	4.85	101.48	0.12
146	MERN18MDS0064EG05	X258492	Lamprophyre	Spilite	645354	5347768	47.50	1.18	13.65	11.60	0.27	4.90	5.98	0.01	0.02	4.11	0.48	0.11	10.35	100.08	2.35
147	MERN18MDS0078BG02	X258431	Lamprophyre		645507	5347994	42.20	0.60	9.59	9.01	0.22	9.90	10.30	0.03	0.05	2.14	0.30	0.28	16.70	101.43	4.03
148	MERN19MDS0152AG01	X261162	Lamprophyre	Spilite	646504	5348319	65.00	0.63	13.50	10.05	0.17	3.42	0.44	0.01	0.01	4.01	0.03	0.21	2.62	100.08	0.02
149	MERN19MDS0152AG01	X261146	Lamprophyre		646504	5348320	46.50	0.52	11.65	9.40	0.21	17.45	9.09	0.02	0.07	1.37	1.22	0.32	3.90	101.93	0.03
150	MERN20MDS127CG04	C079666	Lamprophyre?	Ank-Ser	642344	5346169	35.30	0.31	7.29	7.66	0.35	7.46	15.75	0.01	0.12	1.41	1.57	0.26	23.40	100.99	6.53
151	MERN17MDS0034AG06	X258407	Mafic dike	Spotted	644449	5347294	52.30	1.41	15.65	13.60	0.17	8.80	0.14	0.01	0.04	0.04	1.44	0.10	5.56	99.26	0.02
152	MERN18MDS0068AG01	X258469	Mafic dike	Spilite	645454	5347795	49.60	1.40	13.45	14.70	0.20	5.99	7.92	0.02	0.01	2.97	0.44	0.18	2.53	99.42	0.09
153	MERN19MDS0178BG02	X261164	Mafic dike	Spilite	646610	5347387	64.50	0.62	13.25	9.82	0.17	3.33	0.45	0.01	0.01	3.98	0.03	0.21	2.51	98.87	0.02
154	MERN18MDS0115AG01	X258464	Mafic dike	Spilite	645851	5347849	48.30	1.02	12.95	11.30	0.26	5.25	7.47	0.02	0.01	2.91	0.05	0.10	9.09	98.74	1.63
155	MERN17MDS0023AG04	X258401	Powell Quartz-Diorite		644441	5347230	66.10	0.78	12.95	6.35	0.10	3.67	1.35	0.01	0.04	3.08	0.98	0.15	3.01	98.56	0.15
156	MERN17MDS0034BG07	X258408	Powell Quartz-Diorite		644456	5347292	59.20	0.80	14.60	7.52	0.13	4.51	2.74	0.01	0.03	3.01	1.27	0.12	5.14	99.07	0.59
157	MERN17MDS0034BG08	X258409	Powell Quartz-Diorite		644458	5347309	59.10	0.95	15.25	10.25	0.10	6.12	0.82	0.01	0.03	2.65	1.02	0.14	4.34	100.77	0.14
158	MERN17MDS0035AG02	X258483	Powell Quartz-Diorite	Spilite	644426	5347363	63.60	1.32	14.85	8.33	0.04	4.88	0.55	0.01	0.01	4.52	0.16	0.36	2.89	101.5	0.02
159	MERN17MDS0040AG01	X258410	Powell Quartz-Diorite	Spotted	644388	5347283	57.90	0.84	15.05	12.95	0.14	5.97	0.18	0.01	0.05	0.17	1.75	0.14	4.63	99.77	0.01
160	MERN17MDS0045CG03	X258414	Powell Quartz-Diorite	Spilite	644363	5347485	52.90	0.68	16.65	10.50	0.19	6.32	2.05	0.01	0.01	4.57	0.13	0.11	5.05	99.18	0.38
161	MERN17MDS0045CG06	X258415	Powell Quartz-Diorite	Spilite	644363	5347485	52.80	0.86	16.25	9.62	0.18	5.82	2.55	0.01	0.01	4.73	0.12	0.12	5.13	98.21	0.47
162	MERN18MDS0104AG01	X258467	Powell Quartz-Diorite	Spotted	644494	5347556	58.50	0.84	14.35	12.25	0.11	6.67	0.22	0.01	0.04	0.08	1.48	0.12	4.69	99.35	0.02

	Field Number	Lab ID	Rock Type	Alteration	UTM-East	UTM-North	S_%	H20+_%	S.G.	Ag ppm	As ppm	Au_ppm	Ba ppm	Bi ppm	Cd ppm	Ce ppm	Co ppm	Cr ppm	Cs ppm	Cu ppm	Dy ppm
Method					NAD 83	NAD 83	S-IR08	OA-IR06	OA-GRA08b	ME-4ACD81	ME-MS42	Au-ICP21	ME-MS81	ME-MS42	ME-4ACD81	ME-MS81	ME-4ACD8	ME-MS81	ME-MS81	ME-4ACD81	ME-MS81
Detection Limit							0.01	0.01		0.5	0.1		0.5	0.01	0.5	0.1	1	1	0.05	1	0.05
125	MERN20MDS201AG03	C079658	Andesite	Spotted	645265	5348054	<0.01	5.79	2.95	0.25	0.2		299	0.02	0.8	21.5	8	30	0.38	27	3.21
126	MERN17MDS0030AG02	X258481	Andesite	Spotted	645036	5347711	0.04		2.77												
127	MERN17MDS0031AG07i	X258485	Andesite	Spilite	645240	5347733	0.01		2.64												
128	MERN17MDS0031AG07ii	X261051	Andesite	Spotted	645240	5347733	<0.01		2.74												
129	MERN17MDS0064DG04	X258482	Andesite	Spilite	645355	5347769	0.01		2.7												
130	MERN18MDS0084CG01	X258432	Andesite	Spotted	645667	5348114	0.03	4.34	2.77	0.25	0.2		101.5		0.25	19.7	23	20	0.19	364	3.86
131	MERN18MDS0085EG11	X258436	Andesite	Chl	645776	5348159	0.01	5.07	2.89	0.25	0.6		229		0.25	34.6	16	10	0.32	8	5.14
132	MERN18MDS0108AG01	X258470	Andesite	Spilite	645622	5347834	0.03		2.7	0.25	0.2		137	0.19	0.25	37.2	8	10	0.13	110	6.58
133	MERN18MDS0109AG01	X258474	Andesite	Spotted	645563	5347825	0.04		2.79	0.25	0.1		260	0.03	0.25	36.5	3	10	0.19	9	6.43
134	MERN18MDS0112AG01	X258494	Andesite	Spilite	645748	5347867	0.18		2.7	0.25	2.3		79.5	0.13	2.1	8.4	31	150	0.09	288	3.03
135	MERN18MDS0113AG01	X258478	Andesite	Spilite	645805	5347679	0.02		2.69	0.25	0.3		68.4	0.01	0.5	29.2	23	5	0.22	12	4.67
136	MERN18MDS0114AG01	X258493	Andesite	Spotted	645819	5347735	0.01		2.76												
137	MERN18MDS0114AG02	X258475	Andesite	Spotted	645819	5347735	0.12		2.69	0.25	1.1		236	0.59	0.8	27.8	18	10	0.38	120	4.06
138	MERN18MDS0118AG01	X258466	Andesite	Spilite	645590	5347983	0.45		2.71												
139	MERN18MDS0118AG02	X258491	Andesite	Spilite	645590	5347983	0.13		2.73	0.25	0.4		21.1	0.03	0.6	33.1	23	10	0.07	108	4.92
140	MERN19MDS0153BG03	X261149	Andesite	Spilite	646297	5348043	0.01			<0.5	0.2		72.9	0.02	0.6	28.6	15	10	0.17	6	4.1
141	MERN18MDS0119AG01	X258462	Andesite		645630	5348024	0.15		2.65	0.25	0.1		282	1.17	0.25	61	9	10	0.21	1310	6.31
142	MERN18MDS0085CG07	X258435	Mafic tuff	Spotted	645724	5348195	0.36	6.09	2.82	0.25	0.4		383		0.25	4.9	21	50	0.32	299	1.34
143	MERN18MDS0085CG12i	X258488	Mafic tuff	Spotted	645737	5348188	0.04		2.73												
144	MERN18MDS0085CG12ii	X258487	Mafic tuff	Chl	645737	5348188	0.04		2.7												
145	MERN18MDS0115BG03	X258459	Mafic tuff	Spotted	645851	5347849	0.01		2.68	0.25	0.1		850	0.04	0.25	14.5	17	30	0.65	13	2.53
146	MERN18MDS0064EG05	X258492	Lamprophyre	Spilite	645354	5347768	0.03		2.69	0.25	0.2		164.5	0.01	1.5	10.1	30	100	0.26	63	2.42
147	MERN18MDS0078BG02	X258431	Lamprophyre		645507	5347994	0.05	2.59	2.8	0.25	0.1		451		0.25	25.8	29	770	0.17	4	2.88
148	MERN19MDS0152AG01	X261162	Lamprophyre	Spilite	646504	5348319	<0.01			0.25	0.2		7.8	0.01	<0.5	25.2	4	10	0.06	2	5.61
149	MERN19MDS0152AG01	X261146	Lamprophyre		646504	5348320	0.01			0.25	0.2		612	0.03	0.6	27.9	57	1620	0.23	87	3.15
150	MERN20MDS127CG04	C079666	Lamprophyre?	Ank-Ser	642344	5346169	0.04	0.96	2.89												
151	MERN17MDS0034AG06	X258407	Mafic dike	Spotted	644449	5347294	0.01	7.12	2.83	0.25	0.1		344	0.05	0.25	14.5	25	40	0.52	29	3.39
152	MERN18MDS0068AG01	X258469	Mafic dike	Spilite	645454	5347795	0.11		2.8	0.25	0.4		116	0.02	0.25	33.7	47	60	0.23	67	4.02
153	MERN19MDS0178BG02	X261164	Mafic dike	Spilite	646610	5347387	<0.01			0.25	0.7		9.3	0.01	<0.5	28.1	5	10	0.07	4	6.06
154	MERN18MDS0115AG01	X258464	Mafic dike	Spilite	645851	5347849	0.04		2.72	0.25	0.1		33.5	0.02	0.5	11.4	28	90	0.07	78	2.86
155	MERN17MDS0023AG04	X258401	Powell Quartz-Diorite		644441	5347230	0.02	2.51	2.72	0.25	0.6		344	0.08	0.25	34	8	20	0.37	15	4.43
156	MERN17MDS0034BG07	X258408	Powell Quartz-Diorite		644456	5347292	0.03	3.49	2.88	0.25	0.1		280	0.05	0.25	29.7	18	30	0.47	44	4.37
157	MERN17MDS0034BG08	X258409	Powell Quartz-Diorite		644458	5347309	0.01	4.69	2.87	0.25	0.2		240	0.03	0.6	35.4	22	30	0.5	86	4.64
158	MERN17MDS0035AG02	X258483	Powell Quartz-Diorite	Spilite	644426	5347363	0.02		2.7												
159	MERN17MDS0040AG01	X258410	Powell Quartz-Diorite	Spotted	644388	5347283	0.01	5.67	2.85	0.25	0.1		426	0.03	0.25	9.5	21	20	0.39	33	3.09
160	MERN17MDS0045CG03	X258414	Powell Quartz-Diorite	Spilite	644363	5347485	0.01	4.27	2.72	0.25	0.1		66.5	0.02	0.25	19.2	28	50	0.19	9	2.58
161	MERN17MDS0045CG06	X258415	Powell Quartz-Diorite	Spilite	644363	5347485	0.01	4.26	2.79	0.25	0.1		66.7	0.02	0.25	19.7	26	40	0.18	7	2.98
162	MERN18MDS0104AG01	X258467	Powell Quartz-Diorite	Spotted	644494	5347556	0.005		2.75	0.25	0.2		315	0.02	0.25	31.2	21	20	0.6	96	3.66

	Field Number	Lab ID	Rock Type	Alteration	UTM-East	UTM-North	Er ppm	Eu ppm	Ga_ppm	Gd_ppm	Ge_ppm	Hf_ppm	Hg_ppm	Ho_ppm	In_ppm	La_ppm	Li_ppm	Lu_ppm	Mo_ppm	Nb_ppm	Nd_ppm
Method					**NAD 83**	**NAD 83**	**ME-MS81**	**ME-MS81**	**ME-MS81**	**ME-MS81**	**ME-MS81**	**ME-MS81**	**ME-MS42**	**ME-MS81**	**ME-MS42**	**ME-MS81**	**ME-4ACD81**	**ME-MS81**	**ME-4ACD81**	**ME-MS81**	**ME-MS81**
Detection Limit							**0.03**	**0.03**	**0.1**	**0.05**	**5**	**0.2**	**0.005**	**0.01**	**0.005**	**0.1**	**10**	**0.01**	**1**	**0.2**	**0.1**
125	MERN20MDS201AG03	C079658	Andesite	Spotted	645265	5348054	2.41	0.91	19.4	3.05	<5	4	<0.005	0.73	0.089	8.3	20	0.39	<1	7.1	13.1
126	MERN17MDS0030AG02	X258481	Andesite	Spotted	645036	5347711															
127	MERN17MDS0031AG07i	X258485	Andesite	Spilite	645240	5347733															
128	MERN17MDS0031AG07ii	X261051	Andesite	Spotted	645240	5347733															
129	MERN17MDS0064DG04	X258482	Andesite	Spilite	645355	5347769															
130	MERN18MDS0084CG01	X258432	Andesite	Spotted	645667	5348114	2.57	0.44	17.7	3.61	2.5	3.2		0.82		7.7	30	0.33	2	5.2	11.8
131	MERN18MDS0085EG11	X258436	Andesite	Chl	645776	5348159	2.67	0.75	17.9	4.99	2.5	4		0.91		14.9	20	0.46	1	7.2	19.4
132	MERN18MDS0108AG01	X258470	Andesite	Spilite	645622	5347834	4.41	1.17	20.6	6.25	2.5	5	0.0025	1.49	0.067	16.9	20	0.66	0.5	8.5	22.7
133	MERN18MDS0109AG01	X258474	Andesite	Spotted	645563	5347825	4.64	1.13	19.3	6.18	2.5	5.5	0.0025	1.45	0.021	16.4	10	0.7	0.5	10.2	22.2
134	MERN18MDS0112AG01	X258494	Andesite	Spilite	645748	5347867	1.89	1.07	18.2	2.68	2.5	1.5	0.0025	0.67	0.147	3.9	20	0.3	0.5	3.7	5.8
135	MERN18MDS0113AG01	X258478	Andesite	Spilite	645805	5347679	2.97	1.22	19.5	4.56	2.5	3.5	0.0025	1	0.06	14.2	30	0.44	0.5	6.1	16.3
136	MERN18MDS0114AG01	X258493	Andesite	Spotted	645819	5347735															
137	MERN18MDS0114AG02	X258475	Andesite	Spotted	645819	5347735	2.73	0.7	20.6	4.16	2.5	3.5	0.0025	0.89	0.128	13.3	40	0.44	0.5	6.3	16.2
138	MERN18MDS0118AG01	X258466	Andesite	Spilite	645590	5347983															
139	MERN18MDS0118AG02	X258491	Andesite	Spilite	645590	5347983	3.19	1.35	18.9	4.91	2.5	3.9	0.0025	1.07	0.032	15.2	20	0.5	1	7.9	19.7
140	MERN19MDS0153BG03	X261149	Andesite	Spilite	646297	5348043	2.45	0.65	17.4	3.94	<5	3.4	<0.005	0.83	0.059	12.6	20	0.34	1	5.6	15.7
141	MERN18MDS0119AG01	X258462	Andesite		645630	5348024	3.38	1.42	11	7.34	2.5	3.5	0.0025	1.29	0.106	27.8	10	0.51	41	8.1	32.3
142	MERN18MDS0085CG07	X258435	Mafic tuff	Spotted	645724	5348195	0.94	0.45	19.1	1.16	2.5	0.7		0.3		2.3	20	0.15	0.5	1.5	2.9
143	MERN18MDS0085CG12i	X258488	Mafic tuff	Spotted	645737	5348188															
144	MERN18MDS0085CG12ii	X258487	Mafic tuff	Chl	645737	5348188															
145	MERN18MDS0115BG03	X258459	Mafic tuff	Spotted	645851	5347849	1.73	0.87	21.4	2.65	2.5	2.4	0.0025	0.63	0.022	5.9	20	0.34	1	4.7	9.2
146	MERN18MDS0064EG05	X258492	Lamprophyre	Spilite	645354	5347768	1.57	0.77	16.2	2.28	2.5	1.4	0.0025	0.52	0.03	4.8	10	0.25	0.5	3	6.6
147	MERN18MDS0078BG02	X258431	Lamprophyre		645507	5347994	1.63	1.12	11.3	3.42	2.5	1.7		0.6		11.4	40	0.22	0.5	2.6	15.4
148	MERN19MDS0152AG01	X261162	Lamprophyre	Spilite	646504	5348319	3.94	1.09	22.5	5.28	<5	3.8	<0.005	1.21	0.041	13	20	0.61	1	8.2	17.6
149	MERN19MDS0152AG01	X261146	Lamprophyre		646504	5348320	1.77	1.55	13.3	3.8	<5	2	<0.005	0.63	0.011	11.6	30	0.26	<1	3	17.2
150	MERN20MDS127CG04	C079666	Lamprophyre?	Ank-Ser	642344	5346169															
151	MERN17MDS0034AG06	X258407	Mafic dike	Spotted	644449	5347294	2.33	0.5	22.4	2.99	2.5	3.1	0	0.76	0.03	6.9	50	0.38	0.5	6.9	9.1
152	MERN18MDS0068AG01	X258469	Mafic dike	Spilite	645454	5347795	2.5	1.06	17.3	4.3	2.5	2.8	0.0025	0.9	0.009	17.1	20	0.38	1	9.6	18.4
153	MERN19MDS0178BG02	X261164	Mafic dike	Spilite	646610	5347387	4.04	1.09	22	5.35	<5	3.8	<0.005	1.29	0.04	13.1	20	0.66	1	10.1	18.5
154	MERN18MDS0115AG01	X258464	Mafic dike	Spilite	645851	5347849	1.89	1.01	16.2	2.6	2.5	1.6	0.0025	0.62	0.152	5.2	20	0.31	0.5	3.5	7.5
155	MERN17MDS0023AG04	X258401	Powell Quartz-Diorite		644441	5347230	2.77	1.08	15.4	4.47	2.5	4.5	0	0.94	0.02	17.6	20	0.43	1	7	18.6
156	MERN17MDS0034BG07	X258408	Powell Quartz-Diorite		644456	5347292	2.63	0.92	16.8	4.08	2.5	4.2	0	0.91	0.02	14.3	20	0.4	0.5	6.7	16.5
157	MERN17MDS0034BG08	X258409	Powell Quartz-Diorite		644458	5347309	2.86	1.12	17.9	5.28	2.5	3.9	0	1.03	0.03	20.2	30	0.42	1	6.1	20.3
158	MERN17MDS0035AG02	X258483	Powell Quartz-Diorite	Spilite	644426	5347363															
159	MERN17MDS0040AG01	X258410	Powell Quartz-Diorite	Spotted	644388	5347283	2.07	0.36	17.4	2.33	2.5	3.4	0.01	0.7	0.08	4.7	30	0.33	0.5	5.7	6.7
160	MERN17MDS0045CG03	X258414	Powell Quartz-Diorite	Spilite	644363	5347485	1.59	0.77	16.7	2.52	2.5	2.3	0	0.54	0.05	9.2	30	0.22	0.5	3.4	10.5
161	MERN17MDS0045CG06	X258415	Powell Quartz-Diorite	Spilite	644363	5347485	1.86	1.02	16.4	2.85	2.5	2.4	0	0.63	0.05	9.3	30	0.27	0.5	4	11.4
162	MERN18MDS0104AG01	X258467	Powell Quartz-Diorite	Spotted	644494	5347556	2.55	0.64	17.7	3.92	2.5	3.9	0.0025	0.83	0.037	14.9	40	0.4	1	5.8	17.3

	Field Number	Lab ID	Rock Type	Alteration	UTM-East	UTM-North	Ni_ppm	Pb_ppm	Rb_ppm	Re_ppm	Sb_ppm	Sc_ppm	Se_ppm	Sm_ppm	Sn_ppm	Sr_ppm	Ta_ppm	Tb_ppm	Te_ppm	Th_ppm	Tl_ppm
Method					**NAD 83**	**NAD 83**	**ME-4ACD81**	**ME-4ACD81**	**ME-MS81**	**ME-MS42**	**ME-MS42**	**ME-4ACD81**	**ME-MS42**	**ME-MS81**	**ME-MS81**	**ME-MS81**	**ME-MS81**	**ME-MS81**	**ME-MS42**	**ME-MS81**	**ME-MS42**
Detection Limit							**1**	**2**	**0.2**	**0.001**	**0.05**	**1**	**0.2**	**0.03**	**1**	**0.1**	**0.1**	**0.01**	**0.01**	**0.05**	**0.02**
125	MERN20MDS201AG03	C079658	Andesite	Spotted	645265	5348054	21	3	39.2	0.001	<0.05	26	<0.2	3.43	23	9.6	0.5	0.51	0.01	1.52	<0.02
126	MERN17MDS0030AG02	X258481	Andesite	Spotted	645036	5347711															
127	MERN17MDS0031AG07i	X258485	Andesite	Spilite	645240	5347733															
128	MERN17MDS0031AG07ii	X261051	Andesite	Spotted	645240	5347733															
129	MERN17MDS0064DG04	X258482	Andesite	Spilite	645355	5347769															
130	MERN18MDS0084CG01	X258432	Andesite	Spotted	645667	5348114	12	3	7.3			15		2.98	1	7.4	0.4	0.56		1.35	
131	MERN18MDS0085EG11	X258436	Andesite	Chl	645776	5348159	17	1	26.8			23		4.45	3	6.1	0.6	0.79		1.71	
132	MERN18MDS0108AG01	X258470	Andesite	Spilite	645622	5347834	10	1	7.8	0.001	0.05	17	0.1	5.85	3	20.1	0.5	1.13	0.13	2.11	0.01
133	MERN18MDS0109AG01	X258474	Andesite	Spotted	645563	5347825	1	4	12.9	0.0005	0.05	18	0.1	5.68	3	28.3	0.6	1.1	0.01	2.55	0.01
134	MERN18MDS0112AG01	X258494	Andesite	Spilite	645748	5347867	27	1	1.2	0.001	0.05	36	0.4	1.95	12	108.5	0.2	0.53	0.01	0.55	0.01
135	MERN18MDS0113AG01	X258478	Andesite	Spilite	645805	5347679	13	1	1.9	0.001	0.025	21	0.1	3.92	2	39.6	0.4	0.8	0.01	1.8	0.01
136	MERN18MDS0114AG01	X258493	Andesite	Spotted	645819	5347735															
137	MERN18MDS0114AG02	X258475	Andesite	Spotted	645819	5347735	13	1	19.1	<0.001	0.07	20	0.1	3.98	10	8.9	0.4	0.7	0.53	1.67	0.01
138	MERN18MDS0118AG01	X258466	Andesite	Spilite	645590	5347983															
139	MERN18MDS0118AG02	X258491	Andesite	Spilite	645590	5347983	21	1	0.5	0.001	0.025	23	0.3	4.83	1	53.4	0.5	0.85	0.09	1.78	0.01
140	MERN19MDS0153BG03	X261149	Andesite	Spilite	646297	5348043	10	<2	4.5	0.001	<0.05	19	<0.2	4.21	3	28	0.5	0.66	<0.01	1.73	<0.02
141	MERN18MDS0119AG01	X258462	Andesite		645630	5348024	6	3	18.3	0.041	0.05	20	0.7	7.53	3	29.5	0.5	1.08	1.76	2.14	0.01
142	MERN18MDS0085CG07	X258435	Mafic tuff	Spotted	645724	5348195	16	1	29.1			27		0.78	8	6.1	0.1	0.2		0.28	
143	MERN18MDS0085CG12i	X258488	Mafic tuff	Spotted	645737	5348188															
144	MERN18MDS0085CG12ii	X258487	Mafic tuff	Chl	645737	5348188															
145	MERN18MDS0115BG03	X258459	Mafic tuff	Spotted	645851	5347849	23	1	33.6	0.003	0.08	25	0.1	2.26	4	26.4	0.3	0.44	0.04	1.1	0.01
146	MERN18MDS0064EG05	X258492	Lamprophyre	Spilite	645354	5347768	16	1	10.1	0.001	0.05	35	0.1	1.82	1	107.5	0.2	0.4	0.01	0.49	0.01
147	MERN18MDS0078BG02	X258431	Lamprophyre		645507	5347994	147	3	7.4			26		3.63	1	232	0.2	0.43		1.29	
148	MERN19MDS0152AG01	X261162	Lamprophyre	Spilite	646504	5348319	<1	<2	0.3	<0.001	<0.05	18	<0.2	5.05	2	21.7	0.6	0.79	<0.01	1.63	<0.02
149	MERN19MDS0152AG01	X261146	Lamprophyre		646504	5348320	502	4	15.9	<0.001	<0.05	24	<0.2	4.01	1	196	0.2	0.54	0.01	1.49	<0.02
150	MERN20MDS127CG04	C079666	Lamprophyre?	Ank-Ser	642344	5346169															
151	MERN17MDS0034AG06	X258407	Mafic dike	Spotted	644449	5347294	17	1	25	0	0.03	33	0.1	2.59	7	4.3	0.3	0.51	0.01	1.36	0.01
152	MERN18MDS0068AG01	X258469	Mafic dike	Spilite	645454	5347795	44	1	11.3	0.0005	0.025	40	0.3	4.17	1	208	0.5	0.72	0.01	2.42	0.01
153	MERN19MDS0178BG02	X261164	Mafic dike	Spilite	646610	5347387	<1	<2	0.4	0.001	<0.05	18	<0.2	5.09	2	22.6	0.5	0.87	0.01	1.64	<0.02
154	MERN18MDS0115AG01	X258464	Mafic dike	Spilite	645851	5347849	24	1	0.8	0.001	0.06	33	0.1	2.19	12	154.5	0.2	0.47	0.01	0.58	0.01
155	MERN17MDS0023AG04	X258401	Powell Quartz-Diorite		644441	5347230	11	1	17.6	0	0.03	16	0.1	4.34	2	46.5	0.5	0.76	0.01	2.96	0.01
156	MERN17MDS0034BG07	X258408	Powell Quartz-Diorite		644456	5347292	23	1	24.5	0	0.03	18	0.1	3.86	2	50.9	0.4	0.67	0.01	2.47	0.01
157	MERN17MDS0034BG08	X258409	Powell Quartz-Diorite		644458	5347309	29	1	20.8	0	0.03	18	0.1	4.66	2	40.7	0.4	0.82	0.01	1.98	0.01
158	MERN17MDS0035AG02	X258483	Powell Quartz-Diorite	Spilite	644426	5347363															
159	MERN17MDS0040AG01	X258410	Powell Quartz-Diorite	Spotted	644388	5347283	24	2	26.8	0	0.03	15	0.1	1.77	6	6.7	0.4	0.5	0.01	1.84	0.01
160	MERN17MDS0045CG03	X258414	Powell Quartz-Diorite	Spilite	644363	5347485	53	4	3	0	0.03	26	0.1	2.45	1	101.5	0.2	0.42	0.01	1.04	0.01
161	MERN17MDS0045CG06	X258415	Powell Quartz-Diorite	Spilite	644363	5347485	49	2	2.5	0	0.03	26	0.1	2.99	1	123	0.2	0.47	0.01	1.07	0.01
162	MERN18MDS0104AG01	X258467	Powell Quartz-Diorite	Spotted	644494	5347556	22	1	25.9	0.0005	0.06	15	0.1	4.02	4	6.3	0.4	0.65	0.01	2.07	0.01

	Field Number	Lab ID	Rock Type	Alteration	UTM-East	UTM-North	Tm_ppm	U_ppm	V_ppm	W_ppm	Y_ppm	Yb_ppm	Zn_ppm	Zr_ppm
Method					**NAD 83**	**NAD 83**	**ME-MS81**	**ME-MS81**	**ME-MS81**	**ME-MS81**	**ME-MS81**	**ME-MS81**	**ME4ACD81**	**ME-MS81**
Detection Limit							**0.01**	**0.05**	**5**	**1**	**0.1**	**0.03**	**2**	**2**
125	MERN20MDS201AG03	C079658	Andesite	Spotted	645265	5348054	0.33	0.39	227	3	19.8	2.55	252	146
126	MERN17MDS0030AG02	X258481	Andesite	Spotted	645036	5347711					43.7			197
127	MERN17MDS0031AG07i	X258485	Andesite	Spilite	645240	5347733					23.8			139
128	MERN17MDS0031AG07ii	X261051	Andesite	Spotted	645240	5347733					23.7			145
129	MERN17MDS0064DG04	X258482	Andesite	Spilite	645355	5347769					28.5			149
130	MERN18MDS0084CG01	X258432	Andesite	Spotted	645667	5348114		0.39	171	3	21.3	2.14	263	117
131	MERN18MDS0085EG11	X258436	Andesite	Chl	645776	5348159		0.46	133	2	23.7	2.71	152	146
132	MERN18MDS0108AG01	X258470	Andesite	Spilite	645622	5347834	0.65	0.58	38	1	37.2	4.28	196	219
133	MERN18MDS0109AG01	X258474	Andesite	Spotted	645563	5347825	0.68	0.7	8	0.5	37.3	4.51	191	247
134	MERN18MDS0112AG01	X258494	Andesite	Spilite	645748	5347867	0.3	0.16	376	1	16.1	1.97	401	55
135	MERN18MDS0113AG01	X258478	Andesite	Spilite	645805	5347679	0.45	0.43	272	1	26.8	2.96	187	158
136	MERN18MDS0114AG01	X258493	Andesite	Spotted	645819	5347735					31.9			151
137	MERN18MDS0114AG02	X258475	Andesite	Spotted	645819	5347735	0.42	0.51	232	4	23	2.68	268	154
138	MERN18MDS0118AG01	X258466	Andesite	Spilite	645590	5347983					31.9			159
139	MERN18MDS0118AG02	X258491	Andesite	Spilite	645590	5347983	0.48	0.43	181	1	27.7	3.21	174	171
140	MERN19MDS0153BG03	X261149	Andesite	Spilite	646297	5348043	0.33	0.44	226	1	22	2.03	366	139
141	MERN18MDS0119AG01	X258462	Andesite		645630	5348024	0.53	0.67	166	7	30.6	2.85	84	134
142	MERN18MDS0085CG07	X258435	Mafic tuff	Spotted	645724	5348195		0.1	267	2	7.6	0.9	223	22
143	MERN18MDS0085CG12i	X258488	Mafic tuff	Spotted	645737	5348188					11.1			26
144	MERN18MDS0085CG12ii	X258487	Mafic tuff	Chl	645737	5348188					10.4			26
145	MERN18MDS0115BG03	X258459	Mafic tuff	Spotted	645851	5347849	0.26	0.33	209	1	15.1	1.77	201	87
146	MERN18MDS0064EG05	X258492	Lamprophyre	Spilite	645354	5347768	0.24	0.13	324	0.5	13.8	1.68	166	48
147	MERN18MDS0078BG02	X258431	Lamprophyre		645507	5347994		0.46	189	1	13.9	1.48	221	58
148	MERN19MDS0152AG01	X261162	Lamprophyre	Spilite	646504	5348319	0.55	0.48	6	1	33	4.02	74	144
149	MERN19MDS0152AG01	X261146	Lamprophyre		646504	5348320	0.28	0.52	206	1	17.3	1.71	144	71
150	MERN20MDS127CG04	C079666	Lamprophyre?	Ank-Ser	642344	5346169					22.3			61
151	MERN17MDS0034AG06	X258407	Mafic dike	Spotted	644449	5347294	0.33	0.47	305	2	17.6	2.37	292	113
152	MERN18MDS0068AG01	X258469	Mafic dike	Spilite	645454	5347795	0.39	0.36	366	0.5	22.1	2.41	118	105
153	MERN19MDS0178BG02	X261164	Mafic dike	Spilite	646610	5347387	0.63	0.44	<5	1	33.9	4.25	70	142
154	MERN18MDS0115AG01	X258464	Mafic dike	Spilite	645851	5347849	0.29	0.16	281	0.5	16.1	1.94	224	59
155	MERN17MDS0023AG04	X258401	Powell Quartz-Diorite		644441	5347230	0.4	0.54	117	0.5	23.4	2.84	80	168
156	MERN17MDS0034BG07	X258408	Powell Quartz-Diorite		644456	5347292	0.35	0.55	163	1	21.9	2.8	136	153
157	MERN17MDS0034BG08	X258409	Powell Quartz-Diorite		644458	5347309	0.41	0.52	178	2	24.1	3	170	145
158	MERN17MDS0035AG02	X258483	Powell Quartz-Diorite	Spilite	644426	5347363					40.4			175
159	MERN17MDS0040AG01	X258410	Powell Quartz-Diorite	Spotted	644388	5347283	0.3	0.46	143	8	16.7	2.21	161	133
160	MERN17MDS0045CG03	X258414	Powell Quartz-Diorite	Spilite	644363	5347485	0.19	0.24	160	1	12.8	1.49	132	84
161	MERN17MDS0045CG06	X258415	Powell Quartz-Diorite	Spilite	644363	5347485	0.27	0.27	207	4	15.4	1.77	123	85
162	MERN18MDS0104AG01	X258467	Powell Quartz-Diorite	Spotted	644494	5347556	0.38	0.54	188	2	22.1	2.56	150	174

A 3-3: Whole-rock $\delta^{18}O$ results

Sample	ALS	d18O (Vs Smow)	Occurrence/Deposit	Vein Type	Lithology	Alteration	Easting	Northing
MERN18MDS0085CG12i	X258488	4.2	Anglo A Zone	Cu-Ag	Mafic tuff	Spotted	645737	5348188
MERN18MDS0085CG12ii	X258487	4.5	Anglo A Zone	Cu-Ag	Mafic tuff	Chl	645737	5348188
MERN18MDS085CG07	X258435	3.3	Anglo A Zone	Cu-Ag	Mafic tuff	Spotted	645724	5348195
MERN18MDS085BG01	X258433	5.8	Anglo A-Zone	Cu-Ag	Qtz-phyric rhyolite	Spotted	645738	5348189
MERN18MDS085BG02	X258434	5.8	Anglo A-Zone	Cu-Ag	Qtz-phyric rhyolite	Spotted	645723	5348170
MERN18MDS085EG11	X258436	4.6	Anglo A-Zone	Cu-Ag	Andesite	Chl	645776	5348159
MERN18MDS0098AG05	X258442	4.5	Background		Andesite	Spilite	644616	5348043
MERN18MDS0098AG07	X258448	4.4	Background		Andesite	Spilite	644616	5348043
MERN18MDS0099AG05i	X258489	3.1	Background		Andesite	Chlorite	644451	5347921
MERN18MDS0099AG05ii	X261052	3.8	Background		Andesite	Chlorite	644451	5347921
MERN18MDS0099AG05iii	X258486	3.5	Background		Andesite	Spotted	644451	5347921
MERN18MDS0113AG01	X258478	5.0	Background		Andesite	Spilite	645805	5347679
MERN18MDS0118AG01	X258466	4.9	Background		Andesite	Spilite	645590	5347983
MERN18MDS0118AG02	X258491	5.0	Background		Andesite	Spilite	645590	5347983
MERN18MDS0119AG01	X258462	5.6	Background		Andesite		645630	5348024
MERN17MDS0045AG02	X258413	5.5	Background		Aphyric rhyolite	Ser	644405	5347521
MERN17MDS0041AG03	X258411	7.8	Background		Powell Tonalite	Spilite	644674	5347418
MERN18MDS0087AG01	X258444	7.3	Background		Powell Tonalite	Spotted	644635	5347296
MERN18MDS0110AG01	X258497	6.8	Background		Qtz-phyric rhyolite	Spilite	645673	5347845
MERN20MDS200BG01	C079656	8.2	E	Au	Joliet tonalite	Spotted	645997	5347208
MERN19MDS0128BG04	X261175	7.9	E-W Shear Zone	Au	Powell Tonalite	Ank-Ser	644626	5347380
MERN19MDS0128BG02	X261173	7.8	E-W Shear Zone	Au	Powell Tonalite	Ank-Ser	644626	5347381
MERN19MDS0128BG03	X261174	7.9	E-W Shear Zone	Au	Powell Tonalite	Ank-Ser	644626	5347381
MERN19MDS0128BG05	X261176	7.9	E-W Shear Zone	Au	Powell Tonalite	Ank-Ser	644626	5347382
MERN19MDS0128BG06	x261177	7.6	E-W Shear Zone	Au	Powell Tonalite	Ank-Ser	644626	5347382
MERN19MDS0128BG07	X261178	7.7	E-W Shear Zone	Au	Powell Tonalite	Ank-Ser	644626	5347382
MERN19MDS0128BG08	X261179	7.9	E-W Shear Zone	Au	Powell Tonalite	Ank-Ser	644626	5347382
MERN19MDS0125GG60	X261078	4.2	Joliet Breccia	Cu-Ag	Andesite	Spilite	646452	5347937
MERN19MDS0125GG61	X261073	4.0	Joliet Breccia	Cu-Ag	Andesite	Spilite	646493	5347917
MERN19MDS0125GG62	X261072	5.2	Joliet Breccia	Cu-Ag	Andesite	Spilite	646421	5347973
MERN19MDS0125AG52	X261120	3.3	Joliet Breccia	Cu-Ag	Andesite (clast)	Spotted	646522	5347784
MERN19MDS0125AG53	X261119	2.9	Joliet Breccia	Cu-Ag	Andesite (clast)	Spotted	646522	5347784
MERN19MDS0125FG63	X261071	7.8	Joliet Breccia	Cu-Ag	Aphyric felsic dike	Ank-Ser	646426	5347987
MERN19MDS0125AG49	X261126	6.6	Joliet Breccia	Cu-Ag	Qtz-phyric rhyolite dike	Spilite	646586	5347789
MERN19MDS0125AG49	X261127	7.0	Joliet Breccia	Cu-Ag	Qtz-phyric rhyolite dike	Spotted	646586	5347789
MERN19MDS0125DG42	X261131	7.0	Joliet Breccia	Cu-Ag	Qtz-phyric rhyolite dike	Spilite	646712	5347827
MERN19MDS0125DG43	X261129	7.5	Joliet Breccia	Cu-Ag	Qtz-phyric rhyolite dike	Ser	646712	5347827
MERN20MDS201AG01	C079657	5.4	Powell D-Zone	Cu-Ag	Andesite	Spilite	645265	5348054
MERN20MDS201AG03	C079658	4.8	Powell D-Zone	Cu-Ag	Andesite	Spotted	645265	5348054
MERN20MDS201BG08	C079661	6.5	Powell D-Zone	Cu-Ag	Joliet tonalite	Ser	645262	5348013
MERN17MDS0031AG07i	X258485	4.3	Powell F-Zone	Cu-Ag	Andesite	Spilite	645240	5347733
MERN17MDS0031AG07ii	X261051	4.2	Powell F-Zone	Cu-Ag	Andesite	Spotted	645240	5347733

Sample	ALS	d18O (Vs Smow)	Occurrence/Deposit	Vein Type	Lithology	Alteration	Easting	Northing
MERN18MDS086AG04	X258438	3.7	Powell F-Zone	Cu-Ag	Aphyric felsic dike	Ser	645190	5347767
MERN18MDS086AG05	X258439	3.6	Powell F-Zone	Cu-Ag	Aphyric felsic dike	Spotted	645190	5347765
MERN18MDS086AG08	X258440	3.6	Powell F-Zone	Cu-Ag	Aphyric felsic dike	Spotted	645186	5347742
MERN17MDS0061DG05	X258416	4.7	Powell F-Zone	Cu-Ag	Qtz-phyric rhyolite	Spotted	645168	5347780
MERN17MDS0061DG06	X258417	4.5	Powell F-Zone	Cu-Ag	Qtz-phyric rhyolite	Spotted	645166	5347775
MERN17MDS0035BG03	X258461	6.1	Powell Rouyn	Au	Aphyric rhyolite		644426	5347363
MERN17MDS0073AG01	X258418	7.3	Powell Rouyn	Au	Powell Tonalite	Spilite	644512	5347244
MERN19MDS0129AG07	X261180	6.5	Powell-Rouyn	Au	Aphyric rhyolite	Ser	644505	5347412
MERN19MDS0129AG08	X261181	7.1	Powell-Rouyn	Au	Aphyric rhyolite	Ser	644504	5347410
MERN19MDS0129AG09	X261182	6.7	Powell-Rouyn	Au	Aphyric rhyolite	Ser	644503	5347409
MERN19MDS0129AG10	X261183	7.0	Powell-Rouyn	Au	Aphyric rhyolite	Ser	644503	5347408
MERN19MDS0129AG11	X261184	6.5	Powell-Rouyn	Au	Aphyric rhyolite	Ser	644503	5347408
MERN19MDS0129AG12	X261185	7.3	Powell-Rouyn	Au	Aphyric rhyolite	Ser	644503	5347408
MERN19MDS0129AG13	X261186	6.8	Powell-Rouyn	Au	Aphyric rhyolite	Ser	644502	5347407
MERN19MDS0129AG14	X261187	7.0	Powell-Rouyn	Au	Aphyric rhyolite	Ser	644502	5347407
MERN19MDS0129AG15	X261188	6.7	Powell-Rouyn	Au	Aphyric rhyolite	Ser	644502	5347407
MERN19MDS0129AG16	X261189	6.4	Powell-Rouyn	Au	Aphyric rhyolite	Ser	644510	5347419
MERN19MDS0129AG16 (DUPLICATE)	X261195	6.8	Powell-Rouyn	Au	Aphyric rhyolite	Ser	644510	5347419
MERN19MDS0129AG18	X261190	6.8	Powell-Rouyn	Au	Aphyric rhyolite	Ser	644556	5347359
MERN19MDS0129AG19	X261191	6.7	Powell-Rouyn	Au	Aphyric rhyolite	Ser	644555	5347358
MERN19MDS0129AG20	X261192	7.0	Powell-Rouyn	Au	Aphyric rhyolite	Ser	644554	5347358
MERN19MDS0129AG21	X261193	6.4	Powell-Rouyn	Au	Aphyric rhyolite	Ser	644551	5347357
MERN19MDS0129AG23	X261194	6.8	Powell-Rouyn	Au	Aphyric rhyolite	Ser	644546	5347353
MERN20MDS127CG04	C079666	5.8	Silidor	Au	Lamprophyre?	Ank-Ser	642344	5346169
MERN20MDS127AG01	C079662	7.0	Silidor	Au	Powell Tonalite	Ank-Ser	642390	5346179
MERN20MDS127AG02	C079664	7.3	Silidor	Au	Powell Tonalite	Ank-Ser	642390	5346179
MERN20MDS127AG02	C079663	6.9	Silidor	Au	Powell Tonalite	Ank-Ser	642390	5346179
MERN20MDS127AG03	C079665	7.4	Silidor	Au	Powell Tonalite	Ank-Ser	642390	5346179
MERN20MDS127AG06	C079667	8.7	Silidor	Au	Powell Tonalite	Ank-Ser	642348	5346189
MERN20MDS127AG07	C079668	7.7	Silidor	Au	Powell Tonalite	Ank-Ser	642348	5346189
MERN20MDS127AG08	C079669	8.0	Silidor	Au	Powell Tonalite	Ank-Ser	642347	5346188
MERN20MDS127AG09	C079670	8.3	Silidor	Au	Powell Tonalite	Ank-Ser	642347	5346188
MERN20MDS186BG13	C079653	9.0	Vox	Au	Joliet tonalite	Hmt	645742	5347150
MERN20MDS186AG04	C079672	10.3	Vox	Au	Qtz-phyric rhyolite dike	Ank-Ser	645699	5347175
MERN20MDS186AG05	X261198	9.3	Vox	Au	Qtz-phyric rhyolite dike	Ank-Ser	645696	5347174
MERN20MDS186AG06	X261199	10.1	Vox	Au	Qtz-phyric rhyolite dike	Ank-Ser	645693	5347172
MERN20MDS186AG07	C079676	9.6	Vox	Au	Qtz-phyric rhyolite dike	Ank-Ser	645708	5347170
MERN20MDS186AG08	C079675	9.4	Vox	Au	Qtz-phyric rhyolite dike	Ank-Ser	645709	5347171
MERN20MDS186AG09	X261200	9.5	Vox	Au	Qtz-phyric rhyolite dike	Ank-Ser	645710	5347172
MERN20MDS186AG10	C079651	9.3	Vox	Au	Qtz-phyric rhyolite dike	Ank-Ser	645717	5347173
MERN20MDS186AG11	C079652	9.2	Vox	Au	Qtz-phyric rhyolite dike	Ank-Ser	645720	5347175
MERN20MDS186AG12	C079674	8.5	Vox	Au	Qtz-phyric rhyolite dike	Ank-Ser	645728	5347180
MERN20MDS186CG14	C079654	7.6	Vox	Au	Qtz-phyric rhyolite dike	Spotted	645800	5347138

A 3-4: Quartz $\delta^{18}O$ results

Sample	Vein Type	Description	d18O (Vs Smow)
MERN17MDS0061AG04	Cu-Ag	Powell F-Zone	7.3
MERN18BEQ0003AG01	Cu-Ag	Powell F-Zone	6.4
MERN18BEQ0003AG02	Cu-Ag	Powell F-Zone	6.6
MERN19MDS0125BG55b	Cu-Ag	Joliet Breccia	7.6
MERN20MDS0197AG01	Cu-Ag	Here Cu Vein	8.8
MERN19MDS0182AG01	Cu-Ag	Anglo D Zone	8.9
MERN20MDS0201AG06	Cu-Ag	Powell D Zone	9.4
MERN19MDS0180AG01	Cu-Ag	Anglo C Zone	9.0
MERN19MDS0128BG01	Au	E-W shear vein Mt Powell	10.6
MERN18BEQ0002AG05	Au	E-W shear vein Mt Powell	10.5
MERN19MDS0129AG04	Au	Powell-Rouyn Au vein	10.8
MERN18BEQ0002AG04	Au	Powell-Rouyn Au vein	10.2
MERN19MDS0129AG01	Au	Powell-Rouyn Au vein	11.1
MERN18BEQ002AG01	Au	vein network in FW of Powell-Rouyn	9.7
MERN18BEQ002AG02A	Au	vein network in FW of Powell-Rouyn	9.4
MERN18BEQ002AG02B	Au	vein network in FW of Powell-Rouyn	9.3
MERN18BEQ002AG03	Au	vein network in FW of Powell-Rouyn	9.4
MERN19MDS0127AG14	Au	Silidor	11.2
MERN19MDS0186AG02	Au	Vox Vein	12.6

A 3-5: SEM-EDS Chlorite and Carbonate data

ID	Spectrum	Lithology	Alteration	Location	SiO2	TiO2	Al2O3	FeO	MnO	MgO	CaO	Na2O	K2O	ZnO	NiO	No. of oxygens	Si	Al iv	Al vi	Ti	Fe3+	Fe2+	Mn	Mg
100AG01_area 5	Chl 1	Basalt	Spotted	Background	23.54	0.05	21.69	15.95	0.12	9.75	0.09	0.32	0.00	0.00	0.07	28	5.68	2.32	3.97	0.01	0.84	2.38	0.02	3.51
100AG01_area 5	Chl 2	Basalt	Spotted	Background	23.49	0.00	22.30	15.71	0.13	10.22	0.00	0.25	0.01	0.05	0.00	28	5.61	2.39	4.00	0.00	0.83	2.31	0.03	3.64
100AG01_area 5	Chl 4	Basalt	Spotted	Background	23.58	0.05	21.96	15.83	0.01	10.24	0.06	0.30	0.00	0.05	0.14	28	5.64	2.36	3.94	0.01	0.81	2.36	0.00	3.65
100AG01_area 5	Chl 5	Basalt	Spotted	Background	23.28	0.06	22.44	16.02	0.08	9.96	0.01	0.30	0.04	0.02	0.03	28	5.57	2.43	4.01	0.01	0.81	2.40	0.02	3.55
100AG01_area 8	Chl 1	Basalt	Spotted	Background	23.01	0.05	23.04	15.76	0.11	9.82	0.02	0.33	0.05	0.03	0.06	28	5.50	2.50	4.10	0.01	0.80	2.34	0.02	3.50
100AG01_area 8	Chl 2	Basalt	Spotted	Background	23.51	0.00	22.10	15.63	0.09	10.19	0.11	0.41	0.08	0.04	0.00	28	5.62	2.38	3.96	0.00	0.77	2.35	0.02	3.63
100AG01_area 8	Chl 3	Basalt	Spotted	Background	22.94	0.01	23.37	15.44	0.12	10.07	0.00	0.32	0.00	0.00	0.00	28	5.46	2.54	4.14	0.00	0.81	2.27	0.02	3.58
100AG01_area 8	Chl 4	Basalt	Spotted	Background	22.97	0.00	23.21	16.23	0.10	9.44	0.00	0.14	0.03	0.00	0.02	28	5.50	2.50	4.17	0.00	0.88	2.37	0.02	3.37
100AG01_area 8	Chl 5	Basalt	Spotted	Background	22.69	0.05	22.72	16.65	0.02	9.50	0.08	0.31	0.00	0.00	0.02	28	5.47	2.53	4.04	0.01	0.77	2.59	0.00	3.42
100AG01_area 8	Chl 6	Basalt	Spotted	Background	23.66	0.05	22.61	15.07	0.11	10.39	0.01	0.34	0.00	0.00	0.08	28	5.61	2.39	4.04	0.01	0.84	2.15	0.02	3.67
100AG01_area 8	Chl 7	Basalt	Spotted	Background	23.70	0.07	21.50	15.90	0.17	10.37	0.05	0.25	0.03	0.00	0.03	28	5.69	2.31	3.87	0.01	0.81	2.38	0.03	3.71
105AG01_area 1	Chl 1	Mafic dike	Carb	Background	25.00	0.00	18.64	7.84	0.07	21.87	0.08	0.62	0.01	0.18	0.04	28	5.66	2.34	2.66	0.00	0.05	1.43	0.01	7.38
105AG01_area 1	Chl 2	Mafic dike	Carb	Background	25.02	0.03	18.69	8.31	0.09	21.67	0.08	0.54	0.00	0.03	0.08	28	5.66	2.34	2.66	0.01	0.08	1.49	0.02	7.30
105AG01_area 1	Chl 3	Mafic dike	Carb	Background	26.34	0.02	16.67	7.10	0.02	23.86	0.07	0.49	0.00	0.04	0.00	28	5.91	2.09	2.33	0.00	0.04	1.29	0.00	7.97
105AG01_area 2	Chl 1	Mafic dike	Carb	Background	26.49	0.00	16.87	6.92	0.05	23.36	0.18	0.54	0.01	0.17	0.01	28	5.93	2.07	2.41	0.00	0.09	1.21	0.01	7.80
105AG01_area 2	Chl 2	Mafic dike	Carb	Background	26.35	0.05	16.39	7.27	0.06	23.92	0.04	0.56	0.01	0.04	0.05	28	5.91	2.09	2.27	0.01	0.00	1.36	0.01	8.00
105AG01_area 2	Chl 3	Mafic dike	Carb	Background	24.71	0.07	17.03	9.17	0.04	22.79	0.02	0.46	0.00	0.00	0.02	28	5.64	2.36	2.25	0.01	0.00	1.85	0.01	7.75
105AG01_area 2	Chl 4	Mafic dike	Carb	Background	25.02	0.00	19.44	7.57	0.01	22.00	0.03	0.43	0.02	0.01	0.09	28	5.61	2.39	2.78	0.00	0.13	1.29	0.00	7.36
116AG01_area 8	Chl 1	Cu-Zn-Ag Vein	-	Cu-Zn-Ag Vein	21.88	0.00	21.79	11.28	0.12	15.06	0.07	0.42	0.00	0.00	0.05	28	5.28	2.72	3.55	0.00	0.37	1.91	0.03	5.42
116AG01_area 8	Chl 2	Cu-Zn-Ag Vein	-	Cu-Zn-Ag Vein	22.80	0.04	21.70	16.37	0.12	10.71	0.07	0.01	0.00	0.03	0.00	28	5.53	2.47	3.82	0.01	0.74	2.58	0.03	3.87
116AG01_area 8	Chl 3	Cu-Zn-Ag Vein	-	Cu-Zn-Ag Vein	23.07	0.04	23.72	12.46	0.07	12.55	0.00	0.41	0.04	0.08	0.07	28	5.39	2.61	4.04	0.01	0.70	1.74	0.01	4.37
116AG01_area 8	Chl 4	Cu-Zn-Ag Vein	-	Cu-Zn-Ag Vein	22.98	0.05	23.58	13.13	0.09	12.19	0.01	0.35	0.00	0.02	0.01	28	5.40	2.60	4.03	0.01	0.72	1.86	0.02	4.27
116AG01_area 9	Chl 1	Cu-Zn-Ag Vein	-	Cu-Zn-Ag Vein	22.72	0.02	22.81	13.96	0.12	12.32	0.00	0.59	0.08	0.02	0.02	28	5.38	2.62	3.83	0.00	0.53	2.23	0.02	4.35
116AG01_area 9	Chl 2	Cu-Zn-Ag Vein	-	Cu-Zn-Ag Vein	22.84	0.03	22.92	13.68	0.23	12.40	0.06	0.29	0.01	0.11	0.08	28	5.40	2.60	3.87	0.01	0.64	2.07	0.05	4.37
116AG01_area 9	Chl 3	Cu-Zn-Ag Vein	-	Cu-Zn-Ag Vein	23.16	0.06	23.14	13.47	0.07	12.14	0.00	0.33	0.20	0.06	0.00	28	5.44	2.56	3.96	0.01	0.68	1.97	0.01	4.25
116AG01_area 9	Chl 4	Cu-Zn-Ag Vein	-	Cu-Zn-Ag Vein	22.92	0.01	23.28	13.48	0.09	12.27	0.04	0.53	0.00	0.00	0.00	28	5.39	2.61	3.95	0.00	0.62	2.03	0.02	4.30
116AG01_area 9	Chl 5	Cu-Zn-Ag Vein	-	Cu-Zn-Ag Vein	23.84	0.03	24.49	11.68	0.14	11.57	0.01	0.48	0.25	0.10	0.00	28	5.50	2.50	4.30	0.01	0.86	1.40	0.03	3.98
116AG01_area 9	Chl 6	Cu-Zn-Ag Vein	-	Cu-Zn-Ag Vein	22.74	0.00	22.28	14.72	0.19	12.18	0.00	0.30	0.05	0.02	0.00	28	5.42	2.58	3.77	0.00	0.58	2.35	0.04	4.33
116AG01_area 9	Chl 7	Cu-Zn-Ag Vein	-	Cu-Zn-Ag Vein	21.88	0.03	22.75	15.38	0.09	11.98	0.00	0.26	0.02	0.00	0.03	28	5.26	2.74	3.78	0.01	0.52	2.57	0.02	4.29
123AG01_area 1	Chl 1	Cu-Zn-Ag Vein	-	Cu-Zn-Ag Vein	23.39	0.01	22.35	15.70	0.21	10.11	0.00	0.20	0.00	0.04	0.00	28	5.60	2.40	4.02	0.00	0.85	2.30	0.04	3.61
123AG01_area 1	Chl 2	Cu-Zn-Ag Vein	-	Cu-Zn-Ag Vein	23.05	0.02	22.22	16.28	0.23	10.05	0.01	0.21	0.00	0.01	0.01	28	5.55	2.45	3.96	0.00	0.78	2.49	0.05	3.61
123AG01_area 1	Chl 3	Cu-Zn-Ag Vein	-	Cu-Zn-Ag Vein	22.82	0.05	22.44	16.45	0.24	9.85	0.00	0.23	0.00	0.01	0.02	28	5.50	2.50	3.98	0.01	0.77	2.55	0.05	3.54
123AG01_area 1	Chl 4	Cu-Zn-Ag Vein	-	Cu-Zn-Ag Vein	23.59	0.01	22.34	15.72	0.23	9.81	0.04	0.27	0.01	0.04	0.02	28	5.64	2.36	4.05	0.00	0.87	2.28	0.05	3.50
123AG01_area 1	Chl 5	Cu-Zn-Ag Vein	-	Cu-Zn-Ag Vein	23.38	0.02	21.97	15.99	0.25	10.11	0.02	0.26	0.03	0.00	0.00	28	5.62	2.38	3.95	0.00	0.80	2.41	0.05	3.62
123AG01_area 1	Chl 6	Cu-Zn-Ag Vein	-	Cu-Zn-Ag Vein	23.28	0.02	22.29	15.87	0.23	10.10	0.00	0.34	0.02	0.00	0.00	28	5.58	2.42	3.98	0.00	0.78	2.40	0.05	3.61
123AG01_area 1	Chl 7	Cu-Zn-Ag Vein	-	Cu-Zn-Ag Vein	22.55	0.02	16.64	15.80	0.14	11.62	0.00	0.25	0.01	0.05	0.00	28	5.92	2.08	3.12	0.00	0.52	2.95	0.03	4.54
123AG01_area 2	Chl 1	Cu-Zn-Ag Vein	-	Cu-Zn-Ag Vein	24.01	0.06	21.65	16.14	0.23	9.36	0.00	0.28	0.02	0.00	0.00	28	5.77	2.23	4.02	0.01	0.93	2.32	0.05	3.35
123AG01_area 2	Chl 2	Cu-Zn-Ag Vein	-	Cu-Zn-Ag Vein	23.15	0.01	21.95	15.83	0.22	10.07	0.01	0.33	0.12	0.00	0.01	28	5.59	2.41	3.95	0.00	0.76	2.44	0.04	3.62
123AG01_area 2	Chl 3	Cu-Zn-Ag Vein	-	Cu-Zn-Ag Vein	24.22	0.03	20.73	15.79	0.22	10.97	0.01	0.29	0.01	0.00	0.02	28	5.79	2.21	3.73	0.01	0.78	2.38	0.04	3.91
123AG01_area 2	Chl 4	Cu-Zn-Ag Vein	-	Cu-Zn-Ag Vein	23.38	0.01	22.41	15.89	0.22	10.00	0.00	0.23	0.02	0.02	0.01	28	5.59	2.41	4.02	0.00	0.83	2.35	0.04	3.57
123AG01_area 2	Chl 5	Cu-Zn-Ag Vein	-	Cu-Zn-Ag Vein	23.36	0.01	22.19	15.71	0.24	10.32	0.01	0.22	0.02	0.05	0.01	28	5.60	2.40	3.97	0.00	0.81	2.34	0.05	3.69
123AG01_area 2	Chl 6	Cu-Zn-Ag Vein	-	Cu-Zn-Ag Vein	23.02	0.06	22.02	16.42	0.20	10.18	0.00	0.20	0.01	0.02	0.00	28	5.55	2.45	3.90	0.01	0.76	2.55	0.04	3.66

ID	Spectrum	Lithology	Alteration	Location	Ni	Zn	Ca	Na	K	OH*	Total	Fe/Fe+Mg	Variety
100AG01_area 5	Chl 1	Basalt	Spotted	Background	0.01	0.00	0.02	0.30	0.00	16	35.06	0.48	pycnochlorite
100AG01_area 5	Chl 2	Basalt	Spotted	Background	0.00	0.01	0.00	0.23	0.01	16	35.06	0.46	pycnochlorite
100AG01_area 5	Chl 4	Basalt	Spotted	Background	0.03	0.01	0.02	0.28	0.00	16	35.10	0.46	pycnochlorite
100AG01_area 5	Chl 5	Basalt	Spotted	Background	0.01	0.00	0.00	0.28	0.02	16	35.11	0.47	ripidolite
100AG01_area 8	Chl 1	Basalt	Spotted	Background	0.01	0.01	0.01	0.30	0.03	16	35.13	0.47	ripidolite
100AG01_area 8	Chl 2	Basalt	Spotted	Background	0.00	0.01	0.03	0.38	0.05	16	35.20	0.46	pycnochlorite
100AG01_area 8	Chl 3	Basalt	Spotted	Background	0.00	0.00	0.00	0.30	0.00	16	35.11	0.46	ripidolite
100AG01_area 8	Chl 4	Basalt	Spotted	Background	0.00	0.00	0.00	0.13	0.02	16	34.97	0.49	ripidolite
100AG01_area 8	Chl 5	Basalt	Spotted	Background	0.00	0.00	0.02	0.29	0.00	16	35.16	0.50	ripidolite
100AG01_area 8	Chl 6	Basalt	Spotted	Background	0.02	0.00	0.00	0.31	0.00	16	35.07	0.45	pycnochlorite
100AG01_area 8	Chl 7	Basalt	Spotted	Background	0.01	0.00	0.01	0.23	0.02	16	35.09	0.46	pycnochlorite
105AG01_area 1	Chl 1	Mafic dike	Carb	Background	0.01	0.03	0.02	0.54	0.01	16	36.13	0.17	clinochlore
105AG01_area 1	Chl 2	Mafic dike	Carb	Background	0.01	0.01	0.02	0.48	0.00	16	36.08	0.18	clinochlore
105AG01_area 1	Chl 3	Mafic dike	Carb	Background	0.00	0.01	0.02	0.43	0.00	16	36.10	0.14	clinochlore
105AG01_area 2	Chl 1	Mafic dike	Carb	Background	0.00	0.03	0.04	0.47	0.00	16	36.06	0.14	clinochlore
105AG01_area 2	Chl 2	Mafic dike	Carb	Background	0.01	0.01	0.01	0.48	0.00	16	36.17	0.15	clinochlore
105AG01_area 2	Chl 3	Mafic dike	Carb	Background	0.00	0.00	0.01	0.41	0.00	16	36.30	0.19	clinochlore
105AG01_area 2	Chl 4	Mafic dike	Carb	Background	0.02	0.00	0.01	0.38	0.01	16	35.97	0.16	clinochlore
116AG01_area 8	Chl 1	Cu-Zn-Ag Vein	-	Cu-Zn-Ag Vein	0.01	0.00	0.02	0.39	0.00	16	35.69	0.30	ripidolite
116AG01_area 8	Chl 2	Cu-Zn-Ag Vein	-	Cu-Zn-Ag Vein	0.00	0.01	0.02	0.01	0.00	16	35.08	0.46	ripidolite
116AG01_area 8	Chl 3	Cu-Zn-Ag Vein	-	Cu-Zn-Ag Vein	0.01	0.01	0.00	0.38	0.02	16	35.29	0.36	ripidolite
116AG01_area 8	Chl 4	Cu-Zn-Ag Vein	-	Cu-Zn-Ag Vein	0.00	0.00	0.00	0.32	0.00	16	35.23	0.38	ripidolite
116AG01_area 9	Chl 1	Cu-Zn-Ag Vein	-	Cu-Zn-Ag Vein	0.00	0.00	0.00	0.54	0.05	16	35.56	0.39	ripidolite
116AG01_area 9	Chl 2	Cu-Zn-Ag Vein	-	Cu-Zn-Ag Vein	0.01	0.02	0.02	0.27	0.01	16	35.32	0.38	ripidolite
116AG01_area 9	Chl 3	Cu-Zn-Ag Vein	-	Cu-Zn-Ag Vein	0.00	0.01	0.00	0.30	0.12	16	35.31	0.38	ripidolite
116AG01_area 9	Chl 4	Cu-Zn-Ag Vein	-	Cu-Zn-Ag Vein	0.00	0.00	0.01	0.48	0.00	16	35.41	0.38	ripidolite
116AG01_area 9	Chl 5	Cu-Zn-Ag Vein	-	Cu-Zn-Ag Vein	0.00	0.02	0.00	0.43	0.15	16	35.16	0.36	ripidolite
116AG01_area 9	Chl 6	Cu-Zn-Ag Vein	-	Cu-Zn-Ag Vein	0.00	0.00	0.00	0.28	0.03	16	35.39	0.40	ripidolite
116AG01_area 9	Chl 7	Cu-Zn-Ag Vein	-	Cu-Zn-Ag Vein	0.01	0.00	0.00	0.24	0.01	16	35.45	0.42	ripidolite
123AG01_area 1	Chl 1	Cu-Zn-Ag Vein	-	Cu-Zn-Ag Vein	0.00	0.01	0.00	0.19	0.00	16	35.02	0.47	pycnochlorite
123AG01_area 1	Chl 2	Cu-Zn-Ag Vein	-	Cu-Zn-Ag Vein	0.00	0.00	0.00	0.20	0.00	16	35.10	0.48	ripidolite
123AG01_area 1	Chl 3	Cu-Zn-Ag Vein	-	Cu-Zn-Ag Vein	0.00	0.00	0.00	0.22	0.00	16	35.13	0.48	ripidolite
123AG01_area 1	Chl 4	Cu-Zn-Ag Vein	-	Cu-Zn-Ag Vein	0.00	0.01	0.01	0.25	0.01	16	35.02	0.47	pycnochlorite
123AG01_area 1	Chl 5	Cu-Zn-Ag Vein	-	Cu-Zn-Ag Vein	0.00	0.00	0.00	0.24	0.02	16	35.10	0.47	pycnochlorite
123AG01_area 1	Chl 6	Cu-Zn-Ag Vein	-	Cu-Zn-Ag Vein	0.00	0.00	0.00	0.32	0.01	16	35.15	0.47	ripidolite
123AG01_area 1	Chl 7	Cu-Zn-Ag Vein	-	Cu-Zn-Ag Vein	0.00	0.01	0.00	0.26	0.01	16	35.44	0.43	pycnochlorite
123AG01_area 2	Chl 1	Cu-Zn-Ag Vein	-	Cu-Zn-Ag Vein	0.00	0.00	0.00	0.26	0.01	16	34.95	0.49	pycnochlorite
123AG01_area 2	Chl 2	Cu-Zn-Ag Vein	-	Cu-Zn-Ag Vein	0.00	0.00	0.00	0.31	0.08	16	35.20	0.47	ripidolite
123AG01_area 2	Chl 3	Cu-Zn-Ag Vein	-	Cu-Zn-Ag Vein	0.00	0.00	0.00	0.27	0.01	16	35.13	0.45	pycnochlorite
123AG01_area 2	Chl 4	Cu-Zn-Ag Vein	-	Cu-Zn-Ag Vein	0.00	0.00	0.00	0.21	0.01	16	35.05	0.47	ripidolite
123AG01_area 2	Chl 5	Cu-Zn-Ag Vein	-	Cu-Zn-Ag Vein	0.00	0.01	0.00	0.20	0.01	16	35.07	0.46	ripidolite
123AG01_area 2	Chl 6	Cu-Zn-Ag Vein	-	Cu-Zn-Ag Vein	0.00	0.00	0.00	0.19	0.01	16	35.12	0.48	ripidolite

ID	Spectrum	Lithology	Alteration	Location	SiO2	TiO2	Al2O3	FeO	MnO	MgO	CaO	Na2O	K2O	ZnO	NiO	No. of oxygens	Si	Al iv	Al vi	Ti	Fe3+	Fe2+	Mn	Mg
123AG01_area 2	Chl 7	Cu-Zn-Ag Vein	-	Cu-Zn-Ag Vein	23.07	0.05	22.22	16.46	0.22	9.82	0.03	0.23	0.00	0.00	0.02	28	5.56	2.44	3.97	0.01	0.80	2.52	0.04	3.53
123AG01_area 4	Chl 1	Cu-Zn-Ag Vein	-	Cu-Zn-Ag Vein	22.84	0.03	22.22	16.45	0.25	9.89	0.01	0.28	0.02	0.07	0.03	28	5.52	2.48	3.95	0.01	0.74	2.58	0.05	3.56
123AG01_area 4	Chl 2	Cu-Zn-Ag Vein	-	Cu-Zn-Ag Vein	22.95	0.03	22.34	16.17	0.29	9.97	0.02	0.26	0.03	0.01	0.02	28	5.53	2.47	3.97	0.01	0.77	2.49	0.06	3.58
123AG01_area 4	Chl 3	Cu-Zn-Ag Vein	-	Cu-Zn-Ag Vein	23.24	0.02	22.71	15.45	0.21	10.29	0.00	0.27	0.01	0.04	0.04	28	5.54	2.46	4.04	0.00	0.81	2.27	0.04	3.66
123AG01_area 4	Chl 4	Cu-Zn-Ag Vein	-	Cu-Zn-Ag Vein	23.12	0.02	22.29	16.25	0.29	9.90	0.02	0.28	0.00	0.00	0.00	28	5.56	2.44	3.98	0.00	0.79	2.48	0.06	3.55
125AG53_A3	Chl 1	Mafic clast	Spotted	Joliet Breccia	22.74	0.00	23.11	16.83	0.11	8.74	0.00	0.37	0.04	0.00	0.00	28	5.49	2.51	4.18	0.00	0.83	2.57	0.02	3.14
125AG53_A3	Chl 2	Mafic clast	Spotted	Joliet Breccia	23.38	0.00	23.45	15.84	0.23	8.61	0.03	0.34	0.03	0.03	0.01	28	5.58	2.42	4.32	0.00	0.96	2.20	0.05	3.07
125AG53_A3	Chl 3	Mafic clast	Spotted	Joliet Breccia	23.40	0.00	23.79	16.02	0.12	7.86	0.00	0.25	0.55	0.00	0.06	28	5.58	2.42	4.43	0.00	0.97	2.23	0.02	2.80
125AG53_A3	Chl 4	Mafic clast	Spotted	Joliet Breccia	22.66	0.00	23.40	16.91	0.11	8.45	0.00	0.40	0.00	0.00	0.00	28	5.47	2.53	4.25	0.00	0.85	2.56	0.02	3.04
125AG53_A3	Chl 5	Mafic clast	Spotted	Joliet Breccia	23.29	0.01	21.28	17.20	0.15	9.46	0.03	0.35	0.01	0.00	0.13	28	5.66	2.34	3.86	0.00	0.76	2.74	0.03	3.43
125AG53_A3	Chl 6	Mafic clast	Spotted	Joliet Breccia	22.26	0.02	23.50	17.11	0.19	8.27	0.03	0.25	0.01	0.09	0.03	28	5.41	2.59	4.25	0.00	0.85	2.62	0.04	2.99
125AG70_A2	Chl 1	Felsic clast	Spotted	Joliet Breccia	29.10	0.17	21.95	11.80	0.14	7.97	0.00	0.35	0.83	0.07	0.00	28	6.55	1.45	4.58	0.03	1.58	0.64	0.03	2.68
125AG70_A2	Chl 2	Felsic clast	Spotted	Joliet Breccia	23.00	0.08	23.06	16.56	0.24	8.18	0.05	0.44	0.09	0.00	0.00	28	5.55	2.45	4.25	0.01	0.89	2.45	0.05	2.94
125AG70_A2	Chl 3	Felsic clast	Spotted	Joliet Breccia	23.59	0.09	24.27	13.20	0.07	10.28	0.02	0.67	0.05	0.00	0.09	28	5.51	2.49	4.33	0.02	0.87	1.71	0.01	3.58
125AG70_A2	Chl 5	Felsic clast	Spotted	Joliet Breccia	25.47	0.07	22.63	12.80	0.05	10.42	0.05	0.69	0.05	0.00	0.08	28	5.89	2.11	4.21	0.01	1.02	1.46	0.01	3.59
125AG70_A3	Chl 1	Felsic clast	Spotted	Joliet Breccia	23.15	0.15	23.21	14.66	0.08	10.54	0.07	0.48	0.02	0.00	0.00	28	5.48	2.52	4.07	0.03	0.77	2.13	0.02	3.72
125AG70_A3	Chl 2	Felsic clast	Spotted	Joliet Breccia	22.39	0.00	22.36	16.17	0.09	10.69	0.00	0.08	0.06	0.00	0.09	28	5.42	2.58	3.89	0.00	0.70	2.58	0.02	3.86
125AG70_A3	Chl 4	Felsic clast	Spotted	Joliet Breccia	22.82	0.00	21.87	15.91	0.11	10.94	0.01	0.40	0.06	0.02	0.07	28	5.50	2.50	3.80	0.00	0.62	2.59	0.02	3.93
125AG70_A3	Chl 5	Felsic clast	Spotted	Joliet Breccia	23.57	0.00	23.32	14.44	0.16	10.24	0.00	0.39	0.05	0.00	0.00	28	5.57	2.43	4.19	0.00	0.87	1.98	0.03	3.61
125AG70_A3	Chl 6	Felsic clast	Spotted	Joliet Breccia	23.36	0.03	23.13	14.34	0.13	10.50	0.03	0.53	0.03	0.10	0.00	28	5.53	2.47	4.11	0.00	0.79	2.05	0.03	3.71
125AG70_A3	Chl 7	Felsic clast	Spotted	Joliet Breccia	21.90	0.03	22.52	16.37	0.14	10.53	0.02	0.57	0.02	0.03	0.00	28	5.31	2.69	3.85	0.01	0.52	2.80	0.03	3.81
125AG70_A4	Chl 1	Felsic clast	Spotted	Joliet Breccia	23.30	0.00	22.87	14.79	0.10	10.80	0.00	0.41	0.05	0.00	0.00	28	5.53	2.47	4.03	0.00	0.76	2.18	0.02	3.82
125AG70_A4	Chl 2	Felsic clast	Spotted	Joliet Breccia	23.71	0.00	22.88	14.44	0.06	10.95	0.00	0.34	0.03	0.01	0.00	28	5.59	2.41	4.06	0.00	0.83	2.02	0.01	3.85
125AG70_A4	Chl 3	Felsic clast	Spotted	Joliet Breccia	23.37	0.01	23.71	13.80	0.03	10.93	0.02	0.43	0.01	0.06	0.00	28	5.49	2.51	4.18	0.00	0.82	1.89	0.01	3.83
125AG70_A4	Chl 4	Felsic clast	Spotted	Joliet Breccia	23.42	0.24	22.80	14.59	0.05	10.80	0.04	0.29	0.01	0.00	0.08	28	5.54	2.46	4.01	0.04	0.84	2.05	0.01	3.81
125DG47b_A2	Spectrum 6	Felsic dike	Spotted	Joliet Breccia	24.18	0.15	21.47	14.75	0.14	11.32	0.00	0.32	0.00	0.00	0.00	28	5.73	2.27	3.83	0.03	0.81	2.11	0.03	4.00
125DG47b_A2	Spectrum 7	Felsic dike	Spotted	Joliet Breccia	23.42	0.03	23.35	15.13	0.06	10.00	0.04	0.29	0.00	0.00	0.07	28	5.54	2.46	4.18	0.01	0.88	2.11	0.01	3.53
125DG47b_A3	Spectrum 10	Felsic dike	Spotted	Joliet Breccia	22.75	0.00	23.73	15.26	0.13	10.14	0.00	0.40	0.01	0.00	0.01	28	5.40	2.60	4.17	0.00	0.77	2.26	0.03	3.59
125DG47b_A3	Spectrum 11	Felsic dike	Spotted	Joliet Breccia	24.57	0.00	21.13	14.58	0.15	11.74	0.02	0.35	0.01	0.00	0.00	28	5.80	2.20	3.77	0.00	0.79	2.09	0.03	4.13
125DG47b_A3	Spectrum 12	Felsic dike	Spotted	Joliet Breccia	22.80	0.02	21.96	16.41	0.06	10.26	0.00	0.38	0.04	0.00	0.07	28	5.51	2.49	3.87	0.00	0.68	2.64	0.01	3.70
125DG47b_A4	Spectrum 7	Felsic dike	Spotted	Joliet Breccia	23.18	0.00	23.29	15.03	0.05	10.41	0.07	0.41	0.00	0.00	0.01	28	5.49	2.51	4.11	0.00	0.79	2.19	0.01	3.68
125DG47b_A5	Spectrum 10	Felsic dike	Spotted	Joliet Breccia	22.43	0.00	23.88	15.80	0.07	9.52	0.00	0.31	0.00	0.00	0.05	28	5.37	2.63	4.23	0.00	0.81	2.36	0.01	3.40
125DG47b_A5	Spectrum 11	Felsic dike	Spotted	Joliet Breccia	22.23	0.00	24.31	15.71	0.17	9.38	0.02	0.26	0.05	0.00	0.00	28	5.32	2.68	4.30	0.00	0.82	2.33	0.03	3.35
125DG47b_A5	Spectrum 12	Felsic dike	Spotted	Joliet Breccia	22.61	0.00	22.90	16.07	0.09	9.99	0.00	0.26	0.00	0.00	0.05	28	5.45	2.55	4.05	0.00	0.76	2.48	0.02	3.59
125DG47b_A6	Spectrum 8	Felsic dike	Spotted	Joliet Breccia	23.32	0.06	23.82	14.19	0.13	10.40	0.00	0.38	0.00	0.00	0.04	28	5.49	2.51	4.23	0.01	0.87	1.93	0.03	3.65
125DG47b_A6	Spectrum 9	Felsic dike	Spotted	Joliet Breccia	23.24	0.00	23.80	15.32	0.03	9.47	0.00	0.35	0.03	0.00	0.00	28	5.51	2.49	4.29	0.00	0.90	2.13	0.01	3.35
125DG47b_A7	Spectrum 17	Felsic dike	Spotted	Joliet Breccia	22.88	0.00	21.40	16.69	0.09	10.57	0.00	0.35	0.00	0.00	0.03	28	5.55	2.45	3.76	0.00	0.64	2.74	0.02	3.82
125DG47b_A7	Spectrum 18	Felsic dike	Spotted	Joliet Breccia	23.61	0.04	23.40	14.83	0.06	9.93	0.00	0.42	0.00	0.00	0.08	28	5.57	2.43	4.21	0.01	0.89	2.04	0.01	3.49
125DG47b_A7	Spectrum 19	Felsic dike	Spotted	Joliet Breccia	24.05	0.02	21.84	14.62	0.10	11.06	0.00	0.52	0.03	0.00	0.02	28	5.70	2.30	3.91	0.00	0.77	2.12	0.02	3.90
127AG02_area 1	Chl 1	Tonalite	Ank-ser	Silidor	23.16	0.00	22.45	14.25	0.07	12.05	0.26	0.35	0.00	0.05	0.03	28	5.48	2.52	3.83	0.00	0.64	2.18	0.01	4.25
127AG02_area 1	Chl 2	Tonalite	Ank-ser	Silidor	23.68	0.02	21.14	13.77	0.04	12.71	0.95	0.32	0.02	0.08	0.02	28	5.61	2.39	3.59	0.00	0.59	2.14	0.01	4.49
127AG02_area 1	Chl 3	Tonalite	Ank-ser	Silidor	24.54	0.00	20.23	12.13	0.05	15.59	0.38	0.34	0.02	0.04	0.02	28	5.71	2.29	3.31	0.00	0.49	1.87	0.01	5.40
127AG09_A1	Chl 1	Tonalite	Ank-ser	Silidor	24.15	0.01	20.92	13.07	0.06	14.33	0.07	0.30	0.00	0.00	0.01	28	5.66	2.34	3.51	0.00	0.58	1.98	0.01	5.00
127AG09_A1	Chl 2	Tonalite	Ank-ser	Silidor	24.68	0.06	21.12	12.08	0.06	13.81	0.01	0.52	0.00	0.00	0.01	28	5.76	2.24	3.66	0.01	0.68	1.67	0.01	4.80
127AG09_A1	Chl 3	Tonalite	Ank-ser	Silidor	24.28	0.02	21.04	12.49	0.08	14.36	0.04	0.55	0.00	0.05	0.09	28	5.66	2.34	3.53	0.00	0.55	1.89	0.02	4.99

ID	Spectrum	Lithology	Alteration	Location	Ni	Zn	Ca	Na	K	OH*	Total	Fe/Fe+Mg	Variety
123AG01_area 2	Chl 7	Cu-Zn-Ag Vein	-	Cu-Zn-Ag Vein	0.00	0.00	0.01	0.22	0.00	16	35.09	0.48	ripidolite
123AG01_area 4	Chl 1	Cu-Zn-Ag Vein	-	Cu-Zn-Ag Vein	0.01	0.01	0.00	0.27	0.01	16	35.18	0.48	ripidolite
123AG01_area 4	Chl 2	Cu-Zn-Ag Vein	-	Cu-Zn-Ag Vein	0.00	0.00	0.00	0.25	0.02	16	35.15	0.48	ripidolite
123AG01_area 4	Chl 3	Cu-Zn-Ag Vein	-	Cu-Zn-Ag Vein	0.01	0.01	0.00	0.25	0.01	16	35.10	0.46	ripidolite
123AG01_area 4	Chl 4	Cu-Zn-Ag Vein	-	Cu-Zn-Ag Vein	0.00	0.00	0.00	0.26	0.00	16	35.12	0.48	ripidolite
125AG53_A3	Chl 1	Mafic clast	Spotted	Joliet Breccia	0.00	0.00	0.00	0.34	0.03	16	35.12	0.52	ripidolite
125AG53_A3	Chl 2	Mafic clast	Spotted	Joliet Breccia	0.00	0.01	0.01	0.31	0.02	16	34.94	0.51	ripidolite
125AG53_A3	Chl 3	Mafic clast	Spotted	Joliet Breccia	0.01	0.00	0.00	0.23	0.34	16	35.02	0.53	ripidolite
125AG53_A3	Chl 4	Mafic clast	Spotted	Joliet Breccia	0.00	0.00	0.00	0.37	0.00	16	35.09	0.53	ripidolite
125AG53_A3	Chl 5	Mafic clast	Spotted	Joliet Breccia	0.02	0.00	0.01	0.33	0.01	16	35.18	0.50	brunsvigite
125AG53_A3	Chl 6	Mafic clast	Spotted	Joliet Breccia	0.01	0.02	0.01	0.23	0.01	16	35.04	0.54	ripidolite
125AG70_A2	Chl 1	Felsic clast	Spotted	Joliet Breccia	0.00	0.01	0.00	0.30	0.48	16	34.32	0.45	diabantite
125AG70_A2	Chl 2	Felsic clast	Spotted	Joliet Breccia	0.00	0.00	0.01	0.41	0.06	16	35.08	0.53	ripidolite
125AG70_A2	Chl 3	Felsic clast	Spotted	Joliet Breccia	0.02	0.00	0.01	0.61	0.03	16	35.17	0.42	ripidolite
125AG70_A2	Chl 5	Felsic clast	Spotted	Joliet Breccia	0.01	0.00	0.01	0.62	0.03	16	34.98	0.41	pycnochlorite
125AG70_A3	Chl 1	Felsic clast	Spotted	Joliet Breccia	0.00	0.00	0.02	0.44	0.01	16	35.21	0.44	ripidolite
125AG70_A3	Chl 2	Felsic clast	Spotted	Joliet Breccia	0.02	0.00	0.00	0.07	0.04	16	35.18	0.46	ripidolite
125AG70_A3	Chl 4	Felsic clast	Spotted	Joliet Breccia	0.01	0.00	0.00	0.37	0.04	16	35.38	0.45	ripidolite
125AG70_A3	Chl 5	Felsic clast	Spotted	Joliet Breccia	0.00	0.00	0.00	0.36	0.03	16	35.07	0.44	ripidolite
125AG70_A3	Chl 6	Felsic clast	Spotted	Joliet Breccia	0.00	0.02	0.01	0.49	0.02	16	35.21	0.43	ripidolite
125AG70_A3	Chl 7	Felsic clast	Spotted	Joliet Breccia	0.00	0.00	0.01	0.54	0.01	16	35.57	0.47	ripidolite
125AG70_A4	Chl 1	Felsic clast	Spotted	Joliet Breccia	0.00	0.00	0.00	0.38	0.03	16	35.22	0.43	ripidolite
125AG70_A4	Chl 2	Felsic clast	Spotted	Joliet Breccia	0.00	0.00	0.00	0.31	0.02	16	35.10	0.43	ripidolite
125AG70_A4	Chl 3	Felsic clast	Spotted	Joliet Breccia	0.00	0.01	0.00	0.39	0.01	16	35.13	0.41	ripidolite
125AG70_A4	Chl 4	Felsic clast	Spotted	Joliet Breccia	0.02	0.00	0.01	0.27	0.01	16	35.07	0.43	ripidolite
125DG47b_A2	Spectrum 6	Felsic dike	Spotted	Joliet Breccia	0.00	0.00	0.00	0.30	0.00	16	35.10	0.42	pycnochlorite
125DG47b_A2	Spectrum 7	Felsic dike	Spotted	Joliet Breccia	0.01	0.00	0.01	0.26	0.00	16	35.01	0.46	ripidolite
125DG47b_A3	Spectrum 10	Felsic dike	Spotted	Joliet Breccia	0.00	0.00	0.00	0.37	0.01	16	35.19	0.46	ripidolite
125DG47b_A3	Spectrum 11	Felsic dike	Spotted	Joliet Breccia	0.00	0.00	0.00	0.32	0.01	16	35.13	0.41	pycnochlorite
125DG47b_A3	Spectrum 12	Felsic dike	Spotted	Joliet Breccia	0.01	0.00	0.00	0.35	0.03	16	35.30	0.47	ripidolite
125DG47b_A4	Spectrum 7	Felsic dike	Spotted	Joliet Breccia	0.00	0.00	0.02	0.38	0.00	16	35.17	0.45	ripidolite
125DG47b_A5	Spectrum 10	Felsic dike	Spotted	Joliet Breccia	0.01	0.00	0.00	0.29	0.00	16	35.11	0.48	ripidolite
125DG47b_A5	Spectrum 11	Felsic dike	Spotted	Joliet Breccia	0.00	0.00	0.00	0.25	0.03	16	35.10	0.48	ripidolite
125DG47b_A5	Spectrum 12	Felsic dike	Spotted	Joliet Breccia	0.01	0.00	0.00	0.25	0.00	16	35.15	0.47	ripidolite
125DG47b_A6	Spectrum 8	Felsic dike	Spotted	Joliet Breccia	0.01	0.00	0.00	0.35	0.00	16	35.06	0.43	ripidolite
125DG47b_A6	Spectrum 9	Felsic dike	Spotted	Joliet Breccia	0.00	0.00	0.00	0.32	0.02	16	35.01	0.48	ripidolite
125DG47b_A7	Spectrum 17	Felsic dike	Spotted	Joliet Breccia	0.01	0.00	0.00	0.33	0.00	16	35.32	0.47	ripidolite
125DG47b_A7	Spectrum 18	Felsic dike	Spotted	Joliet Breccia	0.01	0.00	0.00	0.38	0.00	16	35.04	0.46	ripidolite
125DG47b_A7	Spectrum 19	Felsic dike	Spotted	Joliet Breccia	0.00	0.00	0.00	0.47	0.02	16	35.22	0.43	pycnochlorite
127AG02_area 1	Chl 1	Tonalite	Ank-ser	Silidor	0.01	0.01	0.07	0.32	0.00	16	35.32	0.40	ripidolite
127AG02_area 1	Chl 2	Tonalite	Ank-ser	Silidor	0.00	0.01	0.24	0.29	0.01	16	35.38	0.38	pycnochlorite
127AG02_area 1	Chl 3	Tonalite	Ank-ser	Silidor	0.00	0.01	0.09	0.30	0.01	16	35.50	0.30	pycnochlorite
127AG09_A1	Chl 1	Tonalite	Ank-ser	Silidor	0.00	0.00	0.02	0.27	0.00	16	35.38	0.34	pycnochlorite
127AG09_A1	Chl 2	Tonalite	Ank-ser	Silidor	0.00	0.00	0.00	0.47	0.00	16	35.32	0.33	pycnochlorite
127AG09_A1	Chl 3	Tonalite	Ank-ser	Silidor	0.02	0.01	0.01	0.50	0.00	16	35.50	0.33	pycnochlorite

ID	Spectrum	Lithology	Alteration	Location	SiO2	TiO2	Al2O3	FeO	MnO	MgO	CaO	Na2O	K2O	ZnO	NiO	No. of oxygens	Si	Al iv	Al vi	Ti	Fe3+	Fe2+	Mn	Mg
127AG09_A1	Chl 4	Tonalite	Ank-ser	Silidor	23.94	0.02	21.62	12.83	0.02	14.18	0.00	0.26	0.00	0.00	0.08	28	5.59	2.41	3.62	0.00	0.62	1.89	0.00	4.94
127AG09_A1	Chl 5	Tonalite	Ank-ser	Silidor	23.27	0.01	21.61	13.11	0.03	14.10	0.03	0.42	0.00	0.02	0.02	28	5.49	2.51	3.57	0.00	0.50	2.09	0.01	4.96
127AG09_A1	Chl 6	Tonalite	Ank-ser	Silidor	23.46	0.02	21.70	13.36	0.00	13.91	0.00	0.48	0.00	0.06	0.00	28	5.51	2.49	3.59	0.00	0.51	2.12	0.00	4.87
127AG09_A2	Chl 1	Tonalite	Ank-ser	Silidor	23.40	0.00	22.05	12.30	0.00	13.55	0.18	0.83	0.05	0.02	0.05	28	5.50	2.50	3.70	0.00	0.48	1.94	0.00	4.75
127AG09_A3	Chl 1	Tonalite	Ank-ser	Silidor	23.84	0.00	20.49	12.80	0.00	15.15	0.00	0.58	0.00	0.10	0.03	28	5.60	2.40	3.33	0.00	0.39	2.12	0.00	5.30
127AG09_A3	Chl 2	Tonalite	Ank-ser	Silidor	24.29	0.02	21.05	11.79	0.01	15.30	0.00	0.53	0.00	0.00	0.11	28	5.63	2.37	3.47	0.00	0.50	1.79	0.00	5.29
127AG09_A3	Chl 3	Tonalite	Ank-ser	Silidor	23.29	0.06	20.40	14.10	0.06	14.42	0.00	0.42	0.00	0.00	0.10	28	5.54	2.46	3.31	0.01	0.39	2.41	0.01	5.11
127AG09_A3	Chl 4	Tonalite	Ank-ser	Silidor	24.01	0.06	22.46	12.00	0.04	13.64	0.05	0.46	0.01	0.09	0.14	28	5.56	2.44	3.80	0.01	0.66	1.66	0.01	4.71
127AG09_A3	Chl 5	Tonalite	Ank-ser	Silidor	22.97	0.02	20.57	13.96	0.03	14.04	0.00	0.35	0.00	0.15	0.00	28	5.51	2.49	3.39	0.00	0.43	2.37	0.01	5.02
127AG09_A4	Chl 1	Tonalite	Ank-ser	Silidor	23.83	0.03	21.11	12.71	0.00	14.47	0.08	0.49	0.02	0.17	0.08	28	5.58	2.42	3.49	0.01	0.49	2.00	0.00	5.05
127AG09_A4	Chl 2	Tonalite	Ank-ser	Silidor	23.19	0.02	21.85	12.81	0.00	14.79	0.00	0.42	0.00	0.03	0.03	28	5.43	2.57	3.53	0.00	0.44	2.07	0.00	5.16
127AG09_A4	Chl 3	Tonalite	Ank-ser	Silidor	23.83	0.05	21.99	12.78	0.07	13.50	0.00	0.61	0.01	0.00	0.07	28	5.56	2.44	3.70	0.01	0.58	1.92	0.01	4.70
127AG09_A4	Chl 4	Tonalite	Ank-ser	Silidor	25.38	0.00	19.52	11.70	0.00	16.19	0.01	0.40	0.00	0.05	0.06	28	5.86	2.14	3.25	0.00	0.53	1.73	0.00	5.57
127AG09_A4	Chl 5	Tonalite	Ank-ser	Silidor	22.81	0.01	21.79	13.76	0.06	14.13	0.00	0.24	0.00	0.02	0.11	28	5.40	2.60	3.54	0.00	0.46	2.26	0.01	4.98
127AG09_A4	Chl 6	Tonalite	Ank-ser	Silidor	23.69	0.04	21.76	12.83	0.00	14.08	0.06	0.46	0.00	0.06	0.03	28	5.54	2.46	3.61	0.01	0.54	1.96	0.00	4.90
127AG09_A5	Chl 1	Tonalite	Ank-ser	Silidor	24.34	0.08	22.26	11.76	0.07	13.89	0.00	0.52	0.02	0.00	0.00	28	5.62	2.38	3.78	0.01	0.67	1.60	0.01	4.78
127AG09_A5	Chl 2	Tonalite	Ank-ser	Silidor	24.44	0.04	21.54	12.48	0.00	13.65	0.00	0.47	0.00	0.10	0.11	28	5.69	2.31	3.69	0.01	0.67	1.76	0.00	4.74
127AG09_A5	Chl 3	Tonalite	Ank-ser	Silidor	23.69	0.02	21.71	13.10	0.00	13.81	0.02	0.34	0.00	0.01	0.05	28	5.56	2.44	3.64	0.00	0.59	1.98	0.00	4.83
127AG09_A5	Chl 4	Tonalite	Ank-ser	Silidor	22.71	0.00	20.75	14.71	0.06	13.70	0.02	0.40	0.00	0.21	0.09	28	5.45	2.55	3.38	0.00	0.37	2.58	0.01	4.90
127AG09_A5	Chl 5	Tonalite	Ank-ser	Silidor	24.21	0.00	21.35	12.47	0.02	14.80	0.00	0.25	0.00	0.00	0.11	28	5.62	2.38	3.54	0.00	0.59	1.83	0.00	5.13
127BG11_A1	Chl 1	Mafic dike	Ank-ser	Silidor	24.69	0.00	20.19	9.41	0.00	19.15	0.03	0.41	0.06	0.00	0.08	28	5.62	2.38	3.08	0.00	0.29	1.50	0.00	6.49
127BG11_A1	Chl 2	Mafic dike	Ank-ser	Silidor	25.03	0.03	20.34	8.65	0.00	19.30	0.04	0.54	0.00	0.08	0.21	28	5.65	2.35	3.11	0.01	0.32	1.32	0.00	6.49
127BG11_A1	Chl 3	Mafic dike	Ank-ser	Silidor	25.93	0.00	18.90	8.25	0.01	20.35	0.04	0.54	0.02	0.00	0.02	28	5.84	2.16	2.91	0.00	0.30	1.25	0.00	6.83
127BG11_A1	Chl 4	Mafic dike	Ank-ser	Silidor	26.18	0.00	18.06	8.26	0.02	21.12	0.02	0.37	0.07	0.00	0.22	28	5.90	2.10	2.73	0.00	0.27	1.29	0.00	7.09
127BG11_A2	Chl 1	Mafic dike	Ank-ser	Silidor	24.18	0.00	19.23	10.38	0.00	18.55	0.04	0.31	0.00	0.13	0.12	28	5.64	2.36	2.96	0.00	0.27	1.76	0.00	6.45
127BG11_A2	Chl 2	Mafic dike	Ank-ser	Silidor	24.50	0.00	20.62	9.16	0.07	18.65	0.09	0.40	0.00	0.25	0.05	28	5.59	2.41	3.18	0.00	0.34	1.40	0.01	6.34
127BG11_A2	Chl 3	Mafic dike	Ank-ser	Silidor	24.67	0.02	19.60	10.34	0.00	18.55	0.03	0.46	0.02	0.00	0.11	28	5.66	2.34	3.01	0.00	0.28	1.70	0.00	6.35
127BG11_A2	Chl 4	Mafic dike	Ank-ser	Silidor	25.14	0.13	19.37	8.67	0.04	19.85	0.23	0.37	0.01	0.17	0.07	28	5.70	2.30	2.93	0.02	0.30	1.35	0.01	6.71
127BG11_A2	Chl 5	Mafic dike	Ank-ser	Silidor	25.14	0.00	19.31	8.71	0.03	19.72	0.12	0.45	0.00	0.00	0.08	28	5.73	2.27	2.96	0.00	0.30	1.37	0.00	6.70
127BG11_A2	Chl 6	Mafic dike	Ank-ser	Silidor	24.18	0.00	20.68	9.41	0.01	18.55	0.06	0.71	0.00	0.10	0.15	28	5.52	2.48	3.14	0.00	0.23	1.57	0.00	6.32
127BG11_A2	Chl 7	Mafic dike	Ank-ser	Silidor	24.68	0.01	20.69	8.59	0.00	18.78	0.10	0.56	0.01	0.17	0.12	28	5.60	2.40	3.20	0.00	0.34	1.30	0.00	6.36
127BG11_A3	Chl 1	Mafic dike	Ank-ser	Silidor	25.23	0.00	19.39	8.81	0.08	19.99	0.17	0.44	0.00	0.00	0.11	28	5.71	2.29	2.93	0.00	0.27	1.40	0.01	6.74
127BG11_A3	Chl 2	Mafic dike	Ank-ser	Silidor	25.58	0.00	19.58	9.36	0.05	18.94	0.06	0.32	0.01	0.04	0.11	28	5.79	2.21	3.07	0.00	0.42	1.36	0.01	6.40
127BG11_A3	Chl 3	Mafic dike	Ank-ser	Silidor	24.86	0.01	19.78	9.07	0.02	19.48	0.01	0.48	0.00	0.17	0.16	28	5.65	2.35	3.00	0.00	0.27	1.46	0.00	6.60
127BG11_A4	Chl 1	Mafic dike	Ank-ser	Silidor	25.36	0.03	18.17	8.49	0.03	21.13	0.18	0.50	0.00	0.06	0.16	28	5.77	2.23	2.67	0.01	0.15	1.47	0.01	7.16
127BG11_A4	Chl 2	Mafic dike	Ank-ser	Silidor	24.06	0.05	20.18	10.43	0.05	18.48	0.12	0.44	0.01	0.00	0.06	28	5.53	2.47	3.05	0.01	0.24	1.77	0.01	6.34
127BG11_A4	Chl 3	Mafic dike	Ank-ser	Silidor	24.49	0.03	20.93	9.08	0.06	18.55	0.06	0.51	0.02	0.03	0.10	28	5.56	2.44	3.22	0.01	0.34	1.39	0.01	6.28
127BG11_A4	Chl 4	Mafic dike	Ank-ser	Silidor	24.30	0.07	20.14	9.58	0.07	19.00	0.06	0.59	0.00	0.05	0.13	28	5.55	2.45	3.02	0.01	0.21	1.62	0.01	6.47
127BG11_A5	Chl 1	Mafic dike	Ank-ser	Silidor	24.14	0.08	20.04	10.83	0.01	17.90	0.06	0.47	0.00	0.00	0.16	28	5.57	2.43	3.07	0.01	0.28	1.81	0.00	6.16
127BG11_A5	Chl 2	Mafic dike	Ank-ser	Silidor	26.78	0.06	18.16	7.17	0.04	21.14	0.00	0.50	0.07	0.00	0.06	28	5.99	2.01	2.83	0.01	0.36	0.98	0.01	7.05
127BG11_A5	Chl 3	Mafic dike	Ank-ser	Silidor	25.64	0.07	17.89	8.83	0.05	20.90	0.10	0.45	0.03	0.09	0.17	28	5.82	2.18	2.65	0.01	0.18	1.49	0.01	7.08
127CG08_A2	Chl 1	Mafic dike	Ank-ser	Silidor	23.54	0.03	21.01	9.45	0.02	18.20	0.19	0.60	0.01	0.12	0.21	28	5.43	2.57	3.19	0.00	0.22	1.60	0.00	6.26
127CG08_A4	Chl 1	Mafic dike	Ank-ser	Silidor	24.18	0.00	22.14	9.31	0.03	17.05	0.04	0.56	0.00	0.00	0.44	28	5.50	2.50	3.50	0.00	0.44	1.33	0.00	5.78
127CG08_A4	Chl 2	Mafic dike	Ank-ser	Silidor	23.88	0.00	20.91	9.76	0.04	17.82	0.04	0.47	0.04	0.04	0.37	28	5.50	2.50	3.24	0.00	0.31	1.57	0.01	6.12
127CG08_A4	Chl 3	Mafic dike	Ank-ser	Silidor	23.53	0.03	22.01	9.94	0.00	17.18	0.08	0.63	0.00	0.03	0.39	28	5.39	2.61	3.39	0.00	0.31	1.59	0.00	5.86

ID	Spectrum	Lithology	Alteration	Location	Ni	Zn	Ca	Na	K	OH*	Total	Fe/Fe+Mg	Variety
127AG09_A1	Chl 4	Tonalite	Ank-ser	Silidor	0.02	0.00	0.00	0.23	0.00	16	35.32	0.34	ripidolite
127AG09_A1	Chl 5	Tonalite	Ank-ser	Silidor	0.00	0.00	0.01	0.39	0.00	16	35.53	0.34	ripidolite
127AG09_A1	Chl 6	Tonalite	Ank-ser	Silidor	0.00	0.01	0.00	0.44	0.00	16	35.53	0.35	ripidolite
127AG09_A2	Chl 1	Tonalite	Ank-ser	Silidor	0.01	0.00	0.05	0.75	0.03	16	35.70	0.34	ripidolite
127AG09_A3	Chl 1	Tonalite	Ank-ser	Silidor	0.01	0.02	0.00	0.53	0.00	16	35.70	0.32	ripidolite
127AG09_A3	Chl 2	Tonalite	Ank-ser	Silidor	0.02	0.00	0.00	0.48	0.00	16	35.55	0.30	pycnochlorite
127AG09_A3	Chl 3	Tonalite	Ank-ser	Silidor	0.02	0.00	0.00	0.38	0.00	16	35.65	0.35	ripidolite
127AG09_A3	Chl 4	Tonalite	Ank-ser	Silidor	0.03	0.02	0.01	0.42	0.01	16	35.34	0.33	ripidolite
127AG09_A3	Chl 5	Tonalite	Ank-ser	Silidor	0.00	0.03	0.00	0.33	0.00	16	35.58	0.36	ripidolite
127AG09_A4	Chl 1	Tonalite	Ank-ser	Silidor	0.02	0.03	0.02	0.44	0.01	16	35.56	0.33	ripidolite
127AG09_A4	Chl 2	Tonalite	Ank-ser	Silidor	0.01	0.00	0.00	0.38	0.00	16	35.60	0.33	ripidolite
127AG09_A4	Chl 3	Tonalite	Ank-ser	Silidor	0.01	0.00	0.00	0.56	0.01	16	35.49	0.35	ripidolite
127AG09_A4	Chl 4	Tonalite	Ank-ser	Silidor	0.01	0.01	0.00	0.36	0.00	16	35.46	0.29	pycnochlorite
127AG09_A4	Chl 5	Tonalite	Ank-ser	Silidor	0.02	0.00	0.00	0.22	0.00	16	35.50	0.35	ripidolite
127AG09_A4	Chl 6	Tonalite	Ank-ser	Silidor	0.01	0.01	0.02	0.41	0.00	16	35.47	0.34	ripidolite
127AG09_A5	Chl 1	Tonalite	Ank-ser	Silidor	0.00	0.00	0.00	0.47	0.01	16	35.34	0.32	pycnochlorite
127AG09_A5	Chl 2	Tonalite	Ank-ser	Silidor	0.02	0.02	0.00	0.42	0.00	16	35.32	0.34	pycnochlorite
127AG09_A5	Chl 3	Tonalite	Ank-ser	Silidor	0.01	0.00	0.01	0.31	0.00	16	35.37	0.35	ripidolite
127AG09_A5	Chl 4	Tonalite	Ank-ser	Silidor	0.02	0.04	0.01	0.37	0.00	16	35.67	0.38	ripidolite
127AG09_A5	Chl 5	Tonalite	Ank-ser	Silidor	0.02	0.00	0.00	0.22	0.00	16	35.34	0.32	pycnochlorite
127BG11_A1	Chl 1	Mafic dike	Ank-ser	Silidor	0.01	0.00	0.01	0.36	0.03	16	35.78	0.22	pycnochlorite
127BG11_A1	Chl 2	Mafic dike	Ank-ser	Silidor	0.04	0.01	0.01	0.48	0.00	16	35.78	0.20	pycnochlorite
127BG11_A1	Chl 3	Mafic dike	Ank-ser	Silidor	0.00	0.00	0.01	0.47	0.01	16	35.79	0.19	clinochlore
127BG11_A1	Chl 4	Mafic dike	Ank-ser	Silidor	0.04	0.00	0.01	0.33	0.04	16	35.80	0.18	clinochlore
127BG11_A2	Chl 1	Mafic dike	Ank-ser	Silidor	0.02	0.02	0.01	0.28	0.00	16	35.77	0.24	pycnochlorite
127BG11_A2	Chl 2	Mafic dike	Ank-ser	Silidor	0.01	0.04	0.02	0.35	0.00	16	35.70	0.22	ripidolite
127BG11_A2	Chl 3	Mafic dike	Ank-ser	Silidor	0.02	0.00	0.01	0.41	0.01	16	35.80	0.24	pycnochlorite
127BG11_A2	Chl 4	Mafic dike	Ank-ser	Silidor	0.01	0.03	0.06	0.33	0.01	16	35.75	0.20	clinochlore
127BG11_A2	Chl 5	Mafic dike	Ank-ser	Silidor	0.01	0.00	0.03	0.40	0.00	16	35.77	0.20	clinochlore
127BG11_A2	Chl 6	Mafic dike	Ank-ser	Silidor	0.03	0.02	0.01	0.63	0.00	16	35.95	0.22	ripidolite
127BG11_A2	Chl 7	Mafic dike	Ank-ser	Silidor	0.02	0.03	0.02	0.49	0.01	16	35.76	0.20	pycnochlorite
127BG11_A3	Chl 1	Mafic dike	Ank-ser	Silidor	0.02	0.00	0.04	0.38	0.00	16	35.80	0.20	clinochlore
127BG11_A3	Chl 2	Mafic dike	Ank-ser	Silidor	0.02	0.01	0.02	0.28	0.00	16	35.58	0.22	pycnochlorite
127BG11_A3	Chl 3	Mafic dike	Ank-ser	Silidor	0.03	0.03	0.00	0.42	0.00	16	35.82	0.21	pycnochlorite
127BG11_A4	Chl 1	Mafic dike	Ank-ser	Silidor	0.03	0.01	0.04	0.45	0.00	16	35.98	0.18	clinochlore
127BG11_A4	Chl 2	Mafic dike	Ank-ser	Silidor	0.01	0.00	0.03	0.39	0.01	16	35.85	0.24	ripidolite
127BG11_A4	Chl 3	Mafic dike	Ank-ser	Silidor	0.02	0.01	0.02	0.45	0.01	16	35.75	0.22	ripidolite
127BG11_A4	Chl 4	Mafic dike	Ank-ser	Silidor	0.02	0.01	0.01	0.52	0.00	16	35.92	0.22	ripidolite
127BG11_A5	Chl 1	Mafic dike	Ank-ser	Silidor	0.03	0.00	0.01	0.42	0.00	16	35.81	0.25	ripidolite
127BG11_A5	Chl 2	Mafic dike	Ank-ser	Silidor	0.01	0.00	0.00	0.43	0.04	16	35.72	0.16	clinochlore
127BG11_A5	Chl 3	Mafic dike	Ank-ser	Silidor	0.03	0.01	0.02	0.40	0.02	16	35.92	0.19	clinochlore
127CG08_A2	Chl 1	Mafic dike	Ank-ser	Silidor	0.04	0.02	0.05	0.54	0.00	16	35.93	0.23	ripidolite
127CG08_A4	Chl 1	Mafic dike	Ank-ser	Silidor	0.08	0.00	0.01	0.49	0.00	16	35.64	0.23	ripidolite
127CG08_A4	Chl 2	Mafic dike	Ank-ser	Silidor	0.07	0.01	0.01	0.42	0.02	16	35.77	0.23	ripidolite
127CG08_A4	Chl 3	Mafic dike	Ank-ser	Silidor	0.07	0.01	0.02	0.56	0.00	16	35.82	0.25	ripidolite

ID	Spectrum	Lithology	Alteration	Location	SiO2	TiO2	Al2O3	FeO	MnO	MgO	CaO	Na2O	K2O	ZnO	NiO	No. of oxygens	Si	Al iv	Al vi	Ti	Fe3+	Fe2+	Mn	Mg
127CG08_A4	Chl 4	Mafic dike	Ank-ser	Silidor	23.94	0.03	21.45	8.92	0.04	17.65	0.16	0.83	0.00	0.16	0.32	28	5.48	2.52	3.33	0.01	0.28	1.42	0.01	6.02
180AG01_A1	Spectrum 10	Cu-Zn-Ag Vein	-	Anglo-C	23.95	0.03	21.70	16.19	0.08	9.75	0.06	0.35	0.00	0.00	0.00	28	5.73	2.27	3.97	0.00	0.86	2.38	0.02	3.48
180AG01_A1	Spectrum 11	Cu-Zn-Ag Vein	-	Anglo-C	28.99	0.01	20.55	14.01	0.10	7.49	0.17	0.32	0.03	0.00	0.03	28	6.67	1.33	4.43	0.00	1.64	1.06	0.02	2.57
180AG01_A1	Spectrum 8	Cu-Zn-Ag Vein	-	Anglo-C	24.23	0.04	21.84	15.87	0.08	9.68	0.09	0.38	0.00	0.00	0.01	28	5.77	2.23	4.02	0.01	0.91	2.25	0.02	3.43
180AG01_A1	Spectrum 9	Cu-Zn-Ag Vein	-	Anglo-C	27.77	0.05	20.66	14.67	0.10	7.82	0.14	0.35	0.04	0.00	0.00	28	6.47	1.53	4.32	0.01	1.47	1.39	0.02	2.72
180AG01_A2	Spectrum 1	Cu-Zn-Ag Vein	-	Anglo-C	23.09	0.04	21.61	16.13	0.17	10.71	0.03	0.31	0.00	0.00	0.00	28	5.57	2.43	3.80	0.01	0.69	2.56	0.04	3.85
180AG01_A2	Spectrum 18	Cu-Zn-Ag Vein	-	Anglo-C	23.56	0.04	21.41	15.72	0.12	10.93	0.00	0.38	0.00	0.00	0.01	28	5.65	2.35	3.79	0.01	0.72	2.44	0.02	3.90
180AG01_A2	Spectrum 19	Cu-Zn-Ag Vein	-	Anglo-C	23.94	0.02	20.98	16.00	0.15	10.48	0.05	0.40	0.00	0.00	0.03	28	5.75	2.25	3.79	0.00	0.76	2.45	0.03	3.75
180AG01_A2	Spectrum 2	Cu-Zn-Ag Vein	-	Anglo-C	25.74	0.01	20.81	14.92	0.13	9.70	0.06	0.38	0.00	0.00	0.02	28	6.09	1.91	4.02	0.00	1.08	1.87	0.03	3.42
180AG01_A2	Spectrum 26	Cu-Zn-Ag Vein	-	Anglo-C	23.57	0.04	21.17	15.60	0.18	11.38	0.01	0.38	0.00	0.00	0.03	28	5.64	2.36	3.71	0.01	0.67	2.45	0.04	4.06
180AG01_A2	Spectrum 3	Cu-Zn-Ag Vein	-	Anglo-C	22.96	0.02	21.30	16.40	0.17	10.80	0.03	0.34	0.00	0.00	0.00	28	5.56	2.44	3.73	0.00	0.64	2.68	0.03	3.90
180AG01_A2	Spectrum 5	Cu-Zn-Ag Vein	-	Anglo-C	23.28	0.00	22.13	16.03	0.14	10.15	0.01	0.33	0.00	0.00	0.00	28	5.59	2.41	3.96	0.00	0.78	2.44	0.03	3.63
180AG01_A2	Spectrum 6	Cu-Zn-Ag Vein	-	Anglo-C	23.75	0.00	21.35	16.18	0.08	9.91	0.03	0.43	0.00	0.00	0.03	28	5.72	2.28	3.90	0.00	0.80	2.46	0.02	3.56
180AG01_A2	Spectrum 8	Cu-Zn-Ag Vein	-	Anglo-C	23.04	0.02	21.74	15.94	0.18	10.77	0.04	0.41	0.00	0.00	0.05	28	5.55	2.45	3.81	0.00	0.66	2.55	0.04	3.86
180AG01_A2	Spectrum 9	Cu-Zn-Ag Vein	-	Anglo-C	36.80	0.00	16.09	12.06	0.08	6.19	0.07	0.30	0.00	0.00	0.00	28	8.11	0.00	4.36	0.00	2.22	0.00	0.02	2.03
180AG01_A4	Spectrum 17	Cu-Zn-Ag Vein	-	Anglo-C	23.37	0.03	21.58	16.63	0.15	9.18	0.01	0.38	0.02	0.00	0.02	28	5.68	2.32	3.98	0.00	0.83	2.55	0.03	3.33
180AG01_A6	Spectrum 17	Cu-Zn-Ag Vein	-	Anglo-C	28.58	0.03	19.35	15.04	0.08	7.58	0.38	0.30	0.04	0.00	0.00	28	6.69	1.31	4.19	0.00	1.53	1.42	0.02	2.64
180AG01_A6	Spectrum 9	Cu-Zn-Ag Vein	-	Anglo-C	23.29	0.01	21.00	15.73	0.15	10.53	0.09	0.55	0.06	0.00	0.05	28	5.65	2.35	3.77	0.00	0.66	2.54	0.03	3.81
25AG01ii_A1	Chl 2	Gabbro	Spilite	Background	25.17	0.00	18.55	7.98	0.09	22.15	0.00	0.33	0.02	0.05	0.09	28	5.69	2.31	2.65	0.00	0.12	1.39	0.02	7.46
25AG01ii_A1	Chl 4	Gabbro	Spilite	Background	25.13	0.17	18.71	7.96	0.08	21.79	0.05	0.54	0.00	0.03	0.00	28	5.67	2.33	2.67	0.03	0.11	1.39	0.02	7.32
25AG01ii_A1	Chl 5	Gabbro	Spilite	Background	25.00	0.03	18.22	8.08	0.08	22.36	0.03	0.53	0.01	0.02	0.11	28	5.66	2.34	2.55	0.00	0.02	1.52	0.02	7.55
25AG01ii_A1	Chl 6	Gabbro	Spilite	Background	24.11	0.00	19.34	9.51	0.09	20.39	0.03	0.27	0.00	0.12	0.07	28	5.54	2.46	2.80	0.00	0.14	1.69	0.02	6.98
25AG01ii_A1	Chl 7	Gabbro	Spilite	Background	24.54	0.02	19.36	7.99	0.12	21.81	0.04	0.35	0.01	0.12	0.05	28	5.55	2.45	2.74	0.00	0.10	1.41	0.02	7.36
25AG01ii_A2	Spectrum 10	Gabbro	Spilite	Background	24.95	0.13	19.29	7.56	0.06	21.56	0.10	0.52	0.00	0.07	0.01	28	5.62	2.38	2.78	0.02	0.15	1.28	0.01	7.24
25AG01ii_A2	Spectrum 11	Gabbro	Spilite	Background	24.25	0.13	19.19	8.67	0.17	21.44	0.13	0.32	0.00	0.00	0.09	28	5.52	2.48	2.69	0.02	0.08	1.57	0.03	7.28
25AG01ii_A2	Spectrum 12	Gabbro	Spilite	Background	24.53	0.13	19.04	8.03	0.12	21.83	0.07	0.57	0.00	0.05	0.07	28	5.56	2.44	2.66	0.02	0.03	1.49	0.02	7.37
25AG01ii_A2	Spectrum 9	Gabbro	Spilite	Background	24.12	0.24	18.75	9.16	0.12	21.38	0.06	0.33	0.00	0.00	0.07	28	5.53	2.47	2.60	0.04	0.05	1.70	0.02	7.30
25AG01ii_A3	Chl 1	Gabbro	Spilite	Background	25.78	0.00	17.35	8.12	0.04	22.64	0.05	0.60	0.00	0.00	0.01	28	5.82	2.18	2.45	0.00	0.03	1.50	0.01	7.61
25AG01ii_A3	Chl 2	Gabbro	Spilite	Background	25.76	0.06	17.67	7.96	0.08	22.16	0.11	0.46	0.00	0.13	0.03	28	5.82	2.18	2.55	0.01	0.12	1.38	0.02	7.46
25AG01ii_A3	Chl 3	Gabbro	Spilite	Background	25.85	0.00	17.21	8.13	0.08	22.65	0.00	0.46	0.02	0.01	0.03	28	5.84	2.16	2.45	0.00	0.07	1.47	0.02	7.63
25AG01ii_A3	Chl 4	Gabbro	Spilite	Background	24.90	0.03	18.28	8.50	0.03	21.76	0.03	0.41	0.00	0.20	0.02	28	5.67	2.33	2.60	0.01	0.08	1.54	0.01	7.39
25AG01ii_A3	Chl 5	Gabbro	Spilite	Background	26.34	0.00	17.09	7.84	0.15	22.13	0.25	0.37	0.00	0.06	0.08	28	5.94	2.06	2.52	0.00	0.19	1.29	0.03	7.44
25AG01ii_A3	Chl 6	Gabbro	Spilite	Background	24.32	0.02	19.92	8.54	0.15	20.88	0.00	0.51	0.04	0.00	0.03	28	5.51	2.49	2.86	0.00	0.10	1.51	0.03	7.05
25AG01ii_A4	Chl 1	Gabbro	Spilite	Background	24.90	0.06	18.39	8.49	0.13	21.83	0.05	0.48	0.01	0.02	0.00	28	5.66	2.34	2.60	0.01	0.06	1.55	0.02	7.39
25AG01ii_A4	Chl 2	Gabbro	Spilite	Background	24.94	0.01	18.81	8.24	0.08	21.98	0.03	0.42	0.00	0.00	0.00	28	5.64	2.36	2.67	0.00	0.09	1.47	0.02	7.40
25AG01ii_A4	Chl 3	Gabbro	Spilite	Background	25.19	0.17	18.42	8.23	0.10	21.59	0.12	0.46	0.00	0.03	0.00	28	5.70	2.30	2.65	0.03	0.14	1.42	0.02	7.29
25AG01ii_A4	Chl 4	Gabbro	Spilite	Background	24.72	0.20	18.64	8.34	0.04	21.93	0.11	0.30	0.00	0.00	0.12	28	5.61	2.39	2.61	0.03	0.10	1.48	0.01	7.42
25AG01ii_A4	Chl 5	Gabbro	Spilite	Background	24.86	0.18	18.86	7.75	0.05	21.74	0.04	0.54	0.00	0.08	0.02	28	5.63	2.37	2.69	0.03	0.11	1.36	0.01	7.34
25AG01ii_A4	Chl 7	Gabbro	Spilite	Background	23.93	0.26	18.68	9.33	0.14	21.22	0.09	0.41	0.00	0.00	0.00	28	5.50	2.50	2.59	0.04	0.02	1.78	0.03	7.27
25AG01ii_A5	Chl 1	Gabbro	Spilite	Background	24.69	0.05	19.92	7.75	0.09	21.38	0.01	0.39	0.05	0.00	0.10	28	5.56	2.44	2.88	0.01	0.17	1.29	0.02	7.17
25AG01ii_A5	Chl 2	Gabbro	Spilite	Background	25.10	0.02	18.74	7.71	0.17	22.09	0.00	0.43	0.02	0.00	0.12	28	5.66	2.34	2.68	0.00	0.11	1.35	0.03	7.43
25AG01ii_A5	Chl 3	Gabbro	Spilite	Background	25.31	0.04	18.37	7.76	0.11	21.89	0.10	0.40	0.06	0.01	0.10	28	5.73	2.27	2.66	0.01	0.13	1.34	0.02	7.39
31AG07i_A1	Chl 1	Basalt	Spotted	Powell F-Zone	23.92	0.00	22.48	9.65	0.00	17.75	0.00	0.12	0.01	0.00	0.00	28	5.43	2.57	3.50	0.00	0.48	1.35	0.00	6.00
31AG07i_A1	Chl 2	Basalt	Spotted	Powell F-Zone	24.65	0.00	20.61	12.56	0.00	15.15	0.00	0.08	0.00	0.00	0.00	28	5.73	2.27	3.45	0.00	0.64	1.81	0.00	5.25
31AG07i_A2	Chl 1	Basalt	Spotted	Powell F-Zone	23.84	0.00	22.02	9.69	0.00	18.34	0.00	0.14	0.00	0.00	0.00	28	5.42	2.58	3.37	0.00	0.40	1.44	0.00	6.21

ID	Spectrum	Lithology	Alteration	Location	Ni	Zn	Ca	Na	K	OH*	Total	Fe/Fe+Mg	Variety
127CG08_A4	Chl 4	Mafic dike	Ank-ser	Silidor	0.06	0.03	0.04	0.74	0.00	16	35.92	0.22	ripidolite
180AG01_A1	Spectrum 10	Cu-Zn-Ag Vein	-	Anglo-C	0.00	0.00	0.02	0.33	0.00	16	35.05	0.48	pycnochlorite
180AG01_A1	Spectrum 11	Cu-Zn-Ag Vein	-	Anglo-C	0.01	0.00	0.04	0.28	0.02	16	34.06	0.51	no name
180AG01_A1	Spectrum 8	Cu-Zn-Ag Vein	-	Anglo-C	0.00	0.00	0.02	0.35	0.00	16	35.00	0.48	pycnochlorite
180AG01_A1	Spectrum 9	Cu-Zn-Ag Vein	-	Anglo-C	0.00	0.00	0.03	0.31	0.02	16	34.29	0.51	no name
180AG01_A2	Spectrum 1	Cu-Zn-Ag Vein	-	Anglo-C	0.00	0.00	0.01	0.29	0.00	16	35.25	0.46	ripidolite
180AG01_A2	Spectrum 18	Cu-Zn-Ag Vein	-	Anglo-C	0.00	0.00	0.00	0.36	0.00	16	35.24	0.45	pycnochlorite
180AG01_A2	Spectrum 19	Cu-Zn-Ag Vein	-	Anglo-C	0.01	0.00	0.01	0.37	0.00	16	35.19	0.46	pycnochlorite
180AG01_A2	Spectrum 2	Cu-Zn-Ag Vein	-	Anglo-C	0.00	0.00	0.02	0.35	0.00	16	34.78	0.46	pycnochlorite
180AG01_A2	Spectrum 26	Cu-Zn-Ag Vein	-	Anglo-C	0.00	0.00	0.00	0.36	0.00	16	35.30	0.43	pycnochlorite
180AG01_A2	Spectrum 3	Cu-Zn-Ag Vein	-	Anglo-C	0.00	0.00	0.01	0.32	0.00	16	35.32	0.46	ripidolite
180AG01_A2	Spectrum 5	Cu-Zn-Ag Vein	-	Anglo-C	0.00	0.00	0.00	0.31	0.00	16	35.15	0.47	ripidolite
180AG01_A2	Spectrum 6	Cu-Zn-Ag Vein	-	Anglo-C	0.01	0.00	0.01	0.40	0.00	16	35.16	0.48	pycnochlorite
180AG01_A2	Spectrum 8	Cu-Zn-Ag Vein	-	Anglo-C	0.01	0.00	0.01	0.38	0.00	16	35.32	0.45	ripidolite
180AG01_A2	Spectrum 9	Cu-Zn-Ag Vein	-	Anglo-C	0.00	0.00	0.02	0.25	0.00	16	33.00	0.52	no name
180AG01_A4	Spectrum 17	Cu-Zn-Ag Vein	-	Anglo-C	0.00	0.00	0.00	0.36	0.01	16	35.11	0.50	brunsvigite
180AG01_A6	Spectrum 17	Cu-Zn-Ag Vein	-	Anglo-C	0.00	0.00	0.10	0.27	0.02	16	34.19	0.53	no name
180AG01_A6	Spectrum 9	Cu-Zn-Ag Vein	-	Anglo-C	0.01	0.00	0.02	0.52	0.04	16	35.39	0.46	pycnochlorite
25AG01ii_A1	Chl 2	Gabbro	Spilite	Background	0.02	0.01	0.00	0.29	0.01	16	35.96	0.17	clinochlore
25AG01ii_A1	Chl 4	Gabbro	Spilite	Background	0.00	0.00	0.01	0.47	0.00	16	36.03	0.17	clinochlore
25AG01ii_A1	Chl 5	Gabbro	Spilite	Background	0.02	0.00	0.01	0.47	0.01	16	36.15	0.17	clinochlore
25AG01ii_A1	Chl 6	Gabbro	Spilite	Background	0.01	0.02	0.01	0.24	0.00	16	35.92	0.21	ripidolite
25AG01ii_A1	Chl 7	Gabbro	Spilite	Background	0.01	0.02	0.01	0.31	0.01	16	35.99	0.17	sheridanite
25AG01ii_A2	Spectrum 10	Gabbro	Spilite	Background	0.00	0.01	0.02	0.46	0.00	16	35.98	0.16	clinochlore
25AG01ii_A2	Spectrum 11	Gabbro	Spilite	Background	0.02	0.00	0.03	0.28	0.00	16	36.00	0.18	sheridanite
25AG01ii_A2	Spectrum 12	Gabbro	Spilite	Background	0.01	0.01	0.02	0.50	0.00	16	36.14	0.17	sheridanite
25AG01ii_A2	Spectrum 9	Gabbro	Spilite	Background	0.01	0.00	0.01	0.29	0.00	16	36.04	0.19	sheridanite
25AG01ii_A3	Chl 1	Gabbro	Spilite	Background	0.00	0.00	0.01	0.53	0.00	16	36.15	0.17	clinochlore
25AG01ii_A3	Chl 2	Gabbro	Spilite	Background	0.00	0.02	0.03	0.40	0.00	16	35.99	0.17	clinochlore
25AG01ii_A3	Chl 3	Gabbro	Spilite	Background	0.01	0.00	0.00	0.41	0.01	16	36.06	0.17	clinochlore
25AG01ii_A3	Chl 4	Gabbro	Spilite	Background	0.00	0.03	0.01	0.36	0.00	16	36.03	0.18	clinochlore
25AG01ii_A3	Chl 5	Gabbro	Spilite	Background	0.01	0.01	0.06	0.32	0.00	16	35.88	0.17	clinochlore
25AG01ii_A3	Chl 6	Gabbro	Spilite	Background	0.01	0.00	0.00	0.45	0.02	16	36.04	0.19	sheridanite
25AG01ii_A4	Chl 1	Gabbro	Spilite	Background	0.00	0.00	0.01	0.42	0.01	16	36.08	0.18	clinochlore
25AG01ii_A4	Chl 2	Gabbro	Spilite	Background	0.00	0.00	0.01	0.36	0.00	16	36.02	0.17	clinochlore
25AG01ii_A4	Chl 3	Gabbro	Spilite	Background	0.00	0.01	0.03	0.40	0.00	16	35.98	0.18	clinochlore
25AG01ii_A4	Chl 4	Gabbro	Spilite	Background	0.02	0.00	0.03	0.27	0.00	16	35.97	0.18	clinochlore
25AG01ii_A4	Chl 5	Gabbro	Spilite	Background	0.00	0.01	0.01	0.48	0.00	16	36.04	0.17	clinochlore
25AG01ii_A4	Chl 7	Gabbro	Spilite	Background	0.00	0.00	0.02	0.37	0.00	16	36.11	0.20	sheridanite
25AG01ii_A5	Chl 1	Gabbro	Spilite	Background	0.02	0.00	0.00	0.34	0.03	16	35.93	0.17	sheridanite
25AG01ii_A5	Chl 2	Gabbro	Spilite	Background	0.02	0.00	0.00	0.37	0.01	16	36.01	0.16	clinochlore
25AG01ii_A5	Chl 3	Gabbro	Spilite	Background	0.02	0.00	0.02	0.35	0.03	16	35.97	0.17	clinochlore
31AG07i_A1	Chl 1	Basalt	Spotted	Powell F-Zone	0.00	0.00	0.00	0.11	0.01	16	35.44	0.23	ripidolite
31AG07i_A1	Chl 2	Basalt	Spotted	Powell F-Zone	0.00	0.00	0.00	0.08	0.00	16	35.23	0.32	pycnochlorite
31AG07i_A2	Chl 1	Basalt	Spotted	Powell F-Zone	0.00	0.00	0.00	0.12	0.00	16	35.54	0.23	ripidolite

ID	Spectrum	Lithology	Alteration	Location	SiO2	TiO2	Al2O3	FeO	MnO	MgO	CaO	Na2O	K2O	ZnO	NiO	No. of oxygens	Si	Al iv	Al vi	Ti	Fe3+	Fe2+	Mn	Mg
31AG07i_A2	Chl 2	Basalt	Spotted	Powell F-Zone	24.43	0.00	20.91	12.49	0.00	15.20	0.00	0.08	0.00	0.00	0.00	28	5.68	2.32	3.48	0.00	0.62	1.81	0.00	5.27
31AG07i_A2	Chl 3	Basalt	Spotted	Powell F-Zone	24.17	0.00	21.46	9.63	0.00	18.39	0.00	0.22	0.04	0.00	0.00	28	5.50	2.50	3.30	0.00	0.39	1.44	0.00	6.24
31AG07i_A2	Chl 4	Basalt	Spotted	Powell F-Zone	23.67	0.00	22.85	9.68	0.00	17.58	0.00	0.18	0.00	0.00	0.00	28	5.37	2.63	3.54	0.00	0.46	1.37	0.00	5.95
31AG07i_A4	chl 1	Basalt	Spotted	Powell F-Zone	26.33	0.00	19.79	11.70	0.00	15.31	0.06	0.05	0.00	0.00	0.00	28	6.03	1.97	3.46	0.00	0.81	1.43	0.00	5.23
31AG07i_A4	chl 2	Basalt	Spotted	Powell F-Zone	24.14	0.00	22.25	9.53	0.00	17.70	0.04	0.17	0.05	0.00	0.00	28	5.47	2.53	3.48	0.00	0.48	1.32	0.00	5.98
31AG07i_A4	chl 4	Basalt	Spotted	Powell F-Zone	25.84	0.00	20.49	11.95	0.00	14.85	0.00	0.09	0.05	0.00	0.00	28	5.93	2.07	3.56	0.00	0.80	1.50	0.00	5.08
31AG07i_A4	chl 5	Basalt	Spotted	Powell F-Zone	23.58	0.00	23.05	9.62	0.00	17.69	0.00	0.03	0.02	0.00	0.00	28	5.35	2.65	3.56	0.00	0.49	1.34	0.00	5.98
31AG07ii_A3	Chl 1	Basalt	Spotted	Powell F-Zone	25.09	0.00	21.04	11.41	0.00	15.86	0.00	0.00	0.00	0.00	0.00	28	5.75	2.25	3.51	0.00	0.70	1.49	0.00	5.42
31AG07ii_A3	Chl 2	Basalt	Spotted	Powell F-Zone	24.19	0.00	22.53	8.97	0.00	18.28	0.00	0.00	0.00	0.00	0.00	28	5.46	2.54	3.50	0.00	0.53	1.17	0.00	6.15
31AG07ii_A3	Chl 3	Basalt	Spotted	Powell F-Zone	24.62	0.00	20.19	12.44	0.00	15.86	0.00	0.00	0.00	0.00	0.00	28	5.73	2.27	3.33	0.00	0.59	1.84	0.00	5.51
31AG07ii_A4	Chl 1	Basalt	Spotted	Powell F-Zone	25.09	0.00	20.35	12.43	0.00	15.18	0.02	0.06	0.02	0.00	0.00	28	5.81	2.19	3.44	0.00	0.68	1.73	0.00	5.25
31AG07ii_A4	Chl 2	Basalt	Spotted	Powell F-Zone	23.79	0.00	22.54	9.21	0.00	18.48	0.02	0.07	0.00	0.00	0.00	28	5.38	2.62	3.44	0.00	0.44	1.30	0.00	6.23
31AG07ii_QMAP 4_area	Chl 1	Basalt	Spotted	Powell F-Zone	24.58	0.03	22.58	9.24	0.10	16.72	0.00	0.34	0.35	0.00	0.03	28	5.54	2.46	3.63	0.00	0.53	1.21	0.02	5.62
31AG07ii_QMAP 4_area	Chl 2	Basalt	Spotted	Powell F-Zone	23.39	0.00	21.89	10.07	0.07	18.00	0.00	0.41	0.04	0.08	0.00	28	5.36	2.64	3.31	0.00	0.28	1.65	0.01	6.14
31AG07ii_QMAP 4_area	Chl 3	Basalt	Spotted	Powell F-Zone	26.20	0.03	21.12	8.73	0.05	17.22	0.02	0.32	0.01	0.02	0.06	28	5.86	2.14	3.52	0.01	0.71	0.93	0.01	5.74
31AG07ii_QMAP 4_area	Chl 4	Basalt	Spotted	Powell F-Zone	24.18	0.00	22.21	9.26	0.08	17.77	0.02	0.33	0.02	0.11	0.00	28	5.47	2.53	3.46	0.00	0.45	1.31	0.02	6.00
31AG07ii_QMAP 4_area	Chl 5	Basalt	Spotted	Powell F-Zone	23.81	0.02	22.55	8.91	0.06	18.31	0.00	0.41	0.06	0.00	0.08	28	5.37	2.63	3.43	0.00	0.36	1.33	0.01	6.16
31AG07ii_QMAP 4_area	Chl 1	Basalt	Spotted	Powell F-Zone	23.43	0.04	22.22	10.07	0.06	17.55	0.04	0.37	0.00	0.09	0.06	28	5.36	2.64	3.40	0.01	0.35	1.58	0.01	5.98
31AG07ii_QMAP 4_area	Chl 2	Basalt	Spotted	Powell F-Zone	24.03	0.02	22.24	8.86	0.07	18.26	0.03	0.44	0.06	0.10	0.00	28	5.43	2.57	3.41	0.00	0.37	1.30	0.01	6.15
31AG07ii_QMAP 4_area	Chl 3	Basalt	Spotted	Powell F-Zone	23.17	0.06	22.78	9.02	0.05	18.38	0.02	0.35	0.05	0.03	0.00	28	5.27	2.73	3.42	0.01	0.32	1.40	0.01	6.23
31AG07ii_QMAP 4_area	Chl 4	Basalt	Spotted	Powell F-Zone	23.85	0.03	22.12	9.76	0.09	17.49	0.03	0.41	0.08	0.00	0.05	28	5.43	2.57	3.43	0.01	0.39	1.47	0.02	5.94
31AG07ii_QMAP 4_area	Chl 5	Basalt	Spotted	Powell F-Zone	23.80	0.01	22.45	9.44	0.08	17.84	0.01	0.37	0.04	0.00	0.00	28	5.40	2.60	3.46	0.00	0.39	1.40	0.02	6.03
31AG07ii_QMAP 4_area	Chl 6	Basalt	Spotted	Powell F-Zone	24.00	0.01	22.08	9.35	0.05	17.67	0.00	0.41	0.08	0.11	0.00	28	5.46	2.54	3.44	0.00	0.40	1.38	0.01	5.99
31AG07ii_QMAP 4_area	Chl 1	Basalt	Spotted	Powell F-Zone	23.73	0.00	22.00	8.89	0.08	18.98	0.01	0.37	0.00	0.08	0.04	28	5.37	2.63	3.30	0.00	0.29	1.39	0.02	6.41
31AG07ii_QMAP 4_area	Chl 2	Basalt	Spotted	Powell F-Zone	23.63	0.03	22.37	9.93	0.07	17.54	0.00	0.40	0.00	0.00	0.01	28	5.38	2.62	3.44	0.01	0.38	1.51	0.01	5.95
31AG07ii_QMAP 4_area	Chl 3	Basalt	Spotted	Powell F-Zone	23.86	0.04	22.28	9.12	0.05	17.91	0.01	0.35	0.01	0.18	0.00	28	5.42	2.58	3.45	0.01	0.41	1.32	0.01	6.06
31AG07ii_QMAP 4_area	Chl 4	Basalt	Spotted	Powell F-Zone	23.84	0.03	22.47	9.41	0.07	17.88	0.00	0.31	0.00	0.04	0.00	28	5.40	2.60	3.46	0.00	0.42	1.36	0.01	6.04
48AG02_A1	Chl 1	Cu-Zn-Ag Vein	-	Cu-Zn-Ag Vein	23.71	0.04	22.31	14.44	0.10	10.99	0.05	0.44	0.00	0.03	0.00	28	5.62	2.38	3.97	0.01	0.79	2.08	0.02	3.89
48AG02_A1	Chl 2	Cu-Zn-Ag Vein	-	Cu-Zn-Ag Vein	27.72	0.06	17.91	16.44	0.06	8.21	0.08	0.35	0.00	0.00	0.10	28	6.64	1.36	3.84	0.01	1.31	1.98	0.01	2.93
48AG02_A1	Chl 3	Cu-Zn-Ag Vein	-	Cu-Zn-Ag Vein	22.90	0.00	22.20	14.64	0.14	12.06	0.04	0.38	0.00	0.00	0.01	28	5.46	2.54	3.79	0.00	0.60	2.32	0.03	4.29
48AG02_A3	Chl 1	Cu-Zn-Ag Vein	-	Cu-Zn-Ag Vein	23.77	0.04	22.04	13.79	0.05	12.04	0.00	0.67	0.02	0.01	0.00	28	5.60	2.40	3.83	0.01	0.65	2.07	0.01	4.23
48AG02_A3	Chl 2	Cu-Zn-Ag Vein	-	Cu-Zn-Ag Vein	22.48	0.03	21.66	16.02	0.11	11.47	0.08	0.19	0.00	0.06	0.00	28	5.44	2.56	3.70	0.01	0.59	2.65	0.02	4.14
48AG02_A3	Chl 3	Cu-Zn-Ag Vein	-	Cu-Zn-Ag Vein	23.48	0.01	21.58	14.95	0.13	11.71	0.00	0.27	0.01	0.10	0.00	28	5.61	2.39	3.77	0.00	0.70	2.29	0.03	4.17
48AG02_A3	Chl 4	Cu-Zn-Ag Vein	-	Cu-Zn-Ag Vein	23.23	0.02	19.71	17.93	0.19	9.85	0.03	0.21	0.00	0.04	0.00	28	5.75	2.25	3.59	0.00	0.70	3.02	0.04	3.64
61AG07_area 1	Chl 1	Rhyolite	Spotted	Powell F-Zone	22.50	0.04	23.54	15.19	0.04	10.83	0.00	0.29	0.00	0.00	0.02	28	5.35	2.65	4.06	0.01	0.72	2.31	0.01	3.84
61AG07_area 1	Chl 2	Rhyolite	Spotted	Powell F-Zone	22.97	0.01	23.62	14.42	0.04	10.91	0.00	0.24	0.00	0.15	0.04	28	5.43	2.57	4.13	0.00	0.80	2.05	0.01	3.85
61AG07_area 1	Chl 3	Rhyolite	Spotted	Powell F-Zone	23.43	0.07	23.73	13.86	0.02	11.39	0.06	0.12	0.04	0.00	0.00	28	5.48	2.52	4.13	0.01	0.86	1.85	0.00	3.97
61AG07_area 1	Chl 4	Rhyolite	Spotted	Powell F-Zone	23.73	0.00	23.82	14.15	0.05	9.71	0.03	0.26	0.59	0.12	0.00	28	5.57	2.43	4.31	0.00	0.89	1.89	0.01	3.40
61AG07_area 1	Chl 5	Rhyolite	Spotted	Powell F-Zone	22.73	0.00	23.74	14.93	0.04	10.90	0.00	0.19	0.01	0.00	0.06	28	5.38	2.62	4.11	0.00	0.77	2.18	0.01	3.85
61AG07_area 2	Chl 1	Rhyolite	Spotted	Powell F-Zone	22.78	0.00	23.77	14.69	0.06	10.90	0.00	0.28	0.00	0.00	0.00	28	5.39	2.61	4.13	0.00	0.77	2.14	0.01	3.84
61AG07_area 2	Chl 2	Rhyolite	Spotted	Powell F-Zone	22.49	0.02	23.44	15.13	0.09	10.86	0.01	0.16	0.06	0.09	0.00	28	5.36	2.64	4.05	0.00	0.74	2.28	0.02	3.86
61AG07_area 2	Chl 3	Rhyolite	Spotted	Powell F-Zone	23.71	0.00	24.13	13.52	0.02	10.19	0.05	0.27	0.57	0.11	0.04	28	5.54	2.46	4.32	0.00	0.88	1.76	0.00	3.55
61AG07_area 2	Chl 4	Rhyolite	Spotted	Powell F-Zone	23.09	0.00	23.35	14.84	0.04	10.84	0.00	0.31	0.02	0.00	0.07	28	5.46	2.54	4.08	0.00	0.77	2.16	0.01	3.82
61DG07_area 1	Chl 1	Rhyolite	Spotted	Powell F-Zone	22.99	0.00	23.52	15.26	0.03	10.29	0.03	0.25	0.00	0.02	0.00	28	5.46	2.54	4.15	0.00	0.82	2.21	0.01	3.64
61DG07_area 1	Chl 2	Rhyolite	Spotted	Powell F-Zone	23.06	0.00	23.46	15.64	0.00	9.84	0.05	0.27	0.00	0.00	0.00	28	5.49	2.51	4.18	0.00	0.85	2.26	0.00	3.49

ID	Spectrum	Lithology	Alteration	Location	Ni	Zn	Ca	Na	K	OH*	Total	Fe/Fe+Mg	Variety
31AG07i_A2	Chl 2	Basalt	Spotted	Powell F-Zone	0.00	0.00	0.00	0.07	0.00	16	35.25	0.32	pycnochlorite
31AG07i_A2	Chl 3	Basalt	Spotted	Powell F-Zone	0.00	0.00	0.00	0.19	0.02	16	35.59	0.23	ripidolite
31AG07i_A2	Chl 4	Basalt	Spotted	Powell F-Zone	0.00	0.00	0.00	0.16	0.00	16	35.48	0.24	ripidolite
31AG07i_A4	chl 1	Basalt	Spotted	Powell F-Zone	0.00	0.00	0.01	0.05	0.00	16	34.99	0.30	pycnochlorite
31AG07i_A4	chl 2	Basalt	Spotted	Powell F-Zone	0.00	0.00	0.01	0.15	0.03	16	35.46	0.23	ripidolite
31AG07i_A4	chl 4	Basalt	Spotted	Powell F-Zone	0.00	0.00	0.00	0.08	0.03	16	35.04	0.31	pycnochlorite
31AG07i_A4	chl 5	Basalt	Spotted	Powell F-Zone	0.00	0.00	0.00	0.03	0.01	16	35.41	0.23	ripidolite
31AG07ii_A3	Chl 1	Basalt	Spotted	Powell F-Zone	0.00	0.00	0.00	0.00	0.00	16	35.13	0.29	pycnochlorite
31AG07ii_A3	Chl 2	Basalt	Spotted	Powell F-Zone	0.00	0.00	0.00	0.00	0.00	16	35.34	0.22	ripidolite
31AG07ii_A3	Chl 3	Basalt	Spotted	Powell F-Zone	0.00	0.00	0.00	0.00	0.00	16	35.26	0.31	pycnochlorite
31AG07ii_A4	Chl 1	Basalt	Spotted	Powell F-Zone	0.00	0.00	0.01	0.06	0.01	16	35.17	0.31	pycnochlorite
31AG07ii_A4	Chl 2	Basalt	Spotted	Powell F-Zone	0.00	0.00	0.00	0.06	0.00	16	35.48	0.22	ripidolite
31AG07ii_QMAP 4_area	Chl 1	Basalt	Spotted	Powell F-Zone	0.00	0.00	0.00	0.30	0.20	16	35.52	0.24	ripidolite
31AG07ii_QMAP 4_area	Chl 2	Basalt	Spotted	Powell F-Zone	0.00	0.01	0.00	0.36	0.03	16	35.79	0.24	ripidolite
31AG07ii_QMAP 4_area	Chl 3	Basalt	Spotted	Powell F-Zone	0.01	0.00	0.00	0.28	0.00	16	35.22	0.22	pycnochlorite
31AG07ii_QMAP 4_area	Chl 4	Basalt	Spotted	Powell F-Zone	0.00	0.02	0.01	0.29	0.01	16	35.56	0.23	ripidolite
31AG07ii_QMAP 4_area	Chl 5	Basalt	Spotted	Powell F-Zone	0.01	0.00	0.00	0.36	0.04	16	35.71	0.21	ripidolite
31AG07ii_QMAP 4_area	Chl 1	Basalt	Spotted	Powell F-Zone	0.01	0.02	0.01	0.33	0.00	16	35.69	0.24	ripidolite
31AG07ii_QMAP 4_area	Chl 2	Basalt	Spotted	Powell F-Zone	0.00	0.02	0.01	0.38	0.04	16	35.69	0.21	ripidolite
31AG07ii_QMAP 4_area	Chl 3	Basalt	Spotted	Powell F-Zone	0.00	0.01	0.00	0.31	0.03	16	35.73	0.22	ripidolite
31AG07ii_QMAP 4_area	Chl 4	Basalt	Spotted	Powell F-Zone	0.01	0.00	0.01	0.36	0.05	16	35.67	0.24	ripidolite
31AG07ii_QMAP 4_area	Chl 5	Basalt	Spotted	Powell F-Zone	0.00	0.00	0.00	0.33	0.02	16	35.65	0.23	ripidolite
31AG07ii_QMAP 4_area	Chl 6	Basalt	Spotted	Powell F-Zone	0.00	0.02	0.00	0.36	0.05	16	35.65	0.23	ripidolite
31AG07ii_QMAP 4_area	Chl 1	Basalt	Spotted	Powell F-Zone	0.01	0.01	0.00	0.33	0.00	16	35.75	0.21	ripidolite
31AG07ii_QMAP 4_area	Chl 2	Basalt	Spotted	Powell F-Zone	0.00	0.00	0.00	0.36	0.00	16	35.66	0.24	ripidolite
31AG07ii_QMAP 4_area	Chl 3	Basalt	Spotted	Powell F-Zone	0.00	0.03	0.00	0.31	0.01	16	35.60	0.22	ripidolite
31AG07ii_QMAP 4_area	Chl 4	Basalt	Spotted	Powell F-Zone	0.00	0.01	0.00	0.27	0.00	16	35.58	0.23	ripidolite
48AG02_A1	Chl 1	Cu-Zn-Ag Vein	-	Cu-Zn-Ag Vein	0.00	0.01	0.01	0.41	0.00	16	35.17	0.42	pycnochlorite
48AG02_A1	Chl 2	Cu-Zn-Ag Vein	-	Cu-Zn-Ag Vein	0.02	0.00	0.02	0.33	0.00	16	34.46	0.53	no name
48AG02_A1	Chl 3	Cu-Zn-Ag Vein	-	Cu-Zn-Ag Vein	0.00	0.00	0.01	0.35	0.00	16	35.39	0.41	ripidolite
48AG02_A3	Chl 1	Cu-Zn-Ag Vein	-	Cu-Zn-Ag Vein	0.00	0.00	0.00	0.61	0.01	16	35.42	0.39	pycnochlorite
48AG02_A3	Chl 2	Cu-Zn-Ag Vein	-	Cu-Zn-Ag Vein	0.00	0.01	0.02	0.18	0.00	16	35.33	0.44	ripidolite
48AG02_A3	Chl 3	Cu-Zn-Ag Vein	-	Cu-Zn-Ag Vein	0.00	0.02	0.00	0.25	0.01	16	35.23	0.42	pycnochlorite
48AG02_A3	Chl 4	Cu-Zn-Ag Vein	-	Cu-Zn-Ag Vein	0.00	0.01	0.01	0.20	0.00	16	35.20	0.51	brunsvigite
61AG07_area 1	Chl 1	Rhyolite	Spotted	Powell F-Zone	0.00	0.00	0.00	0.27	0.00	16	35.22	0.44	ripidolite
61AG07_area 1	Chl 2	Rhyolite	Spotted	Powell F-Zone	0.01	0.03	0.00	0.22	0.00	16	35.09	0.43	ripidolite
61AG07_area 1	Chl 3	Rhyolite	Spotted	Powell F-Zone	0.00	0.00	0.02	0.11	0.02	16	34.98	0.41	ripidolite
61AG07_area 1	Chl 4	Rhyolite	Spotted	Powell F-Zone	0.00	0.02	0.01	0.24	0.35	16	35.12	0.45	ripidolite
61AG07_area 1	Chl 5	Rhyolite	Spotted	Powell F-Zone	0.01	0.00	0.00	0.18	0.00	16	35.11	0.43	ripidolite
61AG07_area 2	Chl 1	Rhyolite	Spotted	Powell F-Zone	0.00	0.00	0.00	0.25	0.00	16	35.15	0.43	ripidolite
61AG07_area 2	Chl 2	Rhyolite	Spotted	Powell F-Zone	0.00	0.02	0.00	0.15	0.03	16	35.16	0.44	ripidolite
61AG07_area 2	Chl 3	Rhyolite	Spotted	Powell F-Zone	0.01	0.02	0.01	0.25	0.34	16	35.14	0.43	ripidolite
61AG07_area 2	Chl 4	Rhyolite	Spotted	Powell F-Zone	0.01	0.00	0.00	0.28	0.01	16	35.15	0.43	ripidolite
61DG07_area 1	Chl 1	Rhyolite	Spotted	Powell F-Zone	0.00	0.00	0.01	0.23	0.00	16	35.07	0.45	ripidolite
61DG07_area 1	Chl 2	Rhyolite	Spotted	Powell F-Zone	0.00	0.00	0.01	0.25	0.00	16	35.04	0.47	ripidolite

ID	Spectrum	Lithology	Alteration	Location	SiO2	TiO2	Al2O3	FeO	MnO	MgO	CaO	Na2O	K2O	ZnO	NiO	No. of oxygens	Si	Al iv	Al vi	Ti	Fe3+	Fe2+	Mn	Mg
61DG07_area 1	Chl 3	Rhyolite	Spotted	Powell F-Zone	22.80	0.01	23.77	15.18	0.04	10.19	0.03	0.32	0.00	0.06	0.02	28	5.41	2.59	4.18	0.00	0.80	2.21	0.01	3.61
61DG07_area 1	Chl 4	Rhyolite	Spotted	Powell F-Zone	22.63	0.01	23.61	15.83	0.02	9.89	0.04	0.26	0.02	0.00	0.01	28	5.40	2.60	4.16	0.00	0.80	2.37	0.00	3.52
61DG07_area 1	Chl 5	Rhyolite	Spotted	Powell F-Zone	22.98	0.00	23.64	15.02	0.05	10.45	0.01	0.32	0.00	0.01	0.04	28	5.44	2.56	4.15	0.00	0.80	2.17	0.01	3.69
61DG07_area 1	Chl 6	Rhyolite	Spotted	Powell F-Zone	22.84	0.02	23.96	15.14	0.06	10.17	0.01	0.25	0.01	0.01	0.00	28	5.41	2.59	4.21	0.00	0.83	2.17	0.01	3.59
85BG01_A4	Spectrum 1	Cu-Ag Vein	-	Anglo-A Cu-Zn-Ag	22.49	0.04	22.28	15.47	0.18	11.33	0.04	0.46	0.00	0.00	0.05	28	5.40	2.60	3.80	0.01	0.57	2.54	0.04	4.06
85BG01_A4	Spectrum 2	Cu-Ag Vein	-	Anglo-A Cu-Zn-Ag	24.97	0.03	20.90	14.83	0.18	10.60	0.04	0.40	0.04	0.00	0.03	28	5.92	2.08	3.88	0.01	0.91	2.04	0.04	3.75
85BG01_A4	Spectrum 3	Cu-Ag Vein	-	Anglo-A Cu-Zn-Ag	23.55	0.02	21.96	14.93	0.20	11.15	0.03	0.38	0.00	0.00	0.00	28	5.61	2.39	3.88	0.00	0.74	2.24	0.04	3.96
85BG01_A4	Spectrum 4	Cu-Ag Vein	-	Anglo-A Cu-Zn-Ag	22.34	0.00	22.18	14.06	0.06	13.83	0.00	0.31	0.00	0.00	0.02	28	5.31	2.69	3.58	0.00	0.42	2.37	0.01	4.90
85BG01_A4	Spectrum 5	Cu-Ag Vein	-	Anglo-A Cu-Zn-Ag	22.96	0.02	23.08	15.42	0.19	10.10	0.00	0.51	0.03	0.00	0.09	28	5.47	2.53	4.07	0.00	0.73	2.34	0.04	3.59
85BG01_A4	Spectrum 6	Cu-Ag Vein	-	Anglo-A Cu-Zn-Ag	23.42	0.02	21.79	14.81	0.16	11.75	0.00	0.41	0.02	0.00	0.03	28	5.57	2.43	3.78	0.00	0.66	2.29	0.03	4.17
85BG01_A4	Spectrum 7	Cu-Ag Vein	-	Anglo-A Cu-Zn-Ag	23.24	0.05	20.92	15.95	0.22	10.91	0.03	0.34	0.00	0.00	0.00	28	5.64	2.36	3.71	0.01	0.68	2.56	0.05	3.95
85BG01_A4	Spectrum 8	Cu-Ag Vein	-	Anglo-A Cu-Zn-Ag	22.74	0.00	21.51	15.92	0.17	11.58	0.00	0.32	0.00	0.00	0.00	28	5.49	2.51	3.68	0.00	0.57	2.64	0.03	4.17
85BG01_A5	Spectrum 19	Cu-Ag Vein	-	Anglo-A Cu-Zn-Ag	22.68	0.04	22.19	15.38	0.20	11.48	0.00	0.38	0.00	0.00	0.03	28	5.44	2.56	3.79	0.01	0.60	2.48	0.04	4.10
85BG01_A5	Spectrum 20	Cu-Ag Vein	-	Anglo-A Cu-Zn-Ag	23.38	0.03	22.14	14.66	0.17	11.81	0.02	0.38	0.00	0.00	0.02	28	5.54	2.46	3.82	0.01	0.67	2.23	0.03	4.17
85BG01_A5	Spectrum 21	Cu-Ag Vein	-	Anglo-A Cu-Zn-Ag	23.13	0.00	22.12	15.02	0.18	11.74	0.01	0.31	0.00	0.00	0.02	28	5.51	2.49	3.81	0.00	0.65	2.34	0.04	4.17
85BG01_A5	Spectrum 22	Cu-Ag Vein	-	Anglo-A Cu-Zn-Ag	23.08	0.00	21.95	15.00	0.20	11.82	0.01	0.39	0.01	0.00	0.02	28	5.51	2.49	3.77	0.00	0.61	2.38	0.04	4.20
85BG01_A5	Spectrum 23	Cu-Ag Vein	-	Anglo-A Cu-Zn-Ag	22.85	0.01	22.12	15.18	0.17	11.82	0.00	0.41	0.01	0.00	0.05	28	5.45	2.55	3.76	0.00	0.58	2.45	0.03	4.20
85BG01_A5	Spectrum 24	Cu-Ag Vein	-	Anglo-A Cu-Zn-Ag	23.47	0.02	21.45	14.40	0.18	12.64	0.04	0.43	0.01	0.00	0.00	28	5.57	2.43	3.65	0.00	0.58	2.28	0.04	4.47
85BG01_A5	Spectrum 25	Cu-Ag Vein	-	Anglo-A Cu-Zn-Ag	23.22	0.04	22.12	14.87	0.20	11.65	0.00	0.42	0.02	0.00	0.00	28	5.52	2.48	3.81	0.01	0.65	2.31	0.04	4.13
85BG01_A6	Spectrum 15	Cu-Ag Vein	-	Anglo-A Cu-Zn-Ag	23.46	0.01	21.99	14.81	0.22	11.67	0.02	0.38	0.00	0.00	0.03	28	5.57	2.43	3.81	0.00	0.68	2.26	0.04	4.13
85BG01_A6	Spectrum 16	Cu-Ag Vein	-	Anglo-A Cu-Zn-Ag	22.66	0.00	22.51	15.50	0.21	11.18	0.00	0.29	0.00	0.00	0.00	28	5.43	2.57	3.88	0.00	0.65	2.45	0.04	3.99
85BG01_A6	Spectrum 17	Cu-Ag Vein	-	Anglo-A Cu-Zn-Ag	23.15	0.01	21.32	14.60	0.13	13.03	0.00	0.34	0.02	0.00	0.00	28	5.51	2.49	3.58	0.00	0.53	2.38	0.03	4.63
85BG10_area 2	Chl 1	Rhyolite	Spotted	Anglo-A Cu-Zn-Ag	23.24	0.00	21.96	17.53	0.31	8.17	0.04	0.47	0.00	0.00	0.02	28	5.65	2.35	4.07	0.00	0.84	2.72	0.06	2.96
85BG10_area 2	Chl 2	Rhyolite	Spotted	Anglo-A Cu-Zn-Ag	23.17	0.00	22.60	17.01	0.29	7.93	0.04	0.53	0.00	0.00	0.06	28	5.62	2.38	4.20	0.00	0.88	2.57	0.06	2.87
85BG10_area 2	Chl 3	Rhyolite	Spotted	Anglo-A Cu-Zn-Ag	21.88	0.01	21.93	19.44	0.32	7.24	0.00	0.35	0.00	0.00	0.00	28	5.47	2.53	4.04	0.00	0.75	3.32	0.07	2.70
85BG10_area 2	Chl 4	Rhyolite	Spotted	Anglo-A Cu-Zn-Ag	21.97	0.01	20.97	19.67	0.31	7.79	0.02	0.41	0.05	0.08	0.12	28	5.51	2.49	3.80	0.00	0.62	3.50	0.07	2.91
85CG07ii_area 4	Chl 1	Mafic tuff	Spotted	Anglo-A Cu-Zn-Ag	24.23	0.02	21.08	14.44	0.43	11.39	0.02	0.64	0.10	0.00	0.02	28	5.75	2.25	3.75	0.00	0.68	2.18	0.09	4.03
85CG07ii_area 4	Chl 2	Mafic tuff	Spotted	Anglo-A Cu-Zn-Ag	23.45	0.00	20.98	15.89	0.48	11.03	0.03	0.31	0.06	0.00	0.02	28	5.65	2.35	3.70	0.00	0.66	2.54	0.10	3.96
85CG07ii_area 4	Chl 3	Mafic tuff	Spotted	Anglo-A Cu-Zn-Ag	23.78	0.02	21.41	15.09	0.41	11.08	0.00	0.40	0.00	0.05	0.00	28	5.68	2.32	3.80	0.00	0.73	2.28	0.08	3.94
85CG07ii_area 4	Chl 4	Mafic tuff	Spotted	Anglo-A Cu-Zn-Ag	23.47	0.06	21.46	14.93	0.42	11.59	0.02	0.33	0.00	0.06	0.05	28	5.60	2.40	3.74	0.01	0.68	2.30	0.08	4.13
85CG07ii_area 4	Chl 5	Mafic tuff	Spotted	Anglo-A Cu-Zn-Ag	24.31	0.07	21.68	14.12	0.40	11.55	0.04	0.35	0.01	0.00	0.04	28	5.73	2.27	3.85	0.01	0.80	1.98	0.08	4.05
85CG07ii_QMAP 2_area	Chl 1	Mafic tuff	Spotted	Anglo-A Cu-Zn-Ag	24.04	0.06	21.57	14.56	0.48	11.51	0.00	0.16	0.05	0.00	0.00	28	5.70	2.30	3.82	0.01	0.81	2.08	0.10	4.07
85CG07ii_QMAP 2_area	Chl 2	Mafic tuff	Spotted	Anglo-A Cu-Zn-Ag	24.50	0.07	21.60	14.26	0.42	10.93	0.04	0.34	0.28	0.00	0.04	28	5.78	2.22	3.90	0.01	0.83	1.99	0.08	3.84
85CG07ii_QMAP 2_area	Chl 3	Mafic tuff	Spotted	Anglo-A Cu-Zn-Ag	24.14	0.04	21.94	13.93	0.39	11.59	0.03	0.30	0.05	0.05	0.04	28	5.69	2.31	3.89	0.01	0.80	1.94	0.08	4.07
85CG07ii_QMAP 2_area	Chl 4	Mafic tuff	Spotted	Anglo-A Cu-Zn-Ag	27.51	0.02	19.99	13.50	0.43	10.54	0.02	0.36	0.03	0.00	0.00	28	6.36	1.64	3.94	0.00	1.20	1.41	0.08	3.63
85CG07ii_QMAP 2_area	Chl 5	Mafic tuff	Spotted	Anglo-A Cu-Zn-Ag	24.10	0.00	21.18	14.36	0.45	11.70	0.06	0.32	0.07	0.13	0.01	28	5.72	2.28	3.75	0.00	0.73	2.12	0.09	4.14
85CG07ii_QMAP 2_area	Chl 6	Mafic tuff	Spotted	Anglo-A Cu-Zn-Ag	24.18	0.10	21.53	14.14	0.43	11.85	0.02	0.27	0.00	0.02	0.00	28	5.71	2.29	3.79	0.02	0.79	2.00	0.09	4.17
85CG07ii_QMAP 2_area	Chl 7	Mafic tuff	Spotted	Anglo-A Cu-Zn-Ag	24.22	0.03	21.44	14.02	0.40	11.90	0.07	0.40	0.03	0.02	0.01	28	5.71	2.29	3.78	0.01	0.74	2.03	0.08	4.19
85DG05_A1	Chl 1	Mafic dike	Chlorite	Anglo-A Cu-Zn-Ag	23.85	0.00	20.86	15.82	0.20	11.10	0.02	0.27	0.02	0.00	0.01	28	5.73	2.27	3.72	0.00	0.73	2.44	0.04	3.97
85DG05_A1	Chl 2	Mafic dike	Chlorite	Anglo-A Cu-Zn-Ag	24.05	0.07	21.43	15.55	0.13	10.60	0.01	0.46	0.02	0.00	0.00	28	5.73	2.27	3.85	0.01	0.78	2.32	0.03	3.76
85DG05_A1	Chl 3	Mafic dike	Chlorite	Anglo-A Cu-Zn-Ag	23.42	0.00	21.22	16.12	0.13	10.87	0.00	0.38	0.00	0.00	0.07	28	5.64	2.36	3.75	0.00	0.68	2.57	0.03	3.90
85DG05_A2	Chl 1	Mafic dike	Chlorite	Anglo-A Cu-Zn-Ag	23.70	0.10	21.56	15.18	0.17	10.87	0.11	0.46	0.00	0.05	0.15	28	5.65	2.35	3.82	0.02	0.73	2.30	0.03	3.86
85DG05_A2	Chl 2	Mafic dike	Chlorite	Anglo-A Cu-Zn-Ag	24.20	0.00	21.75	14.89	0.22	10.52	0.08	0.43	0.00	0.00	0.05	28	5.75	2.25	3.95	0.00	0.84	2.12	0.04	3.72
85DG05_A2	Chl 3	Mafic dike	Chlorite	Anglo-A Cu-Zn-Ag	22.71	0.00	21.08	17.06	0.12	10.57	0.00	0.44	0.00	0.00	0.03	28	5.54	2.46	3.68	0.00	0.57	2.91	0.02	3.84
85DG05_A3	Chl 1	Mafic dike	Chlorite	Anglo-A Cu-Zn-Ag	23.22	0.03	21.98	15.94	0.20	10.31	0.04	0.44	0.00	0.00	0.00	28	5.58	2.42	3.90	0.01	0.72	2.48	0.04	3.69

ID	Spectrum	Lithology	Alteration	Location	Ni	Zn	Ca	Na	K	OH*	Total	Fe/Fe+Mg	Variety
61DG07_area 1	Chl 3	Rhyolite	Spotted	Powell F-Zone	0.00	0.01	0.01	0.30	0.00	16	35.13	0.46	ripidolite
61DG07_area 1	Chl 4	Rhyolite	Spotted	Powell F-Zone	0.00	0.00	0.01	0.24	0.01	16	35.11	0.47	ripidolite
61DG07_area 1	Chl 5	Rhyolite	Spotted	Powell F-Zone	0.01	0.00	0.00	0.29	0.00	16	35.12	0.45	ripidolite
61DG07_area 1	Chl 6	Rhyolite	Spotted	Powell F-Zone	0.00	0.00	0.00	0.23	0.01	16	35.06	0.46	ripidolite
85BG01_A4	Spectrum 1	Cu-Ag Vein	-	Anglo-A Cu-Zn-Ag	0.01	0.00	0.01	0.43	0.00	16	35.45	0.43	ripidolite
85BG01_A4	Spectrum 2	Cu-Ag Vein	-	Anglo-A Cu-Zn-Ag	0.01	0.00	0.01	0.37	0.02	16	35.01	0.44	pycnochlorite
85BG01_A4	Spectrum 3	Cu-Ag Vein	-	Anglo-A Cu-Zn-Ag	0.00	0.00	0.01	0.35	0.00	16	35.21	0.43	pycnochlorite
85BG01_A4	Spectrum 4	Cu-Ag Vein	-	Anglo-A Cu-Zn-Ag	0.00	0.00	0.00	0.29	0.00	16	35.58	0.36	ripidolite
85BG01_A4	Spectrum 5	Cu-Ag Vein	-	Anglo-A Cu-Zn-Ag	0.02	0.00	0.00	0.47	0.02	16	35.28	0.46	ripidolite
85BG01_A4	Spectrum 6	Cu-Ag Vein	-	Anglo-A Cu-Zn-Ag	0.01	0.00	0.00	0.38	0.01	16	35.33	0.41	ripidolite
85BG01_A4	Spectrum 7	Cu-Ag Vein	-	Anglo-A Cu-Zn-Ag	0.00	0.00	0.01	0.32	0.00	16	35.27	0.45	pycnochlorite
85BG01_A4	Spectrum 8	Cu-Ag Vein	-	Anglo-A Cu-Zn-Ag	0.00	0.00	0.00	0.30	0.00	16	35.40	0.44	ripidolite
85BG01_A5	Spectrum 19	Cu-Ag Vein	-	Anglo-A Cu-Zn-Ag	0.01	0.00	0.00	0.35	0.00	16	35.39	0.43	ripidolite
85BG01_A5	Spectrum 20	Cu-Ag Vein	-	Anglo-A Cu-Zn-Ag	0.00	0.00	0.01	0.35	0.00	16	35.30	0.41	ripidolite
85BG01_A5	Spectrum 21	Cu-Ag Vein	-	Anglo-A Cu-Zn-Ag	0.00	0.00	0.00	0.29	0.00	16	35.29	0.42	ripidolite
85BG01_A5	Spectrum 22	Cu-Ag Vein	-	Anglo-A Cu-Zn-Ag	0.00	0.00	0.00	0.36	0.01	16	35.37	0.42	ripidolite
85BG01_A5	Spectrum 23	Cu-Ag Vein	-	Anglo-A Cu-Zn-Ag	0.01	0.00	0.00	0.38	0.01	16	35.43	0.42	ripidolite
85BG01_A5	Spectrum 24	Cu-Ag Vein	-	Anglo-A Cu-Zn-Ag	0.00	0.00	0.01	0.40	0.01	16	35.43	0.39	ripidolite
85BG01_A5	Spectrum 25	Cu-Ag Vein	-	Anglo-A Cu-Zn-Ag	0.00	0.00	0.00	0.39	0.01	16	35.34	0.42	ripidolite
85BG01_A6	Spectrum 15	Cu-Ag Vein	-	Anglo-A Cu-Zn-Ag	0.01	0.00	0.01	0.35	0.00	16	35.29	0.42	ripidolite
85BG01_A6	Spectrum 16	Cu-Ag Vein	-	Anglo-A Cu-Zn-Ag	0.00	0.00	0.00	0.27	0.00	16	35.29	0.44	ripidolite
85BG01_A6	Spectrum 17	Cu-Ag Vein	-	Anglo-A Cu-Zn-Ag	0.00	0.00	0.00	0.31	0.01	16	35.47	0.39	ripidolite
85BG10_area 2	Chl 1	Rhyolite	Spotted	Anglo-A Cu-Zn-Ag	0.00	0.00	0.01	0.44	0.00	16	35.12	0.55	brunsvigite
85BG10_area 2	Chl 2	Rhyolite	Spotted	Anglo-A Cu-Zn-Ag	0.01	0.00	0.01	0.50	0.00	16	35.10	0.55	brunsvigite
85BG10_area 2	Chl 3	Rhyolite	Spotted	Anglo-A Cu-Zn-Ag	0.00	0.00	0.00	0.34	0.00	16	35.20	0.60	ripidolite
85BG10_area 2	Chl 4	Rhyolite	Spotted	Anglo-A Cu-Zn-Ag	0.02	0.01	0.01	0.40	0.03	16	35.39	0.59	ripidolite
85CG07ii_area 4	Chl 1	Mafic tuff	Spotted	Anglo-A Cu-Zn-Ag	0.00	0.00	0.01	0.59	0.06	16	35.39	0.42	pycnochlorite
85CG07ii_area 4	Chl 2	Mafic tuff	Spotted	Anglo-A Cu-Zn-Ag	0.00	0.00	0.01	0.29	0.04	16	35.29	0.45	pycnochlorite
85CG07ii_area 4	Chl 3	Mafic tuff	Spotted	Anglo-A Cu-Zn-Ag	0.00	0.01	0.00	0.37	0.00	16	35.23	0.43	pycnochlorite
85CG07ii_area 4	Chl 4	Mafic tuff	Spotted	Anglo-A Cu-Zn-Ag	0.01	0.01	0.01	0.31	0.00	16	35.27	0.42	pycnochlorite
85CG07ii_area 4	Chl 5	Mafic tuff	Spotted	Anglo-A Cu-Zn-Ag	0.01	0.00	0.01	0.32	0.01	16	35.12	0.41	pycnochlorite
85CG07ii_QMAP 2_area	Chl 1	Mafic tuff	Spotted	Anglo-A Cu-Zn-Ag	0.00	0.00	0.00	0.15	0.03	16	35.06	0.42	pycnochlorite
85CG07ii_QMAP 2_area	Chl 2	Mafic tuff	Spotted	Anglo-A Cu-Zn-Ag	0.01	0.00	0.01	0.31	0.17	16	35.15	0.42	pycnochlorite
85CG07ii_QMAP 2_area	Chl 3	Mafic tuff	Spotted	Anglo-A Cu-Zn-Ag	0.01	0.01	0.01	0.27	0.03	16	35.12	0.40	pycnochlorite
85CG07ii_QMAP 2_area	Chl 4	Mafic tuff	Spotted	Anglo-A Cu-Zn-Ag	0.00	0.00	0.00	0.32	0.02	16	34.62	0.42	diabantite
85CG07ii_QMAP 2_area	Chl 5	Mafic tuff	Spotted	Anglo-A Cu-Zn-Ag	0.00	0.02	0.02	0.29	0.04	16	35.21	0.41	pycnochlorite
85CG07ii_QMAP 2_area	Chl 6	Mafic tuff	Spotted	Anglo-A Cu-Zn-Ag	0.00	0.00	0.01	0.25	0.00	16	35.11	0.40	pycnochlorite
85CG07ii_QMAP 2_area	Chl 7	Mafic tuff	Spotted	Anglo-A Cu-Zn-Ag	0.00	0.00	0.02	0.37	0.02	16	35.22	0.40	pycnochlorite
85DG05_A1	Chl 1	Mafic dike	Chlorite	Anglo-A Cu-Zn-Ag	0.00	0.00	0.01	0.25	0.01	16	35.18	0.44	pycnochlorite
85DG05_A1	Chl 2	Mafic dike	Chlorite	Anglo-A Cu-Zn-Ag	0.00	0.00	0.00	0.42	0.01	16	35.19	0.45	pycnochlorite
85DG05_A1	Chl 3	Mafic dike	Chlorite	Anglo-A Cu-Zn-Ag	0.01	0.00	0.00	0.35	0.00	16	35.29	0.45	pycnochlorite
85DG05_A2	Chl 1	Mafic dike	Chlorite	Anglo-A Cu-Zn-Ag	0.03	0.01	0.03	0.43	0.00	16	35.25	0.44	pycnochlorite
85DG05_A2	Chl 2	Mafic dike	Chlorite	Anglo-A Cu-Zn-Ag	0.01	0.00	0.02	0.40	0.00	16	35.10	0.44	pycnochlorite
85DG05_A2	Chl 3	Mafic dike	Chlorite	Anglo-A Cu-Zn-Ag	0.01	0.00	0.00	0.42	0.00	16	35.44	0.48	ripidolite
85DG05_A3	Chl 1	Mafic dike	Chlorite	Anglo-A Cu-Zn-Ag	0.00	0.00	0.01	0.41	0.00	16	35.26	0.46	ripidolite

ID	Spectrum	Lithology	Alteration	Location	SiO2	TiO2	Al2O3	FeO	MnO	MgO	CaO	Na2O	K2O	ZnO	NiO	No. of oxygens	Si	Al iv	Al vi	Ti	Fe3+	Fe2+	Mn	Mg
85DG05_A3	Chl 2	Mafic dike	Chlorite	Anglo-A Cu-Zn-Ag	23.82	0.06	22.06	14.68	0.08	10.67	0.06	0.65	0.01	0.14	0.14	28	5.65	2.35	3.93	0.01	0.74	2.17	0.02	3.77
85DG05_A3	Chl 3	Mafic dike	Chlorite	Anglo-A Cu-Zn-Ag	23.74	0.00	21.68	15.84	0.12	10.12	0.00	0.39	0.00	0.16	0.01	28	5.69	2.31	3.93	0.00	0.80	2.37	0.02	3.62
85DG05_A3	Chl 4	Mafic dike	Chlorite	Anglo-A Cu-Zn-Ag	23.43	0.08	21.64	15.97	0.22	10.03	0.05	0.30	0.04	0.10	0.11	28	5.64	2.36	3.89	0.01	0.79	2.43	0.04	3.60
85DG05_A4	Chl 1	Mafic dike	Chlorite	Anglo-A Cu-Zn-Ag	23.02	0.02	21.11	16.60	0.09	10.82	0.04	0.35	0.03	0.01	0.00	28	5.58	2.42	3.70	0.00	0.62	2.74	0.02	3.91
85DG05_A4	Chl 2	Mafic dike	Chlorite	Anglo-A Cu-Zn-Ag	23.78	0.02	20.87	15.84	0.13	11.16	0.00	0.50	0.02	0.00	0.03	28	5.70	2.30	3.69	0.00	0.66	2.52	0.03	3.99
85DG05_A4	Chl 3	Mafic dike	Chlorite	Anglo-A Cu-Zn-Ag	23.90	0.00	22.11	15.19	0.15	10.42	0.02	0.37	0.00	0.00	0.00	28	5.68	2.32	3.99	0.00	0.84	2.18	0.03	3.69
85DG05_A5	Chl 1	Mafic dike	Chlorite	Anglo-A Cu-Zn-Ag	23.55	0.00	21.75	15.31	0.16	10.72	0.02	0.52	0.02	0.07	0.00	28	5.63	2.37	3.87	0.00	0.71	2.35	0.03	3.82
85DG05_A5	Chl 2	Mafic dike	Chlorite	Anglo-A Cu-Zn-Ag	24.01	0.01	20.95	15.43	0.21	10.68	0.02	0.55	0.07	0.10	0.00	28	5.75	2.25	3.78	0.00	0.72	2.37	0.04	3.82
85DG05_A5	Chl 3	Mafic dike	Chlorite	Anglo-A Cu-Zn-Ag	24.13	0.00	20.52	15.49	0.13	11.41	0.00	0.34	0.00	0.10	0.04	28	5.78	2.22	3.67	0.00	0.72	2.38	0.03	4.07
85DG05_A6	Chl 1	Mafic dike	Chlorite	Anglo-A Cu-Zn-Ag	22.87	0.07	20.37	17.01	0.25	10.56	0.00	0.34	0.00	0.14	0.00	28	5.62	2.38	3.59	0.01	0.60	2.89	0.05	3.87
85DG05_A6	Chl 2	Mafic dike	Chlorite	Anglo-A Cu-Zn-Ag	23.44	0.00	21.79	15.59	0.20	10.41	0.07	0.60	0.07	0.02	0.00	28	5.61	2.39	3.88	0.00	0.68	2.44	0.04	3.72
85DG05_A6	Chl 3	Mafic dike	Chlorite	Anglo-A Cu-Zn-Ag	23.50	0.00	20.96	16.17	0.24	10.82	0.00	0.42	0.00	0.00	0.02	28	5.67	2.33	3.72	0.00	0.67	2.59	0.05	3.89
85DG05_A6	Chl 4	Mafic dike	Chlorite	Anglo-A Cu-Zn-Ag	23.12	0.04	21.72	16.08	0.12	10.52	0.06	0.35	0.02	0.08	0.00	28	5.57	2.43	3.84	0.01	0.70	2.54	0.02	3.78
85DG05_A6	Chl 5	Mafic dike	Chlorite	Anglo-A Cu-Zn-Ag	23.54	0.03	21.82	15.71	0.15	10.37	0.00	0.38	0.00	0.07	0.00	28	5.64	2.36	3.91	0.01	0.78	2.37	0.03	3.70
85DG05_A7	Chl 1	Mafic dike	Chlorite	Anglo-A Cu-Zn-Ag	23.80	0.00	20.85	15.67	0.19	11.26	0.02	0.45	0.00	0.00	0.00	28	5.70	2.30	3.69	0.00	0.67	2.47	0.04	4.02
85DG05_A7	Chl 2	Mafic dike	Chlorite	Anglo-A Cu-Zn-Ag	23.60	0.00	21.34	15.65	0.14	10.94	0.06	0.47	0.00	0.05	0.00	28	5.65	2.35	3.78	0.00	0.69	2.45	0.03	3.91
85DG05_A8	Chl 1	Mafic dike	Chlorite	Anglo-A Cu-Zn-Ag	24.21	0.11	21.43	14.74	0.14	11.14	0.03	0.43	0.00	0.04	0.00	28	5.74	2.26	3.84	0.02	0.80	2.13	0.03	3.94
85DG05_A8	Chl 2	Mafic dike	Chlorite	Anglo-A Cu-Zn-Ag	22.92	0.00	21.52	16.23	0.11	10.62	0.01	0.32	0.00	0.20	0.00	28	5.55	2.45	3.79	0.00	0.67	2.62	0.02	3.84
85DG05_A8	Chl 3	Mafic dike	Chlorite	Anglo-A Cu-Zn-Ag	30.23	0.00	18.43	12.54	0.07	9.34	0.06	1.77	0.00	0.00	0.04	28	6.84	1.16	3.94	0.00	1.20	1.18	0.01	3.15
85DG05_A8	Chl 4	Mafic dike	Chlorite	Anglo-A Cu-Zn-Ag	22.71	0.00	20.37	17.24	0.11	10.88	0.07	0.39	0.00	0.11	0.08	28	5.57	2.43	3.53	0.00	0.52	3.02	0.02	3.98
87AG01_A1	Chl 1	Tonalite	Spotted	Powell-Rouyn	23.71	0.06	21.96	12.21	0.21	14.13	0.00	0.49	0.00	0.12	0.00	28	5.53	2.47	3.65	0.01	0.56	1.82	0.04	4.91
87AG01_A1	Chl 2	Tonalite	Spotted	Powell-Rouyn	23.32	0.04	22.06	12.97	0.15	13.99	0.00	0.50	0.04	0.00	0.02	28	5.46	2.54	3.63	0.01	0.49	2.05	0.03	4.88
87AG01_A1	Chl 3	Tonalite	Spotted	Powell-Rouyn	22.82	0.00	21.80	13.90	0.12	13.42	0.00	0.34	0.02	0.15	0.02	28	5.43	2.57	3.61	0.00	0.49	2.27	0.02	4.76
87AG01_A1	Chl 4	Tonalite	Spotted	Powell-Rouyn	23.12	0.06	22.43	12.63	0.13	14.05	0.00	0.59	0.00	0.09	0.00	28	5.40	2.60	3.66	0.01	0.47	1.99	0.03	4.89
87AG01_A1	Chl 5	Tonalite	Spotted	Powell-Rouyn	23.28	0.00	21.84	13.30	0.14	13.81	0.01	0.43	0.01	0.09	0.00	28	5.48	2.52	3.61	0.00	0.51	2.11	0.03	4.84
87AG01_A1	Chl 6	Tonalite	Spotted	Powell-Rouyn	23.53	0.03	22.19	12.81	0.24	13.73	0.04	0.30	0.04	0.00	0.04	28	5.50	2.50	3.70	0.01	0.60	1.91	0.05	4.79
87AG01_A1	Chl 7	Tonalite	Spotted	Powell-Rouyn	23.63	0.02	21.90	13.05	0.15	13.72	0.06	0.27	0.02	0.05	0.05	28	5.54	2.46	3.67	0.00	0.61	1.95	0.03	4.79
87AG01_A2	Chl 1	Tonalite	Spotted	Powell-Rouyn	23.79	0.10	21.79	12.72	0.09	13.51	0.00	0.37	0.22	0.10	0.12	28	5.57	2.43	3.68	0.02	0.60	1.89	0.02	4.72
87AG01_A2	Chl 2	Tonalite	Spotted	Powell-Rouyn	23.58	0.03	21.30	13.01	0.18	14.34	0.05	0.33	0.05	0.13	0.00	28	5.54	2.46	3.51	0.01	0.51	2.05	0.04	5.02
87AG01_A2	Chl 3	Tonalite	Spotted	Powell-Rouyn	22.78	0.00	21.70	13.76	0.17	13.95	0.02	0.57	0.00	0.00	0.00	28	5.39	2.61	3.52	0.00	0.38	2.34	0.03	4.92
87AG01_A2	Chl 4	Tonalite	Spotted	Powell-Rouyn	23.45	0.01	22.40	12.97	0.12	13.22	0.07	0.56	0.00	0.02	0.00	28	5.49	2.51	3.77	0.00	0.58	1.96	0.02	4.61
87AG01_A2	Chl 5	Tonalite	Spotted	Powell-Rouyn	23.55	0.02	21.85	13.29	0.13	13.46	0.00	0.46	0.07	0.00	0.00	28	5.53	2.47	3.67	0.00	0.56	2.05	0.03	4.71
98AG04_A1	Spectrum 12	Basalt	Spotted	Background	23.80	0.03	19.61	12.94	0.37	15.74	0.09	0.38	0.03	0.00	0.11	28	5.62	2.38	3.13	0.01	0.34	2.22	0.07	5.54
98AG04_A1	Spectrum 6	Basalt	Spotted	Background	23.47	0.08	22.03	12.35	0.25	14.40	0.13	0.46	0.00	0.00	0.02	28	5.47	2.53	3.60	0.01	0.51	1.90	0.05	5.00
98AG04_A1	Spectrum 7	Basalt	Spotted	Background	23.74	0.02	21.80	12.32	0.25	14.64	0.07	0.41	0.02	0.00	0.00	28	5.52	2.48	3.57	0.00	0.52	1.88	0.05	5.08
98AG04_A3	Spectrum 10	Basalt	Spotted	Background	23.36	0.13	22.25	12.47	0.16	14.21	0.06	0.48	0.05	0.00	0.00	28	5.44	2.56	3.64	0.02	0.51	1.92	0.03	4.94
98AG04_A3	Spectrum 11	Basalt	Spotted	Background	23.64	0.04	21.94	12.32	0.35	14.30	0.08	0.48	0.01	0.00	0.00	28	5.51	2.49	3.61	0.01	0.52	1.88	0.07	4.97
98AG04_A3	Spectrum 5	Basalt	Spotted	Background	23.89	0.05	21.45	12.20	0.19	14.82	0.04	0.57	0.06	0.00	0.00	28	5.55	2.45	3.51	0.01	0.47	1.90	0.04	5.13
98AG04_A3	Spectrum 6	Basalt	Spotted	Background	24.14	0.00	20.82	12.34	0.28	15.05	0.03	0.56	0.04	0.00	0.02	28	5.62	2.38	3.41	0.00	0.45	1.95	0.06	5.22
98AG04_A3	Spectrum 7	Basalt	Spotted	Background	23.97	0.01	21.58	12.28	0.29	14.55	0.03	0.44	0.07	0.00	0.07	28	5.57	2.43	3.56	0.00	0.53	1.86	0.06	5.04
98AG04_A3	Spectrum 8	Basalt	Spotted	Background	24.52	0.00	21.80	11.55	0.28	14.19	0.03	0.43	0.47	0.00	0.03	28	5.66	2.34	3.68	0.00	0.58	1.64	0.05	4.88
98AG04_A3	Spectrum 9	Basalt	Spotted	Background	23.44	0.03	21.82	12.88	0.27	14.25	0.05	0.32	0.00	0.00	0.11	28	5.49	2.51	3.58	0.01	0.52	2.00	0.05	4.97
98AG04_A4	Spectrum 1	Basalt	Spotted	Background	26.95	0.12	22.78	9.89	0.27	11.31	0.04	0.59	1.30	0.00	0.08	28	6.04	1.96	4.25	0.02	0.99	0.86	0.05	3.78
98AG04_A4	Spectrum 2	Basalt	Spotted	Background	26.79	0.11	23.59	9.25	0.23	11.45	0.00	0.59	1.32	0.00	0.04	28	5.97	2.03	4.36	0.02	1.01	0.71	0.04	3.81
98AG04_A4	Spectrum 3	Basalt	Spotted	Background	23.70	0.08	21.69	12.54	0.16	14.59	0.03	0.38	0.06	0.00	0.03	28	5.52	2.48	3.55	0.01	0.52	1.93	0.03	5.07

ID	Spectrum	Lithology	Alteration	Location	Ni	Zn	Ca	Na	K	OH*	Total	Fe/Fe+Mg	Variety
85DG05_A3	Chl 2	Mafic dike	Chlorite	Anglo-A Cu-Zn-Ag	0.03	0.02	0.02	0.60	0.01	16	35.31	0.44	pycnochlorite
85DG05_A3	Chl 3	Mafic dike	Chlorite	Anglo-A Cu-Zn-Ag	0.00	0.03	0.00	0.36	0.00	16	35.14	0.47	pycnochlorite
85DG05_A3	Chl 4	Mafic dike	Chlorite	Anglo-A Cu-Zn-Ag	0.02	0.02	0.01	0.28	0.02	16	35.13	0.47	pycnochlorite
85DG05_A4	Chl 1	Mafic dike	Chlorite	Anglo-A Cu-Zn-Ag	0.00	0.00	0.01	0.33	0.02	16	35.35	0.46	ripidolite
85DG05_A4	Chl 2	Mafic dike	Chlorite	Anglo-A Cu-Zn-Ag	0.01	0.00	0.00	0.46	0.01	16	35.36	0.44	pycnochlorite
85DG05_A4	Chl 3	Mafic dike	Chlorite	Anglo-A Cu-Zn-Ag	0.00	0.00	0.01	0.34	0.00	16	35.08	0.45	pycnochlorite
85DG05_A5	Chl 1	Mafic dike	Chlorite	Anglo-A Cu-Zn-Ag	0.00	0.01	0.01	0.48	0.01	16	35.30	0.44	pycnochlorite
85DG05_A5	Chl 2	Mafic dike	Chlorite	Anglo-A Cu-Zn-Ag	0.00	0.02	0.01	0.51	0.04	16	35.31	0.45	pycnochlorite
85DG05_A5	Chl 3	Mafic dike	Chlorite	Anglo-A Cu-Zn-Ag	0.01	0.02	0.00	0.32	0.00	16	35.21	0.43	pycnochlorite
85DG05_A6	Chl 1	Mafic dike	Chlorite	Anglo-A Cu-Zn-Ag	0.00	0.03	0.00	0.32	0.00	16	35.37	0.47	pycnochlorite
85DG05_A6	Chl 2	Mafic dike	Chlorite	Anglo-A Cu-Zn-Ag	0.00	0.00	0.02	0.56	0.04	16	35.38	0.46	pycnochlorite
85DG05_A6	Chl 3	Mafic dike	Chlorite	Anglo-A Cu-Zn-Ag	0.00	0.00	0.00	0.39	0.00	16	35.31	0.46	pycnochlorite
85DG05_A6	Chl 4	Mafic dike	Chlorite	Anglo-A Cu-Zn-Ag	0.00	0.01	0.02	0.33	0.01	16	35.25	0.46	ripidolite
85DG05_A6	Chl 5	Mafic dike	Chlorite	Anglo-A Cu-Zn-Ag	0.00	0.01	0.00	0.35	0.00	16	35.17	0.46	pycnochlorite
85DG05_A7	Chl 1	Mafic dike	Chlorite	Anglo-A Cu-Zn-Ag	0.00	0.00	0.01	0.42	0.00	16	35.32	0.44	pycnochlorite
85DG05_A7	Chl 2	Mafic dike	Chlorite	Anglo-A Cu-Zn-Ag	0.00	0.01	0.02	0.44	0.00	16	35.31	0.45	pycnochlorite
85DG05_A8	Chl 1	Mafic dike	Chlorite	Anglo-A Cu-Zn-Ag	0.00	0.01	0.01	0.40	0.00	16	35.15	0.43	pycnochlorite
85DG05_A8	Chl 2	Mafic dike	Chlorite	Anglo-A Cu-Zn-Ag	0.00	0.04	0.00	0.30	0.00	16	35.28	0.46	ripidolite
85DG05_A8	Chl 3	Mafic dike	Chlorite	Anglo-A Cu-Zn-Ag	0.01	0.00	0.01	1.55	0.00	16	35.06	0.43	diabantite
85DG05_A8	Chl 4	Mafic dike	Chlorite	Anglo-A Cu-Zn-Ag	0.02	0.02	0.02	0.37	0.00	16	35.49	0.47	ripidolite
87AG01_A1	Chl 1	Tonalite	Spotted	Powell-Rouyn	0.00	0.02	0.00	0.44	0.00	16	35.47	0.33	ripidolite
87AG01_A1	Chl 2	Tonalite	Spotted	Powell-Rouyn	0.00	0.00	0.00	0.45	0.02	16	35.56	0.34	ripidolite
87AG01_A1	Chl 3	Tonalite	Spotted	Powell-Rouyn	0.00	0.03	0.00	0.31	0.01	16	35.51	0.37	ripidolite
87AG01_A1	Chl 4	Tonalite	Spotted	Powell-Rouyn	0.00	0.02	0.00	0.53	0.00	16	35.61	0.34	ripidolite
87AG01_A1	Chl 5	Tonalite	Spotted	Powell-Rouyn	0.00	0.02	0.00	0.39	0.01	16	35.52	0.35	ripidolite
87AG01_A1	Chl 6	Tonalite	Spotted	Powell-Rouyn	0.01	0.00	0.01	0.27	0.02	16	35.36	0.34	ripidolite
87AG01_A1	Chl 7	Tonalite	Spotted	Powell-Rouyn	0.01	0.01	0.02	0.25	0.01	16	35.34	0.35	ripidolite
87AG01_A2	Chl 1	Tonalite	Spotted	Powell-Rouyn	0.02	0.02	0.00	0.34	0.13	16	35.43	0.35	ripidolite
87AG01_A2	Chl 2	Tonalite	Spotted	Powell-Rouyn	0.00	0.02	0.01	0.30	0.03	16	35.49	0.34	ripidolite
87AG01_A2	Chl 3	Tonalite	Spotted	Powell-Rouyn	0.00	0.00	0.01	0.52	0.00	16	35.72	0.36	ripidolite
87AG01_A2	Chl 4	Tonalite	Spotted	Powell-Rouyn	0.00	0.00	0.02	0.51	0.00	16	35.48	0.36	ripidolite
87AG01_A2	Chl 5	Tonalite	Spotted	Powell-Rouyn	0.00	0.00	0.00	0.42	0.04	16	35.48	0.36	ripidolite
98AG04_A1	Spectrum 12	Basalt	Spotted	Background	0.02	0.00	0.02	0.35	0.02	16	35.71	0.32	pycnochlorite
98AG04_A1	Spectrum 6	Basalt	Spotted	Background	0.00	0.00	0.03	0.42	0.00	16	35.52	0.32	ripidolite
98AG04_A1	Spectrum 7	Basalt	Spotted	Background	0.00	0.00	0.02	0.37	0.01	16	35.50	0.32	ripidolite
98AG04_A3	Spectrum 10	Basalt	Spotted	Background	0.00	0.00	0.01	0.43	0.03	16	35.54	0.33	ripidolite
98AG04_A3	Spectrum 11	Basalt	Spotted	Background	0.00	0.00	0.02	0.43	0.01	16	35.51	0.33	ripidolite
98AG04_A3	Spectrum 5	Basalt	Spotted	Background	0.00	0.00	0.01	0.51	0.04	16	35.62	0.32	ripidolite
98AG04_A3	Spectrum 6	Basalt	Spotted	Background	0.00	0.00	0.01	0.51	0.02	16	35.63	0.32	pycnochlorite
98AG04_A3	Spectrum 7	Basalt	Spotted	Background	0.01	0.00	0.01	0.40	0.04	16	35.51	0.32	ripidolite
98AG04_A3	Spectrum 8	Basalt	Spotted	Background	0.01	0.00	0.01	0.38	0.28	16	35.52	0.31	pycnochlorite
98AG04_A3	Spectrum 9	Basalt	Spotted	Background	0.02	0.00	0.01	0.29	0.00	16	35.45	0.34	ripidolite
98AG04_A4	Spectrum 1	Basalt	Spotted	Background	0.01	0.00	0.01	0.51	0.74	16	35.24	0.33	pycnochlorite
98AG04_A4	Spectrum 2	Basalt	Spotted	Background	0.01	0.00	0.00	0.51	0.75	16	35.22	0.31	pycnochlorite
98AG04_A4	Spectrum 3	Basalt	Spotted	Background	0.01	0.00	0.01	0.34	0.04	16	35.50	0.33	ripidolite

ID	Spectrum	Lithology	Alteration	Location	SiO2	TiO2	Al2O3	FeO	MnO	MgO	CaO	Na2O	K2O	ZnO	NiO	No. of oxygens	Si	Al iv	Al vi	Ti	Fe3+	Fe2+	Mn	Mg
98AG04_A4	Spectrum 4	Basalt	Spotted	Background	24.11	0.06	21.45	12.52	0.34	14.10	0.01	0.43	0.04	0.00	0.00	28	5.62	2.38	3.59	0.01	0.58	1.86	0.07	4.90
98AG04_A4	Spectrum 5	Basalt	Spotted	Background	23.64	0.06	21.85	12.29	0.29	14.70	0.04	0.32	0.02	0.00	0.00	28	5.50	2.50	3.57	0.01	0.53	1.86	0.06	5.10
98AG04_A4	Spectrum 6	Basalt	Spotted	Background	25.16	0.04	21.05	11.84	0.19	14.53	0.01	0.35	0.02	0.00	0.06	28	5.79	2.21	3.60	0.01	0.70	1.58	0.04	4.99
98AG04_A4	Spectrum 7	Basalt	Spotted	Background	24.23	0.08	21.45	12.07	0.24	14.61	0.00	0.49	0.10	0.00	0.05	28	5.61	2.39	3.55	0.01	0.54	1.79	0.05	5.05
98AG04_A4	Spectrum 8	Basalt	Spotted	Background	23.89	0.08	21.61	12.32	0.28	14.52	0.08	0.35	0.02	0.00	0.06	28	5.56	2.44	3.56	0.01	0.56	1.84	0.06	5.04
98AG04_A4	Spectrum 9	Basalt	Spotted	Background	24.15	0.00	21.35	11.99	0.28	14.94	0.03	0.51	0.07	0.00	0.00	28	5.60	2.40	3.51	0.00	0.50	1.83	0.05	5.16
98AG04_A5	Spectrum 2	Basalt	Spotted	Background	24.66	0.02	21.46	11.45	0.20	14.88	0.05	0.56	0.06	0.00	0.05	28	5.67	2.33	3.58	0.00	0.57	1.63	0.04	5.10
98AG04_A5	Spectrum 3	Basalt	Spotted	Background	23.69	0.00	22.18	12.44	0.35	13.95	0.01	0.57	0.01	0.00	0.00	28	5.51	2.49	3.68	0.00	0.53	1.89	0.07	4.84
98AG04_A5	Spectrum 4	Basalt	Spotted	Background	23.73	0.12	21.33	12.12	0.27	15.24	0.05	0.38	0.05	0.00	0.00	28	5.52	2.48	3.44	0.02	0.47	1.89	0.05	5.29
98AG04_A5	Spectrum 5	Basalt	Spotted	Background	23.48	0.01	22.01	12.48	0.22	14.54	0.00	0.48	0.01	0.00	0.04	28	5.47	2.53	3.59	0.00	0.48	1.95	0.04	5.05
98AG04_A5	Spectrum 6	Basalt	Spotted	Background	23.71	0.03	21.92	12.05	0.30	14.70	0.02	0.58	0.02	0.00	0.00	28	5.50	2.50	3.58	0.01	0.48	1.86	0.06	5.08
98AG08_A1	Spectrum 4	Basalt	Spotted	Background	32.76	0.06	17.82	10.63	0.36	10.02	0.00	0.55	0.27	0.00	0.06	28	7.25	0.75	4.07	0.01	1.71	0.25	0.07	3.30
98AG08_A2	Spectrum 10	Basalt	Spotted	Background	24.04	0.06	20.02	14.57	0.32	13.40	0.03	0.00	0.04	0.00	0.11	28	5.73	2.27	3.42	0.01	0.64	2.27	0.06	4.76
98AG08_A2	Spectrum 15	Basalt	Spotted	Background	23.92	0.08	20.16	14.59	0.33	13.41	0.00	0.00	0.10	0.00	0.00	28	5.70	2.30	3.43	0.01	0.62	2.28	0.07	4.76
98AG08_A2	Spectrum 6	Basalt	Spotted	Background	24.52	0.04	20.57	14.12	0.28	13.14	0.00	0.00	0.07	0.00	0.00	28	5.78	2.22	3.58	0.01	0.74	2.04	0.06	4.62
98AG08_A3	Spectrum 12	Basalt	Spotted	Background	23.65	0.06	20.80	14.56	0.32	13.24	0.00	0.00	0.07	0.00	0.01	28	5.62	2.38	3.52	0.01	0.63	2.26	0.06	4.69
98AG08_A3	Spectrum 13	Basalt	Spotted	Background	23.42	0.00	21.87	12.38	0.28	14.74	0.02	0.49	0.01	0.00	0.10	28	5.46	2.54	3.54	0.00	0.45	1.96	0.06	5.12
98AG08_A3	Spectrum 17	Basalt	Spotted	Background	24.30	0.01	20.22	13.86	0.34	13.90	0.00	0.00	0.05	0.00	0.05	28	5.74	2.26	3.45	0.00	0.65	2.09	0.07	4.90
98AG08_A4	Spectrum 4	Basalt	Spotted	Background	23.98	0.00	20.39	14.35	0.28	13.66	0.02	0.00	0.09	0.00	0.00	28	5.69	2.31	3.45	0.00	0.62	2.23	0.06	4.83
98AG08_A4	Spectrum 5	Basalt	Spotted	Background	22.86	0.01	21.54	13.19	0.30	14.66	0.03	0.37	0.18	0.00	0.04	28	5.39	2.61	3.44	0.00	0.36	2.24	0.06	5.15
99AG01_A1	Chl 1	Basalt	Spilite	Background	24.33	0.00	20.44	14.33	0.11	12.81	0.04	0.56	0.02	0.00	0.06	28	5.75	2.25	3.54	0.00	0.59	2.24	0.02	4.51
99AG01_A1	Chl 2	Basalt	Spilite	Background	22.94	0.04	20.16	16.21	0.13	12.23	0.03	0.49	0.00	0.02	0.00	28	5.57	2.43	3.40	0.01	0.44	2.85	0.03	4.42
99AG01_A1	Chl 3	Basalt	Spilite	Background	25.09	0.00	19.33	14.02	0.16	13.39	0.00	0.58	0.00	0.08	0.00	28	5.92	2.08	3.38	0.00	0.60	2.17	0.03	4.71
99AG01_A2	Chl 1	Basalt	Spilite	Background	25.15	0.02	19.09	13.87	0.10	13.67	0.14	0.53	0.00	0.04	0.00	28	5.94	2.06	3.33	0.00	0.59	2.14	0.02	4.81
99AG01_A2	Chl 2	Basalt	Spilite	Background	24.24	0.00	18.98	15.31	0.13	13.10	0.07	0.51	0.00	0.02	0.00	28	5.82	2.18	3.27	0.00	0.49	2.58	0.03	4.69
99AG01_A2	Chl 3	Basalt	Spilite	Background	23.81	0.10	20.77	14.43	0.22	12.36	0.09	0.51	0.03	0.09	0.00	28	5.67	2.33	3.59	0.02	0.60	2.27	0.04	4.39
99AG01_A2	Chl 4	Basalt	Spilite	Background	24.39	0.00	20.99	14.05	0.11	12.37	0.00	0.51	0.04	0.00	0.04	28	5.75	2.25	3.69	0.00	0.68	2.09	0.02	4.35
99AG01_A4	Chl 1	Basalt	Spilite	Background	24.26	0.03	19.65	13.60	0.15	12.77	0.66	0.57	0.04	0.05	0.12	28	5.80	2.20	3.43	0.01	0.56	2.16	0.03	4.55
99AG01_A4	Chl 2	Basalt	Spilite	Background	25.18	0.02	19.79	13.68	0.08	13.61	0.03	0.25	0.00	0.03	0.00	28	5.91	2.09	3.47	0.00	0.72	1.97	0.02	4.76
99AG01_A4	Chl 3	Basalt	Spilite	Background	23.80	0.02	18.90	16.09	0.13	12.66	0.04	0.60	0.00	0.07	0.01	28	5.76	2.24	3.23	0.00	0.42	2.83	0.03	4.57
99AG01_A4	Chl 4	Basalt	Spilite	Background	23.85	0.01	19.92	15.37	0.12	12.99	0.00	0.20	0.02	0.00	0.00	28	5.71	2.29	3.41	0.00	0.58	2.50	0.02	4.64
99AG01_A4	Chl 5	Basalt	Spilite	Background	24.10	0.01	18.34	15.09	0.16	14.13	0.00	0.35	0.00	0.14	0.00	28	5.81	2.19	3.08	0.00	0.42	2.62	0.03	5.08
54BG02_area 1	Chl 1	Mafic dike/lamprophyre?	Chlorite	Background	26.69	0.06	16.08	6.08	0.10	25.59	0.03	0.37	0.16	0.00	0.04	28	5.91	2.09	2.13	0.01	0.00	1.17	0.02	8.45
54BG02_area 1	Chl 2	Mafic dike/lamprophyre?	Chlorite	Background	26.49	0.04	16.27	6.08	0.15	25.55	0.00	0.45	0.10	0.04	0.03	28	5.87	2.13	2.14	0.01	0.00	1.19	0.03	8.43
54BG02_area 1	Chl 3	Mafic dike/lamprophyre?	Chlorite	Background	26.63	0.09	16.02	5.98	0.10	25.66	0.01	0.42	0.14	0.05	0.06	28	5.90	2.10	2.11	0.02	0.00	1.17	0.02	8.47
54BG02_area 1	Chl 4	Mafic dike/lamprophyre?	Chlorite	Background	25.32	0.02	17.92	6.72	0.14	24.29	0.05	0.41	0.02	0.05	0.04	28	5.65	2.35	2.39	0.00	0.00	1.29	0.03	8.08
54BG02_area 1	Chl 5	Mafic dike/lamprophyre?	Chlorite	Background	25.70	0.05	17.04	6.55	0.12	25.10	0.02	0.42	0.01	0.01	0.04	28	5.72	2.28	2.21	0.01	0.00	1.30	0.02	8.32
54BG02_area 1	Chl 6	Mafic dike/lamprophyre?	Chlorite	Background	25.59	0.03	18.05	6.52	0.14	24.21	0.02	0.41	0.01	0.02	0.02	28	5.70	2.30	2.46	0.00	0.01	1.20	0.03	8.04
54BG02_area 2	Chl 1	Mafic dike/lamprophyre?	Chlorite	Background	25.07	0.00	17.78	6.28	0.11	24.22	0.12	0.56	0.01	0.00	0.06	28	5.63	2.37	2.37	0.00	0.00	1.26	0.02	8.11
54BG02_area 2	Chl 2	Mafic dike/lamprophyre?	Chlorite	Background	24.60	0.02	17.30	6.31	0.12	24.56	0.14	0.58	0.05	0.05	0.02	28	5.55	2.45	2.21	0.00	0.00	1.37	0.02	8.27
54BG02_area 2	Chl 3	Mafic dike/lamprophyre?	Chlorite	Background	25.41	0.02	17.51	6.01	0.08	25.69	0.02	0.47	0.01	0.01	0.03	28	5.61	2.39	2.21	0.00	0.00	1.25	0.01	8.46
54BG02_area 2	Chl 4	Mafic dike/lamprophyre?	Chlorite	Background	26.05	0.00	16.98	6.48	0.11	24.88	0.04	0.41	0.01	0.06	0.00	28	5.80	2.20	2.28	0.00	0.00	1.24	0.02	8.26
54BG02_area 2	Chl 5	Mafic dike/lamprophyre?	Chlorite	Background	25.66	0.00	17.62	6.70	0.16	24.41	0.04	0.41	0.01	0.00	0.03	28	5.72	2.28	2.37	0.00	0.00	1.27	0.03	8.12
54BG02_area 2	Chl 6	Mafic dike/lamprophyre?	Chlorite	Background	25.34	0.02	17.61	6.96	0.13	24.41	0.04	0.39	0.00	0.04	0.05	28	5.66	2.34	2.33	0.00	0.00	1.36	0.03	8.13
54BG02_area 2	Chl 7	Mafic dike/lamprophyre?	Chlorite	Background	25.38	0.03	18.22	6.46	0.13	24.18	0.05	0.39	0.01	0.01	0.05	28	5.66	2.34	2.47	0.00	0.00	1.20	0.03	8.04

ID	Spectrum	Lithology	Alteration	Location	Ni	Zn	Ca	Na	K	OH*	Total	Fe/Fe+Mg	Variety
98AG04_A4	Spectrum 4	Basalt	Spotted	Background	0.00	0.00	0.00	0.39	0.02	16	35.42	0.33	pycnochlorite
98AG04_A4	Spectrum 5	Basalt	Spotted	Background	0.00	0.00	0.01	0.29	0.01	16	35.45	0.32	ripidolite
98AG04_A4	Spectrum 6	Basalt	Spotted	Background	0.01	0.00	0.00	0.31	0.01	16	35.25	0.31	pycnochlorite
98AG04_A4	Spectrum 7	Basalt	Spotted	Background	0.01	0.00	0.00	0.44	0.06	16	35.51	0.32	pycnochlorite
98AG04_A4	Spectrum 8	Basalt	Spotted	Background	0.01	0.00	0.02	0.32	0.01	16	35.43	0.32	ripidolite
98AG04_A4	Spectrum 9	Basalt	Spotted	Background	0.00	0.00	0.01	0.46	0.04	16	35.56	0.31	ripidolite
98AG04_A5	Spectrum 2	Basalt	Spotted	Background	0.01	0.00	0.01	0.50	0.04	16	35.48	0.30	pycnochlorite
98AG04_A5	Spectrum 3	Basalt	Spotted	Background	0.00	0.00	0.00	0.51	0.01	16	35.53	0.33	ripidolite
98AG04_A5	Spectrum 4	Basalt	Spotted	Background	0.00	0.00	0.01	0.34	0.03	16	35.55	0.31	ripidolite
98AG04_A5	Spectrum 5	Basalt	Spotted	Background	0.01	0.00	0.00	0.43	0.01	16	35.56	0.33	ripidolite
98AG04_A5	Spectrum 6	Basalt	Spotted	Background	0.00	0.00	0.00	0.52	0.01	16	35.60	0.32	ripidolite
98AG08_A1	Spectrum 4	Basalt	Spotted	Background	0.01	0.00	0.00	0.47	0.15	16	34.05	0.37	diabantite
98AG08_A2	Spectrum 10	Basalt	Spotted	Background	0.02	0.00	0.01	0.00	0.02	16	35.21	0.38	pycnochlorite
98AG08_A2	Spectrum 15	Basalt	Spotted	Background	0.00	0.00	0.00	0.00	0.06	16	35.24	0.38	pycnochlorite
98AG08_A2	Spectrum 6	Basalt	Spotted	Background	0.00	0.00	0.00	0.00	0.04	16	35.08	0.38	pycnochlorite
98AG08_A3	Spectrum 12	Basalt	Spotted	Background	0.00	0.00	0.00	0.00	0.04	16	35.23	0.38	pycnochlorite
98AG08_A3	Spectrum 13	Basalt	Spotted	Background	0.02	0.00	0.00	0.44	0.01	16	35.61	0.32	ripidolite
98AG08_A3	Spectrum 17	Basalt	Spotted	Background	0.01	0.00	0.00	0.00	0.03	16	35.19	0.36	pycnochlorite
98AG08_A4	Spectrum 4	Basalt	Spotted	Background	0.00	0.00	0.01	0.00	0.05	16	35.25	0.37	pycnochlorite
98AG08_A4	Spectrum 5	Basalt	Spotted	Background	0.01	0.00	0.01	0.34	0.11	16	35.72	0.34	ripidolite
99AG01_A1	Chl 1	Basalt	Spilite	Background	0.01	0.00	0.01	0.51	0.01	16	35.45	0.39	pycnochlorite
99AG01_A1	Chl 2	Basalt	Spilite	Background	0.00	0.00	0.01	0.46	0.00	16	35.62	0.43	ripidolite
99AG01_A1	Chl 3	Basalt	Spilite	Background	0.00	0.01	0.00	0.53	0.00	16	35.44	0.37	pycnochlorite
99AG01_A2	Chl 1	Basalt	Spilite	Background	0.00	0.01	0.04	0.49	0.00	16	35.43	0.36	pycnochlorite
99AG01_A2	Chl 2	Basalt	Spilite	Background	0.00	0.00	0.02	0.47	0.00	16	35.55	0.40	pycnochlorite
99AG01_A2	Chl 3	Basalt	Spilite	Background	0.00	0.02	0.02	0.47	0.02	16	35.43	0.40	pycnochlorite
99AG01_A2	Chl 4	Basalt	Spilite	Background	0.01	0.00	0.00	0.47	0.02	16	35.33	0.39	pycnochlorite
99AG01_A4	Chl 1	Basalt	Spilite	Background	0.02	0.01	0.17	0.53	0.02	16	35.50	0.37	pycnochlorite
99AG01_A4	Chl 2	Basalt	Spilite	Background	0.00	0.01	0.01	0.23	0.00	16	35.18	0.36	pycnochlorite
99AG01_A4	Chl 3	Basalt	Spilite	Background	0.00	0.01	0.01	0.56	0.00	16	35.67	0.42	pycnochlorite
99AG01_A4	Chl 4	Basalt	Spilite	Background	0.00	0.00	0.00	0.19	0.01	16	35.35	0.40	pycnochlorite
99AG01_A4	Chl 5	Basalt	Spilite	Background	0.00	0.02	0.00	0.33	0.00	16	35.59	0.37	pycnochlorite
54BG02_area 1	Chl 1	Mafic dike/lamprophyre?	Chlorite	Background	0.01	0.00	0.01	0.32	0.09	16	36.20	0.12	clinochlore
54BG02_area 1	Chl 2	Mafic dike/lamprophyre?	Chlorite	Background	0.01	0.01	0.00	0.39	0.05	16	36.25	0.12	clinochlore
54BG02_area 1	Chl 3	Mafic dike/lamprophyre?	Chlorite	Background	0.01	0.01	0.00	0.36	0.08	16	36.24	0.12	clinochlore
54BG02_area 1	Chl 4	Mafic dike/lamprophyre?	Chlorite	Background	0.01	0.01	0.01	0.36	0.01	16	36.19	0.14	clinochlore
54BG02_area 1	Chl 5	Mafic dike/lamprophyre?	Chlorite	Background	0.01	0.00	0.01	0.36	0.01	16	36.25	0.14	clinochlore
54BG02_area 1	Chl 6	Mafic dike/lamprophyre?	Chlorite	Background	0.00	0.00	0.01	0.36	0.01	16	36.12	0.13	clinochlore
54BG02_area 2	Chl 1	Mafic dike/lamprophyre?	Chlorite	Background	0.01	0.00	0.03	0.48	0.01	16	36.29	0.13	clinochlore
54BG02_area 2	Chl 2	Mafic dike/lamprophyre?	Chlorite	Background	0.00	0.01	0.03	0.51	0.03	16	36.46	0.14	sheridanite
54BG02_area 2	Chl 3	Mafic dike/lamprophyre?	Chlorite	Background	0.01	0.00	0.00	0.40	0.01	16	36.35	0.13	clinochlore
54BG02_area 2	Chl 4	Mafic dike/lamprophyre?	Chlorite	Background	0.00	0.01	0.01	0.36	0.01	16	36.17	0.13	clinochlore
54BG02_area 2	Chl 5	Mafic dike/lamprophyre?	Chlorite	Background	0.01	0.00	0.01	0.35	0.00	16	36.16	0.14	clinochlore
54BG02_area 2	Chl 6	Mafic dike/lamprophyre?	Chlorite	Background	0.01	0.01	0.01	0.33	0.00	16	36.21	0.14	clinochlore
54BG02_area 2	Chl 7	Mafic dike/lamprophyre?	Chlorite	Background	0.01	0.00	0.01	0.34	0.01	16	36.12	0.13	clinochlore

ID	Spectrum	Lithology	Alteration	Location	SiO2	TiO2	Al2O3	FeO	MnO	MgO	CaO	Na2O	K2O	ZnO	NiO	No. of oxygens	Si	Al iv	Al vi	Ti	Fe3+	Fe2+	Mn	Mg
54BG02_area 2	Chl 8	Mafic dike/lamprophyre?	Chlorite	Background	25.60	0.01	18.01	5.96	0.08	25.19	0.01	0.33	0.00	0.01	0.05	28	5.67	2.33	2.38	0.00	0.00	1.13	0.02	8.31
54BG02_area 2	Chl 9	Mafic dike/lamprophyre?	Chlorite	Background	26.02	0.03	17.05	6.13	0.14	25.22	0.03	0.46	0.01	0.01	0.06	28	5.77	2.23	2.25	0.01	0.00	1.19	0.03	8.33
54BG02_area 2	Chl 10	Mafic dike/lamprophyre?	Chlorite	Background	26.45	0.04	16.86	6.21	0.12	24.84	0.02	0.38	0.13	0.00	0.04	28	5.87	2.13	2.30	0.01	0.02	1.14	0.02	8.22
54BG02_area 2	Chl 11	Mafic dike/lamprophyre?	Chlorite	Background	26.00	0.00	17.21	6.35	0.16	24.97	0.00	0.39	0.01	0.00	0.04	28	5.78	2.22	2.30	0.00	0.00	1.21	0.03	8.27
54BG02_area 2	Chl 12	Mafic dike/lamprophyre?	Chlorite	Background	26.34	0.00	16.85	6.09	0.12	25.31	0.02	0.40	0.00	0.03	0.05	28	5.84	2.16	2.26	0.00	0.00	1.14	0.02	8.36
54BG02_area 2	Chl 13	Mafic dike/lamprophyre?	Chlorite	Background	25.44	0.00	17.87	6.56	0.17	24.35	0.05	0.46	0.00	0.05	0.07	28	5.67	2.33	2.39	0.00	0.00	1.27	0.03	8.09
54BG02_area 3	Chl 1	Mafic dike/lamprophyre?	Chlorite	Background	25.94	0.06	17.24	6.15	0.12	25.02	0.00	0.44	0.13	0.03	0.03	28	5.75	2.25	2.28	0.01	0.00	1.19	0.02	8.27
54BG02_area 3	Chl 2	Mafic dike/lamprophyre?	Chlorite	Background	25.45	0.01	17.91	5.81	0.15	25.09	0.03	0.49	0.00	0.07	0.02	28	5.64	2.36	2.35	0.00	0.00	1.15	0.03	8.29
54BG02_area 3	Chl 3	Mafic dike/lamprophyre?	Chlorite	Background	25.95	0.00	16.36	6.31	0.11	25.44	0.15	0.48	0.04	0.01	0.03	28	5.77	2.23	2.10	0.00	0.00	1.30	0.02	8.44
54BG02_area 3	Chl 4	Mafic dike/lamprophyre?	Chlorite	Background	25.84	0.02	16.91	6.45	0.13	25.25	0.00	0.46	0.01	0.05	0.00	28	5.74	2.26	2.19	0.00	0.00	1.29	0.02	8.36
87CG02_area 1	Chl 1	Felsic dike	Spotted/Carbonate	Powell-Rouyn	30.19	0.07	19.60	29.75	0.00	16.97	0.61	0.00	0.35	0.00	0.79	28	5.73	2.27	2.14	0.01	0.00	4.80	0.00	4.81
87CG02_area 1	Chl 2	Felsic dike	Spotted/Carbonate	Powell-Rouyn	30.05	0.59	23.10	25.65	0.46	18.57	0.00	0.99	0.00	0.08	0.00	28	5.47	2.53	2.48	0.08	0.00	3.98	0.07	5.04
87CG02_area 1	Chl 3	Felsic dike	Spotted/Carbonate	Powell-Rouyn	29.40	0.00	27.11	24.92	0.17	16.24	0.08	0.49	0.52	0.00	0.00	28	5.34	2.66	3.20	0.00	0.16	3.62	0.03	4.40
87CG02_area 1	Chl 4	Felsic dike	Spotted/Carbonate	Powell-Rouyn	29.05	0.00	27.34	27.08	0.00	14.83	0.20	0.26	0.14	0.00	1.33	28	5.29	2.71	3.20	0.00	0.21	3.91	0.00	4.03
87CG02_area 1	Chl 5	Felsic dike	Spotted/Carbonate	Powell-Rouyn	31.19	0.27	22.35	28.58	0.24	16.36	0.00	0.37	0.50	0.00	0.00	28	5.73	2.27	2.60	0.04	0.11	4.28	0.04	4.48
87CG02_area 2	Chl 1	Felsic dike	Spotted/Carbonate	Powell-Rouyn	31.90	0.00	22.47	28.98	0.73	15.43	0.11	0.00	0.00	0.00	0.00	28	5.86	2.14	2.75	0.00	0.34	4.11	0.11	4.23
87CG02_area 2	Chl 2	Felsic dike	Spotted/Carbonate	Powell-Rouyn	29.97	0.23	20.60	30.07	0.00	17.31	0.70	0.34	0.32	0.00	0.46	28	5.57	2.43	2.12	0.03	0.00	4.84	0.00	4.79
87CG02_area 2	Chl 3	Felsic dike	Spotted/Carbonate	Powell-Rouyn	34.60	0.00	19.52	24.91	1.56	15.29	0.58	0.00	0.64	0.00	0.00	28	6.39	1.61	2.70	0.00	0.54	3.31	0.24	4.21
87CG02_area 2	Chl 4	Felsic dike	Spotted/Carbonate	Powell-Rouyn	28.75	0.00	18.86	32.60	0.76	15.73	0.01	0.00	0.11	1.15	1.12	28	5.53	2.47	1.86	0.00	0.00	5.51	0.12	4.51
87CG02_area 2	Chl 5	Felsic dike	Spotted/Carbonate	Powell-Rouyn	29.83	0.47	20.16	30.95	0.65	16.81	0.43	0.53	0.15	0.00	0.00	28	5.56	2.44	2.04	0.07	0.00	5.01	0.10	4.67
87CG02_area 3	Chl 1	Felsic dike	Spotted/Carbonate	Powell-Rouyn	27.27	0.31	25.81	29.07	1.17	14.05	0.76	0.39	0.44	0.00	0.10	28	5.11	2.89	2.85	0.04	0.00	4.62	0.19	3.92
87CG02_area 3	Chl 2	Felsic dike	Spotted/Carbonate	Powell-Rouyn	27.53	0.42	21.04	31.69	0.89	15.41	0.60	0.58	0.00	0.88	0.25	28	5.23	2.77	2.01	0.06	0.00	5.37	0.14	4.36
87CG02_area 3	Chl 3	Felsic dike	Spotted/Carbonate	Powell-Rouyn	30.23	0.00	23.49	25.31	0.59	15.23	0.74	0.00	0.03	3.13	0.00	28	5.64	2.36	2.82	0.00	0.25	3.70	0.09	4.23
87CG02_area 3	Chl 4	Felsic dike	Spotted/Carbonate	Powell-Rouyn	30.72	0.00	19.24	30.35	1.54	16.70	0.25	0.33	0.00	0.00	0.00	28	5.80	2.20	2.10	0.00	0.00	4.87	0.25	4.70
87CG02_area 3	Chl 5	Felsic dike	Spotted/Carbonate	Powell-Rouyn	31.91	0.51	22.82	24.01	0.45	17.78	0.12	1.07	0.38	0.00	0.84	28	5.75	2.25	2.64	0.07	0.09	3.53	0.07	4.77
87CG02_area 3	Chl 6	Felsic dike	Spotted/Carbonate	Powell-Rouyn	30.07	0.00	21.00	30.51	1.03	15.72	0.00	0.83	0.00	0.27	0.00	28	5.63	2.37	2.31	0.00	0.00	4.90	0.16	4.39
87CG02_area 3	Chl 7	Felsic dike	Spotted/Carbonate	Powell-Rouyn	28.07	0.29	24.73	30.77	0.22	14.69	0.00	0.00	0.00	0.00	0.28	28	5.29	2.71	2.79	0.04	0.09	4.76	0.04	4.13
87CG02_area 4	Chl 1	Felsic dike	Spotted/Carbonate	Powell-Rouyn	29.74	0.00	19.43	31.26	1.20	17.06	0.40	0.42	0.07	0.00	0.00	28	5.59	2.41	1.94	0.00	0.00	5.16	0.19	4.78
87CG02_area 4	Chl 2	Felsic dike	Spotted/Carbonate	Powell-Rouyn	32.52	0.00	22.76	26.29	0.17	17.64	0.00	0.00	0.00	0.00	0.00	28	5.88	2.12	2.77	0.00	0.36	3.61	0.03	4.76
87CG02_area 4	Chl 3	Felsic dike	Spotted/Carbonate	Powell-Rouyn	29.62	0.00	20.66	32.32	0.00	15.22	0.08	0.00	0.00	1.07	0.00	28	5.67	2.33	2.32	0.00	0.00	5.17	0.00	4.34
87CG02_area 4	Chl 4	Felsic dike	Spotted/Carbonate	Powell-Rouyn	27.74	0.70	22.48	32.11	0.61	15.31	0.52	0.00	0.00	0.00	0.07	28	5.26	2.74	2.31	0.10	0.00	5.19	0.10	4.33
87CG02_area 4	Chl 5	Felsic dike	Spotted/Carbonate	Powell-Rouyn	28.79	0.00	20.27	30.71	1.27	18.36	0.00	0.21	0.06	0.00	0.00	28	5.38	2.62	1.91	0.00	0.00	5.13	0.20	5.12
87CG02_area 5	Chl 1	Felsic dike	Spotted/Carbonate	Powell-Rouyn	27.89	0.13	17.41	34.74	0.31	18.24	0.27	0.08	0.28	0.10	0.00	28	5.30	2.70	1.30	0.02	0.00	6.12	0.05	5.17
87CG02_area 5	Chl 2	Felsic dike	Spotted/Carbonate	Powell-Rouyn	30.02	0.00	21.36	32.16	1.18	14.21	0.00	0.00	0.00	0.28	0.00	28	5.70	2.30	2.50	0.00	0.11	5.00	0.19	4.02
87CG02_area 5	Chl 3	Felsic dike	Spotted/Carbonate	Powell-Rouyn	27.95	0.00	21.66	30.24	0.38	17.32	0.00	0.10	0.24	1.62	0.00	28	5.26	2.74	2.12	0.00	0.00	5.05	0.06	4.86
87CG02_area 6	Chl 1	Felsic dike	Spotted/Carbonate	Powell-Rouyn	29.93	0.00	22.65	24.67	0.23	15.94	0.00	0.32	0.00	3.17	1.66	28	5.62	2.38	2.66	0.00	0.10	3.77	0.04	4.46
87CG02_area 6	Chl 2	Felsic dike	Spotted/Carbonate	Powell-Rouyn	29.26	0.00	24.72	27.49	0.40	17.58	0.19	0.18	0.00	0.00	0.23	28	5.37	2.63	2.73	0.00	0.02	4.20	0.06	4.81
87CG02_area 6	Chl 3	Felsic dike	Spotted/Carbonate	Powell-Rouyn	36.77	0.00	21.76	20.85	0.23	18.45	0.27	0.32	0.07	0.00	0.00	28	6.43	1.57	2.98	0.00	0.73	2.32	0.03	4.81
87CG02_area 6	Chl 4	Felsic dike	Spotted/Carbonate	Powell-Rouyn	30.81	0.00	20.39	26.93	1.33	14.84	0.00	0.43	0.00	2.48	1.89	28	5.84	2.16	2.41	0.00	0.07	4.20	0.21	4.19
87CG02_area 6	Chl 5	Felsic dike	Spotted/Carbonate	Powell-Rouyn	27.50	0.00	21.24	30.50	0.74	16.80	0.53	0.00	0.00	0.30	0.00	28	5.28	2.72	2.13	0.00	0.00	5.14	0.12	4.81
87CG02_area 6	Chl 6	Felsic dike	Spotted/Carbonate	Powell-Rouyn	32.70	0.00	23.02	23.94	0.43	17.41	0.63	0.00	0.35	0.00	1.72	28	5.87	2.13	2.78	0.00	0.33	3.27	0.06	4.66
87CG02_area 6	Chl 7	Felsic dike	Spotted/Carbonate	Powell-Rouyn	33.48	0.00	21.65	26.12	0.00	18.57	0.00	0.00	0.18	0.00	0.00	28	6.01	1.99	2.63	0.00	0.34	3.59	0.00	4.97
87CG02_area 7	Chl 1	Felsic dike	Spotted/Carbonate	Powell-Rouyn	28.90	0.62	25.76	29.42	1.37	13.74	0.00	0.00	0.00	0.00	0.00	28	5.35	2.65	3.00	0.09	0.29	4.27	0.21	3.79
87CG02_area 7	Chl 2	Felsic dike	Spotted/Carbonate	Powell-Rouyn	29.86	0.19	24.21	25.60	0.81	15.44	0.16	0.78	0.07	2.31	0.00	28	5.51	2.49	2.82	0.03	0.08	3.87	0.13	4.25
87CG02_area 7	Chl 3	Felsic dike	Spotted/Carbonate	Powell-Rouyn	31.25	0.00	21.46	29.94	0.34	16.17	0.00	0.00	0.00	0.00	0.28	28	5.81	2.19	2.53	0.00	0.19	4.47	0.05	4.48

ID	Spectrum	Lithology	Alteration	Location	Ni	Zn	Ca	Na	K	OH*	Total	Fe/Fe+Mg	Variety
54BG02_area 2	Chl 8	Mafic dike/lamprophyre?	Chlorite	Background	0.01	0.00	0.00	0.29	0.00	16	36.14	0.12	clinochlore
54BG02_area 2	Chl 9	Mafic dike/lamprophyre?	Chlorite	Background	0.01	0.00	0.01	0.39	0.00	16	36.22	0.12	clinochlore
54BG02_area 2	Chl 10	Mafic dike/lamprophyre?	Chlorite	Background	0.01	0.00	0.00	0.33	0.07	16	36.12	0.12	clinochlore
54BG02_area 2	Chl 11	Mafic dike/lamprophyre?	Chlorite	Background	0.01	0.00	0.00	0.34	0.01	16	36.16	0.13	clinochlore
54BG02_area 2	Chl 12	Mafic dike/lamprophyre?	Chlorite	Background	0.01	0.00	0.00	0.34	0.00	16	36.15	0.12	clinochlore
54BG02_area 2	Chl 13	Mafic dike/lamprophyre?	Chlorite	Background	0.01	0.01	0.01	0.40	0.00	16	36.21	0.14	clinochlore
54BG02_area 3	Chl 1	Mafic dike/lamprophyre?	Chlorite	Background	0.00	0.01	0.00	0.38	0.07	16	36.24	0.13	clinochlore
54BG02_area 3	Chl 2	Mafic dike/lamprophyre?	Chlorite	Background	0.00	0.01	0.01	0.42	0.00	16	36.26	0.12	clinochlore
54BG02_area 3	Chl 3	Mafic dike/lamprophyre?	Chlorite	Background	0.01	0.00	0.04	0.42	0.03	16	36.34	0.13	clinochlore
54BG02_area 3	Chl 4	Mafic dike/lamprophyre?	Chlorite	Background	0.00	0.01	0.00	0.40	0.00	16	36.28	0.13	clinochlore
87CG02_area 1	Chl 1	Felsic dike	Spotted/Carbonate	Powell-Rouyn	0.12	0.00	0.12	0.00	0.17	16	36.16	0.50	pycnochlorite
87CG02_area 1	Chl 2	Felsic dike	Spotted/Carbonate	Powell-Rouyn	0.00	0.01	0.00	0.70	0.00	16	36.36	0.44	ripidolite
87CG02_area 1	Chl 3	Felsic dike	Spotted/Carbonate	Powell-Rouyn	0.00	0.00	0.02	0.34	0.24	16	36.01	0.46	ripidolite
87CG02_area 1	Chl 4	Felsic dike	Spotted/Carbonate	Powell-Rouyn	0.19	0.00	0.04	0.18	0.07	16	35.83	0.51	ripidolite
87CG02_area 1	Chl 5	Felsic dike	Spotted/Carbonate	Powell-Rouyn	0.00	0.00	0.00	0.26	0.23	16	36.04	0.49	pycnochlorite
87CG02_area 2	Chl 1	Felsic dike	Spotted/Carbonate	Powell-Rouyn	0.00	0.00	0.02	0.00	0.00	16	35.57	0.51	brunsvigite
87CG02_area 2	Chl 2	Felsic dike	Spotted/Carbonate	Powell-Rouyn	0.07	0.00	0.14	0.25	0.15	16	36.39	0.50	ripidolite
87CG02_area 2	Chl 3	Felsic dike	Spotted/Carbonate	Powell-Rouyn	0.00	0.00	0.11	0.00	0.30	16	35.42	0.48	diabantite
87CG02_area 2	Chl 4	Felsic dike	Spotted/Carbonate	Powell-Rouyn	0.17	0.16	0.00	0.00	0.05	16	36.39	0.55	ripidolite
87CG02_area 2	Chl 5	Felsic dike	Spotted/Carbonate	Powell-Rouyn	0.00	0.00	0.09	0.38	0.07	16	36.43	0.52	ripidolite
87CG02_area 3	Chl 1	Felsic dike	Spotted/Carbonate	Powell-Rouyn	0.01	0.00	0.15	0.28	0.21	16	36.28	0.54	ripidolite
87CG02_area 3	Chl 2	Felsic dike	Spotted/Carbonate	Powell-Rouyn	0.04	0.12	0.12	0.42	0.00	16	36.65	0.55	ripidolite
87CG02_area 3	Chl 3	Felsic dike	Spotted/Carbonate	Powell-Rouyn	0.00	0.43	0.15	0.00	0.01	16	35.69	0.48	pycnochlorite
87CG02_area 3	Chl 4	Felsic dike	Spotted/Carbonate	Powell-Rouyn	0.00	0.00	0.05	0.24	0.00	16	36.21	0.51	brunsvigite
87CG02_area 3	Chl 5	Felsic dike	Spotted/Carbonate	Powell-Rouyn	0.12	0.00	0.02	0.74	0.17	16	36.23	0.43	pycnochlorite
87CG02_area 3	Chl 6	Felsic dike	Spotted/Carbonate	Powell-Rouyn	0.00	0.04	0.00	0.60	0.00	16	36.40	0.53	brunsvigite
87CG02_area 3	Chl 7	Felsic dike	Spotted/Carbonate	Powell-Rouyn	0.04	0.00	0.00	0.00	0.00	16	35.89	0.54	ripidolite
87CG02_area 4	Chl 1	Felsic dike	Spotted/Carbonate	Powell-Rouyn	0.00	0.00	0.08	0.30	0.03	16	36.48	0.52	ripidolite
87CG02_area 4	Chl 2	Felsic dike	Spotted/Carbonate	Powell-Rouyn	0.00	0.00	0.00	0.00	0.00	16	35.54	0.46	pycnochlorite
87CG02_area 4	Chl 3	Felsic dike	Spotted/Carbonate	Powell-Rouyn	0.00	0.15	0.02	0.00	0.00	16	36.01	0.54	brunsvigite
87CG02_area 4	Chl 4	Felsic dike	Spotted/Carbonate	Powell-Rouyn	0.01	0.00	0.10	0.00	0.00	16	36.14	0.55	ripidolite
87CG02_area 4	Chl 5	Felsic dike	Spotted/Carbonate	Powell-Rouyn	0.00	0.00	0.00	0.16	0.03	16	36.54	0.50	ripidolite
87CG02_area 5	Chl 1	Felsic dike	Spotted/Carbonate	Powell-Rouyn	0.00	0.01	0.06	0.06	0.13	16	36.91	0.54	ripidolite
87CG02_area 5	Chl 2	Felsic dike	Spotted/Carbonate	Powell-Rouyn	0.00	0.04	0.00	0.00	0.00	16	35.86	0.56	brunsvigite
87CG02_area 5	Chl 3	Felsic dike	Spotted/Carbonate	Powell-Rouyn	0.00	0.23	0.00	0.07	0.12	16	36.49	0.51	ripidolite
87CG02_area 6	Chl 1	Felsic dike	Spotted/Carbonate	Powell-Rouyn	0.25	0.44	0.00	0.23	0.00	16	35.96	0.46	pycnochlorite
87CG02_area 6	Chl 2	Felsic dike	Spotted/Carbonate	Powell-Rouyn	0.03	0.00	0.04	0.13	0.00	16	36.02	0.47	ripidolite
87CG02_area 6	Chl 3	Felsic dike	Spotted/Carbonate	Powell-Rouyn	0.00	0.00	0.05	0.22	0.03	16	35.16	0.39	diabantite
87CG02_area 6	Chl 4	Felsic dike	Spotted/Carbonate	Powell-Rouyn	0.29	0.35	0.00	0.32	0.00	16	36.03	0.50	brunsvigite
87CG02_area 6	Chl 5	Felsic dike	Spotted/Carbonate	Powell-Rouyn	0.00	0.04	0.11	0.00	0.00	16	36.36	0.52	ripidolite
87CG02_area 6	Chl 6	Felsic dike	Spotted/Carbonate	Powell-Rouyn	0.25	0.00	0.12	0.00	0.16	16	35.64	0.44	pycnochlorite
87CG02_area 6	Chl 7	Felsic dike	Spotted/Carbonate	Powell-Rouyn	0.00	0.00	0.00	0.00	0.08	16	35.60	0.44	pycnochlorite
87CG02_area 7	Chl 1	Felsic dike	Spotted/Carbonate	Powell-Rouyn	0.00	0.00	0.00	0.00	0.00	16	35.64	0.55	ripidolite
87CG02_area 7	Chl 2	Felsic dike	Spotted/Carbonate	Powell-Rouyn	0.00	0.31	0.03	0.56	0.03	16	36.11	0.48	ripidolite
87CG02_area 7	Chl 3	Felsic dike	Spotted/Carbonate	Powell-Rouyn	0.04	0.00	0.00	0.00	0.00	16	35.76	0.51	brunsvigite

	Spectrum	Lithology	Location	O	Mg	Ca	Mn	Fe	Fe+Mn
				atm %	atm %	atm %	atm %	atm %	atm %
87CG02_New_A1	Spectrum 29	Felsic dike	Powell-Rouyn Au	50.16	13.02	25.26	3.91	7.03	10.95
87CG02_New_A1	Spectrum 30	Felsic dike	Powell-Rouyn Au	50.23	10.81	27.51	4.30	6.60	10.91
87CG02_New_A1	Spectrum 31	Felsic dike	Powell-Rouyn Au	50.15	14.25	24.10	3.14	6.91	10.05
87CG02_New_A1	Spectrum 32	Felsic dike	Powell-Rouyn Au	50.17	14.04	24.37	3.75	6.66	10.41
87CG02_New_A1	Spectrum 33	Felsic dike	Powell-Rouyn Au	50.23	15.27	23.18	3.66	6.64	10.30
87CG02_New_A1	Spectrum 34	Felsic dike	Powell-Rouyn Au	50.23	11.35	26.05	3.94	7.78	11.72
87CG02_New_A1	Spectrum 35	Felsic dike	Powell-Rouyn Au	50.26	13.88	23.40	3.83	7.22	11.05
87CG02_New_A1	Spectrum 36	Felsic dike	Powell-Rouyn Au	50.21	11.55	25.68	4.17	7.54	11.71
87CG02_New_A1	Spectrum 39	Felsic dike	Powell-Rouyn Au	50.21	14.00	23.84	4.19	6.77	10.96
87CG02_New_A1	Spectrum 40	Felsic dike	Powell-Rouyn Au	50.17	12.76	24.85	4.12	7.21	11.33
87CG02_New_A1	Spectrum 41	Felsic dike	Powell-Rouyn Au	50.23	11.17	26.42	4.43	7.17	11.60
87CG02_New_A2	Spectrum 1	Felsic dike	Powell-Rouyn Au	50.33	12.91	23.90	4.16	7.88	12.04
87CG02_New_A2	Spectrum 2	Felsic dike	Powell-Rouyn Au	50.31	14.69	22.39	3.81	7.21	11.02
87CG02_New_A2	Spectrum 3	Felsic dike	Powell-Rouyn Au	50.57	13.90	23.22	3.82	6.65	10.47
87CG02_New_A2	Spectrum 4	Felsic dike	Powell-Rouyn Au	51.16	11.45	24.26	3.84	5.98	9.82
87CG02_New_A2	Spectrum 5	Felsic dike	Powell-Rouyn Au	50.28	12.70	24.49	4.55	6.99	11.54
87CG02_New_A2	Spectrum 6	Felsic dike	Powell-Rouyn Au	50.53	11.78	25.94	3.71	6.31	10.02
87CG02_New_A2	Spectrum 7	Felsic dike	Powell-Rouyn Au	50.32	12.73	25.24	3.95	6.26	10.21
87CG02_New_A2	Spectrum 8	Felsic dike	Powell-Rouyn Au	50.32	12.89	23.89	4.51	7.19	11.70
87CG02_New_A4	Spectrum 1	Felsic dike	Powell-Rouyn Au	50.24	10.61	26.50	4.63	7.37	12.01
87CG02_New_A4	Spectrum 2	Felsic dike	Powell-Rouyn Au	50.11	13.70	24.58	3.82	6.95	10.76
87CG02_New_A4	Spectrum 3	Felsic dike	Powell-Rouyn Au	50.50	14.20	24.05	3.41	6.58	9.99
87CG02_New_A4	Spectrum 4	Felsic dike	Powell-Rouyn Au	50.30	14.42	22.82	4.47	6.88	11.36
87CG02_New_A4	Spectrum 5	Felsic dike	Powell-Rouyn Au	52.69	11.11	20.80	3.82	5.63	9.45
87CG02_New_A4	Spectrum 6	Felsic dike	Powell-Rouyn Au	50.47	13.24	24.72	3.70	6.07	9.77
87CG02_New_A4	Spectrum 7	Felsic dike	Powell-Rouyn Au	50.14	13.06	24.98	4.08	6.60	10.68
87CG02_New_A4	Spectrum 8	Felsic dike	Powell-Rouyn Au	50.35	14.97	23.01	3.92	6.39	10.31
87CG02_New_A4	Spectrum 9	Felsic dike	Powell-Rouyn Au	50.31	13.63	23.62	4.31	6.79	11.10
87CG02_New_A4	Spectrum 10	Felsic dike	Powell-Rouyn Au	50.27	13.42	24.46	3.54	7.48	11.02
87CG02_New_A4	Spectrum 11	Felsic dike	Powell-Rouyn Au	49.95	13.19	23.97	3.68	7.98	11.67
87CG02_New_A5	Spectrum 1	Felsic dike	Powell-Rouyn Au	50.09	12.54	26.02	3.13	7.62	10.75
87CG02_New_A5	Spectrum 2	Felsic dike	Powell-Rouyn Au	50.21	14.42	23.18	3.40	7.73	11.13
87CG02_New_A5	Spectrum 3	Felsic dike	Powell-Rouyn Au	50.16	11.31	26.94	3.41	7.47	10.88
87CG02_New_A5	Spectrum 4	Felsic dike	Powell-Rouyn Au	50.10	12.96	25.99	3.65	6.05	9.70
87CG02_New_A5	Spectrum 5	Felsic dike	Powell-Rouyn Au	50.23	14.62	23.86	2.88	7.11	10.00
87CG02_New_A5	Spectrum 6	Felsic dike	Powell-Rouyn Au	50.06	13.31	23.83	3.84	7.88	11.72
87CG02_New_A5	Spectrum 7	Felsic dike	Powell-Rouyn Au	50.26	14.95	22.58	3.73	7.44	11.17
87CG02_New_A5	Spectrum 8	Felsic dike	Powell-Rouyn Au	50.46	13.53	23.83	3.86	6.36	10.22
87CG02_New_A5	Spectrum 9	Felsic dike	Powell-Rouyn Au	50.10	12.68	25.15	4.27	6.47	10.74
87CG02_New_A5	Spectrum 10	Felsic dike	Powell-Rouyn Au	50.14	12.49	25.69	3.78	6.49	10.27
87CG02_New_A5	Spectrum 11	Felsic dike	Powell-Rouyn Au	50.16	14.98	22.92	3.53	6.70	10.24
87CG02_New_A5	Spectrum 12	Felsic dike	Powell-Rouyn Au	50.14	13.82	23.77	4.04	7.57	11.61
87CG02_New_A5	Spectrum 13	Felsic dike	Powell-Rouyn Au	50.24	13.32	24.27	3.91	6.39	10.30
87CG02_New_A5	Spectrum 14	Felsic dike	Powell-Rouyn Au	50.33	13.53	24.88	3.60	6.49	10.08
87CG02_New_A5	Spectrum 15	Felsic dike	Powell-Rouyn Au	50.22	11.39	26.37	4.49	6.85	11.34
87CG02_New_A6	Spectrum 1	Felsic dike	Powell-Rouyn Au	51.45	11.13	22.27	4.77	7.23	12.00
87CG02_New_A6	Spectrum 2	Felsic dike	Powell-Rouyn Au	49.90	12.52	25.23	3.97	6.76	10.73
87CG02_New_A6	Spectrum 3	Felsic dike	Powell-Rouyn Au	55.43	9.60	15.97	2.92	4.33	7.25
87CG02_New_A6	Spectrum 4	Felsic dike	Powell-Rouyn Au	50.20	12.43	26.22	3.51	6.92	10.43
87CG02_New_A6	Spectrum 5	Felsic dike	Powell-Rouyn Au	50.25	12.80	24.75	4.40	6.47	10.87
87CG02_New_A7	Spectrum 1	Felsic dike	Powell-Rouyn Au	51.82	10.45	22.69	4.72	6.50	11.22
87CG02_New_A7	Spectrum 2	Felsic dike	Powell-Rouyn Au	50.26	12.85	25.42	4.14	6.74	10.88
87CG02_New_A7	Spectrum 3	Felsic dike	Powell-Rouyn Au	50.60	12.54	23.81	4.34	6.68	11.02
87CG02_New_A7	Spectrum 4	Felsic dike	Powell-Rouyn Au	50.08	12.22	25.28	4.61	6.64	11.26
87CG02_New_A7	Spectrum 5	Felsic dike	Powell-Rouyn Au	50.14	12.19	26.14	3.87	6.47	10.33
87CG02_New_A7	Spectrum 6	Felsic dike	Powell-Rouyn Au	50.45	10.38	26.32	4.96	6.92	11.88
87CG02_New_A7	Spectrum 7	Felsic dike	Powell-Rouyn Au	50.66	14.36	22.00	3.58	6.71	10.29
87CG02_New_A7	Spectrum 8	Felsic dike	Powell-Rouyn Au	50.50	10.94	25.38	4.71	7.30	12.02
87CG02_New_A7	Spectrum 9	Felsic dike	Powell-Rouyn Au	50.28	14.67	23.13	3.63	7.14	10.77
87CG02_New_A7	Spectrum 10	Felsic dike	Powell-Rouyn Au	50.17	13.99	23.68	4.23	6.67	10.90
87CG02_New_A7	Spectrum 11	Felsic dike	Powell-Rouyn Au	50.35	13.25	23.79	4.24	6.69	10.93
87CG02_New_A7	Spectrum 12	Felsic dike	Powell-Rouyn Au	53.94	11.26	18.37	2.75	5.26	8.01
87CG02_New_A7	Spectrum 13	Felsic dike	Powell-Rouyn Au	50.08	12.45	25.02	4.40	6.85	11.25
87CG02_New_A7	Spectrum 14	Felsic dike	Powell-Rouyn Au	50.91	11.95	23.54	4.48	7.05	11.54
87CG02_New_A7	Spectrum 15	Felsic dike	Powell-Rouyn Au	50.25	13.37	24.63	4.11	6.70	10.81
87CG02_New_A7	Spectrum 16	Felsic dike	Powell-Rouyn Au	50.29	11.77	25.06	4.86	7.44	12.29
87CG02_New_A8	Spectrum 1	Felsic dike	Powell-Rouyn Au	50.31	13.64	23.48	4.09	6.69	10.78
87CG02_New_A8	Spectrum 2	Felsic dike	Powell-Rouyn Au	50.25	12.82	23.63	4.36	7.79	12.15
87CG02_New_A8	Spectrum 3	Felsic dike	Powell-Rouyn Au	52.20	12.01	21.28	3.55	5.60	9.16
87CG02_New_A8	Spectrum 4	Felsic dike	Powell-Rouyn Au	50.13	12.34	25.78	4.14	6.33	10.47
87CG02_New_A8	Spectrum 5	Felsic dike	Powell-Rouyn Au	50.36	11.93	26.27	4.29	6.21	10.50
87CG02_New_A8	Spectrum 6	Felsic dike	Powell-Rouyn Au	50.24	13.03	24.83	4.12	6.37	10.48
87CG02_New_A8	Spectrum 7	Felsic dike	Powell-Rouyn Au	50.46	12.84	24.20	4.20	6.75	10.96
87CG02_New_A8	Spectrum 8	Felsic dike	Powell-Rouyn Au	50.93	12.19	23.35	3.75	6.61	10.36

	Spectrum	Lithology	Location	O	Mg	Ca	Mn	Fe	Fe+Mn
				atm %	atm %	atm %	atm %	atm %	atm %
87CG02_New_A8	Spectrum 9	Felsic dike	Powell-Rouyn Au	50.04	12.96	25.40	4.18	6.52	10.70
87CG02_New_A8	Spectrum 10	Felsic dike	Powell-Rouyn Au	51.04	12.45	22.79	4.18	6.81	10.99
87CG02_New_A8	Spectrum 11	Felsic dike	Powell-Rouyn Au	51.43	10.15	23.52	4.60	6.22	10.82
87CG02_New_A8	Spectrum 12	Felsic dike	Powell-Rouyn Au	50.28	13.62	24.19	3.98	6.64	10.62
87CG02_New_A8	Spectrum 16	Felsic dike	Powell-Rouyn Au	50.07	11.67	26.29	4.25	7.02	11.27
87CG02_New_A8	Spectrum 17	Felsic dike	Powell-Rouyn Au	50.60	13.15	23.58	4.62	6.44	11.06
99AG01_New_A1	Spectrum 69	Basalt	Near fault	58.42	0.03	22.53	0.04	0.20	0.24
99AG01_New_A1	Spectrum 70	Basalt	Near fault	58.92	0.00	22.71	0.00	0.13	0.13
99AG01_New_A1	Spectrum 71	Basalt	Near fault	58.13	0.00	23.69	0.00	0.20	0.20
99AG01_New_A1	Spectrum 72	Basalt	Near fault	50.29	11.96	25.11	3.23	8.38	11.60
99AG01_New_A1	Spectrum 73	Basalt	Near fault	50.13	11.48	25.85	1.90	10.30	12.20
99AG01_New_A1	Spectrum 74	Basalt	Near fault	50.29	11.78	24.92	1.44	10.77	12.21
99AG01_New_A2	Spectrum 1	Basalt	Near fault	50.15	12.71	23.99	1.37	9.89	11.27
99AG01_New_A2	Spectrum 2	Basalt	Near fault	50.15	10.69	26.34	2.29	9.93	12.22
99AG01_New_A2	Spectrum 3	Basalt	Near fault	50.11	13.27	23.70	1.63	9.80	11.43
99AG01_New_A2	Spectrum 4	Basalt	Near fault	50.19	10.67	26.66	1.66	10.23	11.89
99AG01_New_A2	Spectrum 5	Basalt	Near fault	50.05	12.67	25.54	2.09	8.80	10.89
99AG01_New_A2	Spectrum 6	Basalt	Near fault	50.16	11.66	25.20	1.82	10.56	12.39
99AG01_New_A2	Spectrum 7	Basalt	Near fault	50.00	12.51	24.67	2.74	9.23	11.97
99AG01_New_A2	Spectrum 8	Basalt	Near fault	49.98	12.66	23.93	2.17	10.22	12.39
99AG01_New_A2	Spectrum 9	Basalt	Near fault	50.24	9.80	27.69	2.79	8.92	11.71
99AG01_New_A2	Spectrum 10	Basalt	Near fault	50.08	11.97	25.41	2.22	9.47	11.69
99AG01_New_A2	Spectrum 11	Basalt	Near fault	50.20	12.56	24.80	1.27	10.21	11.48
99AG01_New_A2	Spectrum 12	Basalt	Near fault	50.19	10.56	26.47	1.47	10.62	12.10
99AG01_New_A2	Spectrum 13	Basalt	Near fault	50.19	12.71	24.70	1.75	9.51	11.25
99AG01_New_A2	Spectrum 14	Basalt	Near fault	50.10	13.17	23.93	3.01	8.56	11.56
99AG01_New_A2	Spectrum 15	Basalt	Near fault	50.22	12.14	25.60	1.14	10.30	11.44
99AG01_New_A2	Spectrum 16	Basalt	Near fault	50.17	13.24	24.68	1.27	9.72	10.99
99AG01_New_A3	Spectrum 1	Basalt	Near fault	50.02	11.09	26.39	1.40	10.57	11.97
99AG01_New_A3	Spectrum 2	Basalt	Near fault	50.20	11.58	25.53	3.86	8.18	12.04
99AG01_New_A3	Spectrum 3	Basalt	Near fault	50.23	0.27	45.88	1.50	0.85	2.35
99AG01_New_A3	Spectrum 4	Basalt	Near fault	50.20	12.05	24.92	2.38	9.46	11.83
99AG01_New_A3	Spectrum 5	Basalt	Near fault	50.21	12.32	25.18	1.76	9.21	10.96
99AG01_New_A3	Spectrum 6	Basalt	Near fault	50.11	12.27	24.58	3.09	8.37	11.45
99AG01_New_A3	Spectrum 7	Basalt	Near fault	50.14	13.18	23.87	1.51	10.06	11.57
99AG01_New_A3	Spectrum 8	Basalt	Near fault	50.29	0.28	45.44	2.66	0.61	3.27
99AG01_New_A3	Spectrum 9	Basalt	Near fault	50.34	0.30	45.63	1.47	0.47	1.93
99AG01_New_A3	Spectrum 10	Basalt	Near fault	50.22	9.85	26.71	3.16	9.06	12.23
99AG01_New_A3	Spectrum 11	Basalt	Near fault	50.23	9.75	26.16	5.00	8.38	13.38
99AG01_New_A3	Spectrum 12	Basalt	Near fault	50.33	12.37	25.48	1.38	9.17	10.55
99AG01_New_A3	Spectrum 13	Basalt	Near fault	50.08	12.89	24.95	1.44	9.96	11.40
99AG01_New_A3	Spectrum 14	Basalt	Near fault	50.03	13.33	22.94	2.27	10.24	12.51
99AG01_New_A3	Spectrum 15	Basalt	Near fault	49.99	12.38	25.88	1.91	8.87	10.78
99AG01_New_A3	Spectrum 16	Basalt	Near fault	50.02	13.78	22.72	1.25	10.55	11.80
99AG01_New_A3	Spectrum 17	Basalt	Near fault	50.03	11.64	23.99	2.33	10.82	13.15
99AG01_New_A3	Spectrum 18	Basalt	Near fault	50.11	12.31	24.68	1.91	9.98	11.89
99AG01_New_A3	Spectrum 19	Basalt	Near fault	50.17	12.69	25.20	1.10	10.17	11.27
99AG01_New_A4	Spectrum 1	Basalt	Near fault	50.23	13.07	23.68	1.80	9.50	11.30
99AG01_New_A4	Spectrum 2	Basalt	Near fault	50.05	11.88	25.88	1.64	9.81	11.46
99AG01_New_A4	Spectrum 3	Basalt	Near fault	50.25	13.05	25.10	2.15	8.75	10.90
99AG01_New_A4	Spectrum 4	Basalt	Near fault	50.20	10.36	27.06	2.28	9.75	12.03
99AG01_New_A4	Spectrum 5	Basalt	Near fault	50.08	10.49	25.65	4.22	9.13	13.35
99AG01_New_A4	Spectrum 6	Basalt	Near fault	50.21	11.60	23.87	4.93	8.29	13.23
99AG01_New_A4	Spectrum 7	Basalt	Near fault	50.26	12.20	23.90	3.78	8.66	12.45
99AG01_New_A4	Spectrum 8	Basalt	Near fault	50.14	12.84	24.91	1.73	9.22	10.95
99AG01_New_A4	Spectrum 9	Basalt	Near fault	50.21	10.76	26.61	1.94	9.82	11.76
99AG01_New_A4	Spectrum 11	Basalt	Near fault	50.27	11.91	25.12	1.60	10.02	11.62
99AG01_New_A5	Spectrum 1	Basalt	Near fault	50.12	11.78	24.98	2.94	9.05	11.99
99AG01_New_A5	Spectrum 2	Basalt	Near fault	50.06	12.17	25.96	2.11	8.70	10.81
99AG01_New_A5	Spectrum 3	Basalt	Near fault	50.16	11.11	26.09	1.79	9.80	11.59
99AG01_New_A5	Spectrum 4	Basalt	Near fault	50.07	12.13	25.82	2.27	8.77	11.03
99AG01_New_A5	Spectrum 5	Basalt	Near fault	50.14	12.90	23.77	1.36	10.67	12.02
99AG01_New_A5	Spectrum 6	Basalt	Near fault	50.27	10.86	26.43	1.39	10.29	11.67
99AG01_New_A5	Spectrum 7	Basalt	Near fault	50.09	12.44	24.20	2.55	9.52	12.08
99AG01_New_A5	Spectrum 8	Basalt	Near fault	50.24	10.20	26.70	1.67	10.57	12.24
99AG01_New_A5	Spectrum 9	Basalt	Near fault	50.14	13.44	23.25	2.07	9.78	11.85
99AG01_New_A5	Spectrum 10	Basalt	Near fault	50.14	13.12	23.00	1.92	11.10	13.03
99AG01_New_A5	Spectrum 11	Basalt	Near fault	50.11	11.78	25.90	2.78	8.35	11.13
99AG01_New_A5	Spectrum 12	Basalt	Near fault	50.21	10.16	26.55	1.83	10.66	12.48
99AG01_New_A5	Spectrum 13	Basalt	Near fault	50.26	12.08	24.66	3.34	8.24	11.58
99AG01_New_A5	Spectrum 19	Basalt	Near fault	58.97	0.06	22.68	0.00	0.16	0.16
99AG01_New_A6	Spectrum 1	Basalt	Near fault	50.19	13.58	24.25	1.80	8.81	10.61
99AG01_New_A6	Spectrum 2	Basalt	Near fault	50.13	12.84	24.28	1.75	9.59	11.35
99AG01_New_A6	Spectrum 3	Basalt	Near fault	50.17	12.50	24.56	2.08	9.54	11.62

	Spectrum	Lithology	Location	O	Mg	Ca	Mn	Fe	Fe+Mn
				atm %	atm %	atm %	atm %	atm %	atm %
99AG01_New_A6	Spectrum 4	Basalt	Near fault	50.10	10.93	26.61	1.31	10.57	11.89
99AG01_New_A6	Spectrum 5	Basalt	Near fault	50.39	12.53	24.69	1.45	9.85	11.29
99AG01_New_A6	Spectrum 6	Basalt	Near fault	50.09	12.43	25.87	1.67	9.16	10.84
99AG01_New_A6	Spectrum 7	Basalt	Near fault	52.14	9.81	19.73	3.10	8.87	11.98
99AG01_New_A6	Spectrum 8	Basalt	Near fault	50.25	11.99	24.36	3.76	8.73	12.49
99AG01_New_A6	Spectrum 9	Basalt	Near fault	50.63	11.01	25.65	2.24	8.89	11.14
99AG01_New_A6	Spectrum 10	Basalt	Near fault	50.19	12.19	24.83	2.72	9.34	12.06
99AG01_New_A6	Spectrum 11	Basalt	Near fault	50.21	12.78	23.90	3.14	8.66	11.80
99AG01_New_A6	Spectrum 12	Basalt	Near fault	50.16	12.94	23.49	2.20	9.65	11.86
99AG01_New_A6	Spectrum 13	Basalt	Near fault	50.11	13.00	24.44	1.53	9.82	11.35
99AG01_New_A6	Spectrum 14	Basalt	Near fault	50.29	12.55	24.26	1.77	10.11	11.88
99AG01_New_A6	Spectrum 15	Basalt	Near fault	50.33	11.75	25.15	3.51	8.02	11.53
99AG01_New_A6	Spectrum 16	Basalt	Near fault	50.31	10.30	26.89	3.49	8.40	11.88
99AG01_New_A7	Spectrum 1	Basalt	Near fault	49.95	12.35	24.34	1.73	10.78	12.51
99AG01_New_A7	Spectrum 2	Basalt	Near fault	50.21	12.34	24.41	1.31	10.66	11.97
99AG01_New_A7	Spectrum 3	Basalt	Near fault	49.98	11.95	25.48	1.82	9.96	11.78
99AG01_New_A7	Spectrum 4	Basalt	Near fault	50.21	12.19	24.63	1.58	9.96	11.54
99AG01_New_A7	Spectrum 5	Basalt	Near fault	50.14	11.71	26.12	2.17	8.53	10.70
99AG01_New_A7	Spectrum 6	Basalt	Near fault	50.17	13.15	23.92	2.48	9.39	11.87
99AG01_New_A7	Spectrum 7	Basalt	Near fault	50.23	12.96	22.61	2.21	11.02	13.24
99AG01_New_A7	Spectrum 8	Basalt	Near fault	50.17	11.18	25.71	2.21	10.47	12.68
99AG01_New_A7	Spectrum 9	Basalt	Near fault	50.39	13.67	22.32	1.81	10.14	11.95
99AG01_New_A7	Spectrum 10	Basalt	Near fault	50.24	10.84	24.31	5.00	8.69	13.69
99AG01_New_A7	Spectrum 11	Basalt	Near fault	50.15	13.61	23.78	2.13	9.09	11.22
99AG01_New_A7	Spectrum 12	Basalt	Near fault	49.96	12.31	25.70	2.65	8.58	11.22
99AG01_New_A7	Spectrum 13	Basalt	Near fault	50.06	11.81	24.60	2.37	10.89	13.25
99AG01_New_A7	Spectrum 14	Basalt	Near fault	50.21	11.49	25.44	1.42	11.00	12.42
99AG01_New_A7	Spectrum 15	Basalt	Near fault	50.19	12.04	24.32	4.17	7.91	12.08
99AG01_New_A7	Spectrum 16	Basalt	Near fault	50.10	13.41	23.13	2.25	10.34	12.59
99AG01_New_A7	Spectrum 17	Basalt	Near fault	50.93	11.86	21.95	3.03	9.17	12.21
99AG01_New_A7	Spectrum 18	Basalt	Near fault	50.11	10.57	25.88	3.12	9.67	12.79
99AG01_New_A7	Spectrum 19	Basalt	Near fault	50.22	10.17	25.27	4.48	9.29	13.76
99AG01_New_A7	Spectrum 20	Basalt	Near fault	50.06	13.58	23.98	1.69	9.37	11.06
99AG01_New_A7	Spectrum 21	Basalt	Near fault	49.98	11.49	25.77	1.31	10.23	11.53
99AG01_New_A7	Spectrum 22	Basalt	Near fault	50.20	12.51	23.83	2.96	8.60	11.56
99AG01_New_A7	Spectrum 23	Basalt	Near fault	50.04	13.76	23.80	1.49	9.65	11.14
105AG01_New_A1	Spectrum 1	Lamprophyre	Background	50.10	18.83	25.12	0.08	4.98	5.06
105AG01_New_A1	Spectrum 2	Lamprophyre	Background	50.14	18.82	25.09	0.35	4.76	5.11
105AG01_New_A1	Spectrum 3	Lamprophyre	Background	50.02	18.70	25.79	0.32	4.32	4.64
105AG01_New_A1	Spectrum 4	Lamprophyre	Background	50.09	19.54	24.85	0.33	4.34	4.67
105AG01_New_A1	Spectrum 5	Lamprophyre	Background	49.94	19.19	24.68	0.22	4.52	4.73
105AG01_New_A1	Spectrum 6	Lamprophyre	Background	50.09	17.36	26.64	0.17	5.05	5.22
105AG01_New_A1	Spectrum 7	Lamprophyre	Background	50.17	18.42	25.28	0.26	5.18	5.43
105AG01_New_A1	Spectrum 8	Lamprophyre	Background	50.09	18.63	25.46	0.17	4.90	5.07
105AG01_New_A1	Spectrum 9	Lamprophyre	Background	50.14	18.61	25.32	0.31	4.97	5.28
105AG01_New_A1	Spectrum 10	Lamprophyre	Background	49.99	19.00	25.38	0.30	4.41	4.71
105AG01_New_A1	Spectrum 11	Lamprophyre	Background	50.19	20.36	23.17	0.27	4.59	4.86
105AG01_New_A1	Spectrum 12	Lamprophyre	Background	50.04	17.09	27.36	0.46	4.53	4.99
105AG01_New_A1	Spectrum 13	Lamprophyre	Background	50.16	18.83	25.05	0.38	4.45	4.82
105AG01_New_A1	Spectrum 14	Lamprophyre	Background	50.24	18.25	25.47	0.14	4.95	5.09
105AG01_New_A1	Spectrum 15	Lamprophyre	Background	50.03	20.08	24.49	0.44	4.00	4.44
105AG01_New_A1	Spectrum 16	Lamprophyre	Background	50.08	19.33	25.04	0.78	3.87	4.65
105AG01_New_A2	Spectrum 1	Lamprophyre	Background	50.06	18.36	25.88	0.35	4.58	4.93
105AG01_New_A2	Spectrum 2	Lamprophyre	Background	50.12	19.11	24.75	0.15	4.72	4.87
105AG01_New_A2	Spectrum 3	Lamprophyre	Background	50.25	19.83	23.59	0.20	4.61	4.81
105AG01_New_A2	Spectrum 4	Lamprophyre	Background	49.98	17.14	27.02	0.20	5.08	5.28
105AG01_New_A2	Spectrum 5	Lamprophyre	Background	49.98	18.23	25.71	0.24	4.96	5.19
105AG01_New_A2	Spectrum 6	Lamprophyre	Background	50.08	18.58	24.84	0.26	4.95	5.21
105AG01_New_A2	Spectrum 7	Lamprophyre	Background	50.36	16.10	27.08	0.35	5.23	5.59
105AG01_New_A2	Spectrum 8	Lamprophyre	Background	50.08	17.61	25.82	0.34	4.96	5.29
105AG01_New_A2	Spectrum 9	Lamprophyre	Background	49.96	17.85	25.88	0.46	5.11	5.57
105AG01_New_A2	Spectrum 10	Lamprophyre	Background	50.06	17.94	25.94	0.33	4.76	5.09
105AG01_New_A2	Spectrum 11	Lamprophyre	Background	50.15	18.04	24.92	0.14	5.25	5.39
105AG01_New_A2	Spectrum 12	Lamprophyre	Background	50.00	18.23	25.48	0.33	5.09	5.41
105AG01_New_A2	Spectrum 13	Lamprophyre	Background	50.11	19.51	23.92	0.27	5.13	5.40
105AG01_New_A3	Spectrum 1	Lamprophyre	Background	50.13	17.90	25.64	0.29	5.17	5.46
105AG01_New_A3	Spectrum 2	Lamprophyre	Background	50.06	18.62	25.55	0.18	4.69	4.87
105AG01_New_A3	Spectrum 3	Lamprophyre	Background	49.96	17.63	27.11	0.48	4.13	4.61
105AG01_New_A3	Spectrum 4	Lamprophyre	Background	50.26	19.57	24.21	0.19	4.66	4.85
105AG01_New_A3	Spectrum 5	Lamprophyre	Background	50.15	19.68	23.60	0.43	5.01	5.45
105AG01_New_A3	Spectrum 6	Lamprophyre	Background	50.22	18.21	25.53	0.28	5.11	5.38
105AG01_New_A3	Spectrum 7	Lamprophyre	Background	50.20	18.38	25.23	0.33	4.77	5.09
105AG01_New_A3	Spectrum 8	Lamprophyre	Background	50.05	19.13	24.43	0.06	5.22	5.27
105AG01_New_A3	Spectrum 9	Lamprophyre	Background	50.00	18.31	25.31	0.41	4.98	5.40

	Spectrum	Lithology	Location	O	Mg	Ca	Mn	Fe	Fe+Mn
				atm %	atm %	atm %	atm %	atm %	atm %
105AG01_New_A3	Spectrum 10	Lamprophyre	Background	50.16	17.42	26.93	0.76	3.94	4.70
105AG01_New_A3	Spectrum 11	Lamprophyre	Background	50.12	18.03	25.74	0.19	4.91	5.11
105AG01_New_A3	Spectrum 12	Lamprophyre	Background	50.07	17.46	26.18	0.32	5.00	5.32
105AG01_New_A3	Spectrum 13	Lamprophyre	Background	50.06	18.04	25.63	0.07	5.26	5.33
105AG01_New_A4	Spectrum 1	Lamprophyre	Background	50.08	17.94	26.15	0.24	4.67	4.91
105AG01_New_A4	Spectrum 2	Lamprophyre	Background	50.05	17.09	26.42	0.27	5.45	5.71
105AG01_New_A4	Spectrum 3	Lamprophyre	Background	50.16	20.10	23.91	0.32	4.35	4.67
105AG01_New_A4	Spectrum 4	Lamprophyre	Background	50.12	17.03	26.95	0.34	4.99	5.33
105AG01_New_A4	Spectrum 5	Lamprophyre	Background	50.23	19.85	23.66	0.34	4.85	5.19
105AG01_New_A4	Spectrum 6	Lamprophyre	Background	50.11	16.88	27.06	0.37	5.12	5.50
105AG01_New_A4	Spectrum 7	Lamprophyre	Background	50.06	19.37	25.02	0.21	4.33	4.54
105AG01_New_A4	Spectrum 8	Lamprophyre	Background	50.07	18.40	25.43	0.33	5.16	5.49
105AG01_New_A4	Spectrum 9	Lamprophyre	Background	50.29	20.21	23.23	0.26	4.92	5.18
105AG01_New_A4	Spectrum 10	Lamprophyre	Background	50.09	20.05	23.09	0.26	5.05	5.31
105AG01_New_A4	Spectrum 11	Lamprophyre	Background	50.01	18.61	25.49	0.41	4.42	4.83
105AG01_New_A4	Spectrum 12	Lamprophyre	Background	50.22	19.93	23.71	0.17	3.93	4.10
105AG01_New_A4	Spectrum 13	Lamprophyre	Background	50.20	17.29	26.52	0.29	4.79	5.08
105AG01_New_A4	Spectrum 14	Lamprophyre	Background	50.08	19.92	24.21	0.37	4.55	4.93
105AG01_New_A4	Spectrum 15	Lamprophyre	Background	49.99	20.13	23.72	0.38	4.35	4.73
105AG01_New_A4	Spectrum 16	Lamprophyre	Background	50.05	18.53	25.85	0.62	3.88	4.51
105AG01_New_A4	Spectrum 17	Lamprophyre	Background	50.26	18.68	24.67	0.15	4.79	4.93
105AG01_New_A4	Spectrum 18	Lamprophyre	Background	50.11	20.42	23.22	0.58	4.75	5.33
105AG01_New_A4	Spectrum 19	Lamprophyre	Background	50.03	18.55	25.51	0.68	3.89	4.57
105AG01_New_A5	Spectrum 1	Lamprophyre	Background	50.09	19.21	24.60	0.37	5.00	5.38
105AG01_New_A5	Spectrum 2	Lamprophyre	Background	50.04	19.05	24.70	0.24	4.91	5.15
105AG01_New_A5	Spectrum 3	Lamprophyre	Background	50.18	19.76	24.62	0.49	4.13	4.63
105AG01_New_A5	Spectrum 4	Lamprophyre	Background	50.14	19.87	23.48	0.53	5.00	5.54
105AG01_New_A5	Spectrum 5	Lamprophyre	Background	50.02	19.20	23.96	0.57	5.29	5.86
105AG01_New_A5	Spectrum 6	Lamprophyre	Background	50.11	16.97	26.92	0.41	5.07	5.48
105AG01_New_A5	Spectrum 7	Lamprophyre	Background	50.28	17.73	25.50	0.36	4.90	5.26
105AG01_New_A5	Spectrum 8	Lamprophyre	Background	50.22	19.95	23.40	0.21	4.90	5.11
105AG01_New_A5	Spectrum 9	Lamprophyre	Background	50.01	19.00	25.38	0.27	4.90	5.17
105AG01_New_A5	Spectrum 10	Lamprophyre	Background	49.97	17.75	26.53	0.41	4.44	4.85
105AG01_New_A5	Spectrum 11	Lamprophyre	Background	50.02	17.48	26.84	0.26	4.54	4.81
105AG01_New_A5	Spectrum 12	Lamprophyre	Background	50.12	17.34	26.32	0.11	5.33	5.44
105AG01_New_A5	Spectrum 13	Lamprophyre	Background	50.10	17.65	26.07	0.36	5.14	5.51
105AG01_New_A5	Spectrum 14	Lamprophyre	Background	50.16	18.83	25.15	0.22	4.44	4.65
105AG01_New_A5	Spectrum 15	Lamprophyre	Background	50.05	18.23	25.22	0.36	5.26	5.62
105AG01_New_A6	Spectrum 1	Lamprophyre	Background	50.21	20.46	23.61	0.16	4.51	4.67
105AG01_New_A6	Spectrum 2	Lamprophyre	Background	50.03	19.27	24.91	0.26	4.71	4.97
105AG01_New_A6	Spectrum 3	Lamprophyre	Background	50.09	18.82	25.42	0.17	4.52	4.70
105AG01_New_A6	Spectrum 4	Lamprophyre	Background	50.06	19.52	24.42	0.64	4.00	4.64
105AG01_New_A6	Spectrum 5	Lamprophyre	Background	50.09	18.72	25.08	0.34	4.95	5.29
105AG01_New_A6	Spectrum 6	Lamprophyre	Background	50.21	17.13	26.68	0.48	4.75	5.24
105AG01_New_A6	Spectrum 7	Lamprophyre	Background	50.04	19.41	25.24	0.66	3.67	4.33
105AG01_New_A6	Spectrum 8	Lamprophyre	Background	50.08	20.54	23.58	0.45	4.35	4.79
105AG01_New_A6	Spectrum 9	Lamprophyre	Background	49.94	19.92	23.51	0.35	5.11	5.46
105AG01_New_A6	Spectrum 10	Lamprophyre	Background	50.16	16.50	26.32	0.35	5.74	6.09
105AG01_New_A6	Spectrum 11	Lamprophyre	Background	50.01	17.68	26.85	0.53	4.00	4.53
105AG01_New_A6	Spectrum 12	Lamprophyre	Background	50.07	17.62	26.69	0.51	4.22	4.73
105AG01_New_A6	Spectrum 13	Lamprophyre	Background	50.06	19.82	24.65	0.31	4.32	4.63
105AG01_New_A6	Spectrum 14	Lamprophyre	Background	50.05	18.56	24.88	0.13	5.20	5.33
105AG01_New_A6	Spectrum 15	Lamprophyre	Background	49.98	18.75	25.02	0.31	4.74	5.05
105AG01_New_A6	Spectrum 16	Lamprophyre	Background	49.97	19.08	25.50	0.22	4.51	4.73
105AG01_New_A6	Spectrum 17	Lamprophyre	Background	50.19	18.85	24.75	0.28	5.19	5.47
105AG01_New_A6	Spectrum 18	Lamprophyre	Background	50.20	19.54	23.79	0.35	4.86	5.21
105AG01_New_A6	Spectrum 19	Lamprophyre	Background	50.33	19.22	24.31	0.33	4.94	5.27
105AG01_New_A6	Spectrum 20	Lamprophyre	Background	50.15	19.27	24.36	0.22	4.72	4.94
105AG01_New_A6	Spectrum 21	Lamprophyre	Background	50.40	20.80	21.71	0.31	4.93	5.24
105AG01_New_A7	Spectrum 1	Lamprophyre	Background	50.14	17.55	26.12	0.79	4.71	5.50
105AG01_New_A7	Spectrum 2	Lamprophyre	Background	50.11	20.19	24.53	0.54	3.59	4.13
105AG01_New_A7	Spectrum 3	Lamprophyre	Background	50.16	20.13	24.20	0.11	4.42	4.54
105AG01_New_A7	Spectrum 4	Lamprophyre	Background	50.16	19.12	24.20	0.35	4.83	5.19
105AG01_New_A7	Spectrum 5	Lamprophyre	Background	50.07	20.17	23.30	0.31	4.86	5.17
105AG01_New_A7	Spectrum 6	Lamprophyre	Background	50.11	17.58	26.84	0.72	3.77	4.49
105AG01_New_A7	Spectrum 7	Lamprophyre	Background	50.09	19.00	25.16	0.15	4.67	4.82
105AG01_New_A7	Spectrum 8	Lamprophyre	Background	50.13	19.67	23.74	0.53	4.45	4.97
105AG01_New_A7	Spectrum 9	Lamprophyre	Background	50.10	15.69	28.32	0.33	4.69	5.01
105AG01_New_A7	Spectrum 10	Lamprophyre	Background	50.11	19.70	23.76	0.42	5.10	5.52
105AG01_New_A7	Spectrum 11	Lamprophyre	Background	50.11	19.91	23.84	0.39	4.54	4.93
105AG01_New_A7	Spectrum 12	Lamprophyre	Background	49.95	18.13	25.82	0.33	5.01	5.35
105AG01_New_A7	Spectrum 13	Lamprophyre	Background	49.95	19.56	24.05	0.54	5.19	5.73
105AG01_New_A7	Spectrum 14	Lamprophyre	Background	50.24	19.83	24.22	0.23	4.19	4.42
105AG01_New_A7	Spectrum 15	Lamprophyre	Background	50.14	19.26	24.22	0.19	4.92	5.11

	Spectrum	Lithology	Location	O	Mg	Ca	Mn	Fe	Fe+Mn
				atm %	atm %	atm %	atm %	atm %	atm %
105AG01_New_A7	Spectrum 16	Lamprophyre	Background	50.03	17.88	26.14	0.29	5.19	5.48
105AG01_New_A7	Spectrum 17	Lamprophyre	Background	50.11	17.66	26.54	0.25	4.99	5.23
105AG01_New_A7	Spectrum 18	Lamprophyre	Background	50.08	16.94	26.72	0.15	5.24	5.39
105AG01_New_A8	Spectrum 1	Lamprophyre	Background	50.03	17.01	25.57	0.77	5.52	6.28
105AG01_New_A8	Spectrum 2	Lamprophyre	Background	49.96	18.05	26.54	0.64	4.02	4.66
105AG01_New_A8	Spectrum 3	Lamprophyre	Background	49.98	19.64	23.93	0.39	5.13	5.52
105AG01_New_A8	Spectrum 4	Lamprophyre	Background	50.18	18.81	25.07	0.24	4.84	5.08
105AG01_New_A8	Spectrum 5	Lamprophyre	Background	49.96	16.61	27.00	0.27	5.30	5.57
105AG01_New_A8	Spectrum 6	Lamprophyre	Background	50.14	19.20	24.34	0.33	5.12	5.46
105AG01_New_A8	Spectrum 7	Lamprophyre	Background	50.08	18.73	25.10	0.65	4.34	4.99
105AG01_New_A8	Spectrum 8	Lamprophyre	Background	50.11	19.63	24.54	0.12	4.47	4.58
105AG01_New_A8	Spectrum 9	Lamprophyre	Background	50.07	19.04	25.09	0.12	4.52	4.64
105AG01_New_A8	Spectrum 10	Lamprophyre	Background	50.02	16.89	26.57	1.06	4.50	5.56
105AG01_New_A8	Spectrum 11	Lamprophyre	Background	50.08	19.91	22.98	0.79	5.20	5.99
105AG01_New_A9	Spectrum 1	Lamprophyre	Background	49.99	17.95	25.61	0.35	4.98	5.33
105AG01_New_A9	Spectrum 2	Lamprophyre	Background	50.22	20.43	23.56	0.55	3.95	4.50
105AG01_New_A9	Spectrum 3	Lamprophyre	Background	50.22	19.72	24.04	0.69	4.20	4.89
105AG01_New_A9	Spectrum 4	Lamprophyre	Background	50.25	17.74	25.88	0.34	4.31	4.65
105AG01_New_A9	Spectrum 5	Lamprophyre	Background	50.07	18.91	24.97	0.28	4.81	5.09
105AG01_New_A9	Spectrum 6	Lamprophyre	Background	50.10	17.73	25.36	0.36	5.85	6.21
105AG01_New_A9	Spectrum 7	Lamprophyre	Background	50.05	17.62	26.03	0.11	5.17	5.28
105AG01_New_A9	Spectrum 8	Lamprophyre	Background	50.02	19.52	24.56	0.04	4.84	4.88
105AG01_New_A9	Spectrum 9	Lamprophyre	Background	50.09	17.48	26.38	0.40	4.46	4.85
105AG01_New_A9	Spectrum 10	Lamprophyre	Background	50.04	18.28	25.56	0.31	4.89	5.20
105AG01_New_A9	Spectrum 11	Lamprophyre	Background	50.15	18.80	25.39	1.05	3.95	5.00
105AG01_New_A9	Spectrum 12	Lamprophyre	Background	50.15	19.14	25.24	0.29	4.35	4.64
105AG01_New_A9	Spectrum 13	Lamprophyre	Background	50.21	19.23	23.34	1.26	4.40	5.66
105AG01_New_A9	Spectrum 14	Lamprophyre	Background	50.05	18.57	25.80	0.37	4.59	4.96
105AG01_New_A9	Spectrum 15	Lamprophyre	Background	50.09	19.48	24.39	0.22	4.70	4.91
105AG01_New_A9	Spectrum 16	Lamprophyre	Background	50.17	17.62	26.25	0.35	4.80	5.15
105AG01_New_A9	Spectrum 17	Lamprophyre	Background	50.13	18.70	24.52	0.39	5.02	5.41
105AG01_New_A10	Spectrum 1	Lamprophyre	Background	50.02	17.96	26.09	0.29	4.89	5.18
105AG01_New_A10	Spectrum 2	Lamprophyre	Background	50.08	17.70	26.63	0.28	4.72	5.00
105AG01_New_A10	Spectrum 3	Lamprophyre	Background	50.15	18.91	25.17	0.26	4.44	4.70
105AG01_New_A10	Spectrum 4	Lamprophyre	Background	50.21	18.95	24.58	0.34	4.57	4.91
105AG01_New_A10	Spectrum 5	Lamprophyre	Background	50.08	19.03	24.73	0.30	5.05	5.35
105AG01_New_A10	Spectrum 6	Lamprophyre	Background	50.06	17.91	25.93	0.38	4.98	5.36
105AG01_New_A10	Spectrum 7	Lamprophyre	Background	50.04	18.70	26.06	0.23	4.15	4.38
105AG01_New_A10	Spectrum 8	Lamprophyre	Background	50.08	20.34	23.83	0.37	4.51	4.88
105AG01_New_A10	Spectrum 9	Lamprophyre	Background	50.10	17.72	26.58	0.32	4.59	4.91
105AG01_New_A10	Spectrum 10	Lamprophyre	Background	50.17	18.90	25.46	0.64	3.53	4.18
105AG01_New_A10	Spectrum 11	Lamprophyre	Background	49.99	18.64	25.68	0.22	4.20	4.42
105AG01_New_A10	Spectrum 12	Lamprophyre	Background	50.04	19.22	25.31	0.13	4.24	4.38
105AG01_New_A10	Spectrum 13	Lamprophyre	Background	50.04	17.25	26.77	0.53	4.69	5.21
105AG01_New_A10	Spectrum 14	Lamprophyre	Background	49.98	18.27	26.03	0.34	4.73	5.07
105AG01_New_A10	Spectrum 15	Lamprophyre	Background	50.07	19.56	24.11	0.37	4.82	5.20
105AG01_New_A10	Spectrum 16	Lamprophyre	Background	50.07	20.18	22.82	0.41	4.90	5.31
105AG01_New_A10	Spectrum 17	Lamprophyre	Background	50.17	18.47	25.08	0.32	5.01	5.34
105AG01_New_A10	Spectrum 18	Lamprophyre	Background	50.07	19.07	25.05	0.32	4.53	4.84
105AG01_New_A10	Spectrum 19	Lamprophyre	Background	50.11	18.48	25.43	0.30	5.18	5.48
105AG01_New_A10	Spectrum 20	Lamprophyre	Background	50.02	17.56	26.73	0.16	4.86	5.02
105AG01_New_A10	Spectrum 21	Lamprophyre	Background	50.03	18.41	25.73	0.30	5.09	5.38
105AG01_New_A10	Spectrum 22	Lamprophyre	Background	50.08	19.08	24.32	0.91	4.63	5.54
105AG01_New_A10	Spectrum 23	Lamprophyre	Background	50.05	17.70	25.97	0.48	4.96	5.43
105AG01_New_A10	Spectrum 24	Lamprophyre	Background	50.02	19.26	24.84	0.46	4.49	4.96
105AG01_New_A10	Spectrum 25	Lamprophyre	Background	50.27	18.01	25.47	0.32	5.03	5.35
105AG01_New_A10	Spectrum 26	Lamprophyre	Background	50.01	19.64	23.21	0.36	5.00	5.36
105AG01_New_A10	Spectrum 27	Lamprophyre	Background	50.14	17.26	26.46	0.43	5.13	5.56
127AG02_New_A2	Spectrum 1	Powell tonalite	Silidor	50.16	14.77	25.37	0.98	7.69	8.67
127AG02_New_A2	Spectrum 2	Powell tonalite	Silidor	50.19	16.58	24.50	0.42	6.94	7.35
127AG02_New_A2	Spectrum 3	Powell tonalite	Silidor	50.15	13.52	25.13	0.34	9.97	10.31
127AG02_New_A2	Spectrum 4	Powell tonalite	Silidor	50.21	16.82	22.74	0.17	8.77	8.94
127AG02_New_A2	Spectrum 5	Powell tonalite	Silidor	50.09	19.40	23.83	0.71	5.11	5.82
127AG02_New_A2	Spectrum 6	Powell tonalite	Silidor	50.10	19.79	23.66	0.37	4.98	5.35
127AG02_New_A2	Spectrum 7	Powell tonalite	Silidor	50.17	13.71	26.09	0.35	8.65	9.00
127AG02_New_A2	Spectrum 8	Powell tonalite	Silidor	50.03	17.16	23.66	0.42	7.38	7.80
127AG02_New_A2	Spectrum 9	Powell tonalite	Silidor	50.24	17.24	23.04	0.53	7.46	7.99
127AG02_New_A2	Spectrum 10	Powell tonalite	Silidor	50.13	15.60	24.89	0.90	7.43	8.33
127AG02_New_A2	Spectrum 11	Powell tonalite	Silidor	50.12	15.76	23.04	1.13	8.60	9.74
127AG02_New_A3	Spectrum 1	Powell tonalite	Silidor	50.13	14.44	25.76	0.82	7.70	8.52
127AG02_New_A3	Spectrum 2	Powell tonalite	Silidor	50.19	16.65	24.77	0.52	6.96	7.48
127AG02_New_A3	Spectrum 3	Powell tonalite	Silidor	50.16	15.21	25.37	0.61	7.59	8.20
127AG02_New_A3	Spectrum 4	Powell tonalite	Silidor	50.32	15.68	24.73	0.23	7.92	8.14
127AG02_New_A3	Spectrum 5	Powell tonalite	Silidor	50.33	18.51	24.80	0.85	4.78	5.63

	Spectrum	Lithology	Location	O	Mg	Ca	Mn	Fe	Fe+Mn
				atm %	atm %	atm %	atm %	atm %	atm %
127AG02_New_A3	Spectrum 6	Powell tonalite	Silidor	50.18	18.31	25.39	0.68	4.61	5.29
127AG02_New_A3	Spectrum 7	Powell tonalite	Silidor	50.10	16.53	24.79	0.26	7.07	7.34
127AG02_New_A3	Spectrum 8	Powell tonalite	Silidor	50.03	15.07	25.65	0.48	7.63	8.11
127AG02_New_A3	Spectrum 9	Powell tonalite	Silidor	50.13	16.08	24.94	0.24	7.72	7.96
127AG02_New_A3	Spectrum 10	Powell tonalite	Silidor	50.24	16.73	24.68	0.36	6.74	7.10
127AG02_New_A3	Spectrum 11	Powell tonalite	Silidor	50.24	17.48	23.70	0.26	7.43	7.69
127AG02_New_A3	Spectrum 12	Powell tonalite	Silidor	50.22	16.23	24.87	0.39	7.34	7.74
127AG02_New_A3	Spectrum 13	Powell tonalite	Silidor	50.30	19.05	24.47	0.51	4.56	5.07
127AG02_New_A3	Spectrum 14	Powell tonalite	Silidor	50.20	18.69	23.76	0.82	5.18	6.00
127AG02_New_A3	Spectrum 15	Powell tonalite	Silidor	50.41	17.82	22.67	0.44	7.09	7.54
127AG02_New_A3	Spectrum 16	Powell tonalite	Silidor	50.17	15.59	22.41	0.97	9.02	9.99
127AG02_New_A3	Spectrum 17	Powell tonalite	Silidor	50.08	19.39	22.37	1.02	5.98	7.00
127AG02_New_A3	Spectrum 18	Powell tonalite	Silidor	50.90	21.93	23.00	0.18	0.62	0.80
127AG02_New_A3	Spectrum 19	Powell tonalite	Silidor	50.08	22.12	25.03	0.22	1.10	1.32
127AG02_New_A3	Spectrum 20	Powell tonalite	Silidor	50.10	21.25	26.78	0.23	0.72	0.95
127AG02_New_A3	Spectrum 21	Powell tonalite	Silidor	50.21	22.09	24.99	0.39	1.06	1.45
127AG02_New_A3	Spectrum 22	Powell tonalite	Silidor	50.06	21.21	26.66	0.39	0.76	1.15
127AG02_New_A3	Spectrum 23	Powell tonalite	Silidor	50.26	16.07	23.24	1.06	7.80	8.86
127AG02_New_A4	Spectrum 1	Powell tonalite	Silidor	50.06	15.75	25.80	0.43	7.05	7.47
127AG02_New_A4	Spectrum 2	Powell tonalite	Silidor	50.20	16.61	23.71	0.28	7.84	8.12
127AG02_New_A4	Spectrum 3	Powell tonalite	Silidor	49.99	17.61	24.11	0.19	6.89	7.07
127AG02_New_A4	Spectrum 4	Powell tonalite	Silidor	50.02	14.89	24.04	0.56	9.18	9.73
127AG02_New_A4	Spectrum 5	Powell tonalite	Silidor	50.27	14.25	25.42	0.83	8.17	9.00
127AG02_New_A4	Spectrum 6	Powell tonalite	Silidor	50.07	13.55	26.54	0.70	8.09	8.80
127AG02_New_A4	Spectrum 7	Powell tonalite	Silidor	50.12	14.73	24.28	0.89	9.06	9.94
127AG02_New_A4	Spectrum 8	Powell tonalite	Silidor	50.08	14.43	25.61	0.15	8.61	8.77
127AG02_New_A4	Spectrum 9	Powell tonalite	Silidor	50.08	15.09	25.43	0.91	7.46	8.37
127AG02_New_A4	Spectrum 10	Powell tonalite	Silidor	50.22	15.74	23.94	0.81	8.37	9.18
127AG02_New_A4	Spectrum 11	Powell tonalite	Silidor	50.27	20.74	25.69	0.79	1.14	1.93
127AG02_New_A4	Spectrum 12	Powell tonalite	Silidor	50.22	22.72	22.88	1.12	1.41	2.53
127AG02_New_A4	Spectrum 13	Powell tonalite	Silidor	50.26	23.07	24.34	0.38	0.82	1.19
127AG02_New_A4	Spectrum 14	Powell tonalite	Silidor	50.18	13.92	25.65	0.40	9.15	9.55
127AG02_New_A4	Spectrum 15	Powell tonalite	Silidor	50.18	15.53	23.88	0.97	8.37	9.34
127AG02_New_A5	Spectrum 1	Powell tonalite	Silidor	50.19	16.02	24.05	0.30	8.48	8.78
127AG02_New_A5	Spectrum 2	Powell tonalite	Silidor	50.28	14.37	25.59	0.81	8.14	8.95
127AG02_New_A5	Spectrum 3	Powell tonalite	Silidor	50.09	13.65	24.86	0.13	10.35	10.49
127AG02_New_A5	Spectrum 4	Powell tonalite	Silidor	50.17	12.46	26.33	0.06	9.94	10.00
127AG02_New_A5	Spectrum 5	Powell tonalite	Silidor	50.20	17.83	26.12	0.50	4.60	5.09
127AG02_New_A5	Spectrum 6	Powell tonalite	Silidor	50.25	19.53	23.27	1.17	4.60	5.77
127AG02_New_A5	Spectrum 7	Powell tonalite	Silidor	50.56	17.44	24.39	0.61	4.72	5.32
127AG02_New_A5	Spectrum 8	Powell tonalite	Silidor	49.99	20.24	22.91	0.32	5.08	5.40
127AG02_New_A5	Spectrum 9	Powell tonalite	Silidor	50.23	19.65	23.96	0.29	4.88	5.17
127AG02_New_A5	Spectrum 10	Powell tonalite	Silidor	50.10	19.18	24.41	1.08	4.27	5.36
127AG02_New_A5	Spectrum 11	Powell tonalite	Silidor	50.35	16.91	23.51	0.12	7.73	7.85
127AG02_New_A5	Spectrum 12	Powell tonalite	Silidor	50.06	15.29	24.41	0.14	9.02	9.16
127AG02_New_A5	Spectrum 13	Powell tonalite	Silidor	50.19	19.62	24.70	0.32	4.07	4.40
127AG02_New_A5	Spectrum 14	Powell tonalite	Silidor	50.03	15.37	24.07	1.04	8.15	9.19
127AG02_New_A5	Spectrum 15	Powell tonalite	Silidor	50.26	19.68	23.84	0.98	4.06	5.04
127AG02_New_A5	Spectrum 16	Powell tonalite	Silidor	50.05	23.40	24.44	0.23	0.85	1.08
127AG02_New_A5	Spectrum 17	Powell tonalite	Silidor	50.22	21.94	25.85	0.24	0.65	0.89
127AG02_New_A5	Spectrum 18	Powell tonalite	Silidor	50.14	16.33	23.26	0.28	8.56	8.84
127AG02_New_A6	Spectrum 1	Powell tonalite	Silidor	50.03	22.39	25.78	0.09	0.86	0.95
127AG02_New_A6	Spectrum 2	Powell tonalite	Silidor	50.12	21.38	26.26	0.30	0.79	1.09
127AG02_New_A6	Spectrum 3	Powell tonalite	Silidor	50.14	21.89	25.26	0.19	0.38	0.58
127AG02_New_A6	Spectrum 5	Powell tonalite	Silidor	50.19	21.79	25.52	0.48	0.86	1.34
127AG02_New_A6	Spectrum 6	Powell tonalite	Silidor	50.16	23.92	23.28	0.45	0.83	1.28
127AG02_New_A6	Spectrum 7	Powell tonalite	Silidor	50.22	23.89	24.00	0.04	0.62	0.67
127AG02_New_A6	Spectrum 8	Powell tonalite	Silidor	50.11	20.38	23.40	0.28	4.57	4.85
127AG02_New_A6	Spectrum 9	Powell tonalite	Silidor	50.33	19.55	22.66	0.52	5.38	5.90
127AG02_New_A6	Spectrum 10	Powell tonalite	Silidor	50.24	20.08	23.44	0.47	4.29	4.76
127AG02_New_A6	Spectrum 11	Powell tonalite	Silidor	49.96	15.94	26.77	0.59	5.87	6.45
127AG02_New_A6	Spectrum 12	Powell tonalite	Silidor	50.02	16.42	25.36	0.77	6.52	7.29
127AG02_New_A6	Spectrum 13	Powell tonalite	Silidor	50.20	19.69	23.25	0.53	5.06	5.59
127AG02_New_A6	Spectrum 14	Powell tonalite	Silidor	50.18	15.15	26.10	0.64	7.17	7.81
127AG02_New_A6	Spectrum 15	Powell tonalite	Silidor	50.43	14.08	25.99	0.24	7.81	8.05
127AG02_New_A6	Spectrum 16	Powell tonalite	Silidor	50.10	20.07	23.34	0.76	4.73	5.49
127AG02_New_A6	Spectrum 18	Powell tonalite	Silidor	50.19	15.36	25.96	0.23	7.07	7.30
127AG02_New_A6	Spectrum 19	Powell tonalite	Silidor	50.17	14.03	24.54	0.00	10.46	10.46
127AG02_New_A6	Spectrum 20	Powell tonalite	Silidor	50.03	14.44	25.89	0.13	8.40	8.53
127AG02_New_A6	Spectrum 21	Powell tonalite	Silidor	50.16	16.36	22.60	0.21	9.41	9.62
127AG02_New_A6	Spectrum 22	Powell tonalite	Silidor	50.09	18.64	24.73	0.24	5.35	5.58
127AG02_New_A6	Spectrum 23	Powell tonalite	Silidor	50.24	14.40	24.25	0.14	9.59	9.73
127AG02_New_A6	Spectrum 24	Powell tonalite	Silidor	50.01	19.76	26.42	0.92	1.32	2.24
127AG02_New_A6	Spectrum 25	Powell tonalite	Silidor	50.01	22.73	25.36	0.23	0.48	0.72

	Spectrum	Lithology	Location	O	Mg	Ca	Mn	Fe	Fe+Mn
				atm %	atm %	atm %	atm %	atm %	atm %
127AG02_New_A7	Spectrum 1	Powell tonalite	Silidor	50.27	14.98	24.73	0.25	8.21	8.46
127AG02_New_A7	Spectrum 2	Powell tonalite	Silidor	50.03	14.94	24.78	0.24	9.30	9.54
127AG02_New_A7	Spectrum 3	Powell tonalite	Silidor	50.13	14.01	25.41	0.32	9.10	9.42
127AG02_New_A7	Spectrum 4	Powell tonalite	Silidor	50.17	16.20	23.40	0.28	8.38	8.66
127AG02_New_A7	Spectrum 5	Powell tonalite	Silidor	50.22	16.90	24.99	0.26	6.43	6.69
127AG02_New_A7	Spectrum 6	Powell tonalite	Silidor	50.40	16.39	23.72	0.30	7.87	8.18
127AG02_New_A7	Spectrum 7	Powell tonalite	Silidor	50.31	14.47	23.32	1.20	8.81	10.00
127AG02_New_A7	Spectrum 8	Powell tonalite	Silidor	50.35	12.68	26.87	0.83	8.32	9.15
127AG02_New_A7	Spectrum 9	Powell tonalite	Silidor	50.14	15.89	24.35	0.91	7.59	8.50
127AG02_New_A7	Spectrum 10	Powell tonalite	Silidor	50.16	13.40	26.15	0.95	8.39	9.35
127AG02_New_A7	Spectrum 11	Powell tonalite	Silidor	50.07	16.09	24.22	0.09	8.19	8.28
127AG02_New_A7	Spectrum 12	Powell tonalite	Silidor	49.98	16.50	24.35	0.03	8.05	8.08
127AG02_New_A7	Spectrum 13	Powell tonalite	Silidor	50.06	16.01	24.08	0.79	7.70	8.49
127AG02_New_A7	Spectrum 14	Powell tonalite	Silidor	50.11	14.53	24.47	0.19	9.92	10.11
127AG02_New_A7	Spectrum 16	Powell tonalite	Silidor	50.15	15.06	24.15	0.91	8.48	9.39
127AG02_New_A7	Spectrum 17	Powell tonalite	Silidor	50.13	16.27	24.51	0.41	7.05	7.46
127AG02_New_A7	Spectrum 18	Powell tonalite	Silidor	50.11	17.49	26.49	0.17	4.91	5.08
127AG02_New_A7	Spectrum 19	Powell tonalite	Silidor	50.25	18.28	24.89	0.66	4.49	5.15
127AG02_New_A7	Spectrum 20	Powell tonalite	Silidor	50.10	18.39	25.28	0.42	5.18	5.60
127AG02_New_A7	Spectrum 21	Powell tonalite	Silidor	49.98	19.07	24.07	0.43	5.24	5.67
127AG02_New_A7	Spectrum 22	Powell tonalite	Silidor	49.93	17.72	25.28	0.57	5.01	5.57
127AG02_New_A7	Spectrum 23	Powell tonalite	Silidor	50.20	17.13	26.11	0.41	5.40	5.81
127AG02_New_A7	Spectrum 24	Powell tonalite	Silidor	50.33	17.67	24.67	0.63	5.50	6.14
127AG02_New_A7	Spectrum 25	Powell tonalite	Silidor	50.13	17.09	25.55	0.73	5.56	6.28
127AG02_New_A7	Spectrum 26	Powell tonalite	Silidor	50.06	17.40	25.03	0.82	5.62	6.44
127AG02_New_A7	Spectrum 27	Powell tonalite	Silidor	50.07	19.08	23.99	0.28	5.63	5.91
127AG02_New_A7	Spectrum 28	Powell tonalite	Silidor	50.03	22.93	24.81	0.18	0.72	0.89
127AG02_New_A7	Spectrum 29	Powell tonalite	Silidor	49.95	21.67	26.83	0.12	0.39	0.51
127AG02_New_A7	Spectrum 30	Powell tonalite	Silidor	50.05	21.84	26.50	0.20	0.55	0.75
127AG02_New_A7	Spectrum 31	Powell tonalite	Silidor	50.30	23.21	23.99	0.11	0.82	0.94
127AG02_New_A7	Spectrum 32	Powell tonalite	Silidor	50.15	22.00	25.86	0.24	0.69	0.93
127AG02_New_A8	Spectrum 1	Powell tonalite	Silidor	49.91	17.15	25.75	0.79	5.34	6.13
127AG02_New_A8	Spectrum 2	Powell tonalite	Silidor	50.19	19.43	24.33	0.58	4.68	5.26
127AG02_New_A8	Spectrum 3	Powell tonalite	Silidor	50.16	16.98	25.90	0.49	5.72	6.21
127AG02_New_A8	Spectrum 4	Powell tonalite	Silidor	50.01	19.15	24.40	0.58	4.55	5.13
127AG02_New_A8	Spectrum 5	Powell tonalite	Silidor	50.09	19.44	23.72	0.59	4.90	5.50
127AG02_New_A8	Spectrum 6	Powell tonalite	Silidor	50.20	18.60	25.13	0.72	4.33	5.05
127AG02_New_A8	Spectrum 7	Powell tonalite	Silidor	50.01	18.40	24.78	0.52	5.09	5.62
127AG02_New_A8	Spectrum 8	Powell tonalite	Silidor	49.98	16.32	26.19	0.34	6.25	6.59
127AG02_New_A8	Spectrum 9	Powell tonalite	Silidor	50.10	16.42	24.94	0.34	6.92	7.25
127AG02_New_A8	Spectrum 10	Powell tonalite	Silidor	50.05	19.82	23.71	0.41	4.80	5.21
127AG02_New_A8	Spectrum 11	Powell tonalite	Silidor	50.07	16.29	24.45	0.43	8.22	8.65
127AG02_New_A8	Spectrum 12	Powell tonalite	Silidor	50.10	15.85	24.38	0.55	8.34	8.89
127AG02_New_A8	Spectrum 13	Powell tonalite	Silidor	50.06	16.56	24.86	0.28	6.99	7.27
127AG02_New_A8	Spectrum 14	Powell tonalite	Silidor	50.14	17.03	24.10	0.51	6.69	7.20
127AG02_New_A8	Spectrum 15	Powell tonalite	Silidor	50.10	16.06	24.63	0.87	7.39	8.25
127AG02_New_A8	Spectrum 16	Powell tonalite	Silidor	50.19	16.48	23.05	0.82	8.32	9.15
127AG02_New_A8	Spectrum 17	Powell tonalite	Silidor	50.08	17.74	25.39	0.62	5.26	5.89
127AG02_New_A8	Spectrum 18	Powell tonalite	Silidor	50.11	20.25	23.60	0.63	4.51	5.13
127AG02_New_A8	Spectrum 19	Powell tonalite	Silidor	49.98	17.01	24.57	0.42	6.63	7.05
127AG02_New_A8	Spectrum 20	Powell tonalite	Silidor	50.01	17.04	24.07	0.61	7.21	7.83
127AG02_New_A8	Spectrum 21	Powell tonalite	Silidor	50.11	15.48	25.37	0.66	7.49	8.15
127AG02_New_A8	Spectrum 22	Powell tonalite	Silidor	50.29	15.15	23.06	1.25	9.35	10.61
127AG02_New_A8	Spectrum 23	Powell tonalite	Silidor	50.24	19.98	23.07	0.60	4.80	5.40
127AG02_New_A9	Spectrum 1	Powell tonalite	Silidor	50.14	22.05	23.93	0.70	1.58	2.28
127AG02_New_A9	Spectrum 2	Powell tonalite	Silidor	50.02	21.05	24.54	0.95	2.02	2.97
127AG02_New_A9	Spectrum 3	Powell tonalite	Silidor	50.01	22.08	24.75	0.65	1.49	2.14
127AG02_New_A9	Spectrum 4	Powell tonalite	Silidor	49.88	22.07	24.57	0.57	1.06	1.63
127AG02_New_A9	Spectrum 5	Powell tonalite	Silidor	50.06	20.73	27.51	0.02	0.79	0.81
127AG02_New_A9	Spectrum 6	Powell tonalite	Silidor	50.03	23.84	23.74	0.20	0.77	0.97
127AG02_New_A9	Spectrum 7	Powell tonalite	Silidor	50.12	18.46	24.99	0.77	5.03	5.80
127AG02_New_A9	Spectrum 8	Powell tonalite	Silidor	50.01	18.67	25.18	0.84	4.75	5.59
127AG02_New_A9	Spectrum 9	Powell tonalite	Silidor	50.36	18.00	25.23	0.31	4.53	4.84
127AG02_New_A9	Spectrum 10	Powell tonalite	Silidor	50.07	19.25	24.39	0.28	5.03	5.31
127AG02_New_A9	Spectrum 11	Powell tonalite	Silidor	50.09	19.49	22.93	0.46	5.61	6.08
127AG02_New_A9	Spectrum 12	Powell tonalite	Silidor	50.05	16.92	24.37	0.36	7.17	7.53
127AG02_New_A9	Spectrum 13	Powell tonalite	Silidor	50.26	17.47	25.30	0.39	5.04	5.43
127AG02_New_A9	Spectrum 14	Powell tonalite	Silidor	50.11	18.73	24.90	0.75	5.07	5.82
127AG02_New_A9	Spectrum 15	Powell tonalite	Silidor	49.93	16.20	24.44	0.71	7.44	8.15
127AG02_New_A9	Spectrum 16	Powell tonalite	Silidor	49.98	14.41	26.23	0.82	7.95	8.77
127AG02_New_A9	Spectrum 17	Powell tonalite	Silidor	50.11	19.17	23.80	0.67	5.02	5.70
127AG02_New_A9	Spectrum 18	Powell tonalite	Silidor	50.15	15.68	23.52	0.87	8.63	9.50
127AG02_New_A9	Spectrum 19	Powell tonalite	Silidor	49.93	19.30	24.62	0.66	4.23	4.89
127AG02_New_A9	Spectrum 20	Powell tonalite	Silidor	50.03	18.89	25.28	0.33	4.54	4.88

	Spectrum	Lithology	Location	O	Mg	Ca	Mn	Fe	Fe+Mn
				atm %	atm %	atm %	atm %	atm %	atm %
127AG02_New_A9	Spectrum 21	Powell tonalite	Silidor	50.28	18.41	24.37	0.57	4.41	4.98
127AG02_New_A9	Spectrum 22	Powell tonalite	Silidor	50.13	21.21	26.07	0.34	0.86	1.20
127AG09_New_A1	Spectrum 1	Mafic dike	Silidor	49.91	15.65	25.29	0.28	7.94	8.22
127AG09_New_A1	Spectrum 2	Mafic dike	Silidor	50.13	18.09	23.93	0.17	6.90	7.07
127AG09_New_A1	Spectrum 3	Mafic dike	Silidor	50.08	18.81	22.67	0.15	6.74	6.89
127AG09_New_A1	Spectrum 4	Mafic dike	Silidor	49.98	14.64	26.45	0.17	8.07	8.24
127AG09_New_A1	Spectrum 5	Mafic dike	Silidor	50.14	16.93	24.53	0.22	7.36	7.58
127AG09_New_A1	Spectrum 6	Mafic dike	Silidor	50.08	14.34	25.51	0.47	8.83	9.31
127AG09_New_A1	Spectrum 7	Mafic dike	Silidor	49.99	16.24	24.46	0.28	7.83	8.12
127AG09_New_A1	Spectrum 8	Mafic dike	Silidor	50.05	16.88	24.96	0.20	7.32	7.53
127AG09_New_A1	Spectrum 9	Mafic dike	Silidor	50.46	15.19	24.83	0.08	7.68	7.77
127AG09_New_A1	Spectrum 10	Mafic dike	Silidor	50.21	17.43	24.25	0.15	6.99	7.14
127AG09_New_A1	Spectrum 11	Mafic dike	Silidor	50.16	17.24	23.29	0.30	7.41	7.71
127AG09_New_A1	Spectrum 12	Mafic dike	Silidor	50.09	17.74	24.04	0.34	6.84	7.18
127AG09_New_A1	Spectrum 13	Mafic dike	Silidor	50.65	15.62	22.98	0.29	7.53	7.82
127AG09_New_A1	Spectrum 14	Mafic dike	Silidor	49.99	14.50	25.85	0.11	8.68	8.79
127AG09_New_A1	Spectrum 15	Mafic dike	Silidor	50.16	18.23	23.94	0.25	6.62	6.88
127AG09_New_A1	Spectrum 16	Mafic dike	Silidor	50.03	17.48	25.52	0.13	5.94	6.06
127AG09_New_A1	Spectrum 17	Mafic dike	Silidor	50.29	15.61	24.22	0.31	8.03	8.34
127AG09_New_A1	Spectrum 19	Mafic dike	Silidor	53.28	12.08	17.97	0.15	5.54	5.69
127AG09_New_A1	Spectrum 20	Mafic dike	Silidor	50.11	17.99	22.99	0.33	7.07	7.40
127AG09_New_A1	Spectrum 21	Mafic dike	Silidor	50.13	18.45	22.99	0.27	6.88	7.14
127AG09_New_A1	Spectrum 22	Mafic dike	Silidor	50.00	16.85	24.57	0.26	7.86	8.12
127AG09_New_A1	Spectrum 23	Mafic dike	Silidor	50.27	14.70	26.44	0.11	7.53	7.64
127AG09_New_A2	Spectrum 1	Mafic dike	Silidor	50.15	18.38	23.06	0.24	7.10	7.34
127AG09_New_A2	Spectrum 2	Mafic dike	Silidor	50.13	16.31	24.41	0.22	7.92	8.14
127AG09_New_A2	Spectrum 3	Mafic dike	Silidor	54.02	13.68	18.60	0.28	4.81	5.09
127AG09_New_A2	Spectrum 4	Mafic dike	Silidor	50.14	20.68	23.96	0.34	3.66	4.00
127AG09_New_A2	Spectrum 5	Mafic dike	Silidor	50.10	18.46	24.33	0.32	5.77	6.09
127AG09_New_A2	Spectrum 6	Mafic dike	Silidor	50.10	22.19	23.73	0.05	2.61	2.66
127AG09_New_A2	Spectrum 7	Mafic dike	Silidor	50.22	17.31	25.68	0.22	5.85	6.07
127AG09_New_A2	Spectrum 8	Mafic dike	Silidor	49.99	21.07	24.59	0.02	3.03	3.05
127AG09_New_A2	Spectrum 9	Mafic dike	Silidor	50.12	17.48	24.21	0.22	6.87	7.09
127AG09_New_A2	Spectrum 10	Mafic dike	Silidor	49.99	16.62	24.27	0.04	7.74	7.78
127AG09_New_A2	Spectrum 11	Mafic dike	Silidor	50.14	18.18	23.74	0.08	6.70	6.78
127AG09_New_A2	Spectrum 12	Mafic dike	Silidor	50.08	17.90	23.93	0.07	7.19	7.26
127AG09_New_A2	Spectrum 13	Mafic dike	Silidor	50.12	15.46	24.81	0.56	7.95	8.51
127AG09_New_A2	Spectrum 14	Mafic dike	Silidor	51.90	16.31	18.58	0.07	7.83	7.90
127AG09_New_A2	Spectrum 15	Mafic dike	Silidor	49.97	16.49	24.01	0.30	8.24	8.54
127AG09_New_A2	Spectrum 16	Mafic dike	Silidor	50.09	18.65	24.71	0.18	5.35	5.53
127AG09_New_A2	Spectrum 17	Mafic dike	Silidor	50.12	17.83	24.37	0.18	6.66	6.84
127AG09_New_A2	Spectrum 18	Mafic dike	Silidor	50.39	17.99	23.46	0.24	5.56	5.80
127AG09_New_A2	Spectrum 19	Mafic dike	Silidor	50.13	17.89	23.33	0.10	7.23	7.33
127AG09_New_A2	Spectrum 20	Mafic dike	Silidor	50.14	18.38	25.88	0.00	5.19	5.19
127AG09_New_A2	Spectrum 21	Mafic dike	Silidor	50.27	17.77	24.00	0.21	6.18	6.38
127AG09_New_A2	Spectrum 22	Mafic dike	Silidor	50.16	21.17	22.86	0.31	3.78	4.09
127AG09_New_A2	Spectrum 24	Mafic dike	Silidor	50.09	18.07	25.04	0.07	5.75	5.82
127AG09_New_A2	Spectrum 25	Mafic dike	Silidor	50.11	17.40	24.64	0.26	6.40	6.66
127AG09_New_A3	Spectrum 1	Mafic dike	Silidor	50.26	16.20	24.67	0.13	8.04	8.17
127AG09_New_A3	Spectrum 2	Mafic dike	Silidor	50.12	17.56	23.81	0.55	6.80	7.35
127AG09_New_A3	Spectrum 3	Mafic dike	Silidor	50.08	16.28	24.47	0.46	7.75	8.21
127AG09_New_A3	Spectrum 4	Mafic dike	Silidor	50.14	16.33	24.46	0.35	7.44	7.79
127AG09_New_A3	Spectrum 5	Mafic dike	Silidor	50.19	18.46	24.01	0.20	6.10	6.31
127AG09_New_A3	Spectrum 6	Mafic dike	Silidor	50.16	16.47	24.96	0.49	6.36	6.85
127AG09_New_A3	Spectrum 7	Mafic dike	Silidor	50.05	18.46	22.71	0.25	7.35	7.60
127AG09_New_A3	Spectrum 8	Mafic dike	Silidor	50.09	16.47	25.01	0.23	7.34	7.57
127AG09_New_A3	Spectrum 9	Mafic dike	Silidor	50.02	16.66	24.63	0.43	7.20	7.62
127AG09_New_A3	Spectrum 10	Mafic dike	Silidor	50.15	17.24	23.06	0.22	7.95	8.17
127AG09_New_A3	Spectrum 11	Mafic dike	Silidor	50.13	16.95	24.15	0.41	7.61	8.02
127AG09_New_A3	Spectrum 12	Mafic dike	Silidor	50.04	17.68	25.93	0.35	5.57	5.92
127AG09_New_A3	Spectrum 13	Mafic dike	Silidor	50.02	17.39	23.52	0.26	7.49	7.75
127AG09_New_A3	Spectrum 14	Mafic dike	Silidor	50.04	15.61	26.30	0.34	7.02	7.36
127AG09_New_A3	Spectrum 15	Mafic dike	Silidor	50.03	17.25	25.10	0.26	6.39	6.66
127AG09_New_A3	Spectrum 16	Mafic dike	Silidor	50.33	17.23	22.95	0.25	7.75	8.01
127AG09_New_A3	Spectrum 17	Mafic dike	Silidor	49.90	17.20	24.14	0.14	7.46	7.60
127AG09_New_A3	Spectrum 18	Mafic dike	Silidor	50.12	18.08	24.74	0.33	5.63	5.96
127AG09_New_A3	Spectrum 19	Mafic dike	Silidor	50.11	15.25	26.32	0.25	7.53	7.79
127AG09_New_A3	Spectrum 20	Mafic dike	Silidor	50.03	17.58	24.07	0.35	6.99	7.34
127AG09_New_A3	Spectrum 21	Mafic dike	Silidor	50.17	16.52	23.72	0.75	7.72	8.48
127AG09_New_A3	Spectrum 22	Mafic dike	Silidor	50.10	19.07	23.40	0.23	5.66	5.89
127AG09_New_A3	Spectrum 23	Mafic dike	Silidor	50.30	16.88	23.14	0.32	7.94	8.27
127AG09_New_A3	Spectrum 24	Mafic dike	Silidor	50.00	15.74	25.22	0.27	7.37	7.64
127AG09_New_A3	Spectrum 25	Mafic dike	Silidor	50.17	16.75	23.78	0.21	8.04	8.25
127AG09_New_A3	Spectrum 26	Mafic dike	Silidor	50.23	16.40	24.33	0.44	7.59	8.03

	Spectrum	Lithology	Location	O	Mg	Ca	Mn	Fe	Fe+Mn
				atm %	atm %	atm %	atm %	atm %	atm %
127AG09_New_A3	Spectrum 27	Mafic dike	Silidor	50.27	18.47	23.75	0.25	6.24	6.49
127AG09_New_A3	Spectrum 28	Mafic dike	Silidor	50.12	16.78	24.57	0.62	6.66	7.28
127AG09_New_A3	Spectrum 29	Mafic dike	Silidor	50.21	18.22	24.56	0.23	5.66	5.89
127AG09_New_A3	Spectrum 30	Mafic dike	Silidor	50.09	18.26	24.89	0.20	5.76	5.95
127AG09_New_A4	Spectrum 1	Mafic dike	Silidor	50.08	19.37	22.41	0.36	6.69	7.05
127AG09_New_A4	Spectrum 2	Mafic dike	Silidor	50.23	18.53	23.34	0.31	6.42	6.74
127AG09_New_A4	Spectrum 3	Mafic dike	Silidor	50.16	15.55	24.72	0.06	8.49	8.56
127AG09_New_A4	Spectrum 4	Mafic dike	Silidor	50.05	17.69	24.81	0.27	6.07	6.35
127AG09_New_A4	Spectrum 5	Mafic dike	Silidor	50.23	15.99	25.60	0.29	6.95	7.24
127AG09_New_A4	Spectrum 6	Mafic dike	Silidor	50.13	17.07	24.73	0.36	7.03	7.38
127AG09_New_A4	Spectrum 7	Mafic dike	Silidor	50.20	18.25	23.44	0.16	6.58	6.75
127AG09_New_A4	Spectrum 8	Mafic dike	Silidor	50.30	17.62	23.74	0.35	6.77	7.12
127AG09_New_A4	Spectrum 9	Mafic dike	Silidor	50.15	16.48	25.47	0.27	6.53	6.80
127AG09_New_A4	Spectrum 10	Mafic dike	Silidor	50.15	18.45	22.85	0.24	7.34	7.59
127AG09_New_A4	Spectrum 11	Mafic dike	Silidor	50.07	16.55	24.35	0.11	7.74	7.85
127AG09_New_A4	Spectrum 12	Mafic dike	Silidor	50.04	15.32	25.70	0.15	8.22	8.37
127AG09_New_A4	Spectrum 13	Mafic dike	Silidor	50.35	17.97	23.16	0.36	6.88	7.24
127AG09_New_A4	Spectrum 14	Mafic dike	Silidor	50.18	16.99	22.98	0.36	7.94	8.30
127AG09_New_A4	Spectrum 15	Mafic dike	Silidor	50.12	16.05	26.12	0.23	6.73	6.96
127AG09_New_A4	Spectrum 16	Mafic dike	Silidor	50.20	15.77	24.67	0.18	8.23	8.41
127AG09_New_A4	Spectrum 17	Mafic dike	Silidor	50.16	17.23	24.40	0.34	6.98	7.32
127AG09_New_A4	Spectrum 18	Mafic dike	Silidor	50.03	15.71	25.27	0.17	8.01	8.18
127AG09_New_A4	Spectrum 19	Mafic dike	Silidor	50.13	18.44	23.86	0.22	6.07	6.29
127AG09_New_A4	Spectrum 20	Mafic dike	Silidor	50.13	15.15	25.88	0.29	7.73	8.02
127AG09_New_A4	Spectrum 21	Mafic dike	Silidor	50.15	15.74	25.41	0.26	7.14	7.40
127AG09_New_A4	Spectrum 22	Mafic dike	Silidor	50.06	18.26	24.05	0.28	6.02	6.29
127AG09_New_A4	Spectrum 23	Mafic dike	Silidor	50.03	17.53	24.47	0.27	6.88	7.15
127AG09_New_A4	Spectrum 24	Mafic dike	Silidor	50.23	18.96	22.72	0.30	6.33	6.63
127AG09_New_A4	Spectrum 25	Mafic dike	Silidor	50.11	18.15	23.23	0.29	6.87	7.17
127AG09_New_A4	Spectrum 26	Mafic dike	Silidor	50.29	17.50	23.72	0.25	6.97	7.22
127AG09_New_A4	Spectrum 27	Mafic dike	Silidor	50.28	19.15	22.79	0.37	6.34	6.71
127AG09_New_A4	Spectrum 28	Mafic dike	Silidor	50.16	18.38	23.62	0.22	6.54	6.76
127AG09_New_A4	Spectrum 29	Mafic dike	Silidor	50.11	17.11	23.96	0.13	7.68	7.81
127AG09_New_A4	Spectrum 30	Mafic dike	Silidor	50.25	17.99	23.19	0.43	6.73	7.17
127AG09_New_A5	Spectrum 1	Mafic dike	Silidor	50.00	15.56	24.56	0.33	8.58	8.91
127AG09_New_A5	Spectrum 2	Mafic dike	Silidor	49.97	15.47	24.65	0.36	8.86	9.22
127AG09_New_A5	Spectrum 3	Mafic dike	Silidor	50.08	16.73	24.53	0.06	7.36	7.42
127AG09_New_A5	Spectrum 4	Mafic dike	Silidor	50.12	17.34	23.45	0.15	7.79	7.94
127AG09_New_A5	Spectrum 5	Mafic dike	Silidor	50.05	16.66	23.86	0.27	8.16	8.43
127AG09_New_A5	Spectrum 6	Mafic dike	Silidor	49.98	17.76	23.23	0.31	7.48	7.78
127AG09_New_A5	Spectrum 7	Mafic dike	Silidor	50.18	14.96	25.70	0.30	8.31	8.61
127AG09_New_A5	Spectrum 8	Mafic dike	Silidor	49.99	17.05	23.45	0.32	7.90	8.21
127AG09_New_A5	Spectrum 9	Mafic dike	Silidor	50.00	16.05	25.03	0.38	7.47	7.84
127AG09_New_A5	Spectrum 10	Mafic dike	Silidor	50.05	15.24	26.61	0.25	6.87	7.13
127AG09_New_A5	Spectrum 11	Mafic dike	Silidor	50.03	18.78	22.85	0.25	6.92	7.17
127AG09_New_A5	Spectrum 12	Mafic dike	Silidor	50.09	15.79	25.31	0.63	7.03	7.66
127AG09_New_A5	Spectrum 13	Mafic dike	Silidor	50.03	16.10	24.68	0.59	7.84	8.43
127AG09_New_A5	Spectrum 14	Mafic dike	Silidor	50.15	18.16	23.59	0.23	6.65	6.88
127AG09_New_A5	Spectrum 15	Mafic dike	Silidor	50.07	19.29	23.74	0.69	5.19	5.87
127AG09_New_A5	Spectrum 16	Mafic dike	Silidor	50.23	15.92	25.77	0.96	6.04	7.00
127AG09_New_A5	Spectrum 17	Mafic dike	Silidor	50.04	16.07	25.32	0.13	7.84	7.97
127AG09_New_A5	Spectrum 18	Mafic dike	Silidor	50.12	17.23	23.48	0.27	8.22	8.49
127AG09_New_A5	Spectrum 19	Mafic dike	Silidor	49.90	17.88	23.09	0.16	7.31	7.47
127AG09_New_A5	Spectrum 20	Mafic dike	Silidor	49.95	17.73	24.32	0.16	6.89	7.06
127AG09_New_A5	Spectrum 21	Mafic dike	Silidor	50.19	16.06	25.21	0.35	7.42	7.77
127AG09_New_A5	Spectrum 22	Mafic dike	Silidor	50.17	16.51	23.90	0.28	7.89	8.17
127AG09_New_A5	Spectrum 23	Mafic dike	Silidor	50.04	16.24	26.33	0.26	6.25	6.51
127AG09_New_A5	Spectrum 24	Mafic dike	Silidor	50.07	16.55	22.90	0.58	8.71	9.29
127AG09_New_A5	Spectrum 25	Mafic dike	Silidor	50.06	15.82	24.03	0.34	8.54	8.88
127AG09_New_A5	Spectrum 26	Mafic dike	Silidor	50.21	16.90	23.41	0.33	7.79	8.11
127AG09_New_A6	Spectrum 1	Mafic dike	Silidor	50.16	17.95	23.27	0.17	7.39	7.56
127AG09_New_A6	Spectrum 2	Mafic dike	Silidor	50.16	19.85	22.75	0.16	5.73	5.89
127AG09_New_A6	Spectrum 3	Mafic dike	Silidor	50.16	19.75	25.22	0.01	3.46	3.47
127AG09_New_A6	Spectrum 4	Mafic dike	Silidor	50.43	17.90	23.25	0.15	6.98	7.12
127AG09_New_A6	Spectrum 5	Mafic dike	Silidor	50.06	15.63	26.77	0.16	6.75	6.92
127AG09_New_A6	Spectrum 6	Mafic dike	Silidor	50.08	16.18	24.61	0.46	7.52	7.98
127AG09_New_A6	Spectrum 7	Mafic dike	Silidor	50.24	17.23	23.65	0.21	7.68	7.89
127AG09_New_A6	Spectrum 8	Mafic dike	Silidor	50.15	16.02	25.13	0.38	7.68	8.06
127AG09_New_A6	Spectrum 9	Mafic dike	Silidor	50.13	19.18	21.71	0.78	7.09	7.87
127AG09_New_A6	Spectrum 10	Mafic dike	Silidor	50.05	16.98	25.91	0.24	5.85	6.09
127AG09_New_A6	Spectrum 11	Mafic dike	Silidor	50.09	19.06	25.05	0.10	4.72	4.82
127AG09_New_A6	Spectrum 12	Mafic dike	Silidor	50.35	20.54	23.44	0.09	3.75	3.84
127AG09_New_A6	Spectrum 13	Mafic dike	Silidor	50.10	20.87	24.11	0.06	3.55	3.61
127AG09_New_A6	Spectrum 14	Mafic dike	Silidor	50.27	16.58	23.01	0.57	8.48	9.05

	Spectrum	Lithology	Location	O	Mg	Ca	Mn	Fe	Fe+Mn
				atm %	atm %	atm %	atm %	atm %	atm %
127AG09_New_A6	Spectrum 15	Mafic dike	Silidor	50.33	18.37	22.38	0.23	7.19	7.42
127AG09_New_A6	Spectrum 16	Mafic dike	Silidor	50.08	17.39	23.98	0.30	7.11	7.41
127AG09_New_A6	Spectrum 17	Mafic dike	Silidor	50.32	19.69	23.75	0.16	4.53	4.68
127AG09_New_A6	Spectrum 18	Mafic dike	Silidor	50.15	19.66	25.17	0.16	3.55	3.71
127AG09_New_A6	Spectrum 19	Mafic dike	Silidor	50.12	14.64	26.29	0.78	7.44	8.22
127AG09_New_A6	Spectrum 20	Mafic dike	Silidor	50.01	16.67	24.95	0.42	7.03	7.45
127AG09_New_A6	Spectrum 21	Mafic dike	Silidor	50.13	16.88	25.12	0.14	7.05	7.19
127AG09_New_A6	Spectrum 22	Mafic dike	Silidor	50.58	19.02	21.02	0.21	6.71	6.92
127AG09_New_A6	Spectrum 23	Mafic dike	Silidor	50.36	17.24	23.78	0.13	6.68	6.80
127AG09_New_A6	Spectrum 24	Mafic dike	Silidor	51.65	18.76	20.60	0.19	4.12	4.31
127AG09_New_A6	Spectrum 25	Mafic dike	Silidor	50.06	18.44	22.49	0.25	7.02	7.27
127AG09_New_A6	Spectrum 26	Mafic dike	Silidor	50.01	16.60	26.01	0.44	6.34	6.78
127BG11_New_A1	Spectrum 1	Mafic dike	Silidor	50.15	18.10	25.00	0.43	5.46	5.90
127BG11_New_A1	Spectrum 2	Mafic dike	Silidor	50.12	19.75	23.66	0.25	5.14	5.39
127BG11_New_A1	Spectrum 3	Mafic dike	Silidor	50.11	19.34	24.27	0.21	5.20	5.41
127BG11_New_A1	Spectrum 4	Mafic dike	Silidor	50.10	17.53	26.45	0.11	5.15	5.26
127BG11_New_A1	Spectrum 5	Mafic dike	Silidor	50.07	17.46	25.87	0.24	5.28	5.52
127BG11_New_A1	Spectrum 6	Mafic dike	Silidor	50.10	17.96	25.67	0.36	5.21	5.57
127BG11_New_A1	Spectrum 7	Mafic dike	Silidor	50.14	18.04	25.04	0.37	5.24	5.60
127BG11_New_A1	Spectrum 8	Mafic dike	Silidor	50.06	16.19	26.98	0.38	5.61	5.99
127BG11_New_A1	Spectrum 9	Mafic dike	Silidor	50.21	17.54	25.81	0.28	5.30	5.58
127BG11_New_A1	Spectrum 10	Mafic dike	Silidor	50.16	18.12	24.91	0.19	5.61	5.81
127BG11_New_A1	Spectrum 11	Mafic dike	Silidor	50.04	18.68	25.39	0.23	5.08	5.31
127BG11_New_A1	Spectrum 12	Mafic dike	Silidor	50.20	18.94	24.12	0.50	5.15	5.65
127BG11_New_A2	Spectrum 1	Mafic dike	Silidor	50.04	19.66	24.16	0.15	5.02	5.17
127BG11_New_A2	Spectrum 2	Mafic dike	Silidor	50.14	19.76	23.89	0.36	5.02	5.38
127BG11_New_A2	Spectrum 3	Mafic dike	Silidor	50.10	17.42	25.61	0.24	5.78	6.01
127BG11_New_A2	Spectrum 4	Mafic dike	Silidor	50.12	18.74	24.70	0.41	5.03	5.44
127BG11_New_A2	Spectrum 5	Mafic dike	Silidor	50.08	18.44	24.10	0.36	5.75	6.11
127BG11_New_A2	Spectrum 6	Mafic dike	Silidor	50.03	17.59	25.14	0.41	6.01	6.42
127BG11_New_A2	Spectrum 7	Mafic dike	Silidor	50.06	18.49	24.20	0.24	5.83	6.08
127BG11_New_A2	Spectrum 8	Mafic dike	Silidor	50.09	19.52	23.69	0.37	4.87	5.24
127BG11_New_A2	Spectrum 9	Mafic dike	Silidor	50.11	18.96	24.85	0.28	4.90	5.18
127BG11_New_A2	Spectrum 10	Mafic dike	Silidor	50.02	19.17	24.39	0.31	5.26	5.56
127BG11_New_A2	Spectrum 11	Mafic dike	Silidor	50.05	19.32	24.66	0.12	5.05	5.16
127BG11_New_A2	Spectrum 12	Mafic dike	Silidor	50.08	20.13	23.64	0.24	5.31	5.55
127BG11_New_A2	Spectrum 13	Mafic dike	Silidor	50.09	18.60	24.91	0.23	5.55	5.78
127BG11_New_A2	Spectrum 14	Mafic dike	Silidor	50.06	19.04	24.14	0.26	5.46	5.72
127BG11_New_A2	Spectrum 15	Mafic dike	Silidor	49.94	18.97	26.03	0.27	3.76	4.02
127BG11_New_A2	Spectrum 16	Mafic dike	Silidor	50.16	19.52	23.84	0.34	5.38	5.72
127BG11_New_A2	Spectrum 17	Mafic dike	Silidor	50.13	17.76	25.43	0.29	5.32	5.61
127BG11_New_A2	Spectrum 18	Mafic dike	Silidor	50.10	17.99	25.08	0.32	5.90	6.21
127BG11_New_A2	Spectrum 19	Mafic dike	Silidor	50.03	18.77	23.67	0.38	6.19	6.56
127BG11_New_A2	Spectrum 20	Mafic dike	Silidor	49.95	19.21	23.98	0.30	5.51	5.81
127BG11_New_A2	Spectrum 21	Mafic dike	Silidor	50.08	17.45	25.91	0.33	5.83	6.16
127BG11_New_A2	Spectrum 22	Mafic dike	Silidor	50.10	19.14	23.91	0.15	5.67	5.82
127BG11_New_A3	Spectrum 1	Mafic dike	Silidor	50.23	19.72	26.49	0.23	2.46	2.69
127BG11_New_A3	Spectrum 2	Mafic dike	Silidor	51.61	20.05	21.75	0.18	2.72	2.90
127BG11_New_A3	Spectrum 3	Mafic dike	Silidor	50.10	19.49	26.88	0.13	2.67	2.79
127BG11_New_A3	Spectrum 4	Mafic dike	Silidor	50.26	22.18	23.41	0.25	2.62	2.87
127BG11_New_A3	Spectrum 5	Mafic dike	Silidor	50.23	21.06	24.40	0.09	3.31	3.40
127BG11_New_A3	Spectrum 6	Mafic dike	Silidor	50.10	18.56	26.87	0.23	3.39	3.62
127BG11_New_A3	Spectrum 7	Mafic dike	Silidor	50.33	23.08	23.00	0.13	2.10	2.23
127BG11_New_A3	Spectrum 8	Mafic dike	Silidor	50.12	18.00	25.14	0.39	5.69	6.08
127BG11_New_A3	Spectrum 9	Mafic dike	Silidor	50.28	18.81	24.48	0.35	4.97	5.32
127BG11_New_A3	Spectrum 10	Mafic dike	Silidor	50.38	23.75	22.20	0.08	1.99	2.07
127BG11_New_A3	Spectrum 11	Mafic dike	Silidor	50.59	22.10	23.23	0.09	2.13	2.22
127BG11_New_A3	Spectrum 12	Mafic dike	Silidor	50.21	18.59	24.30	0.57	5.04	5.61
127BG11_New_A3	Spectrum 13	Mafic dike	Silidor	50.06	18.48	25.04	0.25	5.64	5.88
127BG11_New_A3	Spectrum 14	Mafic dike	Silidor	50.19	19.27	23.32	0.73	5.02	5.75
127BG11_New_A3	Spectrum 15	Mafic dike	Silidor	50.13	17.39	25.05	0.56	5.82	6.38
127BG11_New_A3	Spectrum 16	Mafic dike	Silidor	50.02	22.13	23.58	0.18	3.24	3.41
127BG11_New_A3	Spectrum 17	Mafic dike	Silidor	50.08	19.50	26.78	0.20	2.62	2.82
127BG11_New_A3	Spectrum 18	Mafic dike	Silidor	50.05	19.99	23.20	0.52	5.17	5.69
127BG11_New_A3	Spectrum 19	Mafic dike	Silidor	50.02	17.84	25.10	0.54	5.85	6.39
127BG11_New_A3	Spectrum 20	Mafic dike	Silidor	50.22	20.86	24.19	0.19	3.11	3.31
127BG11_New_A3	Spectrum 21	Mafic dike	Silidor	50.26	19.58	22.05	0.52	6.41	6.93
127BG11_New_A4	Spectrum 1	Mafic dike	Silidor	50.32	18.50	23.72	0.53	5.42	5.96
127BG11_New_A4	Spectrum 2	Mafic dike	Silidor	50.11	19.90	23.53	0.26	5.00	5.26
127BG11_New_A4	Spectrum 3	Mafic dike	Silidor	50.14	18.62	24.18	0.23	5.22	5.45
127BG11_New_A4	Spectrum 4	Mafic dike	Silidor	50.31	18.36	23.68	0.30	5.96	6.27
127BG11_New_A4	Spectrum 5	Mafic dike	Silidor	50.11	18.69	24.70	0.30	5.33	5.63
127BG11_New_A4	Spectrum 6	Mafic dike	Silidor	52.88	15.94	19.72	0.31	4.61	4.92
127BG11_New_A4	Spectrum 7	Mafic dike	Silidor	50.11	17.50	24.70	0.24	6.43	6.67

	Spectrum	Lithology	Location	O	Mg	Ca	Mn	Fe	Fe+Mn
				atm %	atm %	atm %	atm %	atm %	atm %
127BG11_New_A4	Spectrum 8	Mafic dike	Silidor	50.01	18.07	23.58	0.53	6.64	7.17
127BG11_New_A4	Spectrum 9	Mafic dike	Silidor	50.00	18.08	23.65	0.50	6.32	6.82
127BG11_New_A4	Spectrum 10	Mafic dike	Silidor	50.29	17.87	24.96	0.21	5.62	5.83
127BG11_New_A4	Spectrum 11	Mafic dike	Silidor	50.10	20.20	23.67	0.27	4.69	4.96
127BG11_New_A4	Spectrum 12	Mafic dike	Silidor	49.98	23.27	23.10	0.11	2.37	2.48
127BG11_New_A4	Spectrum 13	Mafic dike	Silidor	50.01	22.37	23.50	0.18	2.83	3.02
127BG11_New_A5	Spectrum 1	Mafic dike	Silidor	50.13	20.06	23.40	0.24	5.00	5.24
127BG11_New_A5	Spectrum 2	Mafic dike	Silidor	50.05	17.40	24.93	0.60	6.24	6.84
127BG11_New_A5	Spectrum 3	Mafic dike	Silidor	50.22	17.86	25.39	0.42	5.24	5.67
127BG11_New_A5	Spectrum 4	Mafic dike	Silidor	50.10	15.81	27.35	0.29	5.85	6.14
127BG11_New_A5	Spectrum 5	Mafic dike	Silidor	50.03	16.50	26.04	0.55	6.25	6.80
127BG11_New_A5	Spectrum 6	Mafic dike	Silidor	50.08	20.89	23.85	0.16	3.91	4.07
127BG11_New_A5	Spectrum 7	Mafic dike	Silidor	50.04	18.22	25.78	0.27	4.97	5.24
127BG11_New_A5	Spectrum 8	Mafic dike	Silidor	50.18	19.24	25.11	0.55	4.34	4.89
127BG11_New_A5	Spectrum 9	Mafic dike	Silidor	50.02	15.95	26.15	0.37	6.72	7.09
127BG11_New_A5	Spectrum 10	Mafic dike	Silidor	50.18	18.43	25.50	0.52	4.61	5.13
127BG11_New_A5	Spectrum 11	Mafic dike	Silidor	49.96	18.98	25.31	0.26	4.59	4.85
127BG11_New_A5	Spectrum 12	Mafic dike	Silidor	50.25	16.75	26.04	0.41	5.90	6.31
127BG11_New_A5	Spectrum 13	Mafic dike	Silidor	50.11	18.19	25.56	0.14	4.83	4.97
127BG11_New_A5	Spectrum 14	Mafic dike	Silidor	49.98	20.53	24.03	0.12	4.18	4.29
127BG11_New_A5	Spectrum 15	Mafic dike	Silidor	50.20	17.03	24.73	0.63	6.42	7.04
127BG11_New_A5	Spectrum 16	Mafic dike	Silidor	50.00	15.38	26.06	0.71	7.09	7.81
127BG11_New_A5	Spectrum 17	Mafic dike	Silidor	50.12	18.98	23.61	0.33	5.57	5.90
127BG11_New_A5	Spectrum 18	Mafic dike	Silidor	50.06	17.65	26.63	0.25	4.51	4.76
127BG11_New_A5	Spectrum 19	Mafic dike	Silidor	50.14	17.80	25.21	0.35	5.52	5.88
127BG11_New_A5	Spectrum 20	Mafic dike	Silidor	50.10	18.64	23.27	0.65	6.06	6.71
127BG11_New_A5	Spectrum 21	Mafic dike	Silidor	50.17	20.46	23.53	0.13	5.02	5.15
127BG11_New_A5	Spectrum 22	Mafic dike	Silidor	50.30	21.04	24.32	0.21	3.01	3.22
127BG11_New_A5	Spectrum 27	Mafic dike	Silidor	49.93	17.71	25.73	0.26	5.35	5.62
127BG11_New_A5	Spectrum 28	Mafic dike	Silidor	50.01	17.26	25.09	0.54	6.58	7.12
127BG11_New_A5	Spectrum 29	Mafic dike	Silidor	50.06	16.60	26.46	0.35	5.96	6.31
127BG11_New_A5	Spectrum 30	Mafic dike	Silidor	50.01	18.54	25.79	0.22	4.68	4.90
127BG11_New_A5	Spectrum 31	Mafic dike	Silidor	50.10	21.08	23.75	0.21	4.17	4.37
127BG11_New_A5	Spectrum 32	Mafic dike	Silidor	50.17	15.18	26.88	0.76	6.40	7.16
127BG11_New_A5	Spectrum 33	Mafic dike	Silidor	50.12	16.62	25.00	0.72	6.45	7.17
127BG11_New_A5	Spectrum 34	Mafic dike	Silidor	50.18	15.06	25.51	0.76	7.74	8.50
127BG11_New_A6	Spectrum 1	Mafic dike	Silidor	50.16	19.07	24.06	0.32	5.01	5.33
127BG11_New_A6	Spectrum 2	Mafic dike	Silidor	50.23	17.48	25.60	0.30	5.46	5.76
127BG11_New_A6	Spectrum 3	Mafic dike	Silidor	50.26	17.66	24.61	0.58	5.78	6.36
127BG11_New_A6	Spectrum 4	Mafic dike	Silidor	50.06	18.44	24.45	0.26	5.91	6.17
127BG11_New_A6	Spectrum 5	Mafic dike	Silidor	50.30	19.08	23.33	0.38	6.07	6.45
127BG11_New_A6	Spectrum 6	Mafic dike	Silidor	50.10	19.72	25.06	0.00	4.57	4.57
127BG11_New_A6	Spectrum 7	Mafic dike	Silidor	50.19	20.08	23.19	0.29	5.01	5.31
127BG11_New_A6	Spectrum 8	Mafic dike	Silidor	49.97	17.67	26.31	0.29	4.95	5.25
127BG11_New_A6	Spectrum 9	Mafic dike	Silidor	50.07	18.15	25.52	0.26	5.28	5.54
127BG11_New_A6	Spectrum 10	Mafic dike	Silidor	50.24	20.43	23.59	0.20	4.54	4.74
127BG11_New_A6	Spectrum 11	Mafic dike	Silidor	50.10	19.62	23.16	0.21	5.51	5.72
127BG11_New_A6	Spectrum 12	Mafic dike	Silidor	50.07	17.34	25.81	0.53	5.63	6.17
127BG11_New_A6	Spectrum 13	Mafic dike	Silidor	50.09	17.78	24.17	0.64	6.11	6.75
127BG11_New_A6	Spectrum 14	Mafic dike	Silidor	50.20	20.44	22.45	0.51	5.27	5.78
127BG11_New_A6	Spectrum 15	Mafic dike	Silidor	50.08	19.58	23.45	0.34	4.88	5.22
127BG11_New_A6	Spectrum 16	Mafic dike	Silidor	50.02	17.49	26.39	0.26	5.08	5.33
127BG11_New_A6	Spectrum 17	Mafic dike	Silidor	50.11	19.04	24.13	0.19	5.01	5.20
127BG11_New_A6	Spectrum 18	Mafic dike	Silidor	50.09	17.52	26.72	0.03	4.98	5.01
127BG11_New_A6	Spectrum 19	Mafic dike	Silidor	50.14	20.86	24.21	0.14	3.34	3.48
127BG11_New_A6	Spectrum 20	Mafic dike	Silidor	50.21	18.90	25.26	0.20	4.69	4.89
127BG11_New_A7	Spectrum 1	Mafic dike	Silidor	50.30	17.81	24.63	0.61	5.66	6.27
127BG11_New_A7	Spectrum 2	Mafic dike	Silidor	50.07	18.17	24.95	0.55	5.42	5.97
127BG11_New_A7	Spectrum 3	Mafic dike	Silidor	50.10	17.94	25.46	0.36	5.30	5.66
127BG11_New_A7	Spectrum 4	Mafic dike	Silidor	49.99	18.94	24.80	0.19	4.84	5.04
127BG11_New_A7	Spectrum 5	Mafic dike	Silidor	50.13	19.48	23.40	0.42	5.38	5.80
127BG11_New_A7	Spectrum 6	Mafic dike	Silidor	50.06	19.44	23.77	0.38	5.25	5.63
127BG11_New_A7	Spectrum 7	Mafic dike	Silidor	50.17	19.05	24.69	0.18	4.78	4.96
127BG11_New_A7	Spectrum 8	Mafic dike	Silidor	50.72	17.87	23.26	0.12	5.45	5.57
127BG11_New_A7	Spectrum 9	Mafic dike	Silidor	50.24	15.14	26.01	0.67	7.27	7.94
127BG11_New_A7	Spectrum 10	Mafic dike	Silidor	50.20	18.32	25.74	0.15	4.95	5.10
127BG11_New_A7	Spectrum 11	Mafic dike	Silidor	50.09	17.14	26.76	0.24	5.18	5.41
127BG11_New_A7	Spectrum 12	Mafic dike	Silidor	50.04	19.20	24.40	0.34	5.10	5.44
127BG11_New_A7	Spectrum 13	Mafic dike	Silidor	50.45	20.26	23.90	0.20	3.24	3.44
127BG11_New_A7	Spectrum 14	Mafic dike	Silidor	50.27	22.89	22.75	0.05	2.44	2.49
127BG11_New_A7	Spectrum 15	Mafic dike	Silidor	50.18	18.40	24.31	0.51	5.23	5.74
127BG11_New_A7	Spectrum 16	Mafic dike	Silidor	50.07	17.50	25.63	0.43	5.95	6.38
127BG11_New_A7	Spectrum 17	Mafic dike	Silidor	50.15	16.38	24.93	0.70	6.82	7.51
127BG11_New_A7	Spectrum 18	Mafic dike	Silidor	50.16	19.36	24.28	0.28	4.78	5.06

	Spectrum	Lithology	Location	O	Mg	Ca	Mn	Fe	Fe+Mn
				atm %	atm %	atm %	atm %	atm %	atm %
127BG11_New_A8	Spectrum 1	Mafic dike	Silidor	50.11	19.89	23.31	0.49	5.53	6.02
127BG11_New_A8	Spectrum 2	Mafic dike	Silidor	50.07	20.26	23.14	0.28	5.19	5.47
127BG11_New_A8	Spectrum 3	Mafic dike	Silidor	50.04	18.40	24.67	0.27	5.55	5.83
127BG11_New_A8	Spectrum 4	Mafic dike	Silidor	50.17	18.69	24.41	0.33	5.31	5.64
127BG11_New_A8	Spectrum 5	Mafic dike	Silidor	50.12	23.95	23.09	0.04	1.61	1.65
127BG11_New_A8	Spectrum 6	Mafic dike	Silidor	50.09	20.37	26.41	0.02	1.95	1.97
127BG11_New_A8	Spectrum 7	Mafic dike	Silidor	50.02	19.55	24.10	0.15	5.29	5.44
127BG11_New_A8	Spectrum 8	Mafic dike	Silidor	50.09	18.62	24.95	0.35	5.16	5.52
127BG11_New_A8	Spectrum 9	Mafic dike	Silidor	50.16	16.41	27.07	0.16	5.71	5.88
127BG11_New_A8	Spectrum 10	Mafic dike	Silidor	50.01	19.39	24.58	0.11	4.78	4.89
127BG11_New_A8	Spectrum 11	Mafic dike	Silidor	50.14	18.44	24.84	0.29	5.31	5.60
127BG11_New_A8	Spectrum 12	Mafic dike	Silidor	50.12	17.31	26.28	0.28	5.05	5.34
127BG11_New_A8	Spectrum 13	Mafic dike	Silidor	50.33	19.06	23.55	0.40	5.31	5.71
127BG11_New_A8	Spectrum 14	Mafic dike	Silidor	50.10	17.76	26.28	0.18	4.90	5.08
127BG11_New_A8	Spectrum 15	Mafic dike	Silidor	49.98	16.43	25.14	0.72	6.83	7.54
127BG11_New_A8	Spectrum 16	Mafic dike	Silidor	50.20	16.64	24.86	0.64	6.62	7.27
127BG11_New_A8	Spectrum 17	Mafic dike	Silidor	50.05	17.68	26.81	0.38	4.76	5.14
127BG11_New_A8	Spectrum 18	Mafic dike	Silidor	50.05	18.89	24.32	0.17	5.61	5.78
127BG11_New_A8	Spectrum 19	Mafic dike	Silidor	50.03	18.38	25.68	0.22	5.08	5.31
127BG11_New_A8	Spectrum 20	Mafic dike	Silidor	50.19	17.84	25.10	0.29	5.95	6.24
127BG11_New_A8	Spectrum 21	Mafic dike	Silidor	50.18	17.08	25.81	0.62	5.67	6.28
127BG11_New_A8	Spectrum 22	Mafic dike	Silidor	50.32	18.04	24.73	0.10	5.34	5.44
127BG11_New_A8	Spectrum 23	Mafic dike	Silidor	50.08	18.58	24.33	0.61	5.31	5.92
127BG11_New_A8	Spectrum 24	Mafic dike	Silidor	50.15	21.03	24.36	0.29	3.13	3.42
127BG11_New_A8	Spectrum 25	Mafic dike	Silidor	50.94	20.63	21.83	0.28	3.40	3.68
127BG11_New_A8	Spectrum 26	Mafic dike	Silidor	50.49	20.21	24.42	0.16	2.95	3.12
127CG07_New_A1	Spectrum 1	Mafic dike	Silidor	50.06	18.18	24.45	0.52	5.90	6.43
127CG07_New_A1	Spectrum 2	Mafic dike	Silidor	49.94	17.21	25.89	0.25	5.92	6.17
127CG07_New_A1	Spectrum 3	Mafic dike	Silidor	50.13	19.31	25.00	0.39	4.32	4.71
127CG07_New_A1	Spectrum 4	Mafic dike	Silidor	50.13	19.27	25.05	0.57	3.54	4.11
127CG07_New_A1	Spectrum 5	Mafic dike	Silidor	50.06	18.10	25.93	0.56	4.48	5.04
127CG07_New_A1	Spectrum 6	Mafic dike	Silidor	50.29	17.14	25.30	0.46	6.16	6.63
127CG07_New_A1	Spectrum 7	Mafic dike	Silidor	50.24	19.87	23.12	0.29	5.11	5.40
127CG07_New_A1	Spectrum 8	Mafic dike	Silidor	50.19	19.99	24.57	0.38	4.27	4.65
127CG07_New_A1	Spectrum 9	Mafic dike	Silidor	50.18	19.52	24.45	0.50	4.21	4.72
127CG07_New_A1	Spectrum 10	Mafic dike	Silidor	50.01	20.86	24.00	0.64	3.71	4.35
127CG07_New_A1	Spectrum 11	Mafic dike	Silidor	50.24	21.41	22.30	0.51	3.96	4.47
127CG07_New_A1	Spectrum 12	Mafic dike	Silidor	50.15	18.66	26.21	0.27	3.89	4.16
127CG07_New_A1	Spectrum 13	Mafic dike	Silidor	50.11	17.59	27.37	0.42	4.14	4.57
127CG07_New_A1	Spectrum 14	Mafic dike	Silidor	49.96	21.73	24.17	0.22	2.81	3.03
127CG07_New_A1	Spectrum 15	Mafic dike	Silidor	50.05	21.01	23.23	0.54	4.05	4.59
127CG07_New_A1	Spectrum 16	Mafic dike	Silidor	50.13	19.70	25.33	0.59	3.48	4.07
127CG07_New_A1	Spectrum 17	Mafic dike	Silidor	50.15	19.29	24.71	0.61	4.10	4.70
127CG07_New_A1	Spectrum 18	Mafic dike	Silidor	50.25	15.99	26.45	0.38	6.34	6.72
127CG07_New_A1	Spectrum 19	Mafic dike	Silidor	49.95	16.78	25.74	0.40	6.51	6.91
127CG07_New_A1	Spectrum 20	Mafic dike	Silidor	50.09	18.64	24.12	0.18	5.74	5.92
127CG07_New_A1	Spectrum 21	Mafic dike	Silidor	50.11	19.16	23.48	0.32	5.49	5.81
127CG07_New_A1	Spectrum 22	Mafic dike	Silidor	50.13	18.29	24.23	0.43	6.68	7.11
127CG07_New_A1	Spectrum 23	Mafic dike	Silidor	50.08	17.40	25.63	0.33	5.93	6.26
127CG07_New_A1	Spectrum 24	Mafic dike	Silidor	50.24	19.24	22.94	0.33	5.68	6.00
127CG07_New_A1	Spectrum 25	Mafic dike	Silidor	50.13	18.93	23.34	0.54	5.92	6.46
127CG07_New_A1	Spectrum 26	Mafic dike	Silidor	50.03	19.42	23.36	0.24	5.90	6.14
127CG07_New_A1	Spectrum 27	Mafic dike	Silidor	50.10	15.91	25.79	0.42	6.74	7.16
127CG07_New_A1	Spectrum 28	Mafic dike	Silidor	50.19	16.34	25.66	0.41	6.68	7.09
127CG07_New_A1	Spectrum 29	Mafic dike	Silidor	50.22	15.70	26.88	0.31	6.10	6.41
127CG07_New_A2	Spectrum 1	Mafic dike	Silidor	50.08	20.74	24.13	0.40	3.33	3.72
127CG07_New_A2	Spectrum 2	Mafic dike	Silidor	50.11	20.33	24.47	0.24	3.53	3.78
127CG07_New_A2	Spectrum 3	Mafic dike	Silidor	50.02	20.26	24.43	0.29	3.89	4.18
127CG07_New_A2	Spectrum 4	Mafic dike	Silidor	49.98	18.90	26.46	0.30	3.32	3.61
127CG07_New_A2	Spectrum 5	Mafic dike	Silidor	49.85	19.29	25.05	0.34	4.33	4.67
127CG07_New_A2	Spectrum 6	Mafic dike	Silidor	50.23	21.58	22.51	0.44	3.60	4.04
127CG07_New_A2	Spectrum 7	Mafic dike	Silidor	50.11	19.99	24.83	0.39	3.70	4.09
127CG07_New_A2	Spectrum 8	Mafic dike	Silidor	50.19	18.54	26.09	0.37	3.57	3.94
127CG07_New_A2	Spectrum 9	Mafic dike	Silidor	50.00	18.60	25.70	0.68	4.38	5.05
127CG07_New_A2	Spectrum 10	Mafic dike	Silidor	50.14	21.02	23.45	0.24	3.88	4.12
127CG07_New_A2	Spectrum 11	Mafic dike	Silidor	50.01	21.07	22.97	0.21	4.10	4.31
127CG07_New_A2	Spectrum 12	Mafic dike	Silidor	50.20	19.51	24.81	0.45	3.81	4.26
127CG07_New_A2	Spectrum 13	Mafic dike	Silidor	49.93	20.20	24.91	0.49	3.56	4.04
127CG07_New_A2	Spectrum 14	Mafic dike	Silidor	50.10	20.73	24.73	0.32	2.95	3.27
127CG07_New_A2	Spectrum 15	Mafic dike	Silidor	49.99	18.21	26.25	0.45	4.17	4.62
127CG07_New_A2	Spectrum 16	Mafic dike	Silidor	50.03	20.15	23.67	0.58	4.25	4.83
127CG07_New_A2	Spectrum 17	Mafic dike	Silidor	49.94	18.27	26.52	0.34	3.85	4.19
127CG07_New_A2	Spectrum 18	Mafic dike	Silidor	50.28	19.46	24.30	0.70	4.25	4.95
127CG07_New_A2	Spectrum 19	Mafic dike	Silidor	50.08	18.07	24.01	0.41	6.01	6.42

	Spectrum	Lithology	Location	O	Mg	Ca	Mn	Fe	Fe+Mn
				atm %	atm %	atm %	atm %	atm %	atm %
127CG07_New_A2	Spectrum 20	Mafic dike	Silidor	50.12	16.59	25.95	0.57	6.21	6.77
127CG07_New_A2	Spectrum 21	Mafic dike	Silidor	50.14	15.62	26.21	0.46	6.57	7.04
127CG07_New_A2	Spectrum 22	Mafic dike	Silidor	50.05	18.18	23.93	0.27	6.53	6.80
127CG07_New_A2	Spectrum 23	Mafic dike	Silidor	50.12	19.16	23.75	0.37	5.28	5.64
127CG07_New_A2	Spectrum 24	Mafic dike	Silidor	50.08	18.99	23.37	0.29	5.69	5.97
127CG07_New_A2	Spectrum 25	Mafic dike	Silidor	50.12	18.58	23.16	0.42	6.41	6.83
127CG07_New_A2	Spectrum 26	Mafic dike	Silidor	50.17	17.68	24.06	0.56	6.64	7.19
127CG07_New_A2	Spectrum 27	Mafic dike	Silidor	50.17	18.31	24.51	0.25	5.36	5.61
127CG07_New_A2	Spectrum 28	Mafic dike	Silidor	50.22	18.08	24.68	0.46	5.70	6.16
127CG07_New_A2	Spectrum 29	Mafic dike	Silidor	50.08	19.22	22.95	0.51	5.86	6.37
127CG07_New_A2	Spectrum 30	Mafic dike	Silidor	50.15	15.16	26.86	0.47	6.76	7.23
127CG07_New_A2	Spectrum 31	Mafic dike	Silidor	50.15	17.61	24.08	0.48	6.34	6.83
127CG07_New_A2	Spectrum 32	Mafic dike	Silidor	50.04	17.15	25.49	0.48	5.77	6.24
127CG07_New_A3	Spectrum 1	Mafic dike	Silidor	50.18	20.95	23.13	0.30	3.92	4.23
127CG07_New_A3	Spectrum 2	Mafic dike	Silidor	50.07	21.08	22.89	0.34	3.88	4.21
127CG07_New_A3	Spectrum 3	Mafic dike	Silidor	50.17	18.87	24.34	0.30	5.24	5.54
127CG07_New_A3	Spectrum 4	Mafic dike	Silidor	50.08	16.10	27.00	0.42	5.78	6.20
127CG07_New_A3	Spectrum 5	Mafic dike	Silidor	50.03	18.80	24.55	0.20	5.41	5.61
127CG07_New_A3	Spectrum 6	Mafic dike	Silidor	50.11	17.92	24.81	0.28	5.97	6.25
127CG07_New_A3	Spectrum 7	Mafic dike	Silidor	50.05	18.19	25.00	0.32	5.47	5.80
127CG07_New_A3	Spectrum 8	Mafic dike	Silidor	49.98	18.64	24.21	0.34	5.59	5.93
127CG07_New_A3	Spectrum 9	Mafic dike	Silidor	50.09	17.95	24.52	0.39	5.74	6.14
127CG07_New_A3	Spectrum 10	Mafic dike	Silidor	50.12	18.17	25.37	0.34	5.30	5.64
127CG07_New_A3	Spectrum 11	Mafic dike	Silidor	50.01	18.13	24.91	0.39	5.77	6.17
127CG07_New_A3	Spectrum 12	Mafic dike	Silidor	50.11	18.81	23.61	0.44	5.73	6.17
127CG07_New_A3	Spectrum 13	Mafic dike	Silidor	50.22	18.27	24.54	0.18	5.85	6.03
127CG07_New_A3	Spectrum 14	Mafic dike	Silidor	50.12	19.51	23.70	0.36	5.03	5.38
127CG07_New_A3	Spectrum 15	Mafic dike	Silidor	50.12	18.58	24.46	0.32	5.56	5.88
127CG07_New_A3	Spectrum 16	Mafic dike	Silidor	49.97	18.20	24.67	0.21	5.81	6.02
127CG07_New_A3	Spectrum 17	Mafic dike	Silidor	50.11	18.37	24.19	0.25	6.21	6.46
127CG07_New_A3	Spectrum 18	Mafic dike	Silidor	50.08	19.34	23.95	0.38	5.12	5.51
127CG07_New_A3	Spectrum 19	Mafic dike	Silidor	50.09	19.04	23.78	0.35	5.44	5.79
127CG07_New_A3	Spectrum 20	Mafic dike	Silidor	50.03	18.69	23.98	0.39	6.18	6.56
127CG07_New_A3	Spectrum 21	Mafic dike	Silidor	50.01	18.07	24.37	0.26	5.80	6.07
127CG07_New_A3	Spectrum 22	Mafic dike	Silidor	50.06	18.89	24.39	0.30	5.73	6.03
127CG07_New_A3	Spectrum 23	Mafic dike	Silidor	50.07	17.81	25.78	0.28	5.65	5.93
127CG07_New_A3	Spectrum 24	Mafic dike	Silidor	50.02	18.85	24.63	0.31	5.56	5.87
127CG07_New_A3	Spectrum 25	Mafic dike	Silidor	49.90	18.30	24.89	0.29	5.75	6.04
127CG07_New_A3	Spectrum 26	Mafic dike	Silidor	49.98	16.71	26.32	0.39	5.98	6.36
127CG07_New_A3	Spectrum 27	Mafic dike	Silidor	50.13	16.98	26.39	0.26	5.56	5.82
127CG07_New_A3	Spectrum 28	Mafic dike	Silidor	49.90	18.16	24.29	0.46	6.15	6.60
127CG07_New_A3	Spectrum 29	Mafic dike	Silidor	50.08	18.84	24.76	0.26	5.57	5.83
127CG07_New_A3	Spectrum 30	Mafic dike	Silidor	49.98	18.39	24.08	0.29	5.98	6.26
127CG07_New_A3	Spectrum 31	Mafic dike	Silidor	50.04	16.68	26.60	0.39	5.74	6.13
127CG07_New_A3	Spectrum 32	Mafic dike	Silidor	50.01	16.66	26.04	0.30	6.21	6.51
127CG07_New_A3	Spectrum 33	Mafic dike	Silidor	50.07	17.51	23.78	0.43	7.18	7.61
127CG07_New_A3	Spectrum 34	Mafic dike	Silidor	50.12	19.57	23.27	0.26	5.90	6.16
106BG03_Area 2	Spectrum 2	Mafic Dominate	Joliet Breccia	50.11	0.06	48.64	0.47	0.24	0.71
106BG03_Area 2	Spectrum 7	Mafic Dominate	Joliet Breccia	50.05	0.02	48.61	0.48	0.14	0.62
106BG03_Area 2	Spectrum 6	Mafic Dominate	Joliet Breccia	50.11	0.06	48.88	0.36	0.08	0.44
106BG03_Area 2	Spectrum 5	Mafic Dominate	Joliet Breccia	50.01	0.05	48.69	0.44	0.02	0.46
106BG03_Area 2	Spectrum 3	Mafic Dominate	Joliet Breccia	50.03	0.07	48.91	0.31	0.07	0.38
106BG03_Area 2	Spectrum 4	Mafic Dominate	Joliet Breccia	49.99	0.02	48.93	0.36	0.04	0.40
106BG03_Area 2	Spectrum 1	Mafic Dominate	Joliet Breccia	50.10	0.04	49.25	0.20	0.03	0.23
106BG03_Area 5	Spectrum 1	Mafic Dominate	Joliet Breccia	49.93	0.20	47.60	0.71	0.67	1.38
106BG03_Area 5	Spectrum 3	Mafic Dominate	Joliet Breccia	49.94	0.22	48.00	0.78	0.48	1.25
106BG03_Area 5	Spectrum 2	Mafic Dominate	Joliet Breccia	50.03	0.10	48.11	0.62	0.42	1.04
106BG03_Area 6	Spectrum 15	Mafic Dominate	Joliet Breccia	50.08	0.03	48.92	0.43	0.09	0.52
106BG03_Area 6	Spectrum 18	Mafic Dominate	Joliet Breccia	50.01	0.04	49.11	0.21	0.04	0.25
125BG67i_Carb1a	29	Mafic Dominate	Joliet Breccia		0.63	64.78	2.57	2.23	4.79
125BG67i_Carb1a	35	Mafic Dominate	Joliet Breccia		0.57	64.85	2.93	1.94	4.87
125BG67i_Carb1a	24	Mafic Dominate	Joliet Breccia		0.54	65.39	2.76	1.72	4.48
125BG67i_Carb1a	39	Mafic Dominate	Joliet Breccia		0.56	65.25	2.49	1.72	4.21
125BG67i_Carb1a	23	Mafic Dominate	Joliet Breccia		0.50	65.75	1.98	1.88	3.86
125BG67i_Carb1a	33	Mafic Dominate	Joliet Breccia		0.55	66.20	1.75	1.60	3.36
125BG67i_Carb1a	36	Mafic Dominate	Joliet Breccia		0.53	66.40	1.53	1.06	2.59
125BG67i_Carb1a	22	Mafic Dominate	Joliet Breccia		0.62	66.33	1.43	1.17	2.60
125BG67i_Carb1a	40	Mafic Dominate	Joliet Breccia		0.55	67.10	1.34	1.06	2.40
125BG67i_Carb1a	38	Mafic Dominate	Joliet Breccia		0.48	67.08	1.32	0.99	2.30
125BG67i_Carb1a	25	Mafic Dominate	Joliet Breccia		0.45	67.85	1.27	0.99	2.25
125BG67i_Carb1a	27	Mafic Dominate	Joliet Breccia		0.44	67.10	1.08	0.76	1.84
125BG67i_Carb1a	37	Mafic Dominate	Joliet Breccia		0.49	67.65	0.83	0.73	1.56
125BG67i_Carb1a	21	Mafic Dominate	Joliet Breccia		0.44	67.86	0.96	0.85	1.81
125BG67i_Carb1a	28	Mafic Dominate	Joliet Breccia		0.39	66.76	1.08	0.67	1.75

	Spectrum	Lithology	Location	O	Mg	Ca	Mn	Fe	Fe+Mn
				atm %	atm %	atm %	atm %	atm %	atm %
125BG67i_Carb1a	26	Mafic Dominate	Joliet Breccia		0.49	67.81	0.92	0.53	1.45
125BG67i_Carb1a	31	Mafic Dominate	Joliet Breccia		0.35	68.54	1.04	0.41	1.45
125BG67i_Carb1a	32	Mafic Dominate	Joliet Breccia		0.39	68.41	0.94	0.47	1.40
125BG67i_Carb1a	30	Mafic Dominate	Joliet Breccia		0.46	68.27	0.74	0.46	1.20
125BG67i_Carb2	56	Mafic Dominate	Joliet Breccia		0.57	65.06	3.06	0.33	3.39
125BG67i_Carb2	61	Mafic Dominate	Joliet Breccia		0.49	64.70	3.10	1.39	4.48
125BG67i_Carb2	66	Mafic Dominate	Joliet Breccia		0.58	65.24	2.34	1.50	3.84
125BG67i_Carb2	59	Mafic Dominate	Joliet Breccia		0.59	65.48	2.64	2.07	4.72
125BG67i_Carb2	69	Mafic Dominate	Joliet Breccia		0.58	64.99	2.58	1.45	4.03
125BG67i_Carb2	57	Mafic Dominate	Joliet Breccia		0.67	65.16	1.99	1.49	3.48
125BG67i_Carb2	62	Mafic Dominate	Joliet Breccia		0.63	65.98	1.93	1.67	3.60
125BG67i_Carb2	67	Mafic Dominate	Joliet Breccia		0.65	66.12	2.02	1.45	3.48
125BG67i_Carb2	53	Mafic Dominate	Joliet Breccia		0.56	65.75	1.79	1.29	3.08
125BG67i_Carb2	68	Mafic Dominate	Joliet Breccia		0.47	65.72	2.55	1.69	4.24
125BG67i_Carb2	64	Mafic Dominate	Joliet Breccia		0.63	65.96	1.72	1.06	2.77
125BG67i_Carb2	54	Mafic Dominate	Joliet Breccia		0.54	66.07	1.81	1.38	3.20
125BG67i_Carb2	55	Mafic Dominate	Joliet Breccia		0.57	66.23	1.58	1.41	2.99
125BG67i_Carb2	65	Mafic Dominate	Joliet Breccia		0.49	65.52	1.85	1.49	3.34
125BG67i_Carb2	58	Mafic Dominate	Joliet Breccia		0.52	67.28	1.22	0.92	2.14
125BG67i_Carb2	63	Mafic Dominate	Joliet Breccia		0.51	67.39	1.17	0.83	2.00
125BG67i_Carb2	60	Mafic Dominate	Joliet Breccia		0.36	67.92	0.97	0.84	1.81
125BG67i_Dol 1	7	Mafic Dominate	Joliet Breccia		25.85	40.06	0.00	0.47	0.47
125BG67i_Dol 1	8	Mafic Dominate	Joliet Breccia		25.41	40.31	0.01	0.03	0.04
54G02_Area 2	Cc 2	Powell tonalite	Background	50.11	1.64	45.83	0.23	0.58	0.82
54G02_Area 2	Cc 1	Powell tonalite	Background	50.20	1.33	45.79	0.23	0.54	0.77
54G02_Area 3	Cc 2	Powell tonalite	Background	50.85	1.73	43.79	0.30	0.62	0.92
54G02_Area 3	Cc 1	Powell tonalite	Background	50.45	0.79	46.36	0.69	0.53	1.22
85DG05_Area 1	Cc 1	Mafic Dike	Anglo A	50.00	0.80	45.17	1.40	1.21	2.61
85DG05_Area 1	Cc 6	Mafic Dike	Anglo A	50.27	0.44	45.28	1.43	1.51	2.94
85DG05_Area 1	Cc 7	Mafic Dike	Anglo A	50.33	0.44	44.95	1.53	1.19	2.73
85DG05_Area 1	Cc 2	Mafic Dike	Anglo A	49.99	0.35	45.82	1.46	1.48	2.94
85DG05_Area 1	Cc 3	Mafic Dike	Anglo A	50.09	0.48	46.23	1.20	1.18	2.38
85DG05_Area 1	Cc 5	Mafic Dike	Anglo A	50.12	0.58	45.55	1.10	0.93	2.03
85DG05_Area 1	Cc 4	Mafic Dike	Anglo A	50.14	0.38	45.93	1.33	1.02	2.35
85DG05_Area 2	Cc 3	Mafic Dike	Anglo A	50.22	0.54	44.91	1.78	1.67	3.45
85DG05_Area 2	Cc 2	Mafic Dike	Anglo A	49.99	0.63	45.33	1.51	1.14	2.65
85DG05_Area 2	Cc 1	Mafic Dike	Anglo A	50.35	0.53	44.58	1.67	1.11	2.78
85DG05_Area 2	Cc 4	Mafic Dike	Anglo A	50.29	0.41	45.94	1.21	1.27	2.48
85DG05_Area 3	Cc 6	Mafic Dike	Anglo A	50.24	0.84	44.15	1.50	1.16	2.67
85DG05_Area 3	Cc 2	Mafic Dike	Anglo A	50.27	0.61	45.11	1.58	1.22	2.80
85DG05_Area 3	Cc 4	Mafic Dike	Anglo A	50.10	0.50	44.97	1.32	1.61	2.93
85DG05_Area 3	Cc 1	Mafic Dike	Anglo A	50.12	0.55	44.99	1.40	1.40	2.80
85DG05_Area 3	Cc 5	Mafic Dike	Anglo A	50.21	0.51	45.05	1.35	1.40	2.75
85DG05_Area 3	Cc 3	Mafic Dike	Anglo A	49.96	0.68	45.77	1.22	1.15	2.37
85DG05_Area 4	Cc 9	Mafic Dike	Anglo A	50.08	0.52	44.96	1.87	1.80	3.67
85DG05_Area 4	Cc 5	Mafic Dike	Anglo A	50.28	0.78	44.60	1.57	1.35	2.92
85DG05_Area 4	Cc 1	Mafic Dike	Anglo A	50.19	0.57	45.07	1.66	1.34	3.00
85DG05_Area 4	Cc 6	Mafic Dike	Anglo A	50.02	0.73	45.21	1.42	1.22	2.64
85DG05_Area 4	Cc 3	Mafic Dike	Anglo A	50.36	0.47	44.53	1.56	1.32	2.87
85DG05_Area 4	Cc 2	Mafic Dike	Anglo A	50.10	0.45	45.44	1.41	1.42	2.83
85DG05_Area 4	Cc 7	Mafic Dike	Anglo A	50.04	0.43	46.28	1.21	1.33	2.54
85DG05_Area 4	Cc 8	Mafic Dike	Anglo A	50.34	0.36	45.36	1.44	1.04	2.47
85DG05_Area 4	Cc 4	Mafic Dike	Anglo A	50.06	0.31	46.24	1.34	1.15	2.48
85DG05_Area 5	Cc 4	Mafic Dike	Anglo A	50.05	0.72	44.95	1.58	0.95	2.53
85DG05_Area 5	Cc 2	Mafic Dike	Anglo A	50.09	0.37	45.70	1.53	1.62	3.16
85DG05_Area 5	Cc 1	Mafic Dike	Anglo A	50.16	0.46	45.67	1.55	1.13	2.68
85DG05_Area 5	Cc 7	Mafic Dike	Anglo A	49.96	0.39	46.07	1.39	1.45	2.83
85DG05_Area 5	Cc 9	Mafic Dike	Anglo A	50.13	0.28	45.72	1.68	1.30	2.98
85DG05_Area 5	Cc 8	Mafic Dike	Anglo A	50.11	0.41	46.13	1.42	1.27	2.69
85DG05_Area 5	Cc 6	Mafic Dike	Anglo A	50.01	0.38	46.14	1.44	1.20	2.63
85DG05_Area 5	Cc 3	Mafic Dike	Anglo A	50.09	0.29	46.45	1.23	1.14	2.37
85DG05_Area 5	Cc 5	Mafic Dike	Anglo A	50.27	0.20	46.40	1.43	0.82	2.25
85DG05_Area 6	Cc 7	Mafic Dike	Anglo A	50.02	0.58	45.52	1.50	1.36	2.87
85DG05_Area 6	Cc 6	Mafic Dike	Anglo A	50.17	0.48	45.54	1.44	1.57	3.01
85DG05_Area 6	Cc 5	Mafic Dike	Anglo A	50.09	0.45	45.83	1.44	1.50	2.94
85DG05_Area 6	Cc 4	Mafic Dike	Anglo A	49.99	0.47	45.35	1.44	1.37	2.81
85DG05_Area 6	Cc 2	Mafic Dike	Anglo A	50.28	0.26	45.82	1.46	0.86	2.33
85DG05_Area 6	Cc 3	Mafic Dike	Anglo A	50.13	0.32	46.21	1.35	0.82	2.17
85DG05_Area 6	Cc 1	Mafic Dike	Anglo A	50.06	0.25	47.22	0.76	0.59	1.35
85DG05_Area 7	Cc 4	Mafic Dike	Anglo A	51.97	1.84	36.31	1.38	3.01	4.39
85DG05_Area 7	Cc 3	Mafic Dike	Anglo A	49.90	0.43	45.66	1.69	1.49	3.18
85DG05_Area 7	Cc 1	Mafic Dike	Anglo A	50.01	0.32	45.64	1.72	1.25	2.97
85DG05_Area 7	Cc 2	Mafic Dike	Anglo A	49.96	0.28	46.42	1.39	1.22	2.61
85DG05_Area 8	Cc 2	Mafic Dike	Anglo A	50.17	1.03	44.70	1.44	1.37	2.81

	Spectrum	Lithology	Location	O	Mg	Ca	Mn	Fe	Fe+Mn
				atm %	atm %	atm %	atm %	atm %	atm %
85DG05_Area 8	Cc 3	Mafic Dike	Anglo A	50.07	0.69	45.28	1.30	1.24	2.54
85DG05_Area 8	Cc 5	Mafic Dike	Anglo A	50.10	0.39	45.57	1.64	1.52	3.16
85DG05_Area 8	Cc 1	Mafic Dike	Anglo A	50.13	0.47	45.63	1.48	1.51	2.99
85DG05_Area 8	Cc 4	Mafic Dike	Anglo A	50.28	0.49	46.19	1.12	0.83	1.95
95AG01_Area 5	Ank 2	Basalt	Powell Fault	29.64	13.58	33.90	3.66	15.52	19.18
95AG01_Area 5	Ank 4	Basalt	Powell Fault	29.92	14.63	35.72	5.00	12.80	17.80
95AG01_Area 5	Ank 3	Basalt	Powell Fault	30.21	12.85	35.31	5.01	12.49	17.50
95AG01_Area 5	Ank 1	Basalt	Powell Fault	29.64	11.25	37.22	5.84	14.75	20.59
95AG01_Area 6	Ank 5	Basalt	Powell Fault	30.45	16.63	34.67	2.87	12.13	15.00
95AG01_Area 6	Ank 4	Basalt	Powell Fault	29.67	14.19	33.74	4.62	14.21	18.83
95AG01_Area 6	Ank 1	Basalt	Powell Fault	30.11	14.27	35.86	2.94	12.07	15.01
95AG01_Area 6	Ank 2	Basalt	Powell Fault	29.51	11.57	35.86	6.47	11.47	17.94
95AG01_Area 6	Ank 3	Basalt	Powell Fault	29.47	12.69	37.78	4.37	11.92	16.29
95AG01_Area 7	Ank 2	Basalt	Powell Fault	30.66	16.01	33.07	3.48	14.00	17.49
95AG01_Area 7	Ank 1	Basalt	Powell Fault	29.76	13.68	36.45	4.27	12.43	16.70
95AG01_Area 8	Ank 3	Basalt	Powell Fault	31.00	17.88	33.36	3.37	9.69	13.06
95AG01_Area 8	Ank 5	Basalt	Powell Fault	29.39	14.63	33.40	5.82	14.31	20.13
95AG01_Area 8	Ank 2	Basalt	Powell Fault	29.90	15.18	32.33	2.73	13.57	16.30
95AG01_Area 8	Ank 4	Basalt	Powell Fault	31.37	17.92	35.68	3.20	9.18	12.39
95AG01_Area 8	Ank 6	Basalt	Powell Fault	30.14	14.57	35.06	4.14	11.52	15.66
95AG01_Area 8	Ank 1	Basalt	Powell Fault	30.34	16.07	35.92	2.61	10.43	13.04
95AG01_Area 8	Ank 7	Basalt	Powell Fault	30.32	14.02	36.30	2.78	14.76	17.54
95AG01_Area 8	Ank 8	Basalt	Powell Fault	30.37	13.85	37.04	2.35	13.39	15.74
95AG01_Area 8	Ank 9	Basalt	Powell Fault	30.00	11.18	38.50	2.81	15.30	18.11
95AG01_Area 9	Ank 11	Basalt	Powell Fault	30.24	16.00	33.22	3.23	14.76	17.99
95AG01_Area 9	Ank 14	Basalt	Powell Fault	30.00	16.42	33.03	2.52	12.89	15.41
95AG01_Area 9	Ank 4	Basalt	Powell Fault	31.09	17.95	36.69	3.83	9.11	12.94
95AG01_Area 9	Ank 9	Basalt	Powell Fault	29.77	15.36	35.59	3.51	13.74	17.25
95AG01_Area 9	Ank 3	Basalt	Powell Fault	29.80	14.09	35.14	5.14	14.23	19.38
95AG01_Area 9	Ank 6	Basalt	Powell Fault	30.75	16.19	35.58	4.47	10.69	15.15
95AG01_Area 9	Ank 8	Basalt	Powell Fault	30.59	15.36	36.03	3.44	10.83	14.27
95AG01_Area 9	Ank 7	Basalt	Powell Fault	29.68	13.47	36.13	4.58	13.94	18.51
95AG01_Area 9	Ank 5	Basalt	Powell Fault	30.18	14.88	37.93	5.91	9.40	15.31
95AG01_Area 9	Ank 12	Basalt	Powell Fault	29.88	14.41	38.48	4.64	11.75	16.39
95AG01_Area 9	Ank 10	Basalt	Powell Fault	29.38	14.02	37.52	3.36	11.52	14.88
95AG01_Area 9	Ank 2	Basalt	Powell Fault	29.25	11.09	39.20	3.58	15.45	19.03
95AG01_Area 9	Ank 13	Basalt	Powell Fault	29.37	11.67	38.64	4.40	10.61	15.01
95AG01_Area 9	Ank 1	Basalt	Powell Fault	28.52	10.13	39.32	2.47	14.10	16.58

Chapter 4

4 Volcanic reconstruction of Lower Blake River Group strata of the Powell Block, Rouyn-Noranda Mining District, Québec; Implications for the timing and setting of base metal mineralization

4.1 Abstract

The Powell Block of the Rouyn-Noranda mining district, Abitibi Greenstone belt, hosts the Quemont deposit and separates the world-class Horne deposit from the conventional Cu-Zn VMS deposits of the Flavrian block. Stratigraphic correlations across the Powell and Horne blocks are lacking thus the time-stratigraphic position of these two VMS deposits and origin of their gold enrichment remains uncertain. The Powell Block is subdivided into two distinctive domains (Brownlee and Joliet) separated by a 350 m wide quartz-feldspar porphyritic rhyolite dike, which intruded along a major structure. The Brownlee domain is characterized by bimodal mafic dominated volcanism, whereas the Joliet domain is characterized by an anomalously thick succession of felsic, volcanic and volcaniclastic material. This change in composition, style of volcanism and volume of material suggests a drastic change in magmatic activity with time. Water depth during volcanism was variable but trough cross-bedding, and mud-draped ripples in the Powell tuff member of the Powell formation, Brownlee domain, indicates at least locally an above storm wave base to intertidal setting, suggesting local emergent volcanism. These two domains represent two overlapping volcanic centres, fed by separate vents at different stages during the evolution of the Noranda Volcanic Complex, analogous to modern shield volcanism, along primitive arc or back-arc settings, such as the Kermadec arc. Textural, and chemical similarities of volcanic strata in the Joliet domain and Horne block as well as similar interpreted ages, suggests

they and by extension the VMS deposits they host, are time-stratigraphic equivalent and formed within the district's largest felsic monogenic volcanic centre during voluminous felsic volcanism and concomitant subsidence in a subaqueous setting that was locally emergent. Given this setting, the Au-rich Quemont and Horne deposits may have had a more direct magmatic input resulting in higher Au grades than the Cu-Zn VMS deposits of the Flavrian Block, which formed in a mafic dominated, bimodal, effusive and perhaps, a deeper water volcanic setting.

4.2 Introduction

Rouyn-Noranda, Québec, located in the Abitibi Greenstone Belt is one of the world's premier mining districts. It encompasses the Noranda Volcanic Complex within the 2704-2695 Ma Blake River Group (Spence and De Rosen Spence, 1975; Dimroth et al., 1982; Gibson et al., 2000; Gibson and Galley, 2007; McNicol et al., 2014) which hosts 23 Cu-Zn-Au-Ag VMS deposits (Gibson and Watkinson, 1990; Gibson and Galley, 2007; Monecke et al., 2017; Fig. 4.1). McNicoll et al. (2014) demonstrated that there is a regional time gap in volcanism between 2700 and 2698.5 Ma within the Blake River Group as a whole and this provides a much more precise chronostratigraphic distinction between a Lower and Upper Blake River (see below). On this basis, of 23 VMS deposits within the district, 21 formed during Lower Blake River Group volcanism (2702-2700 Ma) and 2 formed during Upper Blake River Group volcanism (2698.5-2695Ma). Of these only the Horne (167 Mt at 2.99 g/t Au, 15.3 g/t Ag, 0.84% Cu, and 0.63% Zn; combined past production and new measured, indicated and inferred Horne 5 resource; Krushnisky et al., 2020) and Quemont (14 Mt at 5.5 g/t Au, 331 g/t Ag 1.32% Cu, and 2.44% Zn) deposits, both within the Lower Blake River Group strata, are Au-rich (Fig. 4.1; Dubé et al., 2007; Mercier-Langevin et al., 2011; McNicoll et al., 2014). The Noranda Volcanic Complex was subdivided into 5 fault-bounded blocks, which in turn were subdivided into sectors (De Rosen Spence, 1976). The Powell block,

part of which is the focus of this manuscript, is bound by the Beauchastel fault to the north and the Horne Creek fault to the south, both of which are second order splays of the Larder Lake Cadillac fault (Robert, 1989; Jackson et al., 1995; Verpaelst et al., 1995; Carrier et al., 2000; Poulsen, 2017; Fig. 4.1). The Powell block contains the Quemont VMS deposit and separates the world class Horne Deposit (10M oz Au; Kerr and Mason, 1990; Gibson et al., 2000) of the Horne Block to the south from the conventional Cu-Zn-Pb-Ag-Au Noranda-type VMS deposits of the Flavrian Block to the north (Gibson and Galley, 2007; Fig. 4.1). Unlike the VMS deposits of the Flavrian Block, which are predominantly hosted within a bimodal succession of mafic and felsic coherent flows and lesser volcaniclastic rocks (Kerr and Gibson, 1993; Gibson and Galley, 2007), the Quemont and Horne deposits are hosted by thick monolithic successions of coherent rhyolite flows, domes and volcaniclastic rocks (Kerr and Mason, 1990; Kerr and Gibson, 1993; Mercier-Langevin et al., 2011).

Notwithstanding ~100 years of exploration and research, uncertainty remains as to the relative stratigraphic position of the Horne and Quemont deposits and their stratigraphic and temporal relationship to VMS deposits of the Flavrian block (Spence and DeRosen-Spence, 1975; Gibson and Watkinson, 1990; Barrett et al., 1991a; Gibson et al., 2000; Monecke et al., 2008; Moore et al., 2016). This uncertainty is due, in part, to the more pronounced deformation history of the Powell Block, a keystone block between the Flavrian and Horne blocks. Early geological maps of the Powell block by Wilson (1941), Morris (1957–1959), De Rosen-Spence (1976), and Lichtblau (1989) although of high quality, do not provide sufficient structural information or geochronological data to confidently constrain the deformation history, reconstruct the stratigraphy and volcanic history, and establish the metallogeny of Lower Blake River Group strata within the Powell block. Furthermore, recent work by Schofield et al. (2021) has documented

epigenetic styles of base and precious metal mineralization within the block that are of similar age as the Upper Blake River Group but hosted in part by rocks of the Lower Blake River Group. From a metallogenic point of view it is important to distinguish geological features related to the younger mineralizing events from those inherent to the deposition and syn-volcanic alteration of the volcanic hosts.

Given these uncertainties and questions, the goal of this study was to reconstruct the deposition history of the Lower Blake River Group volcanic rocks in a portion of the Powell block and to discuss its implications for the broader metallogeny of Lower Blake River Group volcanic rocks comprising the larger Noranda Volcanic complex. To do this we present results of: 1) detailed stratigraphic mapping at 1:100 scale and compilation mapping at 1:1800 scale over a 24 km^2 area that encompassed Lower Blake River Group strata within the central part of Powell Block, which builds on results of a study of the Joliet breccia (Schofield et al., 2021) and epigenetic veins and hydrothermal alteration by Schofield et al. (submitted; Chapter 3); and 2) new geochemical analyses and U-Pb zircon geochronology; the latter to constrain the temporal evolution of the Lower Blake River Group strata within the Powell Block, and to test and refine correlations with strata of the adjacent Horne and Flavrian blocks.

4.3 Terminology

Volcaniclastic units are classified and named using the granulometric terminology proposed by Fisher (1961). The terms tuff, lapilli-tuff, lapillistone, tuff-breccia and breccia are based on the size and relative abundances of clastic components (fragments and crystals), and as used herein have no genetic implications for the processes of fragmentation, transport and

deposition (e.g. Gibson et al., 1999, White and Houghton, 2006). All the volcanic units in the study area are metamorphosed to greenschist facies, but the "meta" prefix is omitted for brevity.

4.4 Geology of the Rouyn-Noranda Mining District

The Rouyn-Noranda mining district of the Abitibi greenstone belt is comprised of upper and lower Blake River Group rocks (Ayer et al., 2005; Thurston et al., 2008; Fig. 4.1), which are bound to the north and south by the Porcupine Destor and the Larder Lake Cadillac Faults, respectively (Fig. 4.1). These faults are associated with turbiditic sediments of the Cadillac and Kewagama Groups (<2687 Ma; Goutier, 1997; Davis, 2002) and alluvial-fluvial successions of polymictic conglomeratic rocks, cross-bedded sandstone, and alkali-shoshonitic volcanic rocks of the Timiskaming Group (≤2679-2669 Ma; Davis, 2002; Ayer et al., 2005; Thurston et al., 2008), which is locally cut by syenitic-monzonitic intrusions (Poulsen, 2017; Dubé and Mercier-Langevin, 2020).

Historically stratigraphic subdivisions within the Rouyn-Noranda mining district have been lithostratigraphic and chemostratigraphic, which has been defined and redefined numerous times since Wilson (1941). De Rosen Spence (1976) proposed the first informal regional lithostratigraphic classification for the district, and interpreted it to comprise a large, 7–9 km thick, subaqueous, shield-like, volcanic edifice, consisting of one or more volcanoes, with a collective diameter of ~40–50 km known as the Noranda Volcanic Complex. The Noranda Volcanic Complex was interpreted to contain a large subsidence structure, postulated to be an ancient caldera (Lichtblau and Dimroth, 1980; Sangster, 1980; Dimroth et al., 1982; Mueller et al., 2009; Pearson and Daigneault, 2009). Spence (1967) and Spence and de Rosen-Spence (1975), grouped the volcanic units into "cycles", which were subsequently refined and linked to cauldron

development during the evolution of the Noranda Volcanic complex (Gibson, 1989; Gibson and Watkinson, 1990) in accordance with limited U-Pb zircon ages available at that time (Mortensen, 1987; 1993). The term cauldron was proposed by Gibson and Watkinson (1990) because, unlike a caldera, a cauldron it is not constrained by shape or connection with surface volcanism and commonly involves passive, piece meal and asymmetric collapse above a static or rising body of magma (Smith and Bailey, 1968; Williams and McBirney, 1979). The limits of the Noranda cauldron have been interpreted to be the Hunter Creek and Horne Creek Faults to the north and south, respectively, and by the Flavrian pluton and the Dalembert shear zone, to the west and east, respectively (Fig. 4.1; Gibson and Watkinson, 1990).

The Flavrian-Powell Intrusive Complex, along the western margin of the cauldron (Fig. 4.1), is interpreted to be a synvolcanic, subvolcanic intrusion and heat source that drove hydrothermal circulation and the formation of some VMS deposits within the district (Goldie, 1976; Campbell et al., 1981; Kennedy, 1985; Galley, 2003; Gibson and Galley, 2007). In addition, it may have played a more direct role in the formation of the VMS deposits by contributing metals and magmatic fluids to a seawater dominated hydrothermal fluid (Gibson and Watkinson, 1990; Galley, 2003; Gibson and Galley, 2007; Franklin et al., 2005; Sharman et al., 2015). The trondjhemite phases of the Flavrian pluton has been dated at 2700.8 +2.6/-1.0 Ma by Mortensen (1993) and 2700.7 ±0.6 Ma by McNicoll et al., (2014). The trondhjemite phase of the Powell pluton has been dated at 2700.1±1.0 Ma (McNicoll et al., 2014).

4.5 Volcanogenic massive sulfide deposits

Most of the VMS deposits in the Rouyn-Noranda district occur within the central Flavrian block, where the host succession is dominated by bimodal effusive volcanic rocks (Wilson, 1941;

Spence, 1967; Spence and De Rosen Spence, 1975; De Rosen Spence, 1976; Gibson and Watkinson, 1990; Kerr and Gibson, 1993; Monecke et al., 2017). The VMS deposits occur at four specific lithostratigraphic intervals marked by hiatuses in volcanic activity, with most of the VMS deposits associated with the "main contact tuff" and the "C-contact tuff", which are sulfide and chert bearing tuffaceous units (Spence and De Rosen-Spence, 1975; Knuckey et al., 1982; Kalogeropoulos and Scott, 1989). The deposits occur with mafic and felsic volcanic centres that are localized along NE- and NW-striking synvolcanic structures (Simmons, 1973; Scott, 1980; Knuckey et al., 1982; Knuckey and Watkins, 1982; Gibson and Watkinson, 1990; Setterfield et al., 1995; Gibson and Galley, 2007). These deposits are small (<5 million tonnes), base metal-rich (Cu, Zn) lenses that formed largely as mounds on the ancient seafloor and have average Au grades of ≤1 g/t Au (Gibson and Watkinson, 1990; Kerr and Gibson, 1993; Monecke et al., 2017). The roots of these deposits are known to extend for >1km and comprise sulfide stringer veins enveloped in an inner chloritic and outer sericitic discordant pipe-like alteration zone, which in some deposits, extend in to the hanging wall (Wilson, 1941; Riverin and Hodgson, 1980; Hall, 1982; Knuckey et al., 1982; Knuckey and Watkinson, 1982; Riverin et al., 1990; Gibson and Watkinson, 1990; Barrett et al., 1991a; Barrett et al., 1991b; Barrett et al., 1992; Barrett et al., 1993; Galley et al., 1995; Santaguida et al., 1999; Hannington et al., 2003).

The Quemont and Horne VMS deposits occur in monolithic felsic dominated successions and are not associated with tuffaceous marker units (Kerr and Gibson, 1993). The Horne deposit is interpreted to have formed by sub-seafloor sulfide replacement of its host rocks, but there is sparse published information for the Quemont deposit (Weeks, 1967; Kerr and Mason, 1990; Kerr and Gibson, 1993; Gibson and Kerr, 1993; Monecke et al., 2017).

In the Rouyn-Noranda mining district there is no consensus on the time/stratigraphic correlation of strata and VMS deposits across the Flavrian, Powell and Horne fault blocks, particularly across the Horne Creek fault in the southern part of the district (Monecke et al., 2017). Spence and De Rosen Spence (1975) and De Rosen Spence (1976) correlated the Joliet-Quemont rhyolites with the Horne rhyolite, whereas Gibson (1989), Gibson and Watkinson (1990), and Kerr and Gibson (1993) interpreted the Horne rhyolite to be older. McNicoll et al. (2014) based on 19 new U-Pb zircon ages for volcanic and intrusive units demonstrated that VMS deposits of the Noranda district formed during two time-stratigraphic intervals during the 9-million-year evolution of the Blake River Group in Québec, separated by a gap in Blake River Group volcanism from 2700 – 2699.5 Ma. Similarly, Moore et al. (2016) interpreted the strata of the Horne block and everything south to the Larder Lake Cadillac fault to be related to an older caldera named the "Rouyn-Pelletier Caldera Complex", whereas the Flavrian and Powell block were interpreted to be related to a younger "Noranda caldera."

4.6 Deformation and metamorphism

The Southern Abitibi Greenstone belt experienced four deformation events (Dimroth et al., 1983; Hubert et al., 1984; Wilkinson et al., 1999; Daigneault et al., 2002; Ispolatov et al., 2008; Bleeker, 2012; Poulsen, 2017; Bedeaux et al., 2017). The first two events are best documented in the Timmins mining camp, ~200 km NW of the Rouyn-Noranda camp, where they are expressed by angular unconformities between folded and tilted metavolcanic rocks and overlying metasedimentary rocks (Bateman et al., 2008; Dubé and Mercier-Langevin, 2020). The first occurs between the ca. 2730–2704 Ma Deloro-Tisdale Group metavolcanic rocks and the ca. 2685 Ma Porcupine assemblage (Bateman et al., 2008; Dubé and Mercier-Langevin, 2020). The second occurs between the Porcupine and Timiskaming (ca. 2676–2669 Ma) assemblages (Bateman et al.,

2008; Dubé and Mercier-Langevin, 2020). In the Rouyn-Noranda camp, pre-Timiskaming deformation is expressed by an angular unconformity between the folded and tilted ca. 2704–2695 Ma Blake River Group metavolcanic rocks and the ca. 2676–2669 Ma Timiskaming Group (Wilson, 1956; Poulsen, 2017). The third deformation event, which is the most pervasive throughout the Southern Abitibi Greenstone belt, overprints the Timiskaming Group and is characterized by a regional E-W cleavage axial planar to large-scale antiforms and synforms and faults, including the Larder Lake Cadillac and Porcupine Destor Faults (Dimroth et al., 1983; Wilkinson et al., 1999; Daigneault et al., 2002; Bleeker, 2012; Poulsen, 2017; Bedeaux et al., 2017). This post-Timiskaming north-south shortening occurred between ca. 2670–2660 Ma and coincides with peak metamorphism in the southern Abitibi greenstone belt, which occurred between ~2669–2653 Ma (Powell et al., 1995; Piette-Lauzière et al., 2019; Dubé and Mercier-Langevin, 2020). The fourth deformation event is associated with northwest-southeast directed shortening and later dextral transcurrent reactivation of the Larder Lake Cadillac and Porcupine Destor faults (Dimroth et al., 1983; Hubert et al., 1984; Wilkinson et al., 1999; Daigneault et al., 2002; Ispolatov et al., 2008; Bleeker, 2012; Poulsen, 2017; Bedeaux et al., 2017).

The main post-Timiskaming deformation event, which resulted in the formation of regional folds and cleavage, is variably referred to as D1, D2 or D3 in the literature depending on mining district and author (Dimroth et al., 1983; Hubert et al., 1984; Wilkinson et al., 1999; Daigneault et al., 2002; Bleeker, 2012; Poulsen, 2017; Bedeaux et al., 2017; Dubé and Mercier-Langevin, 2020). In accordance with most past studies in the Rouyn-Noranda mining district, the main post-Timiskaming folding event is referred to as “D2” and the dextral transcurrent event as “D3” (Goulet, 1978; Dimroth et al., 1983; Hubert et al., 1984).

4.7 Methodology

Detailed field mapping and sampling was conducted at a scale of 1:100 using aerial drone images. Compilation mapping was completed at a scale of 1:10 000 (Appendix A) using historical maps of Morris (1957–1959), De Rosen Spence (1976), and Lichtblau (1989) and new detailed field mapping to constrain key lithologies. Representative samples of least altered versions of each host lithology were collected for petrographic and geochemical analysis. Geochemical samples were first crushed to 2 mm, split using a riffle splitter, and a 250 g subsample was pulverized to 75 microns and analyzed for whole-rock lithogeochemistry at ALS Geochemistry, Sudbury, Ontario. Samples for complete lithological and alteration characterization were analyzed using five analytical methods to produce a complete suite of major and trace elements, C, S and specific gravity at ALS Geochemistry (***CCPKG01)***. Results are included in Appendix Table A1. Regional lithogeochemical data for key volcanic units of the Noranda volcanic complex for comparison are included in Appendix Table A2. Lithophile element concentrations were obtained using Lithium Borate Fusion followed by ICP-MS analysis and base metal concentrations were obtained using 4-acid digestion, followed by ICP-AES analysis. Aqua regia digestion and ICP-MS analysis were used for select trace elements (As, Bi, Hg, In, Re, Sb, Se, Te, Tl). Specific gravity was calculated on pulverized material. Percent Loss on Ignition (LOI) values represent the difference between the weight of the sample before and after it was placed in an oven at 1000°C for 1 hour. For S and C analysis the sample was combusted in a high frequency Leco Induction Furnace and measured using IR Spectroscopy.

High precision isotope-dilution – thermal ionization mass spectrometry (ID-TIMS) U-Pb zircon geochronology was completed at the Jack Satterly Geochronology Laboratory (JSGL), University of Toronto. Heavy mineral concentrates were obtained at the laboratory using standard

crushing, grinding and Wilfley table methods, followed by magnetic and heavy liquid techniques. Best quality (crack, inclusion, core-free), fresh (least altered) grains of zircon were selected for analysis; details of zircon morphology and quality are summarized in Table 1. Zircon grains underwent chemical abrasion pre-treatment (CA, modified after Mattinson, 2005). Full details of CA pre-treatment and subsequent ^{205}Pb-^{235}U isotopic spiking and dissolution (after Krogh, 1973), and mass spectrometry protocols and parameters are provided in Schofield et al. (2021). Pb and UO_2 were analyzed at the JSGL on a VG354 mass spectrometer using a Daly collector in pulse counting mode. Initial Pb from geological sources above 1 picogram was corrected using the Pb evolution model of Stacey and Kramers (1975). Plotting of concordia diagrams and averaging of age results were carried out using the Isoplot version 3.71 Add-In for MS Excel, of Ludwig (2009). Calculated ages are based on weighted averages of $^{207}Pb/^{206}Pb$ ages (ratios). Although the concordia curve bands shown in Fig. 4.16 incorporate uncertainties in the ^{235}U and ^{238}U decay constants, these are excluded from the final age calculations. All age errors and error ellipses are given at the 2 sigma or 95% level of confidence.

4.8 Stratigraphic relationships of 2702-2700 Ma Blake River Group Strata within the Powell Block

Stratigraphic transects which form the basis of this study were executed within 7 of the best exposed and most accessible fault blocks within the Powell Block (Figs. 4.3 and 4.4). Distinctive volcaniclastic units were used as markers to subdivide the strata into formations and members, to aid correlation across fault blocks and to allow definition of facies and/or thickness variations of units. Table 2 shows a summary of the characteristics of each member, their distribution, thickness and interpreted paleoenvironment. The historic lithostratigraphic terminology for the Powell

Block, defined first by De Rosen Spence (1976) and later modified by Lichtblau (1989) has been maintained and only has been modified where necessary based on new correlations and geochronology from this study (see below). The stratigraphic transects occupy two distinctive domains within the Powell Block. The northern ones (A through F) are herein described as being part of the Brownlee domain and traverse G is within the Joliet domain (Figs. 4.3 and 4.4). The boundary between these domains is defined by a ~350m wide, quartz (5%; 0.5-1mm) and feldspar (1%; 0.5-1mm) porphyritic felsic dike, which occurs for a strike length ~1.5km and is characterized by an aphanitic, spherulitic groundmass, and sharp, irregular, and typically not foliated, contact margins. The age of this dike is uncertain, but it has been interpreted to have been emplaced during the same magmatic event as two identical, parallel dikes to the south, one of which yielded a U-Pb zircon age of 2702 ± 0.8 Ma (McNicoll et al., 2014; Schofield et al., 2021; Fig. 4.3). Collectively these three quartz feldspar porphyritic rhyolite dikes have been referred to as the Quemont Feeder dikes (De Rosen Spence, 1976).

4.8.1 Brownlee domain

The Brownlee domain is characterized by a bimodal, but mafic dominated volcanic succession. Three formations are recognized in the Brownlee domain and are discussed below in sequence from the oldest to the youngest.

4.8.1.1 Brownlee formation

The Brownlee formation is structurally and stratigraphically the lowermost unit in fault blocks 1,2,3,5, and 6. Like all formations of the Brownlee domain, the Brownlee formation is restricted by the Beauchastel fault to the north and has a total strike length of 1.3 km (Fig. 4.3).

The lower part of this formation is cut by tonalite and gabbro of the Powell Intrusive complex to the west, so its true thickness is unknown; the minimum measured apparent thickness is ~360 m (Fig. 4.4). The unit is defined by a massive coherent, flow banded, spherulitic, highly amygdaloidal (~20%), feldspar microphyric rhyolite facies (Fig. 4.5A), and a local heterolithic felsic lapillistone facies that occurs adjacent to a dike that cuts across the rhyolite facies (Fig. 4.5B).

The base of the coherent facies is characterized by lobe-hyaloclastite rhyolite flows. The lobe-hylaclastite flows comprise irregular lobes of massive coherent flow-banded, spherulitic rhyolite (Fig. 4.5A–B) that display an increase in amygdale content towards the lobe margins and are surrounded by thin rims of hyaloclastite (Fig. 4.5C–D). The lapillistone facies is crudely bedded and consists of angular to subrounded fragments, ~2–50 mm in diameter, dominantly composed of flow banded or massive feldspar microphyric rhyolite, angular chloritized fragments with cuspate margins and minor quartz (1–3 mm; 10–15%) porphyritic rhyolite clasts (Fig. 4.5B). The matrix of the lapillistone facies is fine-grained, chloritized, and contains quartz crystals ~10%, ≤1 mm in diameter.

4.8.1.2 Powell formation

The Powell formation is bimodal in composition and subdivided into five members. It consists of dominantly coherent volcanic flows, intercalated with minor (~5%) volcaniclastic units.

4.8.1.2.1 Lower Powell basalt member

The Lower Powell basalt member is the lowermost unit of the Powell formation, which conformably overlies the Brownlee rhyolite formation and it extends for a strike length of 2.8 km (Fig. 4.3). It was previously referred to as the Lower Powell andesite (De Rosen Spence, 1976;

Lichtblau and Dimroth, 1980; Lichtblau, 1989), but the Zr/Ti and Nb/Y ratios indicate that it is basaltic in composition (Pearce, 1996) and therefore we have renamed it the Lower Powell basalt member (Fig. 4.6A). Its apparent thickness approximately doubles from 200–500 m thick in fault blocks 5 and 6 in the southeast to ~600–1100 m in fault blocks 1, 2 and 3 in the northwest (Fig. 4.4). It is amygdaloidal (~1–5%) and dominantly microporphyritic with euhedral feldspar (~1%; 0.5–1mm) microphenocrysts, within a pilotaxitic groundmass comprised of fine-grained albite microlites, quartz and interstitial chlorite (Fig. 4.7A). The unit is subdivided into three facies: massive, pillow and breccia facies, dominated by the massive facies. Pillows typically display well preserved concentric cooling laminations and have minimal hyaloclastite (Fig. 4.7B–C). The massive facies contains parallel cooling laminations (Fig. 4.7D), columnar joints (Fig. 4.7E), and amygdales that increase in concentration and size towards the tops of individual flows: diameters range from 2 mm–1cm on average in the interior to ≥10cm towards the top. The upper contact of the massive facies is typically irregular with finger-like amoeboid lobes grading into a breccia facies. The breccia facies commonly occurs at the tops of flows (Fig. 4.7B) and consists of dominant amoeboid, or subordinate angular blocks of the underlying flow within a hyaloclastite matrix. Individual flows typically range from 5 to 25m thick, but locally may reach apparent thicknesses of 70 to 150m.

4.8.1.2.2 Lower marker member

The lower marker is 5 to 10m in apparent thickness and extends for ~2.5km along strike (Figs. 4.3 and 4.4). It consists of bedded, aphyric rhyolite lapillistone to tuff (Figs. 4.8 and 4.9); normal grading and highly rounded clasts are characteristic features of this member. Reverse grading is indicated in fault block 6, however, by the presence of ~15cm–60cm blocks of aphyric rhyolite located towards the top of this member (Fig. 4.8A). The lower marker member

conformably overlies the Lower Powell basalt and is in turn conformably overlain by the Upper Powell basalt. The lower contact is sharp and irregular as it follows irregularities in the upper surfaces of underlying pillows (Fig. 4.8B). In contrast the upper contact is sharp and planar, consisting of a fine, plane-bedded tuff conformably overlain by massive basalt with cooling cracks which parallel bedding in the underlying tuff (Fig. 4.8C). Clast size ranges from ~35–80mm on average at the base, to ~2–9mm on average towards the top (Fig. 4.10E). Large blocks (~20cm–2m diameter) of broken pillows and locally complete pillows occur at the base of this member (Fig. 4.8D).

4.8.1.2.3 Upper Powell basalt member

The upper Powell basalt conformably overlies the lower marker unit and extends for a strike length of 2.8 km (Fig. 4.3). Its apparent thickness does not vary significantly between fault blocks and ranges from ~150 to 330 m (Fig. 4.4). It is texturally and compositionally similar to the lower Powell basalt member and Zr/Ti and Nb/Y ratios indicate that it is also basaltic in composition (Fig. 4.6A; Pearce, 1996) although it was previously referred to as andesite (De Rosen Spence, 1976; Lichtblau and Dimroth, 1980).

The upper Powell basalt member is subdivided into massive, pillow and breccia facies; the massive facies is dominant. Individual flows range from 5–60m thick. A conformable bed of thinly laminated tuff at the top of the upper Powell basalt member is draped over an amoeboid basalt breccia in fault block 5 directly below the Powell rhyolite member. The amoeboid breccia forms a gradational contact with an underlying massive basalt flow.

4.8.1.2.4 Powell rhyolite member

The Powell rhyolite member has a strike length of ~800 m, a thickness of 30m–140m and is in conformable contact with underlying Powell Andesite and overlying Powell tuff members (Figs. 4.3 and 4.4). It comprises a lower, coherent aphyric rhyolite facies and an upper quartz (1–3 mm; 10-15%) porphyritic rhyolite (Fig. 4.10A), which in turn is subdivided into a lower coherent facies and an upper breccia to tuff breccia facies (Fig. 4.4). The coherent facies is flow banded (Fig. 4.10B), spherulitic and locally columnar jointed. It is characterized by a sharp lower contact and a gradational transition to a brecciated upper contact (Fig. 4.10C–D). The breccia is 1–2m thick and consists of angular, non-vesicular blocks of rhyolite that display a jig-saw fit (Fig. 4.10C) and locally minor clast rotation (Fig. 4.10D), consistent with autoclastic fragmentation of the underlying coherent flow. The matrix between the blocks is commonly infilled with tuff of the overlying Powell tuff member (Fig. 4.10C–D).

The overlying breccia to tuff breccia facies (Fig. 4.10E–F) is most abundant in fault block 5, where it comprises a ~75m thick, crudely bedded unit (Fig. 4.4), with a strike length of ~300m (Fig. 4.3). It shows nine consecutive upward coarsening and then fining sequences (Fig. 4.4). The blocks are subangular to subrounded and consist of non-vesicular quartz-phyric rhyolite, but lesser, highly chloritized, aphanitic fragments (~1–6cm in diameter), which weather recessively, constitute up to 10% of the fragments (Fig. 4.10E). The matrix is fine-grained, chloritized and contains quartz crystals. This facies is overlain by and intercalated with the lower ~40m of the Powell tuff member (Fig. 4.11A–B).

4.8.1.2.5 Powell tuff member

The Powell tuff member was previously subdivided by Lichtblau (1989) into the "Powell tuff" and the "Upper marker tuff" but given that these units are compositionally and texturally identical and grade into each other along strike, this subdivision is deemed unnecessary. The Powell tuff member comprises well sorted and finely laminated tuff and lapilli tuff. It is basaltic in composition based on its Zr/Ti and Nb/Y ratios (Fig. 4.6A; Pearce, 1996). This unit directly overlies and is intercalated with the Powell rhyolite member and is, in turn, overlain by and intercalated with rhyolite of the Héré Creek formation (Fig. 4.4). It has a minimum lateral extent of ~1200 m, and an apparent thickness of ~40m–170 m (Figs. 4.3 and 4.4). The apparent thickness is inflated due to the presence of mafic and felsic sills, and intercalated pillowed and massive mafic flows. In addition, an approximately 10m thick lens of vesicular, amoeboid fragment breccia (Fig. 4.7F), occurs in fault block 5 interbedded with the Powell tuff. The Powell tuff itself can be subdivided into a cross-bedded and graded lapilli tuff and tuff facies and a finely laminated tuff facies. The latter commonly drapes over pillows and fills inter pillow voids, but the former locally truncates the tops of broken pillows.

The cross-bedded and graded lapilli tuff and tuff facies is characterized by ~10–50cm thick beds, displaying normal or reverse to normal grading (Fig. 4.11C), with internal laminations in the upper or lower finer part of the beds. Planar cross-bedding, and scours (Fig. 4.11D) are common. Planar cross-beds commonly have steeply dipping foreset laminae, indicating a unidirectional current from the SE to the NW relative to the current attitude of the folded beds.

In contrast, the finely laminated tuff facies is characterized by ~1–2mm thick planar and well sorted laminae of lapilli tuff and tuff, typically without sedimentary structures (Fig. 4.11E). Loaded symmetrical ripples (Fig. 4.11F), and trough cross-beds (Fig. 4.12G) that were observed

locally indicate bi-directional flow. Convolute bedding and pseudo-nodules beneath blocks of Powell rhyolite indicates local soft sediment deformation during deposition (Fig. 4.11B). In addition, periodic ~1–5 cm thick beds and irregular lenses of monolithic, rounded to sub angular lapilli (Fig. 4.11E) rich in feldspar, scoria shards with bubble wall margins and angular non-vesicular altered glass shards occur within this facies (Fig. 4.11H). Large blocks of feldspar phyric and scoriaceous basalt were observed in fault block 8.

4.8.1.3 Héré Creek rhyolite formation

The Héré Creek formation overlies and is intercalated with the Powell tuff member of the Powell formation (Fig. 4.4). Historic mapping has demonstrated that the Héré Creek rhyolite, although offset by the Beauchastel fault, occurs in both the Flavrian and the Powell Blocks with a total strike length of ~19 km and a thickness of 870–1050m (Wilson, 1941; Morris, 1957–1959; Spence and De Rosen Spence, 1975; De Rosen Spence, 1976; Gibson, 1990). The Zr/Ti and Nb/Y ratios and SiO_2 values of 68.5–75.8% indicate that it is a high-silica rhyolite (Fig. 4.6A; Pearce, 1996). It is characterized by amygdaloidal, spherulitic, aphyric rhyolite, which is subdivided into a basal breccia to lapillistone facies (Fig. 4.12A) and an upper coherent facies (Fig. 4.12B–C).

The lower ~40m–150m of the formation consists of bedded monomictic tuff breccia, breccia and lapillistone beds containing aphyric rhyolite clasts (Fig. 4.12D) and which typically show normal grading (Fig. 4.13). It is composed of very thick beds, ~0.5–2m on average, which are not internally laminated. Fragments are angular, locally flow-banded, spherulitic, non-vesicular and range from ~1cm–40cm in diameter (Fig. 4.12D). The matrix is fine-grained and leucocratic. Basal contacts are sharp with local scours and the intercalated Powell tuff member typically shows convolute bedding. The overlying coherent facies is columnar jointed and consists

of a lower coherent flow banded lobe hyaloclastite rhyolite (Fig. 4.12F) and an upper massive, coherent and featureless rhyolite (Fig. 4.12B).

4.8.2 Joliet domain

Stratigraphic transect G in the Joliet domain differs significantly from those to the north in the Brownlee domain and is characterized by a thick succession of felsic volcanic and volcaniclastic rocks and a complete absence of mafic extrusive volcanic and volcaniclastic rocks (Fig. 4.3). Two formational units were crossed by this transect.

4.8.2.1 Joliet formation

The structurally and stratigraphically lowermost and oldest volcanic unit of the Joliet domain is the Joliet formation, which has an exposed strike length of 2.5km but is restricted to the south by the Horne Creek fault (Fig. 4.3). The Joliet formation is truncated to the west by the Powell Intrusive Complex so, although its true thickness is unknown, the minimum apparent thickness is 1400m. The formation is locally cross-cut by quartz porphyritic (1-2mm diameter; 10-15%) rhyolite sills, which texturally and compositionally resemble the Powell rhyolite formation. It is subdivided into a lower flow banded, coherent facies, which is intercalated with an upper volcaniclastic facies comprised of lapillituff, lapillistone and tuff breccia.

The lower coherent facies is ~1000m thick and consists of feldspar microphyric, spherulitic, amygdaloidal, flow-banded lobe hyaloclastite rhyolite. The intercalated volcaniclastic facies is ~400m thick, poorly sorted and crudely bedded. It comprises flow-banded, and moderately vesicular aphyric rhyolite clasts that strongly resemble the underlying flows, as well as ~10% angular chloritized clasts, and locally ~5–10% quartz-porphyritic rhyolite clasts in an ash-sized matrix. Clast sizes range from <1–10cm diameter (4–5cm on average), with local clasts

up to 40cm in diameter. The clasts are typically angular to subangular and equant to tabular in morphology (Fig. 4.14A). The ash-sized matrix component is ~5–10% and comprises a fine-grained, granular mixture of clastic material, crystal fragments and relict chlorite and sericite altered glassy fragments (Fig. 4.14B–C). The relict glassy fragments are ~1–2mm in diameter and have a fluidal morphology (Fig. 4.14B). This facies is crudely bedded, with bedding defined by variations in clast size, and displays a reverse to normal grading. Scours are present where overlying beds cut down into underlying beds (Fig. 4.14D) and trough-cross bedding has been also observed locally (Fig. 4.14D).

4.8.2.2 Quemont rhyolite formation

The Quemont formation conformably overlies the Joliet formation. It occurs for a strike length of 1.5 km and is restricted to fault block 9 (Fig. 4.3). It has an overall apparent thickness of ~685 m. It is subdivided into a lower polymictic tuff breccia, lapillistone to lapillituff facies and upper coherent quartz-porphyritic rhyolite facies.

The tuff breccia, lapillistone to lapillituff facies is clast supported, poorly sorted and crudely bedded, displaying reverse to normal grading and local scoured contacts. It is poorly sorted with clast sizes ranging from 3cm to 30cm. Clasts are angular to subrounded, and equant to tabular in morphology, comprised of non-vesicular plagioclase microporphyritic rhyolite (95%), basalt (5%) and accidental granophyre. The matrix component is ~10% and consists of fine-grained chloritized glass shards.

The coherent facies is flow banded and quartz (1–2mm; 10%) porphyritic. The contact between the massive facies and the tuff breccia, lapillistone to lapillituff facies is highly irregular and in places appears intrusive. The clastic facies immediately below the massive facies is marked

by the appearance of quartz porphyritic rhyolite clasts and quartz-grains in the matrix. The upper contact of the massive facies is truncated to the north by the Powell fault.

4.9 Lithogeochemistry of volcanic units of the Powell Block

The Th/Yb and Zr/Y ratios indicate the basaltic and rhyolitic volcanic rocks of the Powell Block are of transitional to calc-alkaline affinity (Fig. 4.6B; Ross and Bedard, 2009). All of the lithologies sampled exhibit relatively flat Chondrite normalized REE trends, with negative Nb and Eu anomalies (Fig. 4.6C). The rhyolites are all compositionally similar and are characterized by high silica concentrations (62–81% SiO_2), La/Yb_n ratios of 1.6–3.3, and Yb_n values of 19–29 indicating that they are FIIIa–FIV rhyolites/dacites (Fig. 4.6C–D; Hart et al., 2004). The basalts, formerly referred to as andesites (e.g. De Rosen Spence, 1976), are also all compositionally similar, characterized by $La/Yb_{(CN)}$ values of 1.3–4, and Yb_n values of 7–20.

4.10 Intrusions

Intrusive rocks, by virtue of the cross-cutting relationships they commonly provide, are critical components for the understanding of the stratigraphic evolution of the study area (Fig. 4.16). They include early mafic dikes and sills, early felsic dikes and sills, the Powell Intrusive Complex, the Joliet Intrusive Suite, lamprophyre dikes, syenite dikes and diabase dikes. The younger lamprophyre, syenite and diabase dikes will not be discussed herein as they cross-cut virtually all intrusive and extrusive rocks within the study area and thus are irrelevant to the stratigraphic evolution.

4.10.1 Early mafic dikes/sills

The mafic dikes are mesocratic, aphanitic, highly chloritized and/or carbonatized and weather recessively relative to the host-rocks. They strike NW to ENE and are ≤1m wide. Locally, discordant trails of irregular amoeboid mafic fragments occur within the volcaniclastic units (Fig. 4.15A), which are interpreted to have formed by hydroclastic fragmentation of injected mafic dikes that fragmented and mixed with unconsolidated host volcaniclastic units. The mafic dikes are commonly cross-cut by felsic dikes and may occur as narrow margins on either side of felsic dikes (Fig. 4.15B). The mafic dikes exhibit relatively flat chondrite normalized REE slopes, with $La/Yb_{(CN)}$ values of 2.1–4.7, negative Nb anomalies and a slight negative Eu anomaly (Fig. 4.6). Compositionally, they are basaltic to basaltic-andesite based on their Zr/Ti and Nb/Y ratios (Fig. 4.6; Pearce, 1996) and similar both in composition and texture to the basalt flows of the Powell formation.

4.10.2 Early felsic dikes/sills

The felsic dikes are all leucocratic and spherulitic and are subdivided into three main types: 1) aphyric, aphanitic; 2) quartz-porphyritic; and 3) quartz-feldspar porphyritic. The textures and compositions of these three felsic dike types are comparable to rhyolite in the Héré Creek formation, the Powell rhyolite member of the Powell formation and the rhyolite of Quemont formation, respectively. The dikes are typically moderately chloritized and sericitized, mark stratigraphic offsets, and are cross-cut by the tonalite phase of the Powell Intrusive Complex. They strike ENE and range from 20–350m in thickness (Fig. 4.3). The size of spherulites ranges from ≤1mm to 1cm diameter (Fig. 4.15C). The margins of the dikes are commonly flow-banded, sharp and irregular. Heterolithic breccias occur locally along the margins of some aphyric-aphanitic

dikes and comprise angular fragments of aphyric-aphanitic rhyolite, quartz-porphyritic rhyolite, basalt and abundant angular cuspate chloritized shards (Fig. 4.15D).

The aphyric, aphanitic felsic dikes (Héré Creek rhyolite feeder dikes) are characterized by relatively flat chondrite normalized REE slopes, with $La/Yb_{(CN)}$ values of 1.9–3.2, $Yb_{(CN)}$ values of 19–28, and negative Nb and Eu anomalies, which indicates they are compositionally similar to FIIa/FIV rhyolites (Hart et al., 2004) of transitional to calc-alkaline affinity (Fig. 4.6B; Ross and Bedard, 2009). The northernmost Quemont feeder dike is compositionally very similar. It is a rhyolite/dacite (Pearce, 1996) of transitional to calc-alkaline affinity (Ross and Bedard, 2009), with a relatively flat chondrite-normalized REE pattern, La/Yb(cn) ratios ~2, negative Nb and Eu anomalies, and is classified as an FIV rhyolite (Fig. 4.6C-D; Hart et al., 2004).

4.10.3 Powell Pluton

The Powell pluton, like the Favrian Pluton to the north, is comprised of three main phases, early quartz dioritic phases and younger tonalitic and trondjhemitic phases. The quartz-diorite phase is mesocratic, fine-grained and strongly chloritized. It is characterized by fine-grained anhedral-subhedral, locally granophyric textured albite (~70%; 200-500 μm) and quartz (5-10%; 200-500 μm), interstitial chlorite (~15-20%), subhedral epidote (5-10%; 100-200 μm), and accessory rutile, and pyrite. The quartz-diorite phase is characterized by a relatively flat chondrite normalized REE slope, with La/Yb(cn) ratios of 3.2–4.5, and negative Nb and Eu anomalies and is compositionally similar to the basalt flows. Minor pendants of glomeroporphyritic gabbro and xenolith rich phases are also present. The quartz-dioritic mafic phases cross-cut rhyolite of the Brownlee formation, the Joliet formation and lower Powell basalt member of the Powell formation.

The most volumetrically abundant phases of the Powell intrusive complex are the trondhjemite and tonalite, which cross-cut the older quartz-diorite phase and locally early felsic dikes (both the aphyric and quartz-feldspar porphyritic types). They also cut the Brownlee rhyolite formation and the lower Powell basalt member of the Powell formation and contain altered xenoliths of both units. The tonalite phase is leucocratic, medium grained, and characterized by a granophyric intergrowth of anhedral quartz (35-40%; 0.5-1mm) and albite (45-55%; 0.5-1mm) with chlorite (10-15%), sericite (5-10%), and accessory rutile, pyrite, and chalcopyrite; albite is typically strongly sausseritized. The tonalite locally contains abundant miariolitic cavities (~1cm diameter) filled by quartz and chlorite. It is compositionally similar to the older felsic dikes and rhyolite flows and exhibits relatively flat chondrite normalized REE slopes, with La/Yb(cn) ratios of 2.2–2.9, and negative Nb and Eu anomalies.

4.10.4 Joliet tonalite suite

The Joliet tonalite occurs as dikes and plugs distributed in strata of both the Brownlee and Quemont domains, where they are locally associated with intrusion-related angular breccias (e.g. Joliet breccia; Schofield et al., 2021). The tonalite is porphyritic to glomeroporphyritic, consisting of 40–50 % medium-grained quartz and altered albite phenocrysts within a fine-grained spherulitic groundmass (50–60 %) of quartz, albite, sericite and chlorite. The spherulites show all degrees of recrystallization from sector recrystallized spherulites to quartz grains with irregular to rounded (anhedral) outlines and containing internal radiating feldspar laths. Quartz phenocrysts (10–20 %, 1-3 mm) are euhedral to subhedral and smokey grey. Albite phenocrysts (25–35 %, 2-5 mm) are subhedral to euhedral tabular crystals that are intensely altered to sericite. The groundmass is a fine-grained mosaic of quartz and albite ± fine-grained euhedral pyrite (1–3 %), cross-cut by arcuate perlitic fractures altered to sericite ± chlorite. The Joliet tonalite is compositionally similar

to the Powell tonalite exhibits a relatively flat chondrite normalized REE slope, with La/Yb(cn) ratios of 2.5–3.2, and a negative Nb anomaly.

4.11 U-Pb ID TIMS Zircon Geochronology

4.11.1 Powell rhyolite

A sample of coherent quartz-porphyritic rhyolite from the Powell rhyolite member of the Powell formation yielded a zircon population comprising clear, colourless, short prismatic grains and broken equivalents, locally with minor cracks and inclusions (Figs. 4.3 and 4.17A). U-Pb TIMS analysis for 5 chemically abraded zircon grains from this population overlap tightly with each other and Concordia, and give a weighted average $^{207}Pb/^{206}Pb$ age of 2700.19 ± 0.89 Ma (Fig. 4.17A). This is considered to represent the eruption age of the rhyolite, which overlaps within 2 sigma error with the age of the overlying Pump House rhyolite (Héré Creek rhyolite formation), which was dated by McNicoll et al., (2014) as 2700.3 ± 1.2 Ma age (Fig. 4.18).

4.11.2 Brownlee rhyolite

A sample collected from the coherent aphanitic Brownlee rhyolite flow did not yield zircon suitable for U-Pb geochronology (Figs. 4.3 and 4.19). As an alternative, a sample of a quartz-porphyritic clast from a heterolithic breccia adjacent to a felsic dike which cuts the Brownlee coherent aphanitic rhyolite was sampled (Figs. 4.3 and 4.19) and it yielded a population of good quality, clear, colourless to very pale brown, sharp, zircon prisms (Fig. 4.17B). Most are well-terminated, though some are broken; minor cracks are present, as well as mineral (e.g. apatite), fluid and/or melt inclusions. Chemical abrasion and subsequent analysis of the four best single zircon grains from this population are fully concordant but show a spread of $^{207}Pb/^{206}Pb$ ages from 2694.1 ± 1.8 Ma to 2700.0 ± 1.6 Ma (Fig. 4.17B). The two oldest analyses (Z3, Z4) overlap each

other and give a weighted average age of 2699.7 ± 1.1 Ma (MSWD = 0.27, probability of fit = 60%; Fig. 4.17B). Although the result for fraction Z2 strongly overlaps with Z3 and Z4, it is relatively imprecise, and like the younger result for Z1, they are interpreted to reflect minor secondary Pb-loss. Therefore, we interpret the 2699.7 ± 1.1 Ma age to best represent the crystallization age of the felsic clast in the heterolithic breccia. Although, the weighted average age of this sample is younger than that of the overlying Powell rhyolite, the two ages overlap at the 2 sigma level of uncertainty (Fig. 4.18). Similarly, the mean age of the clast is younger than that of the Powell tonalite (2701.0 ± 0.8 Ma; Schofield et al., 2021), which cross-cuts the Brownlee rhyolite, but again the 2 sigma errors for both ages overlap slightly (Fig. 4.18). The crystallization age of the felsic clast represents the maximum age of formation of the heterolithic breccia and there are two alternative ways to interpret this. One is that the breccia formed at the intrusive margin of an early quartz porphyritic felsic dike (Fig. 4.19) and hence the data provide a maximum age for the emplacement of the dike and minimum constraint on the age of the Brownlee rhyolite. The second option is that the clast was incorporated into a heterolithic lapilli tuff unit that is intercalated with the otherwise aphyric Brownlee rhyolite. In this case the crystallization age would represent a maximum age for eruption of the Brownlee rhyolite. In neither case, however, does the data allow interpretation of a conclusive age bracket for the deposition of the Brownlee rhyolite. In both cases, it may help explain the discrepancies with respect to the ages of the overlying Powell rhyolite and the Powell tonalite which cuts it.

4.11.3 Felsic dikes

Two samples collected of the aphyric, aphanitic rhyolite dikes, (MERN17MDS0033 and MERN17MDS0034) did not yield zircons but they crosscut the Powell quartz-diorite phase and the Powell tonalite phase, as well as the quartz-porphyritic rhyolite of the Powell formation, which

indicates a maximum age constraint of 2700.19 ± 0.89 Ma (Schofield et al., 2021) or 2700.1 ± 1.0 Ma (McNicoll et al., 2014).

4.12 Base metal mineralization

VMS deposits in the Powell Block are restricted to the Joliet domain and include the Au-rich Quemont deposit, which is the second largest deposit in the camp (Table 3). The footwall to the Quemont deposit consists of the Joliet formation (Spence and de Rosen Spence, 1975). The host rock is a lapilli tuff to coarse-grained rhyolite breccia unit comprised of aphyric and quartz porphyritic rhyolite clasts that range from ~3 to >30cm, and the deposit occurs at or near the contact between the host and the overlying coherent flow-banded quartz-porphyritic rhyolite (Spence and de Rosen-Spence, 1975, Ballachey et al., 1952; Taylor, 1953, 1957; Campbell, 1962; Weeks, 1963, 1967; Ryznar et al., 1967). The host unit was interpreted by De Rosen Spence (1976) as unit 3 of the Quemont formation (Quemont breccia II; Lichtblau, 1989) and the overlying flow as unit 4 of the Quemont formation but Weeks (1967) suggested that the coherent quartz-porphyritic rock displays intrusive contacts with the underlying breccia. Partially replaced rhyolite clasts were noted locally within the massive sulfide lens (Scott, 1948; Ryznar et al., 1967). The ore consists of chalcopyrite, sphalerite, pyrite, pyrrhotite, and minor magnetite and galena, and is zoned with chalcopyrite and pyrrhotite dominant at the base and pyrite and sphalerite dominant towards the top of the deposit (Scott, 1948; Taylor, 1957; Ryznar et al., 1967). Gold is correlated with elevated copper concentrations (Scott, 1948). Chlorite alteration occurs in the footwall (up to 20m) and hanging wall of the deposit and is associated with disseminated and vein chalcopyrite mineralization (Scott, 1948; Taylor 1953, 1957; Weeks, 1967). An extensive sericitic and pyritic alteration envelope surrounds the chlorite alteration zone (Taylor, 1957; Weeks, 1967). The

deposit and host-rocks are folded into a west-plunging anticline whose southern limb is truncated by the Horne Creek fault.

Numerous Cu-Zn-Ag prospects and occurrences occur throughout the Brownlee sub block of the Powell block. These include disseminated and vein occurrences of pyrite, chalcopyrite ± pyrrhotite, with accessory galena, sphalerite, and Ag- and Bi-tellurides in lower, 27002-2700Ma strata of the Blake River Group (Schofield et al., submitted). The latter have been interpreted as the deep structural roots of eroded VMS deposits located within upper Blake River Group strata and related to a ca. 2698 Ma magmatic-hydrothermal event (Schofield et al., 2021). The Joliet and Don-Rouyn deposits (Table 3) may be related to this style of mineralization. The Joliet deposit is hosted within the Joliet formation, and it is characterized as a highly siliceous breccia containing disseminated, aggregates (up to 1.2cm in diameter) and veinlets of pyrite, and chalcopyrite (Dresser and Denis, 1949). The mineralized breccia has a pipe-like morphology with a diameter of 50m and a long axis that plunges moderately SSW (Harquail, 1951). The Don-Rouyn Cu deposit is hosted by the trondhjemitic phase of the Powell Intrusive Complex and has been interpreted as an example of an Archean porphyry deposit (Kirkham, 1972; Kotila, 1975; Goldie et al., 1979; Jebrak et al., 1997). It is mineralogically zoned with a siliceous bornite-chalcopyrite-pyrite-molybdenite core, chalcopyrite-pyrite marginal zone and an outermost pyrite zone (Goldie et al., 1979) but the absence of k-silicate aleration and the strong correlation of mineralization with chlorite casts considerable doubt on the proper classification of the deposit.

4.13 Discussion

4.13.1 Lithostratigraphic and chronostratigraphic considerations

The Noranda Volcanic complex encompasses the entire Blake River Group (2704-2695 Ma) at Rouyn-Noranda. Ayer et al. (2005) and Thurston et al. (2008), divided the Blake River group in Ontario and Quebec into Lower and Upper Blake River Groups separated by a break in volcanism circa 2701-2700 Ma. In contrast, McNicoll et al. (2014) used a more extensive geochronological database for volcanic and intrusive units to place the break in Blake River Group volcanism in Quebec at 2700-2698.5 Ma. Schofield et al. (2021) used the gap in volcanism defined by McNicol et al. (2014), to subdivide the Noranda Volcanic complex into lower (2704-2699.5 Ma) and upper (2699.5 – 2695 Ma) units, which are similar in age and duration to the existing temporal subdivision of the entire Blake River Group by Ayer et al. (2005) and Thurston et al. (2008). We propose that the gap in volcanism defined by McNicoll et al. (2014) for the Blake River Group of Quebec is a better constrained division of the entire Blake River Group into Lower (LBRG) and Upper (UBRG) Blake River Groups, terminology that is used herein as it allows a more regional scale context for discussion (Fig. 4.18).

In addition, McNicoll et al. (2014) re-grouped existing lithostratigraphic formations of the Noranda Volcanic complex into 8 informal “formations” based on age. This resulted in a classification that is in part lithostratigraphic and chronostratigraphic and previous lithostratigraphic formations of the Flavrian, Powell and Horne blocks were renamed and grouped into the Horne, Noranda, Camac and Renault-Duffresnoy formations (McNicoll et al., 2014). Unfortunatately the limits and extent of these formations are not mappable in the field so the use of the lithostratigraphic term “formation” in the “time” context applied by McNicoll et al. (2014)

does not meet the criteria for “formation” as defined in the North American Stratigraphic Code (North American Commission on Stratigraphic Nomenclature, 2005). Furthermore, the singular term “Noranda formation” is not appropriate because it has long been subdivided internally into 28 informal lithostratigraphic formations, comprised of units with various ages, compositions, features and aerial extent (De Rosen Spence, 1976; Gibson, 1990; Monecke et al., 2017). For these reasons the discussion of former stratigraphic correlations in the district and of the metallogeny of the Powell block within this lithostratigraphic and time framework, retains the historical lithostratigraphic formations and nomenclature in lieu of the more recent and non-compliant “Noranda and Horne formations”.

The two new U-Pb zircon ages presented in this study, combined with the previously reported 2701.0 ± 0.8 Ma age for the Powell tonalite (Schofield et al., 2021), which crosscuts the Brownlee rhyolite, suggests that strata of the Brownlee domain were deposited prior to 2699 Ma (Fig. 4.18). Similarly, the 2702.0 ± 0.8 Ma age of the Quemont feeder dike (McNicoll et al., 2014), constrains the Joliet formation and Quemont formation of the Joliet domain to ≥2702 Ma. These results indicate that the volcanic strata within the Powell Block belong to the Lower Blake River Group. Likewise, the rhyolitic host rocks within the footwall to the Horne deposit have been dated by McNicoll et al., (2014) as 2702.2 ± 0.9 Ma, indicating a Lower Blake River Group age for the Horne Block as well. In contrast, the ages of the strata within the Flavrian block remain contentious.

4.13.2 Structural evolution of the Powell Block

Key to reconstructing the volcanic history of the Powell Block is understanding its structural evolution, which was described in some detail by Schofield et al., (submitted) and is summarized herein. The volcanic strata of the Powell Block were first tilted (D1?) and offset by

brittle ENE striking faults. The strata were subsequently folded during N-S compression (D2) associated with an E-W striking subvertical cleavage ca. 2670-2660 Ma (Schofield et al., submitted). North over south reverse movement occurred along E-W striking faults during D2 deformation and truncated the limbs of the earlier formed folds. These structures were later reactivated as dextral transcurrent faults during D3 (Schofield et al., submitted). This sequence of deformation events is consistent with what is observed along the Larder Lake Cadillac fault (Dimroth et al., 1983; Hubert et al., 1984; Wilkinson et al., 1999; Daigneault et al., 2002; Ispolatov et al., 2008; Bleeker, 2012; Poulsen, 2017; Bedeaux et al., 2017). Thus, the net result is that the volcanic strata in the study area were folded and transposed into a series of fault blocks, which complicates the interpretation of volcanic facies and thickness variations. Reconstruction of the pre-orogenic configuration of fault blocks based on this sequence of deformation events would result in a set of adjacent fault blocks 1 through 9, in order from northwest to southeast bound by a series of NE striking faults, with an overall NW strike of strata (Fig. 4.20). Some of these ENE striking bounding faults might have originated as synvolcanic structures, which localized the extrusion of local rhyolite domes, discussed in detail below. Of key importance is the contact between the two domains (Brownlee and Joliet), which is marked by a ~350m wide, quartz (5%; 0.5-1mm) and feldspar (1%; 0.5-1mm) porphyritic felsic dike (Quemont feeder dike). The fact that this dike is typically in sharp intrusive contact with the host volcanic strata of both domains and only locally overprinted by minor cross-cutting E-W striking brittle faults with negligible offset, suggests that the bulk of the stratigraphic offset must have occurred prior to the intrusion of this dike, indicating the presence of a Lower Blake River Group age synvolcanic structure.

4.13.3 Interpretation of volcanic lithofacies of the Brownlee domain

4.13.3.1 Brownlee formation

The lobe-hyaloclastite morphology of the Brownlee rhyolite is typical of lower viscosity submarine rhyolite flows (De Rosen Spence et al., 1980; Yamagashi and Dimroth, 1985). This formation is not well exposed in all fault blocks, so it is difficult to assess variations in thickness and facies that could be used to suggest vent proximity. Archean rhyolites can extend for up to 10km from their vent (De Rosen Spence et al., 1980) and the presence of an ENE striking felsic dike swarm at the base of fault Block 5, might indicate the presence of an eruptive centre, although further evidence is lacking.

The dominantly flow banded or massive feldspar microphyric rhyolite clasts within the heterolithic lapillistone facies strongly resemble the coherent facies of the Brownlee formation and are likely locally derived. The texture of the quartz-porphyritic rhyolite clasts, with 10–15%, 1–3mm quartz phenocrysts in an aphanitic groundmass, is typical of rhyolite flows or high-level sills and dikes in the Powell rhyolite member. Coherent quartz-porphyritic rhyolite phases were not observed within the exposed portions of the Brownlee formation, and thus the source of the quartz-porphyritic clasts is unknown. It is interpreted that these clasts were derived from: 1) a local coherent quartz-porphyritic phase of the Brownlee rhyolite formation, that due to intrusion of the Powell Intrusive complex and later deformation, is no longer exposed or removed via erosion; 2) by the intrusion and break-up of a synvolcanic QP rhyolite intrusion(s) into an unconsolidated Brownlee rhyolite breccia that was subsequently redeposited; or 3) an intrusion-related breccia developed along the margins of the younger cross-cutting dike. Crude bedding, and the subangular morphology of the clasts in the intercalated felsic lapillistone facies suggests a proximal deposit,

which was transported via mass flows and is consistent with the first or second interpretation. This unit may have formed by mass wasting from adjacent fault scarps and deposition in a local basin, during synvolcanic tectonic activity, but due to the poorly exposed nature of this unit and uncertain contact relationships it's origin cannot be confidently ascertained.

4.13.3.2 Lower Powell basalt member

The apparent thickness of the Lower Powell Basalt member approximately doubles in fault blocks 1, 2 and 3, compared to fault blocks 5, 6 and 7; its thickness in fault block 4 is uncertain as it is truncated by the Powell Fault. This suggests topographic ponding or restriction of the basalt flows in these fault blocks relative to fault blocks 5,6 and 7. The increased thickness in fault blocks 1,2, and 3 cannot be ascribed to folding, since there is no systematic tectonic thinning of all units in fault blocks 5, 6 and 7 relative to fault blocks 1, 2 and 3. In addition, the higher proportion of massive basalt flows, relative to pillowed flows, and greater thickness of individual flows, as well as locally coarser grain size of the thicker flows, suggests a component of primary topographic ponding in fault blocks 1 and 2. This is also consistent with the work of Lichtblau (1989), who mapped lateral variation in facies, from massive, to pillowed to breccia to indicate a vent source to the west (e.g. Waters, 1960; Dimroth et al., 1978). Assuming that the thickness variation is primary requires: 1) synvolcanic subsidence; and 2) ponding against a topographic high created by the extrusion of the Brownlee rhyolite. The latter is consistent with the interpreted location of the Brownlee rhyolite vent in Fault block 5.

4.13.3.3 Lower marker member

The lower marker member does not exhibit significant variations in thickness between fault blocks and is consistently ~5m–10m thick. However, facies changes such as reverse grading of

large blocks of rhyolite in fault block 6, relative to the typical normal grading observed in fault blocks 3,4 and 5 are consistent with deposition by debris flows that evolved into turbidity currents downslope, as suggested by Lichtblau (1989). The lack of significant thickness variation suggests that deposition of the lower Powell basalt member "levelled-out" topographic variations between the individual fault blocks in the Brownlee domain, but that a slope towards the northwest remained during the deposition of this member. The presence of large blocks and locally completely intact pillows at the base of this unit suggests scouring and encorporation of the underlying basalt flows of the lower Powell basalt member occurred during transport, supporting transport via high-concentration and high-velocity mass-flows (Cas and Wright, 1988). Alternatively, it could be a product of fault scarp collapse. The rhyolite clasts are non-vesicular, and juvenile material is lacking, ruling out an explosive magmatic or phreatomagmatic eruption mechanisms (Fisher and Schmincke, 1984), unless these blocks were ballistically emplaced or were resedimented. A phreatic eruption mechanism or gravitational instability triggered by synvolcanic fault movement or oversteepening of a rhyolite dome are thus the most likely trigger mechanisms (Gibson et al., 1999), and suggests a reactivation of vents and renewal of volcanic activity in the southeast of the Brownlee domain, after the deposition of the Lower Powell basalt member.

4.13.3.4 Upper Powell basalt member

This member does not exhibit significant thickness changes between the fault blocks, suggesting that its deposition was not associated with substantial subsidence. However, a ~60 m thickening of this member in fault block 6 and presence of very thick individual massive flows (40–60m), which are columnar jointed towards the base and grade laterally into irregular lobes suspended in a hyaloclastite matrix towards the southeast, suggests a vent source or ponding (e.g.

Gibson et al., 1999), near the site of the Héré Creek rhyolite feeder dike. Numerous secondary narrow ENE striking narrow brittle faults, which offset lower older flows but not upper younger flows, further supports a zone of synvolcanic faulting within this area (e.g., Dimroth et al., 1978). During the waning stage of this eruptive phase, a thin unit of thinly laminated tuff was deposited in Fault block 5. This suggests a brief hiatus in volcanism associated with suspension sedimentation occurred prior to eruption and emplacement of the overlying Powell rhyolite member. The absence of sulphides within the thin tuff interval suggests that nearby active hydrothermal venting was not associated with deposition of this unit.

4.13.3.5 Powell rhyolite member

Lichtblau (1989) interpreted the Powell rhyolite to be a single flow that erupted from a vent now occupied by the northernmost Quemont feeder dike but the rhyolite appears to be thickest in proximity to ENE striking structures that are marked by the Héré Creek feeder dikes, and thins rapidly with increasing distance away from these structures. The presence of quartz-porphyritic rhyolite clasts within the heterolithic breccias along the margins of the Héré Creek feeder dikes, suggests that earlier quartz-porphyritic Powell rhyolite feeder dikes may have used these same conduits. These earlier quartz-porphyritic intrusive phases interacted directly with the adjacent wet unconsolidated volcaniclastic material or intrusion-induced fragmentation, whereas the later aphyric Héré Creek rhyolite feeder dikes have sharp irregular margins indicating they were insulated from the interaction with wet host rocks. Similar relationships of multiple intrusive events along the same conduits are observed in the synvolcanic McDougall-Despina fault set in the Flavrian block (Setterfield et al., 1995).

The limited aerial extent of the individual flows/domes of the Powell rhyolite member (<500m), and rapid thinning away from the Héré Creek rhyolite feeder dikes, is consistent with a

steep-sided (20º–70º), stubby flow, ridge or dome, which is characteristic of blocky flows or domes (Gibson et al., 1999). The gradational transition between the coherent flow-banded facies and the overlying conformable breccia facies, which at the contact is characterized by angular, monolithic clasts that exhibit jig-saw fit textures, is also consistent with a blocky autoclastic flow top breccia (Gibson et al., 1999). This breccia is draped by thinly laminated plane-bedded tuff, which often forms the matrix between the clasts, consistent with emplacement by submarine fallout and subsequent infiltration into voids within the autoclastic breccia. The overlying, crudely bedded breccia to tuff breccia facies, is dominantly restricted to fault block 5, where it constitutes a ~75m thick unit comprised of 9 consecutive upward coarsening and then fining sequences. This drastic change in thickness and localization to fault block 5 suggests the presence of a topographic basin during emplacement of this unit. The monolithic and angular nature of the blocks, crude bedding and presence of angular chloritized fragments, which are interpreted to be altered glass shards, are consistent with transported flank breccia deposits (Cas and Wright, 1988). Flank breccias can form by gravitational instabilities caused by oversteepening and collapse of the flow/dome, tectonic activity and/or explosive eruptions that trigger collapse and slumping of a flow or dome (e.g. Cas and Wright, 1988; Fisher and Schmincke, 1984). The clasts are non-vesicular, and the only juvenile material appears to be the angular chloritized fragments, which are interpreted to be altered glass shards consistent with a phreatic eruption mechanism (e.g. Fisher and Schmincke, 1984).

4.13.3.6 Powell tuff member

Lichtblau (1989) interpreted the lower part of this unit to be a product of phreatic eruptions associated with the emplacement of the Powell rhyolite member. Lichtblau (1989) also interpreted the upper part of this unit to be the distal equivalent of the Joliet Breccia, which is located along

the northern margin of the northernmost Quemont feeder dike and was interpreted to be a seafloor crater fill deposit formed by a phreatic eruption during the emplacement of the Quemont feeder dike (De Rosen Spence, 1976; Lichtblau and Dimroth, 1980; Lichtblau, 1989). However, De Rosen Spence (1976) had interpreted the composition of the Powell tuff to be andesitic.

This study demonstrates that the lower and upper portions of the Powell tuff are homogeneous and basaltic in composition based on Zr/Ti and Nb/Y ratios (Fig. 4.6), and thus is likely unrelated to the felsic magmatism associated with emplacement of the Quemont feeder dike or the Powell rhyolite. Furthermore, the linkage between the Joliet Breccia and the Powell tuff is fully refuted by new detailed mapping and geochronology by Schofield et al., (2021), which demonstrated that the Joliet Breccia was emplaced as a discordant subsurface magmatic-hydrothermal breccia at ca. 2698 Ma. The presence of large scoriaceous blocks within the Powell tuff adjacent to the Joliet Breccia, however, suggests that this might have fortuitously been the proximal eruption site for the Powell tuff, upon which the Joliet Breccia was superimposed much later. The lapilli sized fragments, which are dispersed throughout the Powell tuff as monolithic lenses or thin beds comprise feldspar, scoria shards with bubble wall margins and angular non-vesicular altered glass shards, and are likely the distal equivalent of the proximal vent material, which was ejected into the water column during eruption. The intercalated basalt flows within the Powell tuff member further support ongoing mafic volcanism during deposition of this unit. The localized deposit of closely packed irregular amoeboid fragments (Fig. 4.7F), at the northern margin of fault block 5, adjacent to the Powell fault, suggests a proximal vent source for the basalt flows at this location. Here, the conformable and gradational transition from irregular amoeboid fragments, with minimal interstitial hyaloclastite, to overlying small pillows is consistent with the transition from volcanic spatter to more effusive pillowed flows during the waning phase of an

eruption, possibly triggered by a decrease in volatile content (Fisher and Schmincke, 1984; Sumner et al., 2005).

The scoriaceous lapilli in the Powell tuff are subordinate relative to the blocky non-vesicular altered glassy shards and consistent with a phreatomagmatic eruption mechanism (Gibson et al., 1999), as opposed to the phreatic eruption mechanism suggested by Lichtblau and Dimroth (1980), and Lichtblau (1989). Explosive hydro-volcanic eruptions typically are interpreted to indicate water depths of <700 m based on models of fuel-coolant interaction (Pecover et al., 1973). The thicker beds in the Powell tuff that are massive or display normal grading, are consistent with deposition by turbidity currents, and the thinly laminated beds, which typically show sediment draping features, are consistent with deposition by suspension sedimentation. The association of these different lithofacies within the Powell tuff, and the presence of juvenile scoria fragments suggest deposition from subaqueous pyroclastic flows, and associated submarine fallout (Fiske and Matsuda, 1964; Yamada, 1973; Gibson et al., 1999). In addition, the presence of doubly graded sequences in the cross-bedded and graded lapilli tuff and tuff facies (Fig. 4.13), is consistent with the internal organization of submarine pyroclastic flow deposits (Fiske and Matsuda, 1964; Yamada, 1973; Gibson et al., 1999). Cross-bedding, and scours, suggest deposition from unidirectional currents from the SE to the NW with respect to the current folded configuration of the rocks (Lichtblau, 1989). The presence of symmetrical ripples, and trough cross-bedding was interpreted to indicate local shallowing of the volcanic edifice to below storm wave base conditions resulting in reworking of the tuff by currents consistent with a water depth of <200m (Lichtblau and Dimroth, 1980; Lichtblau, 1989).

Convolute bedding, observed locally in the Powell tuff in proximity to ENE striking narrow brittle faults, that is often draped by plane bedded tuff, may be a product slumping triggered by

seismic activity associated with synvolcanic faults. The intercalation of the Powell tuff and Powell rhyolite, with decreasing frequency of Powell rhyolite towards the top of the Powell tuff succession, suggests coeval bimodal volcanism and that mafic volcanism, responsible for the Powell tuff, outlasted felsic volcanism associated with the localized emplacement of the Powell rhyolite.

4.13.3.7 Héré Creek rhyolite formation

The intercalation of the Héré Creek formation derived breccias with the Powell tuff member of the Powell formation suggests overlapping coeval bimodal volcanism, with no major hiatus in volcanism between these two formations. However, the occurrence of plane-bedded, laminated mafic tuff suspension deposits intercalated with the mass flow deposits of the Powell tuff suggests brief time breaks between eruptions. This is consistent with the nearly identical ages for the Powell rhyolite member of the Powell formation from this study of 2700.19 ± 0.89 Ma, which is coeval with the Powell tuff member and the rhyolite of the Héré Creek formation ("Pumphouse rhyolite") age of 2700.3 ± 1.2 Ma (McNicoll et al., 2014).

Lichtblau (1989) interpreted the basal breccia to lapillistone facies of the Héré Creek rhyolite formation to have been deposited from turbidity current deposits resulting from slumping during emplacement of the Here Creek rhyolite flow. The basal breccia to lapillistone facies is only observed in fault blocks 4 and 5, which may in part be due to post emplacement deformation and exposure, but could also indicate a localized, primary depositional basin within these fault blocks. The lobe hyaloclastite facies, which overlies the basal breccia to lapillistone facies indicates deposition of this unit occurred subaqueously (e.g. De Rosen Spence et al., 1980). The aphyric rhyolite dikes, which form the boundary between fault blocks 3 and 4, and fault blocks 5 and 6, were interpreted by De Rosen Spence (1976) and Lichtblau (1989) to be the feeders to the

texturally and compositionally similar Héré Creek rhyolite formation. The contacts between the rhyolite dikes and the overlying coherent rhyolite flows were not observed but local mapping indicates that the dikes do not extend into the Héré Creek formation.

4.13.4 Interpretation of the volcanic lithofacies of the Joliet domain

4.13.4.1 Joliet formation

The lobe-hyaloclastite morphology of the Joliet rhyolite is typical of lower viscosity submarine rhyolite flows that typically form gently-sloped (10º–20º) lava shields that rarely attain maximum heights of 500m (e.g. De Rosen Spence et al., 1980). Thus, a minimum thickness of ~1400m for the Joliet lobe hyaloclastite flow suggests that the flow was ponded within a primary depositional basin, as opposed to forming a laterally extensive but relatively low relief plateau.

The matrix of the intercalated tuff breccia to lapillistone volcaniclastic facies near the flow top, which is comprised dominantly of angular chloritized fragments with cuspate margins and fine-grained clastic material is consistent with altered hyaloclastite associated with carapace or flank breccias of lobe-hyaloclastite flows (Gibson et al., 1999). The crude bedding observed in the volcaniclastic facies indicates transport, which is also typical of flank breccias (Gibson et al., 1999). The heterolithic nature indicated locally by the presence of quartz-porphyritic rhyolite clasts, is atypical for flank breccias of rhyolite domes or autobrecciation along flow-tops (Cas and Wright, 1988). However, these clasts appear to be spatially restricted to the cross-cutting quartz porphyritic intrusions, and thus are interpreted to be a result of fragmentation and mixing of the injected dikes and sills with the wet and unconsolidated volcaniclastic host rocks. Alternatively, accidental clasts can be incorporated during mass wasting from adjacent fault scarps during synvolcanic tectonic activity or by hydrothermal becciation adjacent to intrusions. The lack of any

interbedded planar bedded tuff, suggests a continuously volcanically and tectonically active centre without a hiatus in activity to allow for suspension sedimentation.

4.13.4.2 Quemont formation

The Quemont formation was divided into five units by De Rosen Spence (1976) and subsequently subdivided to include three breccia units by Lichtblau and Dimroth (1980) and Lichtblau (1989), which they named Quemont breccia I (unit 1 of De Rosen Spence (1976)) and Quemont breccia II (unit 3 of De Rosen Spence (1976)), separated by a coherent flow banded plagioclase microporphyritic rhyolite facies (~19m thick) rhyolite facies (unit 2 of De Rosen Spence (1976)) and the Joliet breccia (steam breccia of De Rosen Spence (1976)).

De Rosen Spence (1976) interpreted the lower breccias of the Quemont formation to have been deposited during pyroclastic eruptions, followed by the massive facies (unit 4), which she interpreted as an effusive flow fed by the middle Quemont feeder dike. This volcanism was interpreted to be associated with 450m of vertical subsidence along the Quemont feeder dikes, which channeled the flow towards the east (De Rosen Spence, 1976). Similarly, Lichtblau and Dimroth (1980) and Lichtblau (1989) interpreted the Quemont breccia I to have been emplaced as a subaqueous equivalent of a co-ignimbrite lag deposit formed by the collapsed eruption columns of two subaqueous phreatic eruptions that occurred at the site of the middle Quemont feeder dike, with a brief hiatus in volcanism between eruptions to allow deposition of plane bedded tuff. Quemont breccia II was interpreted to be a flow foot breccia of the interpreted Quemont rhyolite flow (Lichtblau, 1989). The Joliet breccia was interpreted as a phreatic breccia related to the emplacement of the northernmost Quemont feeder dike (Lichtblau, 1989; De Rosen Spence, 1976), however, this has been disproved by Schofield et al. (2021) who showed that the Joliet Breccia is a younger (ca. 2698 Ma) magmatic-hydrothermal breccia unrelated to the Quemont formation.

The crude bedding, upward coarsening and fining cycles, and presence of a thin bed of laminated tuff within Quemont breccia I are consistent with vent proximal deposits of pyroclastic eruptions (Fisher and Schmincke, 1984; Cas and Wright, 1988). The dominance of non-vesicular lithic clasts is consistent with a phreatic eruption mechanism as suggested by Lichtblau (1989). The accidental blocks of mafic material and granophyre boulders could be fragments that were ripped from the conduit and/or from underlying strata during eruption, as was suggested by De Rosen Spence (1976).

The only difference between Quemont breccia I and II is the presence of quartz-porphyritic rhyolite clasts and locally quartz phenocrysts within the matrix of Quemont breccia II. The restriction and proximity of Quemont breccia II to the Quemont feeder dike and overlying massive coherent Quemont rhyolite facies suggests that the quartz-porphyritic clasts may have been derived from fragmentation and mixing of quartz-porphyritic rhyolite intrusions and the host rock either synvolcanism (i.e. pepperite) or post-volcanism as a deeper intrusion-related breccia. This is consistent with the observations of Oseguera (2014) who noted the irregularity of the contacts between the middle Quemont feeder dike with a breccia unit, which she described as a monomictic matrix-supported breccia, comprised of poorly sorted, subangular clasts (1–6cm diameter) with distinctive curviplanar margins, of quartz-feldspar porphyritic rhyolite identical to the dike. Oseguera (2014) interpreted this as peperitic contacts between the Quemont Feeder dike and host volcaniclastic facies of Quemont breccia II. This relationship and interpretation questions whether the unit mapped as a coherent Quemont rhyolite flow is truly extrusive, or an intrusion. The truncation of the upper contact of the coherent Quemont flow by the Powell fault further questions whether this unit is intrusive or extrusive. As the lower contact appears, at least in part, to be

intrusive, Quemont breccia II is interpreted as a peperitic contact between an overlying massive coherent Quemont rhyolite flow or intrusion and Quemont breccia I.

4.13.5 Volcanic reconstruction of the LBRG within the Powell Block

The new age constraints, as well as the facies analysis discussed above, suggest that strata of the Joliet and Brownlee domains are a product of two separate volcanic centers that formed during different stages of the evolution of the Noranda Volcanic Complex. A possible modern analogue would be volcanism along primitive arc or back-arc settings, such as the Kermadec arc (Gibson and Galley, 2007). Volcanic rocks in the Joliet domain are interpreted to have developed in an initial subsidence structure, bound to the north by a structure now occupied by the northernmost Quemont feeder dike, during voluminous felsic volcanism associated with the emplacement of the Joliet and Quemont formations at ca. 2702 Ma. Subsequently (~2701 Ma), this structure was reactivated and became the southern structural margin for subsidence of the Brownlee domain during emplacement of the younger Powell formation. De Rosen Spence (1976) estimated that the volcanic edifice had thickened by as much as 5000m in the Powell Block. The presence of pillowed basalt flows and lobe hyaloclastite rhyolite flows throughout the succession indicates that it remained underwater throughout volcanism, which would indicate a minimum water depth of 5500m if subsidence had not occurred (De Rosen Spence, 1976). Evidence for pyroclastic eruptions to form the Powell tuff, and possibly the lower marker, and Powell rhyolite members of the Powell formation, as well as the breccia facies of the Quemont formation is consistent with shallower water depths (<1000m) due to the limiting factor of hydrostatic pressure on explosive volcanism (e.g. McBirney, 1963; McBirney and Murase, 1971; Fisher and Schminke, 1984; Cas and Wright, 1988; Gibson et al., 1999). However, Head and Wilson (2003) argued that small volume submarine pyroclastic activity may be possible up to depths of 3000m. The

occurrence of trough cross-bedding and mud-draped ripples in the Powell tuff indicate at least localized areas with above storm wave base to intertidal settings in the Brownlee domain, suggestive of shallow but variable water depths during volcanism and synvolcanic subsidence as originally proposed by Lichtblau and Dimroth (1980).

4.13.6 Timing and setting of base metal mineralization within the Powell and Horne Blocks

The Cu-Zn-(Ag) veins cross-cut ca. 2702–2699 Ma Lower Blake River Group strata, and, like the Joliet Breccia (Schofield et al., 2021) and the broadly coeval Joliet tonalite suit, are demonstrably younger than their host rocks. The Cu-Zn-(Ag) veins, the Joliet Breccia mineralization, the Don-Rouyn and Joliet deposits share the same metal association, textures, paragenesis, and alteration types and styles as the VMS deposits in the district, consistent with their formation from similar hydrothermal fluids (Schofield et al., 2021). Massive sulfide deposits of comparable age to the Cu-Zn-(Ag) veins and the Joliet Breccia (Schofield et al., 2021) occur within Upper Blake River Group strata in the district (e.g. Mobrun, Bouchard-Hebert; Fig. 4.1). The spatial association of young ca. 2698 Ma intrusions, related magmatic-hydrothermal breccias and Cu-Zn-(Ag) mineral occurrences with early brittle NE striking structures, which are interpreted as synvolcanic structures related to ca. 2702–2699 Ma volcanism (De Rosen Spence, 1976; Lichtblau and Dimroth, 1980; Dimroth et al., 1982), attests to reactivation of these structures. Furthermore, the Don-Rouyn deposit, Joliet breccia and numerous small tonalite intrusions and magmatic-hydrothermal breccias occur within a narrow NE striking corridor along the northern edge of the northernmost Quemont feeder dike, which may reflect a deep basement structural control (Fig. 4.1). The same structural conduits are used throughout the volcanic and hydrothermal history of the Powell Block, and the variations in the characteristics of these base

metal rich deposits and occurrences likely reflect changing physiochemical conditions in time and space as a function of an evolving hydrothermal system and varying depths of emplacement.

The Quemont, Delbridge and Deldona massive sulfide lenses all within Lower Blake River Group strata of the Powell Block formed at or near the seafloor, in a seawater dominated hydrothermal system (Monecke et al., 2017). In contrast, the irregular lenses of tonalite, and associated magmatic-hydrothermal breccias, and vein to disseminated Cu-Zn-(Ag) mineral occurrences and deposits were superimposed on older volcanic strata during burial and resurgent magmatic activity, and thus are inferred to have been emplaced at a relatively deeper crustal level. The breccia pipes and associated magmatic-hydrothermal fluids may never have vented at the seafloor or be directly linked to the VMS deposits at the seafloor, but they are interpreted to be part of the same type of hydrothermal system, analogous to the porphyry–epithermal continuum of modern subaerial volcanic arcs (Sillitoe, 2010; Schofield et al., 2021). Most critically they provide the evidence for the superposition of a younger magmatic system in the same location that was arguably the site of one or more older volcanic centres. This supports the contention of Jorgensen et al. (2023) that long-lived cross-stratal permeability may have been established early but maintained to form a larger, vertically extensive magmatic hydrothermal system.

The anomalous size of the Quemont VMS deposit relative to the VMS deposits of the Flavrian block also has been attributed to a sustained, long lived and uninterrupted hydrothermal system, and its Au-enrichment to a more direct contribution of magmatic fluids and metals, and/or orogenic overprinting (Gibson and Watkinson, 1990; Kerr and Mason, 1990; Hannington et al., 1999; Franklin et al., 2005; Mercier-Langevin et al., 2011). The orogenic gold overprint is local and limited, and thus likely did not significantly contribute to the metal tenor of the Quemont and Horne VMS deposits (Taylor et al., 2014; Krushnisky, 2018; Krushnisky et al., 2020). In addition,

the combined production of the orogenic deposits in the Noranda camp remains significantly less than the approximately 10 Moz of Au produced from the Horne deposit alone (Gibson and Galley, 2007). Observations of Au enrichment at modern vent systems such as the Brothers Volcano, Kermadec Arc, New Zealand (De Ronde et al., 2011), and Susu Knolls, Manus Basin (Yeats et al., 2014), have been interpreted to indicate a magmatic fluid contribution to a seawater dominated hydrothermal system. There have been numerous studies on the Horne deposit presenting several lines of evidence that support gold enrichment through a primary magmatic-hydrothermal contribution (e.g. Kerr and Mason, 1990; Kerr and Gibson, 1993; Sharman et al., 2015; Krushnisky, 2018; Krushnisky et al., 2020). Similar studies are lacking at the Quemont deposit, due to a lack of exposure and unavailable historic data.

4.13.7 Implications for the Rouyn-Noranda mining district

The time-stratigraphic position of VMS deposits in the Horne, Powell and Flavrian Blocks have long been debated. This is due to uncertainties related to the correlation of strata across the Beauchastel and Horne Creek faults, and uncertainties related to the questionable intrusive versus extrusive emplacement of the lithologies that have been sampled for U-Pb zircon TIMS ages and used to constrain the age of strata within the three major fault blocks.

The felsic volcanic and volcaniclastic rocks of the Horne block and Joliet domain are lithologically and geochemically similar and exhibit the same transition from lower aphyric rhyolite flows to an upper volcaniclastic succession with quartz-porphyritic rhyolite clasts (Kerr and Gibson, 1993; Gibson et al., 2000; Monecke et al., 2017). The chondrite normalized REE slopes for rhyolites within the Powell and Horne Block are also similar, and the Joliet rhyolite overlaps best with the Horne rhyolite (Fig. 4.21). Felsic volcaniclastic and coherent rocks of the Horne block were interpreted to be primary and syneruptive pyroclastic deposits with localized

domes and cryptodomes that were emplaced within a linear, graben-like structure now represented by the Horne block (Kerr and Mason, 1990; Gibson and Watkinson, 1990). Similarly, the anomalously thick succession of felsic coherent and volcaniclastic rocks within the Joliet domain suggests they were emplaced within a subsidence structure (e.g. Franklin et al., 2005). In addition, the superimposition of numerous thick felsic volcanic and volcaniclastic units (Joliet, Horne, Quemont, Delbridge, Don, South Dufault and Cyprus rhyolites) within the Joliet domain and eastward indicates the presence of a major, long lived felsic monogenic volcanic centre (De Rosen Spence, 1976).

The lithostratigraphic correlations of the Quemont and Horne formations discussed above along with the geochronologic data of McNicoll et al. (2014) indicate that the Quemont and Horne deposits formed near contemporaneously during LBRG volcanism (Fig. 4.22), as initially interpreted by Spence and De Rosen Spence (1975), and De Rosen (1976). This earlier, LBRG period of volcanism and magmatism resulted in the formation of at least 9 VMS deposits within the district (Fig. 4.22; Corbet, Ansil, West Ansil, Bedford, Horne, Quemont, Fabie, Aldermac, Hébécourt), and may have locally produced the conditions favourable for the formation of Au-rich VMS deposits, such as a more direct magmatic input (Goldie, 1976; Kennedy, 1985; Gibson and Kerr, 1993; Galley, 2003; Gibson and Galley, 2007; McNicoll et al., 2014; Sharman et al., 2015) during voluminous felsic volcanism in the Joliet domain and Horne block. Thus, the two Au-rich VMS deposits of the district, Horne and Quemont, are linked in "time" and spatially to the same major felsic volcanic centre, which contrasts markedly with the bimodal-mafic dominated volcanism of the Brownlee domain and Flavrian block, which host the typical Cu-Zn VMS deposits.

Previous lithostratigraphic interpretations place the VMS deposits of the Flavrian block as coeval with the Quemont and Horne deposits (Spence and De Rosen Spence, 1975; De Rosen Spence, 1976) or coeval with the Quemont deposit and slightly younger than the Horne deposit (Dimroth et al., 1982; Gibson, 1990; Gibson and Watkinson, 1990; Kerr and Gibson, 1993). Because of uncertain geochronological constraints of the Flavrian block, correlations between the strata of the Flavrian and Powell blocks cannot be addressed with certainty. Additional U-Pb zircon dating of presumed Upper Blake River Group age formations within the Flavrian Block are in progress to address this issue.

4.14 Conclusions

The Powell Block is subdivided into, the northern Brownlee domain and the southern Joliet domain, which are separated by a quartz feldspar porphyritic rhyolite dike. These two domains are characterized by different ages and volcanic history. The Brownlee domain is characterized by mafic dominated, bimodal volcanism (ca. 2701.5–2699 Ma) and does not host any known massive sulfide deposits. The Joliet domain is characterized by a thick sequence of coherent and volcaniclastic felsic units (≥2702 Ma) and is host to the Au-rich Quemont VMS deposit. The younger age and mafic dominated volcanism of the Brownlee domain indicates it formed during progressive rifting, whereas the older and compositionally homogeneous Joliet domain represents an earlier phase of rifting with felsic magmatism derived from crustal melts without mafic magmatism. Numerous disseminated to vein style Cu-Zn-(Ag) prospects and occurrences, locally associated with discordant ca. 2698 Ma porphyritic tonalite intrusions and heterolithic subsurface breccias also occur throughout the Powell Block. These prospects and occurrences are interpreted as the deep plumbing system that may have fed VMS deposits forming higher in the stratigraphic pile at ca. 2698–2695 Ma (Schofield et al., 2021). These two styles of base metal mineralization

within the Powell Block, are separated in time, space and crustal level, and are linked to different stages of cauldron development and associated hydrothermal events (e.g., Kerr and Gibson, 1993). Thus, the Powell Block provides a window into the evolution of a volcanogenic hydrothermal system through time and space and provides a glimpse into the deep plumbing system of volcanogenic massive sulfide deposits.

The Au-rich Quemont VMS deposit is coeval with the Horne deposit to the south and both may be related to an earlier subsidence event and the construction of districts's largest monogenic felsic volcanic centre. This stage of cauldron development, may have had a more direct magmatic input (Dubé and Gosselin, 2007; Taylor et al., 2014; Sharman et al., 2015) resulting in higher Au grades than the Cu-Zn VMS deposits of the Flavrian Block, which formed in a mafic dominated bimodal volcanic setting.

4.15 Acknowledgements

Dr. Gérald Riverin and Mr. Jean Goutier are thanked for providing critical historical data. Field assistants Ms. Brittany Courchesne, Mr. Derek Leung, Mr. David Dickson, Mr. Brandon Smith, and Mr. Michael Langa are thanked for eager, competent and able assistance in the field. Yorbeau Resources Inc. are thanked for allowing the use of their rock saw facilities during the field season. Financial support was provided by Metal Earth though a Canada First Research Excellence Fund (CFREF) grant, which comprises a tri-agency initiative of the Natural Sciences and Engineering Research Council (NSERC), Social Sciences and Humanities Research Council (SSHRC), and the Canadian Institutes of Health Research (CIHR). Funding was also provided by federal, provincial, and industry partners of the Mineral Exploration Research Centre (MERC; http://merc.laurentian.ca/research/metal-earth/).

4.16 References

Ayer, J. A., Thurston, P. C., Bateman, R., Dubé, B., Gibson, H. L., Hamilton, M. A., Hathway, B., Hocker, S. M., Houlé, M. G., Hudak, G., Ispolatov, V. O., Lafrance, B., Lesher, C. M., MacDonald, P. J., Péloquin, A.S., Piercey, S.J., Reed, L. E., and Thompson, P. H. 2005. Overview of results from the Greenstone Architecture Project: Discover Abitibi Initiative; Ontario Geological Survey, Open File Report **6154**: 146 p.

Ballachey, A.G., Jamieson, W.D., and Hambleton, J.R. 1952. Mining at Quemont: Transactions of the Canadian Institute of Mining and Metallurgy and of the Mining Society of Nova Scotia. **55**: 47-58.

Barrett, T.J., MacLean, W.H. and Cattalani, S. 1991a. Massive sulphide deposits of the Noranda area Quebec. I. The Horne mine. Canadian Journal of Earth Sciences. **28**: 465-488.

Barrett, T.J., Cattalani, S., Chartrand, F., and Jones, P. 1991b. Massive sulphide deposits of the Noranda area, Quebec. II. The Aldermac mine. Canadian Journal of Earth Sciences. **28**: 1301-1327.

Barrett, T.J., Cattalani, S., Hoy, L., Riopel, J., and Lafleur, P-J. 1992. Massive sulphide deposits of the Noranda area, Quebec. IV. The Mobrun mine. Canadian Journal of Earth Sciences. **29**: 1349-1374.

Barrett, T.J., MacLean, W.H., and Cattalani, S. 1993a. Massive sulphide deposits of the Noranda area, Quebec. V. The Corbet mine. Canadian Journal of Earth Sciences. **30**: 1934-1954.

Barrett, T.J., Cattalani, S. and MacLean, W.H., 1993b, Volcanic lithogeochemistry and alteration of the Delbridge massive sulfide deposit, Noranda, Quebec; Journal of Geochemical Exploration, v. 48, p. 135-173.

Bateman, R., Ayer, J. A., Dube, B. 2008. The Timmins-porcupine gold camp, Ontario: anatomy of an Archean greenstone belt and ontogeny of gold mineralization. Economic Geology. **103** (6): 1285-1308.

Bedeaux, P., Pilote, P., Daigneault, R., Rafini, S. 2017. Synthesis of the structural evolution and associated gold mineralization of the Cadillac Fault, Abitibi, Canada. Ore Geology Reviews. **82**: 49-69.

Bleeker, W. 2012. Lode gold deposits in ancient deformed and metamorphosed terranes: The role of extension in the formation of Timiskaming basins and large gold deposits, Abitibi greenstone belt – a discussion: Ontario Geological Survey Open File Report 6280, 47-1 – 47-12.

Boldy, J. 1968. Geological observations on the Delbridge massive sulphide deposit. The Canadian Mining and Metallurgical Bulletin. **61**: 1045-1054.

Campbell, F. A. 1962. Age of mineralization at Quemont and Horne mines. The Canadian Mining and Metallurgical Bulletin. **5**: 627-630.

Campbell, I.H., Franklin, J. M., Gorton, M.P., Hart, T. R., Scott, S.D. 1981. The role of subvolcanic sills in the generation of massive sulfide deposits. Economic Geology. **76**: 2248-2253.

Carrier, A., Jébrak, M., Angelier, J.,and Holyland, P. 2000. The Silidor deposit, Rouyn-Noranda District, Abitibi belt: Geology, structural evolution, and Paleostress modelling of an Au quartz vein-type deposit in an Archean Trondjhemite. Economic Geology. **95**: 1049-1065.

Cas, R.A.F., and Wright, J.V. 1988. Modern Volcanoes and Volcanic Centres *in*: Volcanic successions modern and ancient: a geological approach to processes, products and successions, 363-409.

Cattalani, S., Maclean, W.H., Barrett, T. J. 1993. Géologie et géochimie du gisement Delbridge, Rouyn-Noranda. Gouvernement du Québec, Ministère de l'énergie et des ressources, Direction générale de l'exploration géologique et minérale, 52 p.

Daigneault, R., Mueller, W. U., and Chown, E. H. 2002. Oblique Archean subduction: accretion and exhumation of an oceanic arc during dextral transpression, Southern Volcanic Zone, Abitibi greenstone belt, Canada. Precambrian Research. **115**: 261-290.

Davis, D.W. 2002. U-Pb geochronology of Archean metasedimentary rocks in the Pontiac and Abitibi subprovinces, Québec, constraints on timing, provenance and regional tectonics; Precambrian Research, **115**: 97-117.

David, J. et al. 2010. Datations U-Pb effectuées dans les sousprovinces d'Ashuanipi, de la Grande d'Opinaca et d'Abitibi en 2008-2009. Ministère des Ressources naturelles et de la Faune Québec, report RP 2010-11, 37 p.

De Ronde et al. 2011. Submarine hydrothermal activity and gold-rich mineralization at Brothers Volcano, Kermadec Arc, New Zealand; Mineralium Deposita, **46**: 541-584.

De Rosen-Spence, A. F. 1976. Stratigraphy, development and petrogenesis of the central Noranda volcanic pile, Noranda, Quebec, Unpublished PhD thesis, Toronto, Canada, University of Toronto, 298 p.

De Rosen Spence, A., Provost, G., Dimroth, E., Gochnauer, K., Owen, V. 1980. Archean subaqueous felsic flows, Rouyn-Noranda, Quebec, Canada, and their Quaternary equivalents. Precambrian Research. **12**: 43-77.

Dimroth, E., Cousineau, P., Leduc, M., Sanschagrin, Y. 1978. Structure and organization of Archean subaqueous basalt flows, Rouyn-Noranda area, Québec, Canada; Canadian Journal of Earth Sciences, 15: **902**-918.

Dimroth, E., Imreh, L., Rocheleau, M., Goulet, N. 1982. Evolution of the south-central part of the Archean Abitibi Belt, Québec. Part I: Stratigraphy and paleogeographic model. Canadian Journal of Earth Sciences. **19**: 1729-1758.

Dimroth, E., Imreh, L., Goulet, N., Rocheleau, M. 1983. Evolution of the south-central segment of the Archean Abitibi Belt, Quebec. Part II: Tectonic evolution and geomechanical model; Canadian Journal of Earth Sciences. **20**: 1355-1373.

Dresser, J.A. and Denis, T.C. 1949. Joliet Quebec Mines Limited (Brownlee Proerty). *In* Geology of Quebec Volume 3: Economic Geology. Quebec Department of Mines, Geological Report 20. 155.

Dubé, B., Gosselin, P., Hannington, M., and Galley, A. 2007. Gold-rich volcanogenic massive sulphide deposits. In: Goodfellow W.D. (ed) Mineral Deposits of Canada: a synthesis of major deposit-types, district metallogeny, the evolution of geological provinces, and exploration methods; Geological Association of Canada, Mineral Deposits Division, Special Publication **5**: 75-94.

Dubé, B., and Gosselin, P. 2007. Greenstone-hosted quartz-carbonate vein deposits. *In* Mineral Deposits of Canada: A Synthesis of Major Deposit-Types, District Metallogeny, the Evolution of Geological Provinces, and Exploration Methods. *Edited by* W.D. Goodfellow. Geological Association of Canada, Mineral Deposits Division. Special Publication **5**: 49-73.

Dubé, B., and Mercier-Langevin, P. 2020. Gold deposits of the Archean Abitibi Greenstone belt, Canada. *In* Geology of the world's major gold deposits and provinces. *Edited by* R.H. Sillitoe, R.J. Goldfard, F. Robert, S.F. Simmons. SEG Special Publication **23**: 669-708.

Fisher, R.V. 1961. Proposed classification of volcaniclastic sediments and rocks. Geological Society of America Bulletin. **72**: 1395-1408.

Fiske, R. S., and Matsuda, T. 1964. Submarine equivalents of ash flows in the Tokiwa formation, Japan. American journal of Science. **262**: 76-106.

Fisher, R.V. and Schminke, H-U. 1984. Pyroclastic rocks. Springer, Berlin Heidelberg New York Tokyo, 1-472.

Franklin, J. M., Gibson, H. L., Jonasson, I. R., and Galley, A. G. 2005. Volcanogenic massive sulfide deposits, Economic Geology 100th anniversary Volume, 523-560.

Galley, A.G., Watkinson, D. H., Jonasson, I.R., and Riverin, G., 1995, The subsea-floor formation of Volcanic-Hosted massive sulfide: Evidence from the Ansil Deposit, Rouyn-Noranda, Canada. Economic Geology, **90**: 2006-2017.

Galley, A. G. 2003. Composite synvolcanic intrusions associated with Precambrian VMS-related hydrothermal systems. Mineralium Deposita. **38**: 443-473.

Gibson, H. L. 1990. The mine sequence of the central Noranda volcanic complex: Geology, alteration, massive sulfide deposits and volcanological reconstruction. Ph. D. thesis, Department of Earth Sciences, Carleton University, Ottawa, Ontario, Canada, 715 p.

Gibson, H. L., and Watkins, D. H. 1990. Volcanogenic massive sulphide deposits of the Noranda Cauldron and Shield Volcano, Quebec, in, Rive, M., Verpaelst, P., Gagnon, Y., Lulin, L.M., Riverin, G., and Simard, A., eds., The Northwest Quebec Polymetallic Belt: A summary of 60 years of mining exploration, Canadian Institute of Mining and Metallurgy. Special Volume **43**: 119-132.

Gibson, H. L., Morton, R. L., and Hudak, G. J. 1999. Submarine volcanic processes, deposits, and environments favorable for the location of volcanic-associated massive sulfide deposits. Reviews in Economic Geology. **8**: 13-51.

Gibson, H. L., Kerr, D. J., and Cattalani, S. 2000. The Horne mine: geology, history, influence on genetic models, and a comparison to the Kidd Creek Mine. Exploration and Mining Geology. **9**: 91-111.

Gibson, H. L., and Galley, A. G. 2007. Volcanogenic massive sulphide deposits of the Archean Noranda District, Quebec, Geological Association of Canada, Mineral Deposits Division. Special Publication **5**: 533-552.

Goldie, R., 1976, The Flavrian and Powell Plutons, Noranda area, Québec: A geological investigation of the Flavrian and Powell Plutons and their relationships to other rocks and structures of the Noranda area; unpublished PhD thesis, Queen's University, Kingston, Ontario; 381 p.

Goldie, R. J., Kotila, B., and Seward, D. 1979. The Don Rouyn mine: An Archean porphyry copper deposit near Noranda, Quebec. Economic Geology. **74**: 1680-1684.

Goodwin, A.M. 1977. Archean volcanism in Superior Province, Canadian Shield. *In* Volcanic Regimes in Canada. *Edited by* W.R.A. Barager, L.C. Coleman, and J.M. Hall. Geological Association of Canada. Special Paper **16**: 205-241.

Goulet, N., 1978, Stratigraphy and structural relationships across the Cadillac-Larder Lake Fault, Rouyn-Beauchastel area, Quebec: unpublished PhD thesis, Queen's University, Kingston, Ontario, 141p.

Goutier, J. 1997. Géologie de la région de Destor, Québec, Ministère des ressources naturelles du Québec, Rapport Géologique RG 96-13, 37p.

Hall, B. V. 1982. Geochemistry of the alteration pipe at the Amulet Upper A deposit, Noranda, Quebec. Canadian Journal of Earth Sciences. **19**: 2060-2084.

Hannington, M.D., Poulsen, K.H., Thompson, J.F.H., and Sillitoe, R.H., 1999, Volcanogenic gold in the massive sulfide environment; in C.T. Barrie, and M.D. Hannington, (eds) Volcanic-Associated Massive Sulfide Deposits: Processes and Examples in Modern and Ancient Settings; Reviews in Economic Geology, 8, p. 325-356.

Hannington, M. D., Santaguida, F., Kjarsgaard, I. M., Cathles, L. M. 2003. Regional-scale hydrothermal alteration in the Central Blake River Group, westerm Abitibi subprovince, Canada: implications for VMS prospectivity. Mineralium Deposita. **38**: 393-422.

Harquail, J. A. 1951. Joliet-Quebec Mines Ltd. Underground drilling program 1950-1951. Quebec Department of Mines, Mineral Deposit Branch, GM20600, 27 p.

Hart, T. R., Gibson, H. L., and Lesher, C. M. 2004. Trace element geochemistry and petrogenesis of felsic volcanic rocks associated with volcanogenic massive Cu-Zn-Pb sulfide deposits. Economic Geology. **99**: 1003-1013.

Head, J.W., and Wilson, L. 2003. Deep submarine pyroclastic eruptions: theory and predicted landforms and deposits. Journal of volcanology and geothermal research. **121**: 155-193.

Hubert, C., Trudel, P., and Gélinas, L. 1984. Archean wrench fault tectonics and structural evolution of the Blake River Group, Abitibi Belt, Quebec. Canadian Journal of Earth Sciences. **21**: 1024-1032.

Ispolatov, V., Lafrance, B., Dubé, B., Creaser, R., and Hamilton, M. 2008. Geologic and structural setting of gold mineralization in the Kirkland Lake-Larder Lake gold belt, Ontario. Economic Geology. **103**: 1309-1340.

Jackson, S.L., Cruden, A.R., White, D., and Milkereit, B. 1995. A seismic-reflection-based regional cross section of the southern Abitibi greenstone belt. Canadian Journal of Earth Sciences. **32**: 135-148.

Jebrak, M., Harnois, L., Carrier, A., and Lafrance, J. 1997. The Don Rouyn-Cu-Au porphyry system; *in* J. F. Couture, and F. Robert eds., Atypical gold deposits in the Abitibi Belt, Geological Association of Canada, Field Trip B5 guide, Ottawa, 1997, 72-78.

Kaloperopoulos, S.I., and Scott, S.D. 1989. Mineralogy and geochemistry of an Archean tuffaceous exhalite: The main contact tuff, Millenbach mine area, Noranda, Québec. Canadian Journal of Earth Sciences. **26**: 88-105.

Kennedy, L. P. 1985. The geology and geochemistry of the Archean Flavrian Pluton, Noranda, Quebec, Unpublished PhD thesis, The University of Western Ontario, London, Ontario, Canada, 491 p.

Kerr, D. J., and Mason, R. 1990. A re-appraisal of the geology and ore deposits of the Horne mine complex at Rouyn-Noranda, Quebec. Candian Institute of Mining and Metallurgy Special Volume **43**: 153-165.

Kerr, D. J., and Gibson, H. L. 1993. A comparison of the Horne volcanogenic massive sulfide deposit and intracauldron deposits of the Mine sequence, Noranda, Quebec. Economic Geology. **88**: 1419-1422.

Kirkham, R.V. 1972. Geology of Copper and Molybdenum deposits; in Report of Activities, Part A, Geological Survey of Canada, Paper 72-1A: 82-87.

Knuckey, M. J., Comba, C.D.A., Riverin, G. 1982. Structure, metal zoning and alteration at the millenbach deposit, Noranda, Quebec. *In* Precambrian Sulphide Deposits. *Edited by* R.W. Hutchinson, C.D. Spence, and J.M. Franklin. Geological Association of Canada Special Paper **25**: 255-295.

Knuckey, M.J., and Watkins, J.J. 1982. The geology of the Corbet massive sulphide deposit Noranda district, Québec, Canada. *In* Precambrian Sulphide Deposits. *Edited by* R.W. Hutchinson, C.D. Spence, and J.M. Franklin. Geological Association of Canada Special Paper **25**: 297-317.

Kotila, B.W. 1975. An Archean porphyry copper deposit: The Don Rouyn mine, Noranda, Québec, Kingston, Ontario. B.Sc. thesis, Queen's University, Kingston, Ontario, 21 p.

Krogh, T.E. 1973. A low contamination method for hydrothermal decomposition of zircon and extraction of U and Pb for isotopic age determinations. Geochimica et Cosmochimica Acta. **37**: 485-494.

Krushnisky, A. 2018. Controls on gold enrichment at the Horne 5 Archean VMS deposit, Abitibi Greenstone Belt, Québec. MSc thesis, Université du Québec, Institute national de la recherché scientifique, Québec City, Québec, Canada, 238 p.

Krushnisky, A., Mercier-Langevin, P., Ross, P.S., Goutier, J., Pilote, C, Bernier, C. 2020. Geology and gold enrichment at the Horne 5 Archean volcanogenic massive sulpide deposit, Abitibi greenstone belt, Québec: a synthesis. *In* Targeted Geoscience Initiative 5: contributions to the understanding of Canadian gold systems. *Edited by* P. Mercier-Langevin, C.J.M. Lawley, S, Castonguay, 31-44. https://doi.org/10.4095/323663

Laurin, J. 2009. Geology, gold mineralization and alteration of the Horne West property Rouyn-Noranda. MSc thesis, Department of Earth Sciences, University of Ottawa, Ottawa, Canada, 172 p.

Lemieux, P., 2007; Propriété South-Dufault, Cyprus, Pinkos, Cantons de Rouyn et de Dufresnoy, SNRC 32D/06 . Ministère des ressources naturelles et de la Faune, Québec, Assessment Report GM 63059, 156 p.

L'Hereux, M. 1992. Caractérisation géochimique des volcanites et d'une cheminée d'alteration dans la partie ouest du bloc de Powell, Rouyn-Noranda, Quebec. MSc thesis, Université du Québec a Chicoutimi, Québec, Canada, 116 p.

Lichtblau, A. P. 1989. Stratigraphy and facies at the south margin of the Archean Noranda Caldera. MSc thesis, L'Université du Québec a Chicoutimi, Québec, Canada, 148 p.

Lichtblau, A. P., and Dimroth, E. 1980. Stratigraphy and facies at the south margin of the Archean Noranda Caldera, Noranda, Quebec. Current research, Part A, Geological Survey of Canada, Paper 80-1A, 68-76.

Ludwig, K.R. 2009. User's manual for Isoplot 3.71 a geochronological toolkit for Excel; Berkeley Geochronological Center. Special Publication **4**, 72 p.

Mattinson, J. 2005. Zircon U-Pb chemical abrasion (CA-TIMS) method: Combined annealing and multi-step partial dissolution analysis for improved precision and accuracy of zircon ages. Chemical Geology. **220**: 47-66.

McBirney, A.R. 1963. Factors governing the nature of submarine volcanism; Bulletin of Volcanology, **30**: 337-363.

McBirney A.R. and Murase, T. 1971. Factors governing the formation of pyroclastic rocks. Bulletin of Volcanology. **34**: 372-384.

McNicoll, V., Goutier, J., Dubé, B., Mercier-Langevin, P., Ross, P. S., Dion, C., Monecke, T., Legault, M., Percival, J., Gibson, H. 2014. U-Pb Geochronology of the Blake River Group, Abitibi Greenstone Belt, Quebec, and implications for base metal exploration. Economic Geology. **109**: 27-59.

Mercier-Langevin, P., Hannington, M., Dubé, B., Bécu, V. 2011. The gold content of volcanogenic massive sulfide deposits, Mineralium Deposita. **46**: 509-539.

Monecke, T., Gibson, H., Dubé, B., Laurin, J., Hannington, M. D., Martin, L. 2008. Geology and volcanic setting of the Horne deposit, Rouyn-Noranda, Québec: Initial results of a new research project. Geological Survey of Canada, Current Research 2008-9, 16 p.

Monecke, T., Gibson, H. L., Goutier, J. 2017. Volcanogenic massive sulfide deposits of the Noranda camp. Reviews in Economic Geology. **19**: 169-223

Moore, L. N., Daigneault, R., Aird, H.M., Banerjee, N.R., Mueller, W.U. 2016. Reconstruction and evolution of Archean intracaldera facies: the Rouyn-Pelletier Caldera Complex of the Blake River Group, Abitibi greenstone belt, Canada, Canadian Journal of Earth Sciences. **53**: 355-377.

Morris, H. R. 1957. Surface Geology Anglo-Rouyn and North Part of Powell-Rouyn properties, Rouyn Twp., N.W. Quebec; unpublished geological map for Héré Fault Copper Ltd., 3 sheets, one inch to 200 feet.

Morris, H.R. 1959. Surface Geology, Joliet Quebec Mines; unpublished geological map, 3 sheets, one inch to 200 feet.

Mortensen, J.K. 1987. Preliminary U-Pb zircon ages for volcanic and plutonic rocks of the Noranda-Lac Abitibi area, Abitibi subprovince, Quebec: Geological Survey of Canada Current Research, Part A, Paper 87-1A, 581-590.

Mortensen, J. K. 1993. U-Pb geochronology of the eastern Abitibi subprovince. Part 2: Noranda-Kirkland Lake area. Canadian Journal of Earth Sciences. **30**: 29-41.

Mueller, W. U., Stix, J., Corcoran, P. L., and Daigneault, R. 2009. Subaqueous calderas in the Archean Abitibi greenstone belt: an overview and new ideas. Ore Geology Reviews. **35**: 4-46.

North American Commission on Stratigraphic Nomenclature. 2005. North American Stratigraphic Code. AAPG Bulletin. **89**: 1547-1591.

Oseguera, O. 2014. The significance of magma mingling and mixing during the formation of the host-rock successions of Archean massive sulfide deposits in the Noranda Camp, Abitibi Subprovince, Quebec. MSc thesis, Colorado School of Mines, Golden, Colorado, 117 p.

Pearce, J.A. 1996. A user's guide to basalt discrimination diagrams, in: Bailes, A.H. (Eds.), Trace Element Geochemistry of Volcanic Rocks: Applications for Massive Sulfide Exploration. Geological Association of Canada, Short Course Notes, **12**: 79-113.

Pearson, V., and Daigneault, R. 2009. An Archean megacaldera complex: The Blake River Group, Abitibi greenstone belt. Precambrian Research. **168**: 66-82.

Pecover, R.S., Buchanan, D.J., and Ashby, D.E. 1973. Fuel-coolant interaction in submarine volcanism. Nature. **245**: 307-308.

Piette-Lauzière, N., Guillmette, C., Bouvier, A., Perrouty, S., Pilote, P., Gaillard, N., Lypaczewski, P., Linnen, R. L., Olivo, G. R. 2019. The timing of prograde metamorphism in the Pontiac Subprovince, Superior craton; implications for Archean geodynamics and gold mineralization. Precambrian Research. **320**: 111-136.

Poulsen, K.H. 2017. The Larder Lake Cadillac Break and its gold districts, Reviews in Economic Geology. **19**: 133-167.

Powell, W.G., Carmichael, D.M., and Hodgson, C.J. 1995. Conditions and timing of metamorphism in the southern Abitibi greenstone belt, Quebec. Canadian Journal of Earth Sciences. **32**: 787-805.

Riverin, G. and Hodgson. C.J., 1980, Wallrock alteration at the Millenbach Cu-Zn Mine, Noranda, Quebec; Economic Geology, v. 75, p.424-444.

Riverin, G., Labrie, M., Salmon, B., Asselin, R., and Gagnon, M., 1990, The Geology of the Ansil deposit, Rouyn-Noranda, Quebec, in, Canadian institute of Mining and metallurgy, Special Volume 43, p. 143-151.

Robert, F. 1989. Structural setting and control of gold-quartz veins of the Val d'Or area, southern Abitibi subprovince. University of Western Australia, Geology Department (Key Centre) and University Extension, short course notes. **24**: 167-209.

Robinson, W.G. 1949. Mining property report for 1948, Eldona Gold Mines Ltd. 7p.

Ross, P. S., and Bedard, J. H. 2009. Magmatic affinity of modern and ancient subalkaline volcanic rocks determined from trace-element discriminant diagrams. Canadian Journal of Earth Sciences. **46**: 823-839. https://doi.org/10.1139/e09-054

Ryznar, G., Campbell, F. A., and Krouse, H. R. 1967. Sulfur isotopes and the origin of the Quemont orebody. Economic Geology. **62**: 664-678.

Sangster, D.F. 1980. Quantitative characteristics of volcanologenic massive sulphide deposits 1. Metal content and size distribution of massive sulphide deposits in volcanic centres. Canadian Institute of Mining and Metallurgy Bulletin. **73**: 74-81.

Santaguida, F., Gibson, H.L. and Watkinson, D.H. 1999. Hydrothermal alteration mineral assemblages associated with volcanic-hosted massive sulphide mineralization in the Noranda area, Quebec. Geological Association – Mineralogical Association of Canada, Sudbury Meeting, 57p.

Schofield, M., Gibson, H., Lafrance, B., Poulsen, K. H., Marsh, J., Hamilton, M. A., Jørgensen, T.R.C. 2021. Recognizing subsurface breccias in Archean terranes: implications for district scale metallogeny; Precambrian Research. **361**, 106264. https://doi.org/10.1016/j.precmres.2021.106264

Scott, J. S. 1948. Quemont mine. Structural geology of Canadian ore deposits, a symposium arranged by a committee of the geology division. Canadian institute of mining and metallurgy, 773-776.

Scott, S.D. 1980. Geology and structural control of Kuroko-type massive sulphide deposits; in The Continental Crust and Its Mineral Deposits, edited by D.W. Strangway; Geological Association of Canada, Special Paper **20**: 705-721

Setterfield, T. N., Hodder, R. W., Gibson, H. L., Watkins, J. J. 1995. The McDougall-Despina Fault set, Noranda, Quebec: Evidence for fault-controlled volcanism and hydrothermal fluid flow. Exploration Mining Geology. **4** (4): 381-393.

Sharman, E. R., Taylor, B. E., Minarik, W. G., Dubé, B., Wing, B. A. 2015. Sulfur isotope and trace element data from ore sulfides in the Noranda district (Abitibi, Canada): implications for volcanogenic massive sulfide deposit genesis. Mineralium Deposita. **50**: 591-606.

Sillitoe, R.H., 2010. Porphyry copper systems. Economic Geology. **105**: 3–41. https://doi.org/10.2113/gsecongeo.105.1.3

Simmons, B.D. 1973. Geology of the Millenbach massive sulphide deposit, Noranda, Québec. Canadian Institute of Mining and Metallurgy Bulletin. **66**: 67-78.

Smith, R.L. and Bailey, R.A. 1968. Resurgent Cauldrons. *In*: Studies in Volcanology, *Edited by* R.R. Coats, R.L. Hay, C.A. Anderson; Gelogical Society of America Memoirs **116**: 613-662.

Spence, C.D. 1967. The Noranda Area. Canadian Institute of Mining and Metallurgy. Centennial Field Excursion Guidebook: 36-39.

Spence, C. D., De Rosen-Spence, A. F. 1975. The place of sulfide mineralization in the volcanic sequence at Noranda, Quebec, Economic Geology. **70**: 90-101.

Stacey, J.S. and Kramers, J.D. 1975. Approximation of terrestrial lead isotope evolution by a two-stage model. Earth and Planetary Science Letters. **26**: 207-221.

Sumner, J.M., Blake, S., Matela, R.J., and Wolff, J.A. 2005. Spatter; Journal of Volcanology and Geothermal Research, **142**: 49-65.

Sun, S.S., and McDonough, W. F. 1989. Chemical and isotopic systematics of oceanic basalts: implications for mantle composition and processes. *In* Magmatism and ocean basins. Edited by A.D. Saunders, and M.J. Norry. Geological Society of London. 313-345.

Taylor, B. 1953. Geology of Quemont Mining Corporation Ltd. Geology and mineral deposits of northwestern Québec. Guidebook Field Trip, No. 10, Annual meeting GSA and GAC, 15 p.

Taylor, B. 1957. Quemont mine, Structural geology of Canadian ore deposits. Geology Division, Canadian Institute of Mining and Metallurgy. **2**: 405-412.

Taylor, B. E., De Kemp, E., Grunsky, E., Martin, L., Maxwell, G., Rigg, D., Goutier, J., Lauzière, K., and Dubé, B. 2014. Three-dimensional visualization of the Archean Horne and Quemont Au-Bearing Volcanogenic Massive Sulfide Hydrothermal Systems, Blake River Group, Québec. Economic Geology. **109**: 183-203.

Thurston, P.C., Ayer, J.A., Goutier, J., and Hamilton, M.A. 2008. Depositional gaps in the Abitibi greenstone belt stratigraphy: A key to exploration for syngenetic mineralization; Economic Geology, **103:** 1097-1134.

Verpaelst, P., Péloquin, S., Adam, E., Barnes, A. E., Ludden, J., Dion, D. J., Hubert, C., Milhereit, B., and Labrie, M. 1995. Seismic reflection profiles across the "Mine Series" in the Noranda camp of the Abitibi belt, eastern Canada, Canadian Journal of Earth Sciences. **32**: 167-176.

Waters, A.C. 1960. Determining direction of flow in basalts; American Journal of Science, **258**: 350-366.

Weeks, R. M. 1963. The relative ages of the chalcopyrite and the rhyolite dykes in the rhyolite dyke zone orebodies at Quemont mine, Québec. MSc thesis, Dalhousie University, Halifax, Nova Scotia, Canada, 143 p.

Weeks, R.M. 1967. Quemont Mining Corporation, Limited, in Abel, M. K., ed., CIMM centennial field excursion northwestern Quebec-northern Ontario: Montreal, Canadian Institute of Mining and Metallurgy, 46-51.

White, J.D.L., and Houghton, B.F. 2006. Primary volcaniclastic rocks. Geology. **34** (8): 677-680.

Wilkinson, L., Cruden, A.R., Krogh, T.E. 1999. Timing and kinematics of post-Timiskaming deformation within the Larder Lake - Cadillac deformation zone, southwest Abitibi greenstone belt, Ontario, Canada. Canadian Journal of Earth Sciences. **36**: 627–647. https://doi.org/10.1139/e99-015

Williams, H., and McBirney, A.R. 1979. Volcanoes. Freeman, Cooper and Company, 397p.

Wilson, M. E. 1941. Geological Survey of Canada Memoir 229, 162 p.

Wilson, M.E. 1956. Early Precambrian rocks of the Timiskaming region, Quebec and Ontario, Canada: Geological Society of America Bulletin, **67**: 1397-1430.

Wilson, R. 2012. Hydrothermal Iron-Carbonate alteration associated with volcanogenic massive sulfide (VMS) deposits in cycle IV of the Noranda Mining Camp, Rouyn-Noranda, Quebec. MSc thesis, University of Ottawa, Ottawa, Ontario, Canada, 329 p.

Yamada, E. 1973. Subaqueous pumice flow deposits in the Onikobe Caldera, Miyagi prefecture, Japan. Journal of the geological society of Japan. **79** (9): 585-597.

Yamagashi, H., and Dimroth, E. 1985. A comparison of Miocene and Archean rhyolite hyaloclastites: Evidence for a hot and fluid rhyolite lava; Journal of volcanology and geothermal research, **23**: 337-355.

Yeats, C. J., Parr, J. M., Binns, R. A., Gemmell, J. B., Scott, S. D. 2014. The SuSu Knolls hydrothermal field, eastern Manus Basin, Papua New Guinea: An active submarine high-sulfidation copper-gold system. Economic Geology. **109**: 2207-2226.

4.17 Tables

Table 4-1: Zircon CA-ID-TIMS U-Pb isotopic data for Powell Block rhyolites.

Fraction	Description	U ppm	Pb^T pg	Pb_c pg	Th/U	$^{206}Pb/^{204}Pb$	$^{206}Pb/^{238}U$	± 2σ	$^{207}Pb/^{235}U$	± 2σ	$^{207}Pb/^{206}Pb$	± 2σ	Ages (Ma) $^{206}Pb/^{238}U$	± 2σ	$^{207}Pb/^{235}U$	± 2σ	$^{207}Pb/^{206}Pb$	± 2σ	Disc. (%)
18MDS-0121; Powell rhyolite																			
Z1	1 clr, cls, brkn tip	120	71.06	0.79	0.477	5133	0.521371	0.001162	13.31405	0.03518	0.185209	0.000197	2705.0	4.9	2702.2	2.5	2700.1	1.8	-0.2
Z2	1 clr, cls, shrt pr, incl	140	82.74	1.51	0.500	3115	0.520560	0.001109	13.29307	0.03602	0.185205	0.000232	2701.6	4.7	2700.7	2.6	2700.0	2.1	-0.1
Z3	1 clr, cls, flat, fct pr, crk, incl	130	77.37	1.70	0.497	2580	0.521989	0.001260	13.32974	0.04008	0.185208	0.000269	2707.6	5.3	2703.3	2.8	2700.1	2.4	-0.3
Z4	1 clr, cls, el, brkn, sq, axial incl	165	98.95	2.22	0.565	2500	0.520629	0.001029	13.29591	0.03640	0.185220	0.000255	2701.8	4.4	2700.9	2.6	2700.2	2.3	-0.1
Z5	1 clr, cls, sq, gemmy, minor incl	141	83.90	1.17	0.505	4038	0.521073	0.001089	13.31006	0.03421	0.185259	0.000214	2703.7	4.6	2701.9	2.4	2700.5	1.9	-0.1
19MDS-0149; Qz-phyric clast in volcaniclastic unit (Brownlee rhyolite)																			
Z1	1 clr, cls, subeq, gemmy pr, minor incl	127	74.73	0.42	0.473	10039	0.518144	0.001657	13.18406	0.04562	0.184543	0.000191	2691.3	7.0	2692.9	3.3	2694.1	1.7	0.1
Z2	1 clr, cls, 2:1 gemmy oz pr, incl	113	66.19	0.28	0.447	13466	0.518895	0.002882	13.23192	0.07656	0.184945	0.000247	2694.5	12.2	2696.3	5.5	2697.7	2.2	0.1
Z3	1 clr, cls, stubby, sq, fct pr, incl	95	56.21	0.24	0.491	13369	0.520008	0.001965	13.27402	0.05283	0.185136	0.000185	2699.2	8.3	2699.3	3.8	2699.4	1.6	0.0
Z4	1 clr, cls, ~flat, fct pr, incl	105	62.36	0.34	0.500	10381	0.519691	0.001358	13.27069	0.03881	0.185202	0.000174	2697.9	5.8	2699.1	2.8	2700.0	1.6	0.1

Notes:
All analyzed fractions represent best optical quality (crack-, inclusion-, core-free), fresh (least altered) grains of zircon.
Zircons were chemically abraded.

Abbreviations: Z - zircon; clr - clear; cls - colourless; crk - cracked; el - elongate; subeq - subequant; pr - prism/prismatic; fct - faceted; oz - oscillatory zoned; brkn - broken; incl - inclusions (rod/bubble/mineral); shrt - short; sq - square cross-section.
Pb^T is total amount (in picograms) of Pb.
Pb_C is total measured common Pb (in picograms) assuming the isotopic composition of laboratory blank: 206/204 - 18.49±0.4%; 207/204 - 15.59±0.4%; 208/204 - 39.36±0.4%.
Pb/U atomic ratios are corrected for spike, fractionation, blank, and, where necessary, initial common Pb; 206Pb/204Pb is corrected for spike and fractionation.
Th/U is model value calculated from radiogenic 208Pb/206Pb ratio and 207Pb/206Pb age, assuming concordance.
Disc. (%) - per cent discordance for the given 207Pb/206Pb age.
Uranium decay constants are from Jaffey et al. (1971).

Table 4-2: Characteristic features of formations and members of LBRG strata of the Powell Block

Formation/ Member	Facies	Definition	Dist.	Thickness	Contact relationships	Geochemistry	Age	Paleoenvironment
Joliet rhyolite	**1a**	Flow banded, spherulitic, amygdaloidal, feldspar microphyric rhyolite lobe hyaloclastite flows.	2.5 km	~680 m	Cross-cut by Powell Intrusive Complex and quartz-porphyritic (1-2mm diameter; 10-15%) rhyolite sills and Quemont feeder dike	SiO2 = 75-78% TiO2 = 0.2 La/Ybn = 2.2-2.5 Ybn = 20-23 Zr/Ti = 0.1 Nb/Y = 0.2 Eu/Eu* = 0.4-0.5	-	Submarine effusive volcanism
	1b	Crudely bedded, polymictic, poorly sorted lapillistone to tuff breccia comprised of angular, non-vesicular clasts of aphyric rhyolite (70%), quartz pyric rhyolite (5-10%), chloritized mafic (10-20%) and sporadic juvenile fragments (1%). Clast size ranges from 1-10cm, with local blocks ≥40cm in diameter. Minimal matrix material (~5-10%) comprised of chloritized and sericitized vesicular glass shards and a granular mixture of finer clastic material.	2.5 km	~320 m	"	-	-	Submarine debris flows (flank breccias)
Quemont rhyolite	**2a**	Tuff breccia, lapillistone to lapilli tuff. Polymictic comprised of quartz-porphyritic rhyolite clasts (60%), chloritized mafic clasts (20-25%), and aphyric rhyolite clasts (15-20%). Massive to crudely bedded, locally displaying reverse to normal grading and occasional scouring. Clasts are subangular to subrounded, dominantly non-vesicular, and equant to tabular in morphology. The matrix component (10%) is fine-grained, comprised of chloritized glass shards.	1.5 km	~270 m	Conformable contact with underlying Joliet formation. Cross-cut by Powell Intrusive Complex and quartz-porphyritic (1-2mm diameter; 10-15%) rhyolite sills and Quemont feeder dike	-	-	Submarine Phreatic eruption?
	2b	Massive flow-banded quartz (1–2 mm; 10%) porphyritic rhyolite.	1.5 km	~415 m	"	SiO_2 = 74-76.8% TiO_2 = 0.2% La/Yb_n = 2.1-2.3 Yb_n = 27-28 Zr/Ti = 0.14-0.18 Nb/Y = 0.26-0.29 Eu/Eu* = 0.7	2702.0 ± 0.8 Ma	Submarine effusive volcanism and/or intrusion

Brownlee Rhyolite	**3a**	Flow banded, spherulitic, amygdaloidal (~20%), feldspar microphyric rhyolite lobe hyaloclastite flows and planar columnar jointed sheeted flows.	1.3 km	~360 m	Cross-cut by Powell Intrusive Complex and aphyric felsic dikes	SiO2 = 65-73% TiO2 = 0.5-0.8 La/Yb_n = 1.9-4.4 Yb_n = 19-29 Zr/Ti = 0.05-0.09 Nb/Y = 0.2 Eu/Eu* = 0.3-0.7	-	Submarine effusive volcanism
	3b	Heterolithic lapillistone, crudely bedded, angular-subrounded fragments ~2mm-50mm diameter, of flow banded or massive feldspar microphyric rhyolite, angular chloritized fragments with cuspate margins and accidental quartz (1-3mm; 10-15%) porphyritic rhyolite. Matirix is fine-grained and contains quartz crystals ~10%, ≤1mm in diameter	1.3 km	~15 m	"	-	2699.7 ± 1.1 Ma	Submarine Debris flow
Lower Powell Andesite	**4**	Amygdaloidal (~1–5%) and dominantly microporphyritic with euhedral feldspar (~1%; 0.5–1mm) microphenocrysts, within a pilotaxitic matrix comprised of fine grained feldspar microlites, quartz and interstitial chlorite. Massive, Pillowed and Brecciated, but massive facies predominates. Individual flows typically range from 5–25m thick, but locally may reach thicknesses of 70–150m.	2.8 km	200-110 m	Contact between brownlee formation and Lower Powell Andesite not observed. Cross-cut by aphyric rhyolite dikes/sills, mafic dikes/sills and lamprophyre dikes	SiO_2 = 53-58% TiO_2 = 1.0-1.4 La/Yb_n = 2.2-4.6 Yb_n = 14-15 Zr/Ti = 0.01-0.02 Nb/Y = 0.2-0.3 Eu/Eu* = 0.6-1.1	-	Submarine effusive volcanism
Lower Marker Unit	**5**	Polymictic, bedded and normally graded aphyric rhyolite lapillistone to tuff. Highly rounded, non-vesicular clasts of aphyric rhyolite. Large blocks (~20cm–2m diameter) of broken pillowed andesite and occasionally complete pillows are incorporated into the base of this member.	~2.5 km	5-10m	Sharp conformable contact with underlying and overlying basalt flows	SiO_2 = 62.4-81.9% TiO_2 = 0.21-0.86 La/Ybn = 2.0-2.6 Ybn = 22-27 Zr/Ti = 0.04-0.15 Nb/Y = 0.20-0.26 Eu/Eu* = 0.3-0.5	-	Submarine Debris flow
Upper Powell Andesite	**6**	Amygdaloidal (~1–5%) and dominantly microporphyritic with euhedral feldspar (~1%; 0.5–1mm) microphenocrysts, within a pilotaxitic matrix comprised of fine grained feldspar microlites, quartz and interstitial chlorite. Massive, Pillowed and Brecciated, but massive facies predominates. Individual flows range from 5m-40m thick.	2.8 km	150-330 m	Sharp conformable contact with overlying Powell rhyolite formation. Cross-cut by aphyric rhyolite dikes/sills, mafic dikes/sills and lamprophyre dikes.	SiO_2 = 52.5-63.5% TiO_2 = 1.1-1.4 La/Yb_n = 1.4-4.4 Yb_n = 12-19 Zr/Ti = 0.01-0.02 Nb/Y = 0.2-0.3 Eu/Eu* = 0.5-1.4	-	Submarine effusive volcanism

Powell Rhyolite	**7a**	Coherent aphyric, spherulitic rhyolite	~800 m	~30-50 m	Cross-cut by aphyric rhyolite dikes/sills	SiO_2 = 64-80% TiO_2 = 0.3-0.7 La/Yb_n = 1.7-3.2 Yb_n = 25-37 Zr/Ti = 0.06-0.17 Nb/Y = 0.22-0.28 Eu/Eu* = 0.2-0.6	-	Stubby rhyolite dome forming along fissure
	7b	Coherent flow-banded, spherulitic, columnar jointed, quartz (1–3 mm; 10-15%) porphyritic rhyolite. Upper contact is characterized by angular jig-saw fit breccia, infiltrated by overlying Powell tuff.	~800 m	~10-30 m	Cross-cut by aphyric rhyolite dikes/sills		2700.19 ± 0.89 Ma	Stubby rhyolite dome forming along fissure
	7c	Crudely bedded, breccia to tuff breccia. The blocks are subangular to subrounded and consist dominantly of non-vesicular quartz-phyric rhyolite, but highly chloritized, aphanitic fragments (~1–6cm in diameter), which weather recessively can make up to 10% of the fragments. The matrix is fine-grained, chloritized and contains quartz crystals. This facies is intercalated with the lower 40m of the Powell tuff member.	~800 m	~25-80 m	Cross-cut by aphyric rhyolite dikes/sills		-	Submarine debris flow from collapsed rhyolite dome
Powell tuff	**8a**	~10-50cm thick beds displaying normal or reverse to normal grading, often internally unlaminated except for the finer upper or lower portion of beds. Planar cross-bedding, and scours are common sedimentary features.	1200 m	40-170 m	Cross-cut by aphyric rhyolite dikes/sills, quartz-phyric rhyolite dikes/sills, gabbro sills and lamprophyre dikes. Interbedded with mafic flows. Breccia facies of Powell rhyolite is intercalated with lower portion of tuff, upper portion is intercalated with basal breccia of Here Creek rhyolite formation.	SiO_2 = 55.8% TiO_2 = 0.81 La/Yb_n = 1.8-2.4 Yb_n = 5-10 Zr/Ti = 0.02 Nb/Y = 0.3 Eu/Eu* = 1.1-1.4	-	Pyroclastic flow from a submarine phreatomagmatic eruption originating in the SE and travelling to the NW

	8b	~1-2mm thick planar and well sorted laminae of lapilli tuff and tuff. Loaded symmetrical ripples, trough cross-bedding locally and minor convolute bedding beneath large blocks of quartz-phyric rhyolite.	1200 m	40-170 m	Cross-cut by aphyric rhyolite dikes/sills, quartz-phyric rhyolite dikes/sills, gabbro sills and lamprophyre dikes. Interbedded with mafic flows. Breccia facies of Powell rhyolite is intercalated with lower portion of tuff.	SiO_2 = 55.8% TiO_2 = 0.81 La/Yb_n = 1.8-2.4 Yb_n = 5-10 Zr/Ti = 0.02 Nb/Y = 0.3 Eu/Eu* = 1.1-1.4	-	Suspension fall out tuff from a submarine phreatomagmatic eruption, with minor reworking by shallow subaqueous currents
Here Creek Rhyolite	**9a**	Bedded monomictic tuff breccia, breccia and lapillistone beds of aphyric rhyolite, which show both reverse and normal grading. Very thickly bedded (0.5–2m), which are not internally laminated. Fragments are angular, occasionally flow-banded, spherulitic and non-vesicular and range in size from ~1cm–40cm in diameter. The matrix is fine-grained and leucocratic. Sharp basal contacts with occasional scours are observed.	~19km	~40-150m	Intercalated with the upper portion of the Powell tuff, sharp conformable contacts.	SiO_2 = 68.5-75.8% TiO_2 = 0.2-0.4% La/Yb_n = 3.1-3.5 Yb_n = 26-35 Zr/Ti = 0.13-0.24 Nb/Y = 0.19-0.32 Eu/Eu* = 0.3-0.6	2700.3 ± 1.2 Ma	Submarine debris flow
	9b	Coherent amygdaloidal, columnar jointer, spherulitic, aphyric rhyolite. Consists of a lower lobe hyaloclastite rhyolite and an upper coherent featureless rhyolite.	~19km	~870-1050m				Submarine effusive volcanism

Table 4-3: Summary of base metal deposits and occurrences within the Powell Block, Rouyn-Noranda.

Mine/*Occurrence*	Lode mineralogy	Discovery (and Production)	Tonnage (t)	Grade	Trend and dip	Length (m)	Width (m)	Depth (m)	Wall-rock alteration
Quemont	Py, Po, Sph, Cpy, Mgt	1945 (1949-1971)	16,650,000	1.2% Cu 1.8% Zn 5.5 g/t Au 18 g/t Ag				61	Chl-Ser
Delbridge	Py, Sph, Cpy, Gn, Tet, Ag, Aspy	1965 (1969-1971)	0.36 Mt	0.55% Cu 8.6% Zn 2.40 g/t Au 68.60 g/t Ag				91	Chl, Ser, Calc, Fe-Carb
Deldona	Py, Sph, Cpy, Tet, Au, El, Aspy, Ag, Tm	1947 (1950-1952)	0.09 Mt	0.3% Cu 5% Zn 4.1 g/t Au 26.00 g/t Ag				152	Chl, Ser, Calc, Fe-Carb
Joliet[1]	Qtz, Ank, Py, Cpy, Au	1922 (1954-1974)	2,818,182	1.12% Cu 8 g/t Ag 0.3 g/t Au	S / moderate		50	200	Chl-Ser
Don-Rouyn	Qtz, Ank, Hmt, Au, Cpy, Py, Mo, Bo	1925 (1958-1980)	36,000,000	0.15% Cu 0.3 - 1 g/t Au					Hmt
Powell F-Zone[2]	Cpy, Qtz, Py, Ag, Sph, Au	1929	25,000	7.88% Cu 98 g/t Ag 0.198 g/t Au	053/88	90	1	-	Spotted (Chl-Ser)
Powell B-Zone	Qtz, Cpy, Po, Py, Ag, Au	1929	-	-	Dissem.			-	Spotted (Chl-Ser)
Powell D-Zone[3]	Qtz, Cpy, Po, Py, Sph, Ag	1929	-	0.08% Cu 0.03% Zn 0.17 g/t Au 6 g/t Ag	Dissem. 045/90	77		-	Spotted (Chl-Ser)
Anglo-A	Qtz, Cpy, Py, Po, Ag	1933	-	-	050/78	75	0.2-0.4	-	Spotted (Chl-Ser)
Anglo-B[4]	Qtz, Py, Cpy	1933	-	3.28% Cu 0.92% Zn 28 g/t Ag	NE/?	17	0.2-0.6	-	Spotted (Chl-Ser)
Anglo-C[3]	Qtz, Cpy, Py, Sph	1933	-	18.6% Cu 0.12% Zn 98.5 g/t Ag	036/?	50	0.2-0.3	-	Spotted (Chl-Ser)
Anglo-D	Qtz, Cpy, Py, Ag	1933	-	-	059/?	36	0.2-0.6	-	Spotted (Chl-Ser)
Anglo-E	Qtz, Cpy, Py	1933	-	0.27% Cu	NE/75				Sil-Carb
Joliet Breccia[5]	Qtz, Cpy, Py, Po, Ag	1922	-	0.03% Cu 0.012% Zn 0.52 g/t Ag 0.01 g/t Au	Dissem.	-	-	-	Spotted (Chl-Ser)
Héré Cu Vein[3]	Qtz, Cpy, Py, Po, Ag		-	0.647% Cu 0.045% Zn 9.77 g/t Ag	060/82				Spotted (Chl-Ser)

[1]Overall ore ressource estimated by Boldy (1977)

[2]Ore reserves calculated by A. Waltz, 1931 (Lichtblau, 1976)

[3]Metal assay data from this study

[4]Metal assay data from drillhole A-102, sampled over 1.22m (Simard, 2009)

[5]Average of 54 samples from Schofield et al., (*in press*), Au is averaged from 15 samples

**Subeconomic occurrences are listed in italics*

4.18 Figures

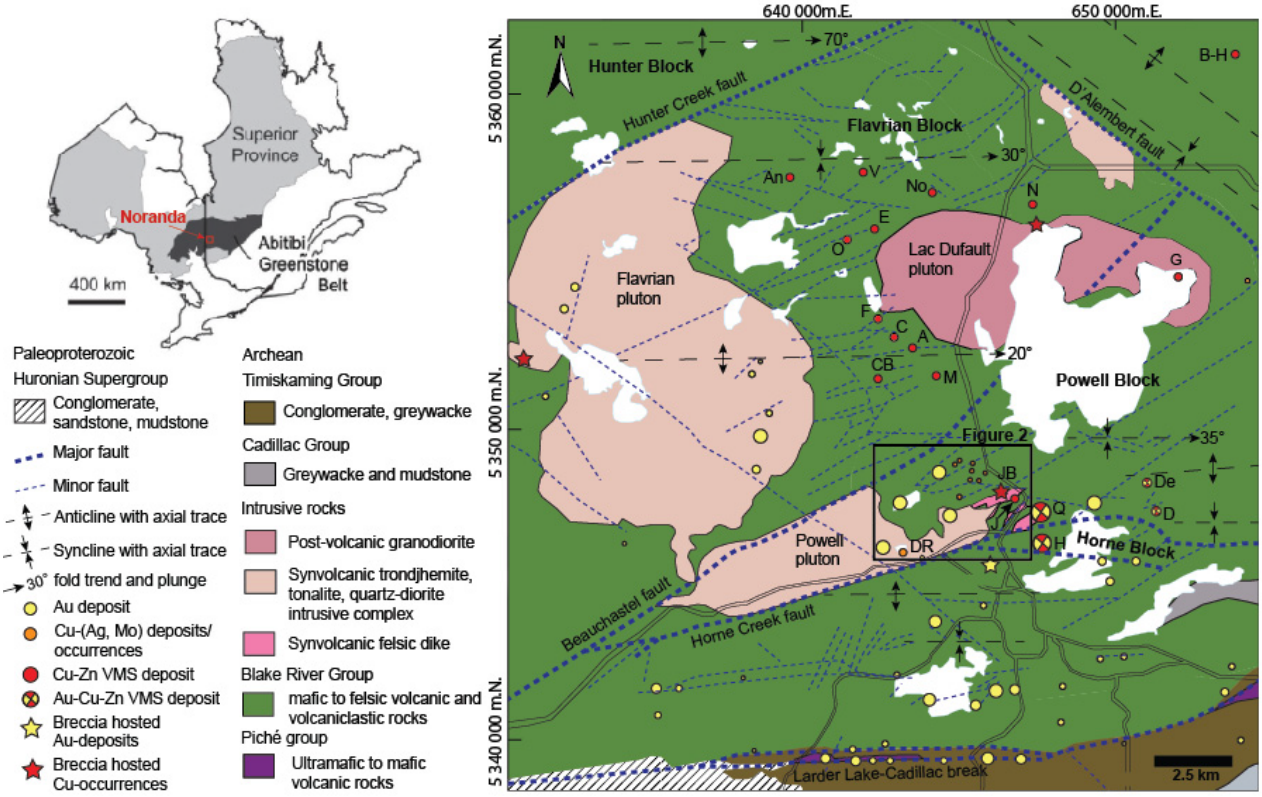

Figure 4.1: Regional geology map of the Rouyn-Noranda mining district.

Regional geology map of the Rouyn-Noranda mining district modified from Schofield et al., (2021) and references therein, showing spatial distribution of the various mineral occurrences and deposits. The yellow circles are scaled to reflect the relative gold content. Abbreviated VMS deposits are: A = Amulet A, An = Ansil, B-H = Bouchard-Hebert, C = Amulet C, CB = Corbet, De = Deldona, D = Delbridge, E = East Waite, F = Amulet F, G = Gallen, H = Horne, J = Joliet, M = Millenbach, No = Norbec, N = Newbec, O = Old Waite, Q = Quemont, V = Vauze. Abbreviation for other deposits are: DR = Don Rouyn; JB = Joliet Breccia. The location for Figure 2 is highlighted by the black rectangle.

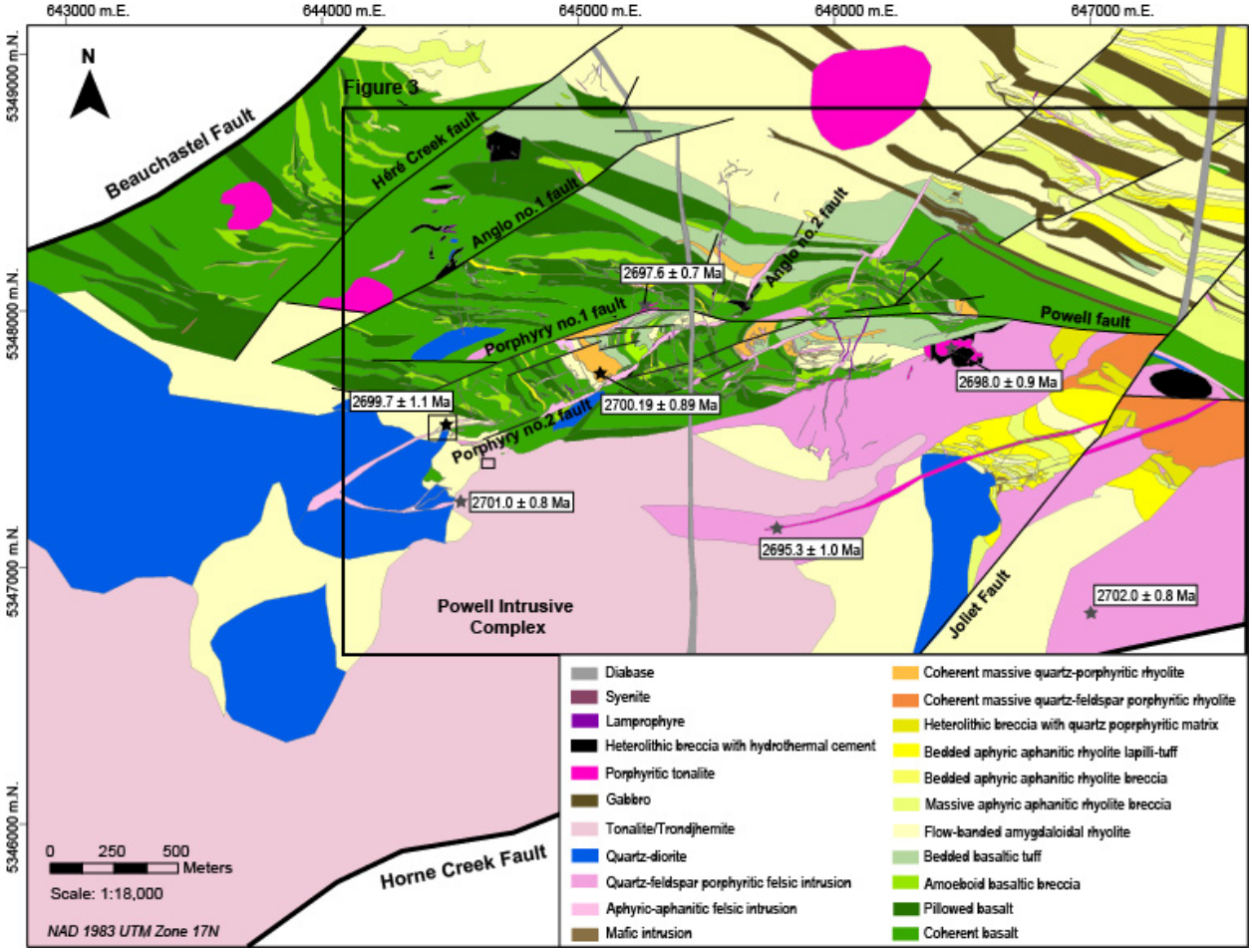

Figure 4.2: Lithological compilation map of the Lower Blake River Group strata of the Powell Block.

Lithological compilation map of the Lower Blake River Group strata of the Powell Block. Sample locations for U-Pb ID TIMS zircon ages are shown as black squares (McNicoll et al., 2014), black circles (Schofield et al., 2021) and black stars (this study). Discordant heterolithic breccias and associated ca. 2698 Ma tonalite intrusions are highlighted in black and bright pink, respectively. Black rectangle shows the location for Figure 3.

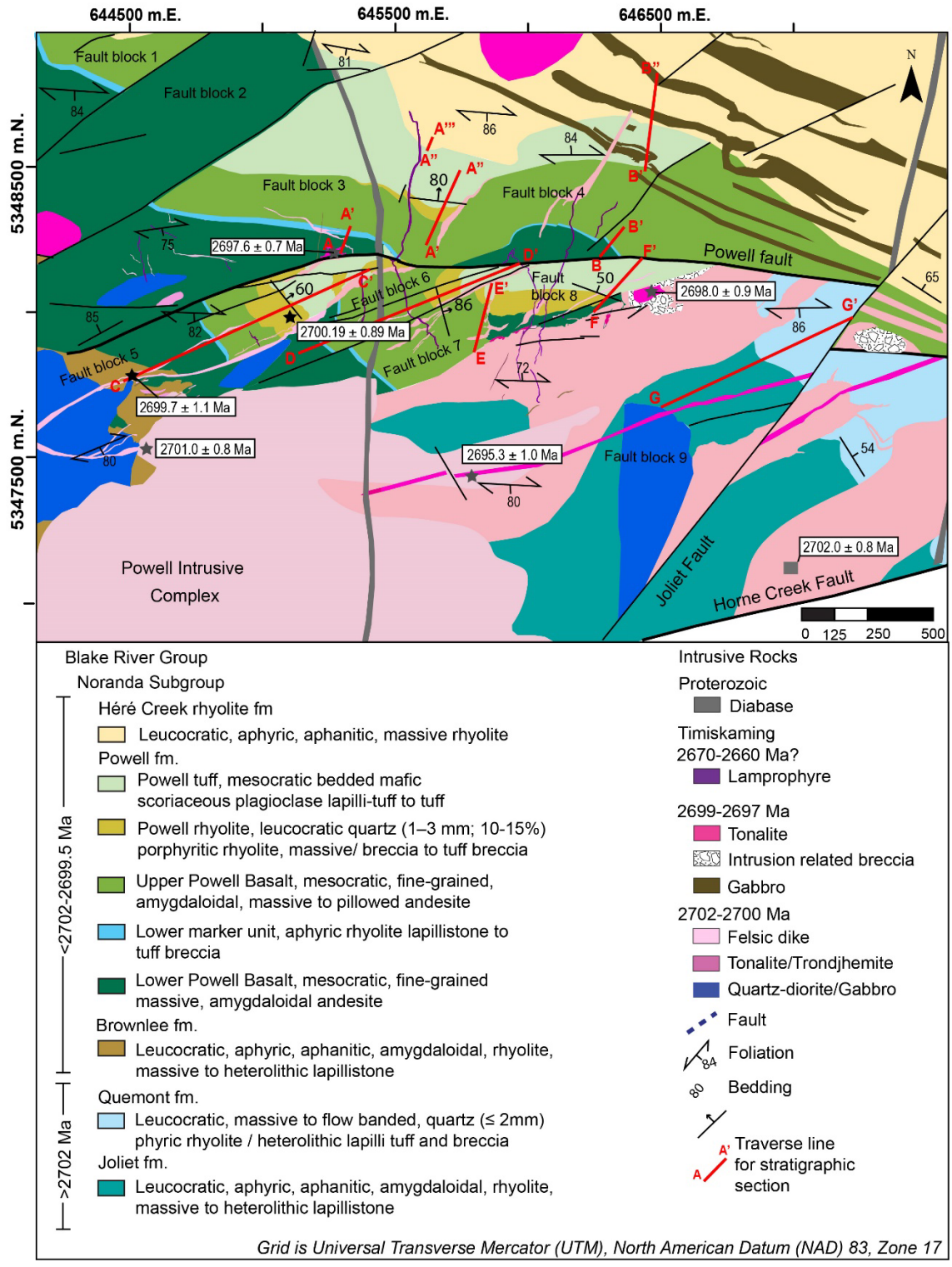

Figure 4.3: Lithostratigraphic map with location of stratigraphic transects.

Lithostratigraphic map showing the internal fault blocks and the locations (red lines) of stratigraphic transects illustrated in Figure 5.

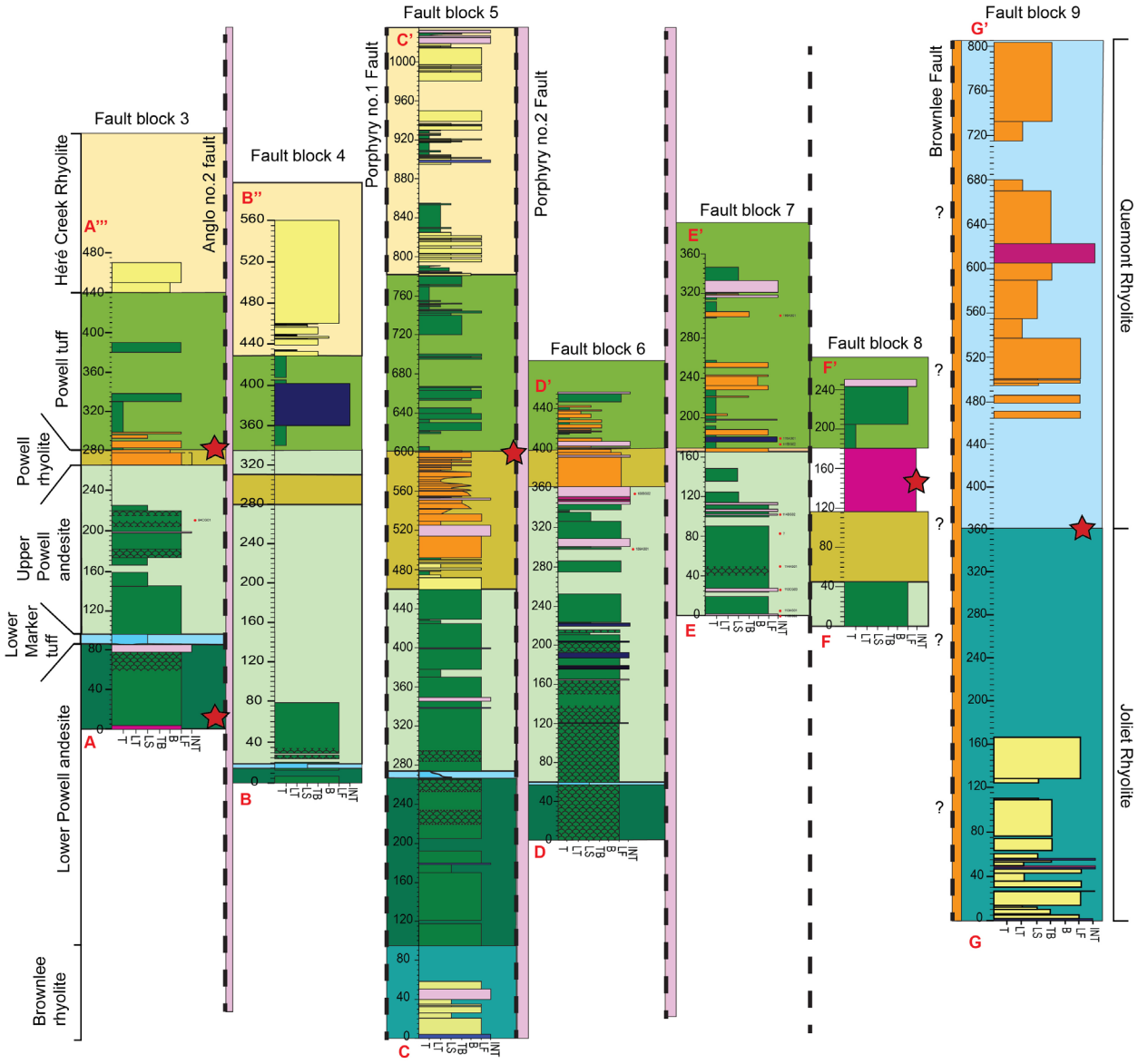

Figure 4.4: Stratigraphic columns for the transects shown in Figure 3.

Stratigraphic columns for the transects in the major fault blocks shown in Figure 3. Apparent thicknesses are as measured in outcrop and have not been corrected for the local steep to moderate dips of strata or for the effects of superimposed tectonic strain. The resulting variations in apparent thicknesses of units, therefore, cannot be interpreted uniquely but this does not affect the portrayal of correct stratigraphic order. Aphyric felsic intrusions shown as light pink, porphyritic felsic intrusions shown as dark pink, and mafic intrusions shown in dark blue. Red stars show locations of subeconomic quartz-sulfide (Cu-Zn-Ag) mineral occurrences. Star in fault block 9 is the Joliet deposit. Abbreviations for scale at bottom of sections: T = tuff, LT = lapilli tuff, LS = lapillistone, TB = tuff breccia, B = breccia, LF = lava flow, INT = intrusive.

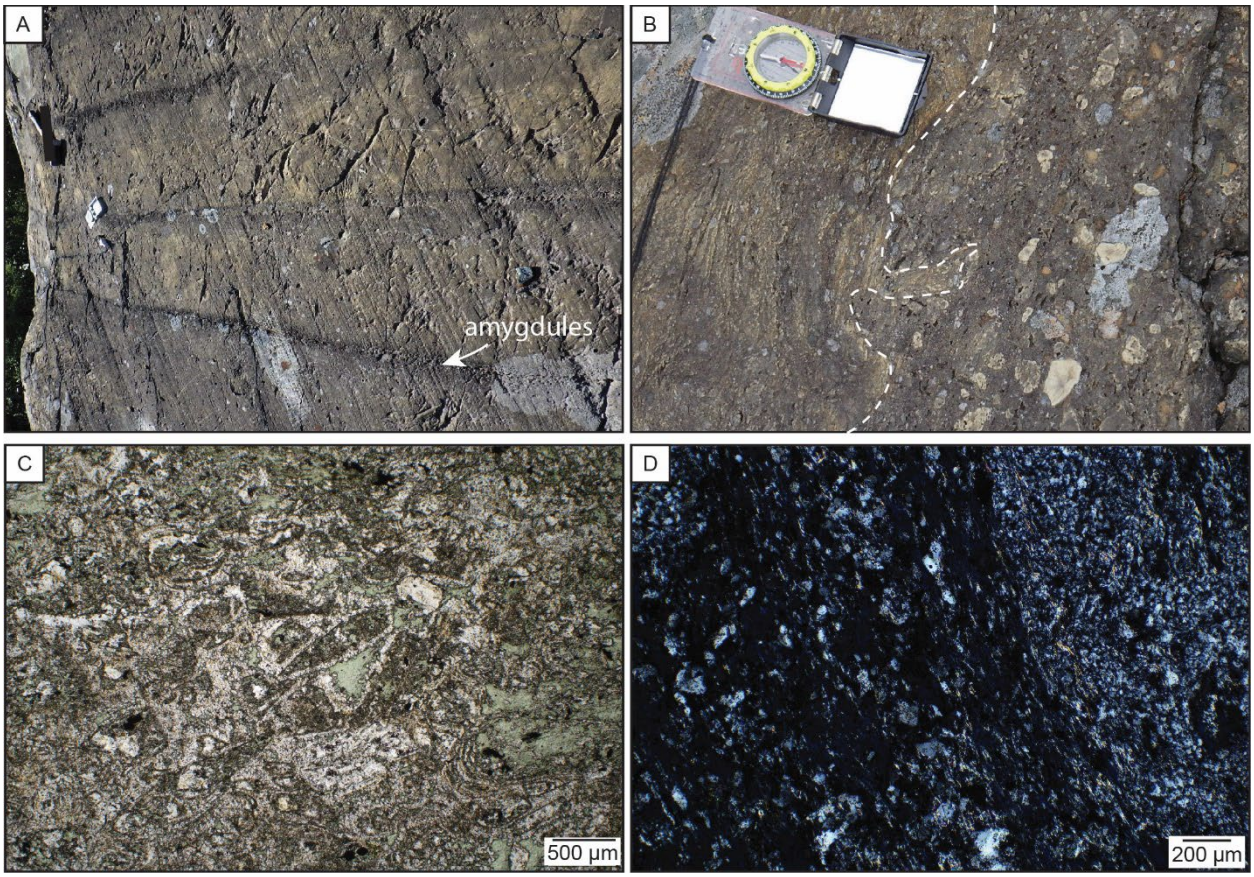

Figure 4.5: Characteristic features of the Brownlee rhyolite formations.

Characteristic features of the Brownlee rhyolite formations. **A)** Proximal facies of massive lobe-hyaloclastite rhyolite flows of the Brownlee rhyolite formation showing increased amygdale content towards the flow top. Compass on left side of image for scale (the diagonal lines are glacial striations on the outcrop surface); **B)** Contact between the massive lobe hyalclastite rhyolite facies and the heterolithic lapillistone facies of the brownlee formation; **C)** Angular chloritized shards in a fine-grained silicic matrix from the margin of a rhyolite lobe (plane-polarized light photomicrograph); **D)** Flow banding comprised of aligned sericitized feldspar microlites and alternating amygdale rich and amygdale poor bands (cross-polarized light photomicrograph).

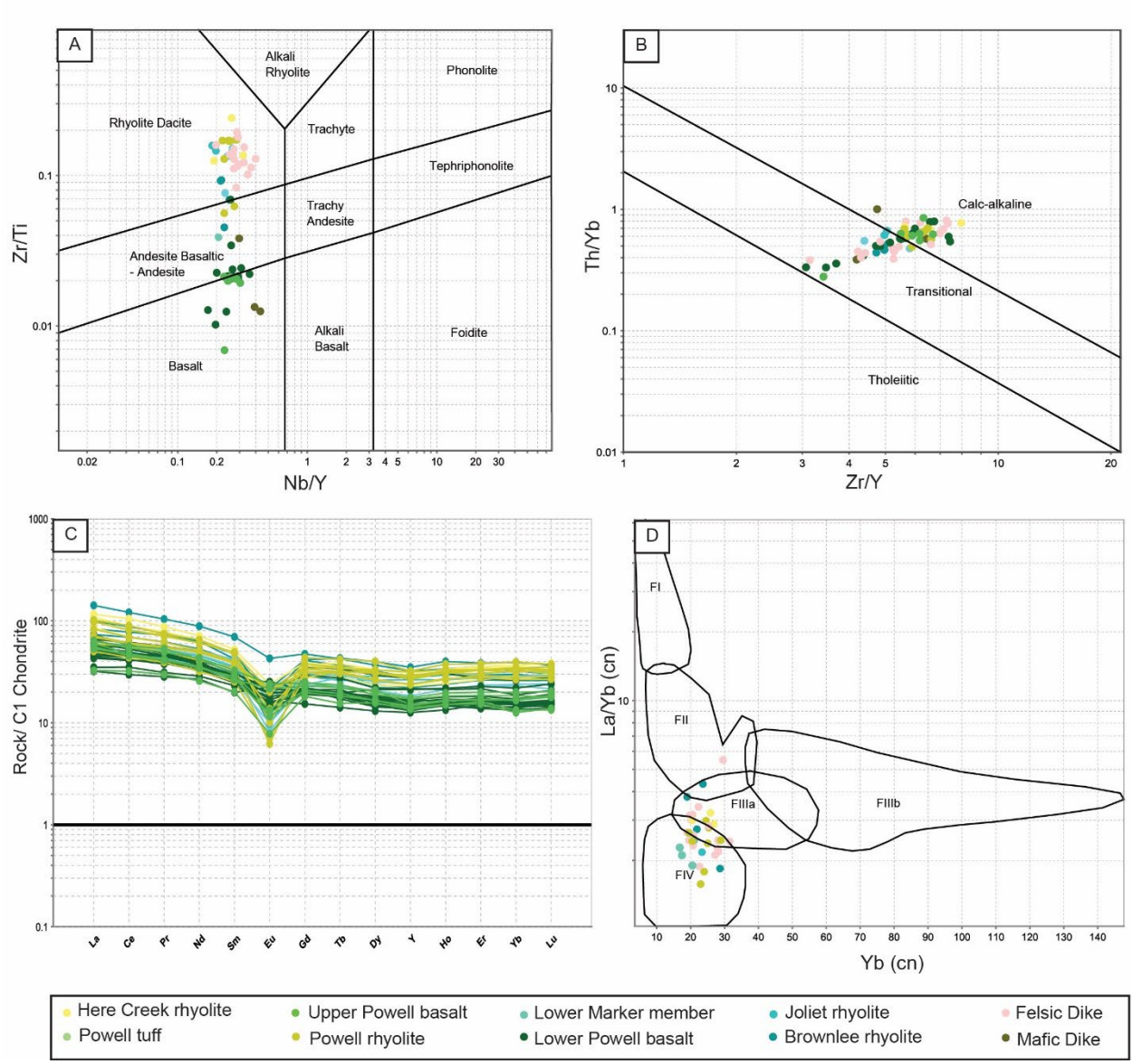

Figure 4.6: Lithogeochemistry data for the main volcanic units of the Powell Block.

Lithogeochemistry data for the main volcanic units of the Powell Block, color coded to match Figure 2; **A)** Rock classification using Zr/Ti and Nb/Y ratios of Pearce (1996); **B)** Magmatic affinity diagram of Ross and Bedard (2009); **C)** Spider plot of immobile trace elements, chondrite normalized using values from Sun and McDonough (1995); **D)** Rhyolite fertility plot of Hart et al., (2004).

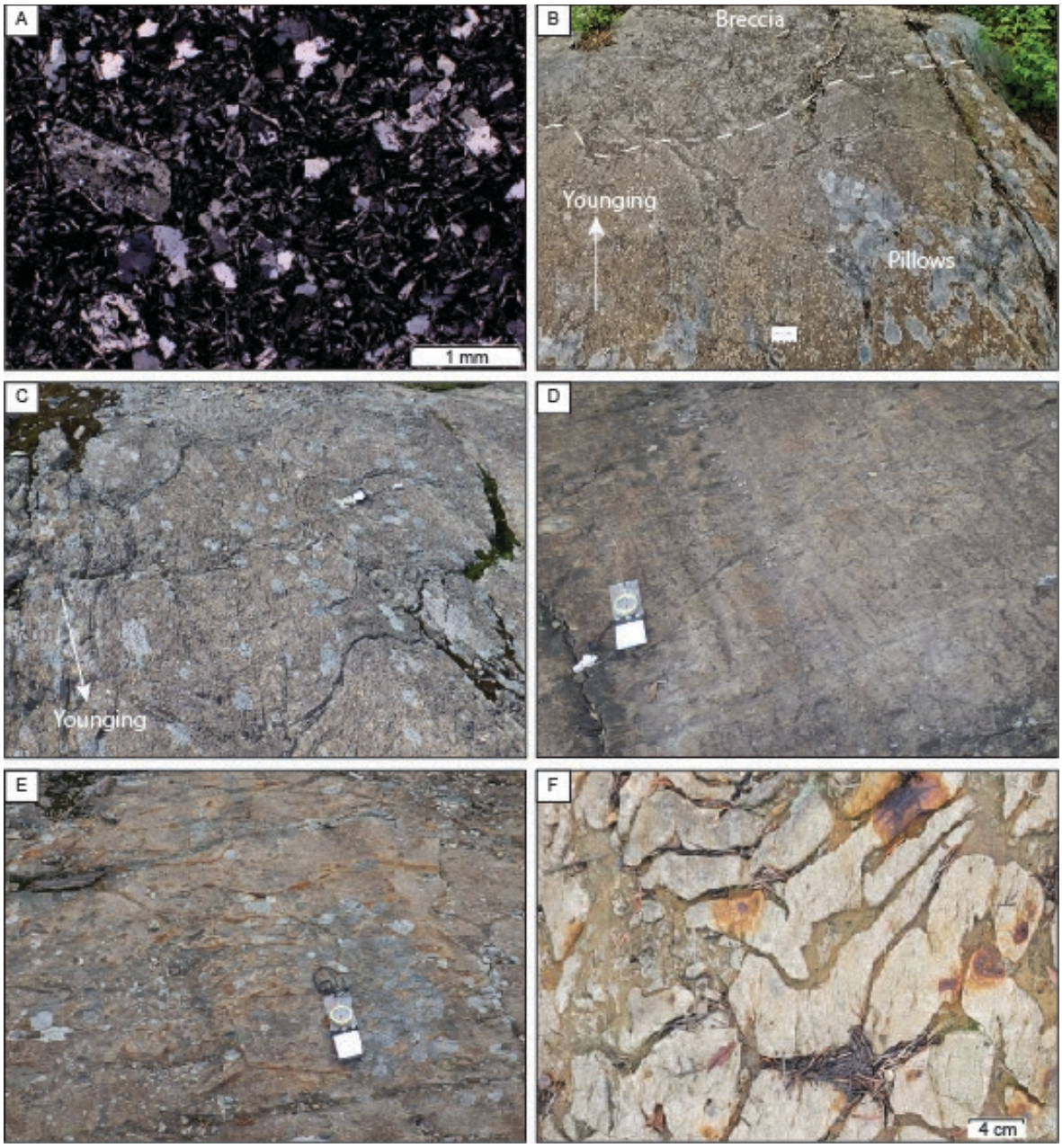

Figure 4.7: Characteristic features of the Lower and Upper Powell Basalt members of the Powell formation.

Characteristic features of the Lower and Upper Powell Basalt members of the Powell formation: **A)** Coherent flow facies showing albite microphenocrysts in a pilotaxitic matrix comprised of albite microlites, and interstitial quartz and chlorite within coherent andesite (cross-polarized light photomicrograph); **B)** Truncated pillows and overlying blocky flow top breccia; **C)** Pillows with concentric cooling laminations, cusps and rounded tops indicating younging direction to the ENE; **D)** Coherent flow facies with parallel cooling laminations; **E)** Coherent flow facies showing columnar jointing with sulfides lining the margins of joints; **F)** Amoeboid fluidal basalt clasts that conform to one another.

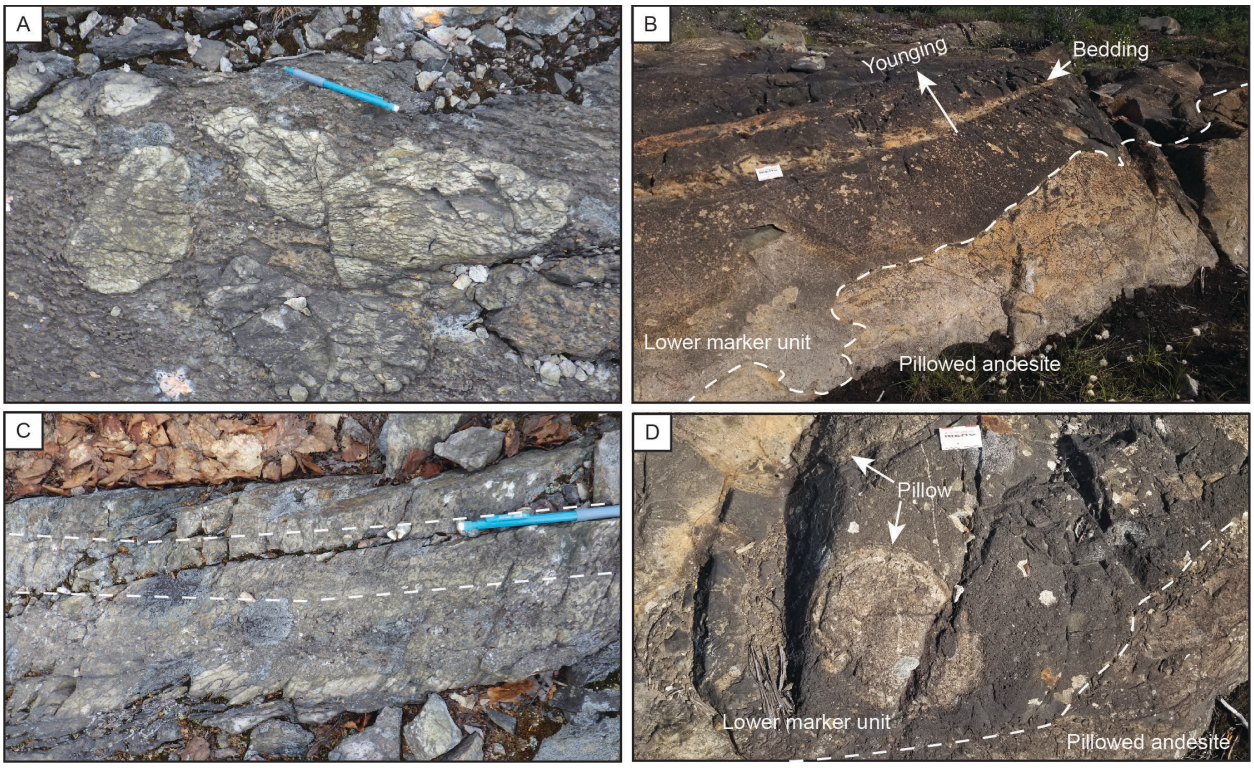

Figure 4.8: Characteristic features of the Lower Marker member of the Powell formation.

Characteristic features of the Lower Marker member of the Powell formation. **A)** Large, rounded blocks of aphyric rhyolite in a fine-grained granular matrix aphyric rhyolite and chlorite; **B)** Bedding and irregular lower contact following an embayment in the underlying pillows; **C)** Finely laminated tuff at the upper contact; **D)** Large blocks of pillowed basalt included in the base of the lower marker unit.

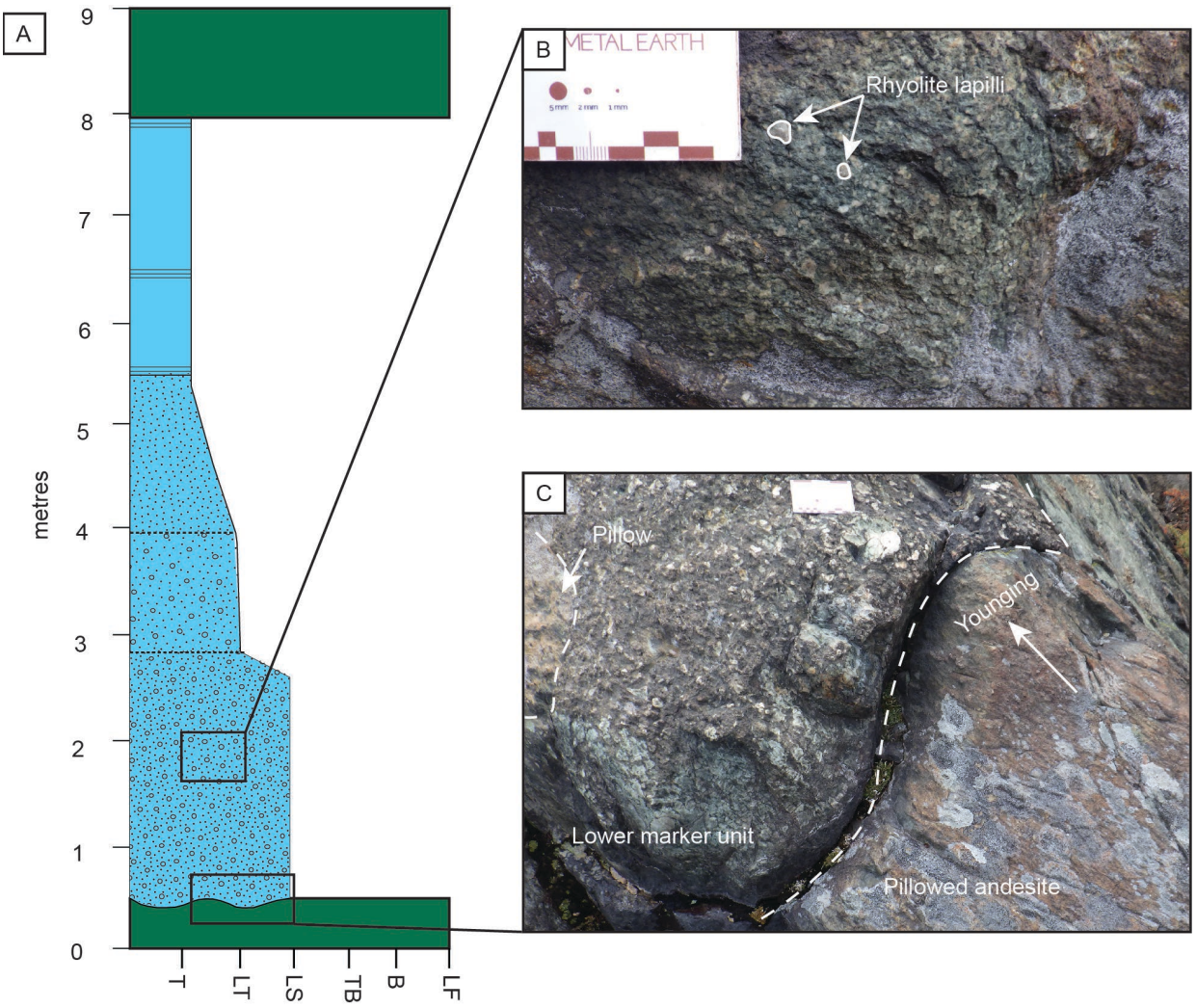

Figure 4.9: Detailed stratigraphic section and photographs of the lower marker member of the Powell formation.

A) Detailed stratigraphic section of the lower marker member in Fault blocks 5. Thickness is as measured in outcrop and not corrected for dip; **B)** Sharp and irregular lower contact following the topography of the underlying pillows; **C)** Rounded lapilli sized clasts of aphyric rhyolite in a fine-grained chloritized matrix.

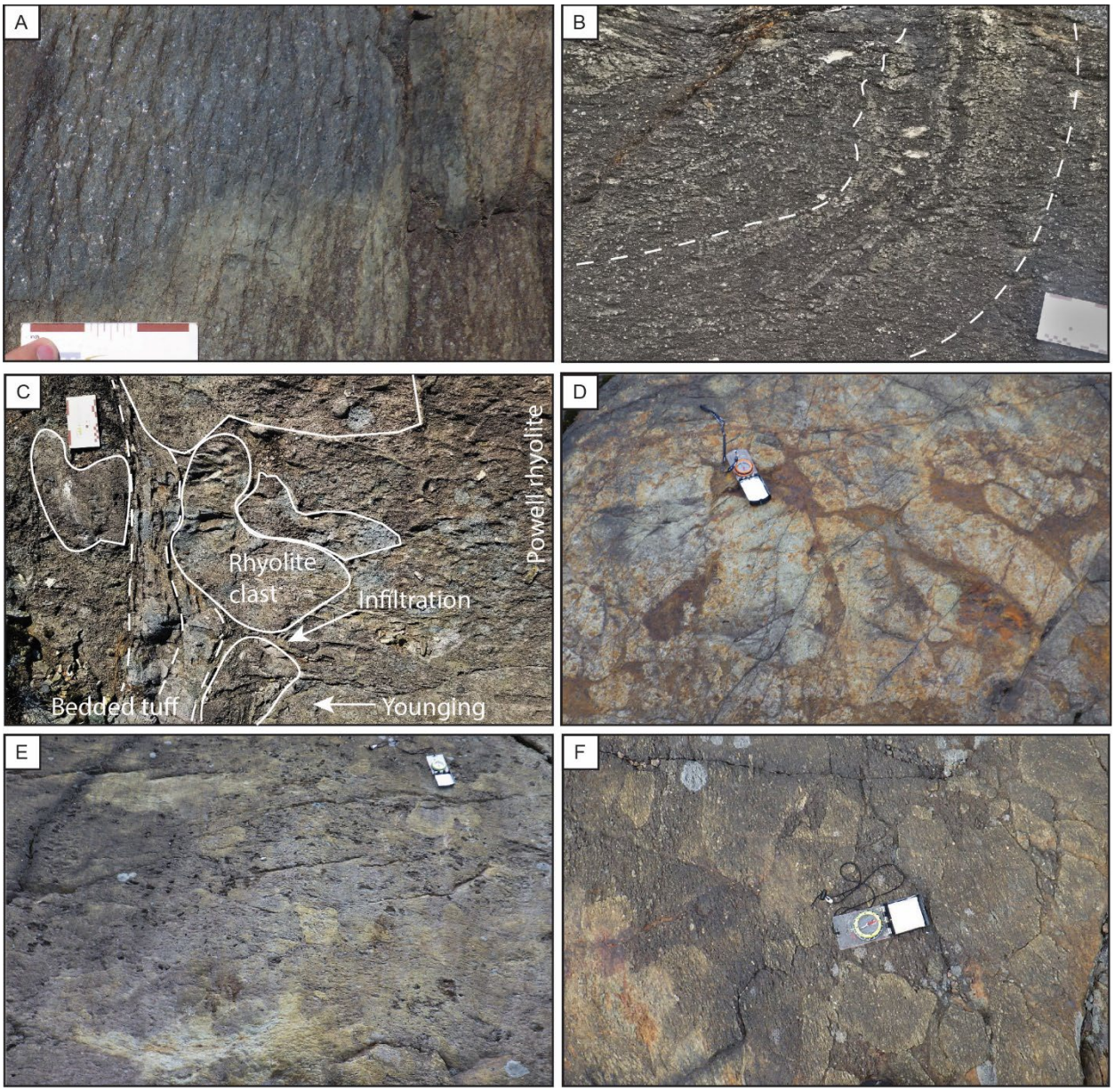

Figure 4.10: Characteristic features of the Powell rhyolite member of the Powell formation.

Characteristic features of the Powell rhyolite member of the Powell formation: **A)** Quartz porphyritic texture consisting of 10-15%, 1–3 mm diameter quartz phenocrysts in a chloritic, aphanitic matrix. Massive facies with metamorphic foliation; **B)** Flow banding within the massive facies; **C)** Top of massive facies showing angular jig-saw fit breccia with tuff from the overlying Powell tuff member between fragments; **D)** Angular breccia at the top of the massive facies showing minor clast rotation and a matrix containing abundant pyrite (brown); **E)** Tuff breccia facies showing dominantly quartz porphyritic rhyolite clasts and minor angular, chloritized and recessively weathered clasts; **F)** Breccia facies showing angular blocks of quartz porphyritic rhyolite in a fine-grained matrix of similar composition.

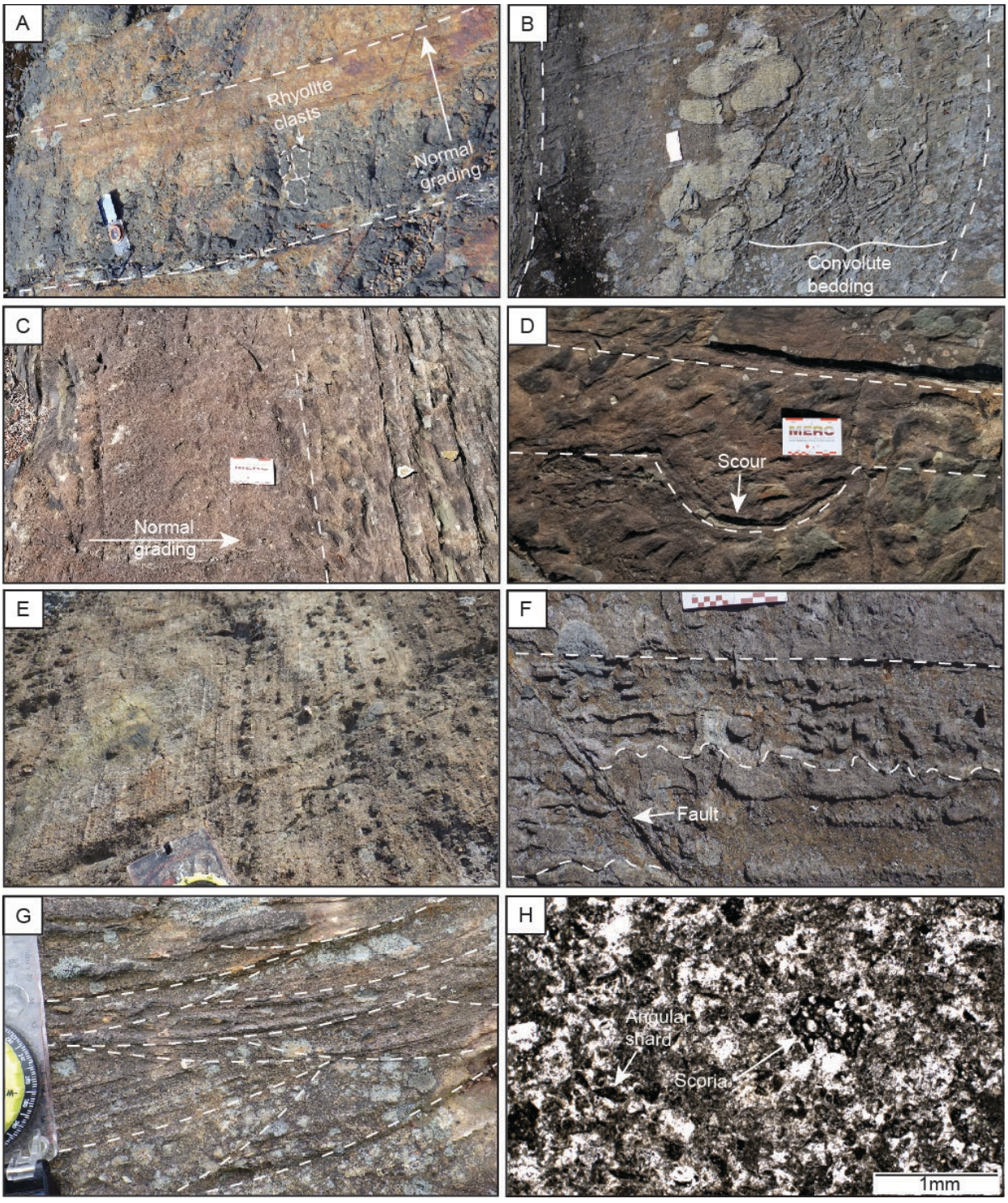

Figure 4.11: Characteristic features of the Powell tuff member of the Powell formation.

Characteristic features of the Powell tuff member of the Powell formation: **A)** Normal graded bed containing clasts of Powell rhyolite in a matrix of Powell tuff; **B)** Convolute bedding beneath large blocks of Powell rhyolite; **C)** Normal grading with thickly bedded coarse tuff overlain by finely

laminated fine tuff; **D)** Sharp scoured contact between beds; **E)** Thinly laminated facies with laminae of rounded scoriaceous lapilli; **F)** Loaded, symmetrical ripples offset by minor brittle fault; **G)** Trough cross-bedding; **H)** Internal textures of lapilli shown in E. Note scoriaceous shards and angular cuspate shards (plane polarized light photomicrograph).

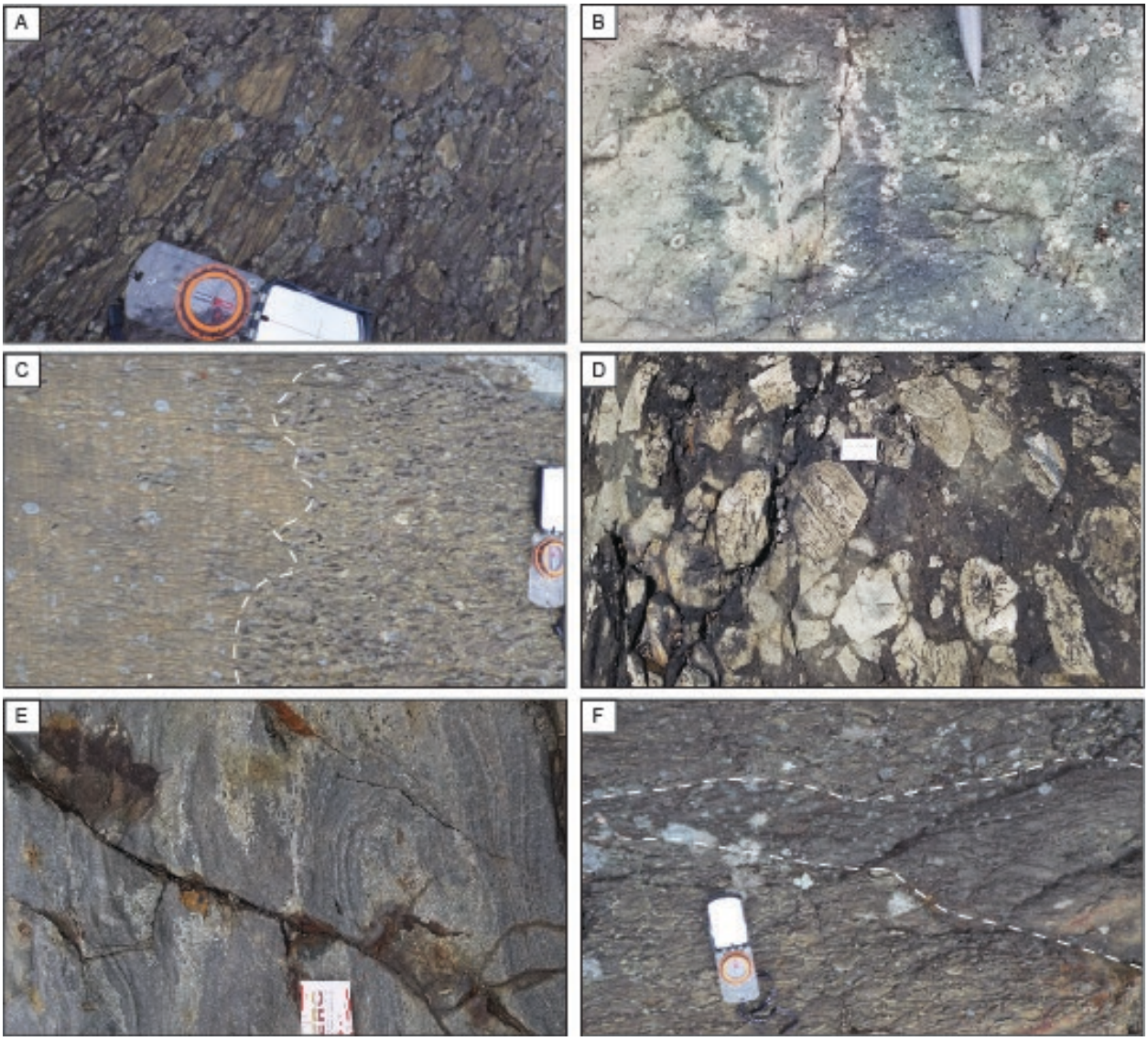

Figure 4.12: Characteristic features of the Héré Creek rhyolite formation.

Characteristic features of the Here Creek rhyolite formation: **A)** Angular monomictic breccia comprised of aphyric rhyolite clasts; **B)** Massive facies showing large spherulites; **C)** Massive facies with hyaloclastite rich upper contact; **D)** Angular monomictic breccia comprised of aphyric rhyolite clasts; **E)** Angular monomictic breccia comprised of aphyric rhyolite clasts, showing local flow banded clasts; **F)** Flow banded lobe of rhyolite surrounded by hyaloclastite.

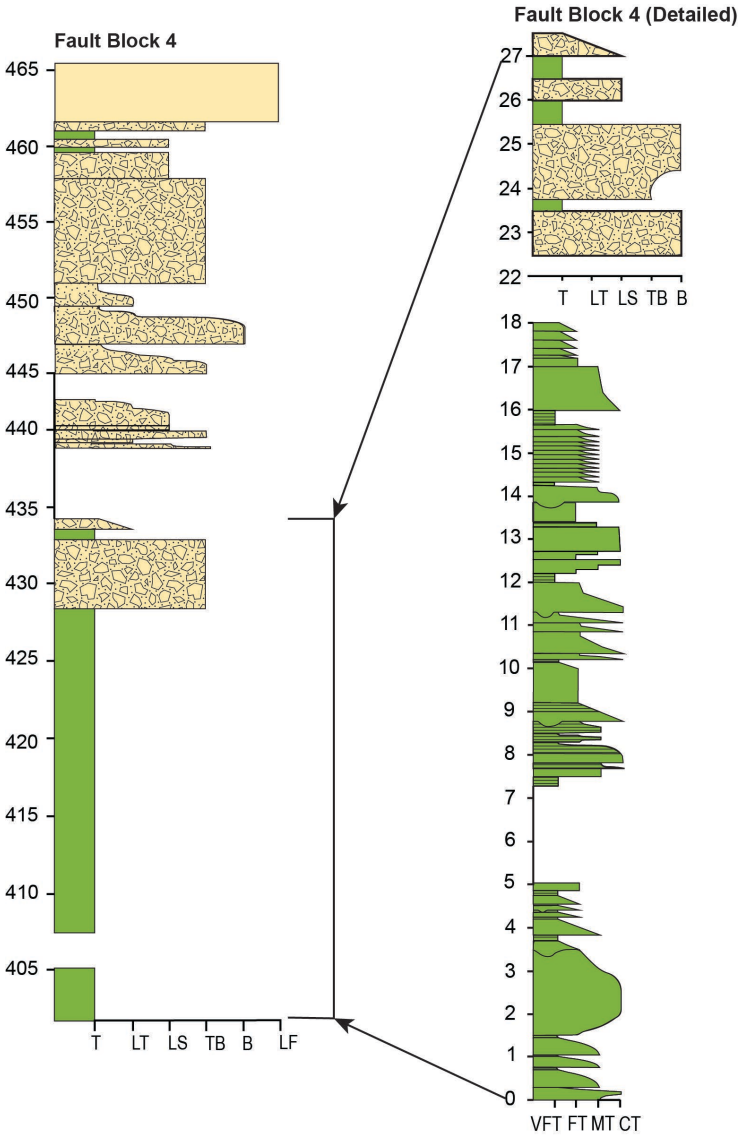

Figure 4.13: Detailed stratigraphic sections of the contact between the Powell and Héré Creek rhyolite formations.

Detailed stratigraphic sections of the contact between the Powell formation (green) and the Héré Creek formation (yellow), in Fault block 4. Thicknesses are as measured and relative and not corrected for dip to be true thicknesses. Note the intercalation of the Powell tuff with the basal rhyolite breccia lithofacies of the Héré Creek formation.

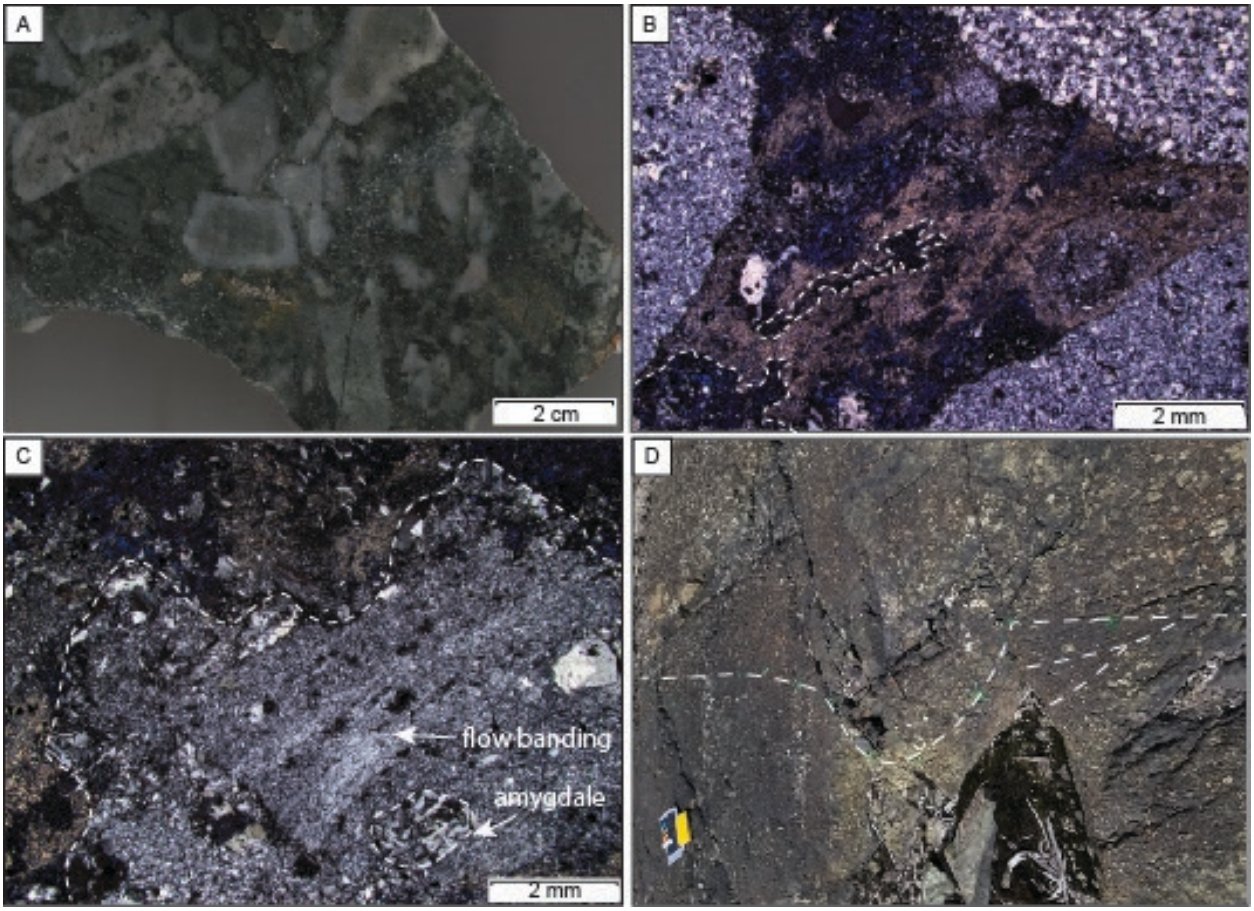

Figure 4.14: Characteristic features of the Joliet formation.

Characteristic features of the Joliet formation. **A)** Polymictic lapillistone showing angular rhyolite clasts with silicified rims in a fine-grained matrix, and a small scoria clast (polished slab); **B)** Matrix of the polymictic lapillistone showing chloritized vesicular altered glass shards (cross-polarized light photomicrograph); **C)** Flow banded and amygdaloidal rhyolite clast from the polymictic lapillistone; **D)** Scoured bedding contact between overlying lapillistone bed and underlying lapilli tuff (outcrop). Trough cross-bedding highlighted in underlying lapillituff.

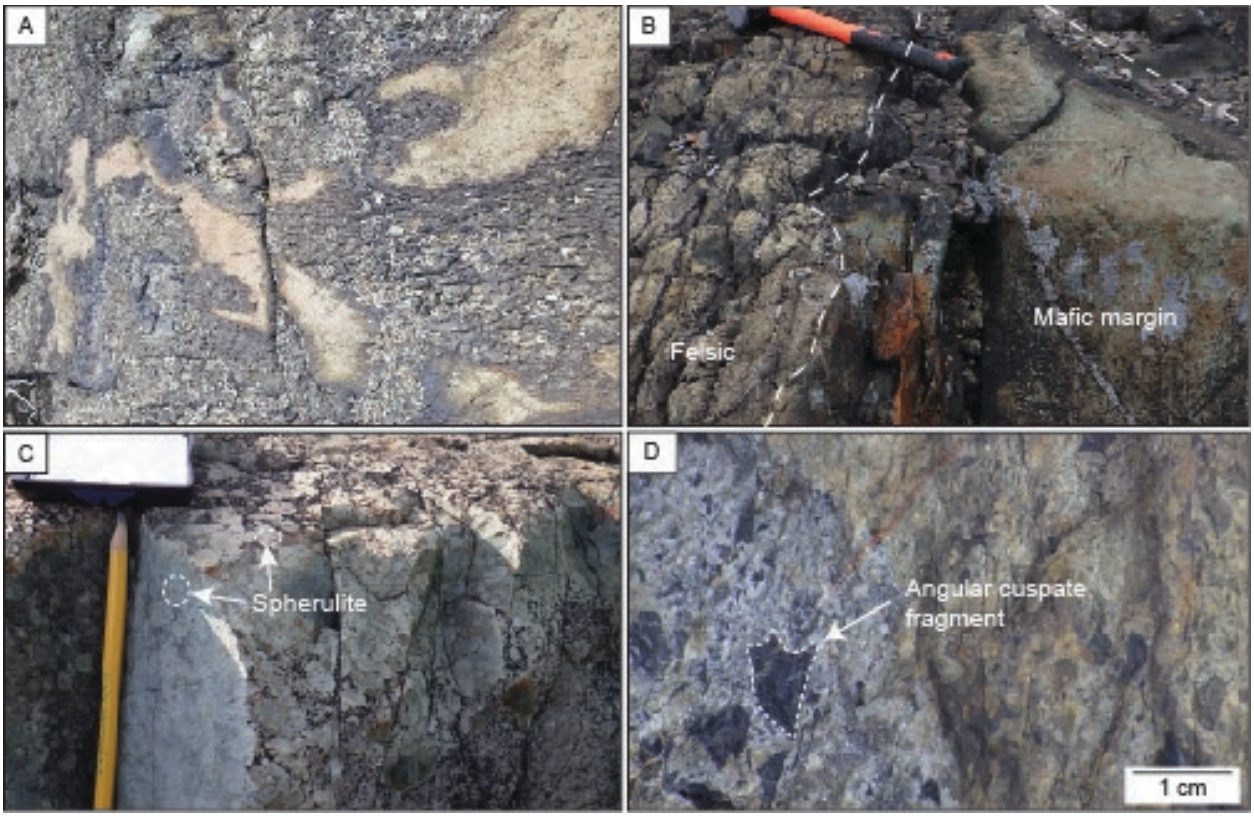

Figure 4.15: Characteristic features of dikes found in the study area.

Characteristic features of the different types of dikes found in the study area: **A)** Irregular amoeboid lenses of mafic dike cross-cutting lapillistone of the Joliet formation (outcrop); **B)** Composite dike with a highly chloritized mafic margin and an aphyric, spherulitic rhyolite core (outcrop); **C)** Large zoned spherulites in aphyric felsic dike (outcrop); **D)** Brecciated margin of aphyric felsic dike, note abundant angular fragments with cuspate margins (outcrop).

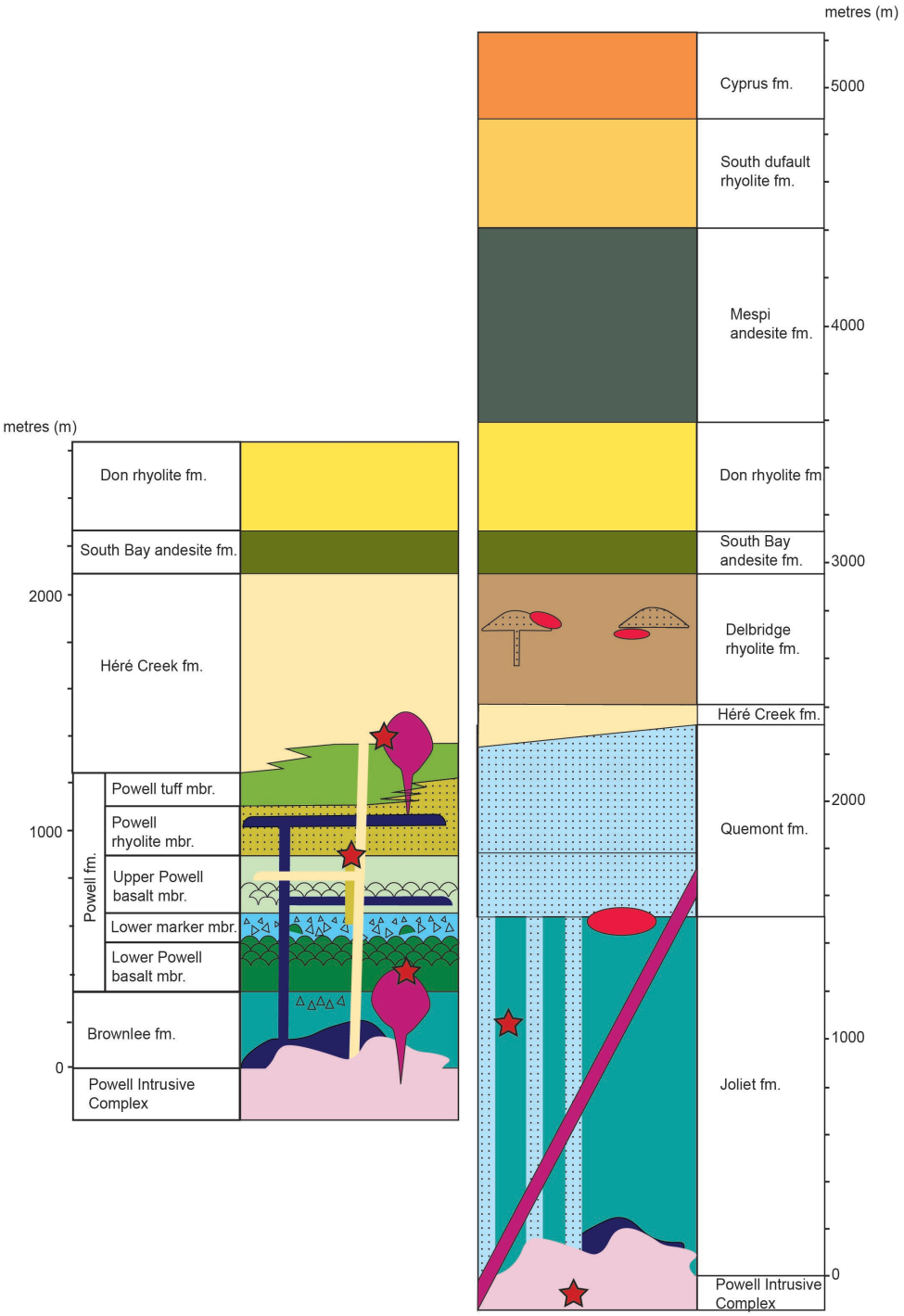

Figure 4.16: Graphical summary of volcanic strata and intrusions within the study area.

Graphical summary of volcanic strata and cross-cutting relationships observed among the intrusive rocks in the study area.

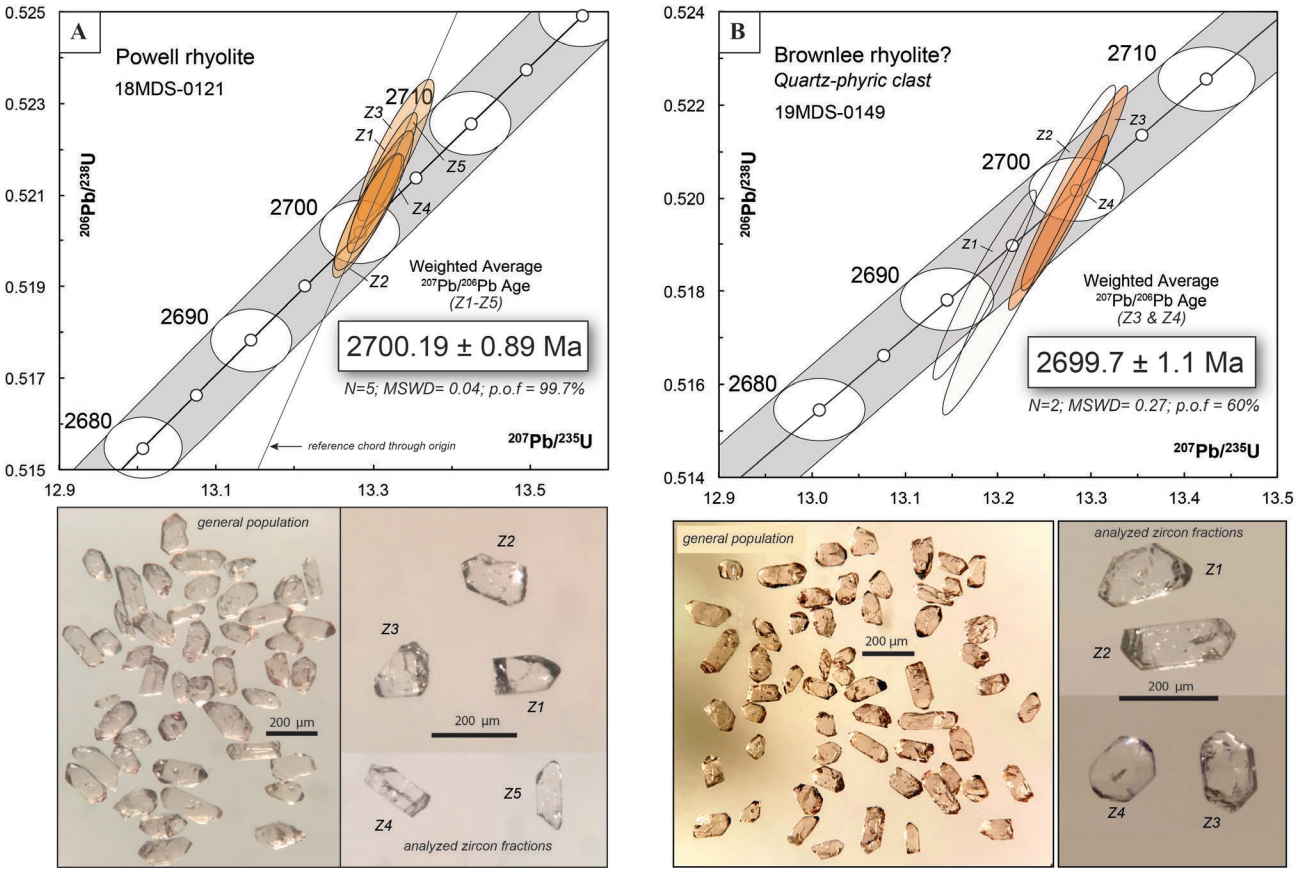

Figure 4.17: Zircon grain images and concordia diagrams for ID-TIMS U-Pb analyses.

Zircon grain images and Concordia diagrams for ID-TIMS U-Pb analyses from the selected rhyolite flows in the Powell Block. **A)** Powell rhyolite; **B)** Brownlee rhyolite.

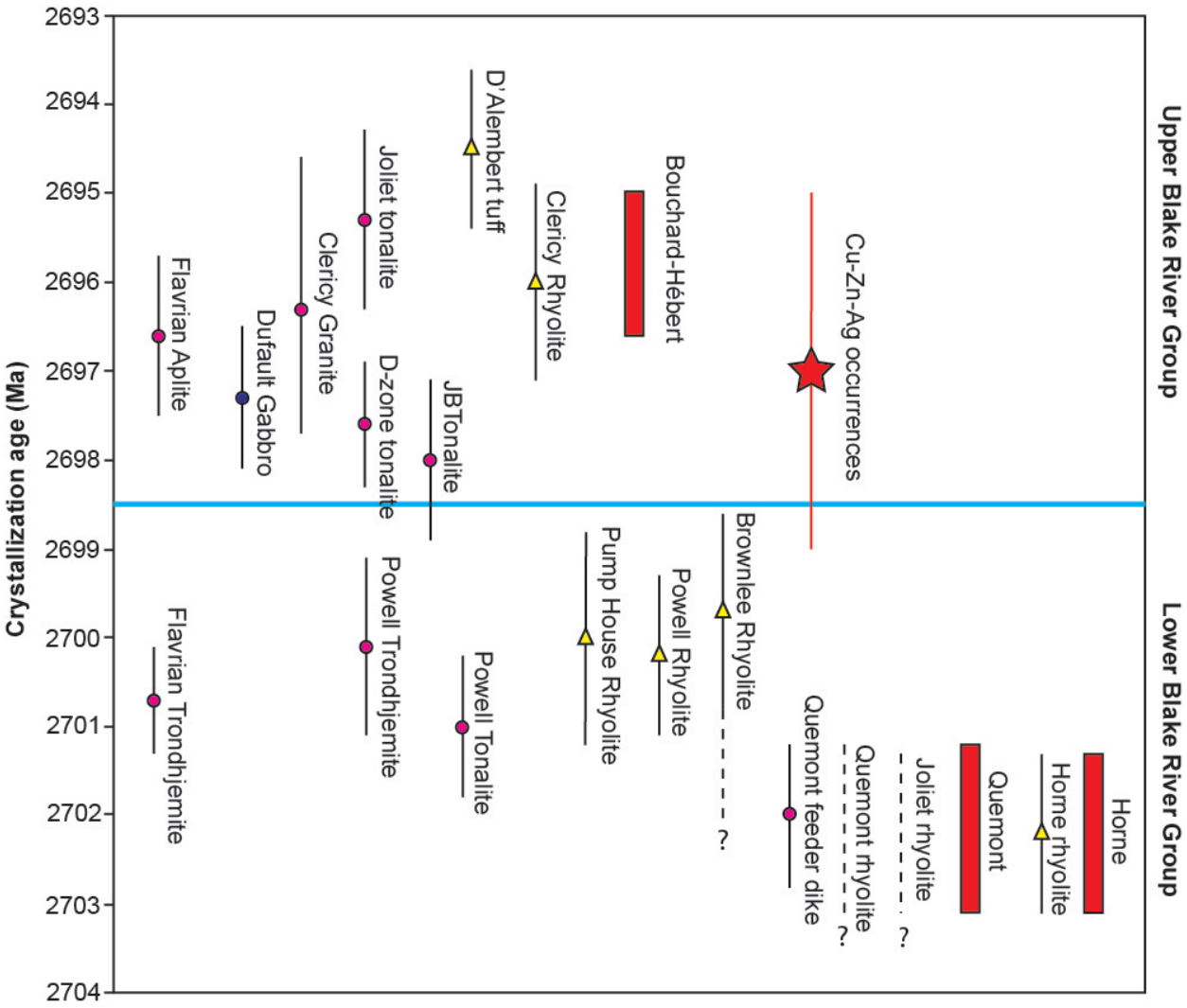

Figure 4.18: Summary diagram showing U-Pb zircon ages for the district.

Summary diagram showing both previous U-Pb zircon ages for the district (McNicoll et al., 2014 and references therein) and new U-Pb TIMS ages from this study. Blue line represents the gap in Blake River Group volcanism from McNicoll et al. (2014), which was used to subdivided everything into Upper and Lower Blake River Group. Red rectangles show age ranges for VMS deposits from McNicoll et al. (2014). Red star shows the interpreted age range of Cu-Zn-Ag prospects from the Powell Block from Schofield et al. (2021). Yellow triangles show ages of felsic volcanic rocks. Pink circles show ages of felsic intrusions. Blue circles show ages of mafic intrusions. Dashed lines are inferred age ranges based on cross-cutting relationships.

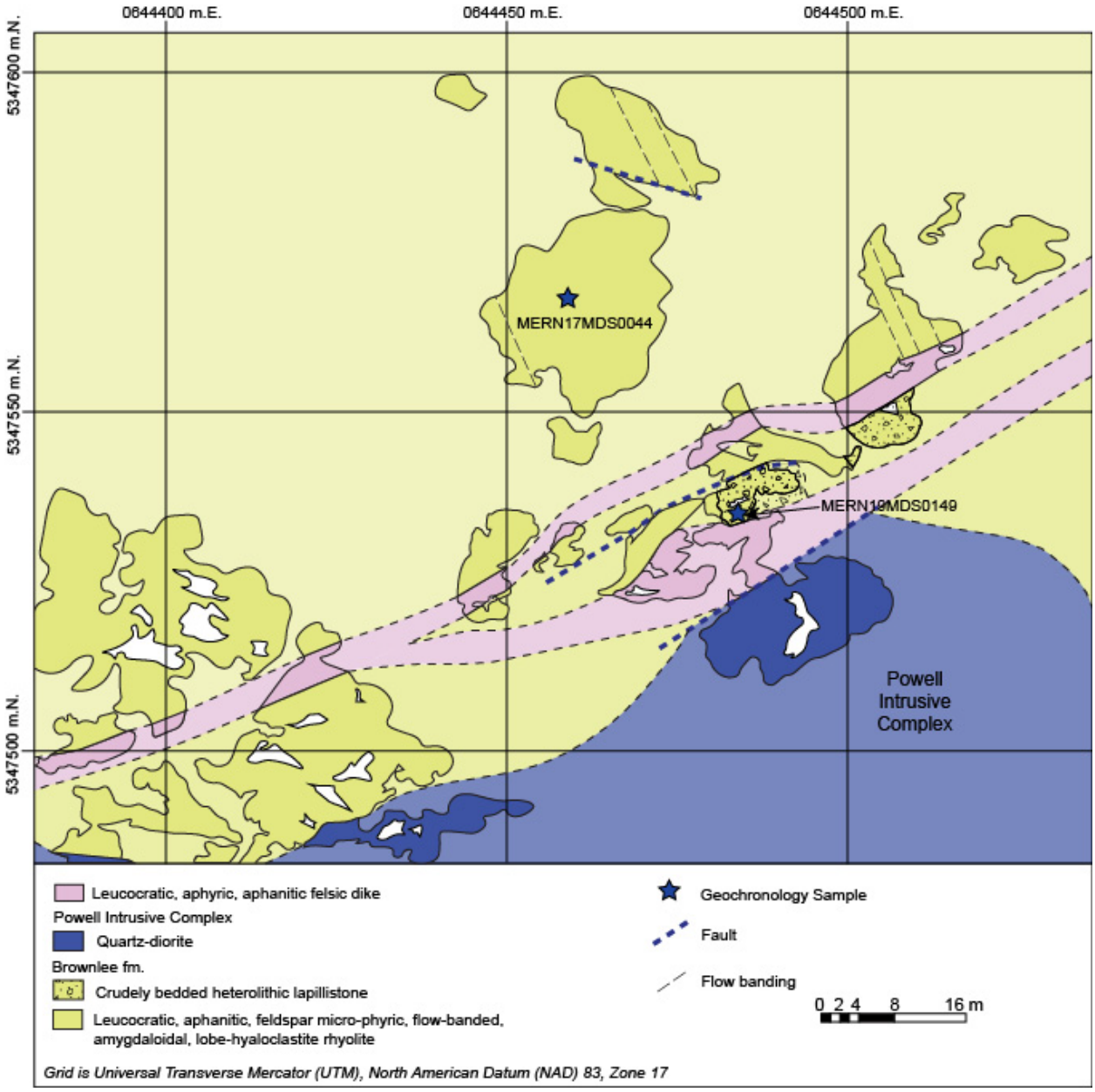

Figure 4.19: Sample location map for Brownlee rhyolite area.

Sample location map for Brownlee rhyolite area. Note the distribution of heterolithic lapillistone adjacent to the cross-cutting felsic dikes. The geochronological sample from site MERN17MDS0044 did not yield zircons.

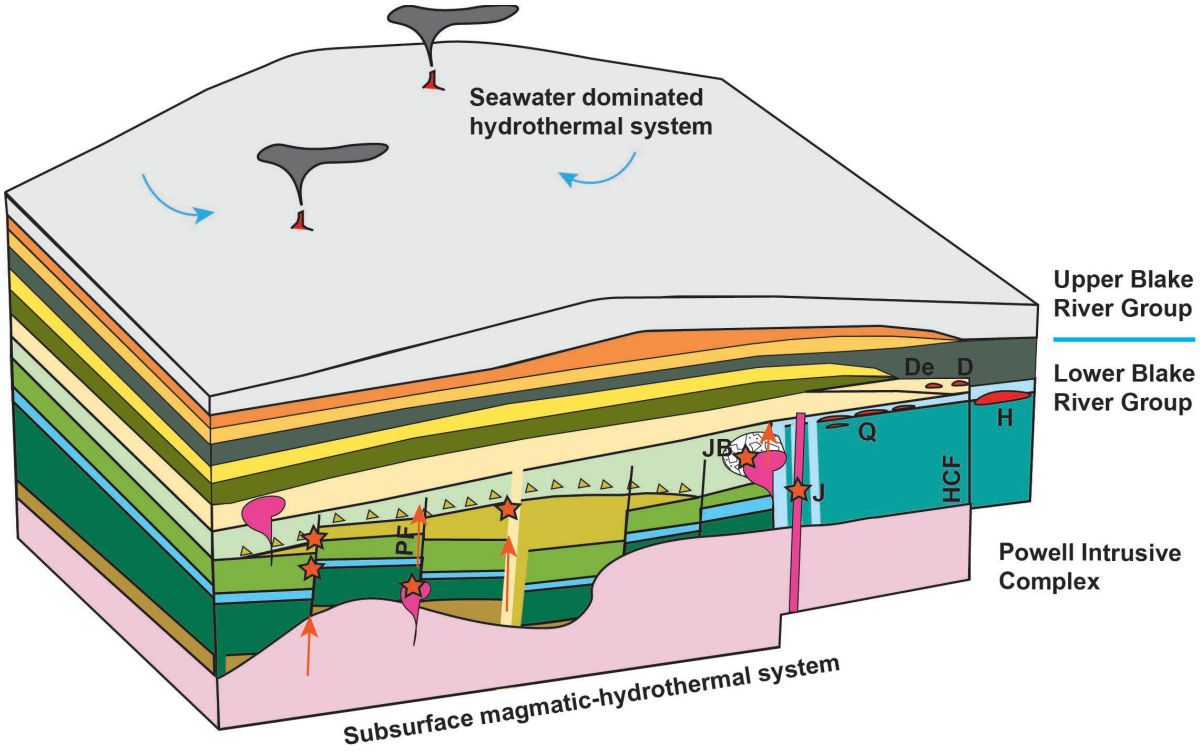

Figure 4.20: Schematic reconstruction of the interpreted hydrothermal system that formed the Cu-Zn-Ag veins.

Schematic reconstruction of the interpreted hydrothermal system that formed the discordant Cu-Zn-Ag veins at ca. 2698 Ma in a subsurface magmatic-hydrothermal regime, relative to potential coeval VMS deposits forming at or near the seafloor at a stratigraphically higher level, in a seawater-dominated hydrothermal system. Not to scale.

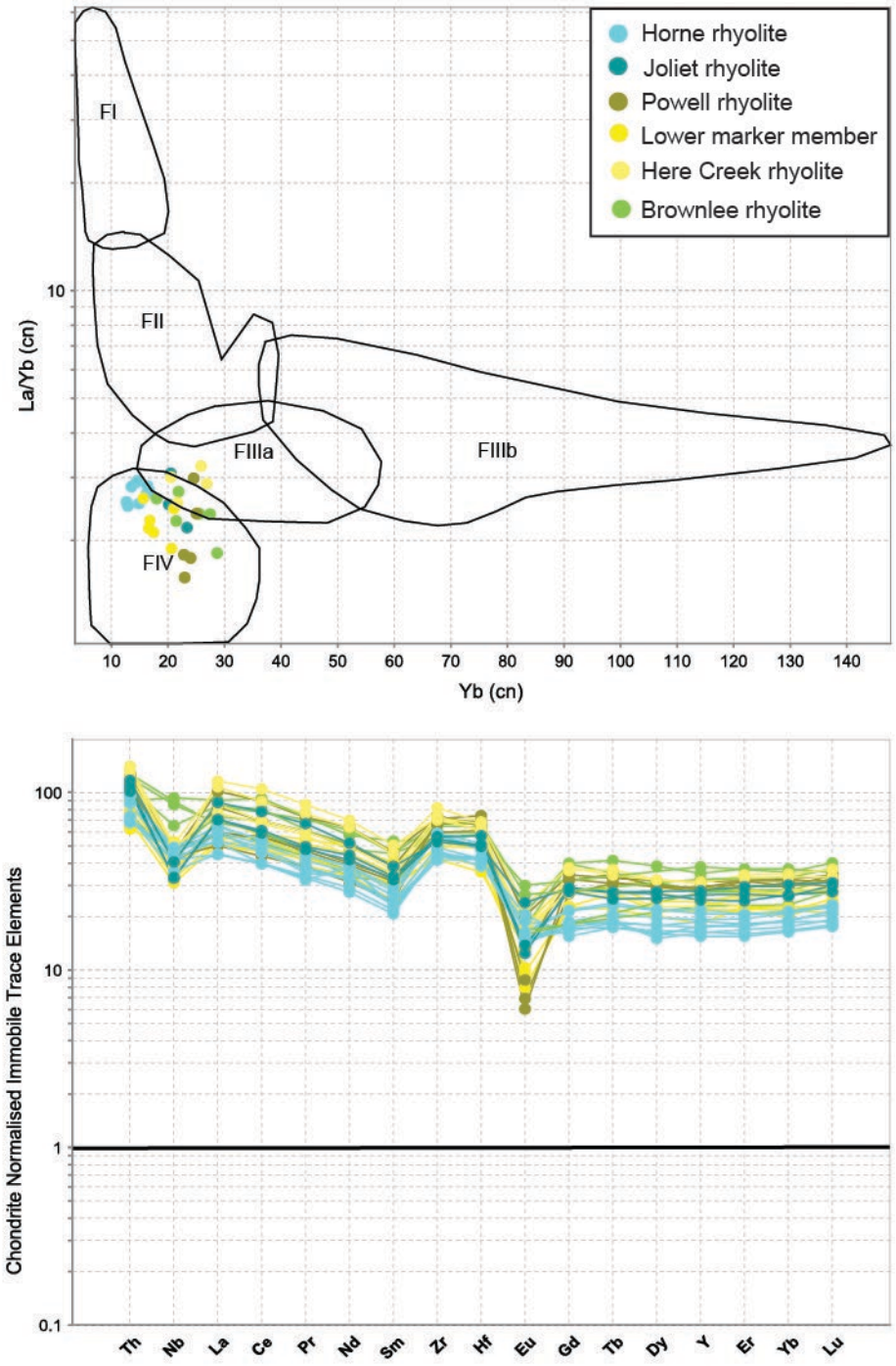

Figure 4.21: Whole rock lithogeochemistry for rhyolite units within the Powell Block compared to the Horne rhyolite.

Whole rock lithogeochemistry for the rhyolite units within the Powell Block, compared to the Horne rhyolite. Horne rhyolite data from Laurin (2009).

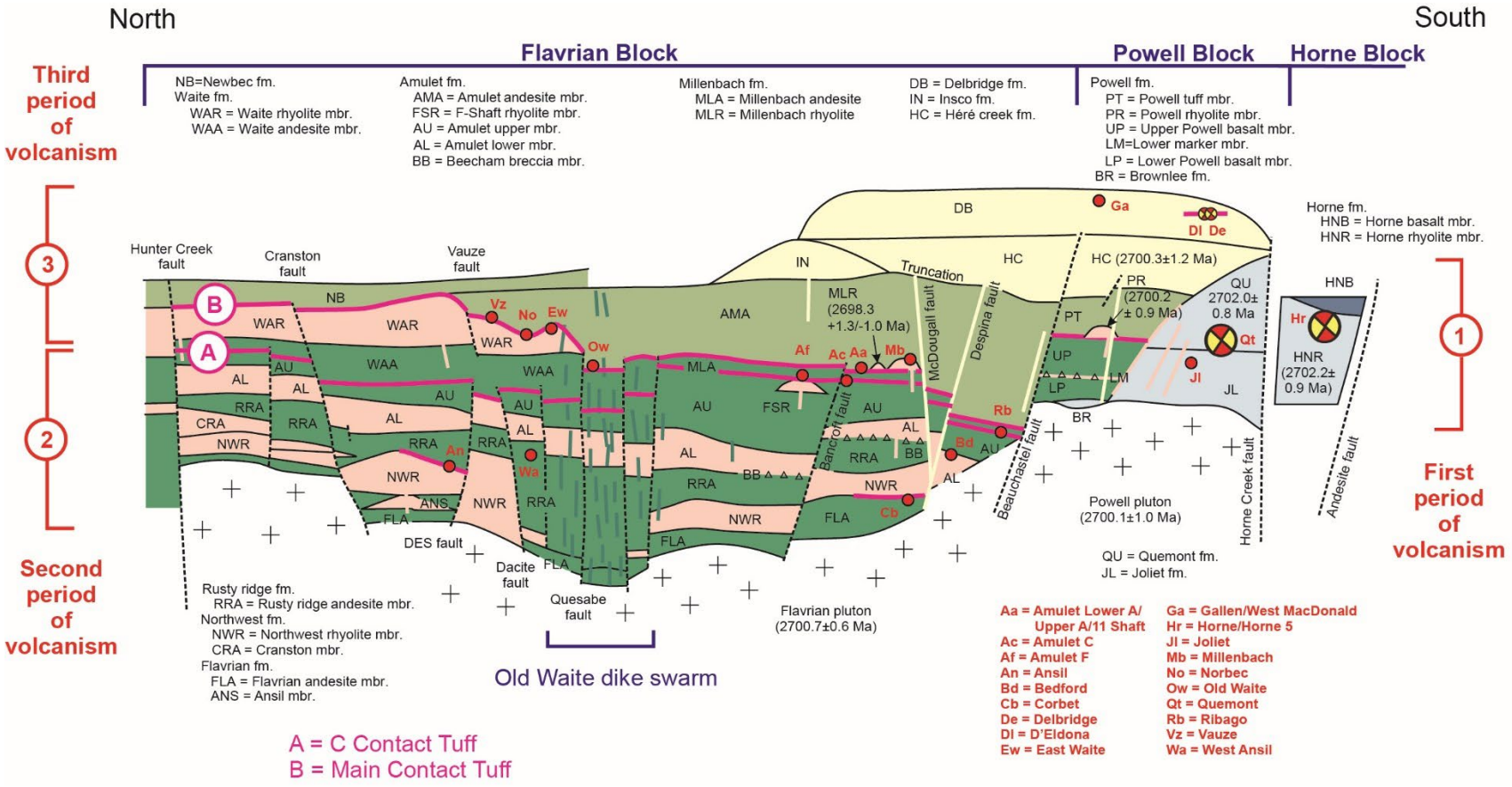

Figure 4.22: Schematic cross-section through the Noranda subsidence structure.

North-south schematic cross section through the Noranda subsidence structure showing the distribution of volcanogenic massive sulfide deposits and summary of U-Pb ID TIMS zircon ages and correlations between fault blocks. Modified from Gibson (1989), Gibson and Watkinson (1990) and Monecke et al. (2017).

4.19 Appendices

A 4-1: Whole-rock lithogeochemistry results of the Powell Block

Number	Lab ID	Formation	Rock Type	Alteration	UTM-East	UTM-North	SiO2 wt%	TiO2 wt%	Al2O3 wt%	Fe2O3t wt%	MnO wt%	MgO wt%	CaO wt%	SrO wt%	BaO wt%	Na2O wt%	K2O wt%	P2O5 wt%	LOI wt%	Total
							ME-ICP06	ME-ICP06	ME-ICP06	ME-ICP06	ME-ICP06	ME-ICP06	ME-ICP06	ME-ICP06	ME-ICP06	ME-ICP06	ME-ICP06	ME-ICP06	OA-GRA05	
							0.01	0.01	0.01	0.01			0.01	0.01	0.01	0.01	0.01	0.01	0.01	
MERN17MDS0035BG03	X258461	Brownlee rhyolite	Rhyolite	Ser-Chl	644426	5347363	63.70	1.16	13.45	9.13	0.05	5.93	0.50	0.01	0.02	1.56	1.02	0.34	3.77	100.63
MERN17MDS0044AG02	X258412	Brownlee rhyolite	Rhyolite	Ser-Chl	644493	5347553	68.60	0.47	11.65	10.45	0.06	2.97	0.13	0.01	0.06	0.08	1.44	0.10	3.08	99.09
MERN17MDS0045AG02	X258413	Brownlee rhyolite	Rhyolite	Ser-Chl	644405	5347521	65.90	0.80	13.30	9.34	0.08	4.58	0.32	0.01	0.05	0.08	2.00	0.27	3.69	100.41
MERN18MDS0104CG04	X258471	Brownlee rhyolite	Rhyolite	Ser-Chl	644494	5347556	69.10	0.52	12.90	8.63	0.06	4.56	0.09	0.01	0.07	0.10	1.77	0.10	3.61	101.51
MERN19MDS0129AG07	X261180	Brownlee rhyolite	Rhyolite	Ser-Chl	644505	5347412	70.60	0.43	10.80	9.18	0.03	2.98	0.12	0.01	0.04	0.11	1.55	0.10	2.99	98.93
MERN19MDS0129AG08	X261181	Brownlee rhyolite	Rhyolite	Ser-Chl	644504	5347410	69.70	0.49	11.95	8.14	0.02	3.45	0.14	0.01	0.04	0.13	1.86	0.11	3.03	99.06
MERN19MDS0129AG09	X261182	Brownlee rhyolite	Rhyolite	Ser-Chl	644503	5347409	70.70	0.46	11.55	8.42	0.02	3.38	0.12	0.01	0.04	0.11	1.73	0.11	3.01	99.65
MERN19MDS0129AG10	X261183	Brownlee rhyolite	Rhyolite	Ser-Chl	644503	5347408	75.80	0.40	10.40	7.68	0.02	3.05	0.12	0.01	0.03	0.11	1.56	0.09	2.63	101.89
MERN19MDS0129AG11	X261184	Brownlee rhyolite	Rhyolite	Ser-Chl	644503	5347408	69.70	0.44	11.40	8.72	0.02	3.40	0.13	0.01	0.04	0.11	1.68	0.10	3.09	98.83
MERN19MDS0129AG12	X261185	Brownlee rhyolite	Rhyolite	Ser-Chl	644503	5347408	72.00	0.44	11.20	7.92	0.02	2.96	0.13	0.01	0.04	0.12	1.82	0.11	2.87	99.63
MERN19MDS0129AG13	X261186	Brownlee rhyolite	Rhyolite	Ser-Chl	644502	5347407	70.00	0.42	10.95	8.82	0.02	3.24	0.13	0.01	0.03	0.10	1.56	0.09	3.04	98.4
MERN19MDS0129AG14	X261187	Brownlee rhyolite	Rhyolite	Ser-Chl	644502	5347407	70.80	0.43	10.50	8.82	0.02	3.18	0.12	0.01	0.03	0.09	1.45	0.09	2.96	98.49
MERN19MDS0129AG15	X261188	Brownlee rhyolite	Rhyolite	Ser-Chl	644502	5347407	70.80	0.42	10.95	8.67	0.02	3.10	0.11	0.01	0.03	0.10	1.62	0.09	2.90	98.81
MERN19MDS0129AG16	X261189	Brownlee rhyolite	Rhyolite	Ser-Chl	644510	5347419	68.30	0.48	12.20	9.39	0.03	3.49	0.14	0.01	0.04	0.12	1.76	0.12	3.24	99.31
MERN19MDS0129AG16 (DUP	X261195	Brownlee rhyolite	Rhyolite	Ser-Chl	644510	5347419	74.20	0.42	10.70	7.09	0.02	2.65	0.12	0.01	0.04	0.12	1.81	0.10	2.61	99.88
MERN19MDS0129AG18	X261190	Brownlee rhyolite	Rhyolite	Ser-Chl	644556	5347359	70.10	0.44	11.45	6.04	0.05	2.97	0.64	0.01	0.03	0.21	2.44	0.10	3.53	98
MERN19MDS0129AG19	X261191	Brownlee rhyolite	Rhyolite	Ser-Chl	644555	5347358	66.00	0.45	11.45	7.25	0.07	3.32	0.69	0.01	0.03	0.13	2.24	0.10	3.82	95.55
MERN19MDS0129AG20	X261192	Brownlee rhyolite	Rhyolite	Ser-Chl	644554	5347358	73.10	0.46	12.20	6.95	0.04	3.24	0.20	0.01	0.03	0.12	2.41	0.12	2.99	101.86
MERN19MDS0129AG21	X261193	Brownlee rhyolite	Rhyolite	Ser-Chl	644551	5347357	66.40	0.43	11.35	9.81	0.05	5.63	0.23	0.01	0.02	0.07	1.11	0.10	3.81	99.01
MERN19MDS0129AG23	X261194	Brownlee rhyolite	Rhyolite	Ser-Chl	644546	5347353	73.30	0.25	11.20	8.14	0.03	2.47	0.03	0.01	0.03	0.27	2.08	0.01	2.57	100.38
MERN19MDS0129AG22	X261139	Brownlee rhyolite	Rhyolite	Ser-Chl	644548	5347355	71.40	0.51	11.95	7.94	0.03	3.44	0.18	0.01	0.03	0.64	1.80	0.10	3.13	101.15
MERN19MDS0155AG01	X261150	Brownlee rhyolite	Rhyolite		644016	5347982	72.00	0.46	11.50	7.13	0.05	2.66	0.36	0.01	0.01	3.60	0.14	0.10	1.99	99.99
MERN19MDS0177BG02	X261160	Joliet rhyolite	Rhyolite		646424	5347442	77.80	0.24	12.00	3.90	0.05	1.67	0.15	0.01	0.02	4.15	0.68	0.04	1.27	101.97
MERN19MDS0178CG03	X261165	Joliet rhyolite	Rhyolite		646611	5347387	75.20	0.23	11.90	3.04	0.03	1.31	0.22	0.01	0.02	4.28	0.79	0.05	1.12	98.19
MERN20MDS0186CG14	C079654	Felsic dike	Rhyolite	Spotted	645800	5347138	69.50	0.43	13.35	4.64	0.03	3.78	0.13	0.01	0.04	1.35	2.03	0.08	2.91	98.27
MERN17MDS0030BG01	X258496	Héré "feeder" dike	Rhyolite		645036	5347711	73.90	0.34	11.40	8.33	0.08	2.23	0.05	0.01	0.08	0.18	1.75	0.07	2.76	101.17
MERN17MDS0033AG03	X258403	Héré "feeder" dike	Rhyolite		644497	5347308	76.30	0.26	10.75	4.87	0.04	2.39	0.17	0.01	0.03	0.10	2.33	0.09	2.50	99.83
MERN17MDS0033AG06	X258419	Héré "feeder" dike	Rhyolite		644491	5347311	74.50	0.26	11.25	6.45	0.07	3.59	0.05	0.01	0.03	0.10	1.99	0.03	2.96	101.28
MERN17MDS0033AG07	X258404	Héré "feeder" dike	Rhyolite		644462	5347319	74.10	0.23	11.05	6.14	0.04	1.12	0.54	0.01	0.03	3.52	1.14	0.04	1.57	99.52
MERN17MDS0033AG09	X258420	Héré "feeder" dike	Rhyolite	Spilite	644451	5347324	75.90	0.25	11.30	5.52	0.02	0.37	0.73	0.01	0.01	5.38	0.55	0.04	0.67	100.75
MERN17MDS0034AG03	X258406	Héré "feeder" dike	Rhyolite		644450	5347291	73.30	0.28	12.00	5.11	0.06	2.80	0.13	0.01	0.03	2.54	1.28	0.05	2.28	99.86
MERN17MDS0050AG01	X258472	Héré "feeder" dike	Rhyolite		644379	5347443	70.70	0.34	11.80	8.15	0.10	2.69	0.04	0.01	0.08	0.11	2.65	0.06	2.74	99.46
MERN18MDS0086AG04	X258438	Héré "feeder" dike	Rhyolite	Not spotted	645190	5347767	73.40	0.35	11.05	7.03	0.05	1.90	0.05	0.01	0.07	0.18	1.83	0.05	2.56	98.52
MERN18MDS0086AG05	X258439	Héré "feeder" dike	Rhyolite	Spotted	645190	5347765	73.50	0.34	10.90	7.60	0.04	2.98	0.07	0.01	0.06	0.14	1.45	0.05	2.91	100.04
MERN18MDS0086AG08	X258440	Héré "feeder" dike	Rhyolite		645186	5347742	75.60	0.37	11.80	5.63	0.02	2.51	0.07	0.01	0.12	0.18	1.92	0.05	2.73	101
MERN18MDS0087CG02	X258445	Héré "feeder" dike	Rhyolite	Spotted	644635	5347296	75.90	0.22	11.45	5.77	0.08	2.53	0.14	0.01	0.02	1.41	1.45	0.03	2.30	101.3
MERN18MDS0098BG09	X258450	Héré "feeder" dike	Rhyolite	Spilite	644647	5348093	75.60	0.31	11.90	4.58	0.07	2.85	0.11	0.01	0.01	4.71	0.05	0.04	1.74	101.96
MERN18MDS0100BG02	X258454	Héré "feeder" dike	Rhyolite	Spotted	644482	5347947	79.00	0.41	4.39	10.45	0.04	1.80	0.20	0.01	0.01	0.02	0.34	0.15	3.33	100.14
MERN18MDS0103BG02	X258490	Héré "feeder" dike	Rhyolite		645415	5347965	72.60	0.35	11.40	6.35	0.07	3.42	0.05	0.01	0.06	0.15	1.77	0.06	2.81	99.09
MERN18MDS0103BG02	X261055	Héré "feeder" dike	Rhyolite		645415	5347965	73.70	0.36	11.60	6.31	0.07	3.36	0.04	0.01	0.06	0.15	1.84	0.06	2.78	100.33
MERN18MDS0104BG03	X261053	Héré "feeder" dike	Rhyolite		644494	5347556	73.40	0.39	13.65	6.13	0.03	2.83	0.08	0.01	0.07	0.12	2.28	0.07	2.85	100.4
MERN18MDS0108BG02	X261059	Héré "feeder" dike	Rhyolite	Spilite	645622	5347834	75.00	0.39	13.65	4.92	0.04	2.77	0.11	0.01	0.01	3.27	0.63	0.07	2.31	101.17
MERN18MDS0113BG02	X258476	Héré "feeder" dike	Rhyolite		645805	5347679	72.10	0.50	13.65	6.53	0.06	3.32	0.12	0.01	0.09	0.94	1.92	0.09	2.77	100.19
MERN18MDS0114BG03	X258498	Héré "feeder" dike	Rhyolite	Spotted	645819	5347735	77.20	0.22	10.60	4.38	0.03	2.42	0.07	0.01	0.03	2.09	1.02	0.04	2.02	100.12
MERN18MDS0103EG05	X258473	Here Creek rhyolite	Rhyolite	Spotted	645415	5347965	75.80	0.22	11.40	5.50	0.03	3.16	0.10	0.01	0.08	0.18	1.87	0.04	2.83	101.21
MERN18MDS0120AG01	X258479	Héré Creek rhyolite	Rhyolite		645686	5348384	75.30	0.35	13.65	4.06	0.09	4.17	0.10	0.01	0.02	0.14	2.06	0.07	3.19	101.35
MERN19MDS0150AG03	X261143	Here Creek rhyolite	Rhyolite		646455	5348483	82.90	0.22	8.96	1.93	0.02	0.71	0.53	0.01	0.01	4.10	0.39	0.01	0.78	100.57
MERN19MDS0150BG02	X261142	Here Creek rhyolite	Rhyolite		646471	5348498	76.60	0.34	11.90	3.25	0.06	1.30	1.29	0.01	0.01	5.11	0.42	0.05	1.65	101.98
MERN19MDS0150CG01	X261141	Here Creek rhyolite	Rhyolite		646482	5348491	71.90	0.40	12.60	5.69	0.08	2.81	0.70	0.01	0.04	3.53	1.07	0.06	2.50	101.38
MERN19MDS0151AG01	X261144	Here Creek rhyolite	Rhyolite		646382	5348652	74.80	0.39	12.10	4.30	0.04	1.01	0.89	0.01	0.05	2.68	1.82	0.06	2.22	100.36
MERN19MDS0151AG02	X261145	Héré Creek rhyolite	Rhyolite		646382	5348652	68.50	0.37	12.00	7.97	0.07	1.19	1.68	0.01	0.02	4.53	0.49	0.07	2.28	99.17
MERN19MDS0165AG01	X261156	Here Creek rhyolite	Rhyolite	Spotted	645687	5348449	71.60	0.39	11.65	5.32	0.04	2.00	0.37	0.01	0.04	3.43	0.91	0.06	2.31	98.12

Number	Lab ID	Formation	Rock Type	Alteration	UTM-East	UTM-North	C %	S %	H20 %	Cl ppm	F ppm	S.G.	Ag ppm	As ppm	Au ppm	Ba ppm	Bi ppm	Cd ppm	Ce ppm	Co ppm
							C-IR07	S-IR08	OA-IR06	Cl-IC881	F-IC881		ME-4ACD81	ME-MS42	Au-ICP21	ME-MS81	ME-MS42	ME-4ACD81	ME-MS81	ME-4ACD81
							0.01	0.01	0.01				0.5	0.1		0.5	0.01	0.5	0.1	1
MERN17MDS0035BG03	X258461	Brownlee rhyolite	Rhyolite	Ser-Chl	644426	5347363	0.02	<0.01		25	820	2.75	0.25	0.2		230	0.05	0.25	37.6	11
MERN17MDS0044AG02	X258412	Brownlee rhyolite	Rhyolite	Ser-Chl	644493	5347553	0.01	0.01	3.94	25	640	2.78	0.25	0.4		509	0.17	0.25	42.3	11
MERN17MDS0045AG02	X258413	Brownlee rhyolite	Rhyolite	Ser-Chl	644405	5347521	0.01	0.04	3.93	25	960	2.76	0.25	0.1		459	0.17	0.25	47.5	12
MERN18MDS0104CG04	X258471	Brownlee rhyolite	Rhyolite	Ser-Chl	644494	5347556	<0.01	0.005		25	920	2.72	0.25	1.1		520	0.06	0.5	53.6	15
MERN19MDS0129AG07	X261180	Brownlee rhyolite	Rhyolite	Ser-Chl	644505	5347412	0.02	0.08	4.55			2.85								
MERN19MDS0129AG08	X261181	Brownlee rhyolite	Rhyolite	Ser-Chl	644504	5347410	0.01	0.02	4.51			2.78								
MERN19MDS0129AG09	X261182	Brownlee rhyolite	Rhyolite	Ser-Chl	644503	5347409	<0.01	0.02	4.25			2.86								
MERN19MDS0129AG10	X261183	Brownlee rhyolite	Rhyolite	Ser-Chl	644503	5347408	0.01	0.02	3.92			2.83								
MERN19MDS0129AG11	X261184	Brownlee rhyolite	Rhyolite	Ser-Chl	644503	5347408	0.01	0.02	4.38			2.79								
MERN19MDS0129AG12	X261185	Brownlee rhyolite	Rhyolite	Ser-Chl	644503	5347408	0.01	<0.01	3.96			2.79								
MERN19MDS0129AG13	X261186	Brownlee rhyolite	Rhyolite	Ser-Chl	644502	5347407	0.01	0.02	4.25			2.79								
MERN19MDS0129AG14	X261187	Brownlee rhyolite	Rhyolite	Ser-Chl	644502	5347407	0.01	0.08	4.02			2.85								
MERN19MDS0129AG15	X261188	Brownlee rhyolite	Rhyolite	Ser-Chl	644502	5347407	0.01	0.04	4.05			2.84								
MERN19MDS0129AG16	X261189	Brownlee rhyolite	Rhyolite	Ser-Chl	644510	5347419	0.01	0.02	4.65			2.8								
MERN19MDS0129AG16 (DUF	X261195	Brownlee rhyolite	Rhyolite	Ser-Chl	644510	5347419	0.01	<0.01	3.39			2.77								
MERN19MDS0129AG18	X261190	Brownlee rhyolite	Rhyolite	Ser-Chl	644556	5347359	0.23	0.03	3.43			2.82								
MERN19MDS0129AG19	X261191	Brownlee rhyolite	Rhyolite	Ser-Chl	644555	5347358	0.27	0.07	3.96			2.73								
MERN19MDS0129AG20	X261192	Brownlee rhyolite	Rhyolite	Ser-Chl	644554	5347358	0.04	0.06	3.83			2.83								
MERN19MDS0129AG21	X261193	Brownlee rhyolite	Rhyolite	Ser-Chl	644551	5347357	0.04	0.02	5.29			2.82								
MERN19MDS0129AG23	X261194	Brownlee rhyolite	Rhyolite	Ser-Chl	644546	5347353	<0.01	0.12	3.45			2.74								
MERN19MDS0129AG22	X261139	Brownlee rhyolite	Rhyolite	Ser-Chl	644548	5347355	0.04	0.03	3.97	170	530	2.82								
MERN19MDS0155AG01	X261150	Brownlee rhyolite	Rhyolite		644016	5347982	0.06	<0.01					0.25	0.1		30.9	0.02	<0.5	74.1	4
MERN19MDS0177BG02	X261160	Joliet rhyolite	Rhyolite		646424	5347442	0.01	<0.01					0.25	0.1		130	0.02	<0.5	36.2	2
MERN19MDS0178CG03	X261165	Joliet rhyolite	Rhyolite		646611	5347387	0.02	<0.01					0.25	0.3		147	0.04	<0.5	37.4	2
MERN20MDS0186CG14	C079654	Felsic dike	Rhyolite	Spotted	645800	5347138	<0.01	<0.01	3.19	90	770	2.78								
MERN17MDS0030BG01	X258496	Héré "feeder" dike	Rhyolite		645036	5347711	<0.01	0.01		<50	330	2.75								
MERN17MDS0033AG03	X258403	Héré "feeder" dike	Rhyolite		644497	5347308	0.02	0.04	2.81	70	680	2.81	0.5	0.8		260	1.43	3	11.4	4
MERN17MDS0033AG06	X258419	Héré "feeder" dike	Rhyolite		644491	5347311	0.01	0.06	3.29	90	580	2.74								
MERN17MDS0033AG07	X258404	Héré "feeder" dike	Rhyolite		644462	5347319	0.1	0.11	1.18	70	300	2.73	0.25	0.2		211	0.18	0.25	31.2	5
MERN17MDS0033AG09	X258420	Héré "feeder" dike	Rhyolite	Spilite	644451	5347324	0.12	0.03	0.46	80	220	2.73								
MERN17MDS0034AG03	X258406	Héré "feeder" dike	Rhyolite		644450	5347291	0.01	0.04	2.25	25	480	2.76	0.25	0.1		305	0.08	0.25	49.3	7
MERN17MDS0050AG01	X258472	Héré "feeder" dike	Rhyolite		644379	5347443	<0.01	0.07		<50	430	2.73								
MERN18MDS0086AG04	X258438	Héré "feeder" dike	Rhyolite	Not spotted	645190	5347767	0.01	0.03	2.68	25	460	2.74	0.25	0.3		630	0.12	0.25	47.3	5
MERN18MDS0086AG05	X258439	Héré "feeder" dike	Rhyolite	Spotted	645190	5347765	0.01	0.01	3.03	25	520	2.73	0.25	0.2		485	0.03	0.25	38.4	8
MERN18MDS0086AG08	X258440	Héré "feeder" dike	Rhyolite		645186	5347742	0.02	0.01	2.62	25	440	2.75	0.25	0.1	<0.001	1085	1.09	0.25	36.3	11
MERN18MDS0087CG02	X258445	Héré "feeder" dike	Rhyolite	Spotted	644635	5347296	0.05	0.01	2.4	50	690	2.7	0.25	0.05		218		0.25	124	2
MERN18MDS0098BG09	X258450	Héré "feeder" dike	Rhyolite	Spilite	644647	5348093	0.01	0.01	1.4	90	230	2.68	0.25	0.05		26.2		0.25	40	5
MERN18MDS0100BG02	X258454	Héré "feeder" dike	Rhyolite	Spotted	644482	5347947	0.02	3.36	1.84	90	400	2.79	7.9	8.4	0.09	113.5		0.25	14.4	43
MERN18MDS0103BG02	X258490	Héré "feeder" dike	Rhyolite		645415	5347965	<0.01	0.01		<50	390	2.74								
MERN18MDS0103BG02	X261055	Héré "feeder" dike	Rhyolite		645415	5347965	<0.01	0.01		<50	380	2.76								
MERN18MDS0104BG03	X261053	Héré "feeder" dike	Rhyolite		644494	5347556	0.005	0.005		25	890	2.74	0.25	0.1		611	0.08	0.25	46.9	9
MERN18MDS0108BG02	X261059	Héré "feeder" dike	Rhyolite	Spilite	645622	5347834	0.12	0.005		25	260	2.72	0.25	0.05		109.5	0.01	0.25	42.6	4
MERN18MDS0113BG02	X258476	Héré "feeder" dike	Rhyolite		645805	5347679	0.01	0.005		70	450	2.73	0.25	<0.1		856	0.03	0.25	37.5	5
MERN18MDS0114BG03	X258498	Héré "feeder" dike	Rhyolite		645819	5347735	<0.01	0.03		<50	280	2.73								
MERN18MDS0103EG05	X258473	Here Creek rhyolite	Rhyolite	Spotted	645415	5347965	<0.01	0.005		50	460	2.79	0.25	0.2		762	0.06	0.25	54.6	7
MERN18MDS0120AG01	X258479	Héré Creek rhyolite	Rhyolite		645686	5348384	0.005	0.005		25	440	2.73	0.25	2		208	0.02	0.25	42.4	1
MERN19MDS0150AG03	X261143	Here Creek rhyolite	Rhyolite		646455	5348483	0.08	<0.01	0.76	130	210	2.71								
MERN19MDS0150BG02	X261142	Here Creek rhyolite	Rhyolite		646471	5348498	0.22	<0.01	1.23	<50	230	2.76								
MERN19MDS0150CG01	X261141	Here Creek rhyolite	Rhyolite		646482	5348491	0.11	0.01	2.65	130	330	2.77								
MERN19MDS0151AG01	X261144	Here Creek rhyolite	Rhyolite		646382	5348652	0.2	<0.01	1.81	<50	350	2.72								
MERN19MDS0151AG02	X261145	Héré Creek rhyolite	Rhyolite		646382	5348652	0.35	<0.01					0.25	0.4		177.5	0.01	<0.5	64.2	2
MERN19MDS0165AG01	X261156	Here Creek rhyolite	Rhyolite	Spotted	645687	5348449	0.14	0.39	2.3	260	350	2.73								

Number	Lab ID	Formation	Rock Type	Alteration	UTM-East	UTM-North	Cr ppm	Cs ppm	Cu ppm	Dy ppm	Er ppm	Eu ppm	Ga_ppm	Gd_ppm	Ge_ppm	Hf_ppm	Hg_ppm	Ho_ppm	In_ppm
							ME-MS81	ME-MS81	ME-4ACD81	ME-MS81	ME-MS81	ME-MS81	ME-MS81	ME-MS81	ME-MS81	ME-MS81	ME-MS42	ME-MS81	ME-MS42
								10	1	0.05	0.03	0.03	0.1	0.05	5	0.2	0.005	0.01	0.005
MERN17MDS0035BG03	X258461	Brownlee rhyolite	Rhyolite	Ser-Chl	644426	5347363	10	0.34	10	7.25	4.38	1.18	21.5	7.01	2.5	4.3	0.0025	1.66	0.018
MERN17MDS0044AG02	X258412	Brownlee rhyolite	Rhyolite	Ser-Chl	644493	5347553	10	0.31	15	9.79	6.15	1.22	18.8	8.21	2.5	7.1	0	2.18	0.02
MERN17MDS0045AG02	X258413	Brownlee rhyolite	Rhyolite	Ser-Chl	644405	5347521	10	0.54	8	7.91	4.69	1	19.9	8.13	2.5	5.3	0	1.73	0.02
MERN18MDS0104CG04	X258471	Brownlee rhyolite	Rhyolite	Ser-Chl	644494	5347556	10	0.31	25	5.83	4.2	0.55	15.3	5.65	2.5	4.8	0.0025	1.3	0.046
MERN19MDS0129AG07	X261180	Brownlee rhyolite	Rhyolite	Ser-Chl	644505	5347412													
MERN19MDS0129AG08	X261181	Brownlee rhyolite	Rhyolite	Ser-Chl	644504	5347410													
MERN19MDS0129AG09	X261182	Brownlee rhyolite	Rhyolite	Ser-Chl	644503	5347409													
MERN19MDS0129AG10	X261183	Brownlee rhyolite	Rhyolite	Ser-Chl	644503	5347408													
MERN19MDS0129AG11	X261184	Brownlee rhyolite	Rhyolite	Ser-Chl	644503	5347408													
MERN19MDS0129AG12	X261185	Brownlee rhyolite	Rhyolite	Ser-Chl	644503	5347408													
MERN19MDS0129AG13	X261186	Brownlee rhyolite	Rhyolite	Ser-Chl	644502	5347407													
MERN19MDS0129AG14	X261187	Brownlee rhyolite	Rhyolite	Ser-Chl	644502	5347407													
MERN19MDS0129AG15	X261188	Brownlee rhyolite	Rhyolite	Ser-Chl	644502	5347407													
MERN19MDS0129AG16	X261189	Brownlee rhyolite	Rhyolite	Ser-Chl	644510	5347419													
MERN19MDS0129AG16 (DUF	X261195	Brownlee rhyolite	Rhyolite	Ser-Chl	644510	5347419													
MERN19MDS0129AG18	X261190	Brownlee rhyolite	Rhyolite	Ser-Chl	644556	5347359													
MERN19MDS0129AG19	X261191	Brownlee rhyolite	Rhyolite	Ser-Chl	644555	5347358													
MERN19MDS0129AG20	X261192	Brownlee rhyolite	Rhyolite	Ser-Chl	644554	5347358													
MERN19MDS0129AG21	X261193	Brownlee rhyolite	Rhyolite	Ser-Chl	644551	5347357													
MERN19MDS0129AG23	X261194	Brownlee rhyolite	Rhyolite	Ser-Chl	644546	5347353													
MERN19MDS0129AG22	X261139	Brownlee rhyolite	Rhyolite	Ser-Chl	644548	5347355													
MERN19MDS0155AG01	X261150	Brownlee rhyolite	Rhyolite		644016	5347982	20	0.05	12	9.05	5.69	2.41	18.8	9.42	<5	6.6	<0.005	1.84	0.031
MERN19MDS0177BG02	X261160	Joliet rhyolite	Rhyolite		646424	5347442	20	0.24	6	6.43	4.42	0.8	16.4	5.67	<5	5.4	<0.005	1.44	0.006
MERN19MDS0178CG03	X261165	Joliet rhyolite	Rhyolite		646611	5347387	30	0.27	2	7.05	4.88	0.72	15.9	5.99	<5	6.1	<0.005	1.6	0.005
MERN20MDS0186CG14	C079654	Felsic dike	Rhyolite	Spotted	645800	5347138													
MERN17MDS0030BG01	X258496	Héré "feeder" dike	Rhyolite		645036	5347711													
MERN17MDS0033AG03	X258403	Héré "feeder" dike	Rhyolite		644497	5347308	10	0.45	13	5.96	3.95	0.67	17.1	4.52	2.5	4.6	0.17	1.31	0.56
MERN17MDS0033AG06	X258419	Héré "feeder" dike	Rhyolite		644491	5347311													
MERN17MDS0033AG07	X258404	Héré "feeder" dike	Rhyolite		644462	5347319	10	0.45	29	6.09	4.32	1.13	19.1	5.35	2.5	4.8	0	1.44	0.01
MERN17MDS0033AG09	X258420	Héré "feeder" dike	Rhyolite	Spilite	644451	5347324													
MERN17MDS0034AG03	X258406	Héré "feeder" dike	Rhyolite		644450	5347291	10	0.41	30	8.33	5.58	1.27	16.9	7.33	2.5	7.9	0.01	1.81	0.01
MERN17MDS0050AG01	X258472	Héré "feeder" dike	Rhyolite		644379	5347443													
MERN18MDS0086AG04	X258438	Héré "feeder" dike	Rhyolite	Not spotted	645190	5347767	10	0.27	25	6.56	4.09	0.31	17.4	6.28	2.5	7	0	1.35	0.02
MERN18MDS0086AG05	X258439	Héré "feeder" dike	Rhyolite	Spotted	645190	5347765	5	0.27	5	6.31	4.49	0.36	15.5	5.19	2.5	6.2	0	1.4	0.02
MERN18MDS0086AG08	X258440	Héré "feeder" dike	Rhyolite		645186	5347742	10	0.31	4	6.58	4.95	0.42	16.9	5.29	2.5	7.1	0	1.53	0.01
MERN18MDS0087CG02	X258445	Héré "feeder" dike	Rhyolite	Spotted	644635	5347296	10	0.34	9	10.75	6.66	2.21	19.5	11.6	2.5	5.4	0	2.27	0.04
MERN18MDS0098BG09	X258450	Héré "feeder" dike	Rhyolite	Spilite	644647	5348093	20	0.05	7	5.88	4.22	1.29	17.8	5.11	2.5	4.8	0	1.29	0.02
MERN18MDS0100BG02	X258454	Héré "feeder" dike	Rhyolite	Spotted	644482	5347947	20	0.11	16000	3.93	2.62	0.67	7.9	3.58	2.5	0.9	0.02	0.9	3.36
MERN18MDS0103BG02	X258490	Héré "feeder" dike	Rhyolite		645415	5347965													
MERN18MDS0103BG02	X261055	Héré "feeder" dike	Rhyolite		645415	5347965													
MERN18MDS0104BG03	X261053	Héré "feeder" dike	Rhyolite		644494	5347556	5	0.44	4	6.02	4.38	0.76	14.5	5.67	2.5	6.1	0.0025	1.39	0.032
MERN18MDS0108BG02	X261059	Héré "feeder" dike	Rhyolite	Spilite	645622	5347834	10	0.16	4	6.08	4.29	1.13	13.7	5.83	2.5	5.9	0.0025	1.4	0.012
MERN18MDS0113BG02	X258476	Héré "feeder" dike	Rhyolite		645805	5347679	10	0.62	36	5.75	4.27	0.82	14.8	5.3	2.5	5.6	0.0025	1.35	0.077
MERN18MDS0114BG03	X258498	Héré "feeder" dike	Rhyolite		645819	5347735													
MERN18MDS0103EG05	X258473	Here Creek rhyolite	Rhyolite	Spotted	645415	5347965	10	0.33	10	8.16	5.69	0.75	16.6	7.45	2.5	7.3	0.0025	1.83	0.022
MERN18MDS0120AG01	X258479	Héré Creek rhyolite	Rhyolite		645686	5348384	5	0.31	37	5.77	4.24	1.03	16	5.59	2.5	6.4	0.0025	1.33	0.014
MERN19MDS0150AG03	X261143	Here Creek rhyolite	Rhyolite		646455	5348483													
MERN19MDS0150BG02	X261142	Here Creek rhyolite	Rhyolite		646471	5348498													
MERN19MDS0150CG01	X261141	Here Creek rhyolite	Rhyolite		646482	5348491													
MERN19MDS0151AG01	X261144	Here Creek rhyolite	Rhyolite		646382	5348652													
MERN19MDS0151AG02	X261145	Héré Creek rhyolite	Rhyolite		646382	5348652	20	0.28	2	8.17	5.49	1.34	19	7.76	<5	7.1	<0.005	1.8	0.021
MERN19MDS0165AG01	X261156	Here Creek rhyolite	Rhyolite	Spotted	645687	5348449													

Number	Lab ID	Formation	Rock Type	Alteration	UTM-East	UTM-North	La_ppm	Li_ppm	Lu_ppm	Mo_ppm	Nb_ppm	Nd_ppm	Ni_ppm	Pb_ppm	Rb_ppm	Re_ppm	Sb_ppm	Sc_ppm	Se_ppm	Sm_ppm
							ME-MS81	ME-4ACD81	ME-MS81	ME-4ACD81	ME-MS81	ME-MS81	ME-4ACD81	ME-4ACD81	ME-MS81	ME-MS42	ME-MS42	ME-4ACD81	ME-MS42	ME-MS81
							0.1	10	0.01	1	0.2	0.1	1	2	0.2	0.001	0.05	1	0.2	0.03
MERN17MDS0035BG03	X258461	Brownlee rhyolite	Rhyolite	Ser-Chl	644426	5347363	15.6	40	0.68	0.5	8.5	22.6	6	2	20.6	0.0005	0.09	24	0.1	5.81
MERN17MDS0044AG02	X258412	Brownlee rhyolite	Rhyolite	Ser-Chl	644493	5347553	17.4	20	0.9	1	11.8	24.2	2	3	24.4	0	0.03	16	0.3	5.96
MERN17MDS0045AG02	X258413	Brownlee rhyolite	Rhyolite	Ser-Chl	644405	5347521	19.7	30	0.69	2	10	28.7	3	3	36.8	0	0.03	15	0.1	6.96
MERN18MDS0104CG04	X258471	Brownlee rhyolite	Rhyolite	Ser-Chl	644494	5347556	23.7	30	0.64	1	8.7	28.8	9	1	28.6	0.0005	0.05	12	0.1	6.25
MERN19MDS0129AG07	X261180	Brownlee rhyolite	Rhyolite	Ser-Chl	644505	5347412														
MERN19MDS0129AG08	X261181	Brownlee rhyolite	Rhyolite	Ser-Chl	644504	5347410														
MERN19MDS0129AG09	X261182	Brownlee rhyolite	Rhyolite	Ser-Chl	644503	5347409														
MERN19MDS0129AG10	X261183	Brownlee rhyolite	Rhyolite	Ser-Chl	644503	5347408														
MERN19MDS0129AG11	X261184	Brownlee rhyolite	Rhyolite	Ser-Chl	644503	5347408														
MERN19MDS0129AG12	X261185	Brownlee rhyolite	Rhyolite	Ser-Chl	644503	5347408														
MERN19MDS0129AG13	X261186	Brownlee rhyolite	Rhyolite	Ser-Chl	644502	5347407														
MERN19MDS0129AG14	X261187	Brownlee rhyolite	Rhyolite	Ser-Chl	644502	5347407														
MERN19MDS0129AG15	X261188	Brownlee rhyolite	Rhyolite	Ser-Chl	644502	5347407														
MERN19MDS0129AG16	X261189	Brownlee rhyolite	Rhyolite	Ser-Chl	644510	5347419														
MERN19MDS0129AG16 (DUF	X261195	Brownlee rhyolite	Rhyolite	Ser-Chl	644510	5347419														
MERN19MDS0129AG18	X261190	Brownlee rhyolite	Rhyolite	Ser-Chl	644556	5347359														
MERN19MDS0129AG19	X261191	Brownlee rhyolite	Rhyolite	Ser-Chl	644555	5347358														
MERN19MDS0129AG20	X261192	Brownlee rhyolite	Rhyolite	Ser-Chl	644554	5347358														
MERN19MDS0129AG21	X261193	Brownlee rhyolite	Rhyolite	Ser-Chl	644551	5347357														
MERN19MDS0129AG23	X261194	Brownlee rhyolite	Rhyolite	Ser-Chl	644546	5347353														
MERN19MDS0129AG22	X261139	Brownlee rhyolite	Rhyolite	Ser-Chl	644548	5347355														
MERN19MDS0155AG01	X261150	Brownlee rhyolite	Rhyolite		644016	5347982	33.6	20	0.74	1	11	40.5	<1	2	2.4	<0.001	<0.05	14	0.2	10.3
MERN19MDS0177BG02	X261160	Joliet rhyolite	Rhyolite		646424	5347442	16.7	10	0.76	2	8.2	19.5	<1	2	12.5	0.001	<0.05	7	<0.2	4.94
MERN19MDS0178CG03	X261165	Joliet rhyolite	Rhyolite		646611	5347387	16.7	10	0.79	2	8.1	20.7	<1	<2	14.8	0.001	<0.05	8	<0.2	5.15
MERN20MDS0186CG14	C079654	Felsic dike	Rhyolite	Spotted	645800	5347138														
MERN17MDS0030BG01	X258496	Héré "feeder" dike	Rhyolite		645036	5347711														
MERN17MDS0033AG03	X258403	Héré "feeder" dike	Rhyolite		644497	5347308	4.9	20	0.59	0.5	12.3	9	6	1	40	0	0.03	14	0.1	2.75
MERN17MDS0033AG06	X258419	Héré "feeder" dike	Rhyolite		644491	5347311														
MERN17MDS0033AG07	X258404	Héré "feeder" dike	Rhyolite		644462	5347319	15.7	10	0.68	3	13.1	19.8	2	2	22.1	0	0.03	11	0.1	4.96
MERN17MDS0033AG09	X258420	Héré "feeder" dike	Rhyolite	Spilite	644451	5347324														
MERN17MDS0034AG03	X258406	Héré "feeder" dike	Rhyolite		644450	5347291	22.6	20	0.84	1	12.9	26.5	1	1	22.4	0	0.03	9	0.3	7.09
MERN17MDS0050AG01	X258472	Héré "feeder" dike	Rhyolite		644379	5347443														
MERN18MDS0086AG04	X258438	Héré "feeder" dike	Rhyolite	Not spotted	645190	5347767	20.5	10	0.67	1	11.4	25.5	1	3	28.7	0	0.38	10	0.2	5.54
MERN18MDS0086AG05	X258439	Héré "feeder" dike	Rhyolite	Spotted	645190	5347765	15.9	10	0.65	1	12.7	20.8	0.5	1	20.5	0	0.05	10	0.2	4.7
MERN18MDS0086AG08	X258440	Héré "feeder" dike	Rhyolite		645186	5347742	14	10	0.78	1	12.5	19.4	3	3	26.7	0	0.03	10	0.1	4.75
MERN18MDS0087CG02	X258445	Héré "feeder" dike	Rhyolite	Spotted	644635	5347296	53.5	30	1	0.5	13.2	61.5	2	1	23.1	0	0.05	12	0.2	12.9
MERN18MDS0098BG09	X258450	Héré "feeder" dike	Rhyolite	Spilite	644647	5348093	16.6	10	0.68	1	12.6	22.3	1	2	0.7	0	0.03	14	0.2	5.3
MERN18MDS0100BG02	X258454	Héré "feeder" dike	Rhyolite	Spotted	644482	5347947	6.1	10	0.31	6	2.1	9.3	4	7	6.5	0	0.1	6	20.8	2.47
MERN18MDS0103BG02	X258490	Héré "feeder" dike	Rhyolite		645415	5347965														
MERN18MDS0103BG02	X261055	Héré "feeder" dike	Rhyolite		645415	5347965														
MERN18MDS0104BG03	X261053	Héré "feeder" dike	Rhyolite		644494	5347556	21.5	20	0.71	0.5	10.9	26	2	1	38.8	0.0005	0.025	11	0.1	6.03
MERN18MDS0108BG02	X261059	Héré "feeder" dike	Rhyolite	Spilite	645622	5347834	19.9	10	0.69	1	9.9	23.3	2	1	10.9	0.0005	0.025	9	0.1	5.7
MERN18MDS0113BG02	X258476	Héré "feeder" dike	Rhyolite		645805	5347679	17.7	20	0.72	0.5	10.1	20.9	4	2	33.9	0.0005	0.025	13	0.1	4.9
MERN18MDS0114BG03	X258498	Héré "feeder" dike	Rhyolite		645819	5347735														
MERN18MDS0103EG05	X258473	Here Creek rhyolite	Rhyolite	Spotted	645415	5347965	25.5	20	0.94	0.5	12.6	29.7	1	1	30.3	0.0005	0.05	9	0.1	6.98
MERN18MDS0120AG01	X258479	Héré Creek rhyolite	Rhyolite		645686	5348384	20.3	20	0.74	0.5	11.5	23.2	1	1	35.3	0.0005	0.025	10	0.1	5.58
MERN19MDS0150AG03	X261143	Here Creek rhyolite	Rhyolite		646455	5348483														
MERN19MDS0150BG02	X261142	Here Creek rhyolite	Rhyolite		646471	5348498														
MERN19MDS0150CG01	X261141	Here Creek rhyolite	Rhyolite		646482	5348491														
MERN19MDS0151AG01	X261144	Here Creek rhyolite	Rhyolite		646382	5348652														
MERN19MDS0151AG02	X261145	Héré Creek rhyolite	Rhyolite		646382	5348652	27.5	20	0.85	1	9.4	32.6	2	<2	9.2	<0.001	<0.05	12	<0.2	7.73
MERN19MDS0165AG01	X261156	Here Creek rhyolite	Rhyolite	Spotted	645687	5348449														

Number	Lab ID	Formation	Rock Type	Alteration	UTM-East	UTM-North	Sn_ppm	Sr_ppm	Ta_ppm	Tb_ppm	Te_ppm	Th_ppm	Tl_ppm	Tm_ppm	U_ppm	V_ppm	W_ppm	Y_ppm	Yb_ppm	Zn_ppm	Zr_ppm
							ME-MS81	ME-MS81	ME-MS81	ME-MS81	ME-MS42	ME-MS81	ME-MS42	ME-MS81	ME-MS81	ME-MS81	ME-MS81	ME-MS81	ME-MS81	ME4ACD81	ME-MS81
							1	0.1	0.1	0.01	0.01	0.05	0.02	0.01	0.05	5	1	0.1	0.03	2	2
MERN17MDS0035BG03	X258461	Brownlee rhyolite	Rhyolite	Ser-Chl	644426	5347363	2	17.6	0.6	1.22	0.02	1.5	0.01	0.67	0.46	61	2	42.5	4.19	78	157
MERN17MDS0044AG02	X258412	Brownlee rhyolite	Rhyolite	Ser-Chl	644493	5347553	4	6.8	0.7	1.55	0.02	2.78	0.01	0.93	0.83	2.5	2	55	6.31	41	260
MERN17MDS0045AG02	X258413	Brownlee rhyolite	Rhyolite	Ser-Chl	644405	5347521	3	10.4	0.6	1.32	0.06	2.23	0.01	0.72	0.65	23	2	43.7	4.81	77	217
MERN18MDS0104CG04	X258471	Brownlee rhyolite	Rhyolite	Ser-Chl	644494	5347556	5	7	0.5	1.02	0.02	2.73	0.01	0.62	0.72	68	2	34.8	4.18	298	215
MERN19MDS0129AG07	X261180	Brownlee rhyolite	Rhyolite	Ser-Chl	644505	5347412												43.5			233
MERN19MDS0129AG08	X261181	Brownlee rhyolite	Rhyolite	Ser-Chl	644504	5347410												47.9			249
MERN19MDS0129AG09	X261182	Brownlee rhyolite	Rhyolite	Ser-Chl	644503	5347409												46.9			250
MERN19MDS0129AG10	X261183	Brownlee rhyolite	Rhyolite	Ser-Chl	644503	5347408												44.3			226
MERN19MDS0129AG11	X261184	Brownlee rhyolite	Rhyolite	Ser-Chl	644503	5347408												46.7			228
MERN19MDS0129AG12	X261185	Brownlee rhyolite	Rhyolite	Ser-Chl	644503	5347408												48.8			238
MERN19MDS0129AG13	X261186	Brownlee rhyolite	Rhyolite	Ser-Chl	644502	5347407												43.2			221
MERN19MDS0129AG14	X261187	Brownlee rhyolite	Rhyolite	Ser-Chl	644502	5347407												47.6			239
MERN19MDS0129AG15	X261188	Brownlee rhyolite	Rhyolite	Ser-Chl	644502	5347407												37.8			228
MERN19MDS0129AG16	X261189	Brownlee rhyolite	Rhyolite	Ser-Chl	644510	5347419												53.2			262
MERN19MDS0129AG16 (DUF	X261195	Brownlee rhyolite	Rhyolite	Ser-Chl	644510	5347419												50.2			228
MERN19MDS0129AG18	X261190	Brownlee rhyolite	Rhyolite	Ser-Chl	644556	5347359												48.2			238
MERN19MDS0129AG19	X261191	Brownlee rhyolite	Rhyolite	Ser-Chl	644555	5347358												47.5			236
MERN19MDS0129AG20	X261192	Brownlee rhyolite	Rhyolite	Ser-Chl	644554	5347358												46.8			244
MERN19MDS0129AG21	X261193	Brownlee rhyolite	Rhyolite	Ser-Chl	644551	5347357												49.8			228
MERN19MDS0129AG23	X261194	Brownlee rhyolite	Rhyolite	Ser-Chl	644546	5347353												40.6			180
MERN19MDS0129AG22	X261139	Brownlee rhyolite	Rhyolite	Ser-Chl	644548	5347355												53			291
MERN19MDS0155AG01	X261150	Brownlee rhyolite	Rhyolite		644016	5347982	1	31.6	0.7	1.53	0.01	2.71	<0.02	0.83	0.68	<5	<1	50.6	5.2	69	257
MERN19MDS0177BG02	X261160	Joliet rhyolite	Rhyolite		646424	5347442	1	29.6	0.7	0.94	0.02	2.95	<0.02	0.73	0.83	8	1	41.6	4.43	30	210
MERN19MDS0178CG03	X261165	Joliet rhyolite	Rhyolite		646611	5347387	1	24.9	0.7	1.03	0.01	3.15	<0.02	0.75	0.92	8	1	43.9	5.14	25	218
MERN20MDS0186CG14	C079654	Felsic dike	Rhyolite	Spotted	645800	5347138												34.5			233
MERN17MDS0030BG01	X258496	Héré "feeder" dike	Rhyolite		645036	5347711												41.9			267
MERN17MDS0033AG03	X258403	Héré "feeder" dike	Rhyolite		644497	5347308	39	6.4	0.7	0.84	0.04	1.85	0.01	0.58	0.42	18	2	33.4	4.12	819	176
MERN17MDS0033AG06	X258419	Héré "feeder" dike	Rhyolite		644491	5347311												32.5			201
MERN17MDS0033AG07	X258404	Héré "feeder" dike	Rhyolite		644462	5347319	5	47.1	0.7	0.98	0.04	2.11	0.01	0.64	0.71	2.5	1	32.8	4.29	77	178
MERN17MDS0033AG09	X258420	Héré "feeder" dike	Rhyolite	Spilite	644451	5347324												47.8			204
MERN17MDS0034AG03	X258406	Héré "feeder" dike	Rhyolite		644450	5347291	2	29.6	0.7	1.35	0.02	4.04	0.01	0.81	0.96	6	1	46.6	6.17	91	289
MERN17MDS0050AG01	X258472	Héré "feeder" dike	Rhyolite		644379	5347443												39			272
MERN18MDS0086AG04	X258438	Héré "feeder" dike	Rhyolite	Not spotted	645190	5347767	3	7.3	0.8	1.08	0.07	3.53	0.01	0.64	0.92	7	3	35.2	4.35	101	256
MERN18MDS0086AG05	X258439	Héré "feeder" dike	Rhyolite	Spotted	645190	5347765	4	5.8	0.6	1.08	0.02	3.63	0.01	0.69	0.89	2.5	2	42.9	4.57	135	243
MERN18MDS0086AG08	X258440	Héré "feeder" dike	Rhyolite		645186	5347742	3	9.5	0.7	1.01	0.81	3.87	0.01	0.75	0.97	6	1	46	4.97	41	285
MERN18MDS0087CG02	X258445	Héré "feeder" dike	Rhyolite	Spotted	644635	5347296	6	11.6	0.8	1.95	0.01	2.48	0.01	1.03	0.81	2.5	1	66.9	6.5	248	210
MERN18MDS0098BG09	X258450	Héré "feeder" dike	Rhyolite	Spilite	644647	5348093	1	27.1	0.7	0.97	0.01	2.02	0.01	0.61	0.53	2.5	1	36.3	4.18	95	189
MERN18MDS0100BG02	X258454	Héré "feeder" dike	Rhyolite	Spotted	644482	5347947	2	5.5	0.05	0.65	1.78	0.3	0.01	0.38	0.23	17	8	27.9	1.99	42	34
MERN18MDS0103BG02	X258490	Héré "feeder" dike	Rhyolite		645415	5347965												43.9			252
MERN18MDS0103BG02	X261055	Héré "feeder" dike	Rhyolite		645415	5347965												43.8			259
MERN18MDS0104BG03	X261053	Héré "feeder" dike	Rhyolite		644494	5347556	6	6.8	0.7	1.03	0.01	3.47	0.01	0.68	0.89	11	3	37.2	4.53	127	273
MERN18MDS0108BG02	X261059	Héré "feeder" dike	Rhyolite	Spilite	645622	5347834	4	14.1	0.6	1.07	0.01	3.02	0.01	0.68	0.78	9	1	36.5	4.42	139	260
MERN18MDS0113BG02	X258476	Héré "feeder" dike	Rhyolite		645805	5347679	7	9.8	0.6	0.95	0.03	2.91	0.01	0.67	0.72	43	1	35.7	4.58	119	249
MERN18MDS0114BG03	X258498	Héré "feeder" dike	Rhyolite		645819	5347735												35.8			258
MERN18MDS0103EG05	X258473	Here Creek rhyolite	Rhyolite	Spotted	645415	5347965	6	7.2	0.8	1.38	0.03	4.04	0.01	0.88	1.04	5	1	48.3	5.91	140	318
MERN18MDS0120AG01	X258479	Héré Creek rhyolite	Rhyolite		645686	5348384	1	11.3	0.7	1.02	0.01	3.49	0.01	0.68	0.92	7	0.5	35.9	4.52	188	286
MERN19MDS0150AG03	X261143	Here Creek rhyolite	Rhyolite		646455	5348483												39.2			214
MERN19MDS0150BG02	X261142	Here Creek rhyolite	Rhyolite		646471	5348498												29			269
MERN19MDS0150CG01	X261141	Here Creek rhyolite	Rhyolite		646482	5348491												50.2			298
MERN19MDS0151AG01	X261144	Here Creek rhyolite	Rhyolite		646382	5348652												48.2			286
MERN19MDS0151AG02	X261145	Héré Creek rhyolite	Rhyolite		646382	5348652	2	54.5	0.7	1.28	<0.01	4.08	<0.02	0.86	1.17	7	1	49.4	5.69	42	278
MERN19MDS0165AG01	X261156	Here Creek rhyolite	Rhyolite	Spotted	645687	5348449												35.1			271

Number	Lab ID	Formation	Rock Type	Alteration	UTM-East	UTM-North	SiO2 wt%	TiO2 wt%	Al2O3 wt%	Fe2O3t wt%	MnO wt%	MgO wt%	CaO wt%	SrO wt%	BaO wt%	Na2O wt%	K2O wt%	P2O5 wt%	LOI wt%	Total
							ME-ICP06	ME-ICP06	ME-ICP06	ME-ICP06	ME-ICP06	ME-ICP06	ME-ICP06	ME-ICP06	ME-ICP06	ME-ICP06	ME-ICP06	ME-ICP06	OA-GRA05	
							0.01	0.01	0.01	0.01			0.01	0.01	0.01	0.01	0.01	0.01	0.01	
MERN19MDS0183AG01	X261169	Here Creek rhyolite	Rhyolite	Spilite	645151	5348837	75.00	0.38	12.40	4.15	0.02	1.95	0.09	0.01	0.02	5.27	0.36	0.05	1.52	101.21
MERN19MDS0184AG01	X261170	Here Creek rhyolite	Rhyolite	Spilite	645088	5348911	75.40	0.37	11.55	3.52	0.03	1.97	0.24	0.01	0.01	5.13	0.23	0.05	1.44	99.94
MERN17MDS0025AG02	X258402	Héré phase of Powell Intrusion	Glomeroporphyritic Gabbro		644899	5347534	41.60	0.72	17.90	11.00	0.17	9.64	9.22	0.01	0.00	1.51	0.02	0.08	6.51	98.39
MERN17MDS0023AG04	X258401	Héré phase of Powell Intrusion	Quartz-Diorite		644441	5347230	66.10	0.78	12.95	6.35	0.10	3.67	1.35	0.01	0.04	3.08	0.98	0.15	3.01	98.56
MERN17MDS0034BG07	X258408	Héré phase of Powell Intrusion	Quartz-Diorite		644456	5347292	59.20	0.80	14.60	7.52	0.13	4.51	2.74	0.01	0.03	3.01	1.27	0.12	5.14	99.07
MERN17MDS0034BG08	X258409	Héré phase of Powell Intrusion	Quartz-Diorite		644458	5347309	59.10	0.95	15.25	10.25	0.10	6.12	0.82	0.01	0.03	2.65	1.02	0.14	4.34	100.77
MERN17MDS0040AG01	X258410	Héré phase of Powell Intrusion	Quartz-Diorite		644388	5347283	57.90	0.84	15.05	12.95	0.14	5.97	0.18	0.01	0.05	0.17	1.75	0.14	4.63	99.77
MERN17MDS0045CG03	X258414	Héré phase of Powell Intrusion	Quartz-Diorite		644363	5347485	52.90	0.68	16.65	10.50	0.19	6.32	2.05	0.01	0.01	4.57	0.13	0.11	5.05	99.18
MERN17MDS0045CG06	X258415	Héré phase of Powell Intrusion	Quartz-Diorite		644363	5347485	52.80	0.86	16.25	9.62	0.18	5.82	2.55	0.01	0.01	4.73	0.12	0.12	5.13	98.21
MERN18MDS0104AG01	X258467	Héré phase of Powell Intrusion	Quartz-Diorite		644494	5347556	58.50	0.84	14.35	12.25	0.11	6.67	0.22	0.01	0.04	0.08	1.48	0.12	4.69	99.35
MERN17MDS0034CG09	X258427	Héré phase of Powell Intrusion	Quartz-Diorite		644458	5347309	58.10	0.88	16.00	10.20	0.10	6.19	0.70	0.01	0.03	2.97	1.13	0.11	4.22	100.64
MERN18MDS0104AG01	X258477	Héré phase of Powell Intrusion	Quartz-Diorite		644494	5347556	58.60	0.88	13.65	12.60	0.11	6.86	0.30	0.01	0.04	0.07	1.31	0.12	4.80	99.89
MERN17MDS0035AG02	X258483	Héré phase of Powell Intrusion		Chlorite	644426	5347363	63.60	1.32	14.85	8.33	0.04	4.88	0.55	0.01	0.01	4.52	0.16	0.36	2.89	101.5
MERN18MDS0106AG01	X261056	Joliet Tonalite	Tonalite		646474	5347884	71.30	0.36	13.65	4.61	0.08	0.78	2.61	0.01	0.01	4.50	0.38	0.10	2.78	101.67
MERN19MDS0125EG09	X261074	Joliet Tonalite	Tonalite		646517	5347856	71.00	0.36	14.25	5.19	0.08	0.87	1.87	0.01	0.02	3.39	0.74	0.11	2.88	100.78
MERN19MDS0125EG28	X261109	Joliet Tonalite	Tonalite		646510	5347862	70.00	0.35	13.95	5.13	0.07	0.79	2.51	0.02	0.01	3.15	0.57	0.11	3.40	100.07
MERN19MDS0141CG04	X261140	Joliet Tonalite	Tonalite		645996	5347739	75.70	0.20	10.90	5.43	0.07	0.77	0.04	0.01	0.02	3.49	1.29	0.03	1.56	99.5
MERN20MDS186BG13	C079653	Joliet Tonalite	Tonalite	Hematite	645742	5347150	77.50	0.18	12.60	3.27	0.05	0.09	0.20	0.01	0.04	5.71	0.89	0.04	0.77	101.35
MERN20MDS200BG01	C079656	Joliet Tonalite	Tonalite	Spotted	645997	5347208	75.70	0.11	11.50	3.23	0.03	0.29	0.87	0.01	0.05	3.51	1.79	0.03	1.55	98.66
MERN20MDS201BG08	C079661	Joliet Tonalite	Tonalite		645262	5348013	70.30	0.29	13.25	7.22	0.12	1.37	0.11	0.01	0.03	0.16	3.12	0.07	3.35	99.39
MERN18MDS0078BG02	X258431	Lamprophyre	Lamprophyre		645507	5347994	42.20	0.60	9.59	9.01	0.22	9.90	10.30	0.03	0.05	2.14	0.30	0.28	16.70	101.43
MERN19MDS0152AG01	X261162	Lamprophyre	Lamprophyre	Spilite	646504	5348319	65.00	0.63	13.50	10.05	0.17	3.42	0.44	0.01	0.01	4.01	0.03	0.21	2.62	100.08
MERN19MDS0152AG01 (lam	X261146	Lamprophyre	Lamprophyre	Spilite	646504	5348320	46.50	0.52	11.65	9.40	0.21	17.45	9.09	0.02	0.07	1.37	1.22	0.32	3.90	101.93
MERN18MDS0064EG05	X258492	Lamprophyre	Lamprophyre	Spilite	645355	5347769	47.50	1.18	13.65	11.60	0.27	4.90	5.98	0.01	0.02	4.11	0.48	0.11	10.35	100.08
MERN20MDS127CG04	C079666	Lamprophyre	Lamprophyre	Ankerite	642344	5346169	35.30	0.31	7.29	7.66	0.35	7.46	15.75	0.01	0.12	1.41	1.57	0.26	23.40	100.99
MERN19MDS0153AG01	X261147	Lower marker unit	Rhyolite				68.90	0.49	11.65	7.91	0.15	5.08	0.08	0.01	0.05	0.22	1.67	0.05	3.58	99.83
MERN18MDS0076CG01	X258456	Lower Marker Unit	rhyolite clast		645222	5347709	80.90	0.24	9.87	4.81	0.03	1.91	0.05	0.01	0.08	0.18	1.70	0.01	2.15	101.93
MERN18MDS0077AG03	X258430	Lower Marker Unit	rhyolite clast		645259	5347730	81.90	0.21	9.07	2.63	0.08	1.87	0.71	0.01	0.03	2.26	0.91	0.04	2.12	101.83
MERN18MDS0097AG01	X258441	Lower Marker Unit	rhyolite lapillistone		644838	5347661	62.40	0.86	14.55	9.92	0.12	5.23	0.15	0.01	0.08	0.97	1.54	0.10	3.95	99.87
MERN18MDS0117AG01	X261058	Lower Marker Unit	rhyolite lapillistone		645269	5348088	73.50	0.48	13.65	5.33	0.11	2.90	0.17	0.01	0.02	3.24	0.88	0.08	2.17	100.83
MERN18MDS0098AG04	X258447	Lower Powell Andesite	Andesite	Spotted	644609	5348031	56.00	1.00	14.95	14.80	0.27	6.96	0.23	0.01	0.04	0.39	1.22	0.16	4.73	100.76
MERN18MDS0098AG05	X258457	Lower Powell Andesite	Andesite	Spotted	644609	5348031	56.80	0.99	15.10	12.45	0.23	6.82	0.28	0.01	0.01	3.34	0.04	0.14	4.10	100.31
MERN18MDS0098AG05	X258442	Lower Powell Andesite	Andesite	Spilite	644616	5348043	57.90	0.98	14.60	11.80	0.22	6.65	0.28	0.01	0.01	3.23	0.05	0.14	4.02	99.88
MERN18MDS0098AG06	X258499	Lower Powell Andesite	Andesite	Spilite	644609	5348031	54.90	0.99	15.30	12.20	0.24	6.96	0.29	0.01	0.01	3.52	0.08	0.18	4.23	98.9
MERN18MDS0098AG07	X258448	Lower Powell Andesite	Andesite	Spilite	644616	5348043	53.00	1.02	15.45	10.30	0.31	6.23	3.37	0.01	0.01	3.73	0.45	0.16	6.14	100.18
MERN18MDS0098AG08	X258449	Lower Powell Andesite	Andesite	Spotted	644616	5348043	54.10	0.98	14.95	14.60	0.25	7.23	0.22	0.01	0.04	0.05	1.53	0.15	5.09	99.21
MERN18MDS0099AG01	X258451	Lower Powell Andesite	Andesite	Spilite	644419	5347923	52.80	1.39	13.75	10.20	0.42	3.98	3.80	0.01	0.01	4.70	0.16	0.34	6.45	98.01
MERN18MDS0099AG02	X258452	Lower Powell Andesite	Andesite	Spotted	644419	5347923	60.20	1.36	14.05	12.90	0.13	4.52	0.80	0.01	0.05	0.12	1.65	0.58	3.93	100.29
MERN18MDS0099AG05i	X258489	Lower Powell Andesite	Andesite		644451	5347922	53.30	1.51	14.60	18.00	0.18	6.31	0.49	0.01	0.02	0.38	0.71	0.37	4.61	100.48
MERN18MDS0099AG05ii	X261052	Lower Powell Andesite	Andesite		644451	5347922	57.80	1.60	15.20	13.90	0.15	4.66	0.63	0.01	0.05	0.13	2.00	0.39	4.18	100.69
MERN18MDS0099AG05iii	X258486	Lower Powell Andesite	Andesite	Spotted	644451	5347922	55.80	1.46	14.45	15.45	0.17	5.42	0.79	0.01	0.03	0.97	0.93	0.37	4.35	100.19
MERN18MDS0100AG01	X258453	Lower Powell Andesite	Andesite	Spotted	644482	5347947	57.90	1.26	12.95	16.15	0.09	4.08	0.74	0.01	0.04	0.04	0.99	0.54	3.91	98.69
MERN18MDS0101AG01	X258460	Lower Powell Andesite	Andesite	Spotted	644602	5347975	60.80	1.27	13.20	13.85	0.12	4.61	0.85	0.01	0.04	0.08	1.46	0.59	3.89	100.76
MERN18MDS0101BG02	X258468	Lower Powell Andesite	Andesite	Spotted	644614	5347950	59.40	1.23	13.35	15.10	0.13	5.81	0.85	0.01	0.03	0.10	1.05	0.56	4.26	101.87
MERN18MDS0124AG01	X258500	Lower Powell Andesite	Andesite		644476	5348228	54.60	1.06	13.65	9.99	0.22	7.35	2.56	0.01	0.01	4.83	0.26	0.17	3.34	100.36
MERN19MDS0153BG02	X261148	Lower Powell Andesite	Andesite	Spilite	646297	5348043	56.50	1.20	14.90	11.20	0.23	6.33	0.26	0.01	0.01	3.46	0.12	0.15	3.98	98.33
MERN19MDS0156AG02	X261151	Lower Powell andesite	Andesite	Spotted	644520	5348365	62.10	0.75	14.15	10.85	0.09	4.38	0.13	0.01	0.07	0.04	2.79	0.11	3.80	99.26
MERN19MDS0156BG03	X261152	Lower Powell Andesite	Andesite	Qtz-Ep-Act	644520	5348365	70.90	0.54	12.75	5.56	0.07	3.32	0.54	0.01	0.03	4.06	0.60	0.09	2.22	100.68
MERN19MDS0157AG02	X261153	Lower Powell andesite	Andesite	epidote	644443	5348237	56.90	0.99	15.70	8.59	0.15	4.65	5.72	0.02	0.01	4.05	0.22	0.18	2.94	100.13
MERN19MDS0157BG03	X261154	Lower Powell Andesite	Andesite	Qtz-Ep-Act	644443	5348237	61.20	0.84	15.35	8.11	0.18	3.41	3.99	0.02	0.02	4.43	0.20	0.13	2.23	100.11
MERN19MDS0158AG01	X261155	Lower Powell andesite	Andesite		644520	5348391	56.80	1.04	15.50	8.05	0.15	5.94	1.34	0.01	0.01	5.32	0.09	0.16	3.90	98.31
MERN20MDS201AG01	C079657	Lower Powell Andesite	Andesite	Spilite	645265	5348054	57.30	1.03	15.80	11.40	0.26	4.69	1.12	0.01	0.02	3.09	0.91	0.17	3.38	99.18
MERN20MDS201AG03	C079658	Lower Powell Andesite	Andesite	Spotted	645265	5348054	54.60	1.10	16.65	13.35	0.29	5.18	1.02	0.01	0.03	0.85	2.04	0.19	4.26	99.57
MERN19MDS0125BG55 LA	X261133	Mafic clast	Andesite		646518	5347800	53.40	1.40	15.60	13.25	0.23	3.33	3.44	0.01	0.04	2.00	1.29	0.21	5.25	99.44
MERN19MDS0125BG55 Chl	X261125	Mafic clast	Andesite	Chlorite	646518	5347800	57.40	1.35	15.00	12.55	0.19	3.43	1.94	0.01	0.02	2.54	0.80	0.22	4.36	99.8
MERN19MDS0125BG54	X261121	Mafic clast	Andesite	Chlorite	646515	5347789	38.40	0.72	19.65	25.60	0.27	5.45	0.50	0.01	0.03	0.55	0.93	0.11	5.87	98.09
MERN19MDS0125AG50	X261134	Mafic clast	Andesite	Chlorite	646527	5347791	45.10	1.20	15.40	25.70	0.24	5.16	0.22	0.01	0.01	0.04	0.06	0.12	5.29	98.55
MERN19MDS0125BG54B	X261122	Mafic clast	Andesite		646515	5347789	45.10	0.64	17.95	14.80	0.32	3.21	5.39	0.01	0.06	1.18	2.23	0.10	7.48	98.47

Number	Lab ID	Formation	Rock Type	Alteration	UTM-East	UTM-North	C %	S %	H20 %	Cl ppm	F ppm	S.G.	Ag ppm	As ppm	Au ppm	Ba ppm	Bi ppm	Cd ppm	Ce ppm	Co ppm
							C-IR07	S-IR08	OA-IR06	Cl-IC881	F-IC881		ME-4ACD81	ME-MS42	Au-ICP21	ME-MS81	ME-MS42	ME-4ACD81	ME-MS81	ME-4ACD81
							0.01	0.01	0.01				0.5	0.1		0.5	0.01	0.5	0.1	1
MERN19MDS0183AG01	X261169	Here Creek rhyolite	Rhyolite	Spilite	645151	5348837	0.01	0.03	1.67	170	290	2.75								
MERN19MDS0184AG01	X261170	Here Creek rhyolite	Rhyolite	Spilite	645088	5348911	0.04	0.01	1.56	180	300	2.75								
MERN17MDS0025AG02	X258402	Glomeroporphyritic Gabb	Glomeroporphyritic Gabbro		644899	5347534	0.59	0.11	5.56	80	230	2.92	0.25	1.5		11.7	0.07	0.25	5.4	56
MERN17MDS0023AG04	X258401	Héré phase of Powell Intr	Quartz-Diorite		644441	5347230	0.15	0.02	2.51	25	720	2.72	0.25	0.6		344	0.08	0.25	34	8
MERN17MDS0034BG07	X258408	Héré phase of Powell Intr	Quartz-Diorite		644456	5347292	0.59	0.03	3.49	25	720	2.88	0.25	0.1		280	0.05	0.25	29.7	18
MERN17MDS0034BG08	X258409	Héré phase of Powell Intr	Quartz-Diorite		644458	5347309	0.14	0.01	4.69	25	970	2.87	0.25	0.2		240	0.03	0.6	35.4	22
MERN17MDS0040AG01	X258410	Héré phase of Powell Intr	Quartz-Diorite		644388	5347283	0.01	0.01	5.67	25	840	2.85	0.25	0.1		426	0.03	0.25	9.5	21
MERN17MDS0045CG03	X258414	Héré phase of Powell Intr	Quartz-Diorite		644363	5347485	0.38	0.01	4.27	25	550	2.72	0.25	0.1		66.5	0.02	0.25	19.2	28
MERN17MDS0045CG06	X258415	Héré phase of Powell Intr	Quartz-Diorite		644363	5347485	0.47	0.01	4.26	25	560	2.79	0.25	0.1		66.7	0.02	0.25	19.7	26
MERN18MDS0104AG01	X258467	Héré phase of Powell Intr	Quartz-Diorite		644494	5347556	0.02	0.005		25	1090	2.75	0.25	0.2		315	0.02	0.25	31.2	21
MERN17MDS0034CG09	X258427	Héré phase of Powell Intr	Quartz-Diorite		644458	5347309	0.12	0.01	4.66	25	1040	2.78	0.25	0.1		235	0.03	0.25	28.4	23
MERN18MDS0104AG01	X258477	Héré phase of Powell Intr	Quartz-Diorite		644494	5347556	0.02	0.005		25	1110	2.78	0.25	1.9		285	0.02	0.5	27	23
MERN17MDS0035AG02	X258483	Héré phase of Powell Intr	usion (Quartz Di	Chlorite	644426	5347363	0.02	0.02		<50	680	2.7								
MERN18MDS0106AG01	X261056	Joliet Tonalite	Tonalite		646474	5347884	0.42	0.1		25	290	2.74	0.25	0.6		89.4	0.05	0.6	33.1	6
MERN19MDS0125EG09	X261074	Joliet Tonalite	Tonalite		646517	5347856	0.33	0.53					0.25	1.4		184	0.3	0.25	37.2	13
MERN19MDS0125EG28	X261109	Joliet Tonalite	Tonalite		646510	5347862	0.46	0.8					0.25	1.1		131.5	0.37	0.25	40.7	10
MERN19MDS0141CG04	X261140	Joliet Tonalite	Tonalite		645996	5347739	0.04	0.07					0.25	0.1		185	0.04	<0.5	51.4	1
MERN20MDS186BG13	C079653	Joliet Tonalite	Tonalite	Hematite	645742	5347150	0.03	0.16	0.51	190	310	2.71								
MERN20MDS200BG01	C079656	Joliet Tonalite	Tonalite	Spotted	645997	5347208	0.18	0.23	0.94	110	650	2.7								
MERN20MDS201BG08	C079661	Joliet Tonalite	Tonalite		645262	5348013	0.01	1.19	3.11	200	310	2.81	0.5	0.1		281	0.43	1.7	29.9	8
MERN18MDS0078BG02	X258431	Lamprophyre	Lamprophyre		645507	5347994	4.03	0.05	2.59	25	990	2.8	0.25	0.1		451		0.25	25.8	29
MERN19MDS0152AG01	X261162	Lamprophyre	Lamprophyre	Spilite	646504	5348319	0.02	<0.01					0.25	0.2		7.8	0.01	<0.5	25.2	4
MERN19MDS0152AG01 (lam	X261146	Lamprophyre	Lamprophyre	Spilite	646504	5348320	0.03	0.01					0.25	0.2		612	0.03	0.6	27.9	57
MERN18MDS0064EG05	X258492	Lamprophyre	Lamprophyre	Spilite	645355	5347769	2.35	0.03		50	140	2.69	0.25	0.2		164.5	0.01	1.5	10.1	30
MERN20MDS127CG04	C079666	Lamprophyre	Lamprophyre	Ankerite	642344	5346169	6.53	0.04	0.96	190	730	2.89								
MERN19MDS0153AG01	X261147	Lower marker unit	Rhyolite				0.01	0.03	4.64	180	430	2.74								
MERN18MDS0076CG01	X258456	Lower Marker Unit	rhyolite clast		645222	5347709	0.01	0.01	2.41	90	350	2.76	0.25	0.05		757		0.25	30.8	8
MERN18MDS0077AG03	X258430	Lower Marker Unit	rhyolite clast		645259	5347730	0.29	0.01	1.1	25	200	2.75	0.25	0.3		243		0.25	28.3	6
MERN18MDS0097AG01	X258441	Lower Marker Unit	rhyolite lapillistone		644838	5347661	0.01	0.01	4.39	25	440	2.68	0.25	0.1		733	0.24	0.25	35.6	13
MERN18MDS0117AG01	X261058	Lower Marker Unit	rhyolite lapillistone		645269	5348088	0.005	0.06		25	300	2.8	0.25	0.3		194	0.05	0.25	35	7
MERN18MDS0098AG04	X258447	Lower Powell Andesite	Andesite	Spotted	644609	5348031	0.01	0.05	6.28	50	520	2.85	0.25	0.3		355		0.25	27.5	29
MERN18MDS0098AG05	X258457	Lower Powell Andesite	Andesite	Spotted	644609	5348031	0.03	0.08	5.71	110	490	2.82	0.25	0.3		15.2		0.25	28.1	31
MERN18MDS0098AG05	X258442	Lower Powell Andesite	Andesite	Spilite	644616	5348043	0.02	0.04	4.62	50	470	2.75	0.25	0.3		21.9	0.13	0.25	33.8	28
MERN18MDS0098AG06	X258499	Lower Powell Andesite	Andesite	Spilite	644609	5348031	0.01	0.01		<50	540	2.78								
MERN18MDS0098AG07	X258448	Lower Powell Andesite	Andesite	Spilite	644616	5348043	0.73	0.01	4.05	25	610	2.67	0.25	0.05		83		0.9	29.2	19
MERN18MDS0098AG08	X258449	Lower Powell Andesite	Andesite	Spotted	644616	5348043	0.02	0.01	6.14	25	790	2.76	0.25	0.05		369		0.25	29.5	24
MERN18MDS0099AG01	X258451	Lower Powell Andesite	Andesite	Spilite	644419	5347923	1.33	0.16	2.68	25	520	2.69	0.25	0.4		62.7		0.9	18.2	18
MERN18MDS0099AG02	X258452	Lower Powell Andesite	Andesite	Spotted	644419	5347923	0.02	0.01	5.37	80	1080	2.78	0.25	0.1		430		0.25	25.5	21
MERN18MDS0099AG05i	X258489	Lower Powell Andesite	Andesite		644451	5347922	<0.01	<0.01		<50	680	2.75								
MERN18MDS0099AG05ii	X261052	Lower Powell Andesite	Andesite		644451	5347922	0.04	<0.01		<50	760	2.74								
MERN18MDS0099AG05iii	X258486	Lower Powell Andesite	Andesite	Spotted	644451	5347922	0.08	0.04		<50	690	2.73								
MERN18MDS0100AG01	X258453	Lower Powell Andesite	Andesite	Spotted	644482	5347947	0.02	0.01	5.73	110	890	3.05	0.25	0.2		370		0.6	25	23
MERN18MDS0101AG01	X258460	Lower Powell Andesite	Andesite	Spotted	644602	5347975	<0.01	0.01		<50	1080	2.75								
MERN18MDS0101BG02	X258468	Lower Powell Andesite	Andesite	Spotted	644614	5347950	0.01	0.08		<50	1090	2.69								
MERN18MDS0124AG01	X258500	Lower Powell Andesite	Andesite		644476	5348228	0.01	0.01		25	610	2.7	0.25	0.2		80.5	0.01	1	32.3	28
MERN19MDS0153BG02	X261148	Lower Powell Andesite	Andesite	Spilite	646297	5348043	0.01	0.33					0.25	5.1		41.7	0.4	<0.5	27.9	25
MERN19MDS0156AG02	X261151	Lower Powell andesite	Andesite	Spotted	644520	5348365	0.01	<0.01	5.17	150	810	2.73								
MERN19MDS0156BG03	X261152	Lower Powell Andesite	Andesite	Qtz-Ep-Act	644520	5348365	0.07	<0.01					0.25	0.5		256	0.01	<0.5	35.7	10
MERN19MDS0157AG02	X261153	Lower Powell andesite	Andesite	epidote	644443	5348237	0.16	<0.01					0.25	0.3		93.7	0.05	<0.5	27.1	24
MERN19MDS0157BG03	X261154	Lower Powell Andesite	Andesite	Qtz-Ep-Act	644443	5348237	0.02	0.34					0.25	0.2		204	0.15	<0.5	30.4	22
MERN19MDS0158AG01	X261155	Lower Powell andesite	Andesite		644520	5348391	0.2	0.01	4.18	<50	490	2.78								
MERN20MDS201AG01	C079657	Lower Powell Andesite	Andesite	Spilite	645265	5348054	0.01	<0.01	4.64	<50	530	2.9	0.25	0.5		142.5	0.01	1.5	32.5	8
MERN20MDS201AG03	C079658	Lower Powell Andesite	Andesite	Spotted	645265	5348054	0.01	<0.01	5.79	200	580	2.95	0.25	0.2		299	0.02	0.8	21.5	8
MERN19MDS0125BG55 LA	X261133	Mafic clast	Andesite		646518	5347800	0.67	0.54		25	600	2.71	0.6	7.1		323	1.74	0.25	33.4	49
MERN19MDS0125BG55 Chl	X261125	Mafic clast	Andesite	Chlorite	646518	5347800	0.35	0.08		25	570	2.77	0.25	0.3		214	0.18	0.25	28.8	13
MERN19MDS0125BG54	X261121	Mafic clast	Andesite	Chlorite	646515	5347789	0.13	0.38		25	510	2.84	2.4	1.8		228	0.45	0.25	43.6	23
MERN19MDS0125AG50	X261134	Mafic clast	Andesite	Chlorite	646527	5347791	0.04	0.02		180	470	2.82	0.25	0.05		22.7	0.06	0.5	9.6	15
MERN19MDS0125BG54B	X261122	Mafic clast	Andesite		646515	5347789	1.23	0.7		25	590	2.74	1.3	4.1		502	1.76	0.25	14.2	25

Number	Lab ID	Formation	Rock Type	Alteration	UTM-East	UTM-North	Cr ppm	Cs ppm	Cu ppm	Dy ppm	Er ppm	Eu ppm	Ga_ppm	Gd_ppm	Ge_ppm	Hf_ppm	Hg_ppm	Ho_ppm	In_ppm	La_ppm
							ME-MS81	ME-MS81	ME-4ACD81	ME-MS81	ME-MS81	ME-MS81	ME-MS81	ME-MS81	ME-MS81	ME-MS81	ME-MS42	ME-MS81	ME-MS42	ME-MS81
								10	1	0.05	0.03	0.03	0.1	0.05	5	0.2	0.005	0.01	0.005	0.1
MERN19MDS0183AG01	X261169	Here Creek rhyolite	Rhyolite	Spilite	645151	5348837														
MERN19MDS0184AG01	X261170	Here Creek rhyolite	Rhyolite	Spilite	645088	5348911														
MERN17MDS0025AG02	X258402	Glomeroporphyritic Gal	Glomeroporphyritic Gabbro		644899	5347534	100	0.14	42	1.99	1.29	0.48	13.5	1.68	2.5	0.8	0.01	0.42	0.01	2.3
MERN17MDS0023AG04	X258401	Héré phase of Powell In	Quartz-Diorite		644441	5347230	20	0.37	15	4.43	2.77	1.08	15.4	4.47	2.5	4.5	0	0.94	0.02	17.6
MERN17MDS0034BG07	X258408	Héré phase of Powell In	Quartz-Diorite		644456	5347292	30	0.47	44	4.37	2.63	0.92	16.8	4.08	2.5	4.2	0	0.91	0.02	14.3
MERN17MDS0034BG08	X258409	Héré phase of Powell In	Quartz-Diorite		644458	5347309	30	0.5	86	4.64	2.86	1.12	17.9	5.28	2.5	3.9	0	1.03	0.03	20.2
MERN17MDS0040AG01	X258410	Héré phase of Powell In	Quartz-Diorite		644388	5347283	20	0.39	33	3.09	2.07	0.36	17.4	2.33	2.5	3.4	0.01	0.7	0.08	4.7
MERN17MDS0045CG03	X258414	Héré phase of Powell In	Quartz-Diorite		644363	5347485	50	0.19	9	2.58	1.59	0.77	16.7	2.52	2.5	2.3	0	0.54	0.05	9.2
MERN17MDS0045CG06	X258415	Héré phase of Powell In	Quartz-Diorite		644363	5347485	40	0.18	7	2.98	1.86	1.02	16.4	2.85	2.5	2.4	0	0.63	0.05	9.3
MERN18MDS0104AG01	X258467	Héré phase of Powell In	Quartz-Diorite		644494	5347556	20	0.6	96	3.66	2.55	0.64	17.7	3.92	2.5	3.9	0.0025	0.83	0.037	14.9
MERN17MDS0034CG09	X258427	Héré phase of Powell In	Quartz-Diorite		644458	5347309	30	0.44	102	4.19	2.47	0.96	16	4.19	2.5	3	0	0.89	0.02	15.6
MERN18MDS0104AG01	X258477	Héré phase of Powell In	Quartz-Diorite		644494	5347556	20	0.57	32	3.66	2.61	0.57	18	3.67	2.5	3.7	0.0025	0.88	0.038	12.5
MERN17MDS0035AG02	X258483	Héré phase of Powell Intrusion (Quartz	Chlorite		644426	5347363														
MERN18MDS0106AG01	X261056	Joliet Tonalite	Tonalite		646474	5347884	10	0.2	19	4.62	3.31	0.93	16.4	4.17	2.5	4.4	0.0025	1.05	0.055	16.3
MERN19MDS0125EG09	X261074	Joliet Tonalite	Tonalite		646517	5347856	30	0.47	57	5.2	3.51	1.3	17.4	5.11	2.5	5.2	0.006	1.19	0.019	16.9
MERN19MDS0125EG28	X261109	Joliet Tonalite	Tonalite		646510	5347862	20	0.34	60	5.48	3.56	1.51	16.8	5.45	2.5	5.1	0.0025	1.2	0.027	19.1
MERN19MDS0141CG04	X261140	Joliet Tonalite	Tonalite		645996	5347739	10	0.72	14	10.7	7.26	1.48	20.2	8.87	<5	8.4	<0.005	2.35	0.013	20
MERN20MDS186BG13	C079653	Joliet Tonalite	Tonalite	Hematite	645742	5347150														
MERN20MDS200BG01	C079656	Joliet Tonalite	Tonalite	Spotted	645997	5347208														
MERN20MDS201BG08	C079661	Joliet Tonalite	Tonalite		645262	5348013	10	0.48	245	4.31	3.16	1.03	17	3.42	<5	4.7	<0.005	0.99	0.094	14.4
MERN18MDS0078BG02	X258431	Lamprophyre	Lamprophyre		645507	5347994	770	0.17	4	2.88	1.63	1.12	11.3	3.42	2.5	1.7		0.6		11.4
MERN19MDS0152AG01	X261162	Lamprophyre	Lamprophyre	Spilite	646504	5348319	10	0.06	2	5.61	3.94	1.09	22.5	5.28	<5	3.8	<0.005	1.21	0.041	13
MERN19MDS0152AG01 (lam	X261146	Lamprophyre	Lamprophyre	Spilite	646504	5348320	1620	0.23	87	3.15	1.77	1.55	13.3	3.8	<5	2	<0.005	0.63	0.011	11.6
MERN18MDS0064EG05	X258492	Lamprophyre	Lamprophyre	Spilite	645355	5347769	100	0.26	63	2.42	1.57	0.77	16.2	2.28	2.5	1.4	0.0025	0.52	0.03	4.8
MERN20MDS127CG04	C079666	Lamprophyre	Lamprophyre	Ankerite	642344	5346169														
MERN19MDS0153AG01	X261147	Lower marker unit	Rhyolite																	
MERN18MDS0076CG01	X258456	Lower Marker Unit	rhyolite clast		645222	5347709	10	0.3	31	5.5	3.65	0.46	13	4.7	2.5	5.2	0	1.17	0.02	12.6
MERN18MDS0077AG03	X258430	Lower Marker Unit	rhyolite clast		645259	5347730	30	0.2	10	5.1	3.74	0.56	8.2	4.67	2.5	5.4		1.16		12.1
MERN18MDS0097AG01	X258441	Lower Marker Unit	rhyolite lapillistone		644838	5347661	10	0.29	4	7.32	4.65	1.03	23.1	6.5	2.5	5.4	0	1.66	0.03	12.9
MERN18MDS0117AG01	X261058	Lower Marker Unit	rhyolite lapillistone		645269	5348088	10	0.31	31	6.18	4.4	0.96	16.6	5.73	2.5	5.1	0.0025	1.45	0.026	17
MERN18MDS0098AG04	X258447	Lower Powell Andesite	Andesite	Spotted	644609	5348031	80	0.41	525	3.64	2.21	0.9	18.5	3.76	2.5	3.1	0	0.8	0.14	10.8
MERN18MDS0098AG05	X258457	Lower Powell Andesite	Andesite	Spotted	644609	5348031	100	0.29	657	3.87	2.65	1.01	18.3	4.12	2.5	3.3	0	0.85	0.17	11.2
MERN18MDS0098AG05	X258442	Lower Powell Andesite	Andesite	Spilite	644616	5348043	80	0.18	444	3.88	2.27	1.2	17.7	4.16	2.5	3.3	0	0.8	0.14	13.3
MERN18MDS0098AG06	X258499	Lower Powell Andesite	Andesite	Spilite	644609	5348031														
MERN18MDS0098AG07	X258448	Lower Powell Andesite	Andesite	Spilite	644616	5348043	80	0.23	9	4.19	2.7	1.13	19.3	3.81	2.5	3.4	0	0.89	0.12	11.7
MERN18MDS0098AG08	X258449	Lower Powell Andesite	Andesite	Spotted	644616	5348043	90	0.62	61	4.35	2.8	0.74	19	4.05	2.5	3.2	0	0.88	0.1	12
MERN18MDS0099AG01	X258451	Lower Powell Andesite	Andesite	Spilite	644419	5347923	20	0.08	336	3.85	2.59	1.26	18.4	3.76	2.5	2.1	0	0.8	0.13	7.6
MERN18MDS0099AG02	X258452	Lower Powell Andesite	Andesite	Spotted	644419	5347923	5	0.31	2	5.39	3.45	1.18	21.1	5.79	2.5	3	0	1.16	0.03	10.5
MERN18MDS0099AG05i	X258489	Lower Powell Andesite	Andesite		644451	5347922														
MERN18MDS0099AG05ii	X261052	Lower Powell Andesite	Andesite		644451	5347922														
MERN18MDS0099AG05iii	X258486	Lower Powell Andesite	Andesite	Spotted	644451	5347922														
MERN18MDS0100AG01	X258453	Lower Powell Andesite	Andesite	Spotted	644482	5347947	5	0.26	6	3.53	2.53	0.73	19	4.22	2.5	2.5	0	0.8	0.06	10.2
MERN18MDS0101AG01	X258460	Lower Powell Andesite	Andesite	Spotted	644602	5347975														
MERN18MDS0101BG02	X258468	Lower Powell Andesite	Andesite	Spotted	644614	5347950														
MERN18MDS0124AG01	X258500	Lower Powell Andesite	Andesite		644476	5348228	50	0.57	2	3.65	2.43	0.89	15.5	3.79	2.5	3.4	0.0025	0.81	0.0025	15.4
MERN19MDS0153BG02	X261148	Lower Powell Andesite	Andesite	Spilite	646297	5348043	10	0.1	37	4.18	2.67	0.84	21.3	4.35	<5	3.7	<0.005	0.93	0.043	12.2
MERN19MDS0156AG02	X261151	Lower Powell andesite	Andesite	Spotted	644520	5348365														
MERN19MDS0156BG03	X261152	Lower Powell Andesite	Andesite	Qtz-Ep-Act	644520	5348365	20	0.28	13	5.21	3.63	0.94	16.7	4.38	<5	5.8	<0.005	1.19	0.005	17.3
MERN19MDS0157AG02	X261153	Lower Powell andesite	Andesite	epidote	644443	5348237	60	0.18	46	4.14	2.44	1.09	18.8	4.23	<5	3.4	<0.005	0.85	0.012	10.8
MERN19MDS0157BG03	X261154	Lower Powell Andesite	Andesite	Qtz-Ep-Act	644443	5348237	30	0.17	126	4.52	2.91	1.09	20.5	4.15	<5	4.3	<0.005	0.98	0.01	13.3
MERN19MDS0158AG01	X261155	Lower Powell andesite	Andesite		644520	5348391														
MERN20MDS201AG01	C079657	Lower Powell Andesite	Andesite	Spilite	645265	5348054	30	0.35	9	4.2	2.62	1.42	15.7	4.18	<5	3.4	<0.005	0.83	0.195	14.2
MERN20MDS201AG03	C079658	Lower Powell Andesite	Andesite	Spotted	645265	5348054	30	0.38	27	3.21	2.41	0.91	19.4	3.05	<5	4	<0.005	0.73	0.089	8.3
MERN19MDS0125BG55 LA	X261133	Mafic clast	Andesite		646518	5347800	10	0.48	184	4.23	2.24	1.9	19.7	5.22	2.5	3.7	0.0025	0.76	0.156	14.1
MERN19MDS0125BG55 Chl	X261125	Mafic clast	Andesite	Chlorite	646518	5347800	10	0.33	69	3.95	2.26	1.58	19.1	5.06	2.5	3.5	0.0025	0.81	0.097	12.4
MERN19MDS0125BG54	X261121	Mafic clast	Andesite	Chlorite	646515	5347789	40	0.29	2580	3.42	1.81	1.51	29.2	4.92	2.5	0.6	0.0025	0.69	0.988	22
MERN19MDS0125AG50	X261134	Mafic clast	Andesite	Chlorite	646527	5347791	120	0.14	145	4.98	3.13	0.54	29.8	3.96	2.5	1.7	0.0025	1.11	0.132	4.3
MERN19MDS0125BG54B	X261122	Mafic clast	Andesite		646515	5347789	40	0.65	159	2.09	1.06	0.63	19.7	1.96	2.5	0.6	0.0025	0.39	0.139	7.2

Number	Lab ID	Formation	Rock Type	Alteration	UTM-East	UTM-North	Li_ppm	Lu_ppm	Mo_ppm	Nb_ppm	Nd_ppm	Ni_ppm	Pb_ppm	Rb_ppm	Re_ppm	Sb_ppm	Sc_ppm	Se_ppm	Sm_ppm	Sn_ppm
							ME-4ACD81	ME-MS81	ME-4ACD81	ME-MS81	ME-MS81	ME-4ACD81	ME-4ACD81	ME-MS81	ME-MS42	ME-MS42	ME-4ACD81	ME-MS42	ME-MS81	ME-MS81
							10	0.01	1	0.2	0.1	1	2	0.2	0.001	0.05	1	0.2	0.03	1
MERN19MDS0183AG01	X261169	Here Creek rhyolite	Rhyolite	Spilite	645151	5348837														
MERN19MDS0184AG01	X261170	Here Creek rhyolite	Rhyolite	Spilite	645088	5348911														
MERN17MDS0025AG02	X258402	Glomeroporphyritic Gabb	Glomeroporphyritic Gabbro		644899	5347534	20	0.17	0.5	1.5	4.2	420	1	0.4	0	0.03	12	0.1	1.32	4
MERN17MDS0023AG04	X258401	Héré phase of Powell Int	Quartz-Diorite		644441	5347230	20	0.43	1	7	18.6	11	1	17.6	0	0.03	16	0.1	4.34	2
MERN17MDS0034BG07	X258408	Héré phase of Powell Int	Quartz-Diorite		644456	5347292	20	0.4	0.5	6.7	16.5	23	1	24.5	0	0.03	18	0.1	3.86	2
MERN17MDS0034BG08	X258409	Héré phase of Powell Int	Quartz-Diorite		644458	5347309	30	0.42	1	6.1	20.3	29	1	20.8	0	0.03	18	0.1	4.66	2
MERN17MDS0040AG01	X258410	Héré phase of Powell Int	Quartz-Diorite		644388	5347283	30	0.33	0.5	5.7	6.7	24	2	26.8	0	0.03	15	0.1	1.77	6
MERN17MDS0045CG03	X258414	Héré phase of Powell Int	Quartz-Diorite		644363	5347485	30	0.22	0.5	3.4	10.5	53	4	3	0	0.03	26	0.1	2.45	1
MERN17MDS0045CG06	X258415	Héré phase of Powell Int	Quartz-Diorite		644363	5347485	30	0.27	0.5	4	11.4	49	2	2.5	0	0.03	26	0.1	2.99	1
MERN18MDS0104AG01	X258467	Héré phase of Powell Int	Quartz-Diorite		644494	5347556	40	0.4	1	5.8	17.3	22	1	25.9	0.0005	0.06	15	0.1	4.02	4
MERN17MDS0034CG09	X258427	Héré phase of Powell Int	Quartz-Diorite		644458	5347309	30	0.35	1	4.9	16.8	30	1	21.4	0	0.03	19	0.1	3.74	2
MERN18MDS0104AG01	X258477	Héré phase of Powell Int	Quartz-Diorite		644494	5347556	40	0.4	0.5	5.8	14.7	25	1	23.2	0.0005	0.05	17	0.1	3.51	4
MERN17MDS0035AG02	X258483	Héré phase of Powell Int	rusion (Quartz I	Chlorite	644426	5347363														
MERN18MDS0106AG01	X261056	Joliet Tonalite	Tonalite		646474	5347884	20	0.58	1	8	17.2	12	1	7.7	0.0005	0.05	9	0.1	4.2	4
MERN19MDS0125EG09	X261074	Joliet Tonalite	Tonalite		646517	5347856	20	0.62	3	9.1	18.9	4	4	15.7	0.0005	0.11	10	0.3	4.76	4
MERN19MDS0125EG28	X261109	Joliet Tonalite	Tonalite		646510	5347862	20	0.6	2	9.1	21	0.5	2	11.5	0.0005	0.07	9	0.5	5.2	3
MERN19MDS0141CG04	X261140	Joliet Tonalite	Tonalite		645996	5347739	10	1.13	1	13.5	32.6	<1	<2	34.1	<0.001	<0.05	11	<0.2	8.26	2
MERN20MDS186BG13	C079653	Joliet Tonalite	Tonalite	Hematite	645742	5347150														
MERN20MDS200BG01	C079656	Joliet Tonalite	Tonalite	Spotted	645997	5347208														
MERN20MDS201BG08	C079661	Joliet Tonalite	Tonalite		645262	5348013	10	0.66	2	8.6	15.7	4	<2	62.5	<0.001	<0.05	8	0.5	3.68	25
MERN18MDS0078BG02	X258431	Lamprophyre	Lamprophyre		645507	5347994	40	0.22	0.5	2.6	15.4	147	3	7.4			26		3.63	1
MERN19MDS0152AG01	X261162	Lamprophyre	Lamprophyre	Spilite	646504	5348319	20	0.61	1	8.2	17.6	<1	<2	0.3	<0.001	<0.05	18	<0.2	5.05	2
MERN19MDS0152AG01 (lam	X261146	Lamprophyre	Lamprophyre	Spilite	646504	5348320	30	0.26	<1	3	17.2	502	4	15.9	<0.001	<0.05	24	<0.2	4.01	1
MERN18MDS0064EG05	X258492	Lamprophyre	Lamprophyre	Spilite	645355	5347769	10	0.25	0.5	3	6.6	16	1	10.1	0.001	0.05	35	0.1	1.82	1
MERN20MDS127CG04	C079666	Lamprophyre	Lamprophyre	Ankerite	642344	5346169														
MERN19MDS0153AG01	X261147	Lower marker unit	Rhyolite																	
MERN18MDS0076CG01	X258456	Lower Marker Unit	rhyolite clast		645222	5347709	10	0.53	1	8.1	16.9	2	4	24.2	0	0.03	10	0.1	4.64	3
MERN18MDS0077AG03	X258430	Lower Marker Unit	rhyolite clast		645259	5347730	10	0.59	3	7.6	15.9	3	2	15.3			8		3.75	1
MERN18MDS0097AG01	X258441	Lower Marker Unit	rhyolite lapillistone		644838	5347661	20	0.69	0.5	9.4	23.2	8	2	23.4	0	0.05	19	0.1	6.19	3
MERN18MDS0117AG01	X261058	Lower Marker Unit	rhyolite lapillistone		645269	5348088	10	0.72	0.5	8.8	21.2	4	1	19.6	0.0005	0.05	15	0.3	5.34	2
MERN18MDS0098AG04	X258447	Lower Powell Andesite	Andesite	Spotted	644609	5348031	30	0.34	1	6.6	14.8	72	1	17.2	0	0.05	19	0.7	3.66	3
MERN18MDS0098AG05	X258457	Lower Powell Andesite	Andesite	Spotted	644609	5348031	30	0.35	2	6.3	15.5	74	1	0.5	0	0.03	21	0.7	3.65	1
MERN18MDS0098AG05	X258442	Lower Powell Andesite	Andesite	Spilite	644616	5348043	30	0.36	1	6.7	18.9	73	3	0.6	0	0.05	21	0.5	4.55	1
MERN18MDS0098AG06	X258499	Lower Powell Andesite	Andesite	Spilite	644609	5348031														
MERN18MDS0098AG07	X258448	Lower Powell Andesite	Andesite	Spilite	644616	5348043	20	0.4	1	6.7	17.2	70	1	9.1	0	0.03	21	0.2	3.83	2
MERN18MDS0098AG08	X258449	Lower Powell Andesite	Andesite	Spotted	644616	5348043	30	0.38	1	6.5	17	71	1	26	0	0.03	22	0.1	4.12	4
MERN18MDS0099AG01	X258451	Lower Powell Andesite	Andesite	Spilite	644419	5347923	10	0.37	1	4.8	12.2	10	6	2.9	0	0.19	29	0.7	2.94	3
MERN18MDS0099AG02	X258452	Lower Powell Andesite	Andesite	Spotted	644419	5347923	20	0.51	1	5.8	16.5	2	1	28	0	0.03	26	0.1	4.48	3
MERN18MDS0099AG05i	X258489	Lower Powell Andesite	Andesite		644451	5347922														
MERN18MDS0099AG05ii	X261052	Lower Powell Andesite	Andesite		644451	5347922														
MERN18MDS0099AG05iii	X258486	Lower Powell Andesite	Andesite	Spotted	644451	5347922														
MERN18MDS0100AG01	X258453	Lower Powell Andesite	Andesite	Spotted	644482	5347947	20	0.34	1	5.1	16.1	1	1	16.3	0	0.03	25	0.2	3.98	2
MERN18MDS0101AG01	X258460	Lower Powell Andesite	Andesite	Spotted	644602	5347975														
MERN18MDS0101BG02	X258468	Lower Powell Andesite	Andesite	Spotted	644614	5347950														
MERN18MDS0124AG01	X258500	Lower Powell Andesite	Andesite		644476	5348228	20	0.37	0.5	6.4	17.5	52	1	6.9	0.0005	0.025	25	0.2	3.97	1
MERN19MDS0153BG02	X261148	Lower Powell Andesite	Andesite	Spilite	646297	5348043	20	0.41	2	6.1	15.9	13	2	2.1	0.001	<0.05	21	0.4	4.39	3
MERN19MDS0156AG02	X261151	Lower Powell andesite	Andesite	Spotted	644520	5348365														
MERN19MDS0156BG03	X261152	Lower Powell Andesite	Andesite	Qtz-Ep-Act	644520	5348365	10	0.59	1	8.5	17.8	11	<2	12.5	<0.001	<0.05	12	<0.2	4.26	<1
MERN19MDS0157AG02	X261153	Lower Powell andesite	Andesite	epidote	644443	5348237	20	0.39	<1	6.3	15.9	41	<2	3.8	0.001	<0.05	21	0.2	4.01	1
MERN19MDS0157BG03	X261154	Lower Powell Andesite	Andesite	Qtz-Ep-Act	644443	5348237	10	0.47	1	6.8	16.6	25	<2	3.3	0.001	<0.05	19	0.7	4.1	6
MERN19MDS0158AG01	X261155	Lower Powell andesite	Andesite		644520	5348391														
MERN20MDS201AG01	C079657	Lower Powell Andesite	Andesite	Spilite	645265	5348054	20	0.38	1	6.2	18.6	29	<2	20.4	0.001	<0.05	22	<0.2	3.79	19
MERN20MDS201AG03	C079658	Lower Powell Andesite	Andesite	Spotted	645265	5348054	20	0.39	<1	7.1	13.1	21	3	39.2	0.001	<0.05	26	<0.2	3.43	23
MERN19MDS0125BG55 LA	X261133	Mafic clast	Andesite		646518	5347800	30	0.35	1	6.4	20	20	1	23.6	0.003	0.025	26	0.6	4.91	9
MERN19MDS0125BG55 Chl	X261125	Mafic clast	Andesite	Chlorite	646518	5347800	30	0.33	1	6.2	17.7	17	1	15.1	0.002	0.025	26	0.2	4.64	9
MERN19MDS0125BG54	X261121	Mafic clast	Andesite	Chlorite	646515	5347789	50	0.26	1	2	21.7	37	2	16.7	0.002	0.07	27	1.6	5.3	11
MERN19MDS0125AG50	X261134	Mafic clast	Andesite	Chlorite	646527	5347791	60	0.52	1	4.5	6.6	19	1	1	0.001	0.025	29	0.1	2.17	7
MERN19MDS0125BG54B	X261122	Mafic clast	Andesite		646515	5347789	30	0.18	0.5	1.7	7.7	28	1	38	0.003	0.05	28	1.1	1.8	13

Number	Lab ID	Formation	Rock Type	Alteration	UTM-East	UTM-North	Sr_ppm	Ta_ppm	Tb_ppm	Te_ppm	Th_ppm	Tl_ppm	Tm_ppm	U_ppm	V_ppm	W_ppm	Y_ppm	Yb_ppm	Zn_ppm	Zr_ppm
							ME-MS81	ME-MS81	ME-MS81	ME-MS42	ME-MS81	ME-MS42	ME-MS81	ME-MS81	ME-MS81	ME-MS81	ME-MS81	ME-MS81	ME4ACD81	ME-MS81
							0.1	0.1	0.01	0.01	0.05	0.02	0.01	0.05	5	1	0.1	0.03	2	2
MERN19MDS0183AG01	X261169	Here Creek rhyolite	Rhyolite	Spilite	645151	5348837											27.3			282
MERN19MDS0184AG01	X261170	Here Creek rhyolite	Rhyolite	Spilite	645088	5348911											55			271
MERN17MDS0025AG02	X258402	Glomeroporphyritic Gat	Glomeroporphyritic Gabbro		644899	5347534	83	0.1	0.31	0.01	0.16	0.01	0.18	0.05	160	1	10.3	1.25	147	25
MERN17MDS0023AG04	X258401	Héré phase of Powell In	Quartz-Diorite		644441	5347230	46.5	0.5	0.76	0.01	2.96	0.01	0.4	0.54	117	0.5	23.4	2.84	80	168
MERN17MDS0034BG07	X258408	Héré phase of Powell In	Quartz-Diorite		644456	5347292	50.9	0.4	0.67	0.01	2.47	0.01	0.35	0.55	163	1	21.9	2.8	136	153
MERN17MDS0034BG08	X258409	Héré phase of Powell In	Quartz-Diorite		644458	5347309	40.7	0.4	0.82	0.01	1.98	0.01	0.41	0.52	178	2	24.1	3	170	145
MERN17MDS0040AG01	X258410	Héré phase of Powell In	Quartz-Diorite		644388	5347283	6.7	0.4	0.5	0.01	1.84	0.01	0.3	0.46	143	8	16.7	2.21	161	133
MERN17MDS0045CG03	X258414	Héré phase of Powell In	Quartz-Diorite		644363	5347485	101.5	0.2	0.42	0.01	1.04	0.01	0.19	0.24	160	1	12.8	1.49	132	84
MERN17MDS0045CG06	X258415	Héré phase of Powell In	Quartz-Diorite		644363	5347485	123	0.2	0.47	0.01	1.07	0.01	0.27	0.27	207	4	15.4	1.77	123	85
MERN18MDS0104AG01	X258467	Héré phase of Powell In	Quartz-Diorite		644494	5347556	6.3	0.4	0.65	0.01	2.07	0.01	0.38	0.54	188	2	22.1	2.56	150	174
MERN17MDS0034CG09	X258427	Héré phase of Powell In	Quartz-Diorite		644458	5347309	34.7	0.3	0.66	0.01	1.66	0.01	0.35	0.42	158	2	19.7	2.57	162	115
MERN18MDS0104AG01	X258477	Héré phase of Powell In	Quartz-Diorite		644494	5347556	6.2	0.4	0.63	0.01	1.85	0.01	0.39	0.49	192	3	22.6	2.58	169	163
MERN17MDS0035AG02	X258483	Héré phase of Powell Intrusion (Quartz I		Chlorite	644426	5347363											40.4			175
MERN18MDS0106AG01	X261056	Joliet Tonalite	Tonalite		646474	5347884	142.5	0.5	0.8	0.01	2.38	0.01	0.49	0.64	19	0.5	28.2	3.46	98	192
MERN19MDS0125EG09	X261074	Joliet Tonalite	Tonalite		646517	5347856	139	0.7	0.86	0.08	2.71	0.01	0.59	0.71	27	1	34	4.16	54	185
MERN19MDS0125EG28	X261109	Joliet Tonalite	Tonalite		646510	5347862	154.5	0.6	0.93	0.06	2.47	0.01	0.57	0.67	25	1	34	3.96	50	185
MERN19MDS0141CG04	X261140	Joliet Tonalite	Tonalite		645996	5347739	24.6	1.1	1.57	0.03	3.44	0.02	1.13	0.91	<5	2	63.9	7.22	43	320
MERN20MDS186BG13	C079653	Joliet Tonalite	Tonalite	Hematite	645742	5347150											85			260
MERN20MDS200BG01	C079656	Joliet Tonalite	Tonalite	Spotted	645997	5347208											104			183
MERN20MDS201BG08	C079661	Joliet Tonalite	Tonalite		645262	5348013	5.7	0.7	0.58	0.18	2.98	0.02	0.52	0.79	34	2	27.9	3.9	433	169
MERN18MDS0078BG02	X258431	Lamprophyre	Lamprophyre		645507	5347994	232	0.2	0.43		1.29			0.46	189	1	13.9	1.48	221	58
MERN19MDS0152AG01	X261162	Lamprophyre	Lamprophyre	Spilite	646504	5348319	21.7	0.6	0.79	<0.01	1.63	<0.02	0.55	0.48	6	1	33	4.02	74	144
MERN19MDS0152AG01 (lam	X261146	Lamprophyre	Lamprophyre	Spilite	646504	5348320	196	0.2	0.54	0.01	1.49	<0.02	0.28	0.52	206	1	17.3	1.71	144	71
MERN18MDS0064EG05	X258492	Lamprophyre	Lamprophyre	Spilite	645355	5347769	107.5	0.2	0.4	0.01	0.49	0.01	0.24	0.13	324	0.5	13.8	1.68	166	48
MERN20MDS127CG04	C079666	Lamprophyre	Lamprophyre	Ankerite	642344	5346169											22.3			61
MERN19MDS0153AG01	X261147	Lower marker unit	Rhyolite														32.3			157
MERN18MDS0076CG01	X258456	Lower Marker Unit	rhyolite clast		645222	5347709	8.5	0.5	1	0.01	2.29	0.01	0.52	0.6	8	1	33.6	3.7	98	193
MERN18MDS0077AG03	X258430	Lower Marker Unit	rhyolite clast		645259	5347730	18.2	0.6	0.82		2.02			0.64	13	1	28.8	3.84	72	190
MERN18MDS0097AG01	X258441	Lower Marker Unit	rhyolite lapillistone		644838	5347661	8.5	0.5	1.3	0.15	2.5	0.01	0.71	0.64	109	1	46	4.54	215	202
MERN18MDS0117AG01	X261058	Lower Marker Unit	rhyolite lapillistone		645269	5348088	21.4	0.5	1.07	0.02	2.21	0.01	0.67	0.57	54	1	37.9	4.63	189	220
MERN18MDS0098AG04	X258447	Lower Powell Andesite	Andesite	Spotted	644609	5348031	4.3	0.3	0.68	0.03	1.24	0.01	0.34	0.31	124	1	22.5	2.15	430	123
MERN18MDS0098AG05	X258457	Lower Powell Andesite	Andesite	Spotted	644609	5348031	12.8	0.3	0.68	0.07	1.28	0.01	0.36	0.32	131	1	24.3	2.4	403	125
MERN18MDS0098AG05	X258442	Lower Powell Andesite	Andesite	Spilite	644616	5348043	13.1	0.3	0.77	0.05	1.31	0.01	0.31	0.34	128	1	22.9	2.3	373	126
MERN18MDS0098AG06	X258499	Lower Powell Andesite	Andesite	Spilite	644609	5348031											23.6			129
MERN18MDS0098AG07	X258448	Lower Powell Andesite	Andesite	Spilite	644616	5348043	44	0.3	0.7	0.01	1.23	0.01	0.36	0.28	133	1	26	2.47	412	126
MERN18MDS0098AG08	X258449	Lower Powell Andesite	Andesite	Spotted	644616	5348043	3.6	0.3	0.73	0.01	1.28	0.01	0.36	0.33	130	1	26.7	2.56	534	126
MERN18MDS0099AG01	X258451	Lower Powell Andesite	Andesite	Spilite	644419	5347923	79.5	0.2	0.7	0.01	0.83	0.01	0.36	0.22	171	1	24.5	2.5	143	85
MERN18MDS0099AG02	X258452	Lower Powell Andesite	Andesite	Spotted	644419	5347923	9.8	0.3	0.99	0.01	1.01	0.01	0.51	0.28	56	1	33.9	3.03	122	104
MERN18MDS0099AG05i	X258489	Lower Powell Andesite	Andesite		644451	5347922											23.2			84
MERN18MDS0099AG05ii	X261052	Lower Powell Andesite	Andesite		644451	5347922											25.1			90
MERN18MDS0099AG05iii	X258486	Lower Powell Andesite	Andesite	Spotted	644451	5347922											22.2			85
MERN18MDS0100AG01	X258453	Lower Powell Andesite	Andesite	Spotted	644482	5347947	10.9	0.2	0.62	0.01	0.91	0.01	0.31	0.25	50	4	21.5	2.18	87	94
MERN18MDS0101AG01	X258460	Lower Powell Andesite	Andesite	Spotted	644602	5347975											29.9			99
MERN18MDS0101BG02	X258468	Lower Powell Andesite	Andesite	Spotted	644614	5347950											29.3			100
MERN18MDS0124AG01	X258500	Lower Powell Andesite	Andesite		644476	5348228	60.2	0.3	0.65	0.01	1.32	0.03	0.38	0.41	198	1	20.7	2.43	81	154
MERN19MDS0153BG02	X261148	Lower Powell Andesite	Andesite	Spilite	646297	5348043	26.3	0.5	0.65	0.1	1.77	<0.02	0.43	0.41	275	1	25.2	2.55	160	151
MERN19MDS0156AG02	X261151	Lower Powell andesite	Andesite	Spotted	644520	5348365											31.1			205
MERN19MDS0156BG03	X261152	Lower Powell Andesite	Andesite	Qtz-Ep-Act	644520	5348365	39.7	0.6	0.71	0.01	2.81	<0.02	0.56	0.72	73	<1	33.2	3.53	42	224
MERN19MDS0157AG02	X261153	Lower Powell andesite	Andesite	epidote	644443	5348237	190.5	0.5	0.68	<0.01	1.42	<0.02	0.36	0.34	196	1	23.8	2.23	74	141
MERN19MDS0157BG03	X261154	Lower Powell Andesite	Andesite	Qtz-Ep-Act	644443	5348237	157	0.5	0.7	0.2	2.17	<0.02	0.45	0.57	166	<1	26.3	2.75	68	173
MERN19MDS0158AG01	X261155	Lower Powell andesite	Andesite		644520	5348391											22.7			131
MERN20MDS201AG01	C079657	Lower Powell Andesite	Andesite	Spilite	645265	5348054	31.3	0.4	0.65	<0.01	1.41	<0.02	0.34	0.37	204	3	23.3	2.43	265	132
MERN20MDS201AG03	C079658	Lower Powell Andesite	Andesite	Spotted	645265	5348054	9.6	0.5	0.51	0.01	1.52	<0.02	0.33	0.39	227	3	19.8	2.55	252	146
MERN19MDS0125BG55 LA	X261133	Mafic clast	Andesite		646518	5347800	54	0.5	0.79	0.14	1.58	0.01	0.34	0.36	393	3	21.9	2.12	174	144
MERN19MDS0125BG55 Chl	X261125	Mafic clast	Andesite	Chlorite	646518	5347800	51.6	0.5	0.68	0.01	1.44	0.01	0.39	0.44	382	3	21.8	2.18	181	136
MERN19MDS0125BG54	X261121	Mafic clast	Andesite	Chlorite	646515	5347789	10.9	0.1	0.6	0.07	0.49	0.01	0.27	0.1	324	4	16.9	1.67	259	23
MERN19MDS0125AG50	X261134	Mafic clast	Andesite	Chlorite	646527	5347791	2.7	0.2	0.77	0.01	0.66	0.01	0.52	0.26	347	8	29.9	3.32	373	59
MERN19MDS0125BG54B	X261122	Mafic clast	Andesite		646515	5347789	49.2	0.1	0.34	0.23	0.62	0.01	0.18	0.58	255	2	10.4	1.08	148	20

Number	Lab ID	Formation	Rock Type	Alteration	UTM-East	UTM-North	SiO2 wt%	TiO2 wt%	Al2O3 wt%	Fe2O3t wt%	MnO wt%	MgO wt%	CaO wt%	SrO wt%	BaO wt%	Na2O wt%	K2O wt%	P2O5 wt%
							ME-ICP06	ME-ICP06	ME-ICP06	ME-ICP06	ME-ICP06	ME-ICP06	ME-ICP06	ME-ICP06	ME-ICP06	ME-ICP06	ME-ICP06	ME-ICP06
							0.01	0.01	0.01	0.01			0.01	0.01	0.01	0.01	0.01	0.01
MERN19MDS0125DG48	X261130	Mafic clast	Andesite	Chlorite	646586	5347789	28.10	1.56	21.00	32.90	0.19	8.06	0.30	0.01	0.01	0.05	0.07	0.22
MERN19MDS0125AG52	X261120	Mafic clast	Andesite	Spotted	646522	5347784	46.20	0.77	19.85	19.35	0.20	4.70	0.19	0.01	0.06	0.40	2.08	0.10
MERN19MDS0125AG53	X261119	Mafic clast	Andesite	Spotted	646522	5347784	44.50	1.01	18.70	22.00	0.19	4.51	0.20	0.01	0.04	0.56	1.39	0.13
MERN17MDS0034AG06	X258407	Mafic dike	Andesite	Chlorite	644449	5347294	52.30	1.41	15.65	13.60	0.17	8.80	0.14	0.01	0.04	0.04	1.44	0.10
MERN18MDS0068AG01	X258469	Mafic Dike	Andesite		645454	5347795	49.60	1.40	13.45	14.70	0.20	5.99	7.92	0.02	0.01	2.97	0.44	0.18
MERN19MDS0178BG02	X261164	Mafic intrusion	Andesite		646611	5347387	64.50	0.62	13.25	9.82	0.17	3.33	0.45	0.01	0.01	3.98	0.03	0.21
MERN18MDS0115AG01	X258464	Mafic Sill	Andesite		645851	5347849	48.30	1.02	12.95	11.30	0.26	5.25	7.47	0.02	0.01	2.91	0.05	0.10
MERN17MDS0033AG10	X258405				644455	5347321	72.30	0.24	11.05	7.88	0.06	2.94	0.03	0.01	0.05	0.08	2.24	0.02
MERN18MDS0085BG01	X258433	Powell Rhyolite	Rhyolite		645738	5348189	76.40	0.27	9.56	6.21	0.07	1.52	0.07	0.01	0.07	0.32	1.74	0.04
MERN18MDS0085BG02	X258434	Powell Rhyolite	Rhyolite		645723	5348170	79.70	0.25	9.53	5.34	0.06	1.03	0.07	0.01	0.08	0.14	1.99	0.04
MERN18MDS0110AG01	X258497	Powell Rhyolite	Rhyolite		645673	5347845	77.10	0.28	13.65	4.94	0.05	2.69	0.05	0.01	0.05	0.74	1.73	0.04
MERN17MDS0061DG05	X258416	Powell Rhyolite	Rhyolite		645168	5347780	75.90	0.28	11.65	7.76	0.03	1.33	0.06	0.01	0.16	0.19	2.05	0.05
MERN17MDS0061DG06	X258417	Powell Rhyolite	Rhyolite		645166	5347775	75.30	0.26	11.05	8.07	0.04	1.72	0.03	0.01	0.10	0.15	1.75	0.05
MERN17MDS0061DG07	X258421	Powell Rhyolite	Rhyolite		645148	5347763	76.20	0.29	11.10	6.18	0.03	1.81	0.06	0.01	0.12	0.16	1.94	0.04
MERN17MDS0061DG08	X258422	Powell Rhyolite	Rhyolite		645141	5347766	77.70	0.26	10.20	5.86	0.04	1.70	0.05	0.01	0.12	0.16	1.82	0.04
MERN17MDS0061DG09	X258423	Powell Rhyolite	Rhyolite		645142	5347760	74.80	0.28	10.90	6.19	0.03	2.24	0.05	0.01	0.09	0.17	1.78	0.04
MERN19MDS0126AG01 (qtz-	X261138	Powell Rhyolite	Rhyolite	Spilite	646496	5348024	71.60	0.36	13.20	4.22	0.07	2.50	0.55	0.01	0.02	4.35	0.89	0.07
MERN19MDS0128BG02	X261173	Powell tonalite	Tonalite	Ankerite-Hematite	644626	5347381	76.20	0.23	11.80	3.81	0.10	0.66	0.83	0.01	0.02	4.50	0.82	0.02
MERN19MDS0128BG03	X261174	Powell tonalite	Tonalite	Ankerite-Hematite	644626	5347381	70.10	0.24	11.25	4.89	0.10	0.98	1.04	0.01	0.02	3.27	1.07	0.02
MERN19MDS0128BG04	X261175	Powell tonalite	Tonalite	Ankerite-Hematite	644626	5347380	77.30	0.23	11.85	4.32	0.11	0.67	0.39	0.01	0.02	4.31	0.93	0.03
MERN19MDS0128BG05	X261176	Powell tonalite	Tonalite	Ankerite-Hematite	644626	5347382	72.20	0.16	10.80	4.50	0.06	1.19	0.48	0.01	0.01	4.10	0.51	0.03
MERN19MDS0128BG06	X261177	Powell tonalite	Tonalite	Ankerite-Hematite	644626	5347382	67.80	0.15	9.85	7.68	0.12	2.00	0.83	0.01	0.01	2.49	0.57	0.02
MERN19MDS0128BG07	X261178	Powell tonalite	Tonalite	Ankerite-Hematite	644626	5347382	73.60	0.20	10.40	5.68	0.15	1.47	1.29	0.01	0.01	3.62	0.70	0.04
MERN19MDS0128BG08	X261179	Powell tonalite	Tonalite	Ankerite-Hematite	644626	5347382	73.90	0.27	11.60	4.82	0.11	0.80	0.53	0.01	0.02	4.33	1.05	0.04
MERN17MDS0041AG03	X258411	Powell Tonalite	Tonalite	Spilite	644674	5347418	75.50	0.26	11.95	4.88	0.05	1.55	0.08	0.01	0.01	4.65	0.34	0.03
MERN17MDS0073AG01	X258418	Powell Tonalite	Tonalite	Spilite	644512	5347244	76.70	0.26	11.70	4.11	0.04	1.32	0.16	0.01	0.01	4.87	0.37	0.06
MERN18MDS0087AG01	X258444	Powell Tonalite	Tonalite	Spotted	644635	5347296	68.90	0.45	13.10	8.22	0.10	3.52	0.20	0.01	0.02	2.31	0.95	0.09
MERN20MDS127AG02_dist h	C079664	Powell Tonalite	Tonalite	Ankerite-Hematite	642390	5346179	78.20	0.31	12.80	1.27	0.03	0.22	0.92	0.01	0.03	5.09	0.91	0.07
MERN20MDS127AG02_prox l	C079663	Powell Tonalite	Tonalite	Ankerite-Hematite	642390	5346179	69.50	0.30	13.30	2.52	0.13	0.79	3.32	0.01	0.03	5.47	0.89	0.06
MERN20MDS127AG01	C079662	Powell tonalite	Tonalite	Ankerite-Hematite	642390	5346179	75.90	0.29	12.55	3.10	0.04	0.74	0.94	0.01	0.02	4.59	0.66	0.06
MERN20MDS127AG03	C079665	Powell tonalite	Tonalite	Ankerite-Hematite	642390	5346179	75.90	0.28	12.70	3.12	0.02	0.61	0.61	0.01	0.02	4.89	0.59	0.04
MERN20MDS127AG06	C079667	Powell tonalite	Tonalite	Ankerite-Hematite	642348	5346189	72.60	0.22	9.38	3.80	0.06	1.13	1.92	0.01	0.01	4.40	0.69	0.02
MERN20MDS127AG07	C079668	Powell tonalite	Tonalite	Ankerite-Hematite	642348	5346189	73.30	0.27	12.10	4.39	0.02	0.65	1.06	0.01	0.02	5.00	0.96	0.05
MERN20MDS127AG08	C079669	Powell tonalite	Tonalite	Ankerite-Hematite	642347	5346188	73.70	0.27	12.30	4.34	0.02	0.71	0.86	0.01	0.02	5.14	0.90	0.05
MERN20MDS127AG09	C079670	Powell tonalite	Tonalite	Ankerite-Hematite	642347	5346188	74.50	0.27	12.50	4.21	0.03	0.63	1.16	0.01	0.01	5.73	0.70	0.06
MERN18MDS0113CG03	X261057	Quartz-phyric rhyolite dike	Rhyolite	Spilite	645805	5347679	77.30	0.23	13.65	3.95	0.04	0.87	1.12	0.01	0.01	5.59	0.06	0.04
MERN19MDS0175AG01	X261158	Quartz-phyric rhyolite sill/dike	Rhyolite	Spilite	646460	5347507	75.20	0.23	10.25	5.74	0.09	1.35	0.36	0.01	0.01	3.95	0.10	0.01
MERN19MDS0125DG01	X261095	Quemont feeder dike	Rhyolite	Spilite	646662	5347897	74.40	0.26	10.80	4.77	0.10	0.58	0.36	0.01	0.01	4.94	0.14	0.02
MERN19MDS0125DG04	X261092	Quemont feeder dike	Rhyolite	Spilite	646610	5347890	75.20	0.28	11.35	5.17	0.13	0.20	0.64	0.01	0.01	5.40	0.32	0.05
MERN19MDS0125DG07	X261093	Quemont feeder dike	Rhyolite	Spilite	646550	5347872	72.50	0.25	10.60	5.43	0.19	0.86	1.06	0.01	0.01	4.70	0.04	0.02
MERN19MDS0125DG23	X261107	Quemont feeder dike	Rhyolite	Spilite	646420	5347791	75.20	0.25	11.50	5.04	0.07	1.23	0.67	0.01	0.01	3.95	0.60	0.03
MERN19MDS0125DG24	X261105	Quemont feeder dike	Rhyolite	Spilite	646403	5347780	75.60	0.24	11.45	5.34	0.06	0.28	1.32	0.01	0.02	5.19	0.52	0.01
MERN19MDS0125DG27	X261110	Quemont feeder dike	Rhyolite	Spilite	646341	5347772	75.70	0.22	10.90	4.13	0.14	0.33	2.57	0.01	0.01	4.99	0.40	0.02
MERN20MDS186AG04	C079672	Quemont feeder dike	Rhyolite	Ankerite-Hematite	645699	5347175	83.50	0.14	7.89	3.17	0.08	0.14	0.52	0.01	0.01	4.26	0.21	0.02
MERN20MDS186AG05	X261198	Quemont feeder dike	Rhyolite	Ankerite-Hematite	645696	5347174	77.30	0.22	10.75	4.56	0.07	0.08	0.32	0.01	0.01	5.80	0.19	0.06
MERN20MDS186AG06	X261199	Quemont feeder dike	Rhyolite	Ankerite-Hematite	645693	5347172	73.80	0.21	10.20	9.30	<0.01	0.13	0.15	0.01	0.01	5.24	0.32	0.04
MERN20MDS186AG07	C079676	Quemont feeder dike	Rhyolite	Ankerite-Hematite	645708	5347170	80.40	0.22	10.25	3.05	0.06	0.20	0.64	0.01	0.06	5.53	0.25	0.06
MERN20MDS186AG08	C079675	Quemont feeder dike	Rhyolite	Ankerite-Hematite	645709	5347171	76.30	0.23	10.45	4.49	0.07	0.30	0.83	0.01	0.07	5.92	0.07	0.06
MERN20MDS186AG09	X261200	Quemont feeder dike	Rhyolite	Ankerite-Hematite	645710	5347172	76.00	0.24	10.80	4.27	0.06	0.58	1.26	0.01	0.01	5.48	0.55	0.06
MERN20MDS186AG10	C079651	Quemont feeder dike	Rhyolite	Ankerite-Hematite	645717	5347173	77.60	0.24	11.35	3.74	0.04	0.17	0.88	0.01	0.01	5.70	0.47	0.03
MERN20MDS186AG11	C079652	Quemont feeder dike	Rhyolite	Ankerite-Hematite	645720	5347175	74.30	0.24	11.05	3.82	0.04	0.38	1.23	0.01	0.01	5.47	0.25	0.04
MERN20MDS186AG12	C079674	Quemont feeder dike	Rhyolite	Ankerite-Hematite	645728	5347180	75.00	0.25	11.40	5.01	0.04	0.16	1.28	0.01	0.02	5.34	0.47	0.03
MERN18MDS0107AG01	X258465	Quemont feeder dyke	Rhyolite		646711	5347834	74.20	0.24	10.90	4.48	0.12	0.34	2.08	0.01	0.06	3.07	1.24	0.04
MERN19MDS0125AG49	X261126	Quemont feeder dyke	Rhyolite		646586	5347789	75.20	0.27	10.75	6.09	0.03	1.44	0.11	0.01	0.02	3.06	0.74	0.03
MERN19MDS0125AG49	X261127	Quemont feeder dyke	Rhyolite	Sericite	646586	5347789	75.90	0.27	10.40	7.10	0.04	1.79	0.05	0.01	0.05	0.31	1.60	0.04
MERN19MDS0125AG70	X261136	Quemont feeder dyke	Rhyolite	Spotted	646551	5347769	74.00	0.26	11.05	7.32	0.05	2.11	0.06	0.01	0.04	0.29	1.64	0.03
MERN19MDS0125AG70 (ser	X261136	Quemont feeder dyke	Rhyolite		646541	5347769	74.00	0.26	11.05	7.32	0.05	2.11	0.06	0.01	0.04	0.29	1.64	0.03
MERN19MDS0125DG42	X261131	Quemont feeder dyke	Rhyolite	Spilite	646712	5347827	76.80	0.26	11.45	5.50	0.09	0.55	0.67	0.01	0.02	4.43	0.47	0.03
MERN19MDS0125DG43	X261129	Quemont feeder dyke	Rhyolite	Sericite	646712	5347827	80.10	0.26	12.20	2.20	0.02	0.31	0.09	0.01	0.14	0.23	3.59	0.04
MERN18MDS0119AG01	X258462	uncertain protolith, strongly sulfidized			645630	5348024	73.30	1.29	10.65	7.23	0.06	1.15	0.44	0.01	0.03	2.97	0.72	0.07

Number	Lab ID	Formation	Rock Type	Alteration	UTM-East	UTM-North	LOI_OA-GRA	Total	C %	S %	H20 %	Cl ppm	F ppm	S.G.	Ag ppm	As ppm	Au ppm	Ba ppm	Bi ppm	Cd ppm
							OA-GRA05		C-IR07	S-IR08	OA-IR06	Cl-IC881	F-IC881		ME-4ACD81	ME-MS42	Au-ICP21	ME-MS81	ME-MS42	ME-4ACD81
							0.01		0.01	0.01	0.01				0.5	0.1		0.5	0.01	0.5
MERN19MDS0125DG48	X261130	Mafic clast	Andesite	Chlorite	646586	5347789	7.11	99.56	0.02	0.17		180	680	2.76	0.7	0.3		23.9	0.67	0.25
MERN19MDS0125AG52	X261120	Mafic clast	Andesite	Spotted	646522	5347784	5.25	99.16	0.03	0.05		25	740	2.72	0.8	0.05		552	0.09	3.1
MERN19MDS0125AG53	X261119	Mafic clast	Andesite	Spotted	646522	5347784	5.16	98.4	0.01	0.26		25	620	2.81	2	1.3		395	0.16	0.25
MERN17MDS0034AG06	X258407	Mafic dike	Andesite	Chlorite	644449	5347294	5.56	99.26	0.02	0.01	7.12	25	1010	2.83	0.25	0.1		344	0.05	0.25
MERN18MDS0068AG01	X258469	Mafic Dike	Andesite		645454	5347795	2.53	99.42	0.09	0.11		480	360	2.8	0.25	0.4		116	0.02	0.25
MERN19MDS0178BG02	X261164	Mafic intrusion	Andesite		646611	5347387	2.51	98.87	0.02	<0.01					0.25	0.7		9.3	0.01	<0.5
MERN18MDS0115AG01	X258464	Mafic Sill	Andesite		645851	5347849	9.09	98.74	1.63	0.04		25	210	2.72	0.25	0.1		33.5	0.02	0.5
MERN17MDS0033AG10	X258405				644455	5347321	3.10	99.99	0.01	0.36	3.22	130	540	2.79	0.25	0.5		415	0.63	0.25
MERN18MDS0085BG01	X258433	Powell Rhyolite	Rhyolite		645738	5348189	2.07	98.34	0.02	0.03	1.94	60	390	2.85	0.25	1.2		620		0.25
MERN18MDS0085BG02	X258434	Powell Rhyolite	Rhyolite		645723	5348170	1.81	100.04	0.02	0.02	2.06	120	350	2.82	0.25	2.4		679		0.25
MERN18MDS0110AG01	X258497	Powell Rhyolite	Rhyolite		645673	5347845	2.56	101.63	0.02	0.005		25	370	2.71	0.25	0.05		350	0.01	0.25
MERN17MDS0061DG05	X258416	Powell Rhyolite	Rhyolite		645168	5347780	2.44	101.9	0.13	0.12	2.75	25	480	2.76	0.25	0.4		1355	0.92	0.25
MERN17MDS0061DG06	X258417	Powell Rhyolite	Rhyolite		645166	5347775	2.49	101.01	0.04	0.07	2.97	25	380	2.78	0.8	0.6		885	0.29	0.25
MERN17MDS0061DG07	X258421	Powell Rhyolite	Rhyolite		645148	5347763	2.37	100.3	0.01	0.01	2.47	60	380	2.81						
MERN17MDS0061DG08	X258422	Powell Rhyolite	Rhyolite		645141	5347766	2.38	100.33	0.04	0.06	2.48	80	450	2.8						
MERN17MDS0061DG09	X258423	Powell Rhyolite	Rhyolite		645142	5347760	2.55	99.12	0.01	0.01	2.95	70	440	2.73						
MERN19MDS0126AG01 (qtz-	X261138	Powell Rhyolite	Rhyolite	Spilite	646496	5348024	2.00	99.83	0.1	0.02				2.76	0.25	0.7		211	0.08	<0.5
MERN19MDS0128BG02	X261173	Powell tonalite	Tonalite	Ankerite-Hematite	644626	5347381	1.81	100.8	0.15	0.01	1.17			2.76						
MERN19MDS0128BG03	X261174	Powell tonalite	Tonalite	Ankerite-Hematite	644626	5347381	2.42	95.4	0.23	0.03	1.82			2.83						
MERN19MDS0128BG04	X261175	Powell tonalite	Tonalite	Ankerite-Hematite	644626	5347380	1.64	101.8	0.07	0.04	1.33			2.82						
MERN19MDS0128BG05	X261176	Powell tonalite	Tonalite	Ankerite-Hematite	644626	5347382	1.93	95.97	0.18	0.03	1.56			2.84						
MERN19MDS0128BG06	X261177	Powell tonalite	Tonalite	Ankerite-Hematite	644626	5347382	3.16	94.68	0.33	0.02	3.22			2.81						
MERN19MDS0128BG07	X261178	Powell tonalite	Tonalite	Ankerite-Hematite	644626	5347382	3.10	100.26	0.53	0.21	2.09			2.76						
MERN19MDS0128BG08	X261179	Powell tonalite	Tonalite	Ankerite-Hematite	644626	5347382	2.09	99.56	0.31	0.21	5.25			2.78						
MERN17MDS0041AG03	X258411	Powell Tonalite	Tonalite	Spilite	644674	5347418	1.60	100.9	0.02	0.01	1.54	25	440	2.67	0.25	0.2		64.3	0.03	0.25
MERN17MDS0073AG01	X258418	Powell Tonalite	Tonalite	Spilite	644512	5347244	1.23	100.83	0.04	0.01	1.18	25	300	2.72	0.25	0.1		56	0.03	0.25
MERN18MDS0087AG01	X258444	Powell Tonalite	Tonalite	Spotted	644635	5347296	2.82	100.68	0.03	0.01	3.32	110	710	2.68	0.25	0.05		129.5		0.25
MERN20MDS127AG02_dist h	C079664	Powell Tonalite	Tonalite	Ankerite-Hematite	642390	5346179	1.31	101.17	0.2	0.21	0.72	170	240	2.63	0.25	0.3		281	0.23	<0.5
MERN20MDS127AG02_prox I	C079663	Powell Tonalite	Tonalite	Ankerite-Hematite	642390	5346179	3.77	100.09	1.03	0.2	0.69	120	240	2.7	0.25	0.3		313	0.22	<0.5
MERN20MDS127AG01	C079662	Powell tonalite	Tonalite	Ankerite-Hematite	642390	5346179	1.74	100.63	0.23	0.13	1.1	140	220	2.72						
MERN20MDS127AG03	C079665	Powell tonalite	Tonalite	Ankerite-Hematite	642390	5346179	1.26	100.04	0.1	0.17	1.09	180	200	2.71						
MERN20MDS127AG06	C079667	Powell tonalite	Tonalite	Ankerite-Hematite	642348	5346189	4.29	98.53	0.71	2.23	0.57	110	210	2.71						
MERN20MDS127AG07	C079668	Powell tonalite	Tonalite	Ankerite-Hematite	642348	5346189	1.70	99.52	0.24	0.88	1.18	100	340	2.73						
MERN20MDS127AG08	C079669	Powell tonalite	Tonalite	Ankerite-Hematite	642347	5346188	1.53	99.84	0.2	0.25	1.12	100	340	2.75						
MERN20MDS127AG09	C079670	Powell tonalite	Tonalite	Ankerite-Hematite	642347	5346188	1.56	101.36	0.29	0.34	0.81	100	250	2.71						
MERN18MDS0113CG03	X261057	Quartz-phyric rhyolite dik	Rhyolite	Spilite	645805	5347679	1.36	101.98	0.2	0.15		25	100	2.72	0.25	0.1		73.1	0.03	0.25
MERN19MDS0175AG01	X261158	Quartz-phyric rhyolite sill	Rhyolite	Spilite	646460	5347507	1.50	98.78	0.08	0.09	1.85	120	240	2.73						
MERN19MDS0125DG01	X261095	Quemont feeder dike	Rhyolite	Spilite	646662	5347897	1.33	97.7	0.12	0.14	1.42			2.8						
MERN19MDS0125DG04	X261092	Quemont feeder dike	Rhyolite	Spilite	646610	5347890	1.42	100.18	0.21	0.28	0.75			2.83						
MERN19MDS0125DG07	X261093	Quemont feeder dike	Rhyolite	Spilite	646550	5347872	2.38	98.04	0.39	0.06	1.63			2.82						
MERN19MDS0125DG23	X261107	Quemont feeder dike	Rhyolite	Spilite	646420	5347791	1.76	100.32	0.11	0.36	2.18			2.78						
MERN19MDS0125DG24	X261105	Quemont feeder dike	Rhyolite	Spilite	646403	5347780	1.41	101.45	0.25	0.04	0.83			2.81						
MERN19MDS0125DG27	X261110	Quemont feeder dike	Rhyolite	Spilite	646341	5347772	2.30	101.72	0.54	0.17	0.88			2.78						
MERN20MDS186AG04	C079672	Quemont feeder dike	Rhyolite	Ankerite-Hematite	645699	5347175	0.85	100.79	0.11	0.1	0.41	90	120	2.77						
MERN20MDS186AG05	X261198	Quemont feeder dike	Rhyolite	Ankerite-Hematite	645696	5347174	0.51	99.87	0.06	0.11	0.43	120	110	2.64						
MERN20MDS186AG06	X261199	Quemont feeder dike	Rhyolite	Ankerite-Hematite	645693	5347172	0.43	99.83	0.02	0.01	0.58	140	150	2.77						
MERN20MDS186AG07	C079676	Quemont feeder dike	Rhyolite	Ankerite-Hematite	645708	5347170	1.10	101.83	0.18	0.37	0.77	80	110	2.71						
MERN20MDS186AG08	C079675	Quemont feeder dike	Rhyolite	Ankerite-Hematite	645709	5347171	1.39	100.19	0.3	0.32	0.62	90	80	2.77						
MERN20MDS186AG09	X261200	Quemont feeder dike	Rhyolite	Ankerite-Hematite	645710	5347172	1.80	101.11	0.45	0.33	0.38	90	260	2.75						
MERN20MDS186AG10	C079651	Quemont feeder dike	Rhyolite	Ankerite-Hematite	645717	5347173	0.84	101.07	0.16	0.15	0.3	80	180	2.71						
MERN20MDS186AG11	C079652	Quemont feeder dike	Rhyolite	Ankerite-Hematite	645720	5347175	1.20	98.03	0.22	0.03	0.64	100	190	2.7						
MERN20MDS186AG12	C079674	Quemont feeder dike	Rhyolite	Ankerite-Hematite	645728	5347180	1.17	100.18	0.22	0.03	0.77	110	190	2.77						
MERN18MDS0107AG01	X258465	Quemont feeder dyke	Rhyolite		646711	5347834	2.79	99.57	0.46	0.02		25	480	2.75	0.25	4.6		497	0.02	0.25
MERN19MDS0125AG49	X261126	Quemont feeder dyke	Rhyolite		646586	5347789	1.89	99.63	0.005	0.6		25	230	2.77	2	0.8		159.5	1.16	0.25
MERN19MDS0125AG49	X261127	Quemont feeder dyke	Rhyolite	Sericite	646586	5347789	2.52	100.07	0.005	0.48		25	340	2.8	1.2	1		435	1.32	0.25
MERN19MDS0125AG70	X261136	Quemont feeder dyke	Rhyolite	Spotted	646551	5347769	2.45	99.3	0.01	0.005					0.25	0.8		338	0.22	0.25
MERN19MDS0125AG70 (ser	X261136	Quemont feeder dyke	Rhyolite		646541	5347769	2.45	99.3	0.01	<0.01					<0.5	0.8		338	0.22	<0.5
MERN19MDS0125DG42	X261131	Quemont feeder dyke	Rhyolite	Spilite	646712	5347827	1.36	101.63	0.12	0.04		25	260	2.72	0.25	0.2		177.5	0.04	0.25
MERN19MDS0125DG43	X261129	Quemont feeder dyke	Rhyolite	Sericite	646712	5347827	1.80	100.98	0.01	0.02		25	1010	2.8	0.25	0.05		1230	0.02	0.25
MERN18MDS0119AG01	X258462	uncertain protolith, strongly sulfidized			645630	5348024	1.61	99.52	<0.01	0.15		70	1720	2.65	0.25	0.1		282	1.17	0.25

Number	Lab ID	Formation	Rock Type	Alteration	UTM-East	UTM-North	Ce ppm	Co ppm	Cr ppm	Cs ppm	Cu ppm	Dy ppm	Er ppm	Eu ppm	Ga_ppm	Gd_ppm	Ge_ppm	Hf_ppm	Hg_ppm
							ME-MS81	ME-4ACD81	ME-MS81	ME-MS81	ME-4ACD81	ME-MS81	ME-MS81	ME-MS81	ME-MS81	ME-MS81	ME-MS81	ME-MS81	ME-MS42
							0.1	1		10	1	0.05	0.03	0.03	0.1	0.05	5	0.2	0.005
MERN19MDS0125DG48	X261130	Mafic clast	Andesite	Chlorite	646586	5347789	32.3	23	10	0.17	316	8.55	5.13	0.74	45.8	7.5	2.5	3.9	0.0025
MERN19MDS0125AG52	X261120	Mafic clast	Andesite	Spotted	646522	5347784	12.5	13	80	0.56	824	3.72	2.17	0.58	27.9	3.22	2.5	0.6	0.0025
MERN19MDS0125AG53	X261119	Mafic clast	Andesite	Spotted	646522	5347784	21.5	22	30	0.45	1500	7.46	4.85	0.98	28.6	5.74	2.5	2	0.005
MERN17MDS0034AG06	X258407	Mafic dike	Andesite	Chlorite	644449	5347294	14.5	25	40	0.52	29	3.39	2.33	0.5	22.4	2.99	2.5	3.1	0
MERN18MDS0068AG01	X258469	Mafic Dike	Andesite		645454	5347795	33.7	47	60	0.23	67	4.02	2.5	1.06	17.3	4.3	2.5	2.8	0.0025
MERN19MDS0178BG02	X261164	Mafic intrusion	Andesite		646611	5347387	28.1	5	10	0.07	4	6.06	4.04	1.09	22	5.35	<5	3.8	<0.005
MERN18MDS0115AG01	X258464	Mafic Sill	Andesite		645851	5347849	11.4	28	90	0.07	78	2.86	1.89	1.01	16.2	2.6	2.5	1.6	0.0025
MERN17MDS0033AG10	X258405				644455	5347321	47.3	7	10	0.95	24	9.63	6.29	1.37	20.6	8.4	2.5	5.5	0
MERN18MDS0085BG01	X258433	Powell Rhyolite	Rhyolite		645738	5348189	26.8	9	10	0.28	476	7.5	5.25	0.4	16.7	5.54	2.5	7.9	
MERN18MDS0085BG02	X258434	Powell Rhyolite	Rhyolite		645723	5348170	34.2	10	20	0.27	123	7.7	4.81	0.35	16.4	6.68	2.5	7.4	
MERN18MDS0110AG01	X258497	Powell Rhyolite	Rhyolite		645673	5347845	42.5	5	5	0.35	3	7.52	5.3	0.77	15.3	6.57	2.5	6.9	0.0025
MERN17MDS0061DG05	X258416	Powell Rhyolite	Rhyolite		645168	5347780	49.7	8	10	0.32	13	9.84	6.06	0.57	16.4	8.67	2.5	7.7	0
MERN17MDS0061DG06	X258417	Powell Rhyolite	Rhyolite		645166	5347775	49.7	10	10	0.32	358	7.81	5.27	0.57	16	7.5	2.5	7.3	0
MERN17MDS0061DG07	X258421	Powell Rhyolite	Rhyolite		645148	5347763													
MERN17MDS0061DG08	X258422	Powell Rhyolite	Rhyolite		645141	5347766													
MERN17MDS0061DG09	X258423	Powell Rhyolite	Rhyolite		645142	5347760													
MERN19MDS0126AG01 (qtz-	X261138	Powell Rhyolite	Rhyolite	Spilite	646496	5348024	54.9	5	20	0.26	50	8.13	5.26	1.17	17.8	7.07	<5	7.2	<0.005
MERN19MDS0128BG02	X261173	Powell tonalite	Tonalite	Ankerite-Her	644626	5347381													
MERN19MDS0128BG03	X261174	Powell tonalite	Tonalite	Ankerite-Her	644626	5347381													
MERN19MDS0128BG04	X261175	Powell tonalite	Tonalite	Ankerite-Her	644626	5347380													
MERN19MDS0128BG05	X261176	Powell tonalite	Tonalite	Ankerite-Her	644626	5347382													
MERN19MDS0128BG06	X261177	Powell tonalite	Tonalite	Ankerite-Her	644626	5347382													
MERN19MDS0128BG07	X261178	Powell tonalite	Tonalite	Ankerite-Her	644626	5347382													
MERN19MDS0128BG08	X261179	Powell tonalite	Tonalite	Ankerite-Her	644626	5347382													
MERN17MDS0041AG03	X258411	Powell Tonalite	Tonalite	Spilite	644674	5347418	52	2	10	0.15	7	8.01	4.97	1.68	19.4	7.51	2.5	5.4	0
MERN17MDS0073AG01	X258418	Powell Tonalite	Tonalite	Spilite	644512	5347244	119	1	10	0.23	24	9.02	5.58	3.46	18.2	10.25	2.5	2.8	0
MERN18MDS0087AG01	X258444	Powell Tonalite	Tonalite	Spotted	644635	5347296	40.2	4	20	0.25	15	7.9	5.38	0.95	22.1	7.01	2.5	5.5	0
MERN20MDS127AG02_dist h	C079664	Powell Tonalite	Tonalite	Ankerite-Her	642390	5346179	32	4	30	0.37	24	4.62	3.52	0.82	13.5	4.1	<5	5.9	<0.005
MERN20MDS127AG02_prox	C079663	Powell Tonalite	Tonalite	Ankerite-Her	642390	5346179	43.5	6	30	0.52	39	4.72	3.48	1.14	16.1	4.65	<5	6.2	<0.005
MERN20MDS127AG01	C079662	Powell tonalite	Tonalite	Ankerite-Her	642390	5346179													
MERN20MDS127AG03	C079665	Powell tonalite	Tonalite	Ankerite-Her	642390	5346179													
MERN20MDS127AG06	C079667	Powell tonalite	Tonalite	Ankerite-Her	642348	5346189													
MERN20MDS127AG07	C079668	Powell tonalite	Tonalite	Ankerite-Her	642348	5346189													
MERN20MDS127AG08	C079669	Powell tonalite	Tonalite	Ankerite-Her	642347	5346188													
MERN20MDS127AG09	C079670	Powell tonalite	Tonalite	Ankerite-Her	642347	5346188													
MERN18MDS0113CG03	X261057	Quartz-phyric rhyolite d	Rhyolite	Spilite	645805	5347679	82.6	4	10	0.08	33	9.96	6.96	1.83	20.7	9.85	2.5	6.6	0.0025
MERN19MDS0175AG01	X261158	Quartz-phyric rhyolite s	Rhyolite	Spilite	646460	5347507													
MERN19MDS0125DG01	X261095	Quemont feeder dike	Rhyolite	Spilite	646662	5347897													
MERN19MDS0125DG04	X261092	Quemont feeder dike	Rhyolite	Spilite	646610	5347890													
MERN19MDS0125DG07	X261093	Quemont feeder dike	Rhyolite	Spilite	646550	5347872													
MERN19MDS0125DG23	X261107	Quemont feeder dike	Rhyolite	Spilite	646420	5347791													
MERN19MDS0125DG24	X261105	Quemont feeder dike	Rhyolite	Spilite	646403	5347780													
MERN19MDS0125DG27	X261110	Quemont feeder dike	Rhyolite	Spilite	646341	5347772													
MERN20MDS186AG04	C079672	Quemont feeder dike	Rhyolite	Ankerite-Her	645699	5347175													
MERN20MDS186AG05	X261198	Quemont feeder dike	Rhyolite	Ankerite-Her	645696	5347174													
MERN20MDS186AG06	X261199	Quemont feeder dike	Rhyolite	Ankerite-Her	645693	5347172													
MERN20MDS186AG07	C079676	Quemont feeder dike	Rhyolite	Ankerite-Her	645708	5347170													
MERN20MDS186AG08	C079675	Quemont feeder dike	Rhyolite	Ankerite-Her	645709	5347171													
MERN20MDS186AG09	X261200	Quemont feeder dike	Rhyolite	Ankerite-Her	645710	5347172													
MERN20MDS186AG10	C079651	Quemont feeder dike	Rhyolite	Ankerite-Her	645717	5347173													
MERN20MDS186AG11	C079652	Quemont feeder dike	Rhyolite	Ankerite-Her	645720	5347175													
MERN20MDS186AG12	C079674	Quemont feeder dike	Rhyolite	Ankerite-Her	645728	5347180													
MERN18MDS0107AG01	X258465	Quemont feeder dyke	Rhyolite		646711	5347834	44.4	0.5	10	0.41	6	8.26	5.84	1.72	20.4	7.46	2.5	5.9	0.0025
MERN19MDS0125AG49	X261126	Quemont feeder dyke	Rhyolite		646586	5347789	48.2	11	20	0.16	2870	8.5	5.59	1.05	16.6	8.09	2.5	6.1	0.01
MERN19MDS0125AG49	X261127	Quemont feeder dyke	Rhyolite	Sericite	646586	5347789	53.7	13	20	0.36	312	8.72	5.57	1.05	20.2	8.98	2.5	6.2	0.0025
MERN19MDS0125AG70	X261136	Quemont feeder dyke	Rhyolite	Spotted	646551	5347769	57.9	6	10	0.44	15	6.66	4.39	1.16	22	7.19	2.5	6.7	0.0025
MERN19MDS0125AG70 (ser	X261136	Quemont feeder dyke	Rhyolite		646541	5347769	57.9	6	10	0.44	15	6.66	4.39	1.16	22	7.19	<5	6.7	<0.005
MERN19MDS0125DG42	X261131	Quemont feeder dyke	Rhyolite	Spilite	646712	5347827	42.9	1	10	0.14	30	8.61	5.74	1.72	18.5	7.8	2.5	6.6	0.0025
MERN19MDS0125DG43	X261129	Quemont feeder dyke	Rhyolite	Sericite	646712	5347827	57.7	0.5	10	1.2	13	9.93	6.56	2.1	27.5	8.74	2.5	8.5	0.0025
MERN18MDS0119AG01	X258462	uncertain protolith, strongly sulfidized			645630	5348024	61	9	10	0.21	1310	6.31	3.38	1.42	11	7.34	2.5	3.5	0.0025

Number	Lab ID	Formation	Rock Type	Alteration	UTM-East	UTM-North	Ho_ppm	In_ppm	La_ppm	Li_ppm	Lu_ppm	Mo_ppm	Nb_ppm	Nd_ppm	Ni_ppm	Pb_ppm	Rb_ppm	Re_ppm	Sb_ppm	Sc_ppm
							ME-MS81	ME-MS42	ME-MS81	ME-4ACD81	ME-MS81	ME-4ACD81	ME-MS81	ME-MS81	ME-4ACD81	ME-4ACD81	ME-MS81	ME-MS42	ME-MS42	ME-4ACD81
							0.01	0.005	0.1	10	0.01	1	0.2	0.1	1	2	0.2	0.001	0.05	1
MERN19MDS0125DG48	X261130	Mafic clast	Andesite	Chlorite	646586	5347789	1.74	0.346	14.8	100	0.74	1	18.5	19.1	15	1	1.9	0.0005	0.025	25
MERN19MDS0125AG52	X261120	Mafic clast	Andesite	Spotted	646522	5347784	0.77	0.339	8.3	50	0.27	0.5	2.6	7.6	22	1	30.1	0.0005	0.025	26
MERN19MDS0125AG53	X261119	Mafic clast	Andesite	Spotted	646522	5347784	1.57	0.714	9.2	50	0.68	1	6	14.2	17	1	22.7	0.0005	0.025	23
MERN17MDS0034AG06	X258407	Mafic dike	Andesite	Chlorite	644449	5347294	0.76	0.03	6.9	50	0.38	0.5	6.9	9.1	17	1	25	0	0.03	33
MERN18MDS0068AG01	X258469	Mafic Dike	Andesite		645454	5347795	0.9	0.009	17.1	20	0.38	1	9.6	18.4	44	1	11.3	0.0005	0.025	40
MERN19MDS0178BG02	X261164	Mafic intrusion	Andesite		646611	5347387	1.29	0.04	13.1	20	0.66	1	10.1	18.5	<1	<2	0.4	0.001	<0.05	18
MERN18MDS0115AG01	X258464	Mafic Sill	Andesite		645851	5347849	0.62	0.152	5.2	20	0.31	0.5	3.5	7.5	24	1	0.8	0.001	0.06	33
MERN17MDS0033AG10	X258405				644455	5347321	2.17	0.02	22.2	20	1.02	1	14.9	26.9	4	1	44.3	0	0.03	13
MERN18MDS0085BG01	X258433	Powell Rhyolite	Rhyolite		645738	5348189	1.66		11.9	10	0.8	3	10.7	14.6	2	3	33.2			9
MERN18MDS0085BG02	X258434	Powell Rhyolite	Rhyolite		645723	5348170	1.69		14.1	10	0.75	2	9.9	18.7	2	1	32			8
MERN18MDS0110AG01	X258497	Powell Rhyolite	Rhyolite		645673	5347845	1.75	0.021	19.6	10	0.87	1	11.3	23.6	2	1	30.6	0.0005	0.025	9
MERN17MDS0061DG05	X258416	Powell Rhyolite	Rhyolite		645168	5347780	2.05	0.01	23.3	10	0.92	1	12.8	27.7	3	2	29.9	0	0.03	9
MERN17MDS0061DG06	X258417	Powell Rhyolite	Rhyolite		645166	5347775	1.69	0.1	23.2	10	0.81	3	11.9	27.6	1	1	26.4	0	0.03	8
MERN17MDS0061DG07	X258421	Powell Rhyolite	Rhyolite		645148	5347763														
MERN17MDS0061DG08	X258422	Powell Rhyolite	Rhyolite		645141	5347766														
MERN17MDS0061DG09	X258423	Powell Rhyolite	Rhyolite		645142	5347760														
MERN19MDS0126AG01 (qtz-	X261138	Powell Rhyolite	Rhyolite	Spilite	646496	5348024	1.81	0.025	24.1	10	0.81	1	11.3	29.8	8	<2	16	<0.001	<0.05	11
MERN19MDS0128BG02	X261173	Powell tonalite	Tonalite	Ankerite-Hematite	644626	5347381														
MERN19MDS0128BG03	X261174	Powell tonalite	Tonalite	Ankerite-Hematite	644626	5347381														
MERN19MDS0128BG04	X261175	Powell tonalite	Tonalite	Ankerite-Hematite	644626	5347380														
MERN19MDS0128BG05	X261176	Powell tonalite	Tonalite	Ankerite-Hematite	644626	5347382														
MERN19MDS0128BG06	X261177	Powell tonalite	Tonalite	Ankerite-Hematite	644626	5347382														
MERN19MDS0128BG07	X261178	Powell tonalite	Tonalite	Ankerite-Hematite	644626	5347382														
MERN19MDS0128BG08	X261179	Powell tonalite	Tonalite	Ankerite-Hematite	644626	5347382														
MERN17MDS0041AG03	X258411	Powell Tonalite	Tonalite	Spilite	644674	5347418	1.7	0.04	23.5	10	0.81	1	12.3	30.7	1	2	7.2	0	0.03	12
MERN17MDS0073AG01	X258418	Powell Tonalite	Tonalite	Spilite	644512	5347244	1.87	0.04	58.9	10	0.69	1	12.2	58.8	2	1	7.6	0	0.03	10
MERN18MDS0087AG01	X258444	Powell Tonalite	Tonalite	Spotted	644635	5347296	1.69	0.05	16.9	40	0.75	0.5	13.3	22.3	2	1	16.1	0	0.03	16
MERN20MDS127AG02_dist h	C079664	Powell Tonalite	Tonalite	Ankerite-Hematite	642390	5346179	1.1	0.008	16.1	<10	0.63	2	8.2	16.5	5	<2	20.5	<0.001	<0.05	6
MERN20MDS127AG02_prox l	C079663	Powell Tonalite	Tonalite	Ankerite-Hematite	642390	5346179	1	0.042	22.4	<10	0.66	2	8.6	22.4	2	<2	23.2	<0.001	<0.05	6
MERN20MDS127AG03	C079662	Powell tonalite	Tonalite	Ankerite-Hematite	642390	5346179														
MERN20MDS127AG06	C079665	Powell tonalite	Tonalite	Ankerite-Hematite	642348	5346189														
MERN20MDS127AG07	C079667	Powell tonalite	Tonalite	Ankerite-Hematite	642348	5346189														
MERN20MDS127AG08	C079668	Powell tonalite	Tonalite	Ankerite-Hematite	642347	5346188														
MERN20MDS127AG09	C079669	Powell tonalite	Tonalite	Ankerite-Hematite	642347	5346188														
MERN18MDS0113CG03	X261057	Quartz-phyric rhyolite dil	Rhyolite	Spilite	645805	5347679	2.23	0.019	32	<10	1.14	1	15.3	41.7	3	2	0.9	0.0005	0.025	12
MERN19MDS0175AG01	X261158	Quartz-phyric rhyolite sil	Rhyolite	Spilite	646460	5347507														
MERN19MDS0125DG01	X261095	Quemont feeder dike	Rhyolite	Spilite	646662	5347897														
MERN19MDS0125DG04	X261092	Quemont feeder dike	Rhyolite	Spilite	646610	5347890														
MERN19MDS0125DG07	X261093	Quemont feeder dike	Rhyolite	Spilite	646550	5347872														
MERN19MDS0125DG23	X261107	Quemont feeder dike	Rhyolite	Spilite	646420	5347791														
MERN19MDS0125DG24	X261105	Quemont feeder dike	Rhyolite	Spilite	646403	5347780														
MERN19MDS0125DG27	X261110	Quemont feeder dike	Rhyolite	Spilite	646341	5347772														
MERN20MDS186AG04	C079672	Quemont feeder dike	Rhyolite	Ankerite-Hematite	645699	5347175														
MERN20MDS186AG05	X261198	Quemont feeder dike	Rhyolite	Ankerite-Hematite	645696	5347174														
MERN20MDS186AG06	X261199	Quemont feeder dike	Rhyolite	Ankerite-Hematite	645693	5347172														
MERN20MDS186AG07	C079676	Quemont feeder dike	Rhyolite	Ankerite-Hematite	645708	5347170														
MERN20MDS186AG08	C079675	Quemont feeder dike	Rhyolite	Ankerite-Hematite	645709	5347171														
MERN20MDS186AG09	X261200	Quemont feeder dike	Rhyolite	Ankerite-Hematite	645710	5347172														
MERN20MDS186AG10	C079651	Quemont feeder dike	Rhyolite	Ankerite-Hematite	645717	5347173														
MERN20MDS186AG11	C079652	Quemont feeder dike	Rhyolite	Ankerite-Hematite	645720	5347175														
MERN20MDS186AG12	C079674	Quemont feeder dike	Rhyolite	Ankerite-Hematite	645728	5347180														
MERN18MDS0107AG01	X258465	Quemont feeder dyke	Rhyolite		646711	5347834	1.9	0.041	20.3	10	0.95	1	14.4	26.1	2	1	25.3	0.0005	0.06	12
MERN19MDS0125AG49	X261126	Quemont feeder dyke	Rhyolite		646586	5347789	1.8	0.826	20.8	20	0.96	1	14	28.8	2	1	11	0.001	0.025	12
MERN19MDS0125AG49	X261127	Quemont feeder dyke	Rhyolite	Sericite	646586	5347789	1.84	0.126	23.5	20	0.97	2	13.3	31.2	6	1	27.1	0.0005	0.025	13
MERN19MDS0125AG70	X261136	Quemont feeder dyke	Rhyolite	Spotted	646551	5347769	1.35	0.059	25.2	20	0.83	1	11.8	32	6	5	26.3	0.0005	0.05	15
MERN19MDS0125AG70 (ser	X261136	Quemont feeder dyke	Rhyolite		646541	5347769	1.35	0.059	25.2	20	0.83	1	11.8	32	6	5	26.3	<0.001	0.05	15
MERN19MDS0125DG42	X261131	Quemont feeder dyke	Rhyolite	Spilite	646712	5347827	1.82	0.055	18.9	20	1.02	2	14.3	26.1	1	1	9.5	0.0005	0.025	12
MERN19MDS0125DG43	X261129	Quemont feeder dyke	Rhyolite	Sericite	646712	5347827	2.23	0.031	25.1	<10	1.16	1	17.9	36.7	3	1	74.1	0.0005	0.025	15
MERN18MDS0119AG01	X258462	uncertain protolith, strongly sulfidized			645630	5348024	1.29	0.106	27.8	10	0.51	41	8.1	32.3	6	3	18.3	0.041	0.05	20

Number	Lab ID	Formation	Rock Type	Alteration	UTM-East	UTM-North	Se_ppm	Sm_ppm	Sn_ppm	Sr_ppm	Ta_ppm	Tb_ppm	Te_ppm	Th_ppm	Tl_ppm	Tm_ppm	U_ppm	V_ppm	W_ppm	Y_ppm
							ME-MS42	ME-MS81	ME-MS81	ME-MS81	ME-MS81	ME-MS81	ME-MS42	ME-MS81	ME-MS42	ME-MS81	ME-MS81	ME-MS81	ME-MS81	ME-MS81
							0.2	0.03	1	0.1	0.1	0.01	0.01	0.05	0.02	0.01	0.05	5	1	0.1
MERN19MDS0125DG48	X261130	Mafic clast	Andesite	Chlorite	646586	5347789	0.4	5.4	13	2.6	0.7	1.35	0.38	1.36	0.01	0.76	0.58	357	42	49.3
MERN19MDS0125AG52	X261120	Mafic clast	Andesite	Spotted	646522	5347784	0.3	2.32	18	20.3	0.1	0.58	0.04	0.39	0.01	0.28	0.14	354	4	20.4
MERN19MDS0125AG53	X261119	Mafic clast	Andesite	Spotted	646522	5347784	1.3	4.34	11	15.5	0.3	1.15	0.06	1.02	0.01	0.75	0.25	338	6	43.6
MERN17MDS0034AG06	X258407	Mafic dike	Andesite	Chlorite	644449	5347294	0.1	2.59	7	4.3	0.3	0.51	0.01	1.36	0.01	0.33	0.47	305	2	17.6
MERN18MDS0068AG01	X258469	Mafic Dike	Andesite		645454	5347795	0.3	4.17	1	208	0.5	0.72	0.01	2.42	0.01	0.39	0.36	366	0.5	22.1
MERN19MDS0178BG02	X261164	Mafic intrusion	Andesite		646611	5347387	<0.2	5.09	2	22.6	0.5	0.87	0.01	1.64	<0.02	0.63	0.44	<5	1	33.9
MERN18MDS0115AG01	X258464	Mafic Sill	Andesite		645851	5347849	0.1	2.19	12	154.5	0.2	0.47	0.01	0.58	0.01	0.29	0.16	281	0.5	16.1
MERN17MDS0033AG10	X258405				644455	5347321	0.3	7.18	28	4.9	0.8	1.6	0.12	2.3	0.01	0.92	0.8	2.5	6	48.7
MERN18MDS0085BG01	X258433	Powell Rhyolite	Rhyolite		645738	5348189		3.76	5	6.8	0.8	1.15		3.34			0.89	22	2	43.2
MERN18MDS0085BG02	X258434	Powell Rhyolite	Rhyolite		645723	5348170		5.08	3	4.5	0.8	1.15		3.18			0.88	12	1	44.7
MERN18MDS0110AG01	X258497	Powell Rhyolite	Rhyolite		645673	5347845	0.1	5.88	3	9.2	0.7	1.29	0.005	3.56	0.01	0.82	0.94	14	1	45.7
MERN17MDS0061DG05	X258416	Powell Rhyolite	Rhyolite		645168	5347780	0.3	7.28	5	6.7	0.8	1.51	0.51	4.21	0.01	0.86	1.03	11	4	50.5
MERN17MDS0061DG06	X258417	Powell Rhyolite	Rhyolite		645166	5347775	1.7	7.25	6	5.5	0.7	1.26	0.16	3.9	0.01	0.78	0.91	11	5	41.7
MERN17MDS0061DG07	X258421	Powell Rhyolite	Rhyolite		645148	5347763														49.5
MERN17MDS0061DG08	X258422	Powell Rhyolite	Rhyolite		645141	5347766														48.3
MERN17MDS0061DG09	X258423	Powell Rhyolite	Rhyolite		645142	5347760														55.5
MERN19MDS0126AG01 (qtz-	X261138	Powell Rhyolite	Rhyolite	Spilite	646496	5348024	<0.2	7.1	1	49.6	0.8	1.23	0.03	3.71	0.02	0.78	1.03	48	1	49.5
MERN19MDS0128BG02	X261173	Powell tonalite	Tonalite	Ankerite-Hematite	644626	5347381														28.1
MERN19MDS0128BG03	X261174	Powell tonalite	Tonalite	Ankerite-Hematite	644626	5347381														23.9
MERN19MDS0128BG04	X261175	Powell tonalite	Tonalite	Ankerite-Hematite	644626	5347380														26.9
MERN19MDS0128BG05	X261176	Powell tonalite	Tonalite	Ankerite-Hematite	644626	5347382														43.4
MERN19MDS0128BG06	X261177	Powell tonalite	Tonalite	Ankerite-Hematite	644626	5347382														148
MERN19MDS0128BG07	X261178	Powell tonalite	Tonalite	Ankerite-Hematite	644626	5347382														95
MERN19MDS0128BG08	X261179	Powell tonalite	Tonalite	Ankerite-Hematite	644626	5347382														48.3
MERN17MDS0041AG03	X258411	Powell Tonalite	Tonalite	Spilite	644674	5347418	0.1	7.15	2	18.6	0.7	1.31	0.02	2.07	0.01	0.72	0.54	2.5	2	40.7
MERN17MDS0073AG01	X258418	Powell Tonalite	Tonalite	Spilite	644512	5347244	0.1	12.2	2	34.7	0.5	1.49	0.02	2.95	0.01	0.75	0.41	2.5	1	45
MERN18MDS0087AG01	X258444	Powell Tonalite	Tonalite	Spotted	644635	5347296	0.1	5.78	4	14.9	0.7	1.48	0.01	1.82	0.01	0.77	0.66	11	1	51.4
MERN20MDS127AG02_dist h	C079664	Powell Tonalite	Tonalite	Ankerite-Hematite	642390	5346179	<0.2	3.69	2	79.4	1.1	0.72	0.08	3.2	<0.02	0.51	0.88	18	2	32.5
MERN20MDS127AG02_prox I	C079663	Powell Tonalite	Tonalite	Ankerite-Hematite	642390	5346179	0.2	5.05	2	109.5	0.7	0.74	0.07	3.72	<0.02	0.58	1	21	15	30.6
MERN20MDS127AG01	C079662	Powell tonalite	Tonalite	Ankerite-Hematite	642390	5346179														35.4
MERN20MDS127AG03	C079665	Powell tonalite	Tonalite	Ankerite-Hematite	642390	5346179														32.3
MERN20MDS127AG06	C079667	Powell tonalite	Tonalite	Ankerite-Hematite	642348	5346189														30.7
MERN20MDS127AG07	C079668	Powell tonalite	Tonalite	Ankerite-Hematite	642348	5346189														34.8
MERN20MDS127AG08	C079669	Powell tonalite	Tonalite	Ankerite-Hematite	642347	5346188														34.4
MERN20MDS127AG09	C079670	Powell tonalite	Tonalite	Ankerite-Hematite	642347	5346188														34.3
MERN18MDS0113CG03	X261057	Quartz-phyric rhyolite d	Rhyolite	Spilite	645805	5347679	0.1	9.99	1	70.1	0.9	1.76	0.02	2.79	0.01	1.08	1.03	2.5	1	57.7
MERN19MDS0175AG01	X261158	Quartz-phyric rhyolite s	Rhyolite	Spilite	646460	5347507														47.5
MERN19MDS0125DG01	X261095	Quemont feeder dike	Rhyolite	Spilite	646662	5347897														48.6
MERN19MDS0125DG04	X261092	Quemont feeder dike	Rhyolite	Spilite	646610	5347890														53.3
MERN19MDS0125DG07	X261093	Quemont feeder dike	Rhyolite	Spilite	646550	5347872														56.9
MERN19MDS0125DG23	X261107	Quemont feeder dike	Rhyolite	Spilite	646420	5347791														55.6
MERN19MDS0125DG24	X261105	Quemont feeder dike	Rhyolite	Spilite	646403	5347780														58.1
MERN19MDS0125DG27	X261110	Quemont feeder dike	Rhyolite	Spilite	646341	5347772														51
MERN20MDS186AG04	C079672	Quemont feeder dike	Rhyolite	Ankerite-Hematite	645699	5347175														30.5
MERN20MDS186AG05	X261198	Quemont feeder dike	Rhyolite	Ankerite-Hematite	645696	5347174														56
MERN20MDS186AG06	X261199	Quemont feeder dike	Rhyolite	Ankerite-Hematite	645693	5347172														70.4
MERN20MDS186AG07	C079676	Quemont feeder dike	Rhyolite	Ankerite-Hematite	645708	5347170														49.7
MERN20MDS186AG08	C079675	Quemont feeder dike	Rhyolite	Ankerite-Hematite	645709	5347171														50
MERN20MDS186AG09	X261200	Quemont feeder dike	Rhyolite	Ankerite-Hematite	645710	5347172														50.2
MERN20MDS186AG10	C079651	Quemont feeder dike	Rhyolite	Ankerite-Hematite	645717	5347173														52.2
MERN20MDS186AG11	C079652	Quemont feeder dike	Rhyolite	Ankerite-Hematite	645720	5347175														55.5
MERN20MDS186AG12	C079674	Quemont feeder dike	Rhyolite	Ankerite-Hematite	645728	5347180														54.4
MERN18MDS0107AG01	X258465	Quemont feeder dyke	Rhyolite		646711	5347834	0.1	6.74	2	51.4	0.8	1.37	0.01	2.43	0.01	0.92	0.65	2.5	1	49.3
MERN19MDS0125AG49	X261126	Quemont feeder dyke	Rhyolite		646586	5347789	1.7	7.08	9	21.8	0.9	1.43	0.8	2.47	0.01	0.92	0.85	8	3	52.3
MERN19MDS0125AG49	X261127	Quemont feeder dyke	Rhyolite	Sericite	646586	5347789	0.7	7.86	13	11	0.9	1.47	0.91	2.5	0.01	0.93	0.93	12	3	52.8
MERN19MDS0125AG70	X261136	Quemont feeder dyke	Rhyolite	Spotted	646551	5347769	0.1	8.35	10	11.7	0.9	1.01	0.13	2.53	0.01	0.71	0.92	14	3	36.3
MERN19MDS0125AG70 (ser	X261136	Quemont feeder dyke	Rhyolite		646541	5347769	<0.2	8.35	10	11.7	0.9	1.01	0.13	2.53	<0.02	0.71	0.92	14	3	36.3
MERN19MDS0125DG42	X261131	Quemont feeder dyke	Rhyolite	Spilite	646712	5347827	0.1	7.16	4	56.6	1	1.44	0.01	2.62	0.01	0.94	0.73	2.5	2	52.8
MERN19MDS0125DG43	X261129	Quemont feeder dyke	Rhyolite	Sericite	646712	5347827	0.1	8.37	18	20.3	1.1	1.61	0.01	3.76	0.02	1.1	0.83	2.5	2	62.6
MERN18MDS0119AG01	X258462	uncertain protolith, strongly sulfidized			645630	5348024	0.7	7.53	3	29.5	0.5	1.08	1.76	2.14	0.01	0.53	0.67	166	7	30.6

Number	Lab ID	Formation	Rock Type	Alteration	UTM-East	UTM-North	Yb_ppm	Zn_ppm	Zr_ppm
							ME-MS81	ME4ACD81	ME-MS81
							0.03	2	2
MERN19MDS0125DG48	X261130	Mafic clast	Andesite	Chlorite	646586	5347789	4.89	285	148
MERN19MDS0125AG52	X261120	Mafic clast	Andesite	Spotted	646522	5347784	1.84	363	25
MERN19MDS0125AG53	X261119	Mafic clast	Andesite	Spotted	646522	5347784	4.36	233	71
MERN17MDS0034AG06	X258407	Mafic dike	Andesite	Chlorite	644449	5347294	2.37	292	113
MERN18MDS0068AG01	X258469	Mafic Dike	Andesite		645454	5347795	2.41	118	105
MERN19MDS0178BG02	X261164	Mafic intrusion	Andesite		646611	5347387	4.25	70	142
MERN18MDS0115AG01	X258464	Mafic Sill	Andesite		645851	5347849	1.94	224	59
MERN17MDS0033AG10	X258405				644455	5347321	6.76	268	203
MERN18MDS0085BG01	X258433	Powell Rhyolite	Rhyolite		645738	5348189	5.05	68	275
MERN18MDS0085BG02	X258434	Powell Rhyolite	Rhyolite		645723	5348170	5.28	43	256
MERN18MDS0110AG01	X258497	Powell Rhyolite	Rhyolite		645673	5347845	5.51	136	287
MERN17MDS0061DG05	X258416	Powell Rhyolite	Rhyolite		645168	5347780	6.36	89	284
MERN17MDS0061DG06	X258417	Powell Rhyolite	Rhyolite		645166	5347775	5.58	107	270
MERN17MDS0061DG07	X258421	Powell Rhyolite	Rhyolite		645148	5347763			307
MERN17MDS0061DG08	X258422	Powell Rhyolite	Rhyolite		645141	5347766			250
MERN17MDS0061DG09	X258423	Powell Rhyolite	Rhyolite		645142	5347760			300
MERN19MDS0126AG01 (qtz-	X261138	Powell Rhyolite	Rhyolite	Spilite	646496	5348024	5.4	74	278
MERN19MDS0128BG02	X261173	Powell tonalite	Tonalite	Ankerite-Hemati	644626	5347381			238
MERN19MDS0128BG03	X261174	Powell tonalite	Tonalite	Ankerite-Hemati	644626	5347381			179
MERN19MDS0128BG04	X261175	Powell tonalite	Tonalite	Ankerite-Hemati	644626	5347380			176
MERN19MDS0128BG05	X261176	Powell tonalite	Tonalite	Ankerite-Hemati	644626	5347382			266
MERN19MDS0128BG06	X261177	Powell tonalite	Tonalite	Ankerite-Hemati	644626	5347382			283
MERN19MDS0128BG07	X261178	Powell tonalite	Tonalite	Ankerite-Hemati	644626	5347382			287
MERN19MDS0128BG08	X261179	Powell tonalite	Tonalite	Ankerite-Hemati	644626	5347382			163
MERN17MDS0041AG03	X258411	Powell Tonalite	Tonalite	Spilite	644674	5347418	5.36	149	192
MERN17MDS0073AG01	X258418	Powell Tonalite	Tonalite	Spilite	644512	5347244	5.07	111	101
MERN18MDS0087AG01	X258444	Powell Tonalite	Tonalite	Spotted	644635	5347296	5.15	371	212
MERN20MDS127AG02_dist h	C079664	Powell Tonalite	Tonalite	Ankerite-Hemati	642390	5346179	3.9	6	208
MERN20MDS127AG02_prox l	C079663	Powell Tonalite	Tonalite	Ankerite-Hemati	642390	5346179	4.03	12	217
MERN20MDS127AG01	C079662	Powell tonalite	Tonalite	Ankerite-Hemati	642390	5346179			202
MERN20MDS127AG03	C079665	Powell tonalite	Tonalite	Ankerite-Hemati	642390	5346179			192
MERN20MDS127AG06	C079667	Powell tonalite	Tonalite	Ankerite-Hemati	642348	5346189			143
MERN20MDS127AG07	C079668	Powell tonalite	Tonalite	Ankerite-Hemati	642348	5346189			166
MERN20MDS127AG08	C079669	Powell tonalite	Tonalite	Ankerite-Hemati	642347	5346188			177
MERN20MDS127AG09	C079670	Powell tonalite	Tonalite	Ankerite-Hemati	642347	5346188			175
MERN18MDS0113CG03	X261057	Quartz-phyric rhyolite c	Rhyolite	Spilite	645805	5347679	7.34	32	280
MERN19MDS0175AG01	X261158	Quartz-phyric rhyolite s	Rhyolite	Spilite	646460	5347507			236
MERN19MDS0125DG01	X261095	Quemont feeder dike	Rhyolite	Spilite	646662	5347897			209
MERN19MDS0125DG04	X261092	Quemont feeder dike	Rhyolite	Spilite	646610	5347890			221
MERN19MDS0125DG07	X261093	Quemont feeder dike	Rhyolite	Spilite	646550	5347872			212
MERN19MDS0125DG23	X261107	Quemont feeder dike	Rhyolite	Spilite	646420	5347791			221
MERN19MDS0125DG24	X261105	Quemont feeder dike	Rhyolite	Spilite	646403	5347780			236
MERN19MDS0125DG27	X261110	Quemont feeder dike	Rhyolite	Spilite	646341	5347772			215
MERN20MDS186AG04	C079672	Quemont feeder dike	Rhyolite	Ankerite-Hemati	645699	5347175			133
MERN20MDS186AG05	X261198	Quemont feeder dike	Rhyolite	Ankerite-Hemati	645696	5347174			239
MERN20MDS186AG06	X261199	Quemont feeder dike	Rhyolite	Ankerite-Hemati	645693	5347172			219
MERN20MDS186AG07	C079676	Quemont feeder dike	Rhyolite	Ankerite-Hemati	645708	5347170			213
MERN20MDS186AG08	C079675	Quemont feeder dike	Rhyolite	Ankerite-Hemati	645709	5347171			221
MERN20MDS186AG09	X261200	Quemont feeder dike	Rhyolite	Ankerite-Hemati	645710	5347172			231
MERN20MDS186AG10	C079651	Quemont feeder dike	Rhyolite	Ankerite-Hemati	645717	5347173			229
MERN20MDS186AG11	C079652	Quemont feeder dike	Rhyolite	Ankerite-Hemati	645720	5347175			237
MERN20MDS186AG12	C079674	Quemont feeder dike	Rhyolite	Ankerite-Hemati	645728	5347180			243
MERN18MDS0107AG01	X258465	Quemont feeder dyke	Rhyolite		646711	5347834	6.21	65	259
MERN19MDS0125AG49	X261126	Quemont feeder dyke	Rhyolite		646586	5347789	6.16	52	225
MERN19MDS0125AG49	X261127	Quemont feeder dyke	Rhyolite	Sericite	646586	5347789	5.55	63	223
MERN19MDS0125AG70	X261136	Quemont feeder dyke	Rhyolite	Spotted	646551	5347769	4.91	71	240
MERN19MDS0125AG70 (ser	X261136	Quemont feeder dyke	Rhyolite		646541	5347769	4.91	71	240
MERN19MDS0125DG42	X261131	Quemont feeder dyke	Rhyolite	Spilite	646712	5347827	5.98	102	233
MERN19MDS0125DG43	X261129	Quemont feeder dyke	Rhyolite	Sericite	646712	5347827	6.93	29	303
MERN18MDS0119AG01	X258462	uncertain protolith, strongly sulfidized			645630	5348024	2.85	84	134

Number	Lab ID	Formation	Rock Type	Alteration	UTM-East	UTM-North	SiO2 wt%	TiO2 wt%	Al2O3 wt%	Fe2O3t wt%	MnO wt%	MgO wt%	CaO wt%	SrO wt%	BaO wt%	Na2O wt%	K2O wt%	P2O5 wt%
							ME-ICP06	ME-ICP06	ME-ICP06	ME-ICP06	ME-ICP06	ME-ICP06	ME-ICP06	ME-ICP06	ME-ICP06	ME-ICP06	ME-ICP06	ME-ICP06
							0.01	0.01	0.01	0.01			0.01	0.01	0.01	0.05	0.01	0.01
MERN18MDS0085CG07	X258435	Upper Marker Unit	Mafic tuff	Spotted	645724	5348195	55.30	0.68	15.25	17.30	0.52	5.17	0.17	0.01	0.05	0.65	1.43	0.08
MERN18MDS0085CG12ii	X258487	Upper Marker Unit	Mafic tuff	Chlorite	645737	5348188	50.20	0.73	17.30	19.95	0.36	3.76	0.12	0.01	0.07	0.30	2.15	0.09
MERN18MDS0085CG12i	X258488	Upper Marker Unit	Mafic tuff		645737	5348188	50.40	0.75	17.85	21.10	0.38	3.98	0.11	0.01	0.07	0.29	2.10	0.10
MERN18MDS0115BG03	X258459	Upper Marker Unit	Felsic tuff		645851	5347849	55.80	0.81	17.30	11.30	0.12	6.67	1.02	0.01	0.09	1.46	1.93	0.13
MERN18MDS0114AG02	X258475	Upper Powell Andesite	Andesite	Spotted	645819	5347735	60.90	1.24	13.65	12.20	0.11	6.65	0.35	0.01	0.03	0.12	1.06	0.23
MERN18MDS0108AG01	X258470	Upper Powell Andesite	Andesite		645622	5347834	63.70	0.65	14.80	8.83	0.15	3.85	0.36	0.01	0.02	4.13	0.49	0.21
MERN18MDS0109AG01	X258474	Upper Powell Andesite	Andesite		645563	5347825	69.60	0.66	13.65	5.98	0.10	3.06	0.32	0.01	0.03	4.07	0.72	0.23
MERN17MDS0064DG04	X258482	Upper Powell Andesite	Andesite	Not spotted	645355	5347769	63.20	1.23	14.95	8.37	0.10	5.97	0.26	0.01	0.01	4.50	0.04	0.18
MERN18MDS0085EG11	X258436	Upper Powell Andesite	Andesite	Not spotted	645776	5348159	58.30	1.26	13.05	14.50	0.27	4.75	0.44	0.01	0.03	0.09	1.17	0.31
MERN17MDS0031AG07ii	X261051	Upper Powell Andesite	Andesite	Spotted	645240	5347733	54.80	1.22	14.90	12.25	0.12	8.92	0.26	0.01	0.02	0.69	0.61	0.17
MERN18MDS0084CG01	X258432	Upper Powell Andesite	Andesite	Spotted	645667	5348114	63.90	0.98	11.10	15.60	0.19	4.26	0.27	0.01	0.01	0.46	0.33	0.15
MERN18MDS0112AG01	X258494	Upper Powell Andesite	Andesite	Not spotted	645748	5347867	52.50	1.33	13.65	11.35	0.24	7.78	1.63	0.01	0.01	3.97	0.08	0.14
MERN18MDS0113AG01	X258478	Upper Powell Andesite	Andesite	Least altered	645805	5347679	59.10	1.24	13.65	9.49	0.12	6.55	0.47	0.01	0.01	4.16	0.10	0.17
MERN17MDS0030AG02	X258481	Upper Powell Andesite	Andesite		645036	5347711	63.00	0.74	13.85	11.80	0.10	3.71	0.31	0.01	0.06	0.18	1.65	0.26
MERN18MDS0118AG02	X258491	Upper Powell Andesite	Andesite	Not spotted	645590	5347983	61.00	1.39	13.65	9.69	0.20	4.01	0.97	0.01	0.01	4.55	0.04	0.36
MERN18MDS0114AG01	X258493	Upper Powell Andesite	Andesite	Spotted	645819	5347735	60.00	1.21	13.50	12.50	0.09	5.06	0.79	0.01	0.04	0.46	1.24	0.32
MERN18MDS0118AG01	X258466	Upper Powell Andesite	Andesite	Spotted	645590	5347983	59.70	1.39	14.50	10.05	0.08	4.16	0.72	0.01	0.01	4.05	0.27	0.36
MERN17MDS0031AG07i	X258485	Upper Powell Andesite	Andesite		645240	5347733	62.30	1.20	14.70	8.08	0.20	5.94	0.42	0.01	0.01	4.44	0.09	0.16
MERN19MDS0153BG03	X261149	Upper Powell Andesite			646297	5348043	63.50	1.10	13.25	8.05	0.13	5.00	0.26	0.01	0.01	3.55	0.22	0.15

Number	Lab ID	Formation	Rock Type	Alteration	UTM-East	UTM-North	LOI_OA-GRA	Total	C_C-IR07_%	S_S-IR08_%	H20+_OA-IR(	Cl_Cl-IC881_	F_F-IC881_p	S.G.	Ag ppm	As ppm	Au ppm	Ba ppm	Bi ppm	Cd ppm
							OA-GRA05		C-IR07	S-IR08	OA-IR06				ME-4ACD81	ME-MS42	Au-ICP21	ME-MS81	ME-MS42	ME-4ACD81
							0.01		0.01	0.01	0.01				0.5	0.1		0.5	0.01	0.5
MERN18MDS0085CG07	X258435	Upper Marker Unit	Mafic tuff	Spotted	645724	5348195	4.42	101.02	0.03	0.36	6.09	120	520	2.82	0.25	0.4		383		0.25
MERN18MDS0085CG12ii	X258487	Upper Marker Unit	Mafic tuff	Chlorite	645737	5348188	4.28	99.32	0.01	0.04		140	690	2.7						
MERN18MDS0085CG12i	X258488	Upper Marker Unit	Mafic tuff		645737	5348188	4.38	101.52	<0.01	0.04		140	680	2.73						
MERN18MDS0115BG03	X258459	Upper Marker Unit	Felsic tuff		645851	5347849	4.85	101.48	0.12	0.01		25	490	2.68	0.25	0.1		850	0.04	0.25
MERN18MDS0114AG02	X258475	Upper Powell Andesite	Andesite	Spotted	645819	5347735	4.62	101.31	0.03	0.12		50	800	2.69	0.25	1.1		236	0.59	0.8
MERN18MDS0108AG01	X258470	Upper Powell Andesite	Andesite		645622	5347834	3.25	100.44	0.18	0.03		25	410	2.7	0.25	0.2		137	0.19	0.25
MERN18MDS0109AG01	X258474	Upper Powell Andesite	Andesite		645563	5347825	2.33	100.75	<0.01	0.04		25	320	2.79	0.25	0.1		260	0.03	0.25
MERN17MDS0064DG04	X258482	Upper Powell Andesite	Andesite	Not spotted	645355	5347769	3.17	101.97	0.04	0.01		<50	330	2.7						
MERN18MDS0085EG11	X258436	Upper Powell Andesite	Andesite	Not spotted	645776	5348159	4.03	98.2	0.02	0.01	5.07	110	650	2.89	0.25	0.6		229		0.25
MERN17MDS0031AG07ii	X261051	Upper Powell Andesite	Andesite	Spotted	645240	5347733	5.34	99.3	0.05	<0.01		<50	470	2.74						
MERN18MDS0084CG01	X258432	Upper Powell Andesite	Andesite	Spotted	645667	5348114	3.60	100.85	0.03	0.03	4.34	170	560	2.77	0.25	0.2		101.5		0.25
MERN18MDS0112AG01	X258494	Upper Powell Andesite	Andesite	Not spotted	645748	5347867	5.05	100.71	0.27	0.18		25	350	2.7	0.25	2.3		79.5	0.13	2.1
MERN18MDS0113AG01	X258478	Upper Powell Andesite	Andesite	Least altered	645805	5347679	3.86	100.32	0.06	0.02		25	530	2.69	0.25	0.3		68.4	0.01	0.5
MERN17MDS0030AG02	X258481	Upper Powell Andesite	Andesite		645036	5347711	3.80	99.46	0.01	0.04		<50	610	2.77						
MERN18MDS0118AG02	X258491	Upper Powell Andesite	Andesite	Not spotted	645590	5347983	2.98	99.35	0.08	0.13		25	1280	2.73	0.25	0.4		21.1	0.03	0.6
MERN18MDS0114AG01	X258493	Upper Powell Andesite	Andesite	Spotted	645819	5347735	4.38	99.59	0.16	0.01		<50	660	2.76						
MERN18MDS0118AG01	X258466	Upper Powell Andesite	Andesite	Spotted	645590	5347983	3.19	98.48	0.06	0.45		<50	970	2.71						
MERN17MDS0031AG07i	X258485	Upper Powell Andesite	Andesite		645240	5347733	3.83	101.36	0.26	0.01		<50	350	2.64						
MERN19MDS0153BG03	X261149	Upper Powell Andesite			646297	5348043	2.83	98.05	0.02	0.01					<0.5	0.2		72.9	0.02	0.6

Number	Lab ID	Formation	Rock Type	Alteration	UTM-East	UTM-North	Ce ppm	Co ppm	Cr ppm	Cs ppm	Cu ppm	Dy ppm	Er ppm	Eu ppm	Ga_ppm	Gd_ppm	Ge_ppm	Hf_ppm	Hg_ppm
							ME-MS81	ME-4ACD81	ME-MS81	ME-MS81	ME-4ACD81	ME-MS81	ME-MS81	ME-MS81	ME-MS81	ME-MS81	ME-MS81	ME-MS81	ME-MS42
							0.1	1		10	1	0.05	0.03	0.03	0.1	0.05	5	0.2	0.005
MERN18MDS0085CG07	X258435	Upper Marker Unit	Mafic tuff	Spotted	645724	5348195	4.9	21	50	0.32	299	1.34	0.94	0.45	19.1	1.16	2.5	0.7	
MERN18MDS0085CG12ii	X258487	Upper Marker Unit	Mafic tuff	Chlorite	645737	5348188													
MERN18MDS0085CG12i	X258488	Upper Marker Unit	Mafic tuff		645737	5348188													
MERN18MDS0115BG03	X258459	Upper Marker Unit	Felsic tuff		645851	5347849	14.5	17	30	0.65	13	2.53	1.73	0.87	21.4	2.65	2.5	2.4	0.0025
MERN18MDS0114AG02	X258475	Upper Powell Andesite	Andesite	Spotted	645819	5347735	27.8	18	10	0.38	120	4.06	2.73	0.7	20.6	4.16	2.5	3.5	0.0025
MERN18MDS0108AG01	X258470	Upper Powell Andesite	Andesite		645622	5347834	37.2	8	10	0.13	110	6.58	4.41	1.17	20.6	6.25	2.5	5	0.0025
MERN18MDS0109AG01	X258474	Upper Powell Andesite	Andesite		645563	5347825	36.5	3	10	0.19	9	6.43	4.64	1.13	19.3	6.18	2.5	5.5	0.0025
MERN17MDS0064DG04	X258482	Upper Powell Andesite	Andesite	Not spotted	645355	5347769													
MERN18MDS0085EG11	X258436	Upper Powell Andesite	Andesite	Not spotted	645776	5348159	34.6	16	10	0.32	8	5.14	2.67	0.75	17.9	4.99	2.5	4	
MERN17MDS0031AG07ii	X261051	Upper Powell Andesite	Andesite	Spotted	645240	5347733													
MERN18MDS0084CG01	X258432	Upper Powell Andesite	Andesite	Spotted	645667	5348114	19.7	23	20	0.19	364	3.86	2.57	0.44	17.7	3.61	2.5	3.2	
MERN18MDS0112AG01	X258494	Upper Powell Andesite	Andesite	Not spotted	645748	5347867	8.4	31	150	0.09	288	3.03	1.89	1.07	18.2	2.68	2.5	1.5	0.0025
MERN18MDS0113AG01	X258478	Upper Powell Andesite	Andesite	Least alterec	645805	5347679	29.2	23	5	0.22	12	4.67	2.97	1.22	19.5	4.56	2.5	3.5	0.0025
MERN17MDS0030AG02	X258481	Upper Powell Andesite	Andesite		645036	5347711													
MERN18MDS0118AG02	X258491	Upper Powell Andesite	Andesite	Not spotted	645590	5347983	33.1	23	10	0.07	108	4.92	3.19	1.35	18.9	4.91	2.5	3.9	0.0025
MERN18MDS0114AG01	X258493	Upper Powell Andesite	Andesite	Spotted	645819	5347735													
MERN18MDS0118AG01	X258466	Upper Powell Andesite	Andesite	Spotted	645590	5347983													
MERN17MDS0031AG07i	X258485	Upper Powell Andesite	Andesite		645240	5347733													
MERN19MDS0153BG03	X261149	Upper Powell Andesite			646297	5348043	28.6	15	10	0.17	6	4.1	2.45	0.65	17.4	3.94	<5	3.4	<0.005

Number	Lab ID	Formation	Rock Type	Alteration	UTM-East	UTM-North	Ho_ppm	In_ppm	La_ppm	Li_ppm	Lu_ppm	Mo_ppm	Nb_ppm	Nd_ppm	Ni_ppm	Pb_ppm	Rb_ppm	Re_ppm	Sb_ppm	Sc_ppm
							ME-MS81	ME-MS42	ME-MS81	ME-4ACD81	ME-MS81	ME-4ACD81	ME-MS81	ME-MS81	ME-4ACD81	ME-4ACD81	ME-MS81	ME-MS42	ME-MS42	ME-4ACD81
							0.01	0.005	0.1	10	0.01	1	0.2	0.1	1	2	0.2	0.001	0.05	1
MERN18MDS0085CG07	X258435	Upper Marker Unit	Mafic tuff	Spotted	645724	5348195	0.3		2.3	20	0.15	0.5	1.5	2.9	16	1	29.1			27
MERN18MDS0085CG12ii	X258487	Upper Marker Unit	Mafic tuff	Chlorite	645737	5348188														
MERN18MDS0085CG12i	X258488	Upper Marker Unit	Mafic tuff		645737	5348188														
MERN18MDS0115BG03	X258459	Upper Marker Unit	Felsic tuff		645851	5347849	0.63	0.022	5.9	20	0.34	1	4.7	9.2	23	1	33.6	0.003	0.08	25
MERN18MDS0114AG02	X258475	Upper Powell Andesite	Andesite	Spotted	645819	5347735	0.89	0.128	13.3	40	0.44	0.5	6.3	16.2	13	1	19.1	<0.001	0.07	20
MERN18MDS0108AG01	X258470	Upper Powell Andesite	Andesite		645622	5347834	1.49	0.067	16.9	20	0.66	0.5	8.5	22.7	10	1	7.8	0.001	0.05	17
MERN18MDS0109AG01	X258474	Upper Powell Andesite	Andesite		645563	5347825	1.45	0.021	16.4	10	0.7	0.5	10.2	22.2	1	4	12.9	0.0005	0.05	18
MERN17MDS0064DG04	X258482	Upper Powell Andesite	Andesite	Not spotted	645355	5347769														
MERN18MDS0085EG11	X258436	Upper Powell Andesite	Andesite	Not spotted	645776	5348159	0.91		14.9	20	0.46	1	7.2	19.4	17	1	26.8			23
MERN17MDS0031AG07ii	X261051	Upper Powell Andesite	Andesite	Spotted	645240	5347733														
MERN18MDS0084CG01	X258432	Upper Powell Andesite	Andesite	Spotted	645667	5348114	0.82		7.7	30	0.33	2	5.2	11.8	12	3	7.3			15
MERN18MDS0112AG01	X258494	Upper Powell Andesite	Andesite	Not spotted	645748	5347867	0.67	0.147	3.9	20	0.3	0.5	3.7	5.8	27	1	1.2	0.001	0.05	36
MERN18MDS0113AG01	X258478	Upper Powell Andesite	Andesite	Least altered	645805	5347679	1	0.06	14.2	30	0.44	0.5	6.1	16.3	13	1	1.9	0.001	0.025	21
MERN17MDS0030AG02	X258481	Upper Powell Andesite	Andesite		645036	5347711														
MERN18MDS0118AG02	X258491	Upper Powell Andesite	Andesite	Not spotted	645590	5347983	1.07	0.032	15.2	20	0.5	1	7.9	19.7	21	1	0.5	0.001	0.025	23
MERN18MDS0114AG01	X258493	Upper Powell Andesite	Andesite	Spotted	645819	5347735														
MERN18MDS0118AG01	X258466	Upper Powell Andesite	Andesite	Spotted	645590	5347983														
MERN17MDS0031AG07i	X258485	Upper Powell Andesite	Andesite		645240	5347733														
MERN19MDS0153BG03	X261149	Upper Powell Andesite			646297	5348043	0.83	0.059	12.6	20	0.34	1	5.6	15.7	10	<2	4.5	0.001	<0.05	19

Number	Lab ID	Formation	Rock Type	Alteration	UTM-East	UTM-North	Se_ppm	Sm_ppm	Sn_ppm	Sr_ppm	Ta_ppm	Tb_ppm	Te_ppm	Th_ppm	Tl_ppm	Tm_ppm	U_ppm	V_ppm	W_ppm	Y_ppm
							ME-MS42	ME-MS81	ME-MS81	ME-MS81	ME-MS81	ME-MS81	ME-MS42	ME-MS81	ME-MS42	ME-MS81	ME-MS81	ME-MS81	ME-MS81	ME-MS81
							0.2	0.03	1	0.1	0.1	0.01	0.01	0.05	0.02	0.01	0.05	5	1	0.1
MERN18MDS0085CG07	X258435	Upper Marker Unit	Mafic tuff	Spotted	645724	5348195		0.78	8	6.1	0.1	0.2		0.28			0.1	267	2	7.6
MERN18MDS0085CG12ii	X258487	Upper Marker Unit	Mafic tuff	Chlorite	645737	5348188														10.4
MERN18MDS0085CG12i	X258488	Upper Marker Unit	Mafic tuff		645737	5348188														11.1
MERN18MDS0115BG03	X258459	Upper Marker Unit	Felsic tuff		645851	5347849	0.1	2.26	4	26.4	0.3	0.44	0.04	1.1	0.01	0.26	0.33	209	1	15.1
MERN18MDS0114AG02	X258475	Upper Powell Andesite	Andesite	Spotted	645819	5347735	0.1	3.98	10	8.9	0.4	0.7	0.53	1.67	0.01	0.42	0.51	232	4	23
MERN18MDS0108AG01	X258470	Upper Powell Andesite	Andesite		645622	5347834	0.1	5.85	3	20.1	0.5	1.13	0.13	2.11	0.01	0.65	0.58	38	1	37.2
MERN18MDS0109AG01	X258474	Upper Powell Andesite	Andesite		645563	5347825	0.1	5.68	3	28.3	0.6	1.1	0.01	2.55	0.01	0.68	0.7	8	0.5	37.3
MERN17MDS0064DG04	X258482	Upper Powell Andesite	Andesite	Not spotted	645355	5347769														28.5
MERN18MDS0085EG11	X258436	Upper Powell Andesite	Andesite	Not spotted	645776	5348159		4.45	3	6.1	0.6	0.79		1.71			0.46	133	2	23.7
MERN17MDS0031AG07ii	X261051	Upper Powell Andesite	Andesite	Spotted	645240	5347733														23.7
MERN18MDS0084CG01	X258432	Upper Powell Andesite	Andesite	Spotted	645667	5348114		2.98	1	7.4	0.4	0.56		1.35			0.39	171	3	21.3
MERN18MDS0112AG01	X258494	Upper Powell Andesite	Andesite	Not spotted	645748	5347867	0.4	1.95	12	108.5	0.2	0.53	0.01	0.55	0.01	0.3	0.16	376	1	16.1
MERN18MDS0113AG01	X258478	Upper Powell Andesite	Andesite	Least altered	645805	5347679	0.1	3.92	2	39.6	0.4	0.8	0.01	1.8	0.01	0.45	0.43	272	1	26.8
MERN17MDS0030AG02	X258481	Upper Powell Andesite	Andesite		645036	5347711														43.7
MERN18MDS0118AG02	X258491	Upper Powell Andesite	Andesite	Not spotted	645590	5347983	0.3	4.83	1	53.4	0.5	0.85	0.09	1.78	0.01	0.48	0.43	181	1	27.7
MERN18MDS0114AG01	X258493	Upper Powell Andesite	Andesite	Spotted	645819	5347735														31.9
MERN18MDS0118AG01	X258466	Upper Powell Andesite	Andesite	Spotted	645590	5347983														31.9
MERN17MDS0031AG07i	X258485	Upper Powell Andesite	Andesite		645240	5347733														23.8
MERN19MDS0153BG03	X261149	Upper Powell Andesite			646297	5348043	<0.2	4.21	3	28	0.5	0.66	<0.01	1.73	<0.02	0.33	0.44	226	1	22

Number	Lab ID	Formation	Rock Type	Alteration	UTM-East	UTM-North	Yb_ppm	Zn_ppm	Zr_ppm
							ME-MS81	ME4ACD81	ME-MS81
							0.03	2	2
MERN18MDS0085CG07	X258435	Upper Marker Unit	Mafic tuff	Spotted	645724	5348195	0.9	223	22
MERN18MDS0085CG12ii	X258487	Upper Marker Unit	Mafic tuff	Chlorite	645737	5348188			26
MERN18MDS0085CG12i	X258488	Upper Marker Unit	Mafic tuff		645737	5348188			26
MERN18MDS0115BG03	X258459	Upper Marker Unit	Felsic tuff		645851	5347849	1.77	201	87
MERN18MDS0114AG02	X258475	Upper Powell Andesite	Andesite	Spotted	645819	5347735	2.68	268	154
MERN18MDS0108AG01	X258470	Upper Powell Andesite	Andesite		645622	5347834	4.28	196	219
MERN18MDS0109AG01	X258474	Upper Powell Andesite	Andesite		645563	5347825	4.51	191	247
MERN17MDS0064DG04	X258482	Upper Powell Andesite	Andesite	Not spotted	645355	5347769			149
MERN18MDS0085EG11	X258436	Upper Powell Andesite	Andesite	Not spotted	645776	5348159	2.71	152	146
MERN17MDS0031AG07ii	X261051	Upper Powell Andesite	Andesite	Spotted	645240	5347733			145
MERN18MDS0084CG01	X258432	Upper Powell Andesite	Andesite	Spotted	645667	5348114	2.14	263	117
MERN18MDS0112AG01	X258494	Upper Powell Andesite	Andesite	Not spotted	645748	5347867	1.97	401	55
MERN18MDS0113AG01	X258478	Upper Powell Andesite	Andesite	Least altered	645805	5347679	2.96	187	158
MERN17MDS0030AG02	X258481	Upper Powell Andesite	Andesite		645036	5347711			197
MERN18MDS0118AG02	X258491	Upper Powell Andesite	Andesite	Not spotted	645590	5347983	3.21	174	171
MERN18MDS0114AG01	X258493	Upper Powell Andesite	Andesite	Spotted	645819	5347735			151
MERN18MDS0118AG01	X258466	Upper Powell Andesite	Andesite	Spotted	645590	5347983			159
MERN17MDS0031AG07i	X258485	Upper Powell Andesite	Andesite		645240	5347733			139
MERN19MDS0153BG03	X261149	Upper Powell Andesite			646297	5348043	2.03	366	139

A 4-2: Regional whole-rock lithogeochemistry comparison

Sample	Source	Formation	UTM-East	UTM-North	SiO2 %	TiO2%	Al2O3%	Fe2O3%	MnO%	MgO%	CaO%	Na2O%	K2O%	P2O5%	LOI%	Total	S%	CO2%	Au ppb	Ag ppm	Cu ppm	Zn ppm	Pb ppm	Mn ppm
					FUS-ICP	FUS-ICP	FUS-ICP	FUS-ICP	FUS-ICP	FUS-ICP	FUS-ICP	FUS-ICP	FUS-ICP	FUS-ICP	FUS-ICP				FA-AA					
MERN19TRJ0328AG01	Joergensen 2019	Horne rhyolite	646479	5346280	70.4	0.37	13.15	7.25	0.33	0.77	0.18	0.23	2.86	0.07	3.48	99.13	2.27	<0.01		<0.5	99	3030	13	
HWWR035	Laurin 2009	Horne rhyolite			74.51	0.292	12.03	3.97	0.075	0.59	1.94	4.56	0.7	0.06	2.26	101	0.65	0.86	9	<0.5	33.4	46.3	7	501
HWWR036	Laurin 2009	Horne rhyolite			74.06	0.281	11.72	2.84	0.058	0.35	1.87	4.5	0.9	0.05	2.14	98.76	0.46	0.94	<5	<0.5	33.5	51.5	7	401
HWWR039	Laurin 2009	Horne rhyolite			73.11	0.287	12.04	3.65	0.085	0.69	3.07	4.3	0.85	0.06	2.6	100.7	0.09	1.61	7	<0.5	111	48.1	8	584
HWWR040	Laurin 2009	Horne rhyolite			72.46	0.307	12.52	3.4	0.084	0.57	3.47	3.91	1.2	0.06	2.66	100.6	0.15	1.67	<5	<0.5	90.7	35.3	5	539
HWWR044	Laurin 2009	Horne rhyolite			72.7	0.303	12.5	2.74	0.201	0.73	3.04	4.7	0.78	0.05	2.74	100.5	0.56	1.44	8	<0.5	19.8	32.5	5	1310
HWWR068	Laurin 2009	Horne rhyolite			59.51	0.648	14.36	8.13	1.69	1.48	4.25	1.34	2.52	0.12	5.17	99.23	2.24	2.06	265	2.2	94.4	154	13	>10000
HWWR067	Laurin 2009	Horne rhyolite			65.33	0.488	13.56	5.88	0.55	1.44	6	1.48	1.57	0.09	9.56	99.94	0.2	1.67	<5	<0.5	65.8	140	18	3690
HWWR093	Laurin 2009	Horne rhyolite			66.638	0.469	13.13	5.51	0.041	0.21	0.2	0.41	3.56	0.14	4.04	94.4	3.48	<0.01	214	<0.5	70.9	3750	34	256
HWWR061	Laurin 2009	Horne rhyolite			66.8	0.456	14.07	5.89	0.351	1.03	3.17	1.66	1.87	0.07	3.55	98.93	2.15	0.35	60	<0.5	94.8	150	13	2320
HWWR112	Laurin 2009	Horne rhyolite			64.46	0.342	11.61	13.49	0.032	0.34	0.14	0.22	3.01	0.08	6.92	100.6	8.9	<0.01	1030	<0.5	355	103	25	234
HWWR111	Laurin 2009	Horne rhyolite			68.42	0.378	12.93	8.78	0.043	0.37	0.16	0.19	3.1	0.07	4.75	99.19	4.71	<0.01	>3000	<0.5	137	93.8	7	291
MERN19MDS0177BG02	Schofield 2019	Joliet rhyolite	646424	5347442	77.80	0.24	12.00	3.90	0.05	1.67	0.15	4.15	0.68	0.04	1.27	101.97	<0.01	0.01		0.25	6	30	2	
MERN19MDS0178CG03	Schofield 2019	Joliet rhyolite	646611	5347387	75.20	0.23	11.90	3.04	0.03	1.31	0.22	4.28	0.79	0.05	1.12	98.19	<0.01	0.02		0.25	2	25	<2	
MERN17TRJ0239AG01	Joergensen 2019	Joliet rhyolite	646189	5346698	75.8	0.1	11.2	3	0.04	0.36	1.91	5.27	0.71	0.01	1.95	100.38	0.18	0.4		<0.5	9	12	3	
MERN18TRJ0240AG01	Joergensen 2019	Joliet rhyolite	646169	5346968	70	0.65	13.9	4.25	0.11	1.33	1.76	6.4	0.07	0.14	1.68	100.3	0.02	0.22		<0.5	37	405	<2	
MERN17MDS0044AG02	Schofield 2017	Brownlee rhyolite	644493	5347553	68.60	0.47	11.65	10.45	0.06	2.97	0.13	0.08	1.44	0.10	3.08	99.09	0.01	0.01		0.25	15	41	3	
MERN17MDS0045AG02	Schofield 2017	Brownlee rhyolite	644405	5347521	65.90	0.80	13.30	9.34	0.08	4.58	0.32	0.08	2.00	0.27	3.69	100.41	0.04	0.01		0.25	8	77	3	
8050	Lhereux	Brownlee rhyolite	643418	5347696	72.50	0.41	11.06	6.24	0.08	4.16	0.64	1.18	1.11	0.25		99.85	0.01	1.17			5	54		
8052	Lhereux	Brownlee rhyolite	643995	5347962	71.80	0.63	11.83	7.39	0.05	2.70	0.45	1.85	1.18	0.28		99.96	0.01	1.04			4	45		
8093	Lhereux	Brownlee rhyolite	644683	5347483	70.60	0.48	12.41	6.49	0.09	3.20	0.32	4.30	0.31	0.33		99.83	0.01	1.40			5	187		
115690	Lhereux	Brownlee rhyolite			75.80	0.43	10.41	5.47	0.02	2.40	0.29	1.26	1.80	0.29		99.82	0.01	1.56			2	26		
115691	Lhereux	Brownlee rhyolite			72.80	0.51	12.13	4.93	0.04	2.67	0.58	3.88	0.67	0.32		99.91	0.01	1.61			2	33		
MERN18MDS0085BG01	Schofield 2018	Powell Rhyolite	645738	5348189	76.40	0.27	9.56	6.21	0.07	1.52	0.07	0.32	1.74	0.04	2.07	98.34	0.03	0.02		0.25	476	68	3	
MERN18MDS0085BG02	Schofield 2018	Powell Rhyolite	645723	5348170	79.70	0.25	9.53	5.34	0.06	1.03	0.07	0.14	1.99	0.04	1.81	100.04	0.02	0.02		0.25	123	43	1	
MERN18MDS0110AG01	Schofield 2018	Powell Rhyolite	645673	5347845	77.10	0.28	13.65	4.94	0.05	2.69	0.05	0.74	1.73	0.04	2.56	101.63	0.005	0.02		0.25	3	136	1	
MERN19MDS0126AG01 (qtz-f	Schofield 2019	Powell Rhyolite	646496	5348024	71.60	0.36	13.20	4.22	0.07	2.50	0.55	4.35	0.89	0.07	2.00	99.83	0.02	0.1		0.25	50	74	<2	
8068	Lhereux	Powell Rhyolite	645680	5348170	79.90	0.36	9.29	5.94	0.06	1.05	0.16	0.20	1.82	0.23		100.48	0.01	1.04			60	39		
8332	Lhereux	Powell Rhyolite	645599	5348141	77.80	0.36	8.79	5.53	0.08	2.44	0.22	1.93	1.09	0.24		99.89	0.01	0.07			50	65		
8081	Lhereux	Lower Marker Unit	644794	5348139	66.90	0.78	11.74	11.84	0.13	3.90	0.25	0.24	1.53	0.28		99.84	0.01	1.24			25	174		
8084	Lhereux	Lower Marker Unit	644606	5348173	67.10	0.74	11.42	12.74	0.10	3.62	0.21	0.23	1.36	0.25		99.83	0.01	0.97			16	116		
MERN18MDS0076CG01	Schofield 2018	Lower Marker Unit	645222	5347709	80.90	0.24	9.87	4.81	0.03	1.91	0.05	0.18	1.70	0.01	2.15	101.93	0.01	0.01		0.25	31	98	4	
MERN18MDS0077AG03	Schofield 2018	Lower Marker Unit	645259	5347730	81.90	0.21	9.07	2.63	0.08	1.87	0.71	2.26	0.91	0.04	2.12	101.83	0.01	0.29		0.25	10	72	2	
MERN18MDS0097AG01	Schofield 2018	Lower Marker Unit	644838	5347661	62.40	0.86	14.55	9.92	0.12	5.23	0.15	0.97	1.54	0.10	3.95	99.87	0.01	0.01		0.25	4	215	2	
MERN18MDS0117AG01	Schofield 2018	Lower Marker Unit	645269	5348088	73.50	0.48	13.65	5.33	0.11	2.90	0.17	3.24	0.88	0.08	2.17	100.83	0.06	0.005		0.25	31	189	1	
MERN18MDS0103EG05	Schofield 2018	Here Creek rhyolite	645415	5347965	75.80	0.22	11.40	5.50	0.03	3.16	0.10	0.18	1.87	0.04	2.83	101.21	0.005	<0.01		0.25	10	140	1	
MERN18MDS0120AG01	Schofield 2018	Héré Creek rhyolite	645686	5348384	75.30	0.35	13.65	4.06	0.09	4.17	0.10	0.14	2.06	0.07	3.19	101.35	0.005	0.005		0.25	37	188	1	
MERN19MDS0151AG02	Schofield 2019	Héré Creek rhyolite	646382	5348652	68.50	0.37	12.00	7.97	0.07	1.19	1.68	4.53	0.49	0.07	2.28	99.17	<0.01	0.35		0.25	2	42	<2	
MERN18TRJ0248AG01	Joergensen 2019	Here Creek rhyolite	645505	5350251	76	0.36	11.85	4.53	0.06	0.99	1.16	3.71	1.11	0.07	1.96	101.83	<0.01	0.23		<0.5	3	74	<2	
MERN18TRJ0269AG01	Joergensen 2019	Northwest rhyolite	638583	5358516	71.4	0.67	13.3	6.24	0.25	1.52	0.95	5.61	0.04	0.21	1.35	101.54	<0.01	0.02		<0.5	1	49	<2	
NOR-55	Lesher et al 1986	Northwest rhyolite			70.10	0.45	12.40	8.72	0.20	4.76	0.42	1.51	1.40	0.07		100.03								
MERN18TRJ0268AG01	Joergensen 2019	Rusty Ridge Andesite	638789	5358154	55	1.57	14.45	11.9	0.18	4.46	4.5	4.56	0.24	0.21	2.44	99.54	0.01	0.03		<0.5	93	166	<2	
MERN18TRJ0267AG01	Joergensen 2019	Amulet rhyolite	639227	5357808	74.5	0.32	12	5.04	0.08	1.76	0.22	3.39	1.87	0.04	1.68	100.95	<0.01	0.03		<0.5	5	71	4	
MERN18TRJ0257AG01	Joergensen 2019	Amulet rhyolite	642383	5351526	64.3	1.06	13.1	13.8	0.28	2.57	0.47	0.07	1.71	0.32	3.39	101.11	<0.01	0.02		<0.5	106	240	<2	
915-4	Lesher et al 1986	Amulet rhyolite			71.7	0.58	13.2	6.82	0.1	3.48	0.26	1.99	1.73	0.14		100.00								
MERN18TRJ0265AG01	Joergensen 2019	Waite Andesite	640825	5356812	59.6	1.03	13.85	8.15	0.16	5.37	4.73	4.47	0.22	0.13	2.22	99.96	<0.01	0.02		<0.5	2	66	3	
915-1	Lesher et al 1986	Waite rhyolite			73.2	0.33	12.1	7.56	0.15	1.53	**0.56**	**3.31**	1.21	0.08		100.03								
MERN18TRJ0264AG01	Joergensen 2019	Waite rhyolite	641211	5357014	76.4	0.22	10.8	3.91	0.04	1.04	1.27	3.33	1.32	0.01	1.49	99.88	<0.01	0.11		<0.5	1	53	<2	
MERN18TRJ0263AG01	Joergensen 2019	Amulet Andesite	642268	5355599	48.9	0.95	17.05	11.1	0.19	9.25	3.22	4.12	0.98	0.12	4.03	99.98	0.02	0.03		<0.5	2	156	<2	

Sample	Source	Formation	UTM-East	UTM-North	As ppm	Sb ppm	Cd ppm	Bi ppm	Co ppm	Ni ppm	Cr ppm	V ppm	Mo ppm	Ga ppm	In ppm	Sn ppm	Tl ppm	W ppm	Hg ppm	Ba ppm	Rb ppm	Sr ppm	Th ppm
MERN19TRJ0328AG01	Joergensen 2019	Horne rhyolite	646479	5346280	7.9	0.34	6.4	0.09	6	2	<10	27	1	16.9	0.341	7	0.06	1	0.025	372	69.9	10.9	2.38
HWWR035	Laurin 2009	Horne rhyolite			<0.5	<0.2	<0.2	<0.1	2.8	<20	167	<5	3	16	<0.1	1	0.11	57	<5	140	19	48	2.52
HWWR036	Laurin 2009	Horne rhyolite			<0.5	<0.2	<0.2	0.2	4.8	<20	184	<5	5	16	<0.1	1	0.19	1.3	<5	158	27	42	2.77
HWWR039	Laurin 2009	Horne rhyolite			<0.5	<0.2	<0.2	0.3	3.1	<20	121	<5	2	16	<0.1	6	0.06	2.2	<5	159	21	55	2.76
HWWR040	Laurin 2009	Horne rhyolite			<0.5	<0.2	<0.2	0.3	3.3	<20	140	<5	3	17	0.2	1	0.2	0.6	<5	204	30	66	2.79
HWWR044	Laurin 2009	Horne rhyolite			0.5	<0.2	<0.2	0.5	2.9	<20	194	6	2	14	<0.1	2	0.53	0.8	<5	133	27	59	1.96
HWWR068	Laurin 2009	Horne rhyolite			5.9	0.3	<0.2	1.4	15	<20	69	81	4	20	0.1	2	0.32	1.5	9	258	67	63	1.87
HWWR067	Laurin 2009	Horne rhyolite			<0.5	0.9	<0.2	0.7	8.8	<20	118	78	4	19	<0.1	2	0.14	1.5	<5	173	48	91	2.1
HWWR093	Laurin 2009	Horne rhyolite			25.7	<0.2	12.2	0.2	5.3	<20	50	17	<2	16	<0.1	3	0.31	0.8	69	179	68	22	1.81
HWWR061	Laurin 2009	Horne rhyolite			2.1	<0.2	<0.2	0.2	7.8	<20	91	39	3	18	0.1	2	0.73	1	9	363	56	96	2.51
HWWR112	Laurin 2009	Horne rhyolite			25.1	<0.2	<0.2	0.1	6.2	<20	66	22	<2	16	0.3	2	0.52	1	12	383	66	12	2.06
HWWR111	Laurin 2009	Horne rhyolite			3	<0.2	<0.2	<0.1	6.9	<20	38	24	<2	18	0.3	5	0.29	1.1	17	598	62	14	2.14
MERN19MDS0177BG02	Schofield 2019	Joliet rhyolite	646424	5347442	0.1	<0.05	<0.5	0.02	2	<1	20	8	2	16.4	0.006	1	<0.02	1	<0.005	130	12.5	29.6	2.95
MERN19MDS0178CG03	Schofield 2019	Joliet rhyolite	646611	5347387	0.3	<0.05	<0.5	0.04	2	<1	30	8	2	15.9	0.005	1	<0.02	1	<0.005	147	14.8	24.9	3.15
MERN17TRJ0239AG01	Joergensen 2019	Joliet rhyolite	646189	5346698	0.4	0.07	<0.5	0.08	3	2	30	<5	3	24.2	0.005	3	<0.02	5	<0.005	136.5	26.3	95	7.45
MERN18TRJ0240AG01	Joergensen 2019	Joliet rhyolite	646169	5346968	0.6	<0.05	3.9	0.05	9	6	20	44	1	18.8	0.122	2	<0.02	1	0.026	44	1.2	72.7	3.4
MERN17MDS0044AG02	Schofield 2017	Brownlee rhyolite	644493	5347553	0.4	0.03	0.25	0.17	11	2	10	2.5	1	18.8	0.02	4	0.01	2	0	509	24.4	6.8	2.78
MERN17MDS0045AG02	Schofield 2017	Brownlee rhyolite	644405	5347521	0.1	0.03	0.25	0.17	12	3	10	23	2	19.9	0.02	3	0.01	2	0	459	36.8	10.4	2.23
8050	Lhereux	Brownlee rhyolite	643418	5347696					7.8	9	3.9									318	24	24	3.7
8052	Lhereux	Brownlee rhyolite	643995	5347962					4.3	5	4.7									170	12	43	3.1
8093	Lhereux	Brownlee rhyolite	644683	5347483					1.9	5	6.0									22	<5	51	2.6
115690	Lhereux	Brownlee rhyolite							3.9	5	2.4									458	31	36	3.3
115691	Lhereux	Brownlee rhyolite							5.8	4	4.0									111	12	30	3.5
MERN18MDS0085BG01	Schofield 2018	Powell Rhyolite	645738	5348189	1.2		0.25		9	2	10	22	3	16.7		5		2		620	33.2	6.8	3.34
MERN18MDS0085BG02	Schofield 2018	Powell Rhyolite	645723	5348170	2.4		0.25		10	2	20	12	2	16.4		3		1		679	32	4.5	3.18
MERN18MDS0110AG01	Schofield 2018	Powell Rhyolite	645673	5347845	0.05	0.025	0.25	0.01	5	2	5	14	1	15.3	0.021	3	0.01	1	0.0025	350	30.6	9.2	3.56
MERN19MDS0126AG01 (qtz-f	Schofield 2019	Powell Rhyolite	646496	5348024	0.7	<0.05	<0.5	0.08	5	8	20	48	1	17.8	0.025	1	0.02	1	<0.005	211	16	49.6	3.71
8068	Lhereux	Powell Rhyolite	645680	5348170					7.8	4	2.9									731	28	18	3.7
8332	Lhereux	Powell Rhyolite	645599	5348141																			
8081	Lhereux	Lower Marker Unit	644794	5348139					16.4	13	1.6									568	28	17	1.9
8084	Lhereux	Lower Marker Unit	644606	5348173					17.1	14	1.1									422	24	19	1.8
MERN18MDS0076CG01	Schofield 2018	Lower Marker Unit	645222	5347709	0.05	0.03	0.25		8	2	10	8	1	13	0.02	3	0.01	1	0	757	24.2	8.5	2.29
MERN18MDS0077AG03	Schofield 2018	Lower Marker Unit	645259	5347730	0.3		0.25		6	3	30	13	3	8.2		1		1		243	15.3	18.2	2.02
MERN18MDS0097AG01	Schofield 2018	Lower Marker Unit	644838	5347661	0.1	0.05	0.25	0.24	13	8	10	109	0.5	23.1	0.03	3	0.01	1	0	733	23.4	8.5	2.5
MERN18MDS0117AG01	Schofield 2018	Lower Marker Unit	645269	5348088	0.3	0.05	0.25	0.05	7	4	10	54	0.5	16.6	0.026	2	0.01	1	0.0025	194	19.6	21.4	2.21
MERN18MDS0103EG05	Schofield 2018	Here Creek rhyolite	645415	5347965	0.2	0.05	0.25	0.06	7	1	10	5	0.5	16.6	0.022	6	0.01	1	0.0025	762	30.3	7.2	4.04
MERN18MDS0120AG01	Schofield 2018	Héré Creek rhyolite	645686	5348384	2	0.025	0.25	0.02	1	1	5	7	0.5	16	0.014	1	0.01	0.5	0.0025	208	35.3	11.3	3.49
MERN19MDS0151AG02	Schofield 2019	Héré Creek rhyolite	646382	5348652	0.4	<0.05	<0.5	0.01	2	2	20	7	1	19	0.021	2	<0.02	1	<0.005	177.5	9.2	54.5	4.08
MERN18TRJ0248AG01	Joergensen 2019	Here Creek rhyolite	645505	5350251	0.2	<0.05	<0.5	0.02	5	1	30	7	2	15.3	0.009	1	<0.02	1	<0.005	271	17.4	58.4	3.74
MERN18TRJ0269AG01	Joergensen 2019	Northwest rhyolite	638583	5358516	0.1	<0.05	<0.5	0.02	4	1	20	6	1	17.7	0.114	6	<0.02	1	<0.005	46.5	0.6	23.4	2.24
NOR-55	Lesher et al 1986	Northwest rhyolite									94									240	24	8	3.2
MERN18TRJ0268AG01	Joergensen 2019	Rusty Ridge Andesite	638789	5358154	<0.1	<0.05	<0.5	0.02	27	10	10	326	1	19.6	0.018	1	<0.02	1	<0.005	143.5	2.4	148.5	1.11
MERN18TRJ0267AG01	Joergensen 2019	Amulet rhyolite	639227	5357808	0.1	<0.05	<0.5	0.03	2	<1	20	<5	2	21.8	0.029	3	<0.02	1	<0.005	417	31.5	26	3.06
MERN18TRJ0257AG01	Joergensen 2019	Amulet rhyolite	642383	5351526	0.1	<0.05	<0.5	0.01	11	1	10	37	1	22.1	0.051	5	<0.02	1	<0.005	316	27.3	5.4	1.72
915-4	Lesher et al 1986	Amulet rhyolite									6									550	30	16	2.7
MERN18TRJ0265AG01	Joergensen 2019	Waite Andesite	640825	5356812	<0.1	<0.05	<0.5	0.01	26	49	50	269	1	19.7	0.008	1	<0.02	1	<0.005	68.5	4.1	82.9	1.5
915-1	Lesher et al 1986	Waite rhyolite									<5									420	21	17	2.6
MERN18TRJ0264AG01	Joergensen 2019	Waite rhyolite	641211	5357014	0.3	<0.05	<0.5	0.02	2	2	30	<5	2	19.3	0.009	1	<0.02	1	<0.005	344	41.4	82	2.64
MERN18TRJ0263AG01	Joergensen 2019	Amulet Andesite	642268	5355599	<0.1	<0.05	<0.5	0.02	31	55	150	242	1	20.4	0.008	2	<0.02	1	<0.005	374	19.4	69.9	0.89
MERN18TRJ0260AG01	Joergensen 2019	Amulet Andesite	642306	5353553	0.2	<0.05	<0.5	0.03	15	44	40	230	1	23.1	0.013	2	0.05	1	<0.005	420	38.9	200	1.7

Sample	Source	Formation	UTM-East	UTM-North	U ppm	Sc ppm	B ppm	Be ppm	Cs ppm	Li ppm	Ta ppm	Hf ppm	Nb ppm	Zr ppm	Y ppm	Ge ppm	La ppm	Ce ppm	Pr ppm	Nd ppm	Sm ppm	Eu ppm	Gd ppm
MERN19TRJ0328AG01	Joergensen 2019	Horne rhyolite	646479	5346280	0.66	11			0.84	10	0.6	4.6	9.7	183	23.1	<5	4.3	9.9	1.33	6.4	1.54	0.79	2.07
HWWR035	Laurin 2009	Horne rhyolite			0.68	9	14	1	1	8	0.67	4.6	11.1	170	27.2	0.8	14.1	28	3.52	15	3.56	0.822	3.79
HWWR036	Laurin 2009	Horne rhyolite			0.88	9	5	<1	1.2	5	0.74	5.2	11.5	224	30.1	0.9	14.3	31.3	3.93	16.7	3.99	0.849	3.86
HWWR039	Laurin 2009	Horne rhyolite			0.7	10	11	<1	1.3	8	0.7	5.1	11.9	220	34.5	1.2	15.3	33	4.22	17.9	4.24	0.95	4.42
HWWR040	Laurin 2009	Horne rhyolite			0.69	11	16	<1	1.6	7	0.71	5.5	12.1	229	32.6	1.2	15.1	33.4	4.25	18	4.47	0.951	4.46
HWWR044	Laurin 2009	Horne rhyolite			0.6	10	<1	1	1	5	0.69	4.5	11.9	161	27.9	1.1	12.4	24.4	3.05	17.9	3.49	0.875	3.39
HWWR068	Laurin 2009	Horne rhyolite			0.48	17	19	1	2	13	0.52	3.8	10	173	23.4	1.8	8.95	21.7	2.91	12.2	3.18	1.64	3.26
HWWR067	Laurin 2009	Horne rhyolite			0.57	14	12	1	1.8	13	0.52	4.1	8.9	178	24.3	2.3	10.7	24.4	3.23	13.6	3.33	1.09	3.53
HWWR093	Laurin 2009	Horne rhyolite			0.72	13	29	<1	1	3	0.5	3.9	8	152	24	0.7	11.7	25.7	3.03	13.4	3.38	2.52	3.52
HWWR061	Laurin 2009	Horne rhyolite			0.66	13	10	1	1.7	12	0.75	4.5	10.6	168	25.5	1.4	12.6	29	3.35	15.6	3.65	0.843	3.74
HWWR112	Laurin 2009	Horne rhyolite			0.74	9	13	<1	1.1	5	0.53	4.4	10.3	179	25.8	1.4	10.6	24.2	3.14	12.8	3.17	1.19	3.18
HWWR111	Laurin 2009	Horne rhyolite			0.61	10	19	<1	1.2	6	0.59	4.5	10.1	190	29.5	1.7	13.8	29.7	3.61	15.3	3.71	0.821	3.6
MERN19MDS0177BG02	Schofield 2019	Joliet rhyolite	646424	5347442	0.83	7			0.24	10	0.7	5.4	8.2	210	41.6	<5	16.7	36.2	4.54	19.5	4.94	0.8	5.67
MERN19MDS0178CG03	Schofield 2019	Joliet rhyolite	646611	5347387	0.92	8			0.27	10	0.7	6.1	8.1	218	43.9	<5	16.7	37.4	4.71	20.7	5.15	0.72	5.99
MERN17TRJ0239AG01	Joergensen 2019	Joliet rhyolite	646189	5346698	1.93	2			0.61	10	2.3	11.5	31.9	336	113	<5	55.1	132	17.85	71	17.6	1.72	20.1
MERN18TRJ0240AG01	Joergensen 2019	Joliet rhyolite	646169	5346968	0.91	14			0.09	10	0.7	5.3	10	204	38.9	<5	20.8	47.8	6.35	24.2	5.86	1.39	5.93
MERN17MDS0044AG02	Schofield 2017	Brownlee rhyolite	644493	5347553	0.83	16			0.31	20	0.7	7.1	11.8	260	55	2.5	17.4	42.3	5.770	24.2	5.96	1.22	8.21
MERN17MDS0045AG02	Schofield 2017	Brownlee rhyolite	644405	5347521	0.65	15			0.54	30	0.6	5.3	10	217	43.7	2.5	19.7	47.5	6.690	28.7	6.96	1	8.13
8050	Lhereux	Brownlee rhyolite	643418	5347696	0.9	11.1			0.39		0.9	6.3	22	230	36		15.5	31.8		17.1	4.63	0.97	
8052	Lhereux	Brownlee rhyolite	643995	5347962	0.7	17.4			0.27		0.8	7.1	16	259	51		20.0	49.3		22.3	6.94	1.54	
8093	Lhereux	Brownlee rhyolite	644683	5347483	0.7	16.1			0.30		1.0	6.1	23	212	60		21.4	56.8		26.8	8.15	1.74	
115690	Lhereux	Brownlee rhyolite			0.9	9.6			0.39		1.0	5.9	20	237	40		15.1	38.0		18.8	4.35	0.38	
115691	Lhereux	Brownlee rhyolite			0.9	10.7			0.25		0.6	6.8	21	251	43		16.0	37.3		15.6	4.84	0.92	
MERN18MDS0085BG01	Schofield 2018	Powell Rhyolite	645738	5348189	0.89	9			0.28	10	0.8	7.9	10.7	275	43.2	2.5	11.9	26.8	3.650	14.6	3.76	0.4	5.54
MERN18MDS0085BG02	Schofield 2018	Powell Rhyolite	645723	5348170	0.88	8			0.27	10	0.8	7.4	9.9	256	44.7	2.5	14.1	34.2	4.650	18.7	5.08	0.35	6.68
MERN18MDS0110AG01	Schofield 2018	Powell Rhyolite	645673	5347845	0.94	9			0.35	10	0.7	6.9	11.3	287	45.7	2.5	19.6	42.5	5.71	23.6	5.88	0.77	6.57
MERN19MDS0126AG01 (qtz-f	Schofield 2019	Powell Rhyolite	646496	5348024	1.03	11			0.26	10	0.8	7.2	11.3	278	49.5	<5	24.1	54.9	6.88	29.8	7.1	1.17	7.07
8068	Lhereux	Powell Rhyolite	645680	5348170	0.9	7.9			0.18		0.8	6.5	12	231	47		13.7	34.5		18.1	4.85	0.51	
8332	Lhereux	Powell Rhyolite	645599	5348141																			
8081	Lhereux	Lower Marker Unit	644794	5348139	0.5	16.0			0.40		0.6	4.1	13	172	38		11.8	29.3		17.0	4.46	0.60	
8084	Lhereux	Lower Marker Unit	644606	5348173	0.4	15.5			0.29		0.6	3.8	12	163	35		13.5	33.9		16.5	4.81	0.77	
MERN18MDS0076CG01	Schofield 2018	Lower Marker Unit	645222	5347709	0.6	10			0.3	10	0.5	5.2	8.1	193	33.6	2.5	12.6	30.8	3.970	16.9	4.64	0.46	4.7
MERN18MDS0077AG03	Schofield 2018	Lower Marker Unit	645259	5347730	0.64	8			0.2	10	0.6	5.4	7.6	190	28.8	2.5	12.1	28.3	3.660	15.9	3.75	0.56	4.67
MERN18MDS0097AG01	Schofield 2018	Lower Marker Unit	644838	5347661	0.64	19			0.29	20	0.5	5.4	9.4	202	46	2.5	12.9	35.6	5.190	23.2	6.19	1.03	6.5
MERN18MDS0117AG01	Schofield 2018	Lower Marker Unit	645269	5348088	0.57	15			0.31	10	0.5	5.1	8.8	220	37.9	2.5	17	35	4.87	21.2	5.34	0.96	5.73
MERN18MDS0103EG05	Schofield 2018	Here Creek rhyolite	645415	5347965	1.04	9			0.33	20	0.8	7.3	12.6	318	48.3	2.5	25.5	54.6	7.23	29.7	6.98	0.75	7.45
MERN18MDS0120AG01	Schofield 2018	Héré Creek rhyolite	645686	5348384	0.92	10			0.31	20	0.7	6.4	11.5	286	35.9	2.5	20.3	42.4	5.72	23.2	5.58	1.03	5.59
MERN19MDS0151AG02	Schofield 2019	Héré Creek rhyolite	646382	5348652	1.17	12			0.28	20	0.7	7.1	9.4	278	49.4	<5	27.5	64.2	8.12	32.6	7.73	1.34	7.76
MERN18TRJ0248AG01	Joergensen 2019	Here Creek rhyolite	645505	5350251	0.93	9			0.19	10	0.8	6.6	12.2	271	38.9	<5	18.2	41	5.46	20.5	5.17	0.94	5.85
MERN18TRJ0269AG01	Joergensen 2019	Northwest rhyolite	638583	5358516	0.64	18			0.04	10	0.7	6.4	10.1	238	51.8	<5	19.6	44.8	6.39	29.2	7.45	1.46	8.67
NOR-55	Lesher et al 1986	Northwest rhyolite			0.63	11.1						8.5		372	97		26.1	71		38	11.1	1.76	
MERN18TRJ0268AG01	Joergensen 2019	Rusty Ridge Andesite	638789	5358154	0.29	31			0.11	10	0.4	3.2	6.5	129	30.3	<5	9.5	24.8	3.57	14.9	4.36	1.36	5.35
MERN18TRJ0267AG01	Joergensen 2019	Amulet rhyolite	639227	5357808	0.85	14			0.17	10	1.1	9.2	16.5	364	73.6	<5	26.8	66.3	9.62	38	10.4	2.23	12.25
MERN18TRJ0257AG01	Joergensen 2019	Amulet rhyolite	642383	5351526	0.44	19			0.41	10	0.7	4.9	9.6	193	38.7	<5	19.4	42.5	7.17	28.1	7.19	1.38	7.1
915-4	Lesher et al 1986	Amulet rhyolite			0.9	17					0.8	6.8		275	44		18.9	44		28	6.54	1.09	
MERN18TRJ0265AG01	Joergensen 2019	Waite Andesite	640825	5356812	0.38	24			0.34	10	0.4	2.9	5.2	114	19	<5	11.9	25.5	3.37	13.7	3.45	1.08	3.64
915-1	Lesher et al 1986	Waite rhyolite			0.8	15					0.7	7		285	52		14.7	37		22	6.44	1.7	
MERN18TRJ0264AG01	Joergensen 2019	Waite rhyolite	641211	5357014	0.68	11			0.47	10	0.9	7.3	12.9	285	51.9	<5	20.8	51.2	7.23	28.3	7.22	1.37	7.7
MERN18TRJ0263AG01	Joergensen 2019	Amulet Andesite	642268	5355599	0.21	25			0.45	40	0.3	2.1	4.1	83	14.8	<5	8	19.2	2.69	11.1	2.61	0.64	3
MERN18TRJ0260AG01	Joergensen 2019	Amulet Andesite	642306	5353553	0.47	23			0.24	10	0.6	4.3	7.4	179	27	<5	14.5	34.5	4.81	18.7	4.75	1.44	5.19

Sample	Source	Formation	UTM-East	UTM-North	Tb ppm	Dy ppm	Ho ppm	Er ppm	Tm ppm	Yb ppm	Lu ppm
MERN19TRJ0328AG01	Joergensen 2019	Horne rhyolite	646479	5346280	0.42	3.8	0.86	2.86	0.47	3.71	0.48
HWWR035	Laurin 2009	Horne rhyolite			0.69	4.54	0.98	3.02	0.476	3.21	0.549
HWWR036	Laurin 2009	Horne rhyolite			0.77	5.01	1.04	3.22	0.513	3.55	0.575
HWWR039	Laurin 2009	Horne rhyolite			0.86	5.52	1.12	3.42	0.527	3.6	0.593
HWWR040	Laurin 2009	Horne rhyolite			0.89	5.58	1.14	3.41	0.535	3.66	0.592
HWWR044	Laurin 2009	Horne rhyolite			0.69	3.99	0.9	2.91	0.526	3.27	0.524
HWWR068	Laurin 2009	Horne rhyolite			0.63	4.06	0.84	2.63	0.432	2.95	0.45
HWWR067	Laurin 2009	Horne rhyolite			0.65	4.08	0.84	2.56	0.408	2.79	0.446
HWWR093	Laurin 2009	Horne rhyolite			0.64	4.08	0.85	2.65	0.414	2.72	0.433
HWWR061	Laurin 2009	Horne rhyolite			0.71	3.82	0.89	2.79	0.536	2.98	0.489
HWWR112	Laurin 2009	Horne rhyolite			0.65	4.23	0.86	2.64	0.419	2.84	0.456
HWWR111	Laurin 2009	Horne rhyolite			0.7	4.5	0.95	3	0.474	3.17	0.475
MERN19MDS0177BG02	Schofield 2019	Joliet rhyolite	646424	5347442	0.94	6.43	1.44	4.42	0.73	4.43	0.76
MERN19MDS0178CG03	Schofield 2019	Joliet rhyolite	646611	5347387	1.03	7.05	1.6	4.88	0.75	5.14	0.79
MERN17TRJ0239AG01	Joergensen 2019	Joliet rhyolite	646189	5346698	3.32	21	4.4	12.45	1.98	12.85	1.95
MERN18TRJ0240AG01	Joergensen 2019	Joliet rhyolite	646169	5346968	1.02	6.84	1.42	4.05	0.65	4.51	0.7
MERN17MDS0044AG02	Schofield 2017	Brownlee rhyolite	644493	5347553	1.55	9.79	2.18	6.15	0.93	6.31	0.9
MERN17MDS0045AG02	Schofield 2017	Brownlee rhyolite	644405	5347521	1.32	7.91	1.73	4.69	0.72	4.81	0.69
8050	Lhereux	Brownlee rhyolite	643418	5347696						3.96	0.71
8052	Lhereux	Brownlee rhyolite	643995	5347962						5.63	0.95
8093	Lhereux	Brownlee rhyolite	644683	5347483						6.04	1.02
115690	Lhereux	Brownlee rhyolite								4.32	0.74
115691	Lhereux	Brownlee rhyolite								4.72	0.84
MERN18MDS0085BG01	Schofield 2018	Powell Rhyolite	645738	5348189	1.15	7.5	1.66	5.25		5.05	0.8
MERN18MDS0085BG02	Schofield 2018	Powell Rhyolite	645723	5348170	1.15	7.7	1.69	4.81		5.28	0.75
MERN18MDS0110AG01	Schofield 2018	Powell Rhyolite	645673	5347845	1.29	7.52	1.75	5.3	0.82	5.51	0.87
MERN19MDS0126AG01 (qtz-f	Schofield 2019	Powell Rhyolite	646496	5348024	1.23	8.13	1.81	5.26	0.78	5.4	0.81
8068	Lhereux	Powell Rhyolite	645680	5348170						5.02	0.87
8332	Lhereux	Powell Rhyolite	645599	5348141							
8081	Lhereux	Lower Marker Unit	644794	5348139						3.65	0.64
8084	Lhereux	Lower Marker Unit	644606	5348173						3.44	0.61
MERN18MDS0076CG01	Schofield 2018	Lower Marker Unit	645222	5347709	1	5.5	1.17	3.65	0.52	3.7	0.53
MERN18MDS0077AG03	Schofield 2018	Lower Marker Unit	645259	5347730	0.82	5.1	1.16	3.74		3.84	0.59
MERN18MDS0097AG01	Schofield 2018	Lower Marker Unit	644838	5347661	1.3	7.32	1.66	4.65	0.71	4.54	0.69
MERN18MDS0117AG01	Schofield 2018	Lower Marker Unit	645269	5348088	1.07	6.18	1.45	4.4	0.67	4.63	0.72
MERN18MDS0103EG05	Schofield 2018	Here Creek rhyolite	645415	5347965	1.38	8.16	1.83	5.69	0.88	5.91	0.94
MERN18MDS0120AG01	Schofield 2018	Héré Creek rhyolite	645686	5348384	1.02	5.77	1.33	4.24	0.68	4.52	0.74
MERN19MDS0151AG02	Schofield 2019	Héré Creek rhyolite	646382	5348652	1.28	8.17	1.8	5.49	0.86	5.69	0.85
MERN18TRJ0248AG01	Joergensen 2019	Here Creek rhyolite	645505	5350251	1.01	6.96	1.41	4.21	0.68	4.77	0.74
MERN18TRJ0269AG01	Joergensen 2019	Northwest rhyolite	638583	5358516	1.46	9.48	1.9	6.12	0.86	5.85	0.81
NOR-55	Lesher et al 1986	Northwest rhyolite			2.6					12.3	1.9
MERN18TRJ0268AG01	Joergensen 2019	Rusty Ridge Andesite	638789	5358154	0.81	5.46	1.17	3.32	0.51	3.38	0.48
MERN18TRJ0267AG01	Joergensen 2019	Amulet rhyolite	639227	5357808	1.95	12.65	2.77	7.65	1.24	8.28	1.28
MERN18TRJ0257AG01	Joergensen 2019	Amulet rhyolite	642383	5351526	1.16	7.14	1.51	4.25	0.66	4.53	0.7
915-4	Lesher et al 1986	Amulet rhyolite			1.12					5.35	0.85
MERN18TRJ0265AG01	Joergensen 2019	Waite Andesite	640825	5356812	0.5	3.53	0.75	2.12	0.34	2.24	0.33
915-1	Lesher et al 1986	Waite rhyolite			1.38					6.33	1
MERN18TRJ0264AG01	Joergensen 2019	Waite rhyolite	641211	5357014	1.41	9.37	1.98	5.59	0.9	6.08	0.93
MERN18TRJ0263AG01	Joergensen 2019	Amulet Andesite	642268	5355599	0.46	2.9	0.54	1.49	0.22	1.48	0.26
MERN18TRJ0260AG01	Joergensen 2019	Amulet Andesite	642306	5353553	0.8	4.67	0.99	2.76	0.4	2.87	0.44

Chapter 5

5 Concluding statements

5.1 Conclusions

This thesis presents a revised stratigraphic, structural and metallogenic interpretation of the Powell block of the Rouyn-Noranda mining district. Using new zircon CA-ID TIMS U-Pb ages, lithogeochemistry and detailed mapping, the Powell Block is subdivided into two domains, the northern Brownlee domain and the southern Joliet domain, which are separated by a quartz feldspar porphyritic rhyolite dike. These two fault blocks consist of lower Blake River Group volcanic strata that differ slightly in age and volcanic history. The Brownlee domain is characterized by mafic dominated, bimodal volcanism (~2701 Ma), whereas the Joliet domain is characterized by a thick sequence of felsic coherent and volcaniclastic units (≥2702 Ma). The Powell Block underwent two major base metal mineralizing hydrothermal events. The older event occurred during lower Blake River Group volcanism and is restricted to the Joliet domain. It is expressed by formation of the Quemont Au-rich VMS deposit. The Au-rich Quemont VMS deposit is coeval with the Au-rich Horne deposit to the south and is related to early subsidence and voluminous felsic volcanism. This event may have led to a greater input of magmatic-hydrothermal fluid to the base metal mineralizing fluids, possibly due to a more volatile rich magma source, proximity to magmatic source, and/or enhanced structural permeability linked to cauldron subsidence and proximity to the transcrustal Horne Creek Fault, resulting in higher Au grades for the Quemont and Horne deposits relative to the conventional Cu-Zn VMS deposits of the Flavrian Block to the north, which formed in a mafic dominated bimodal volcanic setting.

The formerly enigmatic quartz-Cu-Zn-Ag veins and Joliet breccia are related to an Upper Blake River Group, ca. 2699~2695 Ma, magmatic-hydrothermal event, which was superimposed on older Lower Blake River Group volcanic strata, with variations in individual deposit characteristics reflecting differences in depth of formation and proximity to magmatic source. Other similar breccia hosted mineral occurrences elsewhere in the Rouyn-Noranda mining district include the St. Jude breccia and possibly the Newbec breccia, which are both spatially associated with intrusions. The lateral zoning of alteration types, compositional gains and losses, metal tenor, as well as their relative timing within the quartz-Cu-Zn-Ag veins and Joliet Breccia are similar to VMS footwall alteration zones within the district and elsewhere. The VMS deposits hosted by the Upper Blake River Group (e.g. Mobrun, Bouchard-Hebert) are broadly coeval with the timing of these ca. 2698 Ma discordant mineral occurrences. Thus, within the context of the metallogeny of the larger Rouyn-Noranda mining district these vein-style, to breccia hosted occurrences, may be part of a broad continuum of subsurface magmatic-hydrothermal deposits and seafloor VMS deposits, akin to the porphyry-intermediate sulfidation epithermal continuum of modern subaerial volcanic arcs.

Alteration and mineralization associated with gold-quartz-carbonate orogenic veins overprint the early discordant quartz-Cu-Zn-Ag veins and breccia. Field relationships, contrasting alteration mineral associations, lithogeochemical and isotopic alteration signatures, metal tenors and $\delta^{18}O_{quartz}$ values for both vein styles suggest that the quartz-Cu-Zn-Ag veins formed earlier than the gold-quartz-carbonate veins and that the two are genetically unrelated. Detailed structural mapping indicates that the gold-quartz-carbonate veins were emplaced along NNW striking mafic dikes during early D_2 N-S shortening at ca. 2670–2660 Ma, roughly 30 to 40 m.y. after the the emplacement of the quartz-Cu-Zn-Ag veins. Despite the different chronology of the two vein

systems, pre-existing structures controlled the hydrothermal fluid flow and ultimately dictated the orientation of the two vein types and their subsequent deformation style. The superposition of these three mineralization styles attests to the continued reactivation of fundamental structures during the evolution of the Noranda volcanic complex and its hydrothermal systems.

5.1 Future work

In Chapter 2, a magmatic-hydrothermal origin for the Joliet breccia and associated mineralization was documented based on field relationships, petrography and a new zircon CA-ID TIMS U-Pb age for a spatially associated tonalite. A magmatic input could be further assessed using LA-ICP-MS trace element maps, $\Delta^{33}S$ and $\delta^{34}S$ values of pyrite and a fluid inclusion study of the hydrothermal quartz cement.

In Chapter 3, a new alteration style was documented consisting of ovoid clusters of fine-grained concentrically zoned sericite and albite within a chloritic matrix. This alteration style is related to the ca. 2698 Ma magmatic-hydrothermal event that formed the Joliet Breccia and numerous subeconomic quartz-Cu-Zn-Ag veins. It shares some similarities with retrogressed cordierite porphyroblastic dalamatianite alteration found within the amphibolite facies contact metamorphic aureole of the Lac Dufault pluton in the Flavrian block (De Rosen Spence, 1969), however, it is widespread in the Powell block, is not limited to any known contact aureole, nor has any preserved cordierite been observed. Similar alteration spots of unknown origin have been reported at the Corbet deposit (Knuckey and Watkins, 1982) and are overprinting the No.14 lens of the Millenbach VMS deposit (Riverin, 1977). A detailed metamorphic study of the Powell Block would provide a better context to interpret whether this spotted texture consists of retrogressed

porphyroblasts of cordierite or another metamorphic mineral, or whether they are a result of patchy alteration that is preferentially nucleating on pre-existing feldspar phenocrysts as interpreted in this study. In addition, the absolute timing of the gold-quartz-carbonate veins has not been determined. The only age reported in the literature is 2562 ± 12 Ma using Pb-Pb in pyrite (Carignan and Gariépy, 1993), which was interpreted as a reset age (Carrier et al., 2000). Thus, U-Pb dating of accessory minerals (monazite, xenotime) could provide further constraints on the formation of the deposits.

In Chapter 4, the structural and stratigraphic framework for the Powell Block is presented and a comparison is made between the Powell and Horne Blocks. However, because of outstanding issues with the chronostratigraphic framework of the Flavrian block, uncertainty remains regarding correlations between the Powell and Flavrian blocks. Additional U-Pb zircon dating of presumed Upper Blake River Group age formations (Millenbach, and Insco rhyolite) within the Flavrian Block are in progress to address this issue.

5.2 References

Carignan, J., and Gariépy, C., 1993, Pb isotope geochemistry of the Silidor and Launay gold deposits: Implications for the source of Archean Au in the Abitibi Subprovince: Economic Geology, v. 82, 1931-1957.

Carrier, A., Jébrak, M., Angelier, J., Holyland, P., 2000, The Silidor deposit, Rouyn-Noranda District, Abitibi Belt: geology, structural evolution, and paleostress modeling of an Au

quartz vein-type deposit in an Archean trondjhemite; Economic Geology, v. 95, p. 1049-1065.

De Rosen-Spence, A., 1969, Genèse des roches à cordierite-anthophyllite des gisements cupro-zincifères de la région de Rouyn-Noranda, Québec, Canada; Canadian Journal of Earth Sciences, v. 6, p. 1339–1345.

Knuckey, M.J., and Watkins, J.J., 1982, The geology of the Corbet massive sulphide deposit Noranda district, Québec, Canada; *in* R.W. Hutchinson, C.D. Spence, and J.M. Franklin eds., Precambrian Sulphide Deposits, Geological Association of Canada Special Paper 25, p. 297-317.

Riverin, G., 1977, Wall-rock alteration at the Millenbach mine, Noranda, Québec; unpublished PhD thesis, Queen's University, Kingston, Ontario.

Appendices

Appendix A

Schofield, M.D. 2022. Lithostratigraphic map of the Lac Marlon area, Powell Block, Rouyn-Noranda, Québec, 1:10, 1000.

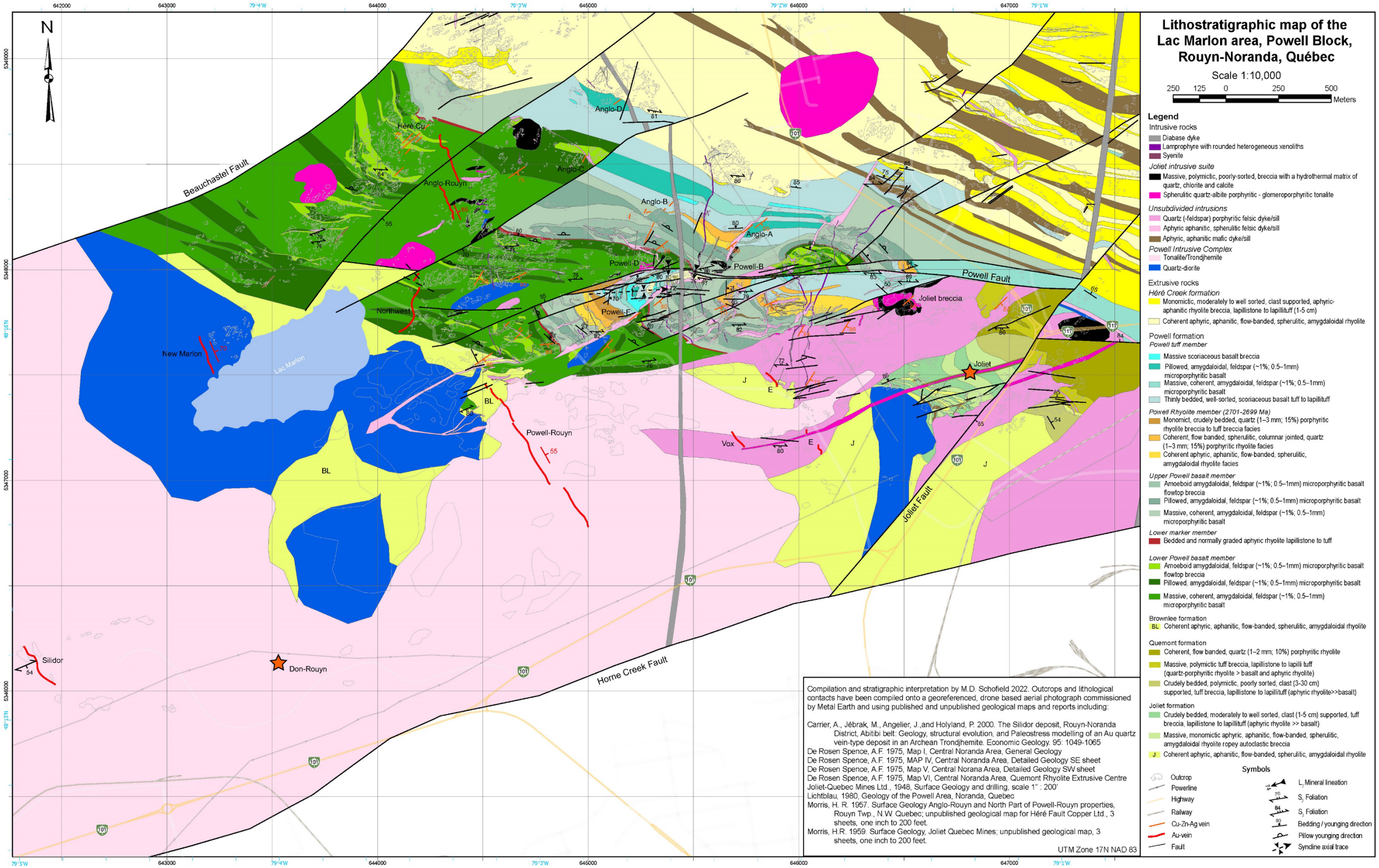

Lithostratigraphic map of the Lac Marlon area, Powell Block, Rouyn-Noranda, Québec

Scale 1:10,000

250 125 0 250 500 Meters

Legend

Intrusive rocks
- Diabase dyke
- Lamprophyre with rounded heterogeneous xenoliths
- Syenite

Joliet intrusive suite
- Massive, polymictic, poorly-sorted, breccia with a hydrothermal matrix of quartz, chlorite and calcite
- Spherulitic quartz-albite porphyritic - glomeroporphyritic tonalite

Unsubdivided intrusions
- Quartz (-feldspar) porphyritic felsic dyke/sill
- Aphyric aphanitic, spherulitic felsic dyke/sill
- Aphyric, aphanitic mafic dyke/sill

Powell Intrusive Complex
- Tonalite/Trondjhemite
- Quartz-diorite

Extrusive rocks

Héré Creek formation
- Monomictic, moderately to well sorted, clast supported, aphyric-aphanitic rhyolite breccia, lapillistone to lapillituff (1-5 cm)
- Coherent aphyric, aphanitic, flow-banded, spherulitic, amygdaloidal rhyolite

Powell formation

Powell tuff member
- Massive scoriaceous basalt breccia
- Pillowed, amygdaloidal, feldspar (~1%; 0.5–1mm) microporphyritic basalt
- Massive, coherent, amygdaloidal, feldspar (~1%; 0.5–1mm) microporphyritic basalt
- Thinly bedded, well-sorted, scoriaceous basalt tuff to lapillituff

Powell Rhyolite member (2701-2699 Ma)
- Monomict, crudely bedded, quartz (1–3 mm; 15%) porphyritic rhyolite breccia to tuff breccia facies
- Coherent, flow banded, spherulitic, columnar jointed, quartz (1–3 mm; 15%) porphyritic rhyolite facies
- Coherent aphyric, aphanitic, flow-banded, spherulitic, amygdaloidal rhyolite facies

Upper Powell basalt member
- Amoeboid amygdaloidal, feldspar (~1%; 0.5–1mm) microporphyritic basalt flowtop breccia
- Pillowed, amygdaloidal, feldspar (~1%; 0.5–1mm) microporphyritic basalt
- Massive, coherent, amygdaloidal, feldspar (~1%; 0.5–1mm) microporphyritic basalt

Lower marker member
- Bedded and normally graded aphyric rhyolite lapillistone to tuff

Lower Powell basalt member
- Amoeboid amygdaloidal, feldspar (~1%; 0.5–1mm) microporphyritic basalt flowtop breccia
- Pillowed, amygdaloidal, feldspar (~1%; 0.5–1mm) microporphyritic basalt
- Massive, coherent, amygdaloidal, feldspar (~1%; 0.5–1mm) microporphyritic basalt

Brownlee formation
- BL Coherent aphyric, aphanitic, flow-banded, spherulitic, amygdaloidal rhyolite

Quemont formation
- Coherent, flow banded, quartz (1–2 mm; 10%) porphyritic rhyolite
- Massive, polymictic tuff breccia, lapillistone to lapilli tuff (quartz-porphyritic rhyolite > basalt and aphyric rhyolite)
- Crudely bedded, polymictic, poorly sorted, clast (3-30 cm) supported, tuff breccia, lapillistone to lapillituff (aphyric rhyolite>>basalt)

Joliet formation
- Crudely bedded, moderately to well sorted, clast (1-5 cm) supported, tuff breccia, lapillistone to lapillituff (aphyric rhyolite >> basalt)
- Massive, monomictic aphyric, aphanitic, flow-banded, spherulitic, amygdaloidal rhyolite ropey autoclastic breccia
- J Coherent aphyric, aphanitic, flow-banded, spherulitic, amygdaloidal rhyolite

Symbols

- Outcrop
- Powerline
- Highway
- Railway
- Cu-Zn-Ag vein
- Au-vein
- Fault
- L_2 Mineral lineation
- S_2 Foliation
- S_3 Foliation
- Bedding / younging direction
- Pillow younging direction
- Syncline axial trace

Compilation and stratigraphic interpretation by M.D. Schofield 2022. Outcrops and lithological contacts have been compiled onto a georeferenced, drone based aerial photograph commissioned by Metal Earth and using published and unpublished geological maps and reports including:

Carrier, A., Jébrak, M., Angelier, J.,and Holyland, P. 2000. The Silidor deposit, Rouyn-Noranda District, Abitibi belt: Geology, structural evolution, and Paleostress modelling of an Au quartz vein-type deposit in an Archean Trondjhemite. Economic Geology. 95: 1049-1065
De Rosen Spence, A.F. 1975, Map I, Central Noranda Area, General Geology
De Rosen Spence, A.F. 1975, MAP IV, Central Noranda Area, Detailed Geology SE sheet
De Rosen Spence, A.F. 1975, Map V, Central Norana Area, Detailed Geology SW sheet
De Rosen Spence, A.F. 1975, Map VI, Central Noranda Area, Quemont Rhyolite Extrusive Centre
Joliet-Quebec Mines Ltd., 1948, Surface Geology and drilling, scale 1" : 200'
Lichtblau, 1980, Geology of the Powell Area, Noranda, Quebec
Morris, H. R. 1957. Surface Geology Anglo-Rouyn and North Part of Powell-Rouyn properties, Rouyn Twp., N.W. Quebec; unpublished geological map for Héré Fault Copper Ltd., 3 sheets, one inch to 200 feet.
Morris, H.R. 1959. Surface Geology, Joliet Quebec Mines; unpublished geological map, 3 sheets, one inch to 200 feet.

UTM Zone 17N NAD 83